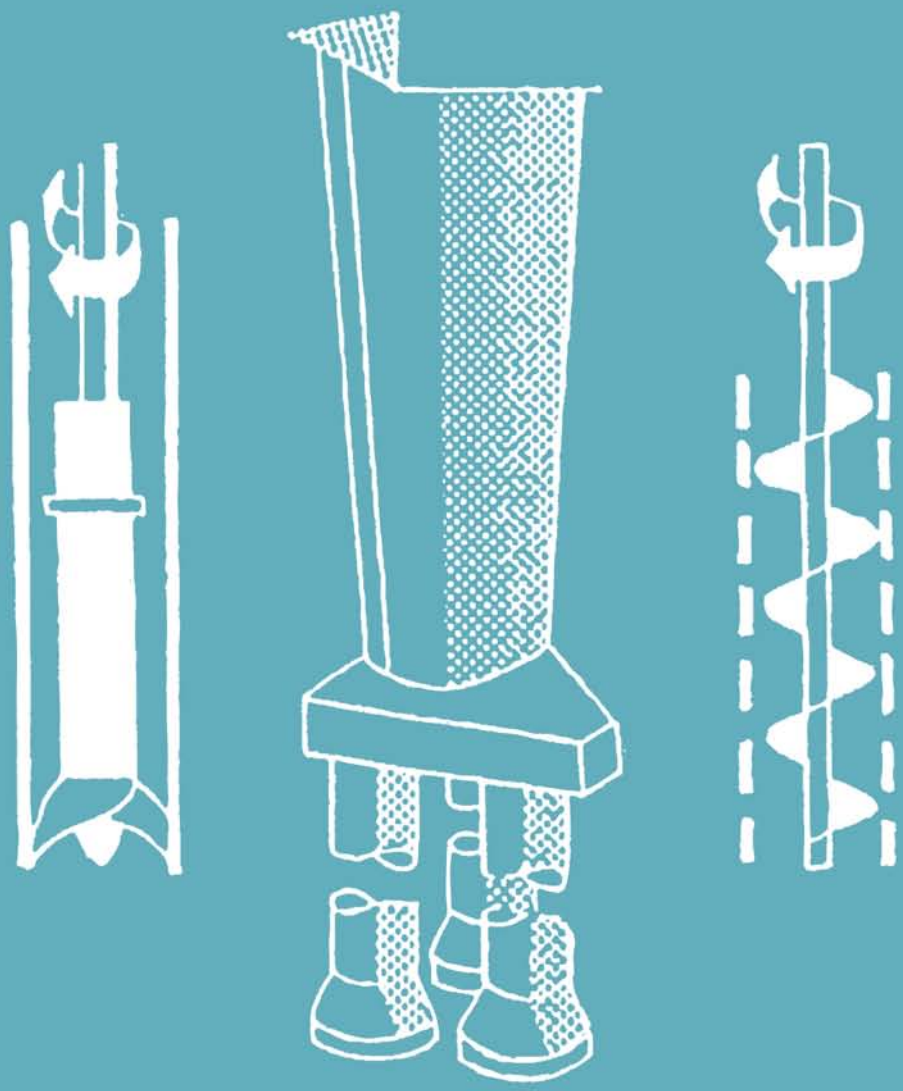

W.F. VAN IMPE AND P.O. VAN IMPE – EDITORS

DEEP FOUNDATIONS ON BORED AND AUGER PILES

CRC Press
Taylor & Francis Group
A BALKEMA BOOK

DEEP FOUNDATIONS ON BORED AND AUGER PILES

PROCEEDINGS OF THE FIFTH INTERNATIONAL SYMPOSIUM ON DEEP FOUNDATIONS ON BORED AND AUGER PILES (BAP V), GHENT, BELGIUM, 8–10 SEPTEMBER, 2008

Deep Foundations on Bored and Auger Piles

Editors

W.F. Van Impe
Laboratory of Geotechnics, Ghent University, Zwijnaarde, Belgium

P.O. Van Impe
AGE, Erpe-Mere, Belgium

CRC Press
Taylor & Francis Group
Boca Raton London New York Leiden

CRC Press is an imprint of the
Taylor & Francis Group, an **informa** business

A BALKEMA BOOK

CRC Press/Balkema is an imprint of the Taylor & Francis Group, an informa business

Typeset by Vikatan Publishing Solutions (P) Ltd., Chennai, India.
Printed and bound in Great Britain by Antony Rowe (A CPI-group Company), Chippenham, Wiltshire

Published by: CRC Press/Balkema
P.O. Box 447, 2300 AK Leiden, The Netherlands
e-mail: Pub.NL@taylorandfrancis.com
www.crcpress.com – www.taylorandfrancis.co.uk – www.balkema.nl

ISBN: 978-0-415-47556-3 (Hbk + CD-rom)
ISBN: 978-0-203-88287-0 (ebook)

Deep Foundations on Bored and Auger Piles – Van Impe & Van Impe (eds)
© 2009 Taylor & Francis Group, London, ISBN 978-0-415-47556-3

Table of contents

Deep Foundations on Bored and Auger Piles – Van Impe & Van Impe (eds)
© 2009 Taylor & Francis Group, London, ISBN 978-0-415-47556-3

Preface

On a five-yearly basis and starting in 1988, the Bored and Auger Pile Seminars have been organized in Ghent.

The intriguing complexity of the soil-pile interaction and its related load-settlement behaviour do justify such specialized topic meetings, especially in case of bored and even more of screw piles.
Contractors, designers and academicians complied once more in the proceedings their new approaches and developments of the last five years, elucidating the today's state-of-the-art from pile installation, pile testing and pile capacity-evaluation point of view.
Newly implemented topics such as energy pile concepts are involved as well in this edition of the BAP events. For sure, this might indeed become a much more relevant issue in the coming decade.

This fifth Bored an Auger Pile Seminar hopefully will also contribute to a better and more efficient professional interaction of specialized contractors, designers and academicians gathering in the discussion sessions this week.

It's the main editor's pleasure to thank sincerely all members of the Scientific and the Organizing Committee in preparing this fifth BAP event. For the continuous follow up of the Seminar's organizing details as well as the lay-out of the proceedings, the laboratory scientific staff Dr ir P. Van Impe, ir R.D. Verastegui F., ir G. Di Emidio; L. Barbetti and the technical-administrative staff Mrs. K. Crombeen, Mrs. L. Van Cauwenberge, Mrs. H. De Cooman, Mr. B. Van Impe, Mr. F. Van Boxstael and Mr. J. Van der Perre should be acknowledged.

The Scientific Committee equally returns thanks to all authors and discussion contributors allowing for a high level proceeding edition and the undoubtfully related intriguin discussion sessions pitching the expectations high.

Prof. Dr ir W.F. Van Impe
Seminar-Coordinator

Deep Foundations on Bored and Auger Piles – Van Impe & Van Impe (eds)
© 2009 Taylor & Francis Group, London, ISBN 978-0-415-47556-3

Scientific advisory committee

F. De Cock (Belgium)
R. Ellman (USA)
B. Lehane (Australia)
H. Brandl (Austria)
F. Van Tol (The Netherlands)
V. Fioravante (Italy)
A. Holeyman (Belgium)
R. Katzenbach (Germany)
W. Van Impe (Belgium)
P. Van Impe (Belgium)

Special lecture

Deep Foundations on Bored and Auger Piles – Van Impe & Van Impe (eds)
© 2009 Taylor & Francis Group, London, ISBN 978-0-415-47556-3

Geotechnical engineering issues related to the Messina Strait Crossing

G. Fiammenghi
Messina Strait Company Ltd., Italy

M. Jamiolkowski
Technical University of Torino, Italy

W.F. Van Impe
Laboratory of Geotechnics, Ghent University, Zwijnaarde, Belgium

ABSTRACT: In this paper, the geotechnical engineering issues involved in the Messina strait crossing by means of a one-span suspension bridge, are summarized. The relevant discussion topics with this respect deal with the soil data collection and with the design soil parameters' evaluation. A summary of the foundation engineering concepts relevant to the bridge design is also supplemented.

1 INTRODUCTION

A stable connection between Italy mainland and Sicily Island has always been longed for by the population, as already pictured, see Fig. 1, Vullo (1999), in a fresco showing a temporary bridge across the Messina Straits, built by the Roman army in the 3rd century B.C.

The modern history of a permanent Strait crossing sets off, approximately in 1885, with an underground tunnel project by the civil engineer Navona.

Ever since and throughout the 20th century many plans and schemes have followed one another, aimed at pursuing the most suitable design concept and intended to develop its feasibility study.

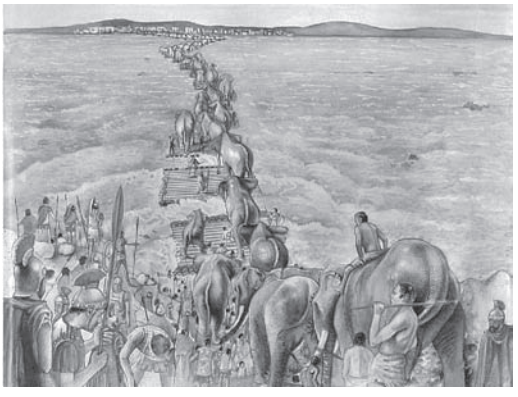

Figure 1. Bridging the Strait: an ancient dream. The temporary bridge built by the Roman army in 3rd century B.C.

The significant action heading towards this goal was the setting up, in 1981, of the Messina Strait Company Ltd (MSC) with the assignment of selecting the most beneficial solution, followed by the progress of a preliminary, yet suitable design, as a starting point for the international bid for general contractors entrusted to design and build a permanent Strait crossing.

Over the period 1981 to 1985, the MSC completed a comprehensive comparative study of the following four solutions:

- Underground tunnel
- Floating submarine tunnel
- Two-span suspension bridge
- One span suspension bridge.

The choice of the one span highway and railway suspension bridge whose cross-section, as shown in Fig. 2 was the decisive effect of the studies, based on the following considerations:

- The hostile environment of the Messina Straits, e.g.; seismicity, sea currents, on-shore and off-shore terrain morphology
- The costs-benefits issues
- The environmental impact
- The vulnerability to extreme events.

For the period 1985 to 1992, the design of the one-span bridge, along with the related highway and

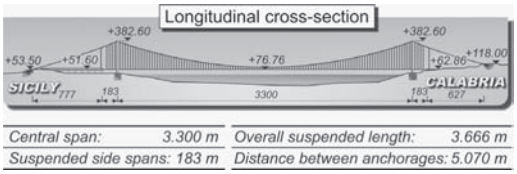

Figure 2. General arrangement of the suspension bridge.

	Calabria	Sicilia
Highway infrastructures:	9.8 Km	10.5 Km
Railway infrastructures:	4.6 Km	15.2 Km

Figure 3. Bridge and access infrastructure.

railway infrastructures, shown in Fig. 3, was completed allowing calling for general contractor biddings.

The following years were mainly devoted to the project's political and financial issues, even though some additional studies were enhanced in relation to: design earthquake, aerodynamic bridge deck optimization and railway runnabilty.

The most recent actions, events and activities on the status of the project, can be summarized as follows:

- 2003. The project of the Bridge is approved by CIPE (Economic Planning Governmental Committee).
- 2004 to 2006, MSC implements the bid to select the General Contractor.
- 2006. The contract is assigned to a Consortium led by IMPREGILO Ltd with the general tasks of: final design and construction of the bridge.
- 2006 the consultants for the project management and control, environmental monitoring and assurance brokerage are appointed.
- Spring 2006. Italian general elections won by Left Wing coalition. The new Government did not consider the construction of the Bridge of priority interest.
- Spring 2008. New Italian general elections won by the Right Wing. The new Government pronounces the intent to build the bridge.

In the following, the writers present a synthesis of the geotechnical issues of the suspension bridge focusing their attention on the geotechnical site characterization and on the adopted foundation system.

2 GEOTECHNICAL SITE CHARACTERISATION

2.1 *Introductory Remarks*

Making reference to Section 2.2 examining the Straits Geology, this Section deals with the geotechnical site characterization at four locations: two tower foundations and two anchor blocks, where the one span bridge interacts with the underlying geomaterials.

The chronological sequence of the depositional history of soils and rocks formations along the planned location of the bridge is summarized in Fig. 4. The in situ and laboratory soil investigation campaigns carried out in late seventies and in the eighties were aimed at determining the physical and mechanical properties of geomaterials which will likely interact more directly with the bridge foundations and with the anchor blocks under static and earthquake generated loadings.

2.2 *Geotechnical investigations*

In addition to various geological borings (series C on the Calabria shore and S on the Sicily shore), reaching depths between 50 and 200 m and discussed in Section 2.2, a series of geotechnical borings (BH series) and in situ tests were carried out on both banks of the Straits, to achieve the essential information for a safe and optimal foundation design.

The programme of the geotechnical investigations is summarized in Tab. 1, while Figs. 5 and 6 report the location of the geotechnical borings and the in situ tests carried out along the bridge axis, together with some geological borings of C and S series, crucial for the foundation design.

The information gained from BH, C and S borings allowed identifying the most important soil profiles for the locations of the towers foundations are shown in Figs. 7 and 8.

Figure 4. Soil deposits encountered across Messina Straits.

Table 1. Soil investigation programme.

	CALABRIA		SICILY	
	Foundation	Anchor	Foundation	Anchor
Borings (1)	4	3	3	1
Holes for SPT's (2)	4	4	4	4
Holes for LPT's (2)	4	4	4	4
Shafts for PLT's (3)	None	1	None	1
Pumping test	1	None	1	None
CPT's	None	None	2	3
DMT's	None	None	1	3
CH (4)	1	1	1	1
SASW	1	1	1	1

(1) depth 90 to 100 m
(2) depth 50 m, with rod energy measurements
(3) 2.5 m in diameter cased shaft, depth 18 m, plate diameter 800 mm
(4) 3 holes, depth of each 100 m

BH = Boring with sampling
SPT = Standard penetration test
LPT = Large penetration test
PLT = Plate load test
CPT = Static cone penetration test
CH = Seismic waves velocity measurement in cross-hole
SASW = Spectral analysis of surface waves
DMT = Flat Marchetti dilatometer

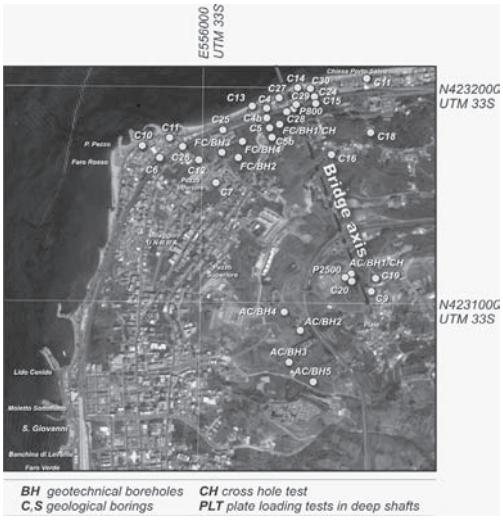

Figure 5. Soil investigation on Calabria Shore.

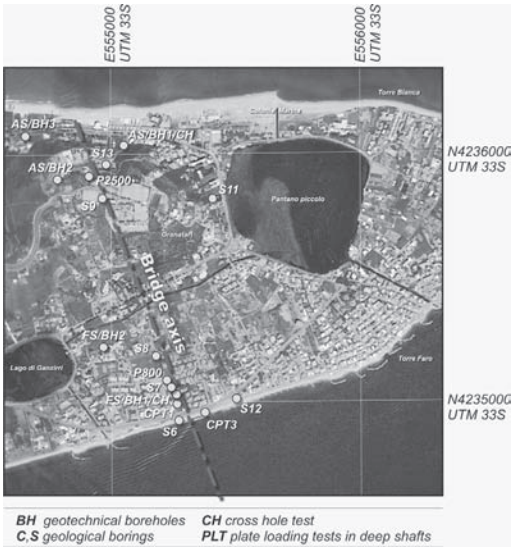

Figure 6. Soil investigation on Sicilia shore.

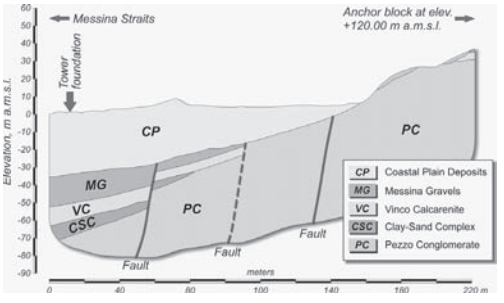

Figure 7. Soil profile at Calabria Shore.

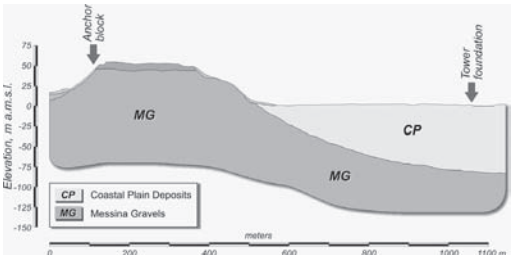

Figure 8. Soild profile at Sicilia Shore.

The Sicily tower, see Fig 8, is laying on 50 to 70 m of thick sand and gravel Coastal Plane (CP) deposits of Holocene age overlaying more than 150 m thick sand and gravel deposit of medium Pleistocene age, locally named Messina Gravels (MG).

The Calabria tower foundation soil profile, see Fig. 7, appears more complex. Here, the sandy and gravely soils, belonging to the CP and MG formations

with thickness of 35 to 45 m, overlay the Calcarenite di Vinco (CV) of the upper Pliocene age and the Sandy-Clayey Complex (SCC) of medium to lower Pliocene age.

Overall the thickness of such geological units, laying directly on the soft rock formation of large thickness (>150 m), locally named Conglomerato di Pezzo (PC), does not exceed ≅ 35 to 50 m.

As to the soil formation, relevant to the anchor block design, MG and PC are respectively on both Sicilia and Calabria shores. The information obtained from BH borings series were supported and enhanced by the results of a variety of in situ tests listed in Tab. 1. Among them, considering that on both sides of the Straits, the foundations design deals with difficult to sample geomaterials, the following two are worth to be mentioned:

- The dynamic Large Penetration Test (LPT), developed in relation to concern that the dimensions of gravely particles can false the blow/count obtained from the Standard Penetration Tests (SPT).
- The measurements of the shear (V_s) and compression (V_p) waves velocity by means of Cross Hole (CH) tests, which now days plays a crucial role in geotechnical site characterization. In the examined case, the V_s and V_p measurements permitted the evaluation in situ of the small strain shear modulus G_0, porosity n, and an estimate of the bulk density γ.

As to LPT, the sampler used as penetration tool, see Fig. 9, had ID =110 mm, OD =140 mm and housed a plastic liner 5 mm thick. It was driven to penetrate 450 mm below the borehole bottom, using fall weight (W) of 5592 N and drop height (H) of 500 mm. Analogously, to SPT also during the LPT, the number of blows necessary to penetrate every 300 mm had been recorded.

To calibrate the LPT and compare its results against SPT, parallel tests with both devices were performed in the well documented uniform Po river sand (Baldi et al. 1988 and 1989) whose grain size distribution is shown in Fig. 10. The results of said calibration tests are presented in Fig.11.

All SPT's and LPT's both at the Po river and at the Messina Straits sites, were carried out in cased boreholes filled with bentonite slurry and having a diameter of 75 mm and 200 mm respectively. During all the tests, the driving energy delivered to the rods was measured using an instrumented 1-m long rod segment located at the top of the string, see Schmertmann and Palacios (1979).

Examples of SPT and LPT results measured at the Straits sites as well as at the Po river site are summarized in Figs. 11 to 15. These figures besides the SPT and LPT blow/counts, report also the V_s trend

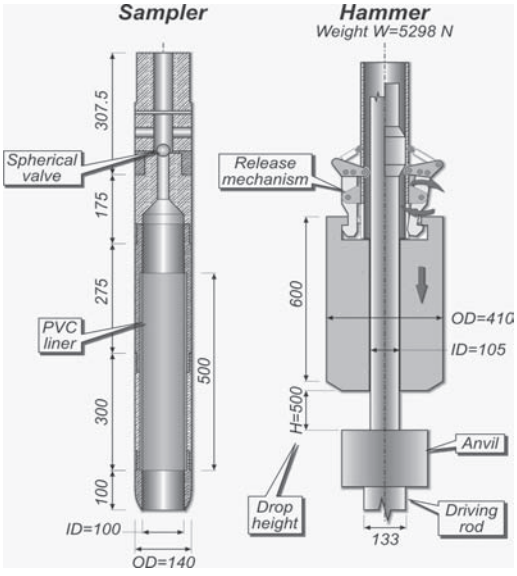

Figure 9. Large penetration test equipment.

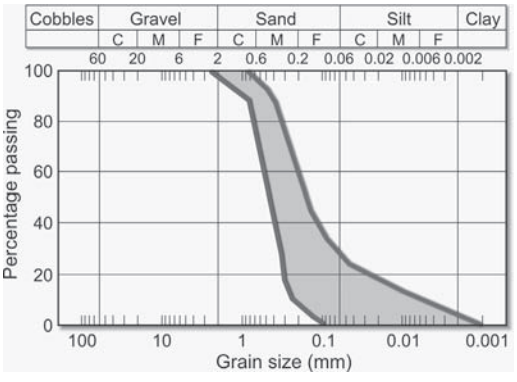

Figure 10. Soil grading at Po River Site.

with depth together with the energy ratio (ER) for both penetration devices. The ER is defined driving the energy measured divided by its theoretical value WH. At all the mentioned sites the yielded ER values resulted quite uniform ranging between 60 and 65 percent and 80 to 85 percent for SPT and LPT respectively, see Fig. 16.

As to geophysical tests, they mainly consisted in 100-m deep cross-hole (CH) tests carried out at 1-m depth intervals. Each test involved three 5-m spaced boreholes, properly equipped: one housing the source and the other carrying the receivers. This arrangement allowed to compute the V_s and V_p velocities using a true time interval method which combined with

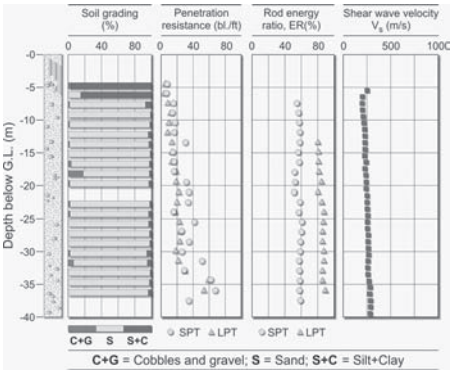

Figure 11. Soil profile at Po River Site.

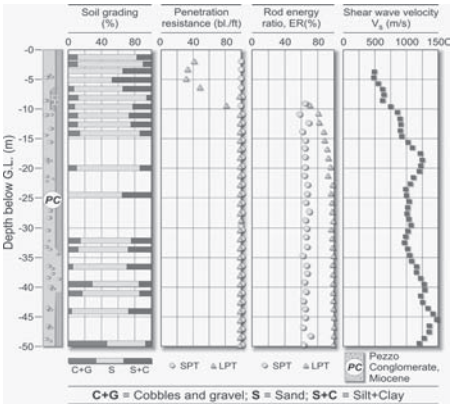

Figure 12. Soil profile at Calabria anchor site.

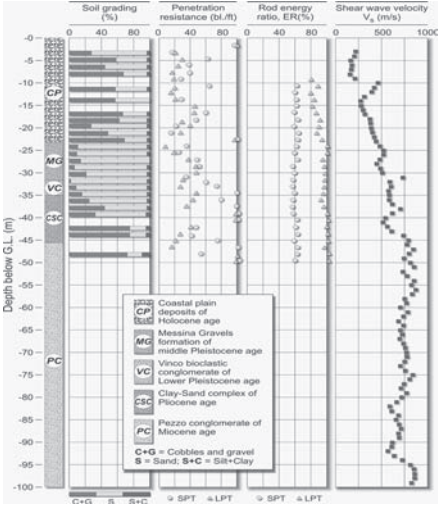

Figure 13. Soil profile at Calabria tower site.

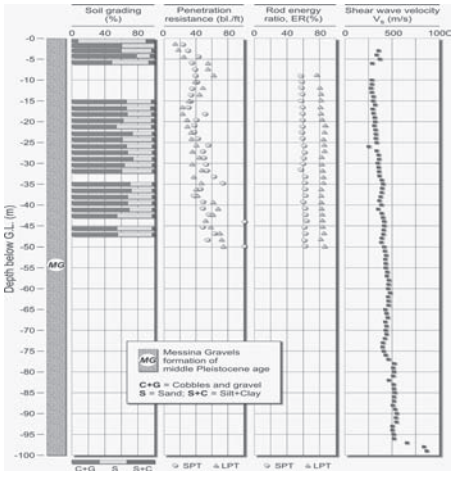

Figure 14. Soil profile at Sicilia anchor site.

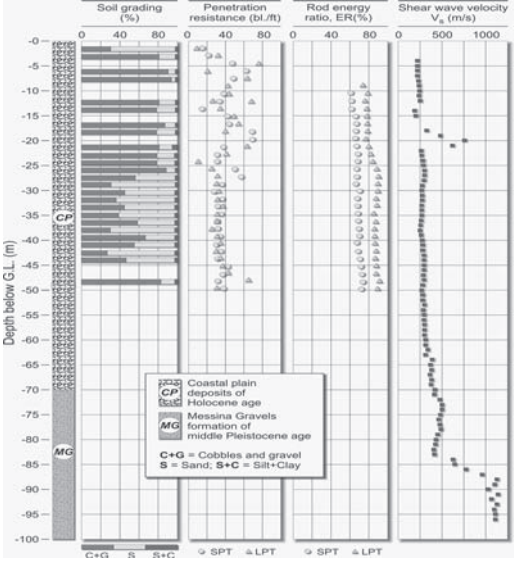

Figure 15. Soil profile at Sicilia tower.

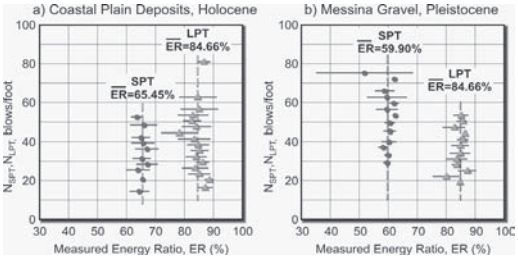

Figure 16. Values of energy ratio measured in Coastal Plain Deposits (a) and in Messina Gravel formation (b).

accurate measurements of the boreholes deviations from the verticality, together with their azimuths, provided reliable results.

In addition to CH tests, the Spectral Analyses of Surface Waves (SASW) method, see Nazarian and Stokoe (1983), was also attempted to assess the V_s in situ via surface geophysics. Fig. 17 shows the V_s measured in the MG at the Sicily anchor site in CH test and by SASW. Both tests yield almost identical values except for the depth between 50 and 55 m where CH tests suggest the presence of a cemented layer not detected by SASW.

During borings and pumping tests, cfr. Tab.1, the ground water level (GWL) conditions at the four pertinent locations were framed. At the towers locations, where the existing ground level (GL) corresponds to an elevation in the order of 1 to 3 m above m.s.l., the GWL is encountered at a depth ranging between 1 and 2 m. At the Sicily anchor block location, the GWL was not found within a depth relevant to the design, while on the Calabria anchor block area was found around 6 to 10 m below GL.

As to laboratory testing, because undisturbed sampling by freezing technique [Yoshimi et al. (1977, 1978, 1984), Yoshimi (2000), Kokusho and Tanaka (1994)] were rescheduled to the final design stage, only a limited number of laboratory tests were carried out, their largest part aimed at determining the classification and the index soil properties. In addition, some testing were carried out on reconstituted material to mark out the sand and gravel stiffness belonging to the CP deposits. These material specimens, properly scalped to a maximum grain size of 10 mm, prepared by under compaction, were subject to resonant column (RCT) and triaxial compression (TX-C) tests, see: ISMES (1985), Ferrante (1988), Jamiolkowski et al. (2002).

2.3 *Engineering properties*

The discussion on the engineering properties of the soils encountered across the Messina Straits is mostly focused on the coarse grained materials belonging to CP and MG deposits. Actually, their characteristics resulted to control the preliminary design of the two towers foundations and of the Sicily anchor block, both under static and earthquake generated loadings.

The preliminary design of the Calabria anchor block embedded in the CP formation, where both SPT and LPT gave always refusal and the CH yielded the V_s higher than 800 m/s, was guided by this in situ tests outcome. A more detailed geotechnical characterization of the PC by seismic and electrical resistivity tomography as well as through laboratory tests was postponed to the final design stage.

As to the classification and index properties tests, in the following are summarized the available information:

a. CP and MG deposits have similar mineralogical composition because both of them were originated by the disruption and the erosion of the same rock formation and deposited in a similar, shallow sea and coastal environment. The predominant minerals are feldspar (44%), quartz (25%) followed by mica (2%) and various rock fragments (29%).
b. The grain size characteristics can be inferred from the grading curves reported in Figs. 18 through 20. Moreover, in Tab. 2, some additional pieces

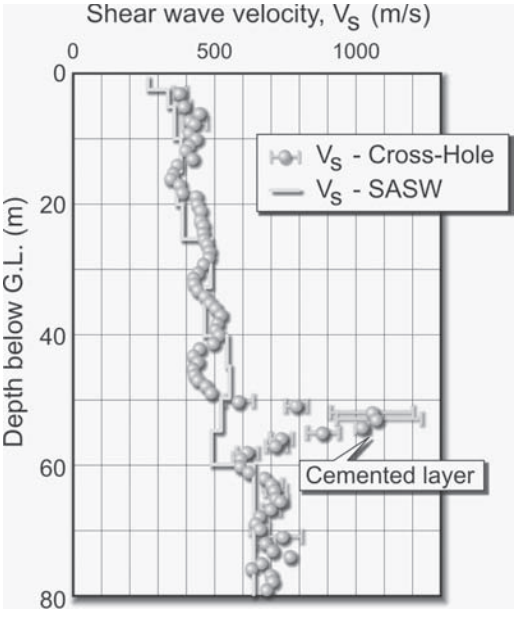

Figure 17. Shear wave velocity measured by two different methods at Sicilian anchor site.

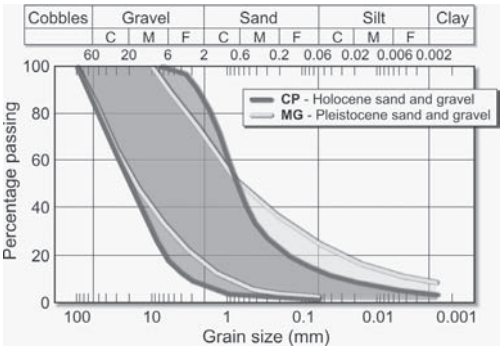

Figure 18. Sicilia tower foundation and anchor.

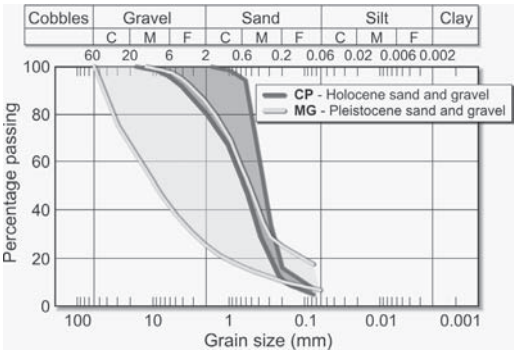

Figure 19. Calabria tower foundation. Grading of the CP and MG deposits.

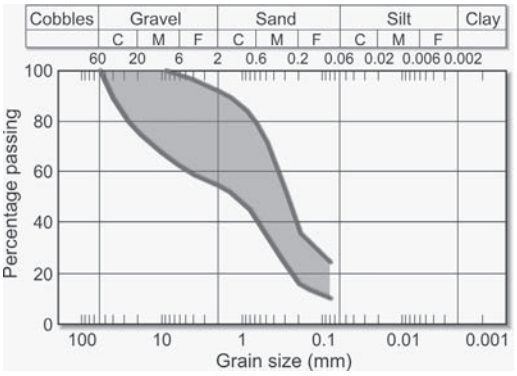

Figure 20. Calabria anchor block. Grading of the disaggregated PC.

Table 2. CP and MG sands and gravel; salient feature of their gradings.

				Gravel (%)		Sand (%)		Fines (%)		D_{50} (mm)		D_{max} (mm)		Tests N.
				mean	st.dev.	mean	st.dev.	mean	st.dev.	from	to	mean	st.dev.	
Tower foundation	Holocene	CPD	BH	58.0	22.1	34.4	18.4	8.6	6.7	0.53	9.60	47.0	17.1	46
			LPT	65.5	22.5	31.7	21.6	2.8	2.2	0.60	21.30	57.9	24.1	73
			SPT	59.6	17.4	36.4	16.7	4.0	2.1	0.60	15.00	30.1	8.1	103
	Pleistocene	MGF	BH	57.1	16.3	36.3	16.4	6.6	3.3	0.92	44.00	56.3	22.2	35
			LPT	85.7	13.2	12.7	12.2	1.7	1.2	7.00	20.00	73.3	26.6	6
			SPT	56.3	11.9	39.0	12.6	4.7	1.0	1.00	11.00	38.3	7.5	6
Anchor block	Pleistocene	MGF	BH	56.9	14.9	33.5	11.9	9.6	6.7	0.20	12.00	39.9	12.4	74
			LPT	67.0	11.5	30.4	9.6	4.0	2.8	0.54	36.00	57.0	22.1	115
			SPT	57.1	9.8	36.5	9.3	6.4	2.1	0.95	7.50	31.3	8.2	117

of information on the grading of the CP and MG deposits as encountered on the Sicily shore, are exposedAs to PC formation it consists in a succession of horizons, from very weakly to weakly cemented conglomerates and sandstone incorporating rare inclusions of siltstone. The cementing matrix of the sand-silt type proves rich of filosilicate components. The clasts of conglomerate and grains sandstone consist of poorly rounded fragments of underlying crystalline granite and gneiss basement. The point load tests carried out on the cores extracted from the borings at the Calabria anchor block yielded values ranging between 0.7 and 1.1 MPa for the conglomerate and between 0.3 and 0.4 MPa for the sandstone.

c. As to bulk density γ, because of the lack of undisturbed sampling, its determination, at the time of the preliminary design, was limited to measurements carried out in situ, during the excavation of the shafts for deep plate loading tests in the MG and PC formations at the Sicily and the Calabria block anchor locations respectively. The obtained values of γ range from 18 to 21 kN/m^3 and from 1.9 to 2.2 kN/m^3, in MG and PC respectively.

Such values were measured above the phreatic surface in soils whose natural water content Wn varied between 2.5 and 4.5 % in MG and from 4 to 11% in PC.

More recently, Foti et al. (2002) have developed a method allowing evaluating the soil porosity (n) in situ based on the seismic wave velocity (V_s, V_p) measurements. The method employs Biot's (1956) theory of poroelasticity for low frequency range and is applicable to fully saturated geomaterials.

The formula to compute n is reported here below:

$$n = \frac{\rho_s - \left[\rho_s^2 - \frac{4(\rho_s - \rho_f)K_f}{V_p^2 - 2\left(\frac{1-\nu_s}{1-2\nu_s}\right)V_s^2}\right]^{0.5}}{2(\rho_s - \rho_f)} \quad (1)$$

n = connected porosity

Table 3. Void ratio and bulk density from seismic tests.

Formation	Void ratio[2] e (–)	Bulk density[3] γ (kN/m^3)	Depth range (m)
Coastal Plain Deposits	0.35 to 0.42	21.0 to 21.8	5 to 60
Messina Gravels	0.28 to 0.40	21.0 to 22.1	20 to 100
Pezzo Conglomerate	0.15 to 0.20	22.5 to 23.8	45 to 100[4]

Notes: [1] Cross hole tests; [2] By means of equation 1), Foti et al. (2002); [3] From computed *e*, assuming full saturation and adopting $G_s = 2.67$; [4] At Calabrian tower location.

ρ_s = soil particles mass
ρ_f = pore fluid density
K_f = bulk modulus of pore fluid
w_s = Poisson ratio of soil skeleton

Equation …1) was validated in a number of fine grained saturated deposits where the computed values of porosity or void ratio (e) were compared against values measured in laboratory on high quality undisturbed samples, see Foti and Lancellotta (2004), and Arroyo et al. (2006).

Tab. 3 gives typical values of e evaluated below the phreatic surface for the Straits deposits based on CH tests results. Moreover, this table reports also an estimate of γ assuming a full saturation and adopting $\rho_s = 2.67$.

d. During the preliminary design stage, in early eighties, the estimate of the relative density (D_r) in situ for the sandy and gravely soils was inferred from SPT results, based on the empirical correlation developed for sands and given by Skempton (1986). In late nineties, Cubrinovski and Ishihara (1999) developed a specific empirical correlation for gravely geomaterials which was calibrated in Japan against the relative density of undisturbed samples retrieved by means of in situ soil freezing.

The correlation assumes that the energy ratio ER is equal to 78%, typical in the Japanese practice. Consequently, the N_{SPT} and N_{LPT} values used to compute D_r were corrected multiplying the blow/count by the ER measured divided by 78%.

The relationships allowing the estimation of D_r suggested by Cubrinovski and Ishihara (1999) are the following:

$$D_r^2 = \frac{(N1)_{78}}{C_d} \tag{2}$$

$$C_d = \frac{9}{e_{max} - e_{min}} \tag{2a}$$

$$e_{max} - e_{min} = 0.23 + \frac{0.06}{D_{50}} \tag{2b}$$

$$N_1 = \left(\frac{Pa}{\sigma'_{vo}} \right)^{0.5} N_{SPT} \tag{2c}$$

$$(N_1)_{78} = \left(\frac{ER}{78} \right) N_1 \tag{2d}$$

Where:

N_1 = SPT and LPT blow/count normalized according to Liao and Whitman (1986) with respect to the effective overburden stress σ'_{vo}.
P_a = reference stress equal to 98.1 kPa
ER = measured energy ratio in percent
e_{max} = maximum void ratio
e_{min} = minimum void ratio
D_{50} = mean grain size in mm

Figs. 21 and 22 show the comparison between values of D_r evaluated by means of the above formulae. The exposed results suggest that the approach by Skempton (1986) for sands tends in gravely soils to overestimate D_r. However, the issue is whether this overestimation is as pronounced as it comes out from Figs. 21 and 22. We will have the answer when undisturbed samples retrieved on the Straits sites by means of freezing technique become available.

For the time being, the values of the relative density, to be considered as actual for the geomaterials in question, should be those obtained using Cubrinovski and Ishihara (1999) approach, giving for both CP and MG deposits $40 < D_r < 60\%$.

As to the assessment of the stress-strain, strength and hydraulic conductivity characteristics for the preliminary design, considering the coarse grained nature of geomaterials encountered, it was mostly based on the results of in situ tests with some limited

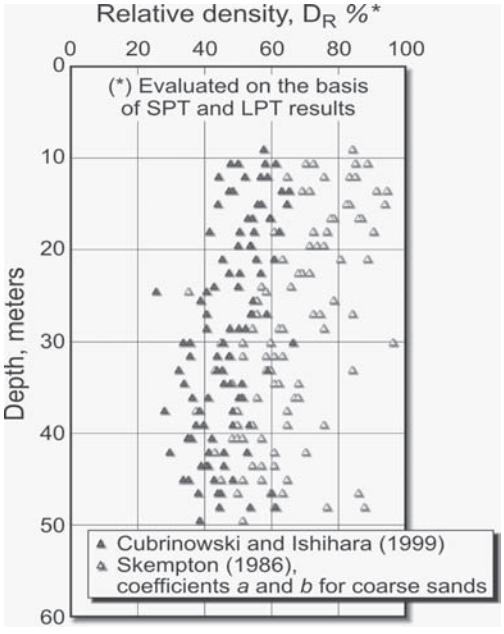

Figure 21. Relative density of Coastal Plain deposits.

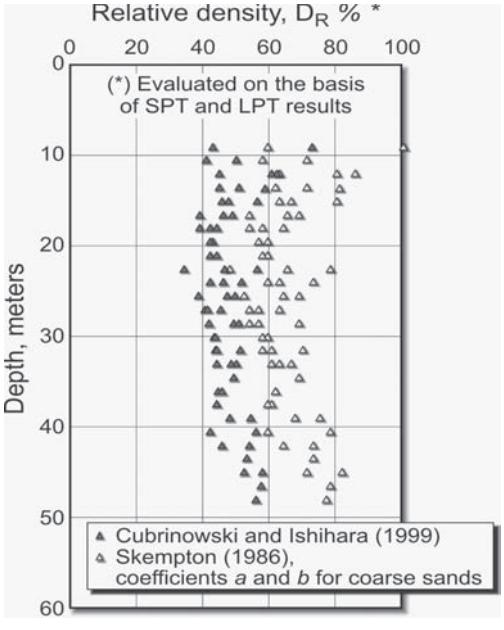

Figure 22. Relative density of Messina Gravel formation.

contribute from the laboratory tests on reconstituted specimens. The available information can be summarized as follows:

a) The small strain shear modulus (G_o) has been obtained from the V_s measured during CH tests by means of the following formula:

$$G_o = V_s^2 \tag{3}$$

The value of shear modulus yielded by eq…3) holds for the shear strain level $\gamma < 1 \times 10^{-3}$ below which the stress-strain relationship can be assumed to be linear [Jardine (1985), Jardine et al. (1991), Tatsuoka et al. (1997), Hight and Leroueil (2002), Jamiolkowski et al. (2005)]. At larger strain, both under monotonic and cyclic loading, the shear modulus is subject to degradation reflecting the non-linearity of the soil behaviour, see Tatsuoka et al. (1997), Darendeli (2001), Jardine et al. (2001), Hight and Leroueil (2002). The relationship $G = f(\gamma)$ has been investigated by means of the RC and TX-C tests on reconstituted specimens of the CP deposits having the D_r ranging between 50 and 60%, see ISMES (1985) and Ferrante (1988).

Fig. 23 shows the relationships between the shear modulus $G(\gamma)$ normalized with respect to

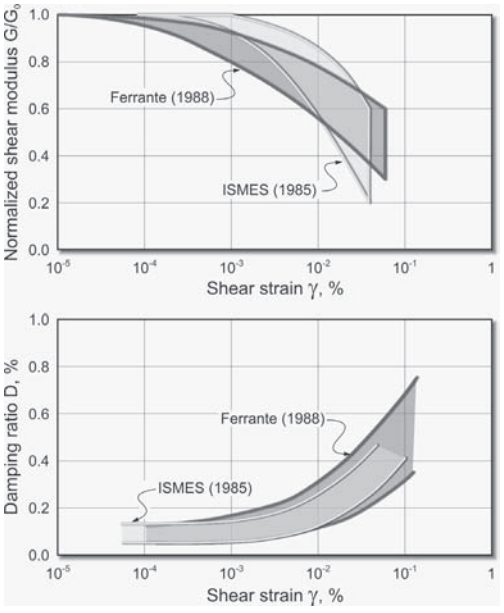

Figure 23. Results of RC tests on reconstituted sand and gravel of CP deposits.

G_o as function of shear strain and shear damping ratio $D = f(\gamma)$ as obtained from the above said laboratory studies, being G a value of shear modulus at $\gamma > 1 \times 10^{-3}$.

Unfortunately, the G values obtained on reconsti tuted specimens, although tested apparently under stress and D_r conditions existing in situ, differ from those in undisturbed state because they do not reflect the influence that depositional and post depositional phenomena, such as structure, aging, or even slight cementation, that all natural deposits to a lesser or larger extent exhibit see Barton et al. (1993), Cresswell (1999). An evident proof is represented by the comparison of V_s measured in CP and MG deposits, respectively of Holocene and medium Pleistocene age.

As already mentioned, these two soils deposited in a similar environment, exhibit similar mineralogical composition, grading and penetration resistance, see Fig. 24, but significantly differ in age, by about 600,000 years.

The reasons for the above differences in V_s, hence in G_o, can be explained by the amount of aging experienced by MG as compared to CP deposits and due to the presence of several forms of very light cementation, see Fig. 25, discovered in the outcrops of the MG formation (Bosi, 1990), but completely absent in the CP deposits, see Crova et al. (1992).

In view of the above and for the time being, the degradation curve of strain dependent shear modulus in the field can be estimated as suggested by Ishihara (1996), benefiting from the plentiful experimental evidences, [Goto et al. (1992, 1994); Yasuda et al. (1994); Hatanaka and Uchida (1995); Ishihara (1996); Lo Presti et al. (2006)] that the G/G_o vs. $\log_{10}\gamma$ curves of undisturbed coarse grained soils are similar in shape to those of the same material in reconstituted state, see for example Fig. 26.

This means that the laboratory determined G_o vs. $\log_{10}\gamma$ curve can be taken as the field degradation curve, normalizing the G with respect to the field G_o value inferred from the V_s measured in situ.

Some additional information about the non linearity of shear modulus can be deduced from the results of loading tests performed on the 800 mm diameter plate at the bottom of the 2.5 m in diameter shafts done at anchor block locations. Although the interpretation of such tests is far from being straightforward, especially, because of the large difference between shaft and plate diameter, it can be worth reporting the ratios of unload-reload modulus G_{ur} inferred form the plate loading tests normalized with respect to G_o obtained at the

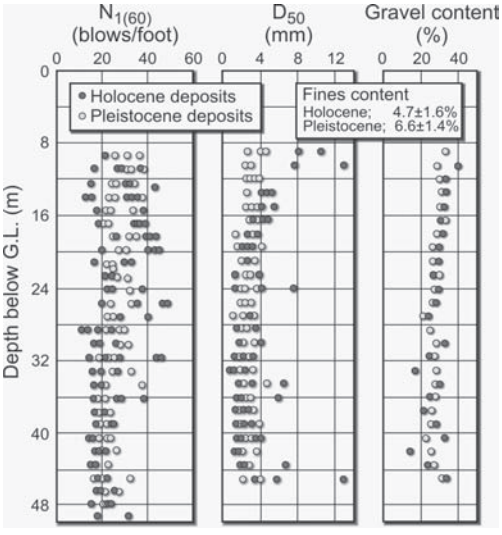

Figure 24. Comparison of CP versus MG deposits.

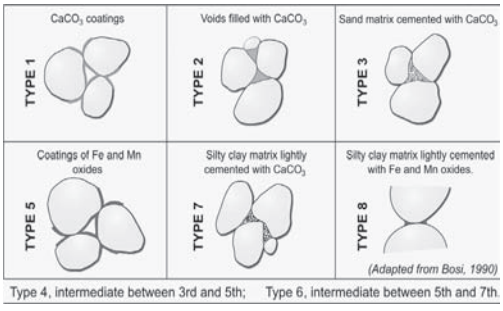

Figure 25. Types of light cementation encountered in MG formation.

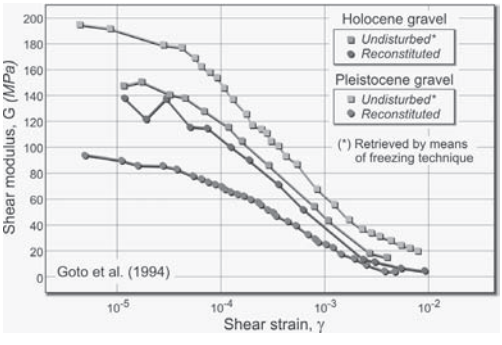

Figure 26. Strain dependent shear modulus; undisturbed vs. reconstituted sandy gravel.

Table 4. Hydraulic conductivity from pumping tests.

Location	$T \cdot 10^{-3}$ (m^2/s)	$k_h \cdot 10^{-3}$ (m/s)	$S \cdot 10^{-3}$ (–)	Gravel + cobbles (%)	Fines (%)
Sicily shore	65	5.0	1.7	44 to 79	3 to 8
Calabria shore	65	2.6	1.7	12 to 80	1 to 16

T = Transmittivity; S = Storage coefficient.

same depth from the V_s. The ratio of G_{ur}/G_o falls in the following range:

- Calabria anchor: $0.40 < G_{ur}/G_o < 0.48$ for $0.05\% < s/D < 0.20\%$
- Sicily anchor: $0.72 < G_{ur}/G_o < 0.93$, for $0.18\% < s/D < 0.24\%$

being:
s = plate settlement
D = plate diameter

b) The drained shear strength has been estimated referring to empirical correlations between large dynamic penetration tests (LPT) and the peak angle of shearing resistance ϕ', for example as the one proposed by Hatanaka and Uchida (1996). According to these authors, the ϕ' value of gravely soil is given by the following relationship:

$$\phi' = C + (20\ N_1)^{0.5}{}_{LPT} \qquad (4)$$

being
N_1 = LPT blow-count normalized with respect to the vertical effective stress σ'_{vo},
C = constant ranging between 17 and 23.

According to Hatanaka and Uchida (1996) Eq. (5) holds also for $(N_1)_{SPT}$ values.

However, it is necessary to recall the readers' attention that also Eq. ...4) has been set up according to the Japanese practice. Therefore, the N_{LPT} and N_{SPT} values used in connection with the correlation in question should be referred to the ER = 78%. Using the results of LPT and SPT obtained in the CP a MG deposits, Jamiolkowski et al. (2002) found $37° > \phi' > 47°$.

An alternative approach to evaluate ϕ' of coarse grained soils consists in the Bolton's (1986) work that put forward the following equation from which ϕ can be estimated:

$$\phi' = \phi'_{cv} = m\ [D_R(Q - \ell n p'_f)] - \qquad (5)$$

where:
ϕ'_{cv} = constant volume angle of friction in degrees
m = dimensionless coefficient equal to 3 or 5 for axisymmetric and plane stress conditions
Q = particle strength parameter
D_r = relative density
p_f' = mean effective stress at failure in kPa.

Keeping in mind the mineralogical composition of the CP and MG deposits, the parameters that can be used in association with Eq. ...5) are:

Q = 9 to 10, $\phi'_{cv} = 35°$, $D_r = 60\%$ and p'_f in the range of practical interest, ranging between 250 and 500 kPa, Eq. …5). With this assumption, Eq. ...5) yields $39° > \phi' > 42°$.

Unlike Eq. …4), Eq. …5) incorporates the framework of the Rowe's (1962) stress-dilatancy theory, rendering the ϕ' stress level at failure dependent, thus implicitly incorporating the features of a curvilinear shear strength envelope.

c) The hydraulic conductivity of the CP deposits was evaluated at two towers locations by pumping tests from the wells supported by the observations of the GWL drawdown in the surrounding piezometers.

The hydrological conditions, considered in the tests interpretation were the unconfined aquifer, with partially penetrating wells and the phreatic surface coincident with the m.s.l.

Pumping wells penetrating CP deposits 25 m and 35 m on the Calabria and Sicily shore respectively having filter along their entire length were employed with piezometers located at 10 m and 20 m from the wells.

Pumping was carried out to attain the flow rate of 0.08 m^3/s in the steady state conditions corresponding to the drawdown in the wells of 0.7 m. In these conditions pumping was carried on for 72 hours, monitoring during this lapse of time the oscillation of the sea level and of the GWL.

The tests results were interpreted in accordance with Todd (1980), disregarding, on account of the modest drawdown, the horizontal flow components. The information assumed from the Pumping tests is shown in Tab. 4.

With the pieces of information given in this Section the readers can get acquainted with the key issues as regards the foundation soils as well as the efforts for their characterization enabling to acquire the geotechnical parameters for the Messina Straits Bridge foundation design.

3 BRIDGE FOUNDATIONS

The bridge main span interacts with the soil at the two towers and at the two anchor blocks locations see Fig. 2 whose foundation seizing was accomplished taking into account the load combinations reported in Tab. 5. In the design have been contemplated the environmental loadings originated by winds and earthquakes which considered levels are reported in the Tab. 6, see: Faccioli (2003), Solari (2003) and Valensize (2003).

The bridge design including its foundations was carried out and intended for a 200 years infrastructure lifetime.

3.1 *Tower foundations*

The steel towers, 382 m high, see Fig. 27, are connected to massive concrete foundations 130 × 60 m in plan placed at the elev. −10 b.m.s.l. within an excavation supported by T-shaped diaphragm walls and is water-proofed by jetgrouting treatment, see Fig. 28.

The loadings transmitted to the soil for two relevant load combinations are summarized in Fig. 29.

The design of the towers foundations was guided by the following circumstances:

- The 16-m deep excavations in gravelly soils with very high hydraulic conductivity, is located close by the Strait shore, see Tab. 4.

Table 5. Loading conditions for towers foundation.

A: Dead load	**C:** Dead load ⊕ 3rd level earthquake
B: Dead load ⊕ Live load ⊕ 3rd level wind	**D*:** Dead load ⊕ 3rd level earthquake ⊕ Lack of lateral confinement on sea side*

(*) Underwater slide within CP deposits on Calabria shore

- With reference to the Calabria tower, the concern that a 3rd level earthquake can trigger a slide of the CP deposits within the steep, circa 1:2, adjacent underwater slope which might induce an unaccepted rotation of the tower towards the Strait.
- The settlements or even the liquefaction of the CP deposits due to the excess pore pressure generated by earthquakes.

The above conditions, together with the high stresses transmitted to the foundation soil, ≅1 MPa under dead+live loads and ≅1.5 MPa, during a third level earthquake, led to the geometry of the towers foundations shown in Figs. 30 through 33.

The intensive jetgrouting treatment, see Fig. 34, employing 1.6 m in diameter columns, foreseen beneath and around the foundations is aimed at preventing the settlements and the liquefaction due to the pore pressure excess triggered by earthquake events.

The diaphragm barretts, penetrating the PC and adopted for the Calabria foundation have been conceived to enhance the rotational stiffness of the foundation and to counteract the tower to tilt towards the Strait during a third level earthquake particularly in case of an underwater slope slide within CP deposits.

The performance of the towers foundations, under static and earthquake loadings, was investigated by means of finite elements (FEM) and finite difference (FDM) numerical models employing GEFDYN and FLAC computer codes, respectively. As to the stress-strain-time behaviour of the materials involved the following assumptions were postulated:

- Visco-elastic, isotropic: concrete, intensive jet grouting beneath the foundations and Pezzo Conglomerate (PC).
- Visco-elastic, cross-anisotropic: external jet grouting with hexagonal array.
- Elasto-plastic, isotropic, with Mohr-Coulomb strength envelope and non-associated flow rule.
- Coastal Plain (CP) and Messina Gravel deposits.

Major computational efforts have been devoted to the Calabria tower foundation where the issues of a

Table 6. Design earthquakes and winds.

Return period (years)	Peak ground Acceleration (freefield)	Wind velocity (at elev. + 70 m a.m.s.l.)	Notes
50 y.	0.12 g	44 m/s	SLS, road and railway traffic
400 y.	0.27 g	47 m/s	SLS, railway traffic only
2000 y.	0.58 g	54 m/s	ULS[1], closed to traffic
>>2000 y.	0.64 g	60 m/s	D-ULS[2], closed to traffic

[1] Minor structural damages, bridge can be re-opened after the event.
[2] Relevant structural damages, bridge needs repairs.

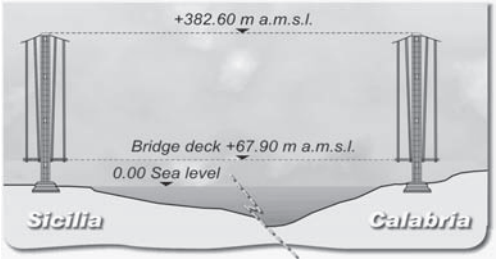

Figure 27. Towers of the one-span suspension bridge over Messina Straits.

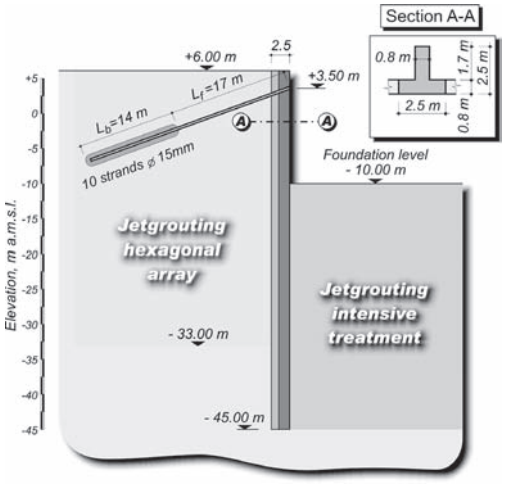

Figure 28. Tower foundations—Earth support for excavations.

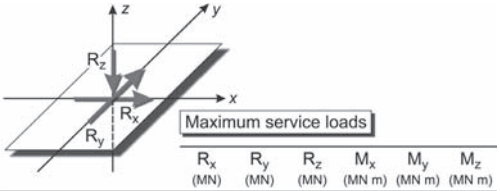

Maximum service loads

	R_x (MN)	R_y (MN)	R_z (MN)	M_x (MN m)	M_y (MN m)	M_z (MN m)
Dead loads	1	0	3790	0	400	0
Live loads	28	0	325	0	1051	0
Wind (3rd lev.)	28	74	22	27114	3412	0

Maximum loads at 3rd level earthquake

	R_x (MN)	R_y (MN)	R_z (MN)	M_x (MN m)	M_y (MN m)	M_z (MN m)
Calabria shore	942	1409	4450	31766	21426	53
Sicilia shore	746	1147	5126	26300	13023	40

(*) at foundation base

Figure 29. Loads on tower foundations*.

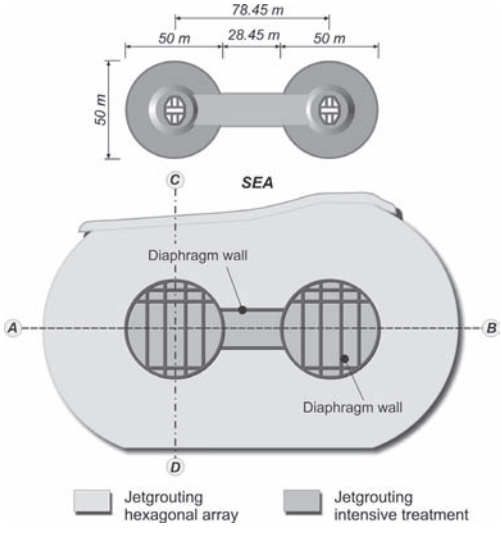

Figure 30. Tower foundation on Calabria shore—Plan view.

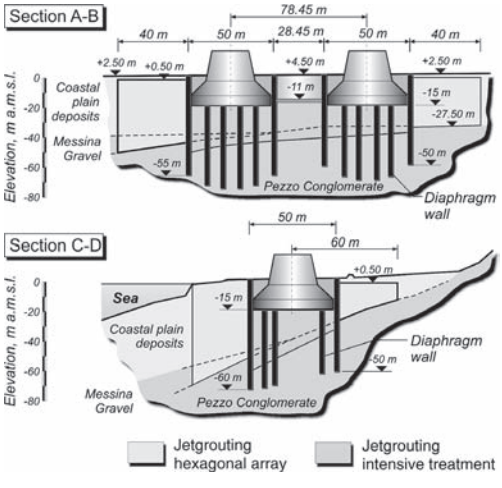

Figure 31. Tower foundation on Calabria shore—Sections.

seismic stability of the underwater slope and of the non-uniform soil stratigraphy, have generated special concern about the permanent displacements, particularly after a third level earthquake.

Given the above, a 3-D FEM was developed to compute the permanent displacement of the foundation under the four loading conditions, as specified in Tab. 5.

A FEM model has been used, with mesh of 19227 elements and 17459 nods, shown in Fig. 35, having dimensions of 140, 280 and 144 meters, respectively for depth, length and width.

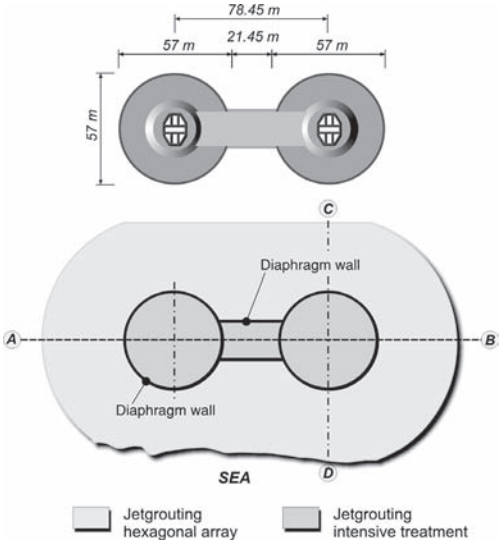

Figure 32. Tower foundation on Sicilia shore—Plan view.

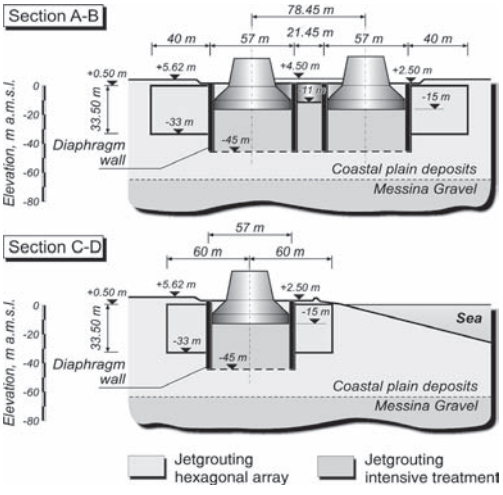

Figure 33. Tower foundation on Sicilia shore—Sections.

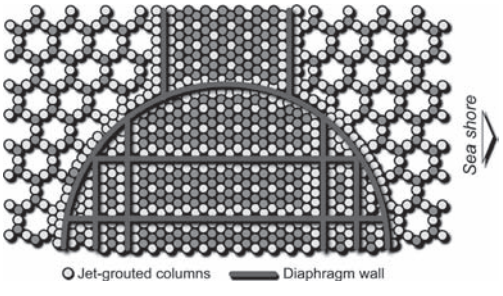

Figure 34. Tower foundations—Jetgrouting treatment scheme.

During the dynamic analyses, aiming at simulating a third level event, the model was subject to a seismic excitation corresponding to the properly scaled El Centro strong motion accelerogram registered during 1979 for the Imperial Valley earthquake.

An example of the output yielded by the dynamic analysis for the loading condition D is reported in Tab. 5. Fig. 35 shows the maximum and permanent displacements of the centre of the foundation; points F_1 and B_1 are located on the slope after the third level earthquake.

As to the Sicilia tower foundation, the deformation analyses were carried out using 2-D FDM, calibrated against both 3-D and 2-D FEM performed for the Calabria tower foundation.

Computed vertical (s_v) and horizontal (s_h) displacements are given in Tab. 7. They have also allowed evaluating the rotation (α) of the two towers towards the Strait under four considered (Tab. 5) loading conditions. Referring to the most severe conditions, D for the Calabria tower and C for the Sicilia tower, the α-values result of the order of 1/1000.

3.2 *Anchor blocks*

The salient features of the anchor blocks, see Fig. 36, are summarized in Tab. 8. The different weight and geometry of the Calabria block, embedded in the PC, as compared to the Sicilian one, embedded in the Messina Gravel deposit, are originated by different mechanical properties of the two geomaterials being considered. Their design has been steered by the following considerations:

- The narrow width of the land between the Strait and the Mediterranean Sea to receive the block on Sicilia shore.
- The temporary earth support of deep excavations more than 50 m required to accommodate the blocks in the ground, see Fig. 36.

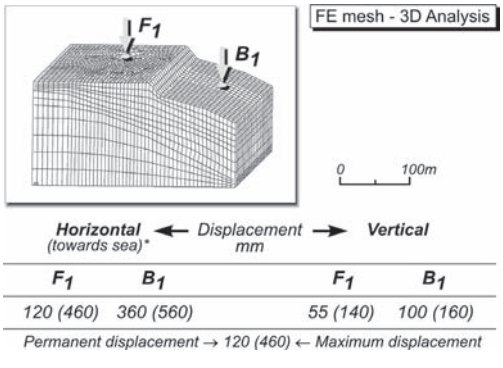

Figure 35. Dynamic FE analyses—Permanent displacements.

Table 7 Tower foundations—Computed displacements.

	Calabria tower				Sicilia tower	
	2-D FDA		3-d FEA		2-d FDA	
Loading conditions	S_v (mm)	S_h (mm)	S_h (mm)	S_v (mm)	S_v (mm)	S_h (mm)
Dead load	15.0	1.5	10.0	0.6	70.0	1.0
Dead load + live load + 3rd level wind	17.0	3.0	10.0	1.0	73.0	3.0
Dead load + 3rd level earthquake	2.0	29.0	12.0	12.0	93.0	37.5
Dead load + 3rd level earthquake lack of confinment	25.0	62.5	55.0	120.0	120.0	90.0

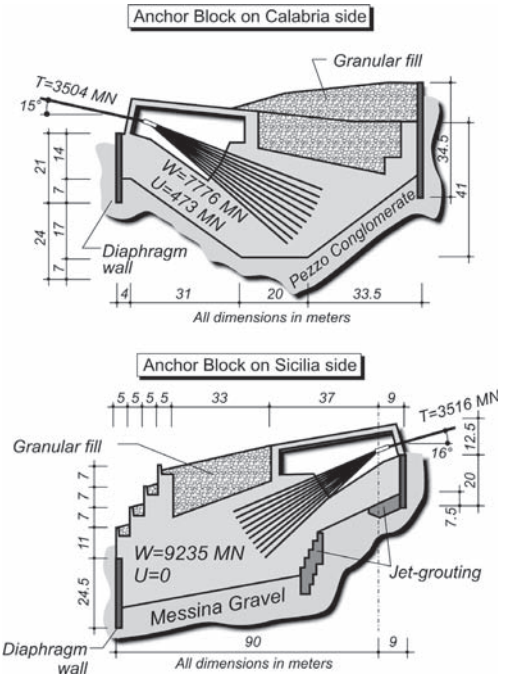

Figure 36. Anchor blocks on Calabria and Sicilia sides.

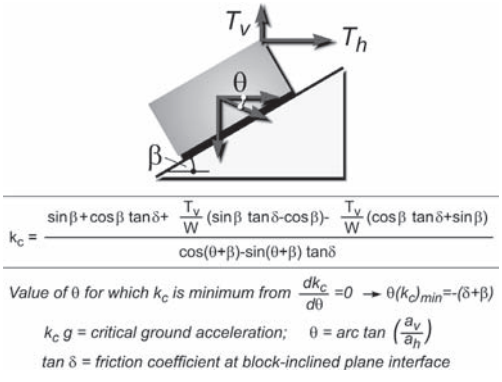

Figure 37. Model of block on inclined plane.

- The need to avoid significant permanent displacements of the blocks after strong earthquakes.

The blocks design was carried out following four different approaches of which, for sake of simplicity, only the following two are briefly examined:

- 2-D coupled pseudostatic FE analysis using the Gefdyn computer code. In this analysis, owing the poor correlation between horizontal (a_h) and vertical (a_v) PGA observed in the recorded strong motion time histories, only the $a_h = 0.32$ m/s^2 was considered. FEM's depth and length were 200 and 300 meters respectively.

  The geotechnical parameters and stress-strain-time behaviour employed in such analyses were similar to those mentioned in connection with the towers design.

  Throughout the analysis, all the phases of the block construction, from the excavation stage to the application, in a static mode, of the earthquake loading assumed to be representative for the third level event (Kramer, 1996), were modeled. For the Calabria anchor block, the analysis under earthquake loading yielded horizontal (s_h) and vertical (s_v) displacement of 60 and 40 millimeters respectively. Similar displacements values were obtained for the Sicily anchor block.
- With the aim of exploring the contingency of permanent anchors displacements during a third

Table 8. Salient anchor blocks features.

			Sicilia	Calabria
Tension load	Horizontal component	T_h , Mn	3382	3382
	Vertical component	T_v , Mn	959	918
	Dead weight	W , Mn	9235	7776
	Buoyancy force	U , Mn	0	473
	Load components ratio	r , Mn	0.41	0.53

$$\text{Load component ratio: } r = \frac{T_h}{G - T_v - U}$$

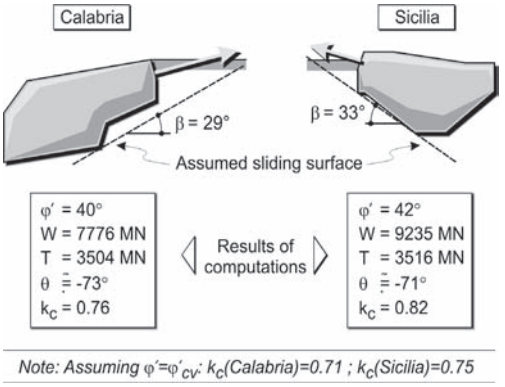

Figure 38. Anchor block: critical seismic coefficient ($k_c = a_c/g$).

level earthquake, a simplified dynamic analysis of a block on an inclined plane (Newmark, 1965, Kramer 1996), see Fig. 37, was carried out, so as to evaluate the critical seismic coefficient $k_c = a_c/g$.

The analyses input and the output data are summarized in Fig. 38, being:

k_c = critical seismic coefficient
g = acceleration of gravity, m/sec^2
a_c = free field peak ground acceleration, m/sec^2
ϕ' = peak angle of shearing resistance of the geomaterial in which block is embedded
ϕ'_{cv} = friction angle at critical state of the geomaterial in which block is embedded
β = sliding plane angle for which $k_c = k_{min}$

The mentioned computations show that k_c is always higher than the actual seismic coefficient k = 0.58. This holds even if one makes a conservative assumption that $\phi' = \phi'_{cv}$.

Therefore, the simplified dynamic analysis indicates that owing to an overall conservative seizing of the anchor blocks, they are not likely to suffer from any significant permanent displacements during a third level earthquake.

REFERENCES

Arroyo, M., Ferreira, C. and Sukolrat, J. (2006). "Dynamic Measurements and Porosity in Saturated Triaxial Specimens". Symposium on Soil Stress-Strain Behaviour: Measurement, Modelling and Analysis, Rome. Ling, Callisto, Leshchínsky and Koseki Eds, Springer, pp. 537–546.

Baldi, G., Jamiolkowski, M., Lo Presti, D.C.F., Manfredini, G. and Rix, G.J. (1989). "Italian Experience in Assessing Shear Wave Velocity from CPT and SPT". Earthquake Geotechnical Engineering, Discussion Session on Influence of Local Conditions on Seismic Response. XII ICSMFE, Rio De Janeiro, Brasil, The Japanese Society of SMFE, pp. 157–168.

Baldi, G., Bruzzi, D., Superbo, S., Battaglio, M. and Jamiolkowski, M. (1988). "Seismic Cone in Po River Sand". ISOPT-1, Orlando, Fla., Vol. 2, pp. 643–650.

Barton, M.E., Mockett, L.D. and Palmer, S.N. (1993). "An Engineering Geological Classification of the Soil-Rock Borderline Materials between Sands and Sandstone". Engineering Geology of Weak Rock 26th Geological Society Annual Conf. Leeds, UK Cripps et al. Eds, Balkema, pp. 125–138.

Biot, M.A. (1956). "Theory of Propagation of Elastic Waves in Fluid-Saturated Porous Solid, I Lower Frequency Range". Journal of Acoustical Society of America, Vol 28, No. 2, pp. 168–178.

Bolton, M.D. (1986). "The Strength and Dilatancy of Sands". Geotechnique, Vol. 36, No. 1, pp. 65–78.

Bosi, C. (1990). "Studio dello stato di aggregazione delle Ghiaie di Messina". Report by Sitec S.r.l., Roma.

Cresswell, A.W. (1999). "Sampling and Strength Testing of Unbonded Locked Sand". Ph.D. Thesis, Southampton University, U.K.

Crova, R., Jamiolkowski, M., Lancellotta, R. and Lo Presti, D.C.F. (1992). "Geotechnical Characterization of Gravelly Soils at Messina Site, Selected Topics". Proceedings of the Wroth Memorial Symposium, Oxford, UK, Houlsby and Schofield Eds, Thomas Telford, pp. 199–218.

Cubrinovski, M. and Ishihara, K. (1999). "Empirical Correlation between SPT-N Value and Relative Density for Sandy Soils". Soils and Foundations, Vol. 39, No. 5, pp. 61–71.

Darendeli, M.B. (2001). "Development of New Family of Normalised Modulus Reduction and Material Damping Reduction Curves". Ph.D. Thesis, University of Texas at Austin, TX, USA.

Faccioli, E. (2003). Seismic Hazard and Design Earthquake. Stretto di Messina Ltd, Internal Report.

Ferrante, G. (1988). "Comportamento in colonna risonante di sabbie frantumabili e della ghiaia di Messina". Politecnico di Torino, Department of Structural and Geotechnical Engineering.

Foti, S. and Lancellotta, R. (2004). "Soil Porosity from Seismic Velocities". Geotechnique, Vol. 54, No. 8, pp. 551–554.

Foti, S., Lai, C.G. and Lancellotta, R. (2002). "Porosity of Fluid Saturated Porous Media from Measured Seismic Wave Velocities". Geotechnique, Vol. 52, No. 5, pp. 359–373.

Goto, S., Suzuki, Y., Nishio, S. and Oh-oka, H. (1992). "Mechanical Properties of Undisturbed Tone-river Gravel

Obtained by in Situ Freezing Method". Soils and Foundations, Vol. 32, No. 3, pp. 15–25.

Goto, S., Nishio, S. and Yoshimi, Y. (1994). "Dynamic Properties of Gravels Sampled by Ground Freezing". Ground Failures under Seismic Conditions. GSP 44, ASCE, pp. 141–157.

Hatanaka, M. and Uchida, A. (1996). "Empirical Correlation Between Penetration Resistance and Internal Friction Angle of Sandy Soils". Soils and Foundations, Vol. 36, No. 4, pp. 1–10.

Hatanaka, M. and Uchida, A. (1995). "Effects of Test Methods on the Cyclic Deformation Characteristics of High Quality Undisturbed Gravel Samples". GSP 56, ASCE, pp. 136–151.

Hight, D.W. and Leroueil, S. (2002). "Characterisation of Soils for Engineering Purposes". Characterisation and Engineering Properties of Natural Soils, Int. Workshop, Singapore, Tan et al. Eds, Swets and Zeitlinger, pp. 255–360.

Ishihara, K. (1996). "Soil Behaviour in Earthquake Geotechnics". Oxford Science Publications.

ISMES (1985). "Results of Laboratory Tests Carried out on Reconstituted Specimens of the Coastal Plain Deposits". R-2685 and R-2690.

Jamiolkowski, M. and Lo Presti, D.C.F. (2002). "Geotechnical Characterisation of Holocene and Pleistocene Messina Sand and Gravel Deposits". Characterisation and Engineering Properties of Natural Soils, Int. Workshop, Singapore, Tan et al Eds, Swets and Zeitlinger, pp. 1087–1119.

Jardine, R.J. (1992). "Some Observations on the Kinematic Nature of Soil Stiffness". Soils and Foundations, Vol. 32, No. 2, pp. 111–124.

Jardine, R.J. (1985). "Investigations of Pile-Soil behaviour with Special Reference to the Foundations of offshore Structures". Ph.D. Thesis, University of London, London. UK.

Jardine, R.J., Kuwano, R., Zdravkovic, L. and Thornton, C. (2001). "Some Fundamental Aspects of the Pre-Failure behaviour of Granular Soils". 2nd Int. Symp. on Pre-Failure Deformation Characteristics of Geomaterials, IS Torino '99 Jamiolkowski et al. eds., Balkema, Vol. 2, pp. 1077–1111.

Kokusho, T. and Tanaka, Y. (1994). "Dynamic Properties of Gravel Layers Investigated by In-situ Freezing Sampling". Ground Failures under Seismic Conditions, GSP 44, ASCE, pp. 121–140.

Kramer, S.L. (1996). Geotechnical earthquake engineering. Prentice Hall.

Liao, S.C. and Whitman, R.V. (1986). "Overburden Correction factors for SPT in Sand". Journal of GED, ASCE, Vol. 112, No. 3, pp. 373–377.

Lo Presti, D., Pallara, O., Froio, F., Rinolfi, A. and Jamiolkowski, M. (2006). "Stress-Strain Strength behaviour of Undisturbed and Reconstituted Gravelly Soils Samples". Rivista Italiana di Geotecnica, Vol. 40, No. 1, pp. 9–27.

Nazarian, S. and Stokoe, K.H. (1983). "Use of the Spectral Analysis of Surface Waves for Determination of Moduli and Thickness of Pavement Systems". Transportation Research Record, No. 954, TRB, Transportation Research Board, Washington, D.C.

Newmark, N.M. (1965). Effects of earthquakes on dams and embankments. 5th Rankine Lecture, Geotechnique, Vol 15, No. 2, pp. 139–159.

Pallara, O. (1995). "Comportamento sforzi-deformazioni di due sabbie soggette alle sollecitazioni monotone e cicliche". Ph.D. Thesis, Politecnico di Torino, Department of Structural and Geotechnical Engineering.

Rowe, P.W. (1962). "The Stress-Dilatancy Relation for Static Equilibrium of an Assembly of Particles in Contact". Proc. Royal Society, 269 A, pp. 500–527.

Schmertmann, J.H. and Palacios, A. (1979). "Energy Dynamics of SPT". Journal of GED, ASCE. Vol. 105, No. GT8, pp. 909–926.

Skempton, A.W. (1986). "Standard Penetration Tests Procedures and the Effects in Sands of Overburden Pressure, Relative Density, Particle Size, Ageing and Overconsolidation". Geotechnique, Vol. 36, No. 3, pp. 425–447.

Solari, G. (2003). Wind Studies. Stretto di Messina Ltd, Internal Report.

Tatsuoka, F., Jardine, R.J., Lo Presti, D.C.F., Di Benedetto, H. and Kokaka, T. (1997). "Characterising the Pre-failure Deformation Properties of Geomaterials". Theme Lecture for Plenary Session No. 1, 14th ICSMFE, Hamburg, Vol. 4, pp. 2129–2164.

Todd, D.K. (1980). "Groundwater Hydrology". Wiley.

Yasuda, N., Otha, N. and Nakamura, A. (1994). "Deformation Characteristics of Undisturbed Riverbed Gravel by In-Situ Freezing Sampling Method". 1st Int. Symp. on Pre-Failure Deformation Characteristics of Geomaterials, IS Hokkaido '94 Sapporo, Japan, Shibuya et al. eds., Balkema, Vol. 1, pp. 41–46.

Yoshimi, Y. (2000). "A Frozen Sample of Sand that did not Melt". Geotech-Year 2000, Developments in Geotechnical Engineering, Bangkok, pp. 293–296.

Yoshimi, Y., Tokimatsu, K., Kaneko, O. and Makihara, Y. (1984). "Undrained Cyclic Shear Strength of a Dense Niigata Sand". Soils and Foundations, Vol. 24, No. 4, pp. 131–145.

Yoshimi, Y., Hatanaka, M. and Oh-oka, H. (1978). "Undisturbed Sampling of Saturated Sands by Freezing". Soils and Foundations, Vol. 18, No. 3, pp. 59–73.

Yoshimi, Y., Hatanaka, M. and Oh-oka, H. (1977). "A Simple Method for Undisturbed Sampling by Freezing". Specialty Session 2 on Soil Sampling 9th ICSMFE, Tokyo, Japan, pp. 23–28.

Valensise, G. (2003). Seismic Settings. Stretto di Messina Ltd, Internal Report.

Vullo, E. (1999). The Biggest Bridge. ITALY-ITALY, N°1.

Keynote lecture 1: Pile design developments

Deep Foundations on Bored and Auger Piles – Van Impe & Van Impe (eds)
© 2009 Taylor & Francis Group, London, ISBN 978-0-415-47556-3

Sense and sensitivity of pile load-deformation behaviour

F.A. De Cock
Geotechnical Expert Office GEO.BE, Belgium

ABSTRACT: The SLS design of piles is often treated in a stepmotherly way. This paper aims to sensitize and to encourage the practitioners to consider more often also the deformability of piled foundations. A summarising database of all well documented load tests available in Belgium on bored and auger piles is included in the paper for documentation. Second, the use of hyperbolic transfer functions as a powerful scientific tool for prediction, analysis, conversion, … of the load-displacement behaviour of single piles is demonstrated by various practical applications. Third, the author is sharing a number of particular experiences with critical or non-critical, expected or not expected deformation behaviour of piled constructions.

1 INTRODUCTION

After 30 years of debate on the Eurocode 7 and the sense and nonsense of the semi-probabilistic design approach, one is actually working in the stage of infiltration of the Eurocodes design philosophy and its application in practice. In December 2004 Eurocode 7: Geotechnical design—Part 1: General rules (EC7-1) was unanimously ratified by the European Member States. On the national level, the involved national bodies and specialists are fully working on the elaboration of the National Annexes, required as link between the EC7-1 and the national standards. Around 2009 (?), after a 2-year calibration period and a further 3-year coexistence period, EC7-1 will become valid in all Member States and the relevant National standards will then have to be withdrawn.

With regard to pile foundation EC7-1 pays quite a lot of attention to the ULS design of single piles and pile groups, in compression, in tension, for lateral loading, … Conversely, the SLS design of piles (vertical displacements of axially loaded piles) is only handled in a rather short subchapter §7.6.4 of EC7-1. Beside some "self-evident" provisions, the most relevant specifications given in this concise subchapter are—in my opinion—the following (EN 1997–1:2004):

- "7.6.4.1(1) Vertical displacements under serviceability limit state conditions shall be assessed and checked against the requirements given in 2.4.8 and 2.4.9."
- "7.6.4.2 (for compression piles) NOTE When the pile toe is placed in a medium-dense or firm layer overlying rock or very hard soil, the partial safety factors for ultimate limit state conditions are normally sufficient to satisfy serviceability limit state conditions."
- "7.6.4.2 (2) Assessment of settlements shall include both the settlement of individual piles and the settlement due to group action."
- "7.6.4.2 (4) When no load results are available for an analysis of the interaction of the piles foundation with the superstructure, the load-settlement performance of individual piles should be assessed on empirically established safe assumptions."
- "7.6.4.3 (for tension piles) NOTE Particular attention should be paid to the elongation of the pile material."

This paper aims:

- to contribute to the understanding of the load-deformation behaviour of piles
- to demonstrate the relevance and importance of considering the SLS both for individual piles as for pile groups
- also to demonstrate the use of transfer functions—in particular of the hyperbolic type—as a practical tool to interpret as well as to predict the pile deformation behaviour.

The paper consists of the following chapters:

- Chapter 2 contains a data-base of well documented pile load tests on bored and auger piles, available in Belgium
- Chapter 3 briefly describes the calculation methods considered in some National design standards (The Netherlands, Germany, France) to assess the load-deformation curve of single piles

– Chapter 4 deals with the use of hyperbolic transfer functions as a powerful tool for analysis, back-calculation, prediction and sensitivity-analysis of the load-settlement curve of single piles of different types and in different soil conditions
– Chapter 5 shows us some illustrations where the deformation behaviour of piles merits to be considered and/or has strongly influenced the design or the behaviour of the structure.

2 PILE LOAD TESTS ON BORED AND AUGER PILES—BELGIAN DATABASE

A database of 27 pile loading tests on displacement screw pile in Western Europe—period 1970–2000—has been set up by De Cock (2001)—see table 1.

A summary of the normalised load-displacement curves included in this database, is given in figure 1.

Since then, 2 extended research programs were conducted in Belgium on screw piles. Within the frame-work of the further elaboration of the EC7-NA guidelines, the BBRI has elaborated a more complete database of Belgian pile load tests. A selection of normalised load-displacement curves (Table 2), subdivided for end bearing and shaft bearing piles and separately for precast driven piles, screw piles and bored/CFA piles is given in de figures 2a to 2g.

Tables 3 and 4 includes indicative values of the relative pile displacement at service load, presuming a factor of safety of 2.0 on the ultimate resistance. Both tables fit quite well with each other.

Table 1. Summarizing table of database (De Cock, 2001).

File No.	Test site and year	Pile Nr	Pile denomination Mean dimensions
A1	Zwevegem 1984	P1	Atlas 36/46—13.05 m
A2		P2	Atlas 36/46—13.05 m
A3	Ghent I 1985	P1	Atlas 36/46—13.05 m
A4		P2	Atlas 36/46—13.50
A5	Oldenburg 1986	P1	Atlas 41/51—9.50 m
A6		P2	Atlas 41/51—7.00 m
A7	Ghent II 1987	P6	Atlas 36/46—12.50 m
A8		P10	Atlas 36/46—12.50 m
A9	Koekelare 1992	P9	Atlas 36/50—13.0 m
A10		P10	Atlas 51/65—13.2 m
A11		P15	Atlas 36/50—13.0 m
A12		P16	Atlas 51/65—13.2 m
F1	Zwolle (NL) 1975	P1	Fundex 45/56—11.0 m
F2	Hamburg 1979	P1	Fundex 42/56—14.0 m
F3	Hamburg 1979	P1	Fundex 44/56—14.8 m
F4		P2	Fundex 44/56—13.8 m
F5	Bremen (D) 1980	P1	Fundex 44/56—6.0 m
F6		P2	Fundex 44/56—8.5 m
F7	Ghent II 1987	P3	Fundex 38/45—13.0 m
F8		P8	Fundex 38/45—13.0 m
O1	Vilvoorde 1993	P3	Omega 41/41—14.0 m
O2		P5	Omega 41/41—8.2 m
O3	Feluy 1997	P2	Omega 36/36—14.5 m cast under gravity
O4		P3	Omega 36/36—14.5 m cast under pressure
O5		P4	Omega B+ 36/60—11.0 m enlarges base
O6		P5	Omega B+ 36/60/70—11.00 m shaft and base enlargement
O7	Paris-St Ouen ‘96	P1	Omega 31/31—7.4 m

Table 2. Summarizing table of database (BBRI).

No.	Soil	Site	Pile id	Description
S1	Sand	LimII	B1	Precast 35 × 35
S2	Sand	LimII	B2	Precast 35 × 35
S3	Sand	LimI	P8	Precast 29 × 29
S4	Sand	Gent	Pre_b	Precast 32 × 32
S12	Sand	LimII	A1bis	Fundex 38/45
S13	Sand	LimII	A2	Olivier 36/51
S14	Sand	LimII	A3	Omega 41/41
S15	Sand	LimII	A4	De Waal 41/41
S16	Sand	LimII	B3	Atlas 36/51
S17	Sand	LimII	B4	Atlas 36/51
S18	Sand	LimII	C2	Olivier 36/51
S19	Sand	LimII	C3	Omega 41/41
S20	Sand	LimII	C4	De Waal 41/41
S26	Sand	Loenhout	S4	CFA with casing diam. 61
S27	Sand		A1	
S28	Sand		C2	
S29	Sand	Gent	CFA_a	CFA diam. 45
S30	Sand	Gent	CFA_b	CFA diam. 45
S31	Sand	KalloIII	C	Bored pile diam. 60, bento
S32	Sand	KalloIII	D	Bored pile diam. 60, bento
C1	Clay	SKW	A1	Precast 35 × 35
C2	Clay	SKW	A4	Precast 35 × 35
C3	Clay	SKW	A2	Fundex 38/45
C4	Clay	SKW	A3	Fundex 38/45
C5	Clay	SKW	B1	De Waal 41/41
C6	Clay	SKW	B2	De Waal 41/41
C7	Clay	SKW	B3	Olivier 36/51
C8	Clay	SKW	B4	Olivier 36/51
C9	Clay	SKW	C1	Omega 41/41
C10	Clay	SKW	C2	Omega 41/41
C11	Clay	SKW	C4	Atlas 36/51
C12	Clay	SKW	C3	Atlas 36/51
C13	Clay	Kortrijk	A	Bored pile diam. 76, bento
C14	Clay	Kortrijk	B	Bored pile diam. 76, bento
C15	Clay	Kortrijk	D	Bored pile diam. 90 casing
C16	Clay	Kortrijk	Z	Bored pile diam. 76 casing

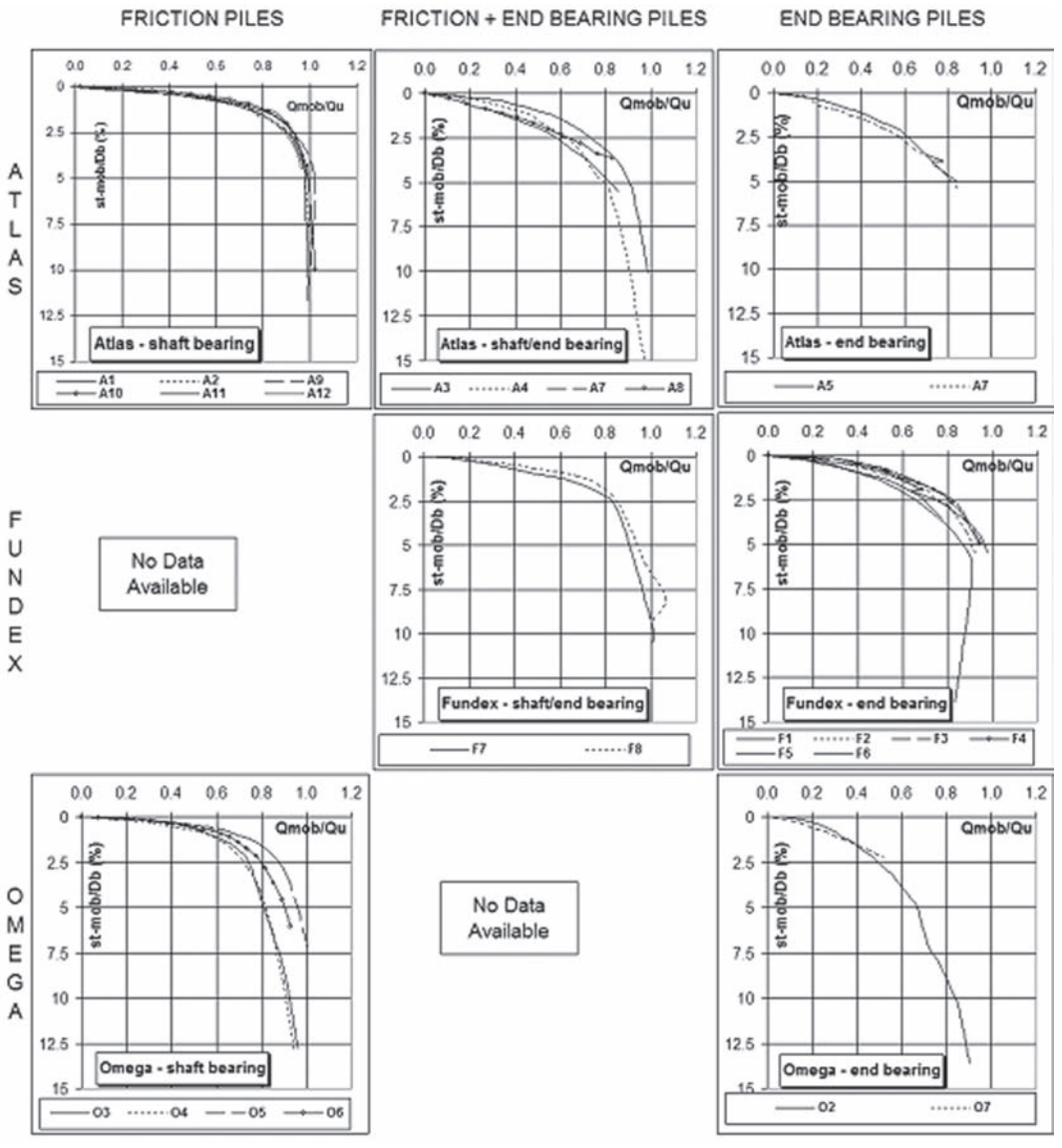

Figure 1. Normalised load-displacement curves for screw piles (De Cock, 2001).

Table 3. Relative displacement at service load for screw piles (De Cock, 2001).

Pile type	Shaft bearing	Shaft + end bearing	End bearing
Atlas	0.5–0.75%	0.75–1.50%	1.5–1.75%
Fundex	No data	0.75–1.0%	0.75–1.25%
Omega	0.5–0.75%	No data	2.0–2.5% *

*The relevance of the data—resulting from 1 short pile (O2) in heterogeneous soil and from 1 pile (O7) with only partial mobilization of the resistances—may be moderate.

Table 4. Relative displacement at service load (BBRI database).

Pile type	Shaft bearing		End bearing
Driven Precast concrete	0.5–0.75%		1.0–2.0%
Screw piles	0.5–1.0%	No data	0.75–1.5%
Bored and CFA	0.5% bentonite 1.0–1.5% casing		0.5–1.5%

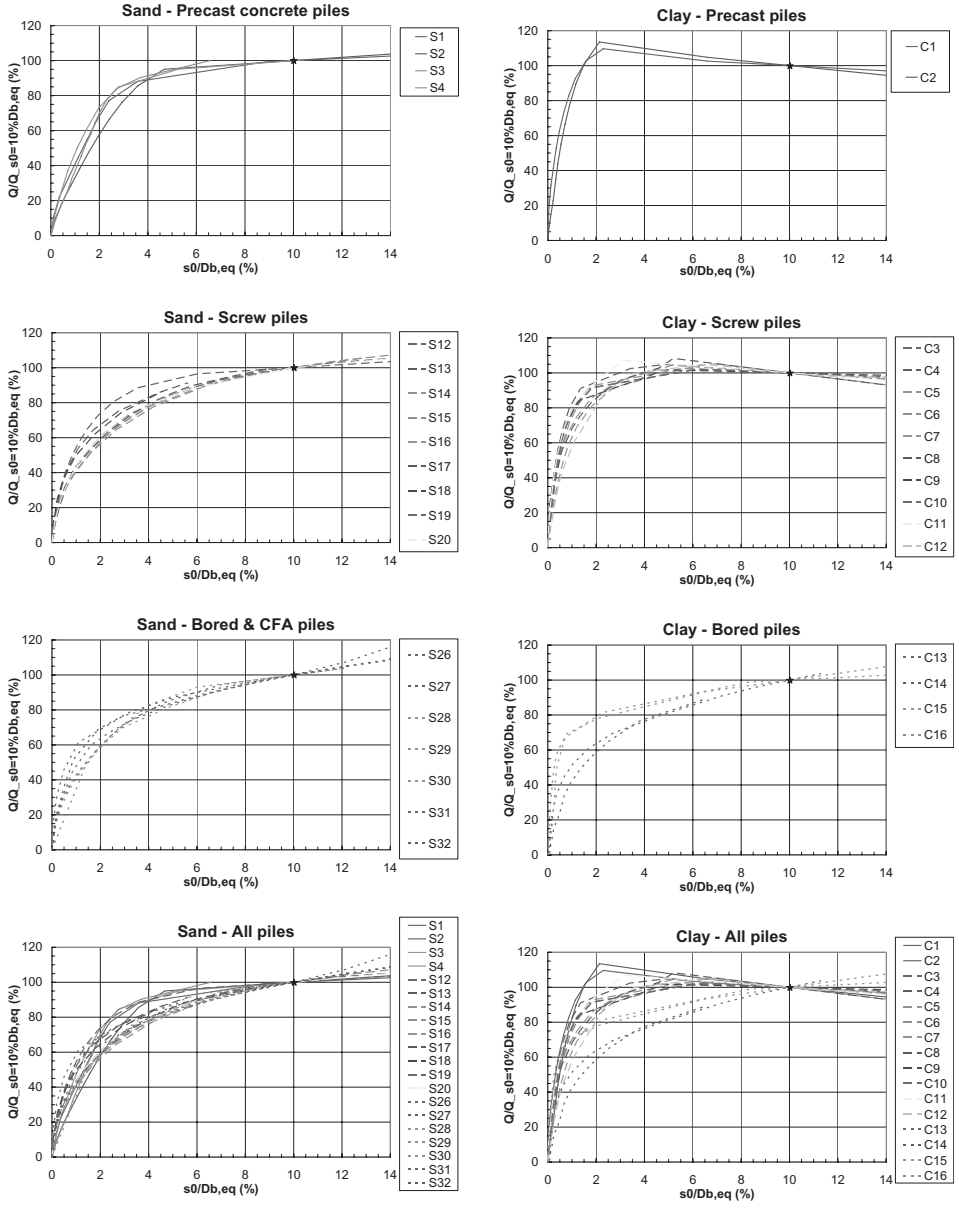

Figure 2a to h. Normalised load-displacement curves for different piles types (BBRI-database).

3 CALCULATION METHODS FOR LOAD-SETTLEMENT BEHAVIOR ON THE BASIS OF IN-SITU SOIL TESTS

A few methods to calculate the load-settlement behaviour are prescribed in European National Codes or Recommendations.

The Dutch piling code NEN 6743 (1993) provides a method to define the design value of the pile head displacement as a function of the mobilised base resistance and shaft resistance, as calculated on the basis of CPT. The method is semi-graphical and based on 2 charts, one for base resistance and one for shaft resistance. Each charts contains 3 normalised load-displacement curves for displacement piles (without making any distinction between e.g. driven piles or screwed piles), for CFA piles and for bored piles respectively.

The German bored piling code DIN 4014 comprises 4 tables, giving values of experience of mobilisation curves for bored piles in non-cohesive soils (based on CPT cone resistances) and in cohesive soils (based on c_u-values).

The French code Fascicule 62-V contains technical rules for the design of foundations of civil engineering structures. It also describes a method to determine the load-displacement curve of a single pile under axial loading, based on bilinear elasto-plastic mobilisation curves, whereby the stiffness factors k_b and k_s for respectively base resistance and shaft resistance result from the work of Frank and Zhao (1982) and are function of the PMT pressuremeter modulus E_M and the diameter D of the pile. The functions are different for non-cohesive and cohesive soils, but the pile type does not interfere.

In particular with regard to the load-settlement prediction of displacement auger piles, one also refers to the former work of Van Impe (1988) published in the first BAP-seminar.

4 HYPERBOLIC TRANSFER FUNCTIONS—GENERALITIES

4.1 *Basic principles*

Every geotechnical engineer is aware of the use of the single hyperbolic function for back-analysis of the pile load-settlement curve. The graphical inverse slope method, as suggested by Chin (1970), allows in many cases for a quite satisfying curve fitting. The main purpose of this curve fitting was and still is to extrapolate the measured load-settlement curves and to allow for a mathematical estimate of the ultimate or asymptotic pile resistance. The method is semi-graphical and based on the conversion of the "measured *Q*-*s*" values into a *s*/*Q* versus *s* diagram. In fact, the basis equation (1)

$$Q = \frac{s}{a + bs} \tag{1}$$

can be transformed into:

$$\frac{s}{Q} = a + b \cdot s \tag{2}$$

which corresponds to a straight line in the *s*/*Q* versus *s* plane. An example of the method is shown in the calculation sheet in figure 3.

Further refinements consist of the search of 2 separate hyperbolic equations (Chin & Vail, 1973) and to be combined for the curve fitting and back-analysis of pile loading tests. But extended and repeated work of Fleming (1972) in the 90's contributed to a much better understanding of the hyperbolic transfer functions and the soil parameters defining these functions. Since then, the hyperbolic function approach has been tested and used by many engineers, mostly with great enthusiasm and satisfaction. Reference is also made to an excellent contribution of Caputo (2003) in the 4th BAP-conference.

The hyperbolic functions have been extensively used by the author during the last decade. For completeness, the theoretical basics are described below.

The transfer functions for respectively base resistance R_b and shaft resistance R_s as a function of the

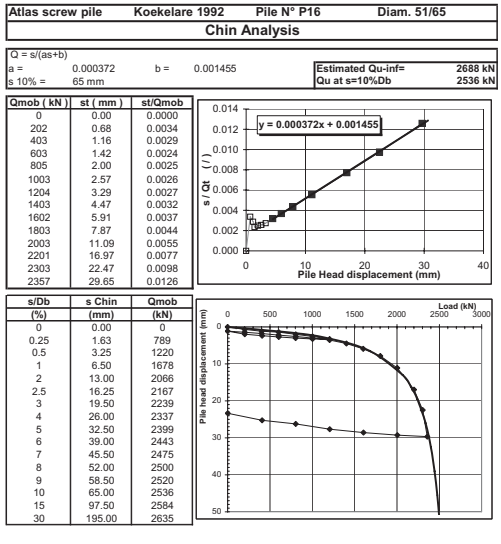

Figure 3. Example of a simple Chin analysis of a pile load test.

base displacement s_b and the shaft displacement s_s are expressed as follows:

$$R_b = \frac{s_b}{K_b + s_b / R_{bu}} \tag{3}$$

$$R_s = \frac{s_s}{K_s + s / R_{su}} \quad \text{or} \quad q_s = \frac{s_s}{K_s + s_s / q_{su}} \tag{4a–4b}$$

The base flexibility factor K_b (dimensions m/kN) corresponds to the tangent slope at the origin of the hyperbolic curve, as shown in figure 4. It also gives, multiplied with R_{bu}, the base displacement at 50% mobilisation of R_{bu}.

On the basis of the settlement formula for circular footings, K_b may be related to the secant modulus E_u (considered at 25% of the ultimate stress) by:

$$K_b = \frac{3 \cdot (1 - \nu^2) \cdot f}{4 \cdot D_b \cdot E_u} \approx \frac{0.54}{D_b \cdot E_u}$$

with $\nu = 0.4$ and $f = 0.85$ (5)

From (5), one deduces the following relation between the base displacement at 50% of R_{bu} and K_b or E_u:

$$s_{50\%} = K_b \cdot R_{bu} = \frac{0.212 \cdot D_b \cdot q_{bu}}{E_u} \tag{6}$$

The shaft resistance flexibility factor K_s (dimensions m/kN) also corresponds to the tangent slope at the origin of a q_s–s_s diagram. With Fleming, one states that K_s is proportional to the pile's shaft diameter D_s and inversely proportional to the ultimate shaft friction R_{su}, and so:

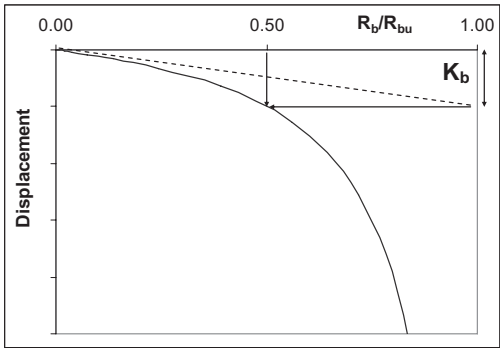

Figure 4. Principle of hyperbolic law.

$$K_s = \frac{M_s \cdot D_s}{R_{su}} \tag{7}$$

with M_s a dimensionless flexibility factor in the nature of an angular rotation. From this one deduces that 50% of the ultimate shaft friction is mobilised at a pile shaft displacement of :

$$s_{50\%} = K_s \cdot R_{su} = M_s \cdot D_s \tag{8}$$

4.2 *Deduction of parameters*

It appears from the above mentioned formulae (4) to (7) that only a few parameters are required to define the various hyperbolic functions:

- R_{bu} or q_{bu}: ultimate pile base resistance, total or unit value
- E_u: secant modulus (at 25% of ultimate stress) of the soil beneath the pile base
- R_{su} or $q_{su,i}$: ultimate pile shaft resistance, total or unit value in the different layers around the pile shaft
- M_s: shaft flexibility factor
- E_c or E_s: pile material modulus (concrete, steel, grout, …)

Some remarks with regard to the parameter choice.

1. The ultimate pile base resistances and pile shaft resistances are in most cases obtained by calculation. An overview of the wide panoply of methods used in Europe resulted from the ERTC3 work in the period 1994–2004. (De Cock 1998, De Cock et al. 2003). It should be mentioned that the required value should be the asymptotic ultimate value at large displacements. However, one can also use the hyperbolic law on the basis of another ultimate value, e.g. at 10% of the pile base, and by deducing R_{bu} from the next correlation at s = 10% of the pile base diameter D_b:

$$R_{b,10\%} = \frac{0.1 D_b}{K_b + 0.1 D_b / R_{bu}} \tag{9}$$

2. For the secant modulus in non-cohesive soils, Caputo (2003) found a correlation factor of 10 between E_u and the average CPT-cone resistance q_c in the proximity of the pile base. According to the author, the correlation should also depend on the soil stress history (e.g. geological overconsolidation) and should also be "pile type" related. There is in fact enough evidence that the soil stiffness may be influenced by the execution method of the pile: e.g. a bored pile may result in some soil reluctance at the pile base, while a driven pile leads

to a densification and prestressing of the pile base layer; the latter results in a much higher deformation modulus. Further literature survey and back-analysis are needed to define suitable correlations, but the following correlations appear to be quite promising in non-cohesive soils:

$$\begin{aligned} E_u &= 4 \text{ to } 6 \times q_c \text{ for bored piles in NC-sands} \\ E_u &= 6 \text{ to } 8 \times q_c \text{ for bored piles in OC-sands} \\ E_u &= 8 \text{ to } 12 \times q_c \text{ for screw piles} \\ E_u &= 15 \text{ to } 20 \times q_c \text{ for driven piles} \end{aligned} \quad (10)$$

For cohesive soils (stiff OC-clays) it was found from back-calculation of screw piles in clay (see below in 5.2.1 and 5.2.2) that—at least for the pile load test—the undrained modulus should be used for the pile base stiffness, and so approximately:

$$E_u = 50 \text{ to } 80\ q_c \quad \text{or} \quad E_u \sim 750 \text{ to } 1.000 \times c_u \quad (11)$$

3. For the shaft flexibility factor, Caputo's statistical analysis (Caputo, 2003) confirmed the findings from Fleming that this factor generally is in the order of 0.001–0.002. This is also confirmed in many of our analysis, with only rare exceptions (see further).
4. The material moduli of elasticity for concrete and steel are supposed to be well known. For concrete several empirical formula relate the elasticity modulus to the compressive strength, as for example:

$$E_{tg} = \sqrt{5600.(0.96); R'_{wj,28,150}} \quad (12)$$

On the other hand, the non-linearity of the material modulus at high concrete or steel stresses should be considered. In particular in the case of tension piles, the question rises whether and when the fissuring of the concrete under tension degrades during the tension test.

5 APPLICATIONS OF HYPERBOLIC TRANSFER FUNCTIONS

5.1 *A multipurpose tool*

When considering base resistance, shaft resistance and pile elasticity separately and by dividing the pile in e.g. 10 or 20 discrete elements, the hyperbolic transfer functions appear to be a fascinating engineering tool. Some of the possible uses are illustrated in the further paragraphs of chapter 5, namely:

5.2 For (class-A) prediction of the LS-curve
5.3 For back-analysis of pile load tests to deduce the adequate design parameters and/or to define calculation methods
5.4 To verify the SLS of a pile foundation (prediction of single pile displacement)
5.5 To convert a pile load test to other pile geometries, e.g. to a larger diameter
5.6 To invert a pile load test from compression to tension, or from bi-directional pile testing to top loaded testing.
5.7 To evaluate the impact of pile type, material, shape, execution method, … on the pile stiffness
5.8 To evaluate the influence of boundary conditions on the pile behaviour, e.g. downdrag, excavation of top layer, …

5.2 *Class A prediction of pile load-deformation*

5.2.1 *Soil testing data*

We used the discrete hyperbolic functions at the occasion of a class A-prediction event that was organised in relation to an extended research program on auger piles in clay, conducted in Belgium (Holeyman, 2001). The results of our predictions were published at the Int. Conference in Istanbul in 2001 (De Cock, 2001).

All in all six different types of ground displacement piles were installed: one prefab concrete pile and five cast-in-place screw types including Fundex, De Wall, Olivier, Omega and Atlas. From each pile type, a series of "short" piles, length approx. 7.5 m, and a "long" pile, length of about 11.5 m, was installed.

Typical CPT data are given in figure 5. CPT-EB2 with electrical cone and CPT-MB12 and CPT-MB23 with mechanical M1 (Dutch cone) are located in the same area, close to pile B2 (long De Waal pile).

5.2.2 *Applied parameters in the prediction*

The ultimate base resistance R_{bu} and the ultimate shaft resistance R_{su}, both considered as the *conventional values* at a relative pile displacement $s = 10\%D_b$ (D_b = pile base diameter) have been deduced from

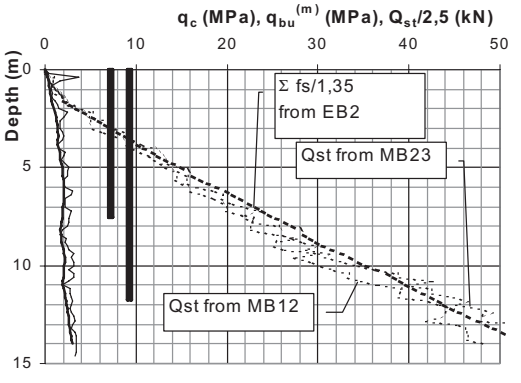

Figure 5. Typical CPT-data and deduced $q_{bu}^{(m)}$ (St-Katelijne-Waver).

the CPT data. According to the Belgian methodology (Holeyman et al. 1997) one defines:

$$R_{bu} = \alpha_b \cdot \varepsilon_b \cdot q_{bu}^{(m)} \cdot A_b \quad \text{or} \\ = \alpha_{b,\text{mean}} \cdot \varepsilon_b \cdot q_{bu,\text{mean}} \cdot A_b \qquad (13a–b)$$

with α_b an empirical (installation) factor taking into account the method of installation of the pile and the soil type;

$$R_{su} = \frac{X_s}{\pi d} \cdot \alpha_s \cdot \Delta Q_{st} \quad \text{or}$$

$$= \frac{X_s}{\pi d} \cdot \sum \alpha_{si} \cdot \Delta Q_{sti} \qquad (14a–b)$$

with a_s an overall empirical factor introducing the effects of pile installation method, the nature and roughness of the pile shaft material and soil structure scale effects.

$$R_{su} = X_s \sum H_i \cdot \eta_{pi} \cdot q_{ci} = X_s \sum H_i \cdot \alpha_{si} \cdot \eta_{pi}^* \cdot q_{ci} \qquad (15)$$

with η_p = an overall empirical factor depending on both soil and pile type. The correlation $\eta_p = q_c/q_{su}$ can be split into a pure soil parameter η_p^* equal to the ratio of q_c and the average unit side friction f_{su}, and a pile/soil dependent empirical factor α_s (as defined above).

Contrary to the traditional Belgian methodology, as used by the BBRI, the unit end bearing resistance in the natural ground conditions has not been calculated using the De Beer method (Van Impe, 1988) which gives $q_{bu}^{(m)}$, but as the mean value of q_c over a depth of $2D_b$ below the pile base (indicated in equation (11b) by $q_{b,\text{mean}}$). Comparison of both values for the various CPT performed in the test pile axis, is given in Figure 6. The De Beer method, which smoothes the q_c-diagram, gives on average 15% lower values than this mean q_c.

The ε_b factor refers to the scale dependent soil shear strength of the fissured clay. It has been deduced from previous research in the considered clay layer to be related to the ratio of the pile diameter D_b to the CPT cone diameter d by:

$$0.476 \le \varepsilon_b \approx 1–0.01(D_b/d - 1) \qquad (16)$$

In the initial prediction, the *pile base area* A_b has been calculated from 1.0 × the external diameter of the auger for Fundex, De Waal and Omega, and from 0.9 × the maximum auger flange diameter for Olivier and Atlas. For clarity, however, in this paper all factors are put = 1.0, incorporating the section reduction factor of $0.9^2 = 0.81$ for Olivier and Atlas in the α_b factor. For $X_s = \pi D_s$, the maximum shaft diameters have been considered for all piles.

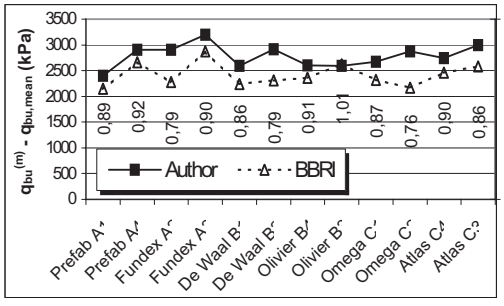

Figure 6. Unit end bearing (without installation factors) from CPT (St-Katelijne-Waver).

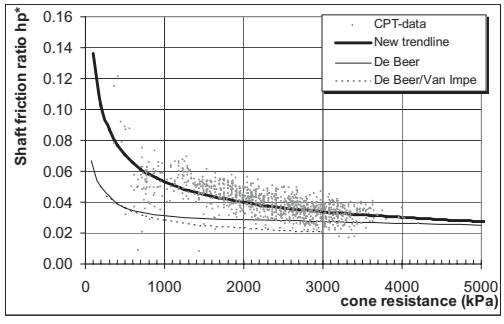

Figure 7a. Shaft friction ratio η_p^* as a function of q_c.

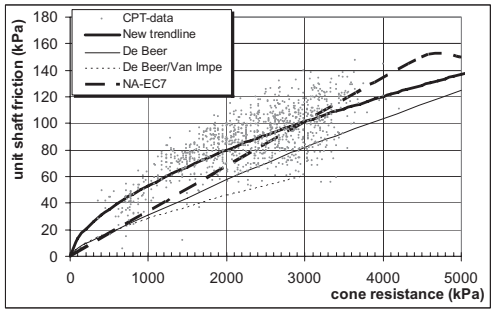

Figure 7b. Unit shaft friction $f_{s,red}$ as a function of q_c.

The $\alpha_{b,\text{mean}}$ factor had been taken = 1.0 for all pile types (but so has now been replaced by 0.81 for Olivier and Atlas).

For α_s, the following values have been used in the prediction: precast piles 0.85, Fundex piles 0.80, De Waal and Omega 1.0, Olivier and Atlas 1.25.

The correlation factor η_{pi}^* has been defined in 2 steps:

– 1st: the measured local friction values f_s from the electrical cone CPT have been reduced by a factor of 1.35 in order to obtain a good correlation

between this reduced integrated local friction $f_{s,red}$ and the total rod friction Q_{st} with the mechanical cones; (see Figure 5);
– 2nd: the relation between $f_{s,red}$ and q_c.has statistically be analysed. Figures 7a and 7b give the collection of the data points, the deduced trend line, the relations earlier suggested by De Beer (1985) and Van Impe (1988), as well as the relation prescribed in the recent Belgian guidelines for the design of compression piles (BBRI, 2008).

From this, one deduces the following trend lines:

$$\eta_p^* = 0.9 \cdot q_c^{-0.41} \quad \text{or} \quad fs,\text{red} = 0.9 \cdot q_c^{0.59} \qquad (17a–b)$$

For the calculation of K_b and K_s, the following values have been adopted:

– E_u = 175 to 225 MPa (≅1000 c_u or ≅70 q_c)
– M_s = 0.0015 for z < 5 m and = 0.001 for z > 5 m.

The E-modulus of the pile's concrete has been taken equal to 30000 MPa, which has appeared later on to be smaller than the values of 35 to 40000 MPa deduced from compression tests on concrete samples.

5.2.3 *Comparison of predictions with SLT-curves*
Figures 8a–8d gives for a selection of 4 piles the comparative charts of the SLT curve ($Q_{t,meas}$) as well as the predicted curves for mobilised base, shaft and total resistance $Q_{b,pred}$, $Q_{s,pred}$ and $Q_{t,pred}$ respectively, all expressed as a function of the pile head displacement s_t.

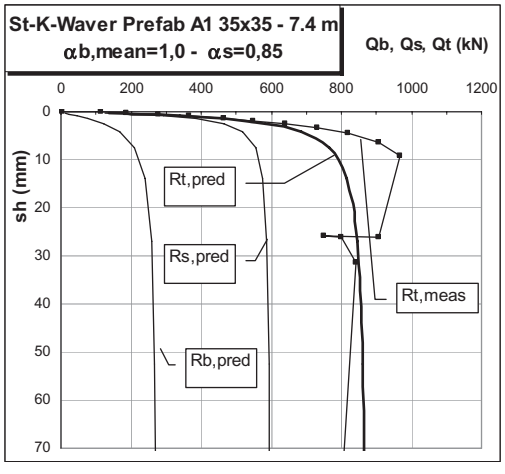

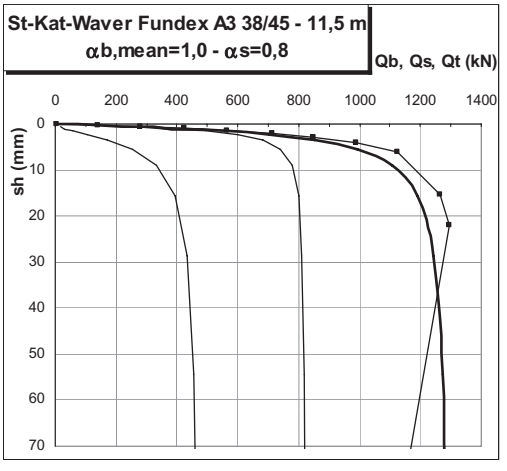

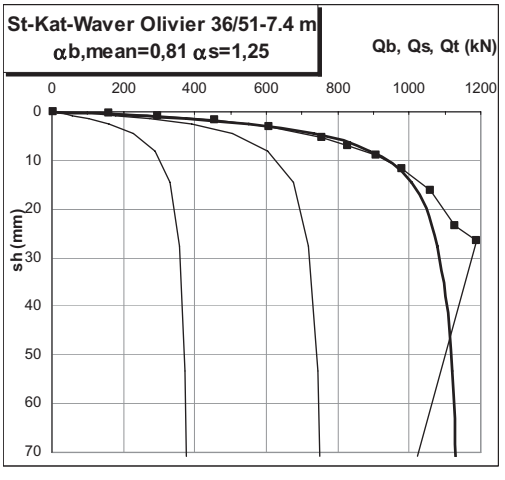

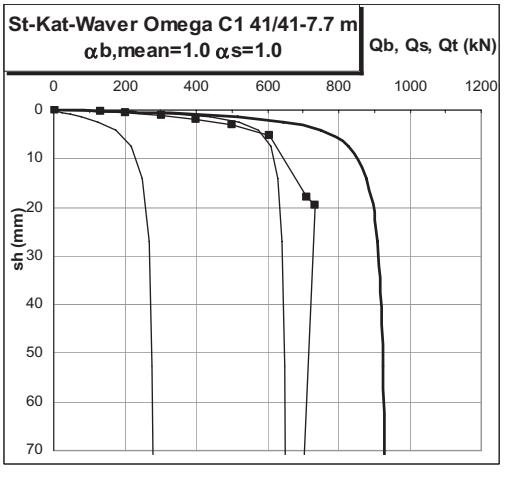

Figures 8a to 8d. Predicted curves of Qb, Qs and Qt and measured total load-displacement curve (St.-Kathelijne-Waver) Screw piles in clay (St-Kathelijne Waver) (De Cock, 2001).

With regard to the measured load-curves, the attention is drawn to the following:

– SLT were performed in 10 to 12 load steps of 60'
– After reaching a peak resistance, piles were further displaced at constant rate of 0.6 to 0.8 mm/min; in all cases the load therefore required decreased more or less significantly to what often is pretended to be the residual resistance.

Comparison of predicted and measured data leads to the following conclusions and remarks:

– All in all, the shape of the predicted curve corresponds fairly well with the observed load-displacement behaviour, considering that the measured displacements at high load levels as well as the peak resistance are very much influenced by the short duration of the load steps and therefore should be handled with caution.
– For prefab and Fundex piles, the prediction of the ultimate total pile resistance as well as of the total stiffness factor (see also the zoomed chart in Figure 8a) may be called perfect.
– For all other piles, the ultimate pile resistance is overestimated by about 15–25%, with a maximum of 50% for the short Atlas pile C4.

5.3 *Back-analysis of pile load tests*

As already explained earlier, only a few parameters are needed to define the required transfer functions for base and shaft resistance. Therefore, curve fitting with the measured load-displacement curves (Q_t, Q_s and Q_b) allows quite easily to obtain the required parameter values to calibrate the chosen design method (e.g. a semi-empirical direct design method based on in situ soil tests such as CPT or PMT).

Some illustrations of such a curve fitting are given in the figures 9a to 9b. For clarity and simplicity, the back-analyses have been performed on the same piles as those reported above for the class A-predictions.

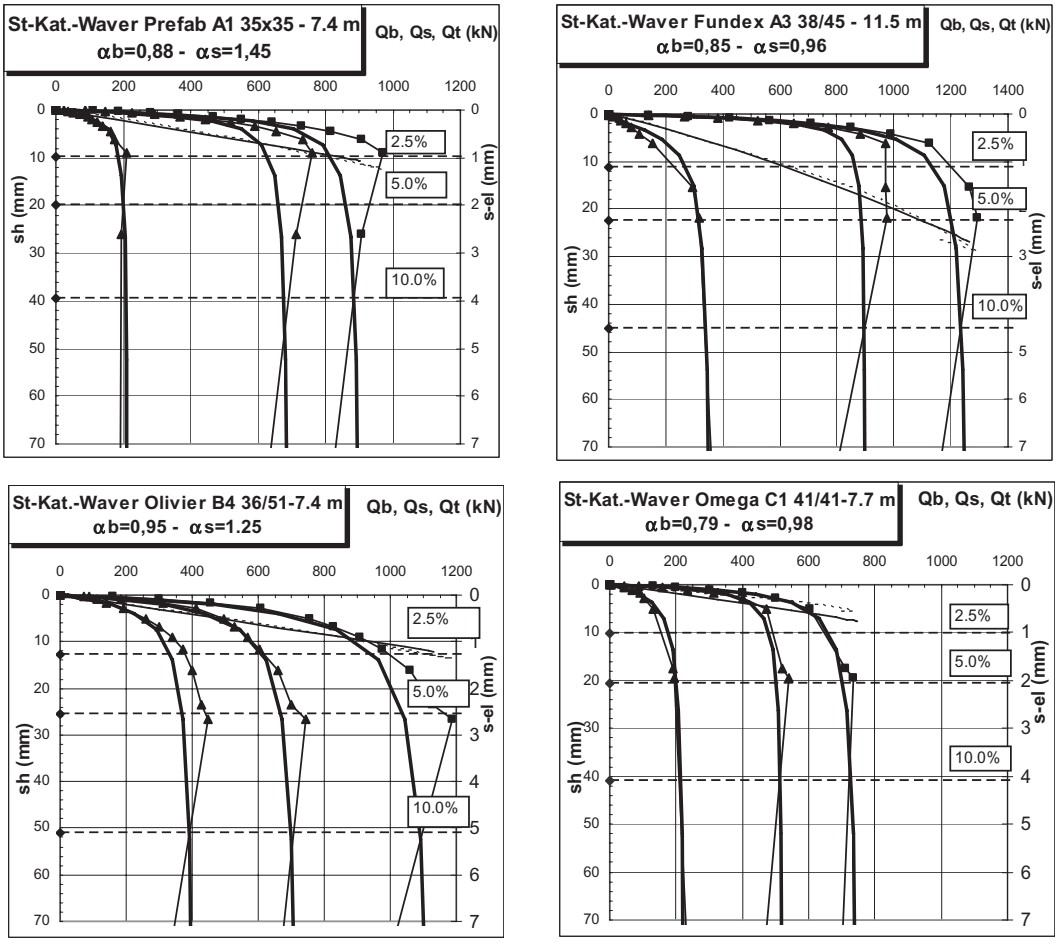

Figure 9a to 9d. Back-analyses of pile load tests. Screw piles in clay (St-Kathelijne Waver).

However, one should keep in mind that there is a slight difference in the definition of the installation factors α_b and α_s used in the back-analysis, which fit into the recently published design guidelines within the EC7-NA (National Application document). Indeed:

– α_b is to be combined, according to equation (11a) with the unit pile base resistance $q^m_{(bu)}$ as calculated according to the De Beer's method and not with an averaged value cone resistance value $q_{c,mean}$
– α_s is to be combined, according to equation (13), with the η^*_p-values as defined in EC7-NA; for the considered case of clay, $\eta^*_p = 1/30\ q_c$ as indicated in figure 7b.

The best estimate of the resulting parameters is indicated in the different figures 9a to 9b. They are also summarised in table 5.

5.4 *SLS design of a single pile*

For the time being, the Belgian EC7-NA document only provides calculation rules for the ULS design of single axially loaded piles in compression. It is the

Table 5. Parameters resulting from back-analysis of pile load tests. Screw piles in clay (St.-Kathelijne-Waver).

Pile	E_c (MPa)	E_b (MPa)	M_s (–)	α_b (–)	α_s (–)
A1 Precast	38.000	130 qc	0.002	0.90	1.80
A3 Fundex	35.000	50 qc	0.002	0.85	0.96
B4 Olivier	25.000	65 qc	0.0045	0.95	1.25
C1 Omega	43.000	50 qc	0.002	0.79	0.98

* pile base resistance is likely to be underestimated and shaft friction overestimated.

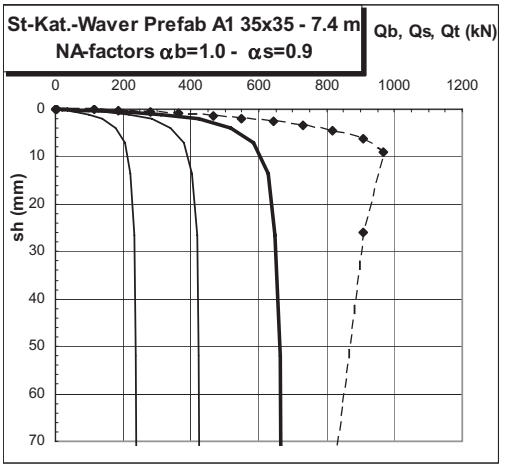

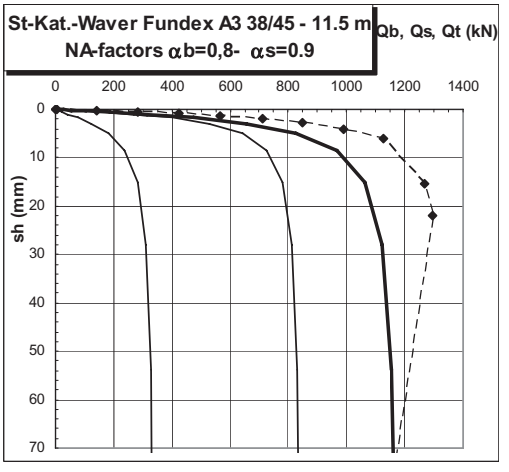

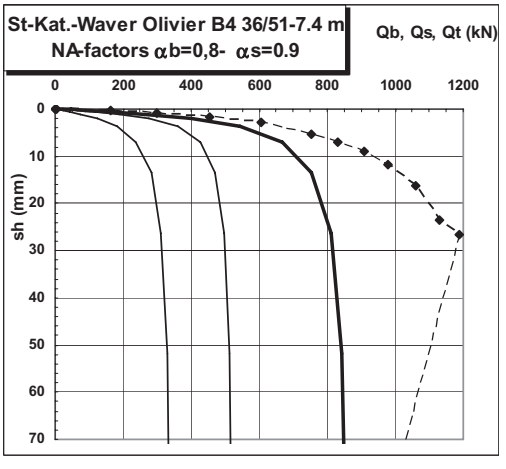

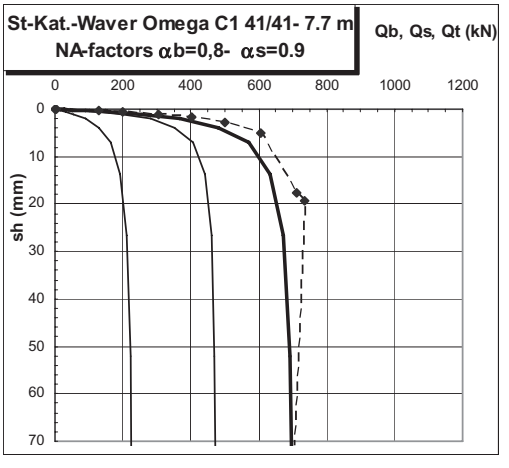

Figure 10a–10d. Calculated curves of Qb, Qs and Qt with factors from EC7-NA and measured total load-displacement curve. Screw piles in clay (St-Kathelijne Waver).

aim of the piling committee to develop in due time also guidelines for the SLS design. The methodology still has to be elaborated and discussed.

In order to get—at least—a feeling of the impact of the ULS design rules on the load-settlement behaviour, for the same 4 piles as considered before, one has now estimated the load-settlement curve using similar hyperbolic functions, with the same stiffness parameters E_b and M_s (and thus also K_b and K_s) as deduced from the curve fitting, but with the α_b and α_s factors as prescribed in the EC7-NA document. For the concrete modulus E_c a "conservative" value of 25.000 MPa has been adopted for all cases. The results are given in figures 10a to 10b.

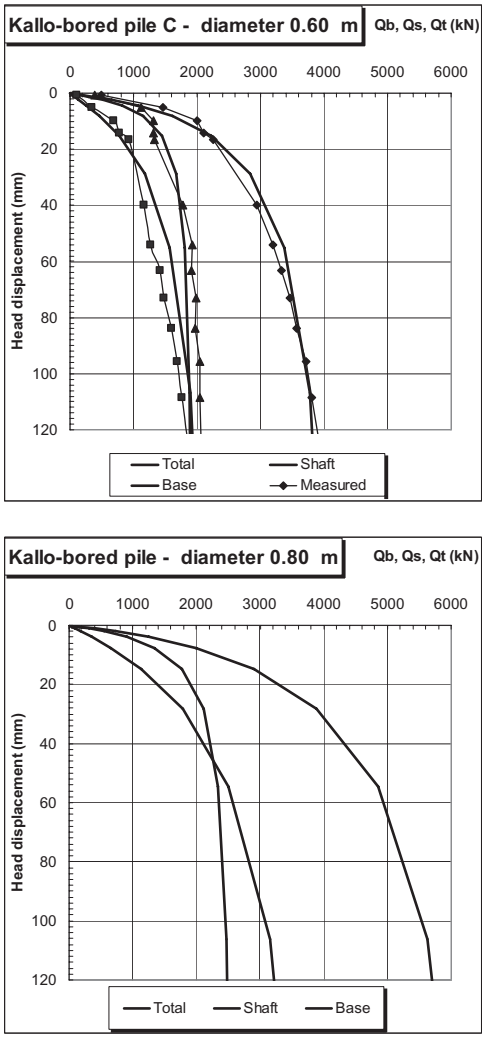

Figure 11. Conversion of pile load test to larger diameter pile.

5.5 *Converting pile load test result to larger diameter—bored piles*

Eurocode 7 (7.6.2.2-(4)) allows for performing design load tests on smaller diameter trial piles, providing a.o. that the trial pile is instrumented in such a manner that the base and shaft resistance can be derived separately from the measurements. The hyperbolic transfer functions are an easy instrument to convert the measured pile-displacement curve for larger (or smaller) diameters. An example is given in figure 11. It is based on the scientific research programme on bored and driven piles in dense sands, conducted at Kallo (De Beer, 1988).

5.6 *Comparison of compression and tension behaviour—shaft grouted auger tube piles*

In 2006–2007 two extended load-testing programmes were performed on so-called CSG-piles (Continuous Shaft Grouted) at the demand of Franki Grondtechnieken BV/The Netherlands. These programmes aimed to define the adequate design parameters for this pile type in accordance to the Dutch piling code NEN 6743 for compression piles and the CUR report 2001 for tension piles. The piles consist of a central steel tube (diameter 140 mm, thickness 10 mm), provided at the base with 1 or several screw blades or with an enlarged drill bit (figure 12). The tube is installed by screwing, while injecting cement-grout through the tube which is mixed with the surrounding soil by the action of the screw blades. After reaching the required depth, additional pressure grouting is performed.

The first test programme, located in Pijnacker, comprised 8 test piles. Two piles—each with a screw blade of 450 mm—were load-tested in both compression and tension. The other 6 piles—either with a screw blade of 350 mm diameter or with a drill bit of 180 mm—were load tested in tension only. All piles were instrumented with 3 tell-tales.

Figure 12. View on the steel tubes for the CSG pile (Franki Grondtechnieken B.V.).

A typical CPT and the configuration of the 2 test piles that will shortly be described below, together with the length of their respective tell-tales, are given in figure 13.

Several disturbances on the tell-tales, the uncertainty about the axial stiffness EA of the piles and the large share of the elastic deformations in the total pile head displacements appeared initially to hinder the interpretation of the test results. Finally, the back-analysis by using the hyperbolic function approach allowed obtaining an acceptable and justified interpretation of the test results. By way of illustration, two analyses are given below.

The test pile TP1 was initially used as a reaction pile for the tension test on the neighbour pile and consequently was compressed in 6 loading-unloading steps up to a maximum test load of 1363 kN; the maximum pile head displacement was 20.4 mm. The "asymptotic" ultimate pile resistance, which is estimated by a simple Chin analysis or a Vanderveen analysis lies in the order of 3250 kN. As this value is far higher than the maximum test load, the accuracy of the extrapolation may be questioned. Moreover, it appears from the tell-tale measurements that the maximum total head-displacement of 20.4 mm was essentially due to the elastic deformation of 18.2 mm, while the displacement of the pile base was only about 2.2 mm. Nevertheless, the curve fitting of the total load-displacement curve as well as of the tell-tale measurements (figure 14), allowed to obtain a fair estimation of the pile stiffness EA (with a quite complex combination of steel tube, steel tell-tales, internal grout and external soil-cement mix), of the soil stiffness factors E_b and M_s and of the design parameters α_b and α_s (in accordance to NEN 4735). Once these parameters were obtained, it was a small challenge to convert the compression test into a tension test, and to compare this tension curve from conversion with the measured curve during the tension test on the same pile. In this conversion, all parameters were kept as deduced from the compression curve fitting. The only parameter that was changed was the pile stiffness factor, for which only the steel section and not the grout sections was considered for the "tension-stiffness". Both the "converted" tension curve and the measured tension curve are shown in figure 15. The correspondence is fairly well.

The results of a second tension test on pile RP2 (diameter tube 140 mm and drill bit 180 mm) as well as the curve fitting are given in figure 16a for the

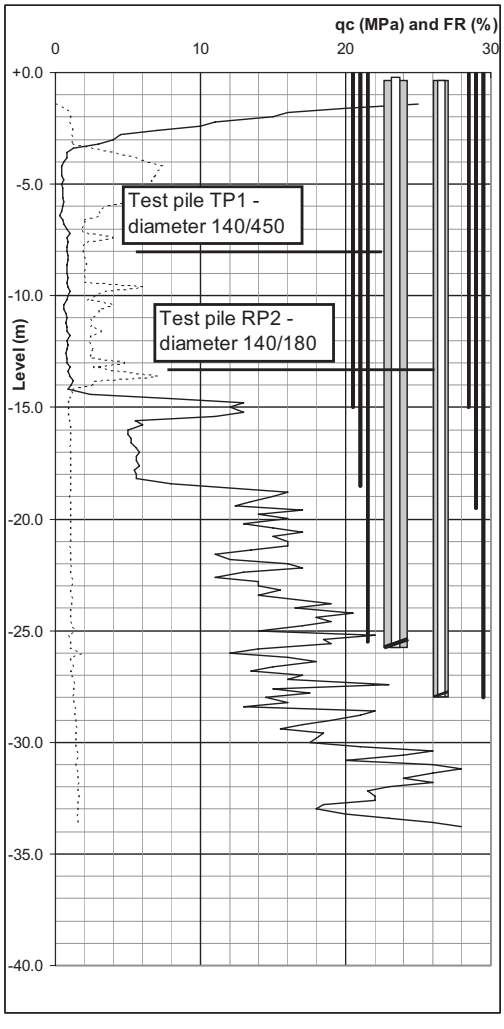

Figure 13. Typical CPT and configuration of piles and tell-tales (Test plot Piijnacker).

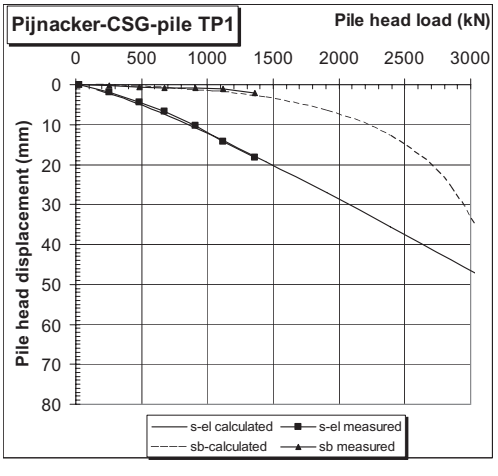

Figure 14. Curve-fitting of the tell-tale measurements (Test plot Pijnacker).

fitting of the tell-tale measurements, and figure 16b for the pile head displacements.

The maximum applied load is 1814 kN, which is about 75% of the estimated "asymptotic" ultimate resistance of 2.400 kN. The pile head displacement at maximum load was 55.0 mm, from which 43.2 mm comes from the elastic elongation and 11.8 mm corresponds to the pile base lifting. These quite high displacements, which are typical for many types of steel tension piles (and anchors), may question the criteria that have to be applied in the ULS as well as the SLS design. One also notices at maximum load of 1814 kN a deviation between the calculated and measured pile elongation s-el. This is mainly due to yielding of the steel at the considered working stresses of well above 450 N/mm².

5.7 *Impact of changes in pile type, material, geometry, execution method,…*

The hyperbolic functions also allow the SLS analysis of changed pile characteristics, such as:

– Changes in pile stiffness EA, e.g. by using a different steel section for steel piles
– Different pile type, e.g. impact driven pile versus auger pile
– Application of post-grouting.

For the latter, we refer to section 6.5, where the application of post-grouted large diameter bored pile is described.

5.8 *Influence of changing boundary conditions*

Also the impact of changing boundary conditions on the pile settlements and safety can be verified on the basis of established transfer functions, e.g.:

– Loss of positive shaft friction due to excavation of the top layers.
– Inversion of positive shaft friction into negative skin friction due to settlements of the surrounding soil.

One refers to section 6.4 for a practical demonstration.

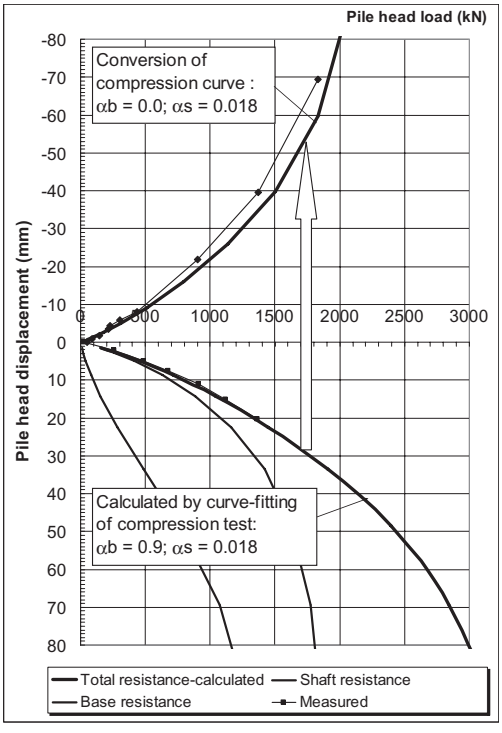

Figure 15. Demonstration of conversion of a compression pile test to a tension curve.

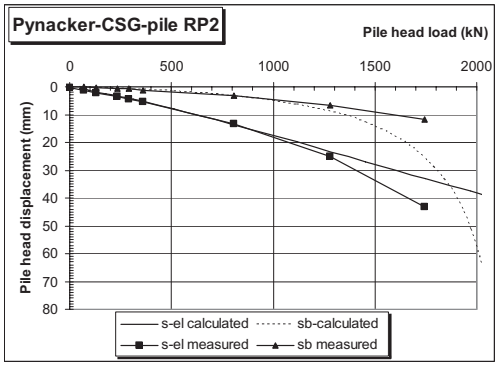

Figure 16a. Curve-fitting of the tell-tale measurements (Test plot Pijnacker).

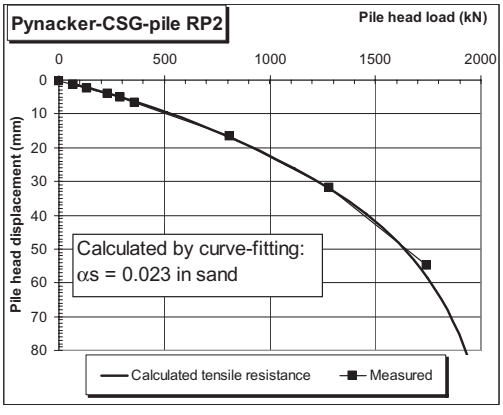

Figure 16b. Curve-fitting of the pile head deformations (Test plot Pijnacker).

6 CASE HISTORIES TO ILLUSTRATE SENSE AND SENSITITY OF PILE DISPLACEMENTS

6.1 *Introduction*

The sensitivity of the structure to displacements of the pile foundations should be verified from the next 3 points of view:

1. the ULS of the pile foundation: what is the real load on the different piles?
2. the ULS of the structure: which stresses are developing in the superstructure due to the displacements of the piles?
3. the SLS of the structure: are the settlements (or heave) of the piles and the pile groups admissible for the structure and its functioning?

In particular with regard to the first and second item, the interaction between structure and pile foundation should be considered. This interaction mainly depends on the stiffness of the superstructure, the stiffness of

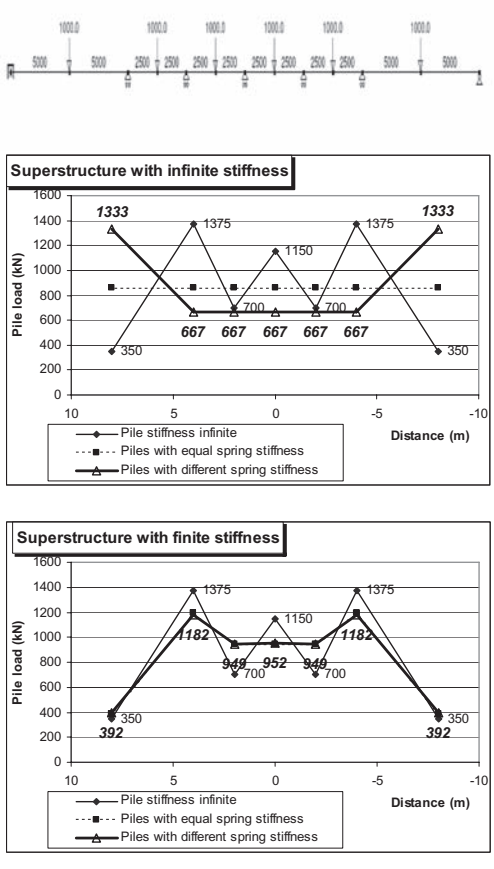

Figure 17. Pile load distribution as a function of stiffness of superstructure and piles. Exercise.

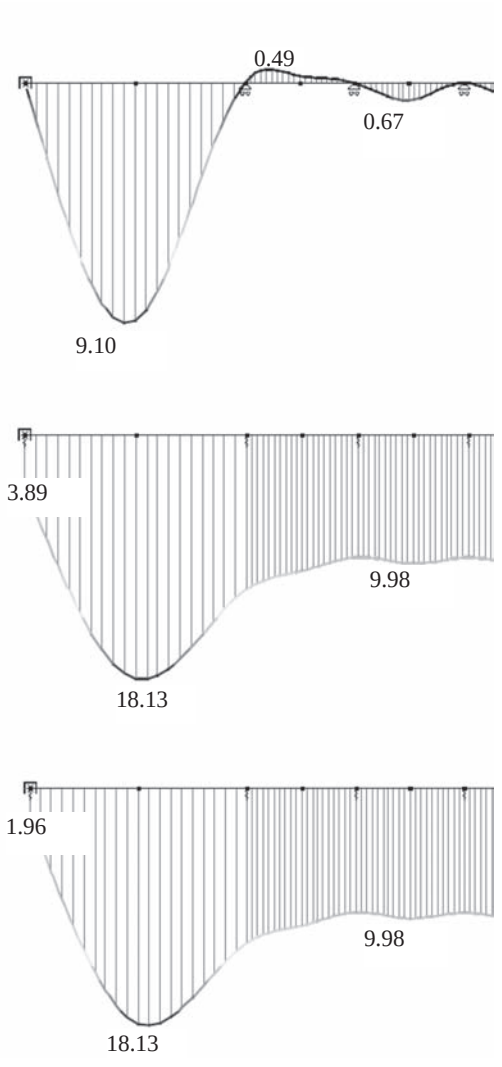

Figure 18. Deformation distribution for combinations 2, 4 and 6. Exercise.

Table 6.

Combination	Stiffness of structure	Stiffness of piles
1	Infinite	Infinite
2	Finite	Infinite
3	Infinite	Finite—100 MN/m
4	Finite	Finite—100 MN/m
5	Infinite	Finite—200 & 100 MN/m
6	Finite	Finite—200 & 100 MN/m

the piles (individually or in group) and the stiffness of the intermittent structure (pile cap, beams, raft…). The very different answers that one can get as a function of the relative stiffness are given in the example of figures 17 and 18. This sensitivity exercise was made in collaboration with the structural design office for a 12-storey apartment building. Six situations are considered for a hypothetic beam of 40 m in length, with 6 column loads of 1.000 kN each and 7 supports (say: 7 piles or pile groups)—see table 6. The stiffness of the beam (=structure) are considered to be either infinite or finite. The supports (piles) have been supposed to be rigid, or to act as (Winkler) springs of equal or different value; the latter case wants to simulate the higher stiffness of peripheral and/or single piles compared to internal piles or pile groups.

A summarise of the pile loads for the various combinations is given in figure 17.

The comparisons, although for a somewhat fictive situation, demonstrate that the load distribution on the different piles is fundamentally dependent onboth structure and pile stiffness. And so are also the bending moments and stresses in the superstructure, on the one hand, and the deformations (settlements) of the structure, on the other hand, as can be seen from the 3 deformation distributions given in figure 18.

6.2 *Heterogeneous soil stratigraphy—Antwerp LB*

In the ‘70 s the strong residential needs nearby the city of Antwerp (located on the right bank of the river Scheldt) gave rise to the development of extensive housing estates in the former polder on the left bank opposite the ancient city centre (figure 19).

By hydraulic or mechanical landfill with sand, the site level was raised from the former polder level of about +1/+2 up to the level +6 to +7. Multiple housing projects were realised in short time and it were golden times for piling contractors, with an extended use of precast concrete piles which were driven into the medium dense or very dense sand layer underneath the polder clay and peat. A typical CPT for the region is given in figure 20.

However, some 30 years later, the new owner of one of the houses had serious doubts about the stability of the house because of various cracking in the sub base as well as in the superstructure. Levelling works revealed an overall tilting of the construction from SW to NE with differential settlements of 92 mm!!! And this in spite of the fact– according to the information from the construction drawings—that the house—with a surface of 4.0×15.0 m²—was built on 14 piles with a capacity of 600 kN. But the reason was quite obvious. The nearby lake, called “Galgenweel” let assume that the subsoil had been disturbed centuries ago, by the occurrence of this “weel = pool, swirl”, which has caused deep erosion of the polder layer and of the underlying sand and later on sedimentation of loose sand-clay deposits. CPT tests at the North side and the South side of the house have confirmed the suspicions and revealed very different soil conditions from the “normal” stratigraphy in the region, with an increasing thickness of the soft layers towards the lake

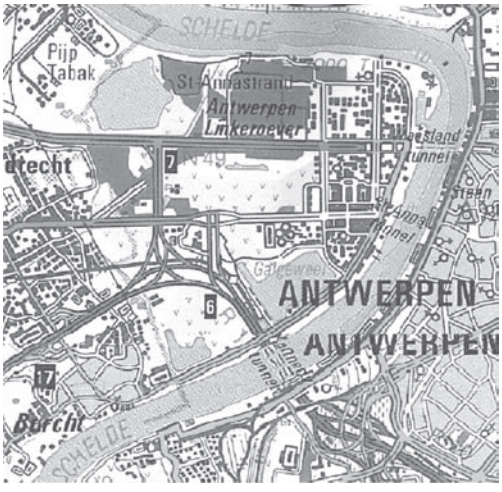

Figure 19. Site map of Antwerp Left Bank, the river Scheldt and the “Galgenweel”.

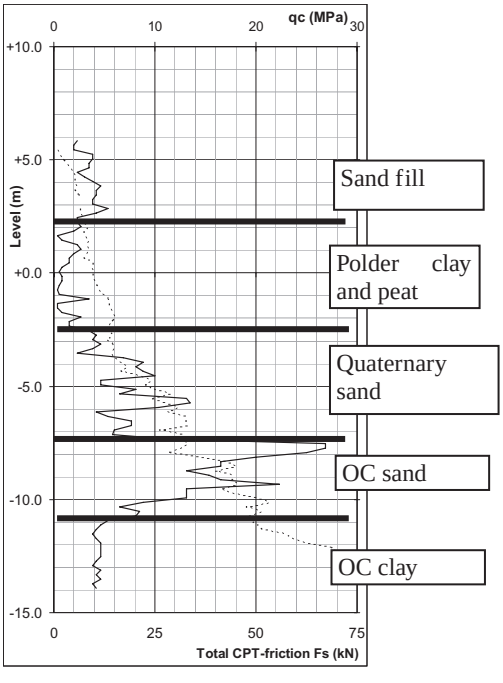

Figure 20. Typical CPT for Antwerp left bank.

(figure 21). Very likely, the piles have been executed too short and the foundations have behaved more like piled raft on a non-consolidated subsoil.

6.3 *Pile load and settlement distribution under uniform stiff high-rise building/Netherlands*

An interesting case history has been reported by Joustra et al. (1977). It concerns a very homogeneous and stiff high-rise building with a surface of 25×47 m², which was founded via a 1.5 m thick concreteslab on 222 prefabricated concrete piles. The piles are 17 m long and have a shaft section of 45×45 cm² and an enlarged base of 72×72 cm². The total building weight is about 290.000 kN, and so the average pile load is of about 1.300 kN/pile (Figure 22) .

Because of the existence of deep compressible layers underneath the pile-bearing sand stratum, some monitoring of the pile settlements and the pile load distribution was performed. The construction scheme is given in figure 23, showing also the location of:

- The piles EL1 to EL5 and ME1 to ME5, which were instrumented with a tell-tale, on the bases of which the head load was calculated
- The measuring points 1 to 10 for observation of the settlements.

Table 7 summarises the results of the tell-tale measurements and the pile loads that have been computed on the basis of the measured elastic shortening.

Figure 24 shows the recorded settlements until ½ year after construction. Settlements in the order of 2.5 cm in the corner points and of 3.7 cm in de centre points were measured.

6.4 *Interaction of foundations of adjacent buildings*

The following case history illustrates the sensitivity even of a pile foundation in interaction with adjacent former or future foundation works, on the one hand, and the possibilities to analyse and to interpret this interaction by using the hyperbolic transfer functions, on the other hand.

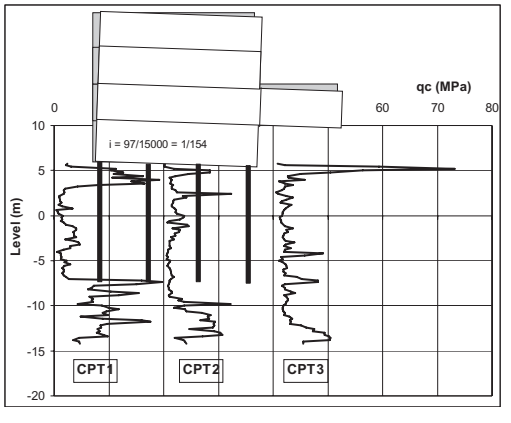

Figure 21. CPT tests and schematic presentation of building subscidence.

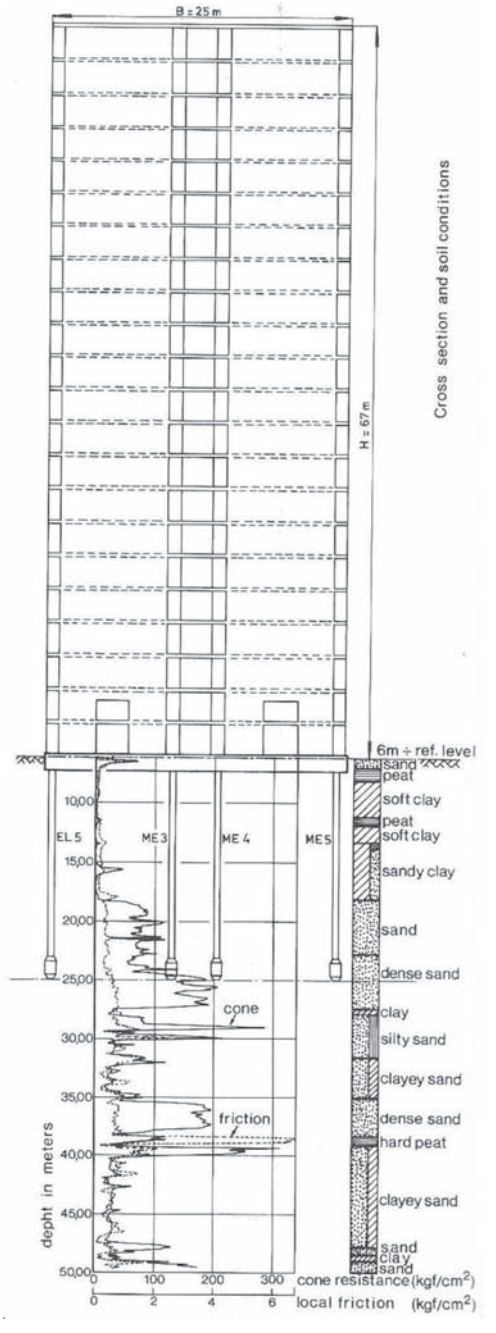

Figure 22. High-rise building—configuration, soil data and pile data (Joustra et al. 1977).

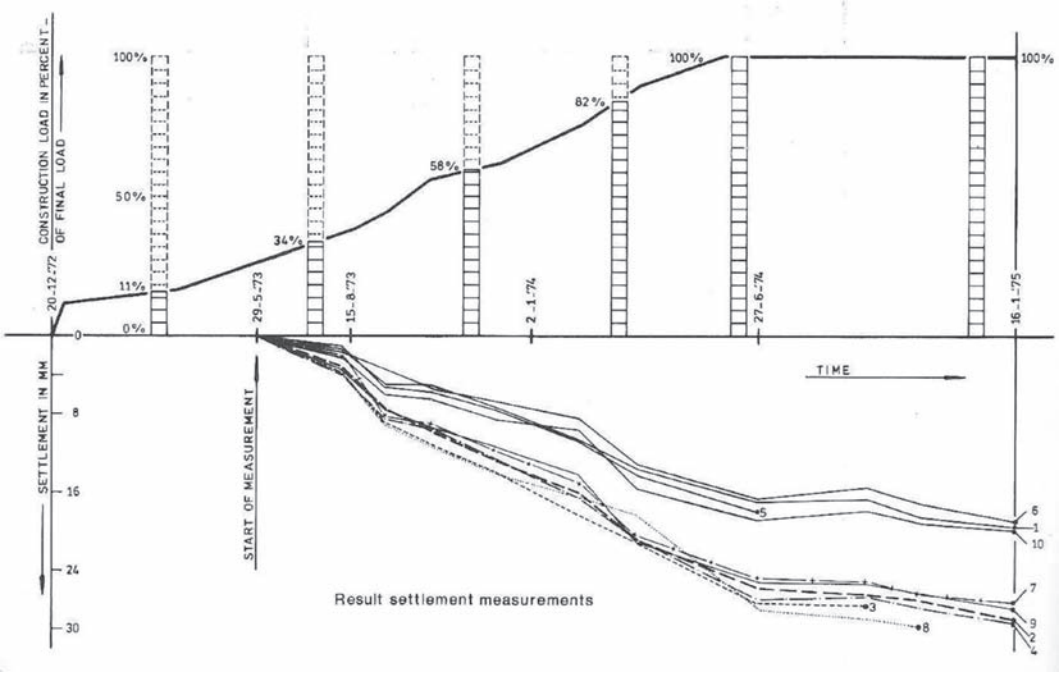

Figure 23. Evolution of settlements during construction.

Table 7. Summary of pile load measurements.

Pile No.	Shortening	Calculated pile load
EL1	2.72 mm	1.780 kN
EL2	1.14 mm	750 kN
EL3	1.47 mm	960 kN
EL4	2.62 mm	1.710 kN
EL5	defective	
EM1	1.20 mm	780 kN
EM2	1.41 mm	920 kN
EM3	1.87 mm	1.210 kN
EM4	1.10 mm	720 kN
EM5	1.91 mm	1.170 kN

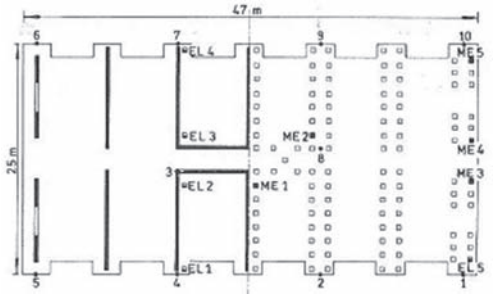

Figure 24. Construction schema and monitoring points.

The case history—which was the subject of a juridical expertise—concerns 3 adjacent houses:

- House No.1 was erected in the 60's and is founded on 21 driven Franki-piles, 500 kN capacity and a length of about 13.5–14.0 m below ground level
- House No. 2 was built in 1989, it includes a sub-base and is founded on 15 Atlas screw piles diameter 36/46 cm, 350 kN capacity and a length of 10 m below ground level
- House No. 3 dates from 1995. The foundation exists of 17 piers ("faux puits"), diameter 1.2 m, 240 kN capacity and a length of 6.9 m.

A schematic cross section parallel to the street and the diagram of the CPT at the location of house No. 2 is given in figure 25.

Quite important damages occurred in house No. 2 due to a tilting of the house towards house No. 3. From the various observations and measurements, the expert deduced what follows:

- a small tilting of house No. 2 resulted in the period 1990–1995 in some small fissuring at the interface with house No. 1.
- in the first week after excavation and concreting of the pier foundation of house No. 3, important new damage and tilting of house No. 2 occurred.
- during and after the erection of house No. 3, a further increase of the damage and tilting of house No. 2 was observed.

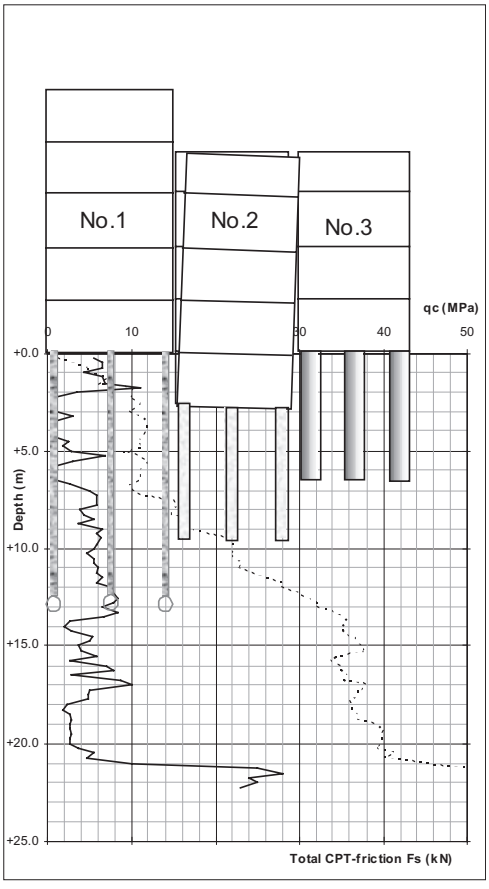

Figure 25. Soil data (CPT at location of building No. 2), pile data and schematic configuration of the 3 adjacent houses.

In 2000, one measures:

- a differential settlement of 5 mm between house 2 and the common wall with house 1
- a tilting of 1/20 of the joint wall of houses 2 and 3, from which the settlement of this common wall is estimated to be in the order of 35–40 mm.

The observed deformations may be explained as follows:

1. the first slight fissuring was caused by the combined effect of:
   - a partial transfer of the load of house 2 to the adjacent piles of house 1—due to some constructive connection between the 2 houses and/or by additional friction on the nearby Franki piles;
   - additional settlements of the pile group by the presence of compressible layer underneath the pile bearing layer.

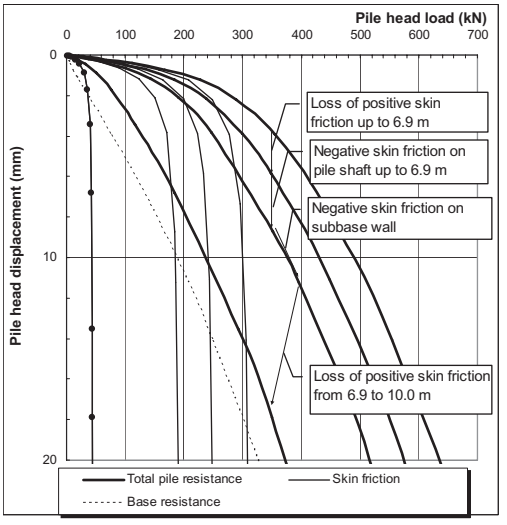

Figure 26. Analysis of the different interactions on the Atlas piles (nearby building 3).

2. possible decompression (stress reduction), decrease of the shear parameters and or subsidence of the soil by the excavation of the piers; this may lead to:
   - loss of the positive shaft friction on the adjacent Atlas piles over the pier lengt and even inversion to negative skin friction on these piles;
   - negative skin friction on the adjacent subbase wall what leads to an additional head load on the pile.
3. additional settlements of the Atlas piles due to the weight of house 3, which causes again negative skin friction on the Atlas piles (particularly beyond the foundation level of the piers) and settlements in the layers underneath the Atlas base level.

The adverse effect of the different interactions on the Atlas piles at the interface of building 2 and 3 may be analysed on the basis of the estimated load-displacement curves for the Atlas piles by using hyperbolic transfer functions. The results of this exercise are given in figure 26.

6.5 *Differential pile behaviour under an hyperstatic architectonic museum building*

The last case history concerns a new prestigious museum building—still under construction—in the city of Antwerp (the so-called MAS—Museum aan de Stroom)—Architects Neutelings-Riedijk/Rotterdam, Consulting Engineers ABT Belgium/Antwerp. The building has a

square footprint of 40×40 m² and contains 10 floor levels with a height of 6 m each (Figure 27). The museum floors—always containing a gallery and a museum room—are stacked in such a way that the MAS becomes a spiral tower. The periphery—with 6-metre high outside glass façades—is conceived as a walking boulevard that remains accessible for everyone, day and night, with panoramic views of the city and the river.

The architectural conception and needs:

- free panoramic view from the peripheral promenades
- museum rooms free of obstacles
- concrete look of walls and ceilings
- high level heights

were a big challenge for the structural concept and resulted in a type of Christmas tree structure consisting of (figures 28 and 29):

- a centre square concrete core of about 12×12 m² with a double function: stability and transfer of building loads to the foundations
- absence of load-bearing façades
- a minimum of load bearing elements in the peripheral galleries and promenade area's
- large projection of the periphery by means of framework or concrete wall-beams.

The overall vertical load on the foundations is maximum about 300.000 kN, from which 205.000 kN is permanent. Almost 85% of the loads is transmitted to the central core, while to other 15% is distributed over a number of "second order" columns and walls. Several options have been considered with regard to the foundation concept. Finally there was chosen for the use of bored shaft grouted bored piles with temporary casing under the central core and for CFA piles for the peripheral loads. Useful data about the behaviour of post-grouted bore piles in the considered tertiary

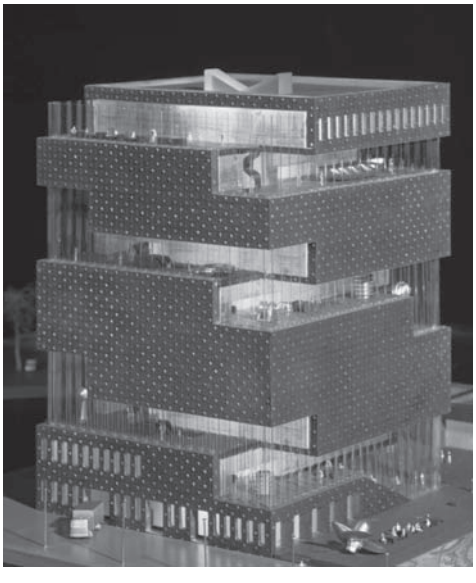

Figure 27. Maquette view of the MAS—museum.

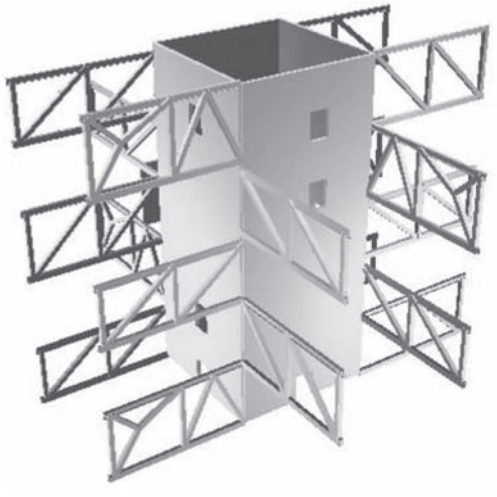

Figure 28. Structural schema.

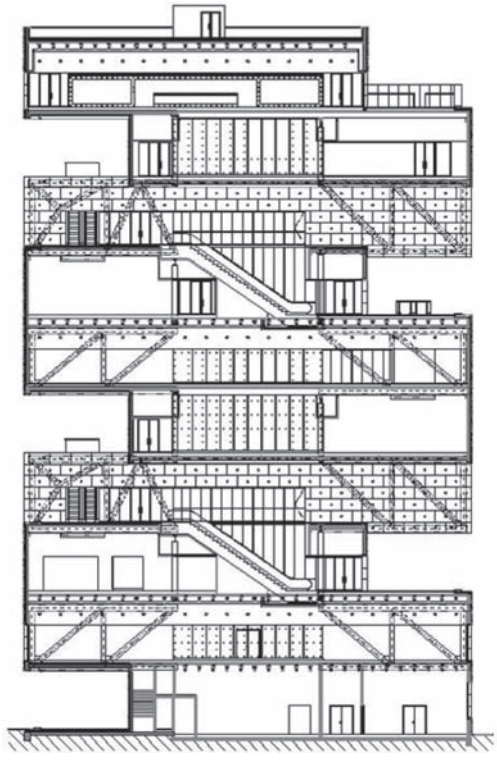

Figure 29. Cross section.

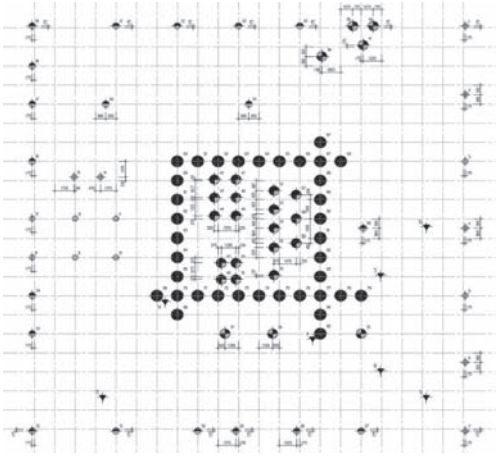

Figure 30. Pile lay-out

sands was gained from the extended bi-directional load testing performed for the HST-tunnel in Antwerp (Maertens et al. 2003) and other literature data. The pile lay-out is given in figure 30.

The main heavy load bearing bored piles have been kept concentrated under the central core. This has the advantage of a direct load transfer without the need for a heavy intermittent repartition slab. The use of shaft grouted piles aimed to increase the individual pile stiffness as well as the pile group stiffness and consequently to reduce the settlements of the central core:

– by the beneficial effect of the shaft grouting, the piles are essentially "friction" piles whereby the individual pile settlement under service load remains small (estimated at about 9 mm)
– the shaft grouting allowed to use relatively short piles, having their base level well away from the deep Boom clay of medium compressibility.

The long term settlements are calculated at about 67 mm for the central pile group and about 16 mm nearby the façades. From these values, about 18 mm respectively 8 mm occurs in the deep clay. In view of these absolute and differential settlements some structural measurements have been taken:

– there are no continuous stiff concrete walls going from central core to façade
– floor slabs between central core an façades are isostatic (hinge supports)
– during the construction period, some particular floor elements are delayed to allow a differential movement of façade and façade.

The settlement of the building are monitored and hopefully some results may be presented during the seminar.

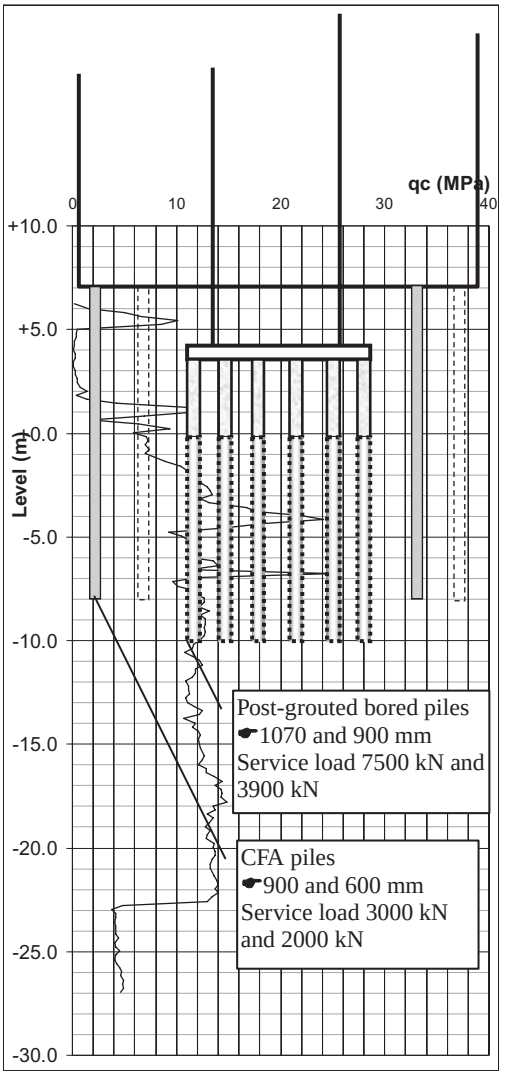

ACKNOWLEDGEMENTS

Our sincere thanks go to ir. Monika De Vos and Noël Huybrechts (BBRI), ir. Ben Notenboom (ABT Belgium) and ir. Bart De Ridder (Studieburo Mouton) for their practical help for supplying practical graphical help for this paper. The author wants also to extend his gratitude to the Flemish government; their financial support and encouragement through IWT (the Institute for the Promotion of Innovation by Science and Technology in Flanders) have stimulated multiple actions to improve the regional geotechnical knowledge and its dissemination across the borders.

REFERENCES

BBRI. 2008. Richtlijnen voor de toepassing van Eurocode 7 in België. Deel 1: Het grondmechanisch ontwerp in uiterste gren-stoestand van axiaal op druk belaste funderingspalen. (Guidelines for the application of Eurocode 7 in Belgium. Part 1: The ULS geotechnical design of axially loaded compression piles). Available on www.sftt-is.bbri.be.

Caputo, V. 2003. Experimental evidence for the validation of load-settlement predictions. *Deep Foundations on Bored and Au-ger Piles, Van Impe (ed). Proc. 4th Intern. Seminar, Ghent, 2–4 June 2003.* Rotterdam: Millpress.

Chin, F.K. 1970. Estimation of the ultimate load op piles from tests not carried to failure. *Proc. 2nd South East Asian Con-ference on Soil Mech. and Found. Eng*. Singapore: 81–92.

Chin, F.K. & Vail, A.J. 1973. Behaviour of piles in alluvium. *Proc. 8th Int. Conf. on Soil. Mech. and Found. Eng.* Moscow, vol 2, part I: 47–52.

CUR. 2001–4. Ontwerpregels voor trekpalen (Design rules for tension piles).

De Beer, E.E. 1985. *In 1985 Golden Jubilee of the ISSMFE, Belgian Society of ISSMFE*. Brussels.

De Beer, E.E. 1988. Different behaviour of bored and driven piles. *Deep Foundations on Bored and Auger Piles, Van Impe (ed). Proc. Intern. Seminar, Ghent, 7–10 June 1988.* Rotterdam: Balkema.

De Cock, F. 1998. Design of axially loaded bored piles—European codes, practice and experience. *Deep Foundations on Bored and Auger Piles, Van Impe (ed). Proc. 3rd Intern. Seminar, Ghent, 19–21 October 1998.* Rotterdam: Balkema.

De Cock, F., Legrand, C. & Huybrechts, N. 2003. Overview of design methods of axially loaded piles in Europe—Report of ERTC3-Piles, ISSMGE Subcommittee. *Proc. XIII ECSMGE, Vanicsek et al. (eds). Prague, August 2003.* Volume 3, pp. 663–715.

De Cock F. 2001. A database approach to overview pile loading tests on displacement screw piles in Western Europe—1970–2000. *In Holeyman, A. (Ed.) Screw Piles—Installation and Design in Stiff Clay. Proceedings of the symposium on screw piles. Brussels. March 2001.* Balkema.

De Cock F. 2001. Class A predictions on the basis of CPT of 10 instrumented screw piles in OC clay. *Proc. XVth International Conference on Soil Mechanics and Geotechnical Engineering. Istanbul*, August 2001.

DIN. 4014: 1990. Bohrpfähle—Herstellung, Bemessung und Tragverhalten (Bored piles—Construction procedure, design and bearing purpose. German code. Berlin: Beuth Verlag.

Fascicule 62-Titre V. Règles Techniques de Conception et de Calcul des Fondations des Ouvrages de Génie Civil (Technical rules for the design of foundations of civil engineering structures). Ministère de l'Equipement du Logement et des Transports. Paris.

Fleming, W.G.K. 1992. A new method for single pile settlement and prediction. *Geotechnique*: vol. 42 (No. 3): 411–425.

Frank, R. & Zhao, S.R. 1982. Estimation par les paramètres pressiométriques de l'enfoncement sous charge axiale de pieux forés dans des sols fins. *Bull. Liaison Labo P. et Ch. 71*: 93–107.

Holeyman, A., e.a. 1997. Design of axially loaded piles—Belgian practice. In F. De Cock & C. Legrand (Ed.), *Design of axially loaded piles-European Practice. Proc. Int. Seminar ERTC3. Brussels 17–18 April*. Balkema.

Holeyman, A.E. (Ed) 2001. Screw Piles—Installation and Design in Stiff Clay. *Proc. Symp. on screw piles. Brussels.* Balkema.

Joustra, K., De Sitter, W.R. & Den Ouden, N.W. 1977. Tall building settlement and pile load measurements. *Proc. 9th Int. Conf. on Soil Mech. and Found. Eng.*—Volume 1: 577–580. Tokyo.

Maertens, J., Theys, F. & Maekelberg, W. 2003. A full-scale test on large diameter bored piles for the construction of the HST-tunnel in Antwerp (Belgium). *Deep Foundations on Bored and Auger Piles, Van Impe (ed). Proc. 4th Intern. Seminar, Ghent, 2–4 June 2003.* Rotterdam: Millpress.

NEN 6743: 1993. Geotechnics—Calculation method for bearing capacity of pile foundation. Compression piles. NNI. 1993.

Van Impe, W.F. 1988. Considerations on the auger pile design. *Deep Foundations on Bored and Auger Piles, Van Impe (ed). Proc. Intern. Seminar, Ghent, 7–10 June 1988.* Rotterdam: Balkema.

Van Impe, W.F., De Beer, E.E. & Lousberg, E. 1988. Prediction of the single pile bearing capacity in granular soils out of CPT-results. *Int. symp. on Penetration Testing I, Orlando. Specialty session on March 24th*: 1–34.

Keynote lecture 2: Bored pile foundations in offshore conditions

Deep Foundations on Bored and Auger Piles – Van Impe & Van Impe (eds)
© 2009 Taylor & Francis Group, London, ISBN 978-0-415-47556-3

Bored pile foundations in offshore conditions

Roderic A. Ellman, Jr., PE & Frederick C. Rhyner, PE
Mueser Rutledge Consulting Engineers, New York, New York, USA

ABSTRACT: Bored pile, aka drilled shaft or drilled pier, foundations are becoming increasingly popular where high axial and lateral load capacity is required. The application of bored pile foundations in offshore (marine) conditions poses unique challenges that engineers and contractors should be aware of with regard to their design and installation. The offshore (marine) environment is typically associated with the need for relatively long length foundation elements that must extend through significant water depth and poor, low strength soils to a competent bearing stratum. These conditions can affect the design of bored piles by offering limited shaft resistance and requiring deep embedment in order to develop pile fixity and resistance to lateral loads. High axial capacity demand usually requires these elements to significantly penetrate into dense soil and rock. Carefully planned site investigations are essential for obtaining the requisite subsurface information needed for design and installation considerations. This paper will discuss a number of the special considerations in the design of bored piles specifically in marine environments, i.e. design parameters for the development of axial and lateral load and consideration for the use of temporary and permanent casing as well as special considerations for their installation, i.e. drilling equipment and installation methods, concrete mix designs and placement, design of rebar cages for constructability and quality control and testing. Several case history examples are mentioned to illustrate these issues.

1 INTRODUCTION

The application of bored pile foundations in offshore (marine) conditions poses unique challenges that engineers and contractors should be aware of with regard to their design and installation. The offshore (marine) environment is typically associated with the need for relatively long length, large diameter, foundation elements that must extend through significant water depth and poor, low strength soils to a competent bearing stratum. These conditions can affect the design of bored piles by offering limited shaft resistance and requiring deep embedment in order to develop pile fixity and resistance to lateral loads. High axial capacity demand usually requires these elements to significantly penetrate into dense soil and rock. Carefully planned site investigations are essential to obtain the requisite subsurface information needed for design and installation considerations.

The use of large diameter drilled shafts is popular on major bridge projects due to increased availability of drilling equipment and skilled contractors and inherent advantages of high capacity shafts in supporting axial and lateral loads. Shaft diameters of up to 4 m (13 ft) and lengths of up to 80 m (260 ft) are no longer unusual. However, such large diameter shafts pose exceptional challenges for construction because of the difficulties in excavating shafts of such size and because of the requirement for underwater placement of large volumes of concrete through dense reinforcing cages.

It is important that engineers involved in such projects be aware of the special challenges associated with marine and offshore construction so that designs can be developed which enhance reliability and minimize risk. In addition, engineers with responsibility for quality control and quality assurance on the project must be fully aware of the critical aspects of foundation construction. The use of design/build procurement for many large bridge projects can foster cooperative efforts between design and construction professionals and typically requires engineers to proactively consider the important aspects of risk, schedule, and quality assurance in deep foundation construction.

This paper will discuss a number of the special considerations in the design and installation of bored piles in a marine environment including:

- Planning site geotechnical investigations
- Equipment and excavation techniques suited to this type of construction
- Design considerations and analysis techniques

- Construction considerations including use of temporary verses permanent casing, design of reinforcement for constructability, concrete placement techniques and concrete mix design
- Design Phase Load Testing.

2 PLANNING SITE GEOTECHNICAL INVESTIGATIONS

In order to obtain sufficient information to characterize the subsurface conditions, all available subsurface data must be reviewed and a subsurface exploration and laboratory testing program appropriate for the proposed structure must be developed. The subsurface exploration program should include a sufficient number of borings to accurately portray the soil profile and depth to bedrock, where appropriate, and include retrieval of disturbed and undisturbed samples, laboratory testing and *in-situ* testing (Ellman and Krhounek, 2001).

2.1 *Standard subsurface exploration techniques*

Disturbed samples are obtained from the split-spoon sampler during performance of the Standard Penetration Test (SPT) in accordance with ASTM D 1586 and AASHTO T-206. Relatively undisturbed thin walled tube samples of cohesive soils are recovered using two methods. The softer strata are sampled by pushing an open ended, thin-walled tube in accordance with ASTM D 1587 and AASHTO T-207. Very stiff soils are recovered using a Pitcher sampler, which is slowly advanced by rotary cutting of an annular space in the soil, surrounding an inner thin-walled tube, allowing the tube to penetrate the hard materials. The tube is located within the outer cutting assembly, and is spring-loaded to recover the "undisturbed" cylinder of soil as the surrounding material is cut away.

2.2 *Laboratory testing*

Representative samples recovered during the exploration program are selected for laboratory evaluation. The laboratory program should consist of classification and index property tests on both disturbed and undisturbed samples, including grain size analyses, Atterberg limits, and natural moisture content determinations. The laboratory program should also include extensive analysis of undisturbed samples, including specific gravity and bulk unit weight determinations, one-dimensional (vertical) consolidations, and strength testing including Unconsolidated-Undrained (U-U) and Consolidated-Undrained (C-U) triaxial shear tests.

2.3 *In-situ testing*

Where appropriate, a subsurface investigation program should also include *in-situ* characterization of soil properties, utilizing the Cone Penetration Test (CPT), the Flat Plate Dilatometer (DMT) and the Pressuremeter (PMT). The Cone Penetration Test is an *in-situ* testing method used to determine the geotechnical engineering properties of soils and delineating soil stratigraphy. The Dilatometer soundings are performed in the softer strata nearer the surface, whereas the Pressuremeter tests are utilized to characterize the hard clays encountered at greater depths.

2.3.1 *Cone Penetration Test (CPT)*

The CPT procedure consists of pushing an instrumented cone tip first into the ground at a controlled rate (usually 2 centimeters/second). The test method should follow the procedures in accordance with ASTM Standard D 3441. CPT offers three main advantages over traditional SPT methods by providing near continuous data, repeatable and reliable penetration data and lower cost allowing more test data at a given site. For more information on Cone Penetration Testing see ASTM Standard D 3441.

2.3.2 *Flat plate dilatometer*

The DMT procedure consists of pushing the blade of the dilatometer to the desired test depth, then slowly inflating and then deflating the membrane in the side of the blade. A specialized limit switch under the membrane activates an audible signal to indicate when the center of the membrane has expanded 0.05 millimeters into the soil (the "A" pressure), 1.10 millimeters into the soil (the "B" pressure), and when the membrane deflates back to an expansion of 0.05 millimeters (the "C" pressure).

Prior to performing the test, the pressures required to expand the membrane to 0.05 and 1.10 millimeters (ΔA and ΔB, respectively) are determined. For more information on Dilatometer testing see FHWA Publication Number SA-91-044 (Briaud and Miran, 1992) and Publication Number FHWA-PA-025+84-24 (Schmertmann, 1988).

2.3.3 *Pressuremeter testing*

Pressuremeter testing is performed in very stiff clay strata. The pressuremeter is a cylindrical probe sheathed with a rubber bladder, which is filled with fluid to expand radially into the soil being tested. An expandable stainless steel jacket protects the bladder from damage during insertion and testing. Performance of the test consists of cutting a socket at the base of the borehole, inserting the pressuremeter probe to the test depth, and expanding the probe incrementally, by volume, by injecting a reasonably non-compressible fluid, using a specially designed,

positive displacement pump at the surface. Similar to the DMT test, the probe is calibrated under atmospheric pressure prior to performing the test. The soil socket is sized to be slightly larger than the diameter of the deflated probe prior to beginning the test. At each volume increment, the fluid pressure is measured at the control unit, which provides a measurement of the soil's resistance to the expansion of the probe. The volume increments are continued until the maximum expansion the probe can safely withstand is reached. From the volume of liquid injected, the radial strain can be determined. By plotting the radial strain versus the corrected pressure, a stress-strain curve is obtained. From these data, soil parameters can be calculated or determined empirically. For more information on Pressuremeter testing see FHWA Publication Number IP-89-008 (Briaud, 1989).

2.4 *Reducing risk*

Bored pile projects in off-shore conditions require particular attention to construction issues during the geotechnical site investigation. In the United States, it is good practice to provide at least two borings at each foundation or bridge pier. In addition to the normal design parameters, critical information related to construction includes:

- Rock characterization and compressive strength
- Groundwater and potential for artesian conditions during construction
- Boulders or cobbles
- Sequence of construction operations and potential effects.

Site characterization limited to obtaining the properties solely for design at the exclusion of construction considerations can result in costly differing site condition claims. For example, many contractors look at the highest unconfined compressive strength of rock to estimate their drilling productivity. Proper sequencing of construction operations can also be critical, especially when there may be multiple contracts on a major project. For example, there is potential for lost ground around the shaft excavation due to running sand or cobbles and boulders and such soil movements can affect nearby operations or existing structures. Pile driving vibrations or vibrations from other sources can interfere with stability of shaft excavations.

One potential method of dealing with uncertainty in subsurface conditions on major bored pile projects is the use of a Geotechnical Baseline Report (GBR). This approach has been used on tunneling projects with success for years and has potential to improve our methods for defining conditions for bidding purposes on bored pile projects. A GBR is issued to specifically define geotechnical conditions as a baseline for bidding so that contractors can more fairly include "contingency" costs in their bid. Vague or exculpatory language is avoided in a GBR so that the basis for each bid is the same. Conditions that are more adverse than defined in the GBR (for example, more than 20 hours spent removing obstructions or boulders) are paid on a unit price basis. The use of a GBR has the potential to reduce the costly litigation associated with differing site conditions and improve the potential for true partnering on major drilled shaft projects (Brown, 2007).

3 EQUIPMENT AND EXCAVATION TECHNIQUES SUITED TO THIS TYPE OF CONSTRUCTION

The high load demands which drive the size and depth of drilled shaft foundations on major bridge projects also tend to drive the construction into deep and hard bearing strata. The marine environment is typically associated with the need for relatively long length, large diameter, foundation elements that must extend through significant water depth and poor, low strength soils to a competent bearing stratum. The depths associated with high capacity foundations sometimes include the need to penetrate through layers of dense glacial till or weathered rock material which may contain boulders and/or cobbles, may be difficult to excavate, or may have special concerns for stability of the excavation during the extended time required to complete the excavation.

Bored piles in offshore conditions will be installed from floating equipment. Other than the typical tools and equipment used for conventional drilled shaft excavation, large and deep excavations are often accomplished with an increased use of:

- Hydraulic casing oscillator
- Reverse circulation drilling (RCD)
- Combination RCD and Kelly Mode
- Combinations of coring, drop chisels and hammer-grab tools in lieu of augers.

3.1 *Hydraulic oscillator drilling*

For large drilled shaft excavations, full length temporary casing is most effectively installed using hydraulic oscillator or rotator equipment, in advance of the excavation (Figure 1). The development of this type of equipment has been instrumental in advancing construction of large deep shafts, because of the large torque and lifting forces that can be generated. In many cases, the thrust applied during removal of the casing requires substantial pile foundations to be installed in support of a template.

Figure 1. Casing oscillator.

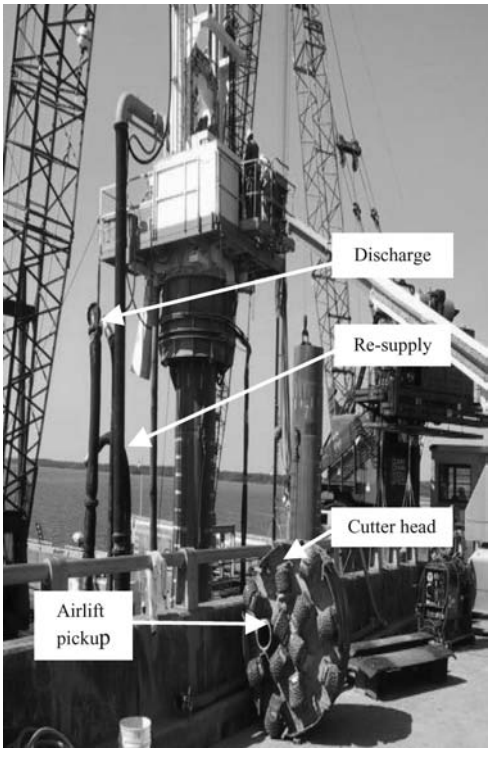

Figure 2. Wirth RCD drill.

3.2 *Reverse Circulation Drilling (RCD)*

RCD techniques are often used to advance shaft excavations to great depth. With RCD (Figures 2 and 3), drilling fluid (usually water) is circulated by lifting the fluid through the center of the drill string, usually with an air-lift pumping system, and with fluid resupplied by pumping into the top of the shaft excavation

Figure 3. Wirth RCD drill used on Oak Creek project, Chicago, Illinois.

from an external reservoir. Cuttings are removed from the base of the excavation by the circulating drilling fluid, which evacuates the material below the cutter head.

An advantage of RCD is that the tool does not need to be cycled in and out of the hole to excavate the soil or rock as would be the case with conventional augers, and for shaft excavations at great depth this advantage can result in improved productivity. However, the time required for setup on each hole is significant.

3.3 *Fly drill*

The Fly drill, also known as the BAUER BFD 3500, was developed and used for the first time on the Victory Bridge project in New Jersey. The importance of the Fly drill was its ability to excavate overburden and extremely hard rock with the same compact machine. The Fly drill operated in either Kelly mode or RCD mode with 266,000 ft-lbs of torque (Hardell, 2005).

3.3.1 *Kelly mode*

When drilling overburden in Kelly mode, the drill rig utilizes a telescoping Kelly bar and a bucket to remove material from the hole (Figure 4). The drill clamps to the top of the casing to resist the reaction of drilling. Once the bucket is full, the drill is unclamped from the casing and the crane swings the drill over the dumpsite and the bucket is dumped. During Kelly mode drilling the Fly drill remains attached to a crane and the crane operator operates the drill.

When a boulder layer was encountered, rock augers and core barrels were used to advance through the

Figure 4. Fly drill operating in Kelly mode, Victory Bridge, New Jersey.

Figure 5. Fly drill in RCD mode, Victory Bridge, New Jersey.

boulders. Many times the casing would not vibrate initially through the boulder layer. This situation required drilling ahead with the Fly drill through the boulder layer. After the boulder layer and the weathered rock below the casing were removed, the casing could then vibrate down to bedrock.

3.3.2 *RCD mode*

Once the overburden was removed from the hole, the Fly drill was transformed to operate in RCD mode (Figure 5) by placing a drill head equipped with roller cutters and 150,000 lbs of static weight on the drill rig. The Fly drill also has hydraulic cylinders which apply 54,000 lbs of down pressure.

The roller cutters crush the hard rock. The cuttings are then lifted to the surface through drill pipe, also known as drill string, by means of an airlift system which works by pumping air down to the bottom of the hole inside two small pipes on the outside of the drill string. Air is then diverted inside the drill string directly above the drill head. This lowers the density of the water inside the drill string, causing the fluid in the drill string to move up. Any material below the drill head is forced up the drill string.

Once the cuttings arrive at the surface, they travel through a pipe leading to a de-sanding system. The de-sanding system separates the cuttings from the water and then pumps clean water back to the hole. On the Victory Bridge project, the airlift system circulated 2906 GPM.

3.4 *Other tools*

Other tools often utilized on large, deep shafts include percussion tools such as drop chisels (Figure 6) or hammergrabs (Figure 7), but productivity with these tools is slow. With large diameter excavations in hard material, chisels can assist in breaking up boulders or large rock fragments left after coring with core barrels or within segmental casing. A hammergrab tool can be more effective at removing large objects within the excavation than rotary drilling equipment.

It is worth noting that the base of the excavation will not be as flat and level as would be accomplished using conventional rotary drilling equipment. However, effective bottom-of-hole cleanout can be accomplished using airlift tools or downhole pumping.

With any drilling method or tool, the possibility exists of losing ground when extending the tool below the bottom of casing in a cohesionless soil. Losing ground refers to excess soil being excavated beyond the nominal diameter of the shaft. Apart from creating a void, the ground loss can undermine nearby existing foundations. Ground loss can be avoided, or at least minimized, by the use of a slurry drilling fluid.

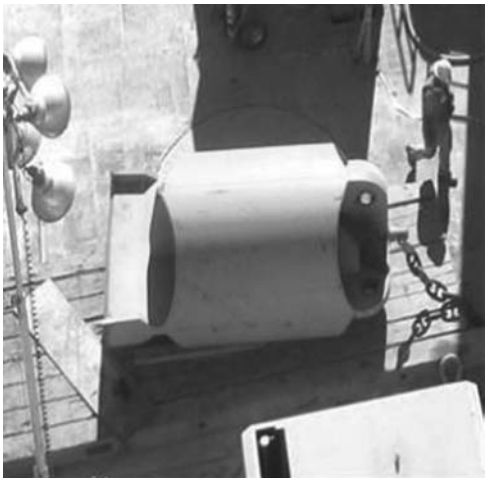

Figure 6. Example of drop chisel.

Figure 7. Example of hammergrab.

4 DESIGN CONSIDERATIONS AND ANALYSIS TECHNIQUES

4.1 *Soil/structure interaction*

In order to evaluate structural response or the performance of a structure under load, we must develop an appropriate soil/structure interaction model of the foundation. The elements that must be considered generally include the pile cap, the drilled shafts and the soil (Figure 8).

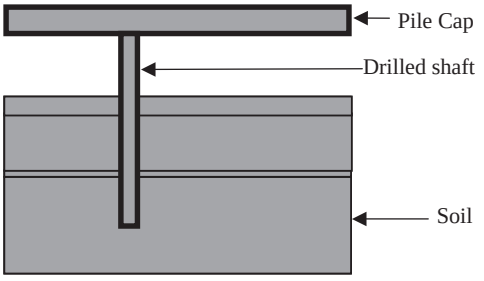

Figure 8. Soil/structure interaction model.

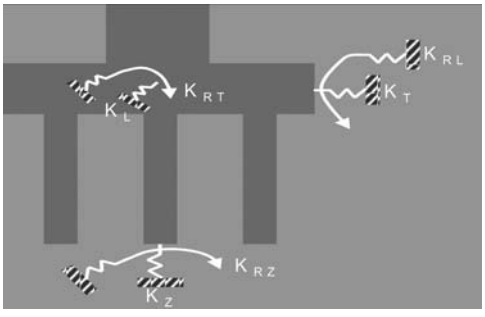

Figure 9. Soil/structure system.

The soil/structure interaction model can be represented by an equivalent model that expresses the soil/structure system as the six degrees of freedom defining the static equilibrium of the system. The soil/structure system is represented by a series of stiffness springs (Figure 9).

Where K_T is the transverse stiffness, K_L is the longitudinal stiffness, K_V is the vertical stiffness, K_{RL} is the longitudinal rocking stiffness, K_{RT} is the transverse rocking stiffness, and K_{RV} is the vertical rocking stiffness.

The corresponding stiffness values can be determined using the software "FB Pier," a nonlinear finite element program developed by the University of Florida's Department of Civil Engineering for the Florida Department of Transportation. The program analyses drilled shaft groups and includes the effect of soil non-linearity. Pile caps are modeled as shell elements, drilled shafts are modeled as beam elements, and the soil is represented as individual nodes spaced along the length of the bored piles. To enhance drilled shaft performance in offshore conditions consideration should be given to the use of permanent casing as this greatly increases the lateral capacity of the bored pile and is helpful in preserving the integrity of the concrete placed within very soft and loose materials.

Soil nodes are represented as nonlinear springs that are modeled by the program using P-Y curves.

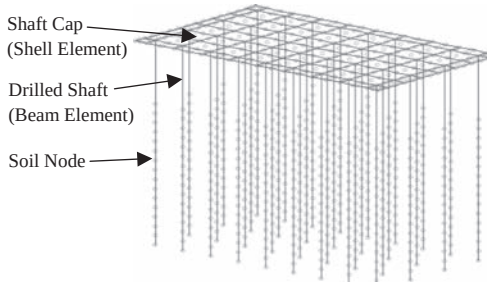

Figure 10. FB pier model.

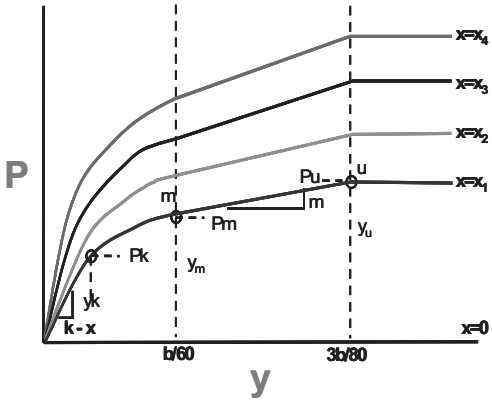

Figure 11. P-Y curves for loading of sand.

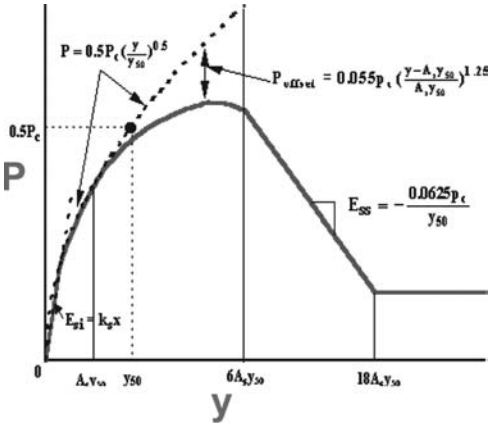

Figure 12. P-Y curve for stiff clay below the water table.

Procedures for developing P-Y curves for sand and clay are included in API RP2 A, 1993 by the American Petroleum Institute. Various examples of P-Y curves are shown in Figures 11–13.

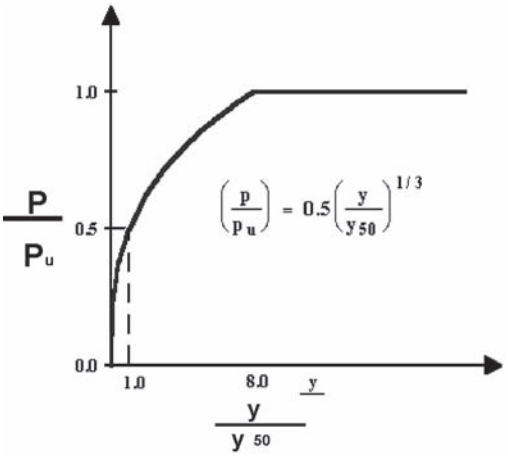

Figure 13. P-Y curve for stiff clay below the water table.

It should be noted that there is some debate over the effects of diameter on the P-Y curves. This is discussed further in the paper, "Diameter Effects On P-Y Curves," by Ignatius Po Lam. Here it is pointed out that there is higher soil resistance with larger diameter elements (>2 feet) especially in a "free head" condition, which is quite common where there is significant free height above the point of fixity (Po Lam, 2006).

4.2 *Seismic kinematic effects*

Due to the nature of offshore conditions, namely, relatively thick deposits of loose, soft materials over relatively dense and stiff materials there is a need to investigate seismic kinematic effects. This considers the bending moments that result at the interface between the two soil strata. As this location may not always be at the point of maximum bending moment from a lateral load analysis, it could govern the bored pile design. Once the required geotechnical properties are established, alternative foundation systems can be evaluated with regard to their affects on the overall performance of the combined structural system, i.e., foundation and superstructure. Performance aspects would include vertical settlement and rotations under dead load, lateral displacements under dead and live loads, dynamic effects under seismic loads including period and frequency of vibrations and kinematic effects on the bored piles.

5 CONSTRUCTION CONSIDERATIONS

5.1 *Permanent casing*

With shaft excavations in excess of 8 ft diameter, the use of permanent casing may be desirable from

Figure 14. Installation of permanent casing.

a constructability standpoint in marine environments (Figure 14). Obviously permanent casing is necessary to form the shaft through water. Once below the mudline, the permanent casing should extend, at least, into firm strata which can provide support for the casing while the remainder of the shaft is excavated without casing. When the shafts extend to rock, it is preferable to extend the permanent casing to rock to facilitate drilling the rock socket. If the casing length exceeds the height of the crane on the project, it is better to design the casing as permanent so as to avoid cutting the casing during withdrawal and/or avoid interference with the tremie or pumped concrete operation. The usual limit for pulling temporary casing on a project is probably 50 to 75 feet.

Large diameter permanent casing is most effectively installed in advance of drilling and most often installed using vibratory hammers (Figure 14), although large offshore-type impact hammers have also been used. If a large hammer is required to install the casing, extraction of a casing would require an even greater force due to the time-dependent setup of the soil resistance in side shear, so it is important to leave it in place. In some cases, the installation of a driven permanent steel pipe, followed by shaft excavation below, may be considered as a type of steel pipe/drilled shaft composite pile. The axial resistance within the depth of permanent casing can be significant in proportion to the overall axial resistance of the shaft and may be included in the design.

5.2 *Temporary casing*

Temporary casing to the full length of the shaft excavation may be used when the risk of excavation collapse is significant or when needed to core rock at shallow depth. For large drilled shaft excavations, full length temporary casing is most effectively installed using hydraulic oscillator or rotator equipment, in advance of the excavation (Figure 15).

Figure 15. Oscillator equipment installing segmental casing.

The casing installed with this equipment is typically high strength steel, often double-wall, with flush fitting joints between segments. Segmental casing is used to achieve the great depths required.

Another reason for using casing is the time required for completion of large deep shafts. This could be a concern if bentonite drilling fluid were used and the exposure time must be limited. Many specifications call for limiting the exposure time to a maximum of four hours for an open hole with bentonite slurry, because of concerns relating to filter cake buildup and subsequent reduction in side shear capacity. The minimum length of time required to complete bottom cleaning operations, place rebar, and start concrete placement in a large shaft can easily exceed this limit. Also, in the United States, the disposal costs for bentonite are about $1.00 per gallon so contractors would prefer to use water.

Designers should be aware that at sites where there is significant thickness of low strength recently deposited alluvium there is the concern of drilled shafts bulging outward due to the pressure of fluid concrete when temporary casings are pulled during drilled shaft construction. The ultimate strength of the soil is calculated using spherical cavity expansion theory and the measured undrained shear strength at locations where DMT testing was performed. This ultimate strength is compared to the fluid pressure of the concrete to generate a “strength ratio.” This strength ratio is similar to a factor of safety. Strength ratios well above 1 indicate that the soil should be strong enough to resist expansion, and strength ratios near or below 1 indicate that the soil would yield and bulging may occur (Goldberg and Camp, 2002).

5.3 *Reinforcement constructability*

Large, heavy reinforcing cages pose construction challenges of lifting, splicing, and placing the cage,

and also from the standpoint of concrete flow through the cage. Multiple cranes, multiple pickup points (Figure 16) or "tipping frames" (Figure 17) may be required to lift the cage. Very long cages may need to be spliced while suspended over the hole, thus greatly increasing the exposure time during which the hole is open without agitation as discussed previously. Extremely congested reinforcing cages pose an impediment to concrete flow and can lead to entrapment of debris or low strength concrete outside the cage.

Some of the key components that can facilitate constructability are:

- Bundle the rebar to increase openings through the cage
- Avoid tight spacing in transverse reinforcing (spirals or hoops) by bundling the bars
- Avoid the use of multiple cages, which pose an extremely difficult condition for concrete placement underwater
- Utilize the permanent steel liner to reduce the longitudinal reinforcement and to provide confinement so that the transverse reinforcement is reduced.

Figure 16. Lifting large reinforcing cage.

Figure 17. Temporary tipping frame to support reinforcing cage on batter.

- A good rule of thumb is to provide a clear opening of at least 5″ between rebar. Unfortunately, seismic demands sometime require closer spacing.

When utilizing a permanent steel liner, the structural design has tremendous potential to improve constructability. In addition, the use of a permanent steel liner for bending stresses can provide a foundation with excellent strength and ductility in flexure for extreme event loads such as seismic or vessel impact forces. When reasonably cleaned using a wire brush or hydro-jet on the interior of the casing after drilling, a good bond at the steel/concrete interface can be achieved. The confinement provided by the steel liner may reduce the need for tightly spaced spirals or hoops.

5.4 *Concrete placement*

Critical issues relating to underwater placement in large or deep drilled shafts include the initiation of flow through the tremie and control of concrete during casing removal. Gravity tremie placement is preferred over sealed pump line systems for deep shafts, although pumping into the top of the gravity tremie provides an excellent delivery system. A sealed pump line in a very deep shaft can result in negative pressures within the line that can lead to segregation and blockage within the line (Yao and Bittner, 2007). For very deep shafts, the use of an open segmental tremie is generally required; a sealed tremie with a closed end plate would be so buoyant and long that control of the empty tremie is difficult.

With an open tremie pipe, the initial charge of concrete is separated from the fluid in the pipe using a plug. The tremie plug will be compressed under very high pressures at depth and should maintain a sufficient width to keep concrete from bypassing the plug.

Even more critical than the plug, is the rate and volume of concrete delivery in the initial concrete charge to the tremie. With the extremely long tremie and large shaft diameter, many cubic yards of concrete may be required to achieve a head of concrete in the shaft above the bottom of the tremie. If a slug of concrete is discharged into the tremie without continuous resupply of concrete or control of the flow from the bottom, the inertia of this initial slug of concrete can result in a very low head of concrete inside the tremie which would result in a breach as the water or slurry flows back into the tremie. This breach can be avoided if the tremie operator can hold the tremie within a few inches of the bottom so as to control the flow from the tremie and maintain a head of concrete within the tremie that exceeds the water head in the shaft. It is important that concrete delivery at this initial stage be provided rapidly and continuously, if possible. Workable concrete for tremie placement in drilled shafts must be a

flowable, cohesive, self consolidating mixture that is easily placed without external vibration. Although the use of the term "self-consolidating concrete" (SCC) has been used in recent years with reference to mixtures with ultra workability in conventional concrete applications, drilled shaft concrete has always been intended as a self consolidating mixture. Traditionally, drilled shafts have been constructed using slump as the sole indication of workability. Alternative methods to describe workability may have application in large diameter drilled shafts.

Concrete mixtures can be designed with high workability by using suitable aggregates and gradation and the proper dosage of water reducing admixtures. Rounded gravel aggregate sources are preferred over crushed stone, and coarse aggregates with a No. 67 or No. 78 gradation are preferred over a No. 57 in terms of workability. Where tight spirals are used, the maximum aggregate size should be lowered to 3/8″ to promote flow. In general, an increase in the sand content in proportion to coarse aggregate will provide increased workability and passing ability with less tendency for segregation; a sand to total aggregate ratio (by volume) from 0.44 to 0.50 has been found to work well in drilled shaft mixtures. Water reducing admixtures in current use include polycarboxylate-based materials, which are preferred over the older naphthalene-based water reducers that have the potential to produce a "flash set".

For large diameter shafts which can often require 300 to 500 m^3 (400 to 650 yd^3) of tremie-placed underwater concrete, retention of workability throughout the duration of the pour is critical. The dosage of retarding or hydration control admixtures must be selected to ensure that the concrete retains adequate workability to allow the tremie placement to be completed. Loss of workability will lead to difficulties in maintaining flow through the tremie, with attendant flaws in the shaft. It must be noted that hydration control is highly temperature dependent.

6 DESIGN PHASE TESTING PROGRAM

Bored piles develop their capacity by a combination of skin friction and end bearing (Figure 18). Initial values for skin friction and end bearing are derived from the subsurface exploration and laboratory testing program and are used to develop a preliminary bored pile design.

A well planned design phase testing program can be used to optimize the preliminary bored pile design by:

- Establishing measured ultimate capacities
- Determining the distribution of skin friction with depth and percentage of end bearing
- Determining strata specific skin friction value for use in the final foundation design.

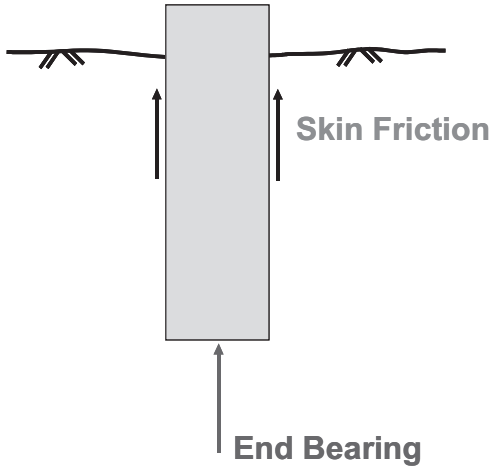

Figure 18. Bored pile capacity development.

Having this data can result in a highly optimized bored pile design and associated significant cost savings.

6.1 *Instrumentation*

Each test pile should be fully instrumented with vibrating wire and/or electrical resistance strain gauges prior to installation. Test pile locations should be established based on subsurface conditions with at least one test pile for each area of differing subsurface conditions.

6.1.1 *Vibrating wire strain gauges*

Geokon Model VSM-4000 surface mounted strain gauges are used on steel piles and Geokon Model VSM-4911 embedment strain gauges are for concrete piles. End clamps for surface mounted strain gauges are welded directly to the Geokon Model VSM-4000 surface mounted strain gauges are used on steel piles and Geokon Model VSM-4911 embedment strain gauges are for concrete piles. End clamps for surface mounted strain gauges are welded directly to the surface of steel piles. Embedment strain gauges are attached directly to a No. 4 size length of rebar, commonly referred to as a sister bar, welded directly to the reinforcing cage of concrete piles. Vibrating wire strain gauges can only record frequency readings over finite time intervals, as the wire has to stop vibrating before a second reading can be recorded. Furthermore, the entire set of vibrating strain gauges must be plucked and read in sequence, i.e., the more vibrating wire strain gauges to be read, the longer the interval required between readings. Therefore, neither continuous nor short time interval data collection is possible.

6.1.2 *Vibrating wire load cells*

Geokon Model 4900 vibrating wire load cells are used to record the applied load of each hydraulic jack during static load tests. These load cells consist of a cylinder of high strength, heat treated steel, with six embedded vibrating wire strain gauges located equidistant around the circumference of the cell. The load cells are used to obtain an accurate measurement of the applied load, and to verify that eccentric loading has not occurred.

6.1.3 *Electrical resistance strain gauge*

Electrical resistance strain gauges can also be used to evaluate short duration type of tests requiring that the gauge continuously record information.

6.1.4 *Linear Variable Differential Transducer (LVDT), dial gauge and other instruments*

LVDTs are used to record displacements of the pile head under load. Three LVDTs are typically positioned concentrically around the head of the pile in a vertical orientation. The LVDTs are connected directly to the test pile, with the moveable probe resting on the reference beam. This insures that the LVDT is compressed as the load is applied. The induced output voltage from the LVDTs is recorded via Geokon Multilogger software.

Dial gauges are used as a secondary method of recording vertical displacement of the test pile under load. These gauges are also connected directly to the test pile, with the probe resting on the reference beam. The dial gauges are read individually at the specified time intervals throughout the load test.

As a backup method of recording vertical displacement, the traditional piano wire, mirror and scale method is used. This involves fixing a mirror and vertical scale to the surface of the pile. Piano wire is then held in a fixed, taut position across the scale by a free hanging weight. A conventional dumpy level is used to monitor uplift, or pull out, of reaction piles as the test load is being applied.

Figure 19. Static axial load test set up.

Figure 20. Statnamic axial load test set up.

Figure 21. Osterberg load cell.

6.2 *Load test procedures*

Various methods can be used to test bored pile axial capacity including static axial load test, Statnamic load tests and Osterberg (O-cell) load test. Bored pile lateral capacity and deflection performance can be determined by static lateral load test and Statnamic load test.

6.2.1 *Static axial load test*

Static axial load testing is performed in accordance with ASTM D-1143. This test can be somewhat difficult in off-shore conditions due to the large load that must be developed and the need for reaction piles (Figure 19).

AASHTO and FHWA recommend that compressive axial load test data be evaluated by the method proposed by Davisson (Davisson, M.T., 1972). The ultimate load that a pile can resist is that which produces a movement of the pile head equal to:

$s = \Delta + D/30$ for piles greater than 24 inches in diameter (FHWA-SA-91–042 Kyfor et al.)

Where: s = Pile head movement (in)
Δ = Elastic deformation or PL/AE (in)
P = Test load (kips)
L = Pile length (in)
A = Cross-sectional area of the pile (sq. in)
E = Modulus of elasticity of the pile material (ksi)
D = Pile diameter (in)

A failure criterion offset line is plotted parallel to the elastic deformation line and the point at which the load-deflection curve intersects the failure criterion line is the ultimate, or failure load.

6.2.2 *Statnamic axial load test*

This test includes an explosive charge with dead weight that instantaneously loads the test pile (Figure 20). The advantage of this test is that a smaller test frame is needed and the length of time to perform the test is much smaller than a conventional static load test.

6.2.3 *Osterberg (O-cell) load test*

The O-cell is a hydraulically driven, high capacity, sacrificial jacking device installed within the bored pile reinforcing cage (Figure 21).

Working in two directions, upward against side-shear and downward against end bearing, the O-cell automatically separates the resistance data.

6.2.4 *Static lateral load test*

Static lateral load testing is performed in accordance with ASTM D-3996. This test includes the application of a horizontal force usually by hydraulic jacks. The test pile head displacement is measured for varying load increments which can be used in assessing the supporting soil's horizontal subgrade modulus and the corresponding point of fixity for the bored pile.

REFERENCES

Ellman, Jr., R. A. and Krhounek, R. C., 2001, "What Structural Engineers Should Know About Soil-Structure Interaction," American Society of Civil Engineers Metropolitan Section, Structures Group 2001 Spring Seminar, New York, New York.

Briaud, J and Miran, J., 1992, "The Flat Dilatometer Test," FHWA, Office of Technology Applications, Washington, D.C.

Schmertmann, J., 1988, "Guidelines for Using the CPT, CPTU and Marchetti DMT for Geotechnical Design, Volumes III and IV," FHWA, Washington, D.C., and Pennsylvania Department of Transportation, Harrisburg, Pennsylvania.

Briaud, J., 1989, "The Pressuremeter Test for Highway Applications," FHWA, Office of Implementation, McLean, Virginia.

Brown, D., 2007, "Construction of Large Drilled Shafts, the 2nd Annual Mike O'Neill Lecture," Deep Foundations Institute Marine Foundations Committee Specialty Seminar, Chicago, Illinois.

Hardell, J. T., 2005, "Construction Techniques Used to Build the Drilled Shafts for the Victory Bridge," Deep Foundations Institute Marine Foundations Committee Specialty Seminar, New York, New York.

Goldberg, A. and Camp, W., 2002, "Drilled Shaft Temporary Casing Evaluation, Cooper River Bridge Replacement Project," Charleston, South Carolina.

Po Lam, I., 2006, "Diameter Effects on P-Y Curves," Earth Mechanics, Inc., Fountain Valley, California.

Yao, S. and Bittner, R. 2007, "Underwater Concrete in Drilled Shafts: The Key Issues and Case Histories," paper accepted for publication, Geotechnical Special Publication, ASCE, 11 p.

Davisson, M.T. (1972), High Capacity Piles, *Proceedings of Lecture Series on Innovations in Foundation Construction*, American Society of Civil Engineers, Illinois Section, Chicago, March 22, pp. 81–112.

Keynote lecture 3: Bored and auger pile testing developments

Deep Foundations on Bored and Auger Piles – Van Impe & Van Impe (eds)
© 2009 Taylor & Francis Group, London, ISBN 978-0-415-47556-3

Relationships between axial capacity and CPT q_c for bored piles in sand

B.M. Lehane
School of Civil & Resource Engineering, University of Western Australia, Australia

ABSTRACT: This paper investigates the relationships between the CPT q_c resistance and the shaft and base resistance of bored piles in sand. An initial review and discussion of some of the factors affecting these relationships is used to assist interpretation of shaft friction measurements obtained in two instrumented augered piles at a sand site in Perth, Australia. A new database of augered piles in Perth sand is then presented and the interpreted base and shaft resistances for the database are examined using the framework established for estimation of shaft friction and previously published numerical predictions for base capacity. The paper's findings challenge commonly held assumptions and provide a means for advancing existing design approaches.

1 INTRODUCTION

Although ground freezing can facilitate the retrieval of undisturbed samples of sand and gravel, the geotechnical profession needs to rely, almost exclusively, on in-situ tests to assess design parameters for coarse grained soil. The Cone Penetration Test (CPT) is a very most popular in-situ test as it enables stratigraphic profiling and also provides measures of soil consistency, which can be incorporated in design approaches. The CPT end resistance (q_c) is commonly used directly in empirical correlations for pile shaft friction and base resistance.

While correlations between the CPT q_c value and pile capacity may be appreciated for displacement piles (given the similarity between a cone and a full displacement pile), the relationship between this q_c value and either the end bearing or shaft resistance of a bored pile is rather less obvious. However, despite the lack of any theoretical basis, most published methods for bored piles in coarse grained soil assume a proportional relationship between q_c and the unit ultimate shaft friction (τ_f) and the end bearing (q_b) i.e.

$$\tau_f = \alpha_s \, q_c \quad \text{or} \quad \tau_f = q_c / \beta_c \tag{1}$$

$$q_{b0.1} = \alpha_b \, q_{c,avg} \tag{2}$$

where α_s (=1/β_c) is an empirical coefficient, $q_{b0.1}$ is the ultimate end bearing resistance defined at a pile base displacement of 10% of the pile diameter and $q_{c,avg}$ is an appropriately averaged q_c value in the vicinity of the pile tip.

The widespread use of equations (1) and (2) in practice, prompted the study presented here into the factors affecting the values of β_c (=1/α_s) and α_b for bored (non-displacement) piles in cohesionless soil. The paper initially provides an overview and discussion of factors affecting shaft and base capacity. Recent studies performed in the centrifuge on wished-in-place piles are then examined and are seen to yield important insights into the factors controlling shaft friction. These insights are employed to assist interpretation of the shaft friction measured in two instrumented augered piles at a sand site in Perth, Australia. A recently compiled database of augered piles, comprising 12 static load tests in Perth sand, is then presented and the interpreted base and shaft resistances are examined using the framework established for estimation of shaft friction and previously published numerical predictions for base capacity. Finally, some recommendations are provided to assist bored pile design in sand.

2 OVERVIEW: SHAFT FRICTION

2.1 *Expressions for shaft friction*

The ultimate shaft friction (τ_f) may be derived from Coulomb's friction equation i.e.

$$\tau_f = \sigma'_{hf} \tan\delta = (\sigma'_{h0} + \Delta\sigma'_{hc} + \Delta\sigma'_{hd}) \tan\delta \tag{3}$$

where σ'_{hf} is the lateral effective stress at peak unit skin friction and δ is the interface friction angle between the soil and the pile shaft. The value of σ'_{hf}

differs from the in-situ lateral effective stress (σ'_{h0}) due to the changes in lateral stress that arise because of pile construction procedures ($\Delta\sigma'_{hc}$) and during shearing at pile-soil interface ($\Delta\sigma'_{hd}$). Equation (3) is more commonly expressed in one of the following forms:

$$\tau_f = (K/K_0)\, K_0\, \sigma'_{v0} \tan\delta \quad \text{with } K = \sigma'_{hf}/\sigma'_{vf} \qquad (4a)$$

$$\tau_f = \beta\, \sigma'_{v0} \quad \text{with } \beta = K \tan\delta \qquad (4b)$$

where K_0 is the coefficient of earth pressure at rest and σ'_{v0} is the free field vertical effective stress. The value of K/K_0 ($= \sigma'_{hf}/\sigma'_{h0}$) would be unity for a 'wished-in-place' pile, if changes in lateral stress during loading ($\Delta\sigma'_{hd}$) were zero. Rollins et al. (2005) backfigured average values of K from axial tension tests on bored piles in sand and gravel. These K values are plotted on Figure 1, where they are seen to be several times the normally consolidated K_0 value ($K_{0,nc}$) at depths less than about 10 m. Backfigured K values reduced systematically with pile length and Rollins et al. (2005) state that this reduction cannot be attributed to a reduction in OCR (and hence K_0) with depth at the respective sites. The same authors also noted that K values in gravel tended to be about 25 to 50% higher than those in sand.

It is evident from Figure 1 and a comparison of equation (1) with equations (3) & (4) that proposed value of β_c ($=1/\alpha_s$) should reflect variations in the values of σ'_{h0}, $\Delta\sigma'_{hc}$, $\Delta\sigma'_{hd}$ and δ. The validity of equation (1) relies on the fact that these lateral stress quantities (or at least those making the largest contribution to σ'_{hf}) can be described approximately as a function of the CPT q_c value.

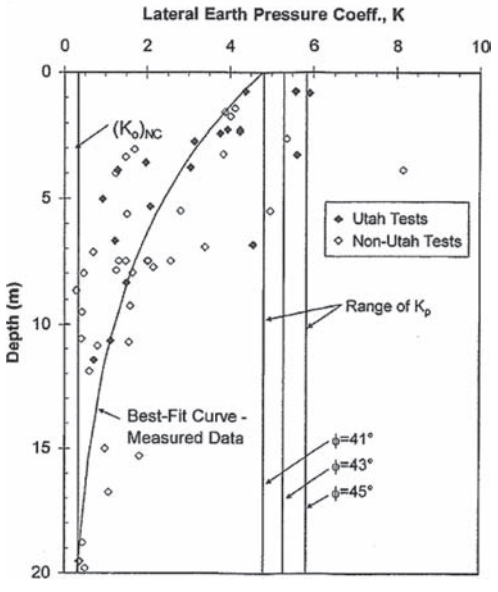

Figure 1. Backfigured K values for bored piles in sand (Rollins et al. 2005).

2.2 *Existing correlations for ß$_c$*

De Cock et al. (2003) discuss the range of β_c ($=1/\alpha_s$) values in use in Europe and provide a plot, shown on Figure 2, summarising currently adopted correlations between τ_f and q_c. This figure highlights the wide range of correlations in use. For example, in a cohesionless soil deposit with a mean q_c value less than 10 MPa, recommended β_c values range from 280 for large diameter piles in France to 95 for continuous flight augered (CFA) piles in Italy; a typical mean value of β_c is 150.

The correlations shown on Figure 2 were derived through backanalyses from specific databases of shaft capacity. Some trends common to the correlations are as follows:

i. The rate of increase in τ_f with q_c reduces as q_c increases i.e. β_c increases with q_c. A limit on the maximum available shaft friction is imposed when q_c exceeds about 15 MPa.
ii. β_c values for continuous flight augered (CFA) piles are the same or slightly lower than those for piles bored using temporary casing.
iii. It follows from (ii) that the variation in construction practices employed across Europe cannot be the only explanation for the range in recommended β_c values.

Houlsby & Hitchman (1988) show that the CPT q_c value correlates directly with the in-situ lateral effective stress (σ'_{h0}) and is relatively independent of σ'_{v0}. The following relationships were proposed for (medium grained) Leighton Buzzard sand at two relative densities (D_r):

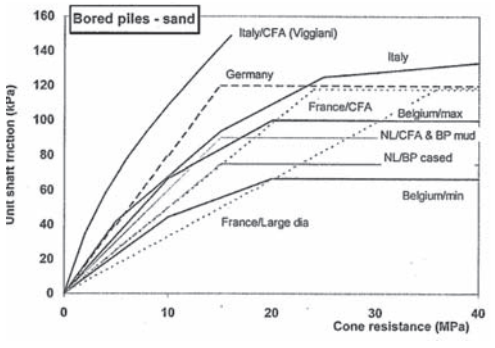

Figure 2. Variation of unit shaft friction with q_c adopted in Europe (De Cock et al. 2003).

$$\frac{q_c}{p_a} = 160\left(\frac{\sigma'_{h0}}{p_a}\right)^{0.6} \quad \text{at } D_r = 54 \pm 7\% \tag{5a}$$

$$\frac{q_c}{p_a} = 230\left(\frac{\sigma'_{h0}}{p_a}\right)^{0.6} \quad \text{at } D_r = 86 \pm 4\% \tag{5b}$$

where p_a is a reference stress equal to atmospheric pressure (=100 kPa).

If both construction related and shearing induced changes in effective stress are assumed to be negligible (i.e. $\Delta\sigma'_{hc}$ and $\Delta\sigma'_{hd} = 0$ in equation 3) so that the lateral effective stress at peak shear stress, σ'_{hf}, is equal to σ'_{h0}, equation (5) may be manipulated to produce relationships between τ_f and q_c for medium dense and dense Leighton Buzzard sand. These relationships are plotted on Figure 3 assuming a (typical) δ value of 35° for a concrete-sand interface.

A comparison of Figure 2 with Figure 3 indicates:

i. The predicted τ_f values on Figure 3 generally fall below the design recommendations on Figure 2, suggesting that σ'_{hf} is larger than σ'_{h0} (i.e. $\Delta\sigma'_{hc}$ + $\Delta\sigma'_{hd}$ is positive). At q_c = 10 MPa, predicted β_c values of 425 ± 125 are well above the β_c range of 95 to 280 used in practice i.e. shaft friction is underestimated by a factor of about 3.
ii. Unlike the trend seen in Figure 3, the current design procedures do not recommend a dependence of β_c on relative density.
iii. Predicted β_c values reduce as q_c increases, whereas β_c values corresponding to the trends shown on Figure 2 increase with q_c.

This comparison provides indirect confirmation that σ'_{hf} for a bored pile in sand is likely to be larger than the in-situ lateral effective stress (σ'_{h0}). The same conclusion was inferred from the backanalyses of Rollins et al. (2005) summarised in Figure 1.

2.3 *Dilation at the shaft-soil interface*

Boulon & Foray (1986) postulated that dilation during shearing of the soil at the pile interface can make a significant contribution to the peak shaft friction. They used a cavity expansion analogy to deduce the following expression for the increase in lateral stress ($\Delta\sigma'_{hd}$) due to a radial expansion equal to *y*:

$$\Delta\sigma'_{hd} = \frac{4Gy}{D} = k_n y \tag{6}$$

here G is the equivalent linear shear modulus of the sand or gravel mass constraining the dilation, D is the pile diameter and k_n is the equivalent normal stiffness. Equation (3) may therefore be written as:

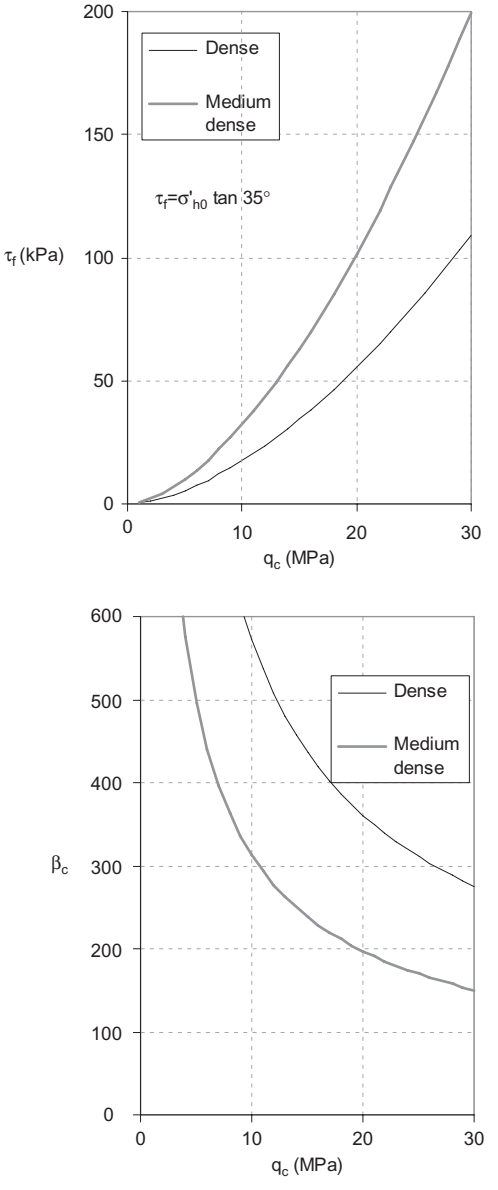

Figure 3. Predicted variation of t_f with q_c in Leighton Buzzard sand assuming $s'_{ho} = s'_{hf}$ and d = d 35°.

$$\begin{aligned}\tau_f &= \sigma'hf \tan\delta \\ &= (\sigma'_{h0} + \Delta\sigma'_{hc} + 4Gy/D) \tan\delta\end{aligned} \tag{7}$$

Visualisation studies reported by Boulon (1988) and Desrues (1991) suggest that the thickness of the dilating zone is independent of the pile diameter and typically varies between about 2 and 10 times the mean sand particle size (D_{50}). The radial expansion, *y*,

must also be independent of the pile diameter and as σ'_{rd} varies in inverse proportion to the pile diameter (equation 6), the relative contribution of dilation to shaft capacity will be much larger for small scale piles than for large diameter piles. It follows that β_c should also vary with pile diameter, although the form of such a variation cannot easily be inferred, given the range of factors contributing to $\Delta\sigma'_{hd}$.

3 OVERVIEW: BASE CAPACITY

Correlations relating the ultimate base resistance of a bored pile in granular soil to the CPT end resistance in the vicinity of its base (q_c) generally take the simple form indicated in equation (2). However, as for β_c values, there is a wide range of α_b factors in use in design practice. For example, De Cock et al. (2003) state that α_b values of between 0.15 and 0.2 are in use in France, Germany and Italy, whereas The Netherlands adopts α_b values of 0.5 and 0.8 for bored and CFA piles respectively. In Belgium, a base factor of between 0.33 and 0.67 is applied to a CPT resistance averaged using the Van Impe-De Beer (1988) procedure.

The ultimate end bearing resistance of a bored pile may be expected to tend towards the q_c resistance after displacements in excess of a few diameters (assuming q_c is relatively uniform with depth). White & Bolton (2005), and others, show that the inferred value of α_b is less than unity partly because the ultimate base resistance is generally defined at a base displacement of 10% of the pile diameter (i.e. $q_{b0.1}$). Xu et al. (2008) examined a relatively large database of $q_{b0.1}$ values for closed and open-ended driven pipe piles in sand and deduced that the value of α_b for a full displacement driven pile is only about 60% of an averaged CPT end resistance ($q_{c,avg}$) and that α_b reduces with the level of soil displacement induced near the base during pile installation. Their proposed design expression, which is given in equation (8), illustrates the impact of soil displacement on the α_b value and suggests that α_b may be as low as 0.15 for a non-displacement pile.

$$q_{b0.1} / q_{c,avg} = 0.15 + 0.45 \times A_{rb,ef} \quad (8a)$$

$$A_{rb,eff} = 1 - FFR \frac{D_i}{D^2} \quad (8b)$$

where D_i is the pipe pile inner diameter and FFR is the final filling ratio (=the incremental filling ratio measured over the final few diameters of pile penetration).

Lee & Salgado (1999) conducted numerical studies to deduce a relationship between $q_{b0.1}$ and q_c. Base load displacement curves were derived using the Finite Element Method (FEM) and a non-linear elastic-plastic constitutive model for sand at various initial stress levels and relative densities. Cone resistance was derived for the same soil conditions using the program CONPOINT (Salgado 1993). Predicted values of α_b are re-plotted on Figure 4 where they are seen to be in general agreement with the 0.15 to 0.2 range employed in practice. However, the predictions show a systematic reduction in α_b with D_r and a moderate reduction of α_b with increasing initial vertical effective stress (σ'_{vi}). The limit imposed on the maximum value of $q_{b0.1}$ (e.g. 15 MPa in The Netherlands) is consistent with the relatively low α_b values predicted at high D_r values.

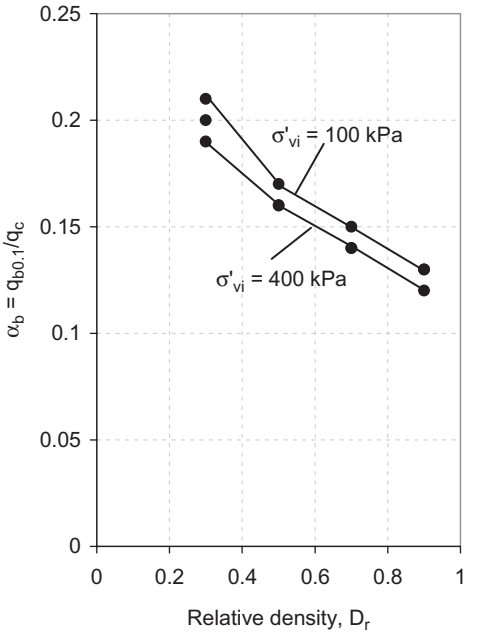

Figure 4. Predicted variation of α_b with relative density and initial stress level (re-plotted from Lee & Salgado 1999).

It is apparent from Figure 4 and the range of α_b values inferred from static load tests that $q_{b0.1}$ does not vary uniquely with q_c i.e. the value of α_b is not constant and is likely to vary with relative density and stress level in addition to the bored pile construction procedure. α_b values indicated by a database of pile load tests conducted in Perth sand are examined later in the paper to explore correlations for base capacity that seek to improve on that given by equation (2).

4 CENTRIFUGE INVESTIGATIONS OF SHAFT CAPACITY

It is instructive to review some trends deduced by Foray et al. (1998) and Lehane et al. (2005) from

centrifuge tests on buried piles with a range of pile diameters in normally consolidated sand. Buried piles were employed in both test series so that the construction related component of lateral stress change ($\Delta\sigma'_{hc}$) could be assumed to be zero and the initial lateral stresses (σ'_{h0}) could be calculated as $K_{0,nc}\sigma'_v$, where $K_{0,nc}$=1–sin ϕ'. Sand grains were glued to the shafts of all piles to create 'fully rough' interfaces.

4.1 *Tests reported by Foray et al. (1998)*

The effects of pile diameter and sand size were investigated for buried piles by Foray et al. (1998). Four piles with diameters of 16 mm, 27 mm, 35 mm and 55 mm were tested and each comprised axial load cells at up to ten separate locations. Typical measured profiles of maximum local shear stress (τ_f) inferred from the measured load distributions are plotted on Figure 5 for two pile diameters (D = 16 mm and 27 mm) tested at 100 g in two dense quartz sands with D_{50} = 0.32 mm and 0.7 mm. These results indicate that, as predicted by equation (7), lower values of τ_f are mobilised by the larger diameter piles, but higher values of τ_f, for a given pile diameter, develop in the coarser sand. Foray et al. (1998) attribute the latter trend, which was also observed by Rollins et al. (2005), to the greater thickness of the dilatant zone at the pile shaft in coarse sand.

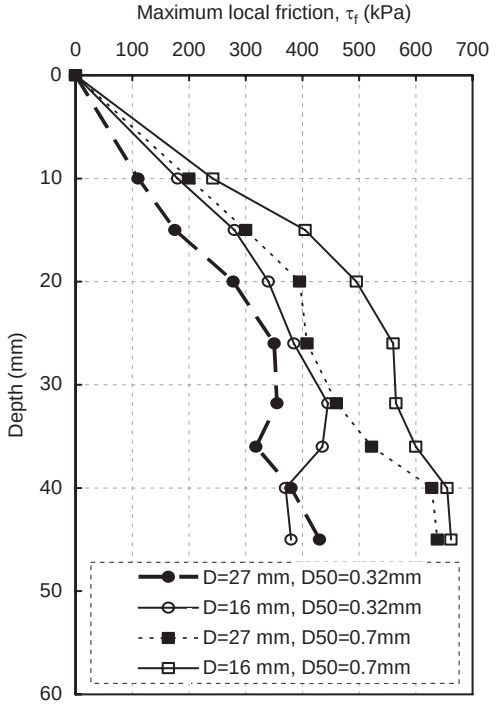

Figure 5. τ_f values measured on buried centrifuge piles in sand (Foray et al. 1998).

4.2 *Tests reported by Lehane et al. (2005)*

The piles employed by Lehane et al. (2005) were 130 mm in length with diameters of 3 mm, 5 mm, 10 mm and 18 mm. The piles were buried in sand, which was subsequently saturated, before being subjected to axial tension loading at *g*-levels of approximately 30 g, 50 g, 100 g and 180 g; these g levels led to average vertical effectives stress levels along the pile shafts of 22 kPa, 37 kPa, 75 kPa and 134 kPa.

The variation of the average peak shear stress, $\tau_{f,av}$ with D measured in all tension tests is shown on Figure 6a. It is evident that, at any given average initial stress level (or g level), $\tau_{f,av}$ reduces with D, with greatest relative reductions occurring at lower diameters. Fig. 6a also shows that, at any given diameter, larger $\tau_{f,av}$ values are mobilised at higher initial stresses. This dependence on initial stress is investigated on Fig. 6b by normalizing the $\tau_{f,av}$ values by their respective

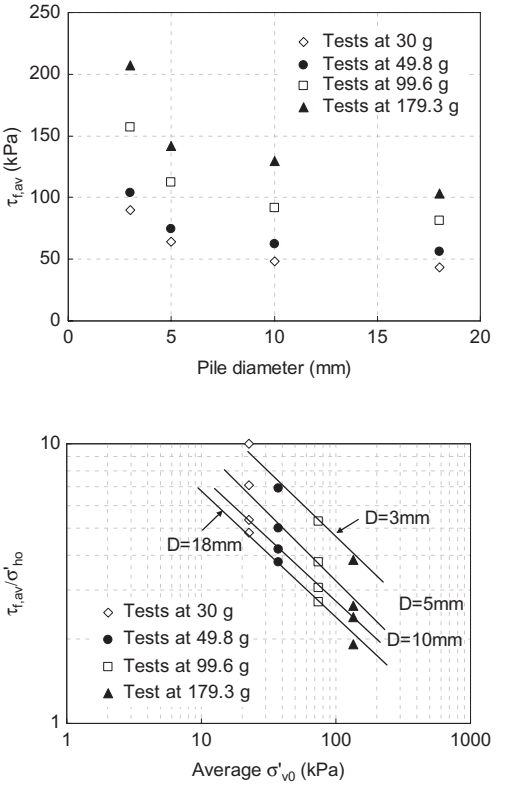

Figure 6. (a) Peak average shear stress variation ($\tau_{f,av}$) with pile diameter, (b) stress level dependence of $\tau_{f,av}$ (Lehane et al. 2005).

initial average lateral effective stress (σ'_{h0}) and plotting this ratio against the average initial vertical effective stress (σ'_{v0}). An in-situ K_0 value of 0.4 was assumed to calculate σ'_{h0}. Figure 6b shows $\tau_{f,av}/\sigma'_{h0}$ ratios reducing as both σ'_{v0} and D increase. This trend, which would not occur if the lateral effective stress on the pile shaft remained constant, is compatible with the inverse dependence of $\Delta\sigma'_{hd}$ given by equation (6) and the tendency for reduced dilatancy as the stress level increases.

The $\tau_{f,av}/\sigma'_{h0}$ ratios plotted on Figure 6 vary between 2 and 10 and are well in excess of the corresponding ratio of 0.7 measured at maximum shear stress in interface shear tests. It is clear, therefore, that the lateral effective stresses acting on the pile shafts at peak tension capacity are substantially higher than the initial values of σ'_{h0}. These average increases in lateral effective stress ($\Delta\sigma'_{hd}$) were estimated using equation (3), assuming tan $\delta = 0.7$ and $\sigma'_{hc} = 0$.

Estimated average $\Delta\sigma'_{hd}$ values are normalized by the mean initial lateral effective stress (σ'_{h0}) and plotted against the pile diameter (D) on Figure 7. This figure provides a graphical illustration of the immense contribution of lateral stress changes during shear to the shaft capacity of small diameter piles. For example, the inferred $\Delta\sigma'_h/\sigma'_{h0}$ value for a pile with D = 3 mm at 30 g (for which the average $\sigma'_{h0} = 9$ kPa) is 14 and the pile derives virtually all of its shaft capacity due to the stress increase that takes place during shearing to failure. Figure 7 also shows that, as implied by equation (6), the value $\Delta\sigma'_{hd}$ (and hence the contribution of dilation) reduces as the diameter increases and the stress level increases.

Lehane et al. (2005) conclude that these $\Delta\sigma'_{hd}$ values can be predicted using equation (6). However, they show that the operational G value for the (small scale) centrifuge piles employed is far lower than the very small strain elastic value (G_0) because the cavity strains (y/D) are well in excess of the strains at which the use of G_0 is appropriate. This study adopted y values measured in sand-sand constant normal stiffness (CNS) shear box tests, which showed that the degree of dilation reduced with increasing normal stiffness, k_n. The following approximate relationship was deduced from these CNS data:

$$y = \frac{y_0}{\left[1+\left(\frac{k_n}{k_{nref}}\right)^{0.75}\right]} \qquad (9)$$

where y_0 is the dilation at peak shear stress in a constant normal load (CNL) test (for which $k_n = 0$) and k_{nref} is a reference constant normal stiffness (corresponding to the k_n value at which $y_{max} = y_0/2$) and had a value of 500 kPa/mm for the particular sand employed in the centrifuge tests.

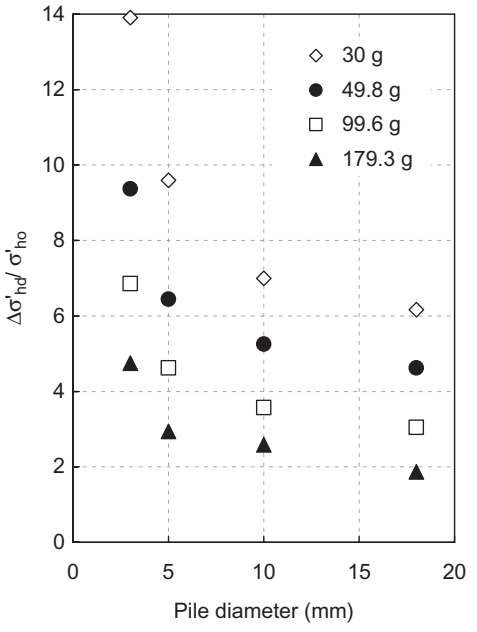

Figure 7. Relative values of $\Delta\sigma'_{hd}$ as a function of pile diameter and stress level (Lehane et al. 2005).

5 SHAFT FRICTION PROFILES AT A PERTH SAND SITE

This section discusses the results of instrumented axial pile load tests in the context of the foregoing review of the various components of shaft friction and their relationship with the CPT q_c value. The test data discussed were obtained at the Shenton Park test bed site in Perth, Western Australia. This site has been investigated extensively (e.g. Lehane et al. 2004, Schneider 2008) using a wide variety of in-situ and laboratory tests and has also been used for other foundation and retaining wall experiments (e.g. Lehane 2008).

5.1 *Ground conditions and pile load test results*

The stratigraphy at the Shenton Park site comprises a 7 m thick deposit of 'Spearwood Dune sand' overlying the 'Tamala Limestone' formation. The dune sand is sub-angular to sub-rounded with D_{50}, D_{60} and D_{10} values of 0.42 mm, 0.47 mm and 0.21 mm respectively. The sand is siliceous and originated from dissolution of the Tamala Limestone, which was eroded, transported, and re-deposited by the wind, probably in the late Pleistocene. The water table is typically at ~6.5 m depth (i.e. just above the top of the limestone) and the sand has a low level of saturation (<15%). which varies seasonally by up to about 5%. As part of a separate study, Schneider (2008) reports the results of about 50

CPTs and 10 seismic CPTs (SCPTS) in the test area, which measured 100 m × 40 m. These tests indicated low horizontal variability, but a strong seasonal effect on the CPT q_c values and on the small strain shear moduli (G_0), inferred from the SCPT shear wave velocities (V_s). Both q_c and G_0 varied from maxima at the end of the dry season to minima at the end of the wet season that were 30% less than the respective maxima.

4 m long, CFA grout piles with diameters of 225 mm and 340 mm were installed in May 2007 and load tested (using a 25 tonne cone truck as reaction) in June 2007. The instrumentation on each pile comprised a steel bar with four levels of strain gauges, placed centrally in the pile bore after grout placement (see Figure 10). The G_0 values and CPT q_c values obtained close to the piles just prior to their installation are plotted on Figures 8 and Figure 10; these data are typical of those obtained towards the end of the Perth dry season. Schneider et al. (2008) attribute the relatively constant value of G_0 seen on Figure 8 to the reducing influence of suction and/or slight cementation with depth.

The shear stress-local pile displacement (τ-w) relationship inferred from the axial load distributions measured on the pile with D = 225mm are plotted on Figure 9. It is apparent that, following an initially stiff response, the rate of increase in shear stress with displacement is approximately linear up to a displacement of about 7 mm (3% of D). Peak shear stresses are not developed until a displacement of 0.08D (on average), which is well in excess of the displacement of between 1% and 3% of D, commonly assumed necessary for the development of peak shaft friction.

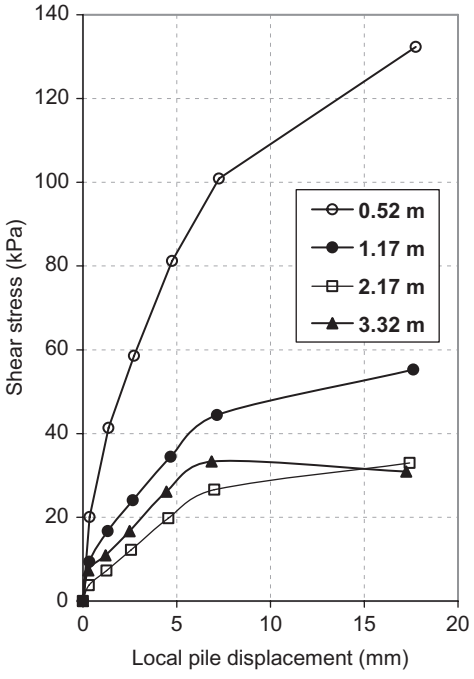

Figure 9. Shear stress displacement (t-z) curves inferred for 225 m diameter pile at Shenton Park.

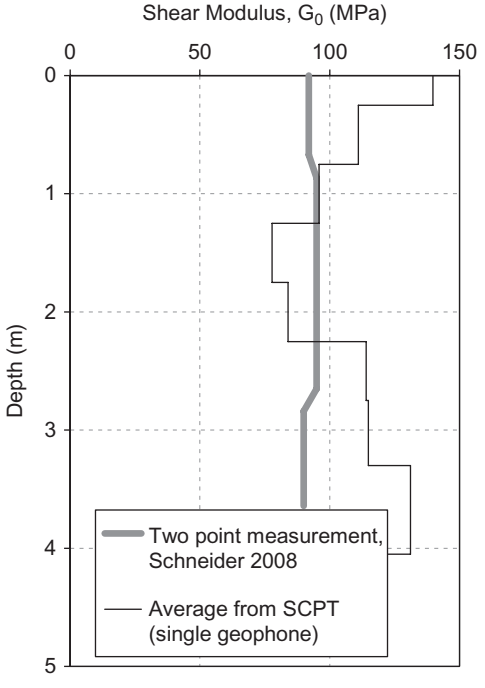

Figure 8. G_0 data at Shenton Park (obtained at time of load tests).

It was only possible to load the 340 mm diameter pile to a head displacement of 5 mm due to the load limit imposed by the available reaction from the CPT truck. The shear stress-displacement relationships measured for this pile were therefore extrapolated to estimate peak frictions (τ_f), which were assumed to be fully developed at a displacement of 15 mm. The distribution with depth of these 'peak' frictions is compared on Figure 10 with the corresponding distribution measured for the 225 mm diameter pile. To assist comparisons, Figure 10 also shows the CPT q_c profile over the same depth interval.

It is apparent that τ_f reduces with depth for both piles, despite the fact that q_c increases with depth at a relatively significant rate. There is clearly not a proportional relationship τ_f and q_c and the value of β_c ($=q_c/\tau_f$) reduces almost tenfold from 0.5 m to 3.3 m.

Over the same depth interval, assuming a pile-sand interface friction angle of 33˚, the lateral stress

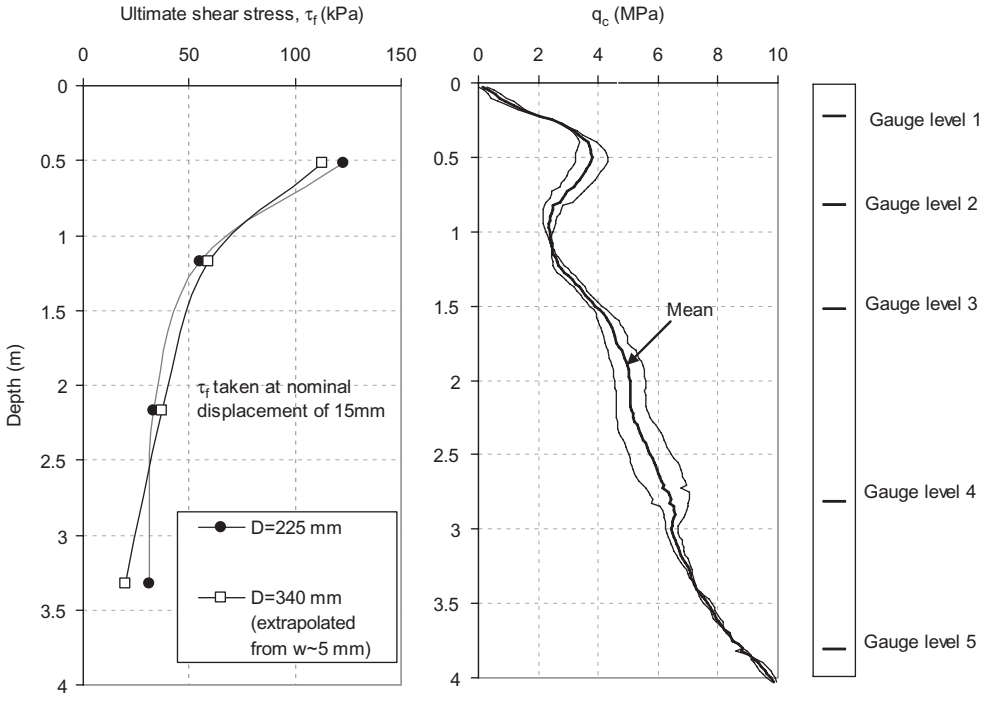

Figure 10. Ultimate shear stress profiled for Shenton Park piles compared with q_c profile.

coefficient K ($=\sigma'_{hf}/\sigma'_{v0}$) reduces from ~12 to ~0.42 i.e. there is a 30-fold reduction.

These observations, which are now examined in further detail, are consistent with the influence of dilation anticipated from the centrifuge test data and the database Rollins et al. (2005).

5.2 *Prediction of τ_f profiles at Shenton Park*

As previously discussed, the contribution of dilation to shaft capacity is related to the degree of dilation (*y*) and the operational shear stiffness (G) of the soil mass constraining this dilation (equation 6). This G value could be inferred at the Shenton Park site using results from self-boring pressuremeter tests (SBPTs), which were conducted within 15 m of the test piles in February 2007 (Schneider et al. 2008). The pressuremeter shear moduli, G_{ph}, derived during the initial (virgin) loading phase in four shallow tests are plotted against cavity strain (ε_c) on Figure 11. The resolution of the strain-gauged feeler arms on the pressuremeter is insufficient to allow the G_0 value to be determined. However, extrapolation of the G_{ph}-ε_c curves to very low strains indicates a G_0 range of 80 MPa and 130 MPa, which is consistent with the range indicated on Figure 8. As illustrated on Figure 11, the measured

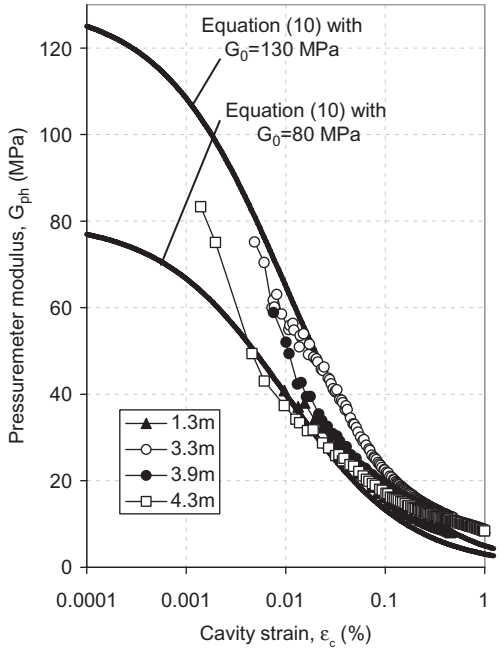

Figure 11. Pressuremeter modulus degradation curves at Shenton Park.

variations of G_{ph} with ε_c may be estimated by the following equation:

$$G_{ph} = \frac{G_o}{\left[1+\left(\frac{e_c}{e_{ref}}\right)^{0.7}\right]} \quad (10)$$

where $G_{ph} = 0.5G_0$ at $\varepsilon_{ref} = 0.01\%$

This expression for G_{ph} predicts the operational radial stiffness around a pile when the dilation at the sand-pile interface (=y) is equal to ε_c D/2. The increase in lateral effective stress due to dilation ($\Delta\sigma'_{hd}$) on the piles at Shenton Park may therefore be estimated from equations (6) and (10) using a relationship such as equation (9) derived from CNS tests. The value of y_0 in equation (9) at the normal stress levels of interest increases with the mean effective particle size (D_{50}), soil relative density (D_r), interface roughness, among other factors.

Based on a consideration of these factors and a review of published direct shear data such as DeJong et al. (2006), Tabucannon (1997), Kelly (2001), a y_0 value of 0.15 mm is estimated for the Shenton Park sand (with D_{50} ~ 0.4 mm) under constant normal stress conditions, when normal stresses are between about 30 kPa and 100 kPa.

Predictions for the value of β_c for the 225 mm diameter piles at Shenton Park were obtained using equation (1) to evaluate τ_f and the mean CPT q_c profile shown on Figure 10. Construction related changes in lateral effective stress ($\Delta\sigma'_{hc}$) were assumed zero while equations (6), (9) and (10) were employed in an iterative fashion to derive $\Delta\sigma'_{hd}$ (assuming y_0 = 0.15 mm). Following the recommendations of Uesugi & Kishida (1986), Lehane et al. (1993) and Dietz (2000), the interface friction angle (δ) between the sand and pile (rough concrete) was set equivalent to the soil-soil constant volume friction angle of 33˚. A profile for the in-situ lateral stress (σ'_{h0}) was assessed based on lift-off pressures measured in SBPTs. The σ'_{h0} profile adopted is shown on Figure 12, where it is seen to provide a close match to the lift-off stress inferred from 4 SBPTs. K_0 values corresponding to this profile vary from 1.25 at 0.5 m depth to 0.48 at 3.5 m depth.

Predictions for β_c were obtained for the inferred range of G_0 moduli at this site and these are compared on Figure 12b with the measured β_c profile. Predicted β_c values increase significantly with depth and range from ~80 at 1 m depth to 220 at 4 m depth. These values are in reasonable agreement with the observed β_c profile and appreciably less than those values derived assuming no dilation (i.e. $\Delta\sigma'_{hd}$ = 0).

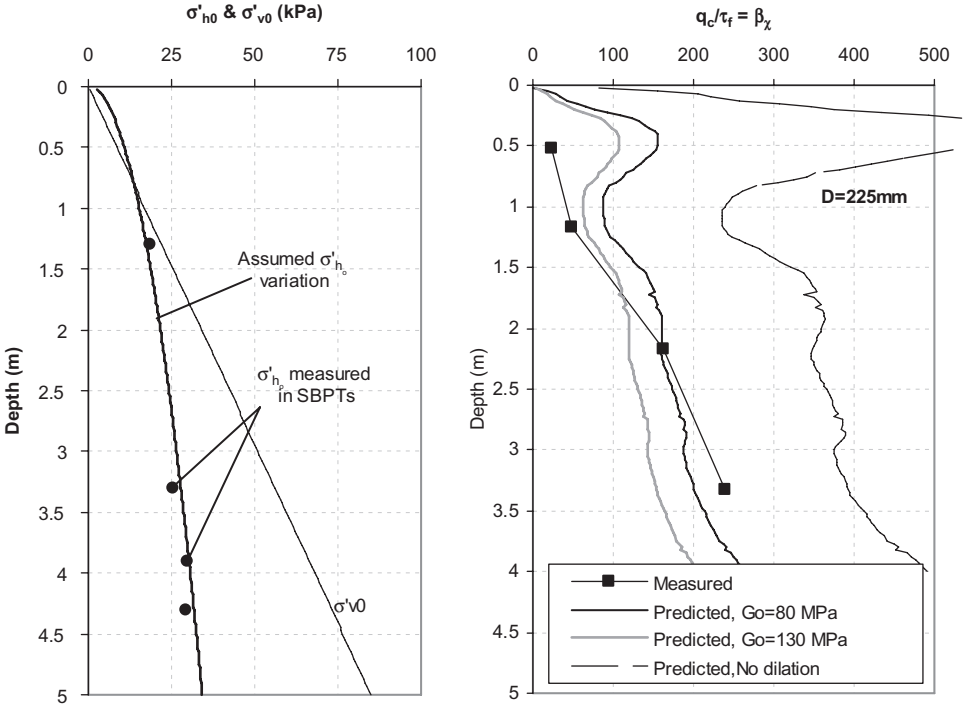

Figure 12. (a) In-situ stresses at Shenton Park and (b) Measured and predicted β_c values.

Deviations between measurements and predictions may be expected due to construction related lateral stresses changes ($\Delta\sigma'_{hc}$), which on the evidence of the match on Figure 12b are not a major component of the ultimate lateral effective stresses.

This analysis highlights the importance of dilation in the development of appropriate correlations for β_c. Such correlations evidently need to incorporate the variable influence of parameters such as the pile diameter, initial stress level, very small strain stiffness, stiffness non-linearity and dilation dependence on radial stiffness. The site specific variability of these parameters combined with construction related lateral stress changes make the formulation of a general expression for β_c difficult; such a range of factors also explains the range of β_c values backfigured from load test databases. One such database is now examined to explore trends for both shaft and base capacity.

6 AUGERED PILES IN PERTH

The shaft friction and end bearing characteristics discussed in the foregoing are now examined using a database of static load test data compiled by the author for augered piles installed in Perth sands.

6.1 *Database summary*

The database, which is summarised in Table 1, comprises 12 tests at 6 separate sand sites in the Perth area (and includes the two tests at Shenton Park, discussed above). All of the piles were installed by Belpile Pty Ltd, which is a Perth-based contractor specialising in the construction of small to medium diameter continuous flight augered (CFA) piles. Belpile's particular appeal is its ability (using a patented procedure) to install belled (=under-reamed) piles in sand above and below the water table. The construction process for the bells involves the use of bentonite pumped through the auger stem and a special under-reaming tool. This process is summarised in Figure 13 and a photo showing the base of an exhumed belled pile constructed in Perth sand is shown on Figure 14.

Investigations involving boreholes, CPTs (and in some cases DMTs) indicated that the ground conditions at all sites comprised fine to medium siliceous sand with average relative densities (D_r) varying from about 15% (in South Perth) to 90% (in Claremont).

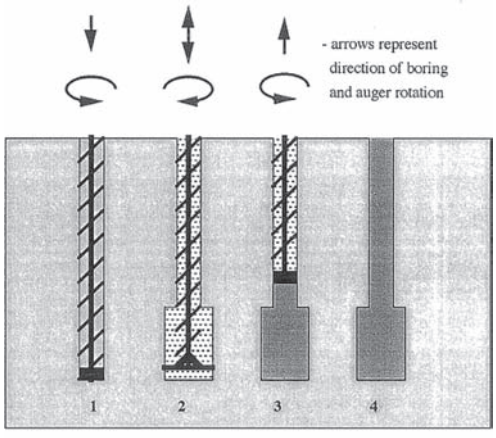

Figure 13. Belpile Pty Ltd construction method (Coutts 2000).

Table 1. Database of load tests on augered piles in Perth sand.

Site	D (mm)	D_{base} (mm)	L (m)	$q_{c,avg}$ (Shaft) (MPa)	$q_{c,tip}$ (Base) (MPa)	Max. disp/D (%)	Comments
Veneto (1)	340	700	8.6	9.7	5	8.1	Tip of pile in silt
Veneto (2)	340	700	4.6	15	15	8.4	
South Beach (South)	450	850	5.5	15	20	2.0	Variable $q_{c,tip}$
South Beach (North)	450	850	5.5	15	30	2.0	Variable $q_{c,tip}$
Claremont	450	850	6.7	6.8	11	6.6	2 identical piles (instrumented)
Dolphin (1)	340	700	5	15	18	7.1	
Dolphin (2)	340	700	9.5	10.6	6	3.9	Tip of pile in silt
South Perth (straight)	340	340	10.5	4	4	16.8	Instrumented
South Perth (belled)	340	700	10.5	4	4	9.6	Instrumented
Shenton Park (1)	225	225	4	5	9	8.0	Instrumented; see Section 5
Shenton Park (2)	340	340	4	5	9	1.5	Instrumented; see Section 5

Figure 14. Exhumed enlarged base of bored pile in Perth Sand.

Nine of the twelve piles in the database had bell diameters (D_{base}) varying from 700 mm to 850 mm with a height of 0.5 m; shaft diameters (D) for belled and straight shafted piles ranged from 225 mm to 450 mm. Six of the twelve piles included instrumented steel bars to allow separation of the shaft and base components of resistance. For these cases, the minimum instrumentation included strain gauges at the pile head and base (or just above the bell in the case of belled piles). Grout with a 28 day cube strength of 40 MPa was employed as the pile material and backanalyses of the strain gauges at the pile heads during load tests indicated grout Youngs moduli (E_{pile}) of 35 ± 5 MPa. All gauges were zeroed just prior to load tests, with the implicit assumption that residual loads were negligible.

Load testing employed anchor piles to provide reaction and followed the Australian Standard maintained load testing procedure, which includes a 6 hour creep stage at the expected working load. A typical measured load displacement relationship is shown on Figure 15.

The RATZ load transfer program (Randolph 2003) was used to match the pile head load-displacement data and the base load-displacement data (when available). These backanalyses adopted:

- Parabolic 't-z' springs representing the variation of shaft shear stress with displacement at 1 m intervals along the pile shaft; the t-z relationships were generated from specified peak shear stresses (τ_f) and equivalent linear soil shear moduli (G).
- An hyperbolic base load-base displacement relationship leading to a linear reduction in secant base stiffness with increasing load level; this relationship was defined by specifying an initial stiffness (k_{bi}) and an ultimate base resistance (q_{bf}).

A wide range of τ_f, G, k_{bi} and q_{bf} values were trialled when seeking a best-fit match to the load-displacement response shown by each database pile. The value of G was assumed to be constant along each pile's shaft to simplify this task (with little loss in accuracy). Unload-reload loops performed as part of the load testing schedule assisted with the assessment of the respective contributions of the base and shaft load in un-instrumented tests.

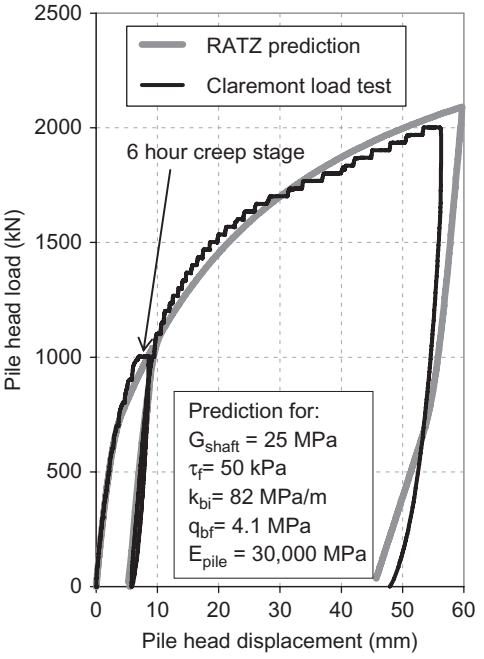

Figure 15. Typical load test in Perth sand and RATZ best-fit prediction.

An example of the kind of match achievable using the RATZ backanalysis is shown on Figure 15 for a load test at Claremont (the load-displacement relationships for the two tests at Claremont were closely comparable). It is seen on Figure 15 that use of the quoted τ_f, G, k_{bi} and q_{bf} parameters led to good agreement for both loading and unloading stages. Many of the load tests were halted prior to achieving a base displacement of 10% of the pile base diameter and therefore the end bearing resistance at this displacement ($q_{b0.1}$) was derived using the hyperbolic expression for base stiffness adopted in RATZ and the best-fit k_{bi} and q_{bf} values. For the example shown on Figure 15, this extrapolation gave $q_{b0.1}$ of 3.18 MPa (=1800 kN) at a base displacement of 85 mm (=D_{base}/10).

Interpreted values of β_c (=$q_{c,avg}/\tau_{f,avg}$) and α_b = $q_{b0.1}/q_{c,tip}$ for the Perth database are plotted against pile embedment on Figures 16 and 17. These are discussed separately in the following sections.

6.2 *Shaft friction factor,* β_c

Figure 16 indicates β_c values increasing from an average of 125 for a pile length (L) of 4 m to about 250 for L = 10 m; the overall database average value is 175.

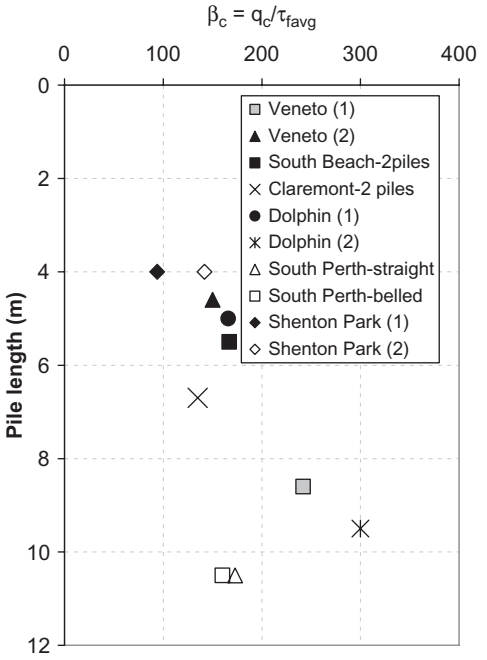

Figure 16. Perth database values of β_c.

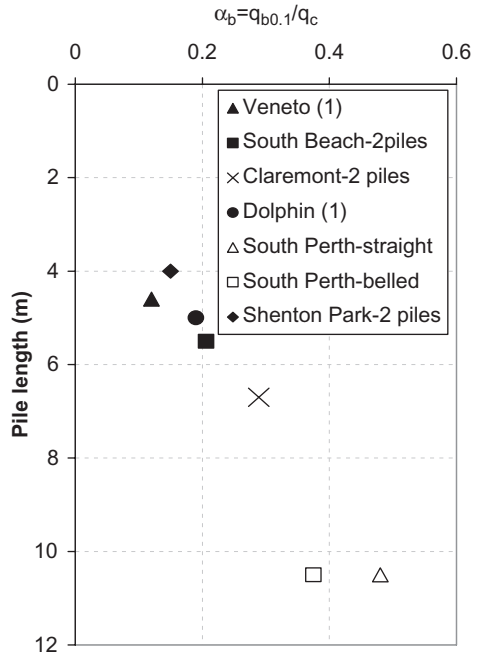

Figure 17. Perth database values of a_b.

The measured/derived values are within the range proposed by existing correlations (such as shown on Figure 2) and the spread of values is consistent with the wide variety of factors affecting the value of β_c (discussed in Section 5). Because of such factors, it is not appropriate to develop a correlation for β_c using the data points on Figure 16. However, some general observations may be made:

i. The observed increase in β_c (or reduction in $\tau_{f,avg}$) is expected because of the reduced influence of the dilation component of shaft friction due to the higher stress levels and stiffness at depth (e.g. see Figures 6 and 12).
ii. The influence of pile diameter on shaft friction (as seen, for example, on Figure 6) is not obvious due to the limited range of shaft diameters in the database. This effect is nonetheless evident at Shenton Park where the 340 mm diameter pile has a large β_c value (or lower friction) than the 225 mm pile.

The discussion in Section 5 and the range of β_c values (inferred for a given construction process in Perth sand) on Figure 16 highlight the continued need for site specific load tests—and their interpretation within the framework described. Use of the β_c value derived from a small scale test pile to estimate the shaft friction of a larger and longer pile will lead to non-conservative design. Conservative estimates for large diameter and deep piles are best obtained using charts such as those shown on Figure 3, which assume no dilation contribution to friction.

6.3 *Base factor,* α_b

Figure 17 indicates a significant variability in the database values of α_b, which apparently increases with pile length from about 0.12 at 4 m to about 0.45 at 10 m. The inference from the discussion in Section 3 is that the value of $q_{b0.1}$ is likely to vary with the (very) large strain stiffness of the soil at the pile base and only reaches the ultimate value of q_c (averaged) at a pile base displacement of a few diameters. From the equation of a rigid punch in an elastic soil, the equivalent elastic operational stiffness at a displacement of 0.1D ($E_{0.1D}$) is given as:

$$E_{0.1D} = (10\pi/4)(1-\nu_2)\, q_{b0.} \qquad (11)$$

For a typical large strain Poissons ratio of 0.4 (Lehane & Fahey 2002), equation (11) simplifies to:

$$E_{0.1D} \sim 10\, q_{b0.1} \qquad (12)$$

The ratio of stiffness (at a given strain) to q_c is well known to reduce with increasing relative density.

Consequently Rix & Stokoe (1991), and others, deduced that, for a given sand deposit, the very small strain (elastic) stiffness varies with q_c raised to a power of 0.25 and the vertical effective stress (σ'_v) raised to a power of 0.5 i.e. there is a relatively weak correlation between small strain stiffness and q_c. At the much higher strain levels operational at pile base displacements of 0.1D, it is likely that 'stiffness' (i.e. $E_{0.1D}$) varies more strongly with q_c.

A statistical analysis of the Perth database combined with the numerical predictions of Lee & Salgado (1999) shown on Figure 4 was performed to derive a correlation between $q_{b0.1}$, q_c and σ'_v. The numerical predictions were included to provide theoretical support for the correlation and also because these predictions encompassed a much wider range of σ'_v values (up to 400 kPa) than that of the database (for which the maximum σ'_v was 125 kPa). The best fit expression deduced is as follows and is shown graphically on Figure 18:

$$q_{b0.1} = (2.4 - 0.7)\, qc^{0.5} \sigma'^{0.25}_v pa^{0.25} \qquad (13)$$

where p_a is reference stress taken equal to atmospheric pressure (=0.1 MPa) with the same units as those employed for q_c and σ'_v. Figure 18 shows that equation (13) provides a reasonable fit to the Perth database and the numerical predictions. The marginally higher $q_{b0.1}$ values of the field piles for a given q_c and σ'_v value may reflect installation related stiffening of the sand near the pile base.

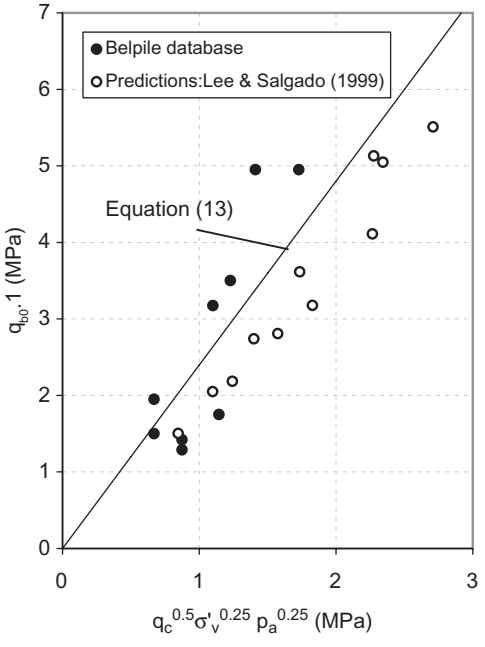

Figure 18. Relationship between $q_{b0.1}$,σ'_v and q_c.

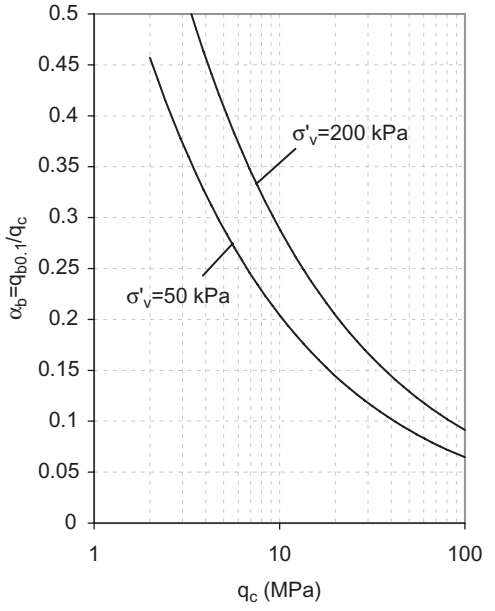

Figure 19. Dependence of α_b on q_c and σ'_v.

The mean variation of α_b with q_c, as implied by equation (13), is shown on Figure 19 for two initial vertical stress levels (σ'_v). This variation highlights the strong reduction of α_b with q_c and the moderate dependence on the pile embedded length (or stress level). In dense sands with q_c between 50 MPa and 100 MPa, equation (13) predicts a respective $q_{b0.1}$ range of only 5.5 MPa to 7.7 MPa i.e. a 40% increase in $q_{b0.1}$ for a doubling in the q_c value.

equation (13) and the mean trend lines shown on Figure 19 are supported by the database of pile tests in Perth sand and by the numerical analysis of wished in place piles in normally consolidated sand. However, as $q_{b0.1}$ is affected by the large strain soil stiffness ($E_{0.1D}$), equation (13) should be used with caution in other sand types such as overconsolidated aged deposits, which may be expected to be appreciably stiffer.

7 CONCLUSIONS

This paper has shown that the unit shaft friction (τ_f) and base resistance ($q_{b0.1}$) of a bored pile in sand do not vary uniquely with the CPT q_c value and consequently empirical correlations employing a single shaft or base multiplier (i.e. β_c and α_b) have poor general reliability.

The value of β_c (=q_c/τ_f) is seen to vary strongly with the dilation contribution to shaft friction and, as

such, increases with the pile diameter and stress level. Prediction of this variation is shown to be possible but cannot generally be performed as it requires knowledge of the site specific non-linear radial stiffness of the sand mass as well as the sand-shaft interface shear characteristic. Static load tests on instrumented test piles interpreted with an understanding of the factors controlling shaft friction provides the most reliable basis for design. A lowerbound estimate of shaft friction may be made assuming that the lateral effective stress at pile failure (σ'_{hf}) is equivalent to the in-situ initial horizontal effective stress (σ'_{h0}).

The base resistance of a bored pile in sand at a displacement of 0.1D ($q_{b0.1}$) is controlled by the large strain stiffness of the sand mass at the pile base. A database of static load tests in Perth sand and numerical predictions for wished-in-place piles indicate that this stiffness varies with $q_c^{0.5}$ $\sigma'_v{}^{0.25}$. The value of α_b consequently reduces as q_c increases and σ'_v reduces.

ACKNOWLEDGEMENTS

The author is indebted to Stuart Coutts of Belpile Pty Ltd for providing all necessary information for the database of augered piles and being an active proponent of static load testing in Perth. The author would also like to acknowledge the assistance provided by staff and students at the University of Western Australia.

REFERENCES

Boulon M. (1988). Numerical and physical behaviour under monotonous and cyclic loading. Modelling Soil-Water-Structure Interactions. In Kolkman et al. (ed). Rotterdam, Balkema, pp. 285–293.

Boulon M. & Foray P. (1986). Physical and numerical simulation of lateral shaft friction along offshore piles in sand. Proc. 3rd international Conference on Numerical Methods in Offshore Piling, Nantes, France, 127–147.

Coutts S.G. (2000). The uplift capacity of an enlarged base pile in sand. MSc thesis, University of Western Australia.

De Cock F., Legrand C. & Huybrechts N. (2003). Overview of design methods of axially loaded piles in Europe—Report of ERTC3-Piles, ISSMGE Subcommittee. Proc., 8th European Conf. on Soil Mech. and Geotech. Eng., Prague, 663–715.

Desrues J. (1991). An introduction to strain localisation in granular media. Proc. Physics of Granular Media, Winter School les Houches, Nova Sciences Publications, 127–142.

DeJong J.T., White D.J. & Randolph M.F. (2006). Microsclae observation and modelling of soil-structure interface behaviour using particle image velocimetry. Soils and Foundations 46(1), 15–28.

Dietz M.S. (2000). Developing an holistic understanding of interface friction using sand within the direct shear apparatus, PhD Thesis, Department of Civil Engineering, University of Bristol, UK.

Foray P., Balachowsky L. & Rault G. (1998). Scale effects in shaft friction due to the localization of deformations. Centrifuge 98, 211–216, Balkema.

Houlsby G.T. & Hitchman (1988). Calibration chamber tests of a cone penetrometer in sand. Geotechnique 38(1), 39–44.

Kelly R. (2001). Development of a large diameter ring shear apparatus and its use for interface testing. PhD dissertation, University of Sydney, Australia.

Lee J.H. & Salgado R. (1999). Determination of pile base resistance in sands. Journal of Geotechnical and Geoenvironmental Engineering, ASCE, 125(8), 673–683.

Lehane B.M., Doherty J. & Schneider J.A. (2008). Settlement prediction for footings on sand. Keynote lecture, Proc. 4th International Symposium on Deformation Characteristics of Geomaterial, IS-Atlanta, Sept. 2008.

Lehane B.M., Gaudin C. & Schneider J.A. (2005). Scale effects on tension capacity for rough piles buries in dense sand. Geotechnique 55(10), 709–719.

Lehane B.M., Ismail M. & Fahey M. (2004). Seasonal dependence of in-situ test parameters in sand above the water table, Geotechnique, 54(3), 215–218.

Lehane B.M., Jardine R.J., Bond A.J. & Frank R. (1993). Mechanisms of shaft friction in sand from instrumented pile tests. J. Geotechnical Engineering., ASCE, 119(1), 19–35.

Randolph M.F. (2003). Ratz program manual version 4.2, Centre for Offshore Foundation Systems, University of Western Australia.

Rix G.J. & Stokoe K.H. (1991). Correlation of initial tangent modulus and cone penetration resistance. Calibration Chamber Testing, Elsevier, 351–361.

Rollins K.M., Clayton R.J., Mikesell R.C. & Blaise B.C. (2005). Drilled shaft side friction in gravely soils. Journal of Geotechnical and Geoenvironmental Engineering, ASCE, 131(8), 987–1003.

Salgado R. (1993). Analysis of penetration resistance in sand. PhD thesis, Dept. of Civil Engineering, Univ. of California, Berkeley.

Schneider J.A. (2008). Analysis of piezocone data for displacement pile design. PhD thesis, University of Western Australia.

Schneider J.A., Fahey M. & Lehane B.M. (2008). Characterisation of an unsaturated sand deposit by in-situ testing. Proc. 3rd International Conf. on site characterisation, Taipei.

Tabucannon J.T. (1997). Shaft resistance of piles in sand. PhD Dissertation, University of Sydney, Australia.

Uesugi, M., & Kishida, H. (1986). Frictional resistance at yield between dry sand and mild steel, Soils and Foundations, 26(4), 139–149.

Van Impe W.A., De Beer E. & Lousberg E. (1988). Prediction of the single bearing capacity in granular soils from CPT results. International Symposium in Penetration testing (ISOPT 1), Speciality Session, Orlando.

White, D.J. & Bolton, M.D. (2005). Comparing CPT and pile base resistance in sand. ICE, Geotechnical Engineering, 158: 3–14.

Xu X., Schneider J.A. & Lehane B.M. (2008). CPT methods for assessment of end bearing of open and closed ended driven piles in siliceous sand. Canadian Geotechnical Journal (in press).

Keynote lecture 4: Energy pile concepts

Deep Foundations on Bored and Auger Piles – Van Impe & Van Impe (eds)
© 2009 Taylor & Francis Group, London, ISBN 978-0-415-47556-3

Energy piles concepts

H. Brandl
Vienna University of Technology, Vienna, Austria

ABSTRACT: Energy foundations, especially energy piles contribute increasingly to environmental protection and provide substantial long-term cost savings and minimised maintenance. The paper deals with thermo-active circuits and design aspects of energy foundations focusing on energy piles. Theoretical aspects refer to the heat transfer between absorber fluid, pile concrete and soil. Case histories and recommendations for absorber pipe installation in energy piles bridge the gap between theory and practice. Furthermore, the benefits of energy foundations are summarised and hints for promoting geothermal energy utilisation are given, gained from 25 years of experience with thermo-active ground structures (energy piles, etc.).

1 INTRODUCTION

At the BAP III-Seminar 1998 the author delivered the Keynote lecture "Energy piles and diaphragm walls for heat transfer from and into the ground". During the past 10 years since then this technology has developed extremely well spreading to many countries Austria has still a pioneering role as indicated in Fig. 1, showing the increase of energy piles between 1984 and 2004. Since the year 2005 more than 6000 energy piles have been installed per year resulting in a total number of presently more than 50 000 energy piles. Moreover, "Energy diaphragm walls" (slurry trench walls) have become a frequently used alternative to energy piles in Austria. Numerous buildings with deep basements and metro lines, e.g. all new stations of the Vienna Metro have "Energy diaphragm walls". They dominate especially in areas with a

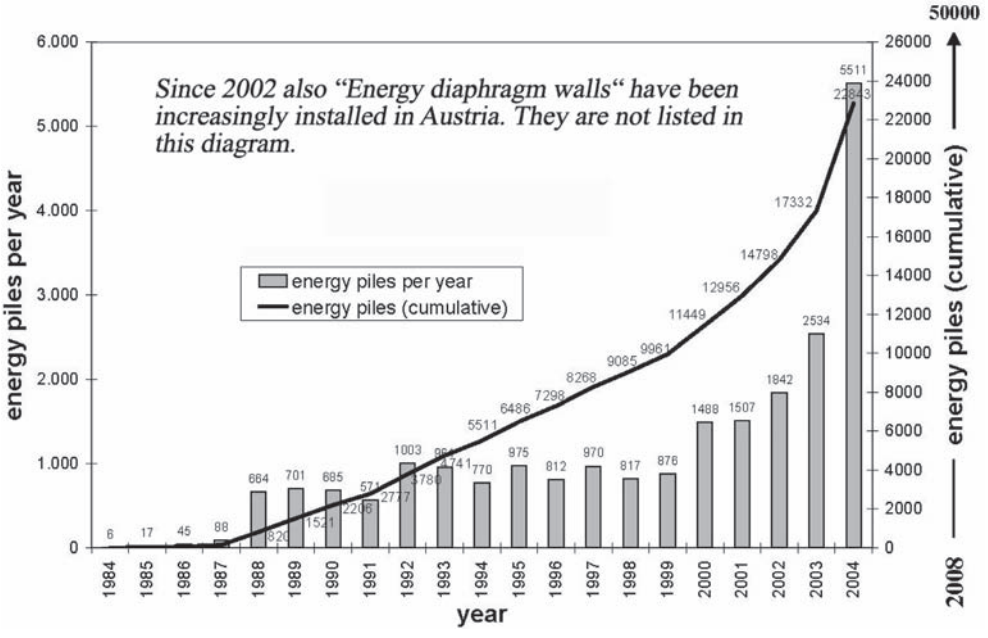

Figure 1. Number of energy piles installed in Austria; since 2005 more than 6000 energy piles per year.

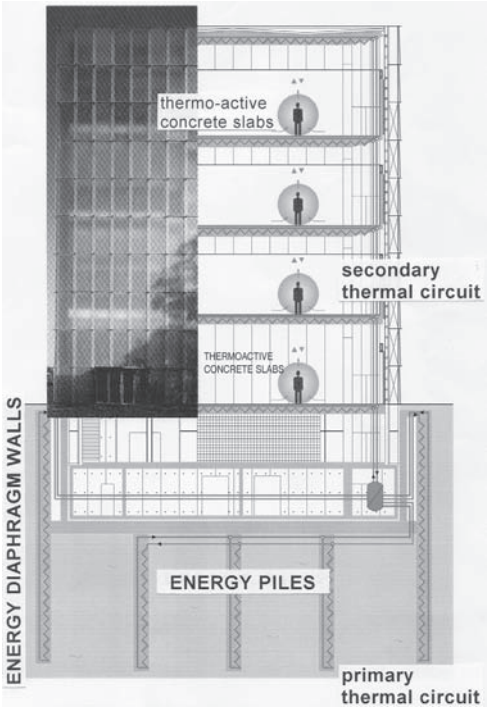

Figure 2. Cross section through an Arts Centre with geothermal cooling and heating: energy diaphragm walls and piled raft (with energy piles).

high groundwater level, whereby concepts combined with energy piles have proved suitable in many cases (Fig. 2).

The dominating ground-sourced elements are energy foundations, but energy tunnels, energy wells, retaining structures etc. are also used. Energy foundations may comprise base slabs, piles barrettes, slurry trench systems (single elements or continuous diaphragm walls), concrete columns, and grouted stone columns. Combinations with near-surface earth collectors and retaining structures are also possible. Thermo-active ground structures or wells can be used for heating and/or cooling buildings of all sizes, as well as for road pavements, bridge decks, etc.

A seasonal operation with an energy balance of heating and cooling has proved to be most economical and environmentally friendly. This would also correspond to changing energy consumption of houses since the 1970s. According to Fig. 3 the required energy for heating has decreased significantly, but on the other hand the energy for cooling is increasing, mainly due to large glass facades and permanently closed windows of modern architecture.

Comparative investigations have disclosed that for a life-time of more than 50 years the operation costs

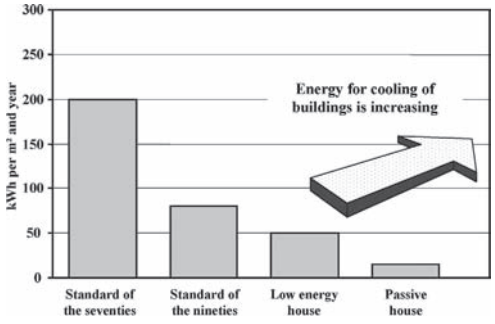

Figure 3. Required energy for the heating of houses in Austria. Improvements since the 1970s.

of houses (especially for residential and office buildings, shopping centres) are significantly higher than the construction costs. Therefore, optimised energy concepts are of greatest importance, also with regard to environmental aspects.

2 THERMO-ACTIVE CIRCUITS FOR ENERGY FOUNDATIONS

A thermo-active system consists of the primary circuit below ground and the secondary circuit in the building (Fig. 2).

The primary circuit contains closed pipework in earth-contact concrete elements (piles, barrettes, diaphragm walls, columns, base slabs, and wells) through which a heat carrier fluid is pumped that exchanges energy from the building with the ground. The heat carrier fluid is a heat transfer medium of either water, water with antifreeze (glycol) or a saline solution. Glycol–water mixtures have proved most suitable, containing also additives to prevent corrosion in the header block, valves, the heat pump, etc. Once cast, the pipings within the underground-contact concrete elements are individually joined to a header and manifold block. They are joined by connecting pipes which, in the case of energy foundations, are normally laid within the blinding beneath the base slab. The secondary circuit is a closed fluid-based building heating or cooling network (secondary pipework) embedded in the floors and walls of the structure or in bridge decks, road structures, platforms, etc.

Commonly, primary and secondary circuits are connected via a heat pump that increases the temperature level, typically from 10–15°C to a level between 25°C and 35°C (Fig. 4).

All that is required for this process is a low application of electrical energy for raising the originally non-usable heat resources to a higher, usable temperature. The principle of a heat pump is similar to

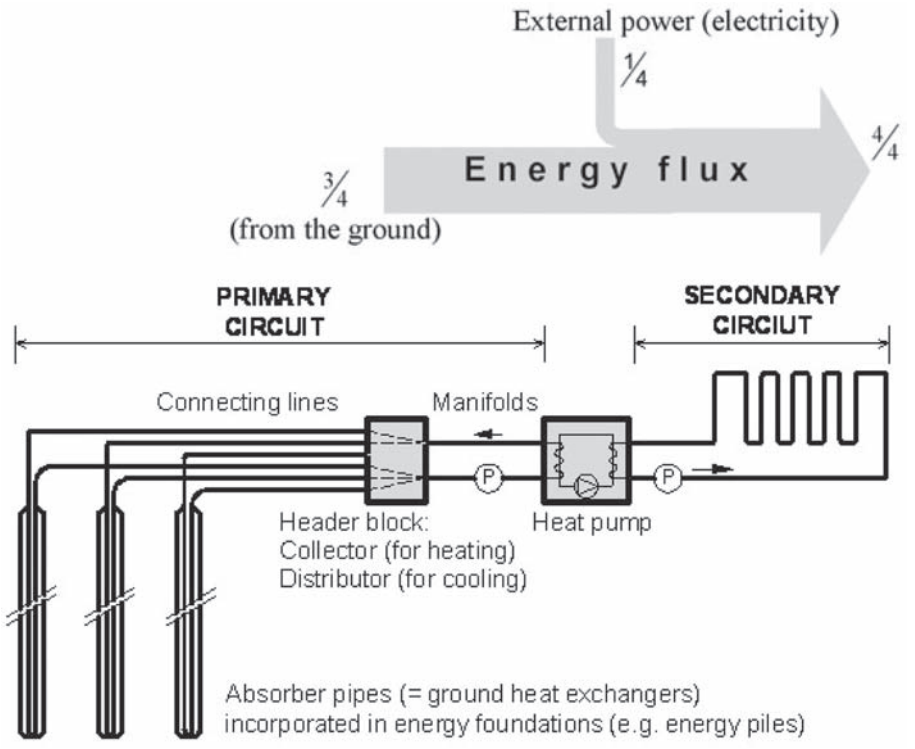

Figure 4. Scheme of a geothermal energy plant with energy piles and an energy flux for COP = 4 of the heat pump. COP = coefficient of performance defining the heat pump efficiency.

that of a reverse refrigerator. In the case of the heat pump, however, both the heat absorption in the evaporator and the heat emission in the condenser occur at a higher temperature, whereby the heating and not the cooling effect is utilised.

The coefficient of performance, COP, of a heat pump is a device parameter and defined by

$$COP = \frac{energy\ output\ after\ heating\ \ pump\,[kW]}{energy\ input\ \ for\ operation\,[kW]} \quad (1)$$

The value of COP = 4 means that from one portion of electrical energy and three portions of environmental energy from the ground four portions of usable energy are derived (Fig. 4).

The efficiency of a heat pump is strongly influenced by the difference between extracted and actually used temperature. A high user temperature (inflow temperature to the heating system of the secondary circuit) and a low extraction temperature (due to insufficient return-flow temperature) in the heat exchanger (primary circuit) reduce its efficiency. For economic reasons a value of COP = 4 should be achieved. Therefore, the usable temperature in the secondary circuit should not exceed 35–45°C, and the extraction temperature in the absorber pipes should not fall below 0–5°C. Consequently, this technology tends to be limited to low temperature heating (and cooling).

The seasonal performance factor (SPF) of a thermo-active system with a heat pump is the ratio of the usable energy output of the system to the energy input required to obtain it. Therefore SPF includes not only the heat pump but also other energy-consuming elements (e.g. circulation pumps). At present, values of SPF = 3.8–4.3 are achieved with standard electric heat pumps. Special devices with direct vaporisation increase SPF by 10–15%.

$$SPF = \frac{useable\ energy\ output\ of\ \ the\ energy\ system\,[kWh]}{energy\ input\ of\ \ the\ energy\ system\,[kWh]} \quad (2)$$

If only heating or only cooling is performed, high-permeability ground and goundwater with a high hydraulic gradient are of advantage. However, the most economical and environmentally friendly is a seasonal operation with an energy balance throughout

the year, hence heating in winter (i.e. heat extraction from the ground) and cooling in summer (i.e. heat sinking/recharging into the ground). In this case low-permeability ground and groundwater with only low hydraulic gradients are favourable.

There is no limitation to the depth of piles as far as the installation of energy absorber systems is concerned. The energy potential increases with depth: hence deeper ground-sourced energy systems are advantageous. The economically minimum length of piles, barrettes or diaphragm wall panels is about 6 m. Energy wells should reach deeper, because they have a lower heat transfer capacity.

3 DESIGN ASPECTS OF ENERGY FOUNDATIONS

Early ecological energy planning for building can often prevent costly refurbishment and renovation in the future. High-quality energy design involves not only heating and cooling (rooms, water) but also lighting, and it requires a multi-objective optimisation.

An optimised energetic-thermal design should also consider the seasonal heat loss from (un-)insulated slab-on grade floors or basement walls. Far more energy and costs are expended in running an inefficiently laid out building than in constructing an efficient one. A proper design should consider the efficiency of the overall building process, including the sustainability of all elements.

For general feasibility studies and pre-design of energy foundations the following assumptions can be made regarding the energy volume that can be extracted from thermo-active energy foundations:

- Pile foundations with piles D = 0.3 to 0.5 m: 40 to 60 W/m run
- Pile foundations with piles D $\geq$ 0,6 m: 35 W/m² earth-contact area
- Diaphragm walls, pile walls (fully embedding the soil): 30 W/m² earth-contact area
- Base slabs: 10 to 30 W/m².

Dry soil makes deeper piles and a larger area of the heat exchanger necessary. Moreover, a seasonal energy balance is required.

The heat that can be extracted from or fed into/ stored in the ground depends on the maximum possible heat flux density in the absorber pipe system. There, the heat transport occurs by forced convection of the fluid (usually an antifreeze—water mixture). In order to optimise the absorber pipe system the following parameters have to be considered:

- Diameter and length of pipes;
- Properties of pipe wall (roughness);
- Heat conductivity, specific heat capacity, density and viscosity of fluid circulating in absorber pipes;
- Flow velocity and flow conditions (laminar-turbulent) within absorber pipes.

Figure 5 gives a schematic overview of the heat transport within a thermo-active system consisting of energy piles. It illustrates that the heat flux $\dot{Q}_{\text{prim}}$ transported by heat carrier fluid in the primary circuit is given by the specific heat capacity c_{prim}, the mass flow $\dot{m}_{\text{prim}}$ and the temperature difference T_{prim}.

Complex ground properties and pile groups require numerical modelling of the geothermal heating/cooling system. Fig. 6 shows for example the daily mean temperatures in Vienna for the year 2001. Such data are needed to design a heating–cooling system whereby it is assumed that heating typically starts at external temperatures lower than 12 C. This provides the heating period for the unsteady numerical models. The seasonal course of the air temperature is simulated by a sinusoidal curve according to the following equation

$$T_{GS} = T_{m,out} + \Delta T_{out} \cos\left[\frac{2\pi}{P}\left(t - \varepsilon_t\right)\right] \qquad (3)$$

where $T_{GS}(t)$ is the ground surface temperature, t is time, $T_{m,out}$ is the average yearly temperature, ΔT_{out} is the temperature amplitude, P is the duration period, and ε_t is the phase displacement.

In the end, the monthly heating and cooling demands have to be compared with the available output, as indicated in Fig. 7.

Moreover, the seasonal course of the absorber fluid temperature (heat carrier fluid temperature) should be predicted.

Usually, a numerical simulation of the geothermal system is recommended for buildings with a heating and cooling demand of more than 50 kW. This rough value decreases to about 20 kW for buildings where rooms have to be cooled throughout the year. Geometric simplification may lead to significant errors in heat calculation. Therefore three-dimensional analyses should be conducted. The simulation should comprise the expected inflow and outflow temperatures at the energy foundations and the temperature distribution in the ground. Numerical models and computer programs should be reliably calibrated, that is on the basis of longterm measurements and experience from other sites, and on physical plausibility. Otherwise wrong results may be gained, even from well-known suppliers. Experience has shown that the results are very sensitive to even small changes in the finite element mesh. Consequently, the importance of numerical simulations lies rather in parametric studies

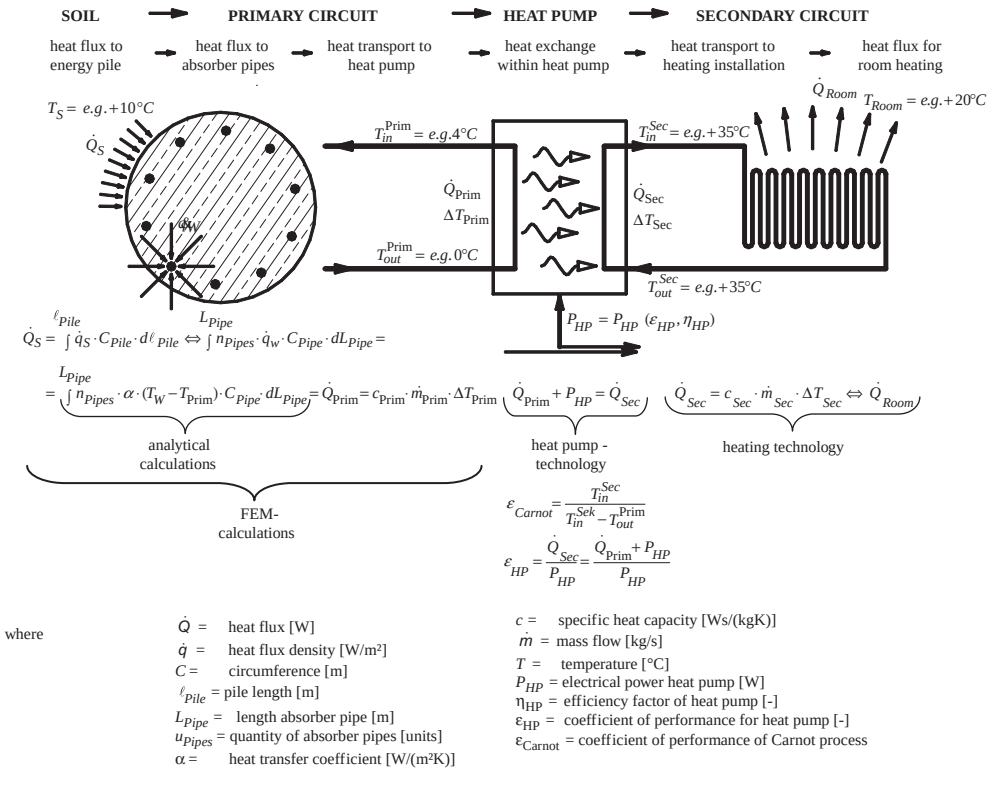

where

$\dot{Q}$ = heat flux [W]
$\dot{q}$ = heat flux density [W/m²]
C = circumference [m]
ℓ_{Pile} = pile length [m]
L_{Pipe} = length absorber pipe [m]
u_{Pipes} = quantity of absorber pipes [units]
α = heat transfer coefficient [W/(m²K)]
c = specific heat capacity [Ws/(kgK)]
$\dot{m}$ = mass flow [kg/s]
T = temperature [°C]
P_{HP} = electrical power heat pump [W]
η_{HP} = efficiency factor of heat pump [-]
ε_{HP} = coefficient of performance for heat pump [-]
ε_{Carnot} = coefficient of performance of Carnot process

Figure 5. Scheme of heat flux balance for heating in an energy pile plant.

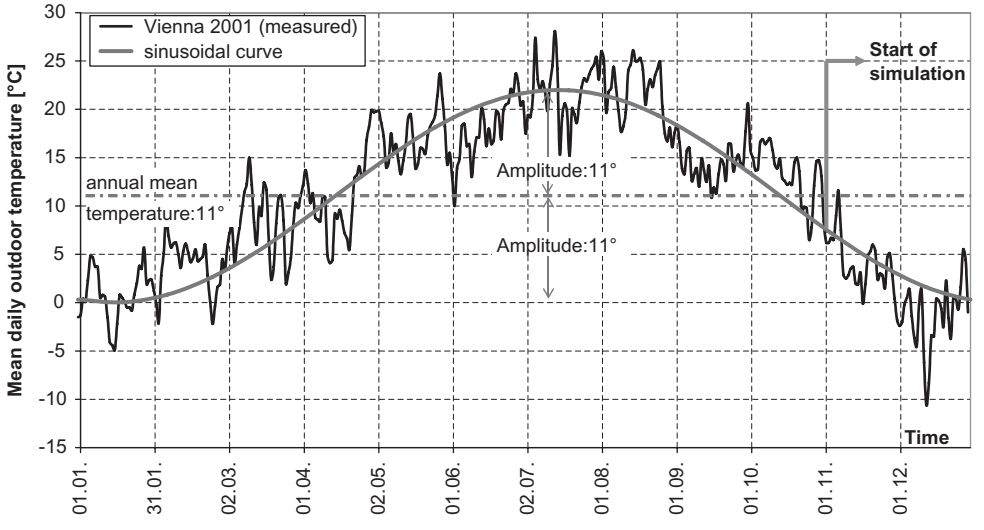

Figure 6. Mean daily outdoor temperatures in Vienna 2001, with idealised sinusoidal curve for numerical calculations.

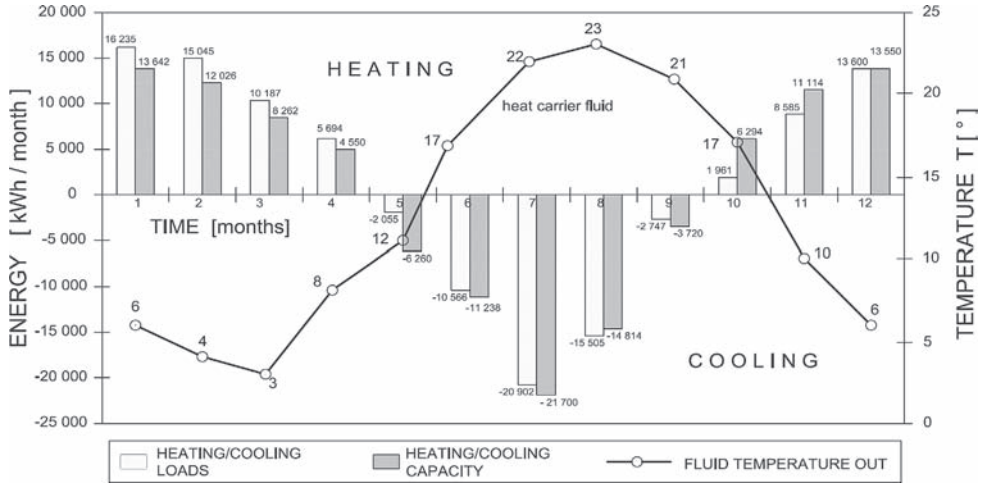

Figure 7. Example of energy demand and output for heating and cooling (annual distribution) of a building founded on energy piles. Temperature of heat carrier fluid is also shown.

(to investigate the influence of specific parameters) than in gaining 'exact' quantitative results.

Calculation of the temperature distribution in the ground due to energy foundations or energy wells is increasingly being demanded by local authorities for environmental risk assessment. This refers mainly to possible influences on adjacent ground properties and on the groundwater by the long-term operation of thermo-active deep foundations.

Monitoring of thermo-active ground-sourced systems is essential for an optimised long-term operation, and to enable sophisticated design of future projects.

Proper geothermal energy utilisation requires an interdisciplinary design, especially in the case of houses. Geotechnical engineer, architect, building equipment (sanitation) designer and installer, heating engineer and specialised plumber should cooperate as early as possible to create the most economical energy system. However, the tender for construction should clearly specify individual performances on the site. It has proved suitable to entrust a geothermally experienced plumber with all details of the primary and secondary circuits, beginning with the mounting of the absorber pipe systems in the foundation elements.

4 HEAT TRANSFER BETWEEN ABSORBER FLUID, PILE CONCRETE AND SOIL

4.1 *General*

Assuming that the walls of the absorber pipes of a ground heat exchanger have the same temperature as the surrounding concrete or soil respectively reduces the complex thermal problem (Fig. 8) to the heat transfer from pipe wall to absorber fluid (heat carrier fluid). This is essentially influenced by the flow behaviour of the fluid, i.e. laminar or turbulent.

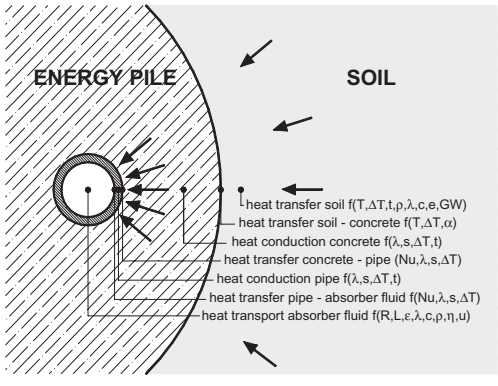

Figure 8. Heat transport from soil to heat carrier fluid within the absorber pipe of an energy pile. (GW = ground water).

Pipe flow is described by two zones (Fig. 9): The transient inflow zone where flow velocity and temperature-profile change with pipe length, followed by the steady-state condition with a constant hydrodynamic and thermal profile. The heat transfer does not change then (at constant thermal conductivity). In absorber pipes in thermo-active foundations, retaining walls, tunnels, pipe wells and roads the steady-state phase dominates. Furthermore, this state is reached already after a short distance. Hence, the

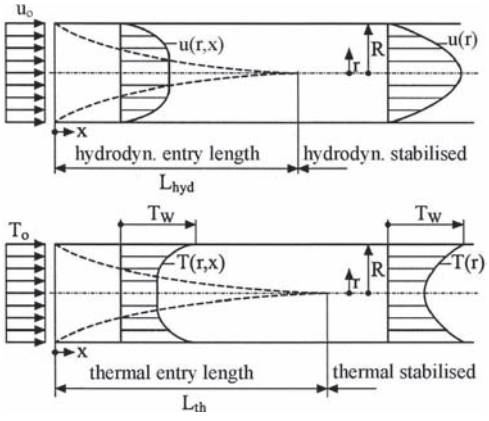

Figure 9. Flow velocity and temperature distribution in absorber pipes filled with heat carrier fluid.

following theoretical considerations are limited to the steady-state flow and heat transfer problem (Adam & Markiewicz, 2002).

Laminar flow in a pipe is based on flow paths with different velocities u and interface friction t that is proportional to the velocity gradient *du/dx* perpendicular to the flow direction. The coefficient of proportionality is the viscosity η that increases with temperature. Figure 10 shows an example of a typical absorber fluid for energy foundations (an antifreeze—water mixture). For this purpose Newton's friction law can be applied:

$$\tau = \eta \frac{du}{dx} \tag{4}$$

The mean velocity of laminar flow is $u_{mean} = 0.5\ u_{max}$, and for turbulent flow $u_{mean} = 0.80$ to $0.85\ u_{max}$. The transition from laminar to turbulent flow condition is described by Reynolds' number

$$\mathrm{Re} = \frac{ud}{\nu} \text{ with } \nu = \frac{\eta}{\rho} \tag{5}$$

where

u = mean velocity [m/s]
d = pipe diameter [m]
υ = cinematic viscosity [m²/s]
η = dynamic viscosity [kg/ms]
ρ = density [kg/m³]

Below the critical Reynolds' number Re = 2300 laminar flow occurs, and above Re > 104 full turbulence exists. Between these boundary values transient conditions occur. Turbulence increases the diffusive transfer of energy, impulse and mass. This effect increases with flow velocity.

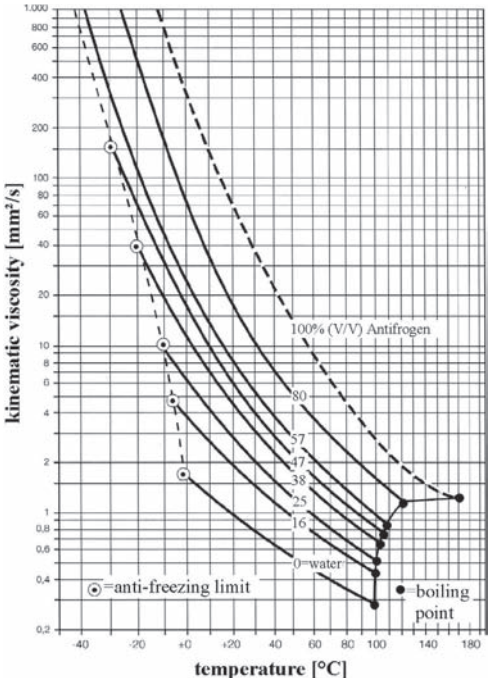

Figure 10. Kinematic viscosity versus temperature for different mixtures of water and Antifrogen L.

4.2 *Heat transfer by convection*

Heat transfer through contact is based on Fourier's law of molecular heat transport which can be written for one-dimensional problems

$$\dot{q} = -\lambda \left(\frac{\partial T}{\partial x} \right) \tag{6}$$

where

$\dot{q}$ = heat flux density [W/m²]
λ = thermal conductivity of the flowing medium [W/(m K)]
T = temperature
x = local coordinate

Heat transfer between masses not moving relative to each other occurs by conduction. Heat transfer by convection is based on differential movements. The latter occur between pipe wall and absorber fluid, whereby molecular heat transfer takes place at the interface:

$$\dot{q}_w = -\lambda \left(\frac{\partial T}{\partial r} \right)_{\text{wall}} \tag{7}$$

where $\dot{q}_w$ is the heat flux density at the pipe wall [W/m²].

The heat transfer between pipe wall and the fluid can be described by the heat transfer coefficient α

$$\alpha = \frac{\dot{q}_w}{T_{\text{wall}} - T_{\text{fluid}}} = \frac{-\lambda\left(\frac{\partial T}{\partial r}\right)_{\text{wall}}}{\Delta T} \tag{8}$$

and by Nusselt's number Nu which is defined as follows:

$$Nu = \frac{\alpha d}{\lambda} = \frac{-\left(\frac{\partial T}{\partial r}\right)_{\text{wall}}}{\frac{\Delta T}{d}} \tag{9}$$

Under turbulent conditions the heat transfer velocity depends not only on the self-velocity of the energy carrier (heat carrier fluid) but also on that of the turbulent fluctuations which is connected to the average flow velocity of the absorber fluid. Consequently, the heat transfer depends also on the flow velocity, and the heat transfer coefficient α is a function of material properties, geometric dimensions, length of heat transfer occurrence, and flow velocity of absorber fluid.

Calculation of the temperature gradient $(\partial T/\partial r)_{\text{wall}}$ at the pipe wall is only possible as long as equation (6) is valid in each point of the absorber fluid. But this applies only to laminar flow without friction or to motionless media. For turbulence, equation (6) is valid only for the pipe wall (according to equation (7)) but not for the interior of the flowing medium. Hitherto, no exact theory exists for this thermal problem; it can be solved only by equations based on experimental data (VDI, 1977).

4.3 *Heat transfer by forced convection*

The absorber pipes of a heat exchanger are part of a closed circuit (primary circuit in Fig. 4) where the flow is created by a pump. Therefore it is called *forced convection*. Commonly, the calculation is based on steady-state conditions, whereby the flow velocities should not be too low.

The flow velocity $u(r)$ within a circuit is different at each point of a cross section. Consequently, the period t for which individual fluid particles remain within a certain absorber pipe section differs. According to equation (12) in (Brandl, 2006) one-dimensional conditions can be described by

$$\rho c \frac{\partial T}{\partial t} = \lambda \frac{\partial^2 T}{\partial r^2} \tag{10}$$

where

þ is the density
c is the specific heat capacity
λ is the thermal conductivity

of the flowing medium. The different time periods of the fluid absorber staying in particular sections are $t = x/u(r)$ with the radial distance r according to Fig. 11. This leads to

$$\rho c\, u(r) \frac{\partial T}{\partial x} = \lambda \frac{1}{r} \frac{\partial}{\partial r}\left(r \frac{\partial T}{\partial r}\right) \tag{11}$$

Furthermore, another dimensionless coefficient is used for parametric studies: the Prandtl number *Pr* as a material-dependent value which is defined as

$$Pr = \frac{\nu}{a} = \frac{\nu \rho c}{\lambda} \tag{12}$$

For $Pr \to 0$ the velocity profile along a flow path *x*, where the heat is transferred, is equivalent to the profile of a piston flow. In the case of $Pr \to \infty$ the velocity profile corresponds to the Hagen-Poiseulle flow (Fig. 11). Common absorber fluids exhibit a value of about

$Pr = 7$ clean water close to the freezing point
$Pr = 70$ viscous fluid, such as water-glycol mixture as anti-freeze medium

Commonly, the heat transfer from concrete or soil to the absorber fluid occurs at a widely constant pipe wall temperature (T_w) along the entire pipe length, *if laminar flow conditions prevail*. For a mean fluid temperature T_m the molecular heat transfer can be described then be equation (14) and Fig. 12 (left).

$$\frac{\partial T}{\partial x} = \frac{T_W - T}{T_W - T_m} \frac{dT_m}{dx} \tag{13}$$

$$\rho c\, u(r) \left(\frac{T_W - T}{T_W - T_m}\right) \frac{dT_m}{dx} = \lambda \frac{1}{r} \frac{\partial}{\partial r}\left(r \frac{\partial T}{\partial r}\right) \tag{14}$$

In the case of constant heat flux density $\dot{q}_w = \alpha (T_w - T_m)$ the heat transfer coefficient α is constant:

$$\alpha = \frac{q_W}{T_W - T_m} = \frac{\lambda}{R} \left(\frac{\partial}{\partial \left(\frac{z}{R}\right)} \left(\frac{T_W - T}{T_W - T_m}\right) \right)_{\text{wall}} \tag{15}$$

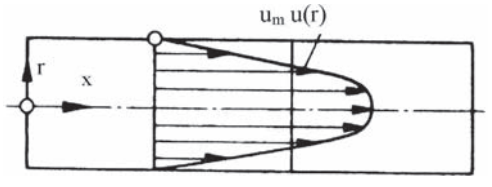

Figure 11. Flow velocity distribution in pipes (Hagen-Poiseuille's parabola).

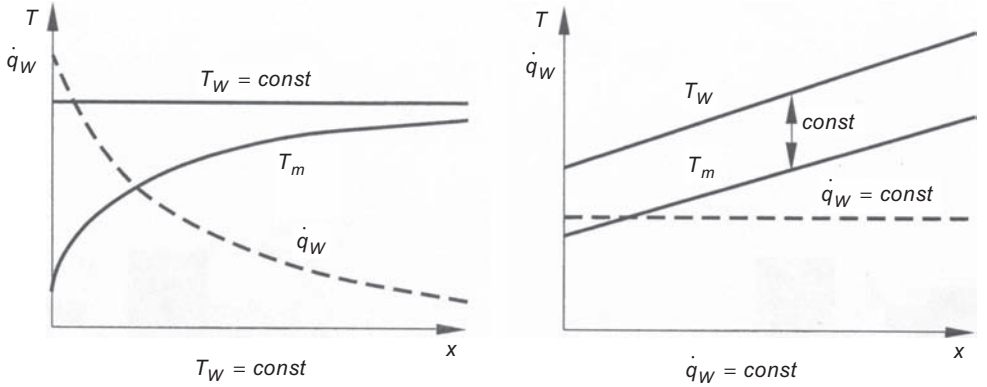

Figure 12. Heat conditions for constant temperature (left) and constant heat flux density (right) at the wall of an absorber pipe.

In this case the temperature difference $T_w - T_m$ is also constant leading to

$$\frac{\partial T}{\partial x} = \frac{dT_W}{dx} = \frac{dT_m}{dx} \tag{16}$$

This finally gives a molecular heat transfer according to equation (17) and Fig. 12 (right).

$$\rho c\, u(r) \frac{dT_m}{dx} = \lambda \frac{1}{r} \frac{\partial}{\partial r}\left(r \frac{\partial T}{\partial r} \right) \tag{17}$$

Turbulent flow conditions in the absorber pipe include a laminar zone close to the pipe wall where the local flow velocity is finally zero (Fig. 13). Equation (4) is then valid only along the pipe wall but not within the core of the flux. The shear stress τ_w along the wall is

$$\tau_W = -\eta \frac{u'}{\varepsilon_l} = \frac{\xi}{8} \rho u_c^2 \tag{18}$$

where
u_c is the flow velocity in the core of the fluid
u' is the flow velocity along the laminar (viscous) edge zone
ξ is the coefficient of flow pressure loss within the pipe system
ε_l is the thickness of the laminar (viscous) edge zone.

Energy and impulse transfer within this core is achieved by so-called *turbulence balls* continually entering and leaving the laminar edge zone, thus undergoing an average velocity change from ucore to u' and vice versa. These oscillating balls have a mass flux density of $\dot{m}_r$, and the shear stress $\dot{\tau}$ along ε_l is

$$\tau' = \dot{m}_r \left(u_c - u' \right) \tag{19}$$

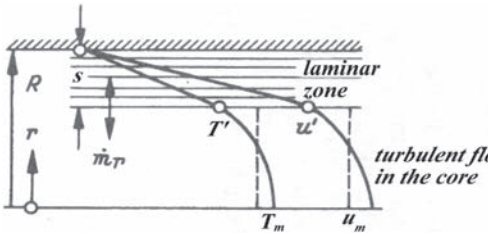

Figure 13. Turbulent flow conditions with a laminar flow area along the wall of an absorber pipe.

In a similar way the heat flux density $\dot{q}$ transferred by these turbulence balls can be expressed by

$$\dot{q}' = \dot{m}_r c \left(T' - T_c \right) \tag{20}$$

The temperature profile in a cross section is similar to the flow velocity profile (Fig. 13). Thus, the heat flux density $\dot{q}_w$ at the pipe wall becomes

$$\dot{q}_W = -\lambda \frac{T'}{\varepsilon_l} = \alpha T_c \text{ or } \alpha = \frac{\dot{q}_W}{T_W - T_c} \tag{21}$$

where
T_c is the temperature in the core of the fluid,
T' is the temperature at the laminar (viscous) edge zone
T_w is the temperature on the wall
ε_l is the thickness of the laminar (viscous) edge zone

Equations (18) to (21) lead to Prandtl's basic equation for the relationship between heat transfer and flow resistance:

$$\frac{Nu}{\mathrm{Re}\,\mathrm{Pr}} = \frac{\xi}{8} \frac{1}{1 + (\mathrm{Pr} - 1) \dfrac{u'}{u_c}} \tag{22}$$

The velocity ratio u'/u_c is then substituted by 12.7 $\sqrt{\xi/8}$, which represents a suitable approach. Further sophistications are based on experimental data leading finally to a formula that also considers the length of the pipe system (Oertel, 2001):

$$Nu_{m,T} = \frac{\frac{\xi}{8}(\mathrm{Re}-1000)\mathrm{Pr}}{1+12{,}7\sqrt{\frac{\xi}{8}}\left(\sqrt[3]{\mathrm{Pr}^2}-1\right)} f \qquad (23)$$

with $$f = 1+\sqrt[3]{\left(\frac{d}{L}\right)^2} \qquad (24)$$

for $0.5 < Pr < 10^4$ and $2300 < \mathrm{Re} < 10^6$, and for $0 < d/L < 1$

Figure 14 considers *laminar and turbulent flow conditions* depending on the dimension-less numbers of Reynolds, Nusselt and Prandtl. When determining these parameters a possible temperature dependence of the material properties has to be taken into account, whereby in practice only the dynamicviscosity is influenced by temperature changes in a relevant way. Thus the Nusselt number becomes

$$Nu = Nu_m \left(\frac{\eta_m}{\eta_w}\right)^{0,14} \qquad (25)$$

where η_m is the dynamic viscosity at a caloric mean temperature T_m,

η_w is the dynamic viscosity at a wall temperature of T_w.

4.4 *Summarising remarks*

The material properties should be related to a mean temperature of $T_m = (T_{inflow} + T_{returnflow})/2$ which considers the inflow and return flow of the absorber fluid into/from the primary circuit.

The heat transfer coefficient α depends on the pipe diameter *d*, the pipe length *L*, the flow velocity u, the viscosity η, the density ρ, and the specific heat capacity c or thermal conductivity λ respectively. For laminar flow it can be determined theoretically; turbulence, however, requires experimental data. The heat transfer coefficient of turbulent flow is always higher than that of laminar flow: $\alpha_{laminar} \leq f(\sqrt{u})$ whereas α turbulent $= f(u^{3/4})$, if equal boundary conditions are assumed. The flow velocity is not only a criterion for the contact period but also for the intensity of a turbulent mixing.

The Nusselt number *Nu* is a valuable criterion to describe the heat transfer intensity from the absorber fluid to a particular section of the absorber pipe. But it does not describe the overall heat extraction (or storage) *Q* of the entire absorber system. For that variable the time period that an absorber fluid circulates within the heat exchanger has also to be considered.

Some guidelines for geothermal energy utilisation recommend creation of turbulent flow in the absorber pipes. However, this should not be generalised. In the case of longer heat extraction (or storage) the critical point is not the heat transfer but the quantity of heat energy economically extracted from or stored in the surrounding soil. High performance pumps, required to create turbulent conditions would therefore reduce

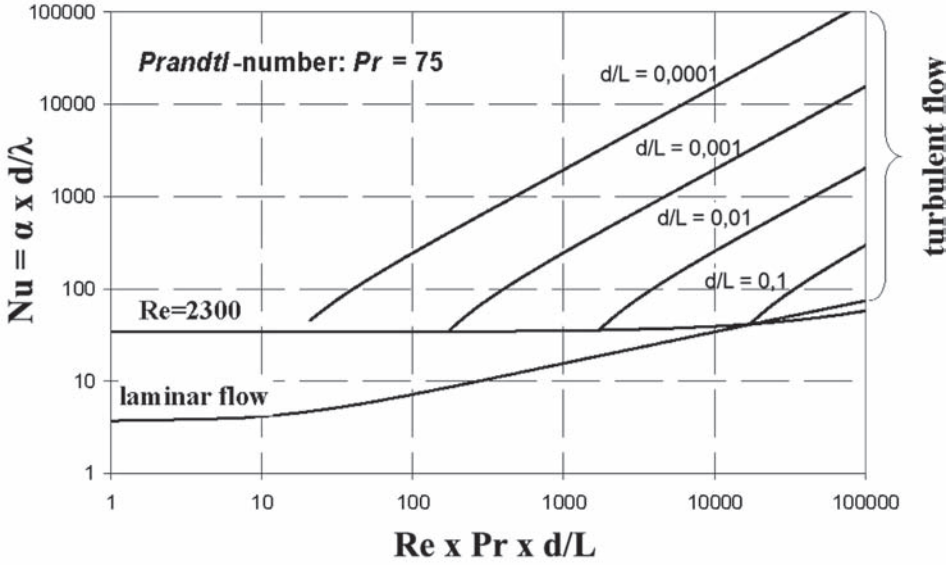

Figure 14. Heat transfer from absorber pipe wall to heat carrier fluid for different conditions.

the seasonal performance factor (SPF) of the overall geothermal system.

Figure 15 illustrates the performance balance of soil and absorber (heat exchanger) per metre run of an energy pile under steady-state conditions. The heat flux density $\dot{q}$ of the soil is compared with that of the absorber, $\dot{q}_w$, whereby the geometric conditions (circumference of pile C_{pile}, circumference absorber pipe C_{pipe}) and the number of absorber pipes has to be considered:

$$\dot{q}C_{pile} \leftrightarrow n\dot{q}_w C_{pipe} = n\alpha(T_w - T_m)C_{pipe} \qquad (26)$$

where n is the number of absorber pipes filled with heat carrier fluid.

Equation (26) does not include the heat transfer through the concrete cover and the pipe wall. This can only be simulated numerically.

4.5 *Numerical simulations*

In order to investigate the influence of individual parameters and their interaction comprehensive comparative studies were conducted (Markiewicz, 2004).

Heat transfer under *laminar flow conditions* depends on how long the fluid stays in the absorber pipes, on the pipe diameter, and on the density and thermal parameters of the absorber fluid.

When *laminar and turbulent flow conditions* are compared directly, the following conclusions can be drawn:

- Heat transfer under turbulent conditions depends significantly more on the input parameters. Under laminar conditions Nusselt's number is rather constant for all parameters.

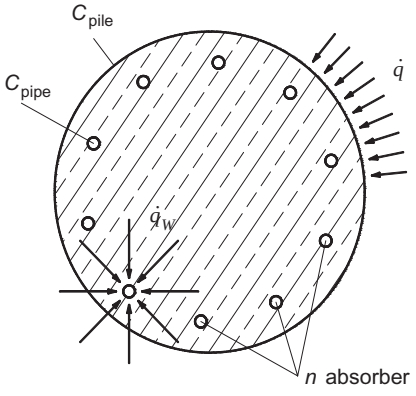

Figure 15. Heat volume balance for an energy pile. C = circumference of pile or pipe; $\dot{q}$ = heat flux density.

- Increasing the concentration of the water-glycol mixture increases the laminar zone, hence reduces the turbulent zone and therefore worsens heat transfer. If pure water is used as absorber fluid, turbulence occurs in nearly all cases, and Nusselt's number is about 15 times higher than for a water-glycol mixture. Nevertheless, in most cases an anti-freeze is unavoidable, because temperatures below 0°C are possible during operation. It should be considered that—when using a heat pump—the fluid temperature at the vaporizer is still about 2°C lower than the inflow temperature. This involves the danger of freezing/icing in the heat pump.
- Under laminar conditions the flow velocity is independent of the pipe diameter. It only depends on pump performance, pump efficiency, pipe length and on the flow parameters (kinematic viscosity and density). Furthermore, it increases with the operating temperature, whereas under turbulent conditions the flow velocity is rather independent of the temperature.
- Under laminar conditions the pipe diameter does not influence the residence period of the heat carrier fluid within the ground heat exchanger (absorber pipes), whereas under turbulence this duration increases with pipe diameter.
- In small-diameter pipes and at low operating temperatures laminar flow occurs practically in all cases.
- If small-diameter pipes are used Nusselt's number can hardly be increased by increasing the pump performance. Hence, installing pumps with higher capacity is then of no use. However, in the case of large-diameter pipes turbulent flow condi-tions can be achieved rapidly by increasing the pump performance. This also increases the heat transfer from absorber pipe wall to absorber fluid.
- With decreasing pipe diameter the total flow resistance that has to be overcome by the pump increases, as pipe wall friction related to the diameter increases. For diameters of d = 2 to 4 cm the pressure remains nearly constant, but for smaller diameters it increases over-proportionally. Furthermore, the pressure increases with low operating temperature because the viscosity of the fluid increases.

5 CASE HISTORIES

5.1 *Heating and cooling of a rehabilitation centre*

Figure 16 shows the ground plan of a case history that was already presented during the BAP III-Seminar (Brandl, 1998). 175 bored piles (D = 1.2 m)

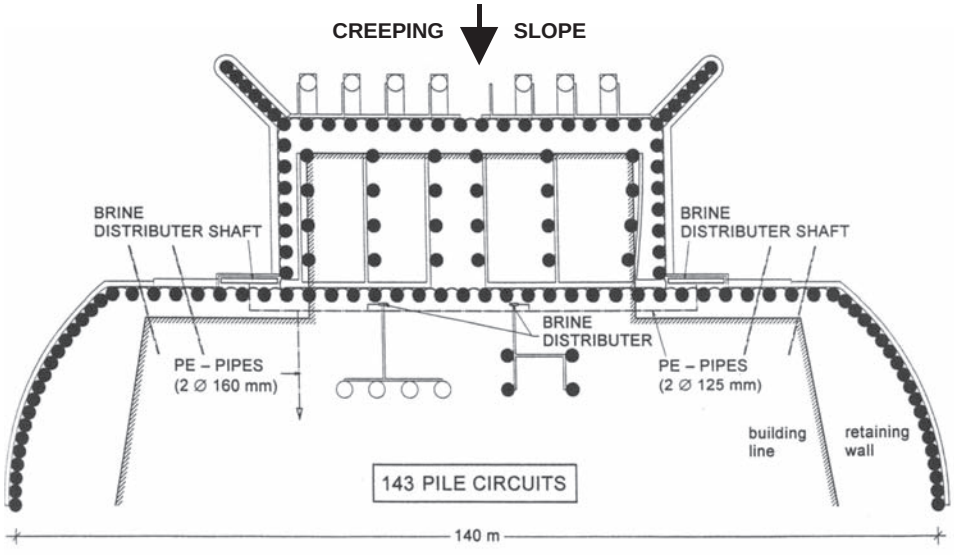

Figure 16. Ground plan of the rehabilitation centre Bad Schallerbach/Austria with energy piles and energy transfer system.

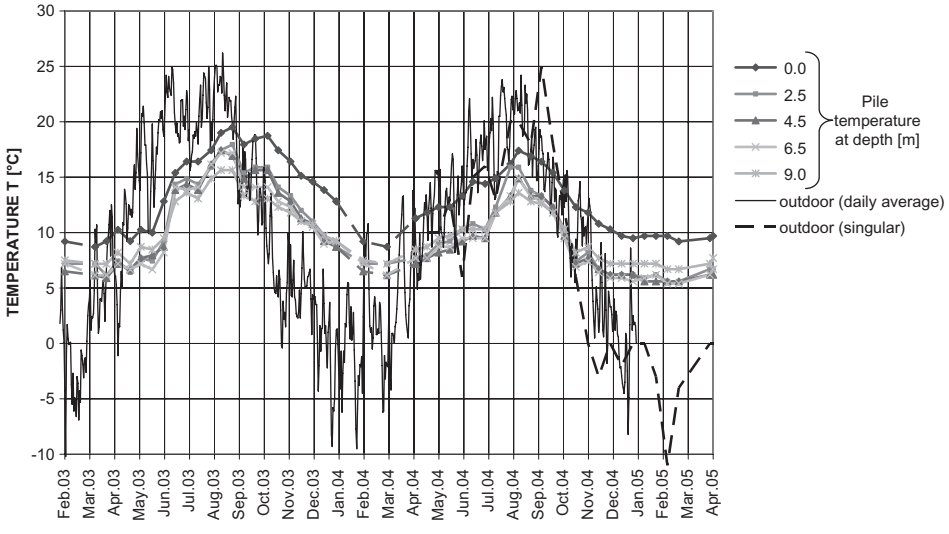

Figure 17. Outdoor temperature near the rehabilitation centre and temperature within energy pile (one of the "measuring piles" in Fig. 16). Strong heat wave in summer 2003; more normal temperature distribution in 2004; cold summer and warm autumn in 2005.

were installed as retaining structure and as foundation elements of a rehabilitation centre situated in a creeping slope. 143 piles are fitted with heat exchangers and hence act as energy piles for heating and cooling.

Since autumn 1997 the energy piles have been under full operation without any problem. Long-term monitoring revealed typical seasonal temperature fluctuations with relatively large amplitudes of maximum and minimum pile temperatures in sum-

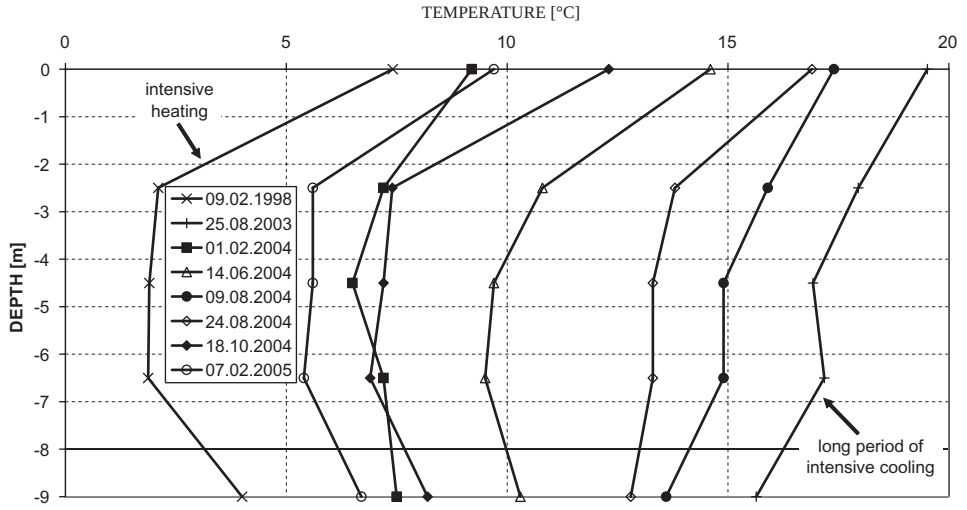

Figure 18. Temperature within energy pile against pile depth; data from long-term operation illustrating the seasonal fluctuation.

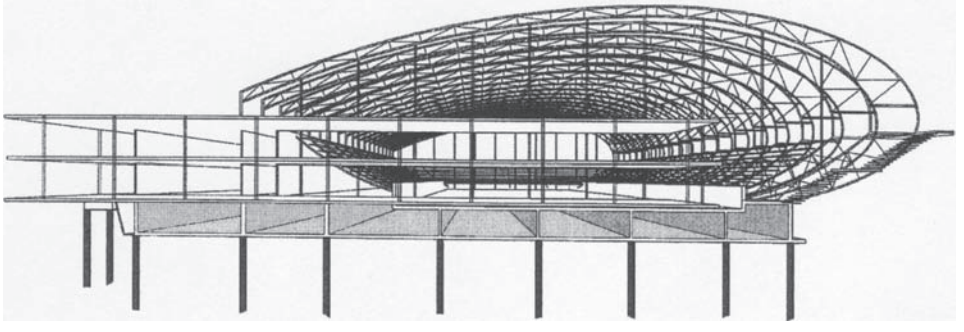

Figure 19. Energy piles for heating and cooling a multi-purpose hall.

mer and winter—as intended for this pilot project. Consequently, the pile temperatures in the subsequent winter were somewhat higher than in the quasi-steady state before. Moreover, Fig. 17 reveals that daily outdoor mean values are needed for a reliable interpretation. Only singular outdoor temperature measurements parallel to pile temperature measurements are not sufficient (indicated in the diagram from April 2004 to April 2005).

In Fig. 18 some temperature curves are selected as examples of heating and cooling periods in relevant years. Immediately after commencing continuous operation of the geothermal system started (with excessive heating); the year 2003 had a very high cooling demand, and there was quasi-steady state in the year 2004/2005.

5.2 *Heating and cooling of a Multi-purpose Hall, of a Spa Hotel, and of a Low-energy Shopping Centre*

A multi-purpose hall with a capacity of 8,000 persons was designed for exhibitions, fairs, and as a sports hall, especially as an ice rink. The latter required intensive cooling and temporary heating. The complex energy management could be solved with energy piles, because piles were already needed for a deep foundation of the structure resting on weak clays (Fig.19). The deep foundation comprises 320 cast in situ concrete piles (bored piles, $D = 0.5$ m) of 18 m length. The piles contain in total about 65 km absorber pipes (HDPE; $d = 25$ mm). This cooling/heating system provides an annual saving of 85,000 m^3 of natural

gas which is equivalent to an environmental relief of 73 tons CO_2.

In the same region a 43 m high Spa Hotel with geothermal heating and cooling was built. The core of the Spa centre comprises four floors with 6,500 m² of spa and fitness zones, and a 2,000 m² bath and sauna world. The energy foundation consists of 357 auger piles, 30 m long and includes 69,000 m of plastic pipes. Groundwater temperature is constant at 12°C. Primary and secondary energy circuits are connected by a 400 kW heat pump. In winter 1.6 GWh are extracted from the ground, corresponding to the energy demand of about 160 modern one-family houses. About the same heat volume is then sunk back into the ground when cooling the building in summer.

In 2007 Austria's first low-energy shopping centre was opened using its pile foundation for heating and cooling. 650 piles of in total 800 bored piles (diameter D = 0.9 m, some piles with D = 1.2 m; depth = 50 m) are equipped with absorber pipes. The subsoil consists of 3 to 5 m sandy gravel underlain by soft sandy-clayey silt (banded) down to 40 m, and finally sand to gravel. The groundwater level lies about 3 m below surface. Thus a significant magnitude of conventional energy can be saved: 4.1 GWh/a of fossil fuel, 61 MWh/a of electrical energy. Furthermore, the energy piles instead of conventional heating/cooling systems save nearly 550 tons of CO_2. Temporary surplus of geothermal energy is fed into the public district energy supply line.

5.3 *Energy tunnels using pile walls*

A tunnel may activate a significantly larger quantity of useable geothermal heat than deep foundations.

The energy can be used for heating and/or cooling railway stations, administration and residential buildings, and for keeping platforms, bridges, passages etc. free from ice in winter. Consequently, shallow tunnels (especially in cut and cover) make a wider application possible than deep-seated tunnels, because the heat transfer between source and user is easier.

The first thermo-active traffic tunnel ("Energy tunnel") was finished in 2003 running through the northern Vienna woods. The 12.8 km long tube was constructed in several sections and after different methods:

- "Cut and cover", consisting of large diameter bored piles, reinforced concrete base slab and roof. In this part "Energy piles" were installed.
- "New Austrian Tunnelling Method" (NATM) with a primary support of reinforced shotcrete, rock bolts and anchors, and a secondary lining of reinforced concrete. In this part "Energy geocomposites" were installed.
- Additionally, "Energy wells" were used to locally reduce the groundwater level.

Along the cut and cover tunnel the primary sidewall lining of the tunnel consists of bored piles, whereby each third pile is used as an energy pile

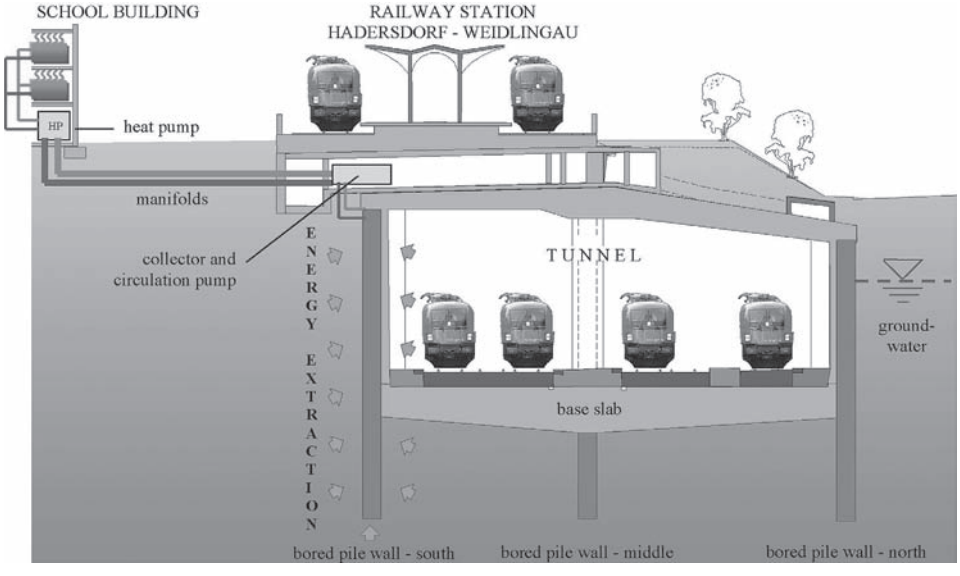

Figure 20. Schematic cross section of an energy plant as thermo-active tunnel ("energy tunnel"). One side wall of cut-and-cover tunnel used as energy wall. Bored pile walls (south-middle-north).

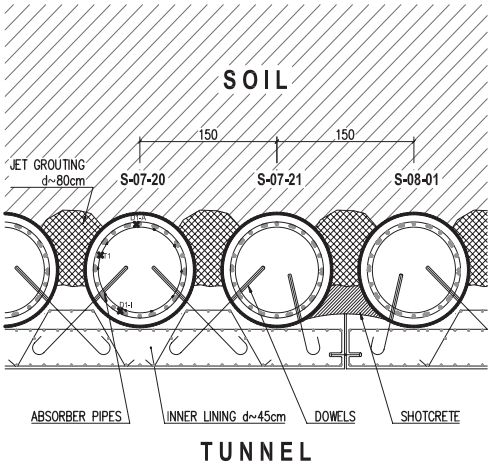

Figure 21. Detail to Fig. 20: Longitudinal section through the energy tunnel wall. The primary lining consists of bored piles with jet-grouted columns in between and is connected to the watertight secondary lining by dowels. Every third pile is equipped with absorber pipes that are situated behind reinforcement bars and thus protected from damage through dowel installation for the inner lining (reinforced concrete panels). Also shown is the location of measurement instruments in pile S-07 – 20.

Table 1. Technical data of the energy plant "LT24—Hadersdorf-Weidlingau".

Annual heating output: MWh	214
Energy piles	59 piles
Mean length: m	17.1
Heating capacity: kW	150
Required antifreeze passage: m^3/h	51.6
Absorber pipes	HDPE. d^o = 25 mm d^i = 20 mm
Absorber circuits	80 units
Absorber pipes in piles — total length: m	9,709
Connecting lines — total length: m	13,754

(Figs. 20, 21). Thus, the energy plant comprises 59 bored piles with a diameter of 1.2 m and an average pile length of about 17.1 m. The intermittent pile wall exhibits jet-grouting columns between the piles.

Pile excavation (by grab) was supported by casings using rotating equipment. The energy piles are equipped with absorber pipes connected to collectors/distributors which are located at a central point of the tunnel. The pipes leading from the piles to the collectors/distributors are placed alongside the cover of the tunnel. The connecting pipes are leading into a collector/distributor room that is easily accessible on top of the cut and cover tunnel and contains the header block with the collector/distributor for all collecting pipes. The manometers allow a detailed watertightness check of all absorber pipes. A manifold with a diameter of 150 mm connects the collectors/distributors with heat pumps in an adjacent school in order to heat the building. Table 1 gives the relevant technical data.

Preliminary calculations yielded an extractable thermal power of about 150 kW in the long term. In one heating period an energy amount of 214 MWh can be gained. Furthermore, the benefits of this new energy concept are both, environmentally friendly and economical: The reduction of natural gas of 34,000 m^3 per year leads to a decrease of annual CO2-emissions of 30 t. Furthermore, annual savings in operation costs of about 10,000 € are achieved—compared to the old natural gas heating system of the school building.

The plant was constructed as a demonstrating project in the context of a major research initiative by the Austrian Government. Due to this scientific background, the plant is intensively instrumented with measurement devices. Six energy piles are fitted with 18 temperature gauges in different levels; additionally, one pile is fitted with combined strain-temperature gauges in five levels for measuring strains and temperature. The aim of this measuring system is to investigate the effects of temperature changes within an energy pile on its bearing capacity and the temperature fluctuation in the energy piles during operation. Moreover, heat carrier fluid passage, total extracted heat, and temperatures in the manifold are monitored. The groundwater temperature surrounding the energy plant is also registered (at different distances). Temperature differences between energy piles (thermo-active and bearing function) and standard piles (only bearing function) have been checked by heat picture photographs. The differences can be registered even after the placement of the secondary lining, i.e. the reinforced concrete cover (Fig. 22).

The operation of the energy plant started in February 2004, and during the first testing phase initial data were obtained which could be used to optimise the absorber system. About 40 MWh of heating energy could be extracted from the energy piles during the first six weeks of operation. Since autumn 2004 the energy system runs permanently for a school near the tunnel. The external air temperature ("outdoor temperature") is used as criterion for regulating the energy system. Down to –5°C the school building can be fully heated with ground source energy. At lower temperatures the existing gas boiler furnace is added.

Figure 23 shows for example the specific strain in the measuring pile S-7–20 at different times plotted for the inner and outer side and the central axis. The zero-reading was before soil excavation in front of the pile wall. Therefore, the curves include both

mechanical and thermal effects, as can be clearly seen from the seasonal differences. The temperature-induced deformations are significantly smaller than those caused by earth pressure, and the natural fluctuation of the tunnel temperature has a greater influence than the temperature changes due to energy extraction/storage in the energy piles. Energy operation even creates a more uniform temperature in the piles, that is, smaller temperature differences between pile head/toe and inner/outer side. This thermal balancing-out reduces the temperature-induced statical moments in the energy piles.

Of course, the energy operation causes a stronger cooling or heating of the piles. But this occurs uniformly, hence causing a volumetric deformation without constraints, and therefore no additional load on the structure.

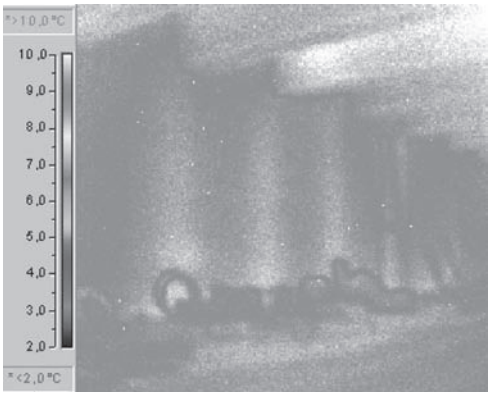

Figure 22. To Figs. 20, 21. Photo taken with a heat camera, showing (equally spaced) colder areas of the inner tunnel lining caused by energy piles.

6 INSTALLATION OF ABSORBER PIPES IN DEEP ENERGY FOUNDATIONS

Experience with energy piles since 25 years and with energy diaphragm walls since 12 years has disclosed that a proper installation of absorber pipes is essential for the long-term behaviour of the thermo-active system. Failures after this construction period are largely negligible.

Installing reinforcement cages fitted with absorber pipes into bored or auger piles, barrettes or diaphragm walls requires the following measures:

- Protection from mechanical damaging, especially in the case of cut by machine and non-deburred reinforcement bars.
- Protection from thermal damaging (during reinforcement welding).
- Exact positioning of the reinforcement cages (orientation of the connecting box).
- Constructing stiff reinforcement cages for deep foundations (e.g. welding of helical reinforcement to vertical rebars of deep piles, barrettes etc.).
- Lifting long reinforcement cages at both ends to prevent damage to the pressurised absorber pipe loops.
- Use of full tremie pipes to place concrete in pile bores; also for dry rotary-bored piles, where commonly self-compacting concrete is placed via a short tremie pipe from the ground surface.

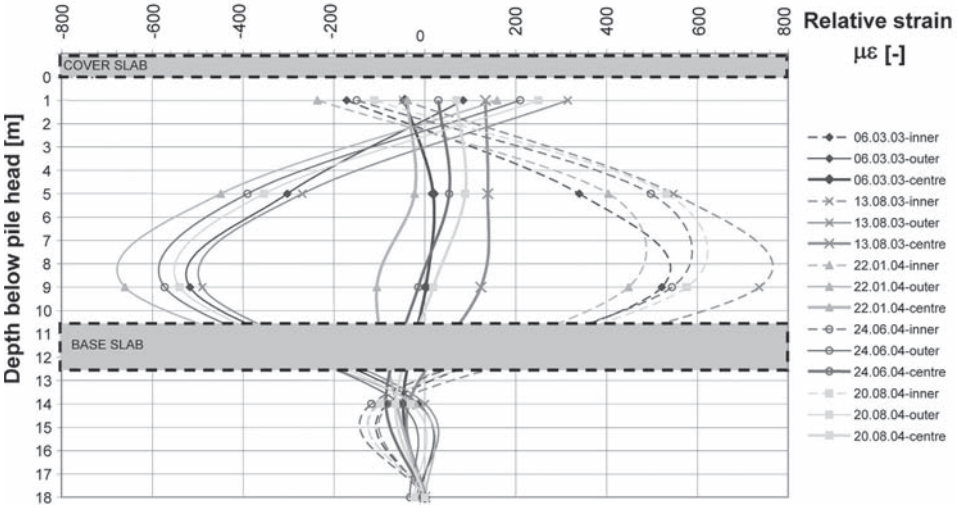

Figure 23. Relative strain along inner and outer (earth-) side and along centre line of an energy pile (S-07–20 in Fig.21).

- Upon the completion of the pipe work fixing on the reinforcement cage, a visual check on the final location of the pipes is imperative to ensure that the floor of the wet pile concrete though the reinforcement cage would not be impaired. The pipe ends near the bottom of the cage should be placed at different levels to help this.
- Very long reinforcement cages fitted with absorber pipes have to be installed in sections which should be coupled by screwing and not welding. The pipes are extended/coupled by electrically welded sleeves. Welding of the reinforcement sections is only unavoidable if a lightening protection element is attached. In such cases the absorber pipes have to be protected during welding by welding mats.
- Cautious insertion and withdrawal of the tremie pipes.
- Protection from torsion and heave of the reinforcement cage during concreting and steel pipe withdrawal.
- Sufficient distance of the absorber pipes from the reinforcement on head and toe of the piles, barrettes, or diaphragm wall panels.
- Special precautions have to be taken for energy piles or diaphragm walls used for cut and cover tunnels or retaining walls if they are covered by a secondary lining. In order to avoid damage of the absorber pipes when installing the connecting nails or dowels, the pipes should be protected by twin bars.

The absorber pipes in the foundation elements shall be kept under pressure in all construction stages. This enables prompt localisation of possible defects and repair in time. The collectors or distributors respectively of the absorber pipes should be fitted with optical flow meters for long-term monitoring of the fluid circulation in the geothermal system.

Special emphasis should be lain on the interface between energy piles and building (Fig. 24). For instance, joints caused by complex construction sequence require detailed planning and most careful execution when situated below the groundwater level. Consequently, it has proved suitable to collect the absorber pipes leading away from the pile heads to the header block in special boxes in order to minimise the openings through foundation rafts. Sealing with resin is also required then.

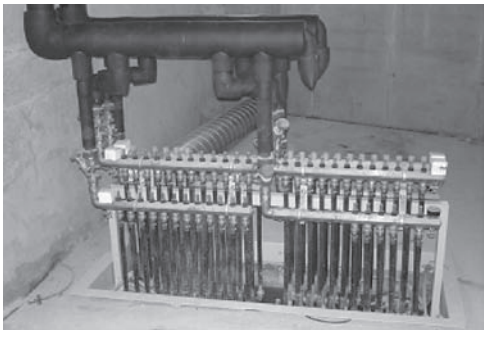

Figure 24. Interface between primary and secondary circuits (header block).

7 BENEFITS OF ENERGY FOUNDATIONS

The benefits of energy foundations and other thermo-active earth-contact structures may be summarised as follows:

- Environmentally friendly (non-polluting, sustainable energy).
- Reduction of fossil energy demand, hence of CO_2-emissions.
- Promoting the compliance with international environment obligations (Kyoto- and Toronto-targets, etc.).
- Economical, at least in the long term.
- Although thermo-active earth-contact structures commonly require similar or slightly higher investment costs, they have lower running costs, hence lower life-cycle costs than conventional systems.
- Low maintenance and long lifetime.
- Geothermal energy systems run fully automated.
- Thanks to the low temperature and pressure in the heat carrier circuits geothermal heating/cooling systems can be operated without risk.
- Closed primary heat carrier circuit embedded in concrete prevents damage of pipework or groundwater pollution.
- Increase of personal comfort in buildings (indoor rooms). The temperature personally felt there—the ambience experienced—consists of air and radiation temperature, which are influenced by wall and floor temperatures. Comfort is enhanced by low-temperature heating of walls and floors exhibiting a large heat-radiating surface.
- Optimal hygrothermal behaviour of buildings (e.g. for museums and arts centres).
- No storage of fossil fuel, no stove and chimney, no visible radiators are needed.
- Geothermal cooling may replace conventional air conditioning which is frequently felt to be loud and unhygienic.
- Geothermal energy may be easily combined with other energy systems.
- Unlike hydroelectricity, geothermal energy is not vulnerable to droughts.
- The cost of geothermal energy is not prone to unpredictable price fluctuations.
- Reduction of energy imports, hence lower dependency on external economical or political situations.
- Positive public image, and in several regions is supported by government grants.

8 PROMOTION OF GEOTHERMAL ENERGY UTILISATION

An early ecological energy planning for buildings can in many cases prevent costly refurbishment and renovation in the future. High-quality energy design involves not only heating and cooling (rooms, water) but also lighting.

Building biology (including building ecology) gains increasing importance in the fight against global warming, depletion of the ozone layer and exploitation of material resources. Building biology has become (or should become!) a multi-disciplinary science combining architecture, civil and geotechnical engineering, physics and chemistry, installation engineering, medicine and related sciences. It considers not only interactions of buildings and human health, but also energy concepts, the life cycle of building materials, sustainability, etc.

Geothermal geotechnics offers a promising alternative to conventional heating/cooling systems, providing solutions to the challenges of today's energy policies.

The targets for renewable energy and for energy buildings can be reached generally only by political measures:

- High taxes on fossil fuels are the most important prerequisite for energy saving and promotion of renewable energy sources.
- In order to promote the installation of thermo-active systems or/and other heating-cooling systems based on renewable energy, the economic incentives for private investors, house owners, companies, but also for public administrators to invest in renewable energy systems should be improved in many countries. A strong support by European Union policy is necessary.
- Legislation.
- Public grants.

Since January 2004 each person who wants to build a family house in Austria receives financial support by the local government only if they present a so-called "energy performance certificate" with low energy number. This number describes the energy consumption (provided heating energy minus heating losses) and is expressed in kWh/m^2 and year. Promotion by public funds is granted only if this energy number is smaller than 50 kWh/m^2 for each floor. At values less than 40, 30, 25, 20, 15 kWh/m^2 the grant increases step by step.

However, if a building is heated/cooled by means of clean, renewable energy, e.g. by geothermal systems, the allowable limit value for energy consumption may be increased. The target of multi-disciplinary innovations should approach heat-and-light systems combined with ground-sourced or solar residual heating/cooling.

Thermo-active structures (including energy foundations) are therefore very helpful in reaching this low energy number. Their installation is widely supported by politicians and media. Consequently, nearly 1000 buildings with energy foundations or retaining/basement walls already exist in Austria.

This "philosophy" is fully supported by the Directive 2002/91/EC of the European Parliament and of the Council on the energy performance of buildings. Thus an energy performance certificate has to be presented if a building with more than 500 m² is sold or rented.

9 CONCLUSIONS

25 years of experience with energy piles has disclosed that such environmentally friendly systems for heating and cooling of buildings have significant advantages over conventional technologies (fossil fuels etc.) and enable sustainable and clean energy consumption. Local climate and ground properties, technological level, the specific use of a building, seasonal fluctuations, environmental conditions and actual energy prices are the main influence parameters of an optimised integral design.

Energy systems based on earth-contact structural elements (energy piles, energy diaphragm walls, etc.) have a double function, and they work most efficiently if the thermo-active elements are in contact with groundwater. Nevertheless, a sufficient seasonal performance factor of the system is achievable even without groundwater, especially for seasonal operation, i.e. heating in winter and cooling in summer. Energy balance is the ideal form of heating/cooling. Moreover, the smaller the temperature difference between ground source energy and used energy, the higher is the seasonal performance factor, hence the efficiency of the thermo-active system. Usually, a temperature difference of only $\Delta T = 2$°C between absorber fluid inflow and return flow from the primary circuit is sufficient for an economical operation of the energy system. Consequently, such geothermal systems represent low-temperature systems. Experience has shown, that the electricity required for operating the entire system commonly varies between 20 to 30% of the total energy output. If no heat pump is necessary (e.g. for free cooling) this value drops to 1 to 3% for merely operating a circulation pump.

Despite overlapping integral design aspects there should be always a clear interface between energy foundations and building (household etc.) regarding responsibility of construction, quality control and assurance. It has proven suitable to consider this already in the tender design.

Proper operation of thermo-active foundation systems does not affect the load capacity of piles or diaphragm walls during geothermal cycles (as already stated in Brandl, 1998). Hence, temperature-induced settlement or heave of buildings with such energy foundations is negligible in relation to displacements caused by static loads.

Commonly, the groundwater temperature is changed by more than ±1°C only within a distance of less than 5 to 10 m to the earth-contact structural elements. These values could be found even for rather large thermo-active ground structures.

The drop out rate of properly installed energy piles is negligible and occurs practically only during construction. In Austria the failure rate usually is less than 2% of the required usable energy output of the entire energy system. If it is more, the construction firms have to pay for reduced quality. However, for safety reasons the energy foundations are commonly designed as if an energy loss of 10 % might occur. This over-design covers failures during the construction period that cannot be repaired and possible long-term failures or losses in the primary and secondary circuit of the energy system. Long-term failures within energy piles can be excluded if they are operated properly. Once, energy piles have passed positively the acceptance tests, no long-term failures could be observed until now.

Proper geothermal energy utilisation requires an inter-disciplinary design, especially in the case of houses. The geotechnical engineer, structural engineer, architect, building services designer and installer, heating engineer and specialised plumber should cooperate as early as possible to create a most economical energy system. In the first phase of operation precise adjustment is recommended to optimise the performance of the engineering system. Furthermore, some operation rules have to be considered (Brandl, 1998, 2006).

REFERENCES

Abu-Hamdeh, N., Khadair, A. & Reeder, R. (2001). A comparison of two methods used to evaluate thermal conductivity for some soils. Int. *Journal of Heat Mass Transfer* 44, No. 14, pp. 1073–1078.

Adam, D. & Markiewicz, R. (2002). Nutzung der geothermischen Energie mittels erdberührter Bauwerke. *Öster. Ingenieur- und Architekten-Zeitschrift*, Vienna Vol. 147, No. 4, 5 and 6.

Brandl, H. (2006). Energy foundations and other thermo-active ground structures. (Rankine-Lecture). *Géotechnique*, Vol. LVI No. 2, pp. 81–122.

Brandl, H. (1998). Energy piles and diaphragm walls for heat transfer from and into ground. *3rd Int. Geotechnical Seminar, Deep Foundations and Auger Piles (BAP III)*. University of Ghent. W.F.Van Impe (ed.). Proc.: A.A. Balkema, Rotterdam, pp. 37–60.

Enercretnägele (2004). Thermoaktive Fundamente. *Nägele-Reports*, Röthis, Austria.

Markiewicz, R. (2004). Numerische und experimentelle Untersuchungen zur Nutzung von geothermischer Energie mittels erdberührter Bauteile und Neuentwicklungen für den Tunnelbau. *Doctoral Thesis*. Institute for Soil Mechanics and Geotechnical Engineering, Vienna University of Technology.

Oertel, H. jr. (Hrsg.) (2001). Prandtl—Führer durch die Strömungslehre. Friedr. Vieweg & Sohn Verlagsges. mbH, Braunschweig, Germany.

Rees, S.W., Adjali, M.H., Zhou, Z., Davies, M. & Thomas, H.R. (2000). Ground heat transfer effects on the thermal performance of earth-contact structures. *Renewable and Sustainable Energy Reviews* 4, pp. 213–265.

Sanger, F.J. (1979). Degree-days and heat conduction in soils. *Proc. 1st Int. Conf. Permafrost*, pp. 253–262.

Sauty, J.P. (1980). An analysis of hydrodispersive transfer in aquifers. *Water Resource Res.* Vol. 18, No. 2, pp. 253–265.

Unterberger, W. et al. (2008). Praktische Erfahrungen beim Bau einer Erdwärmeanlage am Beispiel des Bauloses U2/2. *Betontag 2008*, Proc. Österreich. Vereinigung für Beton- und Bautechnik, Wien.

Verein Deutscher Ingenieure (1997). *VDI-Wärmeatlas*. Springer-Verlag Berlin Heidelberg.

Academics practitioners forum

Deep Foundations on Bored and Auger Piles – Van Impe & Van Impe (eds)
© 2009 Taylor & Francis Group, London, ISBN 978-0-415-47556-3

Summary

H.G. Poulos
Coffey Geotechnics and University of Sydney, Australia

ABSTRACT: This paper summarizes the format and intentions of the Academic—Practitioner Forum to be held during BAP V.

1 INTRODUCTION

There appears to be a persistent gap in communication between geotechnical academics and practitioners. Academics frequently view practitioners as being ignorant of new research findings and clinging to outmoded methods of analysis and design. Conversely, practitioners frequently view academics as "having their heads in the clouds" and undertaking research that is esoteric and not directly applicable to practice. In an effort to bridge the apparent communication gap between academics and practitioners, the International Society for Soil Mechanics and Geotechnical Engineering (ISSMGE) conducted an Academic-Practitioner Forum at their 16th International Conference in Osaka in 2005 (Poulos et al, 2006). Following the success of this event, similar forums have been arranged in other conferences, and this present event during BAP V will continue this recent tradition. It will however focus on issues that are specific to piling.

2 ISSUES TO BE DISCUSSED

The following two questions will be posed during this session, as follows:

1. *Should we continue to develop sophisticated methods of pile design, or else focus on improving the reliability of simpler design methods?*
2. *How reliable is the interpretation of dynamic pile testing of bored and auger piles, compared to that of driven piles? Are there other more reliable yet rapid and economical tests available for bored and auger piles?*

3 PARTICIPANTS

The following persons will participate in the Forum:

a. Academics
   Professor L. G. de Mello, Brazil
   Professor W. Hachich, Brazil
   Prof. C. Viggiani, Italy
b. Practitioners
   Mr. G. Murray, New Zealand
   Mr. G.P. Byrne, South Africa
   Mr. L. Maertens, Belgium

4 FORMAT OF FORUM

The format of the Forum will be as set out in Table 1. The rules for participations are as follows:

- Each person will have no more than 5 minutes for the presentation on each topic.
- No more than 8 slides can be shown during each presentation.

Table 1. Proposed format for Bap V Academic/Practitioner Forum.

Item	Time allowed (minutes)
Introduction by Chairman	8
Discussion of Issue 1 (6*5 minutes)	30
Audience comments	5
Voting on Issue 1	4
Discussion of Issue 2 (6*5 minutes)	30
Audience comments	5
Voting on Issue 2	4
Summary by Chairman	4
Total	90

- At the end of the presentations for each topic, the audience will be asked to give their views on the discussion and to vote for or against a proposition that is put to them regarding that topic.
- At the end of the Forum, the Chairman will summarize the proceedings and offer comments on the outcomes and means by which the academic-practitioner gap can be further reduced.

REFERENCE

Poulos, H.G., Day, P., Valenzuela, L., Crawford, S., Mayne, P., Bolton, M. Tatsuoka, F. and Koseki, J. (2006). "Practitioner/Academic Forum". Prof. 16th Int. Conf. Soil Mechanics and Geotechnical Engineering, Osaka, Millpress, Rotterdam,Vol. 5, 2917–2936.

Discussion session 1: Pile design development & codes

Deep Foundations on Bored and Auger Piles – Van Impe & Van Impe (eds)
© 2009 Taylor & Francis Group, London, ISBN 978-0-415-47556-3

Report of discussion session 1, on pile design development and codes

A.F. van Tol
Delft University of Technology, Delft, The Netherlands
Deltares (former GeoDelft), Delft, The Netherlands

W. Bilfinger
Vecttor Projetos Ltda. Sao Paolo, Brazil

Victor Li
Victor Li & Associates Ltd., Hong Kong

Y. El-Mossallamy
Ain Shams University, Cairo, Egypt
ARCADIS Consultants, Darmstadt, Germany

A. Mandolini
Department of Civil Engineering, Second University of Napoli, Italy

ABSTRACT: This Report of Discussion Session 1 on pile design and development and codes presents the summary of the presentations by the discussion leader and the panelists. These presentations deal respectively with Eurocode 7, pile developments, effects of construction procedure of bored piles and bored piles in difficult soils and piled rafts.

1 INTRODUCTION

For the conference topic 1, Pile Design Development and Codes 20 abstracts were submitted. The themes of these abstracts were analyzed and although it was not always clear what the exact content of the related paper would be, it shows the important subjects in the field of this conference topic. The most important developments from the abstracts are shown in table 1 (some abstracts deal with more then one item).

It appears that the abstracts cover the most important themes of this discussion session. Perhaps it was expected that the imminent introduction of Eurocode 7 would lead to more abstracts on this item.

Table 1. Content of submitted abstracts.

Items	Number	Remarks
Pile capacity	5	Axial and lateral
Installation effects	2	
Piles in difficult soil	5	Bored piles and others
Load displacement	6	Mainly numerical analyses
Piled rafts	2	
Eurocode 7	2	
Others	1	Ground improvement

The content of the presentations of the discussion leader and the panelists was carefully selected in view of important themes in the topic 1 of this conference. The following themes are addressed in these lectures: the introduction of Eurocode 7, pile developments, bored piles in weathered rock, the effect of construction procedure of bored piles and piled rafts. These presentations cover the most relevant aspects of this conference topic. The summaries of these lectures are presented below in this session report.

2 INTRODUCTION OF EUROCODE 7
A.F. VAN TOL

2.1 *General*

Eurocode 7, Geotechnical Design consists of two parts, namely:

- part 1 (EC 7-1), General rules, that was ratified in 2004
- part 2, (EC 7-2), Ground investigation and testing, ratified in 2005.

In addition to these codes, each Member State will issue a National Annex with the selected Design Approach and the magnitude of the partial factors to be applied. Some Member States will also publish a national code with additional requirements. Most Member States finalized these documents in 2007.

The implementation of EC 7-1 is planned stepwise. From 2007 on a period of Coexistence starts, in which Eurocode 7-1 and the existing national codes may be used. From 2010 on these national codes will be withdrawn.

2.2 *Pile design according to EC 7-1*

The important requirements for the design of pile foundations according to the 3 Design Approaches (DA) are given in chapter 2. The corresponding partial factors are presented in Table A.3 for action or the effect of actions (γ_F or γ_E), Table A.4 for ground parameters (γ_M), Tables A.6, A.7 and A.8 for resistances for piles (γ_R) and Table A.9, A.10 and A.11 for the correlation factors ξ.

Section 7 of EC 7-1 is devoted to the design of pile foundations under axial loads. In this section, clauses 7.6.2.2 and 7.6.2.3 deal with the assessment of the Ultimate compressive resistance from respectively static load tests and from ground test results. In this section the correlation factors, to derive a characteristic resistance from a number of static load tests or ground tests, are introduced.

The subsequent requirements for ULS for piles in compression or tension lead to the basic condition that the design value of the Actions F_d does not exceed the design value of the Resistance R_d:

$$F_d < R_d \tag{1}$$

$$F_d = \gamma_F \, . \, F_k \tag{2}$$

$$R_d = R_k/\gamma_t \quad \text{or} \quad R_d = R_{bk}/\gamma_b + R_{sk}/\gamma_s \tag{3}$$

where F_k is the characteristic value of the actions, γF the partial factor on actions, R_k, R_{bk} and R_{sk} are the characteristic values of respectively the total, the base and the shaft resistance and γ_t, γ_b and γ_s the partial factors on respectively the total, the base and the shaft resistance.

The characteristic values of the resistance R are obtained from shall be based on:

- results of static load test (SLT)
- empirical or analytical calculation methods validated by static load test
- results of dynamic load tests, validated by (SLT)
- observed performance, supported by ground investigation and ground testing.

The characteristic values of the resistance are obtained with:

$$Rk = R/\xi \tag{4}$$

where the correlation factor ξ is a statistical factor depending on the number and type of tests.

Table 2 presents the partial factors, from A.6, A.7 and A.8 of Annex A of EC 7-1 for Ultimate Limit State for driven, bored and CFA piles in compression. It is striking that EC 7-1 recommends different partial factors for the different pile types in Design Approach 1 and not in DA 2 and 3. The explanation for the higher partial factors for bored and CFA pile will be the higher uncertainty (installation procedure dependent) regarding the base capacity of these piles compared to driven piles. Although this is an understandable ground, the reason for the absence of this diversion in DA 2 and 3 is not consistent but will probably be explained by the lack of space for diversion, as the safety in these approaches is (nearly) completely located at the action side.

It is interesting to see how the Member States have dealt with this in their National Annex. In some Member States the mentioned uncertainties are covered by installation factors, but the calculation methods, wherein installation factors might appear are not unified in this code. Schuppener (2007) presented an overview of the DA's and partial factors that were chosen by the Member States in their National Annex. The overview is based on a questionnaire and presents the status at January 2007. Table 3 in Schuppener (2007) presents the selected partial factors for bored and driven piles. From this table it appears that 3 Member States, that chose for DA1 follow the recommendation and take higher partial factors for bored then for driven piles (P, IRL, LT) and one vice versa: higher factor for driven then for bored piles (R). It also can be seen that in DA2 two Member States chose higher partial factor for bored then for driven piles (CH, D).

2.3 *Harmonization of Direct CPT-method*

The final goal of the European Standardization project is to harmonize the design of constructions. The questions is of the development of EC 7-1 succeeded to (partly) reach this goal for geotechnical design. After

Table 2. ULS, recommended values in EC 7-1 for γ_b, γ_s, γ_t.

Type of pile	Design approach 1							
	Combination 1			Combination 2			DA2	DA3
Driven	1.0	1.0	1.0	1.3	1.3	1.3	1.1	1.0
Bored	1.25	1.0	1.15	1.6	1.3	1.5	1.1	1.0
CFA	1.1	1.0	1.1	1.45	1.3	1.4	1.1	1.0

the publication of EC 7-1 different committees initiated exercises to design trial examples of standard design situations by representatives of the Member States. Some of these exercises showed a very large scatter in the design results and EC 7 was blamed. The effect of differences in Design Approaches, partial and correlation factors however cannot be responsible for very large deviations. The real reason is the fact that the calculation methods that are not unified in EC 7-1. Therefore, more results can be achieved by trying to harmonize the calculation methods.

As stated above clause 7.6.2.3 of EC 7-1 deals with the assessment of the ultimate compressive resistance from ground test results. In Member States were Cone Penetration Testing is a standard soil investigation technique the method to derive the ultimate pile resistance directly from the cone resistance is generally accepted. Several National codes in Europe apply this direct CPT method to determine the pile capacity (Cock & Legrand, 1997). Eurocode 7, part 2, Ground Investigation and Testing address this method in paragraph 4.3.4.2 and in Annex D.7 an example of the method illustrated. The calculation procedures in different countries, like in the Netherlands, France and Belgium are similar but with some important differences, like e.g. the factors accounting for the installation effects, the pile geometry and the averaging procedures to assess the representative cone resistance for the pile base. The method described in Annex D.7 in EC 7-2 at present is the Dutch method.

The Netherlands, France and Belgium started a working group to harmonize the method. The first action of this group was to gather a reliable database with static pile load tests. At present, the group gathered about 25 well-documented pile load tests on driven prefabricated piles (mostly concrete and some closed ended steel piles) and compared the results of these load tests with the predicted ultimate base and shaft capacity according to the Dutch, French and Belgium method. The next step will be to extend the database with driven, cast in place piles, bored and screwed piles.

The first results show that the Dutch and Belgium methods overestimate the base capacity considerably. The French method is more conservative and fits therefore better. This confirms the findings published by Puppala et al. (2002) based on the database of the Federal Highway Authorities and Xu & Lehane (2005) based on the UWA database.

3 PILE DEVELOPMENTS
W. BILFINGER

The increasingly competitive global market is driving industry towards two critical and opposite, thresholds: to build faster and cheaper, on one side, and, on the other side, to avoid underperformance, failures and mistakes.

For this reason, a segment of this industry is constantly searching for ways to improve the foundations of structures, which, in essence, mean to increase the allowable loads and/or to reduce settlements of piles, leading to proportionally cheaper foundations, without affecting the necessary safety margin.

The development of piles is currently focused on a better understanding of bearing capacity and load-settlement prediction and, to some extend, to improve construction reliability.

To evaluate the real possibilities of improving reliability and the capacity to predict bearing capacity and load-settlement behavior accurately, one has to consider the different factors that affect these pile characteristics.

Normally safety and reliability are affected by:

- Load uncertainties—in this paper, this issue will not be discussed;
- Material uncertainties, including strength and deformability of the pile and the surrounding material. The material uncertainties are normally divided into their intrinsic variability and those associated to representativeness, testing reproducibility, including accuracy and precision;
- Method uncertainties, associated to the design calculations and assumptions.

For practical purpose, pile behavior predictions that include all factors above, with exception of load variability, are based normally on field and laboratory testing of the foundation soil, and a model that uses these inputs. The most common soil testing performed in North and South America for pile design, i.e., bearing capacity and load-settlement prediction, are SPT and CPT tests (Paikowsky, 2002). Less frequently, other types of tests are performed. Comparison between observed and calculated bearing capacities by several methods shows that in roughly 50 years generalized formulae to predict ultimate bearing capacity have not gained significant reliability. Figure 1 presents

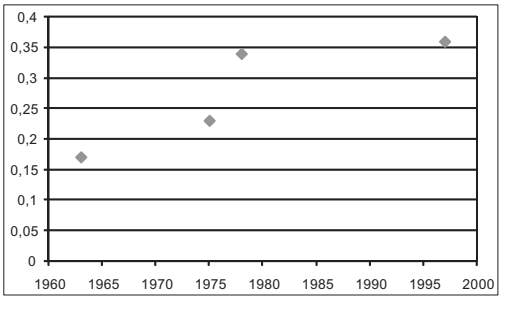

Figure 1. COV associated to different databases.

COV associated to the databases presented by the different authors in their original papers. The data base used by Norlund in 1963 to develop the corresponding bearing capacity calculation method show a proportionally low COV, when compared to other methods. Later tests presented by Paikowsky (2002) lead to COV's between 0,22 and 0,58.

This conclusion is backed by a study by O'Neill's (2001) about side resistance of piles, that concludes that "… much still remains to be learned ... and that site specific load testing should remain an integral part of the design process for driven and drilled shafts".

A way to reduce this variability is to perform site specific load test and calibrate generalized pile behavior prediction methods. A theoretical sound approach is the use of Bayesian inference to combine load tests with predicted bearing capacities (Bacher and Rackwitz, 1982), (Hachich et al. 2008). But often the problem of these approaches is the necessity of performing previous load tests, preferable more than one and, in some cases, high variability of results, even on the safe side (showing, for example, significantly higher loads than predicted), can lead to a theoretical need for higher safety factors.

Another approach is to use information from the site: in the case of bored and auger piles, a direct measurement of installation parameters is complicated, but possible. Interesting and promising results were presented by NeSmith (2003) and Saeki and Ohki (2003), were the installation effort is compared to pile bearing capacity. A statistic analysis comparing probability of failure using not only bearing capacity predictions, but adding the information of the installation effort certainly will show significantly lower probabilities of failure or, in other word, more reliable foundations.

All the efforts of reducing variability and, therefore, reliability, can be seen in a broader view, a part of the initial phases of geotechnical risk management.

Risk management is an effective management and decision tool and is widely used in several engineering activities. The introduction of risk management in geotechnical engineering is recent, but becoming increasingly important. The ITIG (International Tunneling Insurer Group) published recently, together with the ITA (International Tunneling Association), a "Code of Practice for Risk Management of Tunnel Works" (ITIG, 2006), which consists in a rational way to manage risk in tunneling works. Some re-insurers are including the necessity of use of this Code in their contracts, showing that, probably in the near future, risk management will be almost obligatory in tunneling works. This trend, probably, will be expanded to other geotechnical works, including deep foundation engineering.

Considering that risk management will be probably "unavoidable", it is important to realize that risk management does not involve complicated theories or formulation. The key tools for effective risk management are available and the only necessity is systematic use of available information, using a relatively simple methodology.

4 INFLUENCE OF CONSTRUCTION PROCEDURES ON PILE CAPACITY—SOME HONG KONG EXPERIENCE

VICTOR LI

4.1 *Introduction*

Most textbooks on foundation engineering present a picture that the estimation of pile capacity of bored piles is a relatively straight forward exercise. In reality, it is far from being the true story. Figure 2 shows a summary of average shaft friction of bored piles measured in Hong Kong (GEO, 2006). The widespread of data gives a clear message that prediction of pile capacity, or at least the shaft friction, of bored piles is difficult even when the bored pile data in Figure 2 represent bored piles constructed in fairly similar soil conditions in Hong Kong.

The shaft friction τ of a bored pile can be described by a simple relationship.

$$\tau = \sigma_h \tan \delta \qquad (1)$$

where σ_h is the horizontal stress acting on the pile shaft and δ is the friction angle between the soil and pile shaft. Both parameters are highly affected by the method of construction, making the prediction of pile capacity a difficult task. In this note, the author likes to make a point by discussing some case studies in Hong Kong.

4.2 *Use of permanent liner*

In Hong Kong, permanent tubular liners made from a corrugated steel sheet are sometimes used for construction of bored pile to prevent necking of pile shaft during extraction of temporary casing. They are also used routinely for bored piles constructed

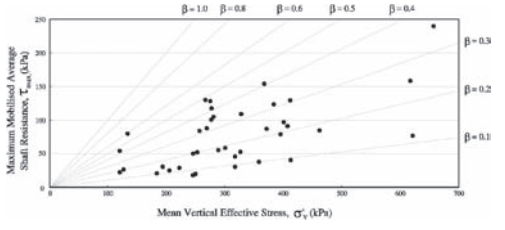

Figure 2. Measured shaft friction of bored piles in Hong Kong (GEO, 2006).

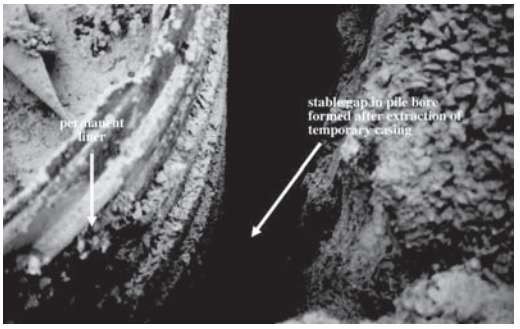

Figure 3. Gap between pile bore and permanent liner.

in cavernous marble formations to prevent loss of concrete into marble cavities. The permanent liner is placed inside the steel casing before concreting inside the permanent liner. As the diameter of the permanent liner is smaller than the temporary steel casing, a gap will be formed between the soils and the permanent liner when the temporary steel casing is extracted during concreting (Fig. 3). Experiences indicate that the gap can remain stable after extraction of temporary casing due to arching effect (Lam & Li, 2003). In this case, shaft friction will be low because σ_h is zero. If collapse of pile bore occurs to fill up the gap, σ_h will drop due to release of stress caused by soil movement towards the permanent liner. Also, δ will be low as the soils filling up the gap are likely to be in a much looser state then their initial states. Lam & Li (2003) reported a case study for a 60 m long, 1.5 m diameter bored pile constructed using a permanent liner. The measured average shaft friction is 17 kPa, which is practically the lowest limit of shaft friction one can obtain according to the data in Figure 2.

4.3 *Concreting rate and setting time of concrete*

As discussed convincingly by Kay & Kalinowksi (1997), the confining stress σ_h in Eq.1 tends to be controlled by contact pressure derived from placement of concrete rather than in-situ earth pressure of soils. The contact pressure of concrete is governed by the rate of pour, setting time and delay of concrete pour, so will be the shaft friction of bored pile. Kay & Kalinowksi (1997) reported a case study of two 1.5 m diameter bored piles constructed at 6 m apart on a Hong Kong site, and apparently using similar construction method. Loading test results indicated that one bored pile gave significantly lower shaft friction than the other. A review of construction records revealed that the bored pile with unexpectedly lower shaft friction had a considerable number of delays in concreting, amounting to 155 minutes in the total 342 minutes placement time, while concreting for the other bored pile with higher shaft friction was completed in 267 minutes with much reduced loss in delay time.

4.4 *Soft interface*

Bored piles and barrettes are often constructed using bentonite slurry for supporting the pile bore. It is commonly recognized that slow rate of excavation and delay in concreting can lead to formation of thick filter cake along the pile bore. Ng et al. (2000) reported a case study of a 39.7 m long test barrette constructed on a Hong Kong site. The soil profile comprised fill, marine deposit, alluvium and completely decomposed granite (CDG). The excavation of the barrette took 62 hours to complete and concreting was commenced 43 hours after completion of excavation. Shaft friction measured along the barrette was low, and particularly so for the CDG layer which gave shaft friction comparably to that of the marine clay layer. Li & Lam (2001) argued that the low shaft friction was likely to be due to the unusually long duration of excavation and long delay in concreting, causing significant relaxation of confining stress (i.e. σ_h), and thick filter cake to be formed along the bored pile (hence low δ). Ng et al. (2000) has therefore made an unintended contribution of demonstrating how poor construction method can lead to low shaft friction.

In summary, use of appropriate method and good control of construction for ensuring high σ_h and δ are important in achieving higher shaft friction of bored piles. Textbook analyses are unfortunately of little help in this respect.

5 PERFORMANCE OF LARGE DIAMETER BORED PILES IN WEATHERED ROCK
Y. EL-MOSSALLAMY

5.1 *Introduction*

Deep foundations using large diameter bored piles have proved in the last two decades to be an economic geotechnical foundation type. The structural serviceability requirements can be fulfilled with relatively fewer piles. This foundation system was successfully applied in different soil conditions.

There is relatively good experience regarding the behavior of bored piles in cohesive and cohesionless soils. In moderately to completely weathered rock as well as rock that is decomposed to residual soil, the load-settlement behavior of bored piles depends on the whole rock formation matrix considering the rock joint system and the shear strength along the presented joints and discontinuities more than on the quality of the intact rock pieces.

5.2 *Case history*

The behavior of large diameter bored piles in moderately to completely weathered rock and residual soils will be briefly presented considering the results of a case history of a bridge foundation in Germany. The subsoil mainly consists of Quaternary formations of silt down to a depth of about 10 m. Below the Quaternary soil; there is a layer of completely weathered limestone and residual soils (silt and clay) with a thickness of about 30 to 40 m. A sublayer of a slightly to moderately weathered limestone bank with a thickness of about 6 m divides the completely weathered layer in an upper and lower sublayers. Moderately to slightly weathered rock formations of limestone and dolomite were found in large depths of about 40 to 50 m beneath the ground surface. The bridge piers were suggested to be founded on large diameter bored piles that should be socketed 2 m in the above mentioned slightly to moderately weathered limestone bank reducing the required pile length to only 25 to 30 m.

To ascertain the adequacy of the pile bearing capacity and determine appropriate design values, pile load tests were conducted on large diameter bored piles. The tested piles are socketed in the suggested bearing layer of the slightly to moderately weathered limestone bank. To avoid the need for a large reaction system, multiple Osterberg cells were applied to conduct the load test. The pile load tests were carried out using two O-Cells that were installed in the different geotechnical subground layers. The load test is carried out in three stages (Fig. 4).

Figure 5 represents the evaluated skin friction in the different layers as well as the measured pile base resistance in the bearing stratum. The measured ultimate skin friction in the alluvial sand and gravel layer reaches about 200 kPa. This value is larger than the maximum value given in DIN 4014 for cohesionless soil, but still lies in the expected range according to experience (e.g. Kempfert 1982 and Dürrwang 1997). In the contrary the measured ultimate skin friction in the residual soils with a value of about

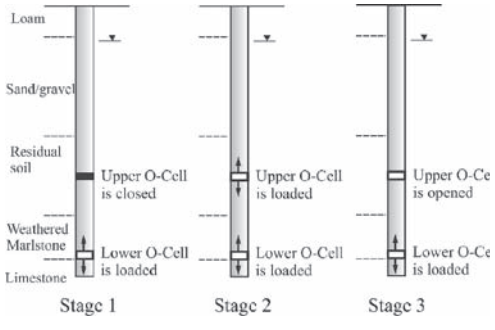

Figure 4. Load stages of the pile load test.

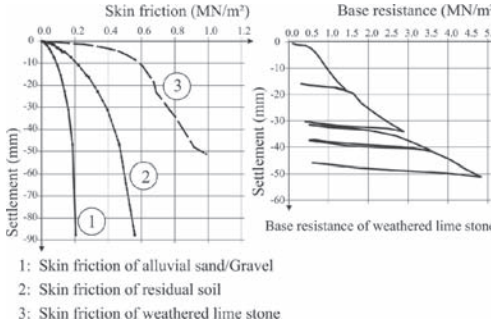

Figure 5. Pile skin friction and base resistance.

600 kPa reaches about 10 times the corresponding value for cohesive soils according to DIN 4014. This high value of skin friction in completely weathered rock and residual soils were measured by other load tests on large diameter bored piles (Dürrwang 1997). These high values are due to the structure of completely weathered rock and residual soils on one hand and the conventional sedimented cohesive soils on the other hand. The residual soils show a dominant dilation performance that leads to increasing horizontal stresses during shearing by pile loading. The increased horizontal confinement stresses cause a large increase of the ultimate skin friction.

The ultimate skin friction in the slightly to moderately weathered lime stone reaches 1000 kPa and lies higher than the given value according to DIN 4014. The ultimate pile base resistance reaches about 4.8 MPa and lies beneath values given by DIN 4014. These results show that the correlation between pile capacity in weathered rock and the uniaxial compressive strength of the intact rock is not accurate to estimate the ultimate capacity of bored piles in such rock formations.

5.3 *Design procedure*

As no possibility does exist to take into account —in an adequate manner— the effect of pile installation by theoretical means, the numerical model as well as soil parameters applied to design the piled foundation of the bridge were first calibrated and adjusted to the results of single pile load tests. The bridge foundations were then designed using the same numerical model and the determined soil and pile/soil parameters. The results of the load test using multi O-Cells give information on pile segments. Therefore, the first design step is to calculate an equivalent top-loaded load-settlement curve from the results of the pile segments. Figure 6 shows the equivalent load-settlement curve that is calculated directly from the pile load test (line 1). Line 2 represents the equivalent load-settlement curve considering the elastic deformation of the pile material. Line 3

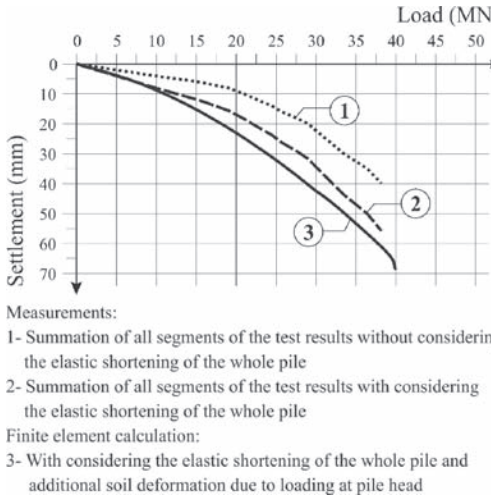

Figure 6. Total load-settlement behavior of the test piles.

demonstrates the calculated equivalent load-settlement curve applying axisymmetric finite element analyses.

The structural design of the superstructure depends mainly on the determined stiffness of the foundations. The pile group action, defined as the settlement of the pile group divided by the settlement of the single pile under the corresponding average load, has a dominant effect on the foundation behavior and should be considered in a realistic manner. Therefore, three dimensional analyses may be necessary in certain conditions to study the foundation behavior using the calibrated pile-soil parameters obtained by the back-calculation of pile load test results. The pile group action depends on pile spacing, the pile length, the number of piles in the group, the depth of compressible layer beneath the pile tip and the applied load level. The pile group action increases with increasing the number of piles in the pile group. It increases with increasing the pile length to pile diameter ratio. It decreases with increasing pile spacing to pile diameter ratio. It decreases with decreasing the depth of compressible layer beneath the pile tip. It decreases with increasing the load level defined as the ratio between applied and ultimate loads.

6 SOME REMARKS ON THE USE OF PILES AS SETTLEMENT REDUCERS
A. MANDOLINI

6.1 *Introduction*

Traditional design methods for piled foundations still concentrate on providing axial capacity from the piles to carry the total structural load. Such an approach gives no credit to the contribution of the raft and is considered to be conservative. Moreover, it is adopted as a common practice by engineers in many countries and prescribed by the majority of existing codes and regulations.

Starting from the pioneering work by Burland et al. (1977), in the last decades a large amount of research has been aimed to the use of piles to control average and differential settlement (respectively, settlement based design approach, SBD, and differential settlement based design approach, DSBD) of an unpiled raft whose bearing capacity is sufficient to carry the total external load with a reasonable factor of safety against failure. In other words, it could be said that the 'piled raft concept' has been conceived for fulfilling SLS requirements ('piles as settlement reducers'), in some way implicitly assuming that the "raft ensures adequate bearing capacity, thus piles have to ensure only adequate increase of stiffness".

If compared with the amount of research carried out on the behaviour of piled raft under service loads, there is no doubt that less attention has been dedicated by researchers to the interaction via soil between piles and raft when approaching failure.

Some recent results show how the matter is more complex as it appears, suggesting that, even in the case of settlement reducing piles, an assessment of the response of a piled raft at failure is suitable to ensure that satisfying SLS requirements does not compromise design requirements in terms of ULS.

6.2 *Interaction between raft and piles at failure*

Depending on how piles are located underneath the raft, they could leave practically unchanged the bearing capacity of the unpiled raft (Q_{UR}) or determine a reduction of its potential contribution because inhibited by their presence. At the same time, piles failing in a group under a load Q_{PG} could reduce their bearing capacity when combined with a raft in contact with soil, for instance as a consequence of the inhibited relative pile-soil relative movement at shallow depth close to the raft; in some cases, they could increase their bearing capacity as a consequence of the surcharge effects due to the contact raft-soil stresses.

In general terms, it could be said that the bearing capacity of a piled raft can be evaluated as:

$$Q_{PR} = \alpha_{UR} \cdot Q_R + \alpha_{PG} \cdot Q_{PG} \quad (1)$$

where α_{UR} and α_{PG} represent respectively the factors affecting the bearing capacities of the unpiled raft Q_{UR} and of the pile group Q_{PG}, both of them conventionally evaluated (for instance, for the pile group: $Q_{PG} = \eta \cdot n \cdot Q_S$, where η = efficiency at failure of the pile group made by n piles having a failure load Q_S).

With reference to the numerical results obtained by 3D FE analyses of vertically loaded piled rafts

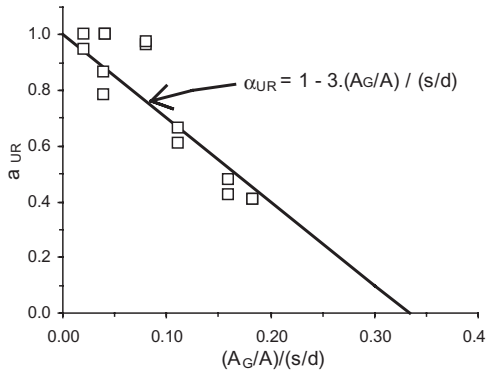

Figure 7. Relationship between α_{UR} and FF.

resting on soft clayey soils, de Sanctis & Mandolini (2006) found that a factor FF can be introduced to better understand the interaction at failure of the two components (raft and piles):

$$FF = \frac{\left(A_G / A\right)}{(s/d)} \qquad (2)$$

where A_G is the area occupied by the piles underneath the raft area A and s/d is the ratio between pile spacing and pile diameter.

Figure 7 groups the numerical results in terms of reduction factor α_{UR} to be applied to Q_{UR} to give the contribution $\alpha_{UR} \cdot Q_{UR}$ of the raft at failure when combined in a piled raft. For all the analysed cases, it was found $\alpha_{PG} \sim 1$.

Data in Figure 7 have been reasonably fitted with a simple linear regression, thus suggesting the following comments: (i) for the case of an unpiled raft ($A_G/A = 0$), $\alpha_{UR} = 1$ as expected; (ii) for the case of piles uniformly spread underneath the raft ($A_G/A \sim 1$) at relatively small spacing ($s/d \sim 3$), $\alpha_{UR} \sim 0$. It follows that $(A_G/A)/(s/d) \sim 1/3$ may be viewed as a critical value for FF corresponding to the transition from a pile group behaviour (i.e., no contribution of the raft is allowed, $\alpha_{UR} = 0$) to a piled raft behaviour (i.e., the raft supplies a fraction $\alpha_{UR} > 0$ of its bearing capacity when unpiled).

It is interesting to note that Cooke (1986) suggested values for $s \sim 3 \cdot d$ as that critical value of the spacing below which a pile group embedded in a clayey soil tends to exhibit 'block' mode of failure instead of individual pile mode of failure.

Putting together all the things, it could be said that for piles uniformly spread underneath the raft ($A_G/A \sim 1$), the adoption of pile spacing ratio $s/d < 3$ yields to 'block' failure of the pile group preventing the raft to contribute; on the other hand, spacing ratio $s/d > 3$ prevents the pile group to fail as a 'block' making the raft able to transfer load directly to the soil.

Let us consider now the case of an unpiled square raft (width B = 17 m) at ground surface resting on a clayey soil (soil shear stiffness G = 10 MPa; undrained shear strength c_u = 100 kPa; Poisson's ratio $\nu = 0,2$) loaded by an external total load Q = 50 MN. The evaluation of failure load in undrained conditions with conventional bearing capacity theory yields to $Q_{UR} \sim 178$ MN, that means $FS_{UR} = Q_{UR}/Q \sim 3,6$. The evaluation of the long term settlement with simple elastic theory yields to $w_{\infty,UR} \sim 108$ mm. Such settlements are considered not admissible (for instance, $w_{adm} = 50$ mm) and hence piles have to be added to reduce settlement.

If bored piles with length L = 30 m and diameter d = 1 are selected, the conventional approach for the evaluation of failure load of the single pile yields to a value $Q_S \sim 4$ MN ($s_{lim} = \alpha \cdot c_u$, $\alpha = 0,35$; $p_{lim} = N_c \cdot c_u$; $N_c = 9$). Assuming an efficiency of the pile group at failure $\eta \sim 0,7$ and neglecting the contribution of the raft in contact with soil (i.e. assuming that all the load is transferred to the soil by only the piles), at least 6^2 piles at spacing s = 3 m are needed ($Q_{PG} = 0,7 \cdot 36 \cdot 4 \sim 100$ MN) to ensure a factor of safety not lesser than 2. The corresponding settlements of the pile group, evaluated by the interaction factor method, yields to a long term settlement $w_{\infty,PG} \sim 39$ mm.

According to Burland (2004), a structure, its foundation and the surrounding ground interact with each other whether or not the designers allow for this interaction. In practice and looking at piled raft behavior, it means that although we decided to neglect raft contribution, it exists!

From quantitative point of view, the "true" factor of safety of the piled raft can be evaluated by using eq. (1):

$$\frac{A_G}{A} = \frac{15^2}{17^2} \approx 0,78; \frac{s}{d} = 3; FF = 0,26; \alpha_{UR} = 0,22$$

$$Q_{PR} = 0,22 \cdot 178 + 1,00 \cdot 100 \approx 140 \text{ MN}; FS_{PR} \approx 2,8$$

The evaluation of the settlement of the piled raft by the PDR method (Poulos, 2000) yields to $w_{PR} \sim 40$ mm.

The example show that the addition of the piles allow to fulfill the design requirement for which they have been added but, at the same time, they limited the contribution of the raft to about 20% of its potential contribution, giving a resulting factor of safety decreased from the initial value for the unpiled raft $FS_{UR} \sim 3,6$ to $FS_{PR} \sim 2,8$.

If only 4^2 piles at spacing s = 5 m are used, the efficiency at failure of the pile group can be assumed

to increase to about 0,8 and the following results come out:

$$\frac{A_G}{A} = \frac{15^2}{17^2} \approx 0,78; \frac{s}{d} = 5; FF = 0,155; \alpha_{UR} = 0,53$$

$$Q_{PR} = 0,53 . 178 + 1,00 . 51 \approx 140\ MN; FS_{PR} \approx 2,9$$

Less piles more spaced slightly increase FS_{PR} leaving practically unchanged $w_{PR} \sim 40$ mm.

7 CONCLUSION

Even for those cases where piles are used to reduce settlements, their presence can affect the bearing capacity of the raft, giving a factor of safety of the combined piled raft smaller than that ensured by the raft when unpiled. Such findings suggest to evaluate always the available bearing capacity in order to check if the requirements fixed by Codes (when allowing innovative design approaches) are satisfied.

REFERENCES

Baecher, G.B. & Rackwitz, R. 1982. Factors of Safety and Pile Load Tests. International Journal for Numerical and Analytical Methods in Geomechanics, v. 6.

Burland, J.B. 2004. Interaction between structural and geotechnical engineer. *New Perspectives in the Design and Construction of Foundation Structures*. Joint Structural Division Annual Seminar, Hong Kong.

Burland, J.B., Broms, B.B. & De Mello, V.F.B. 1977. Behaviour of foundation and structures. State of the Art Report, *Proc. IX ICSMFE*, Tokyo, 2: 495–546.

Cooke, R.W. 1986. Piled raft foundations on stiff clays: A contribution to design philosophy. *Geotechnique*, 36 (2): 169–203.

De Cock, F. & Legrand C., 1997. Design of Axially Loaded piles, European Practice, *Proceedings of the ERTC3* Seminar, Brussels, Belgium, 1997.

De Sanctis, L. & Mandolini, A. 2006. Bearing capacity of piled supported rafts on soft clay soils. *Journal of Geotechnical and Geoenvironmental Engineering*, 132 (12): 1600–1610.

Dürrwang, R. 1997: *Pfahltragfähigkeiten im Grenzbereich Lockerboden/Fels*; Geotechnik Heft 3/97.

Dürrwang, R., Hecht, T., Johmann, S. & El-Mossallamy, Y. 2005. *Die Gründung der Weidatalbrücke; Pfahlprobebelastungen mit der Osterbergzelle*, Pfahlsymposium 2005, Braunschweig: 377–388.

Hachich, W.C., Falconi, F., & Santos, M. S. 2008 Foundation Safety: Incorporating load test results. In: Congresso Luso-Brasileiro, Coimbra.

Kay, J. N. & Kalinowski 1997. "Shaft friction for cast-in-place piles in Hong Kong", *Proc. 2nd International Symposium on Structures and Foundations in Hong Kong*: 1–6.

Kempfert, H.-G. 1982. *Vergleichende Auswertung von Probebelastungen der DB an Großbohrpfählen in nichtbindigem Untergrund*; Geotechnik 1982, Heft 1.

Klosinski, B. & Rychlewski, P. 2003. Analysis of bearing capacity and settlement of CFA Piles. In: Deep Foundations on Bored and Auger Piles—BAP IV, Gent

Lam, J. & Li, K. S. 2003. "Influence of construction method on shaft friction of bored pile—a case study", *Proc. HKIE Geotechnical Division Annual Seminar—Case Histories of Geotechnical Engineering in Hong Kong*: 143–152.

Li, K.S. & Lam, J. 2001. Discussion on "Field studies of well-instrumented barrette in Hong Kong", *Journal of Geotechnical and Geoenvironmental Engineering*, ASCE, 127 5: 466–468.

Mandolini, A., Russo, G. & Viggiani, C. 2005. Pile foundations: experimental investigation, analysis and design. State of the Art Report, *Proc. XVI ICSMGE*, Osaka, 1: 177–213.

Moormann, Chr. 2005. *Pfahltragverhalten in festen und veränderlich festen Gesteinen*, Mitteilung des Institutes für Grundbau und Bodenmechanik, Universität Kassel, Heft Nr. 18: 249–273.

Nesmith, W.M. 2003. Installation effort as an indicator of displacement screw pile capacity. In: Deep Foundations on Bored and Auger Piles—BAP IV, Gent.

Ng, C. W. W., Rigby, D.B. & Ng, S.W.L. 2000. "Field studies of well-instrumented barrette in Hong Kong', *Journal of Geotechnical and Geoenvironmental Engineering*, ASCE, 126[1], 60–73.

Norlund, R. 1963. Bearing Capacity of Piles in Cohesionless Soils. *Journal of the Soil Mechanics and Foundations Division*—ASCE, v. 89, n. SM3

Osterberg, J.O. 2001. *Load testing high capacity piles—what have we learned?* Proceedings of the Fifth International Conference on Deep Foundation Practice, Singapore, April 2001.

O'Neill, M.W. 2001. Side Resistance In Piles and Drilled Shafts. *Journal of Geotechnical and Geoenvironmental Engineering*—ASCE, v. 127, n. 1.

Paikowsky, S.G. 2002. Load and resistance factor design (LRFD) for deep foundations. In: Foundation Design Codes and Soil Investigation in view of International Harmonization and Performance, Kamakura.

Poulos, H.G. 2000. Practical design procedures for piled raft foundations. *Design application of raft foundations*. Hemsley J.A. Editor, Thomas Telford: 452–467.

Puppala, A.J., Wattanasanticharoen, E., Hoyos, L.R., & Satyanarayana, R. 2002. "Use of cone penetration test (CPT) results for accurate assessment of pile capacities". *Proc., NICE2002: 9t h International Conference on Piling and Deep Foundations*, June 3–5, 2002, Nice, France, pp. 575–580.

Schuppener, B. 2007. Eurocode 7: Geotechnical design—part 1: General rules—its implementation in the European Member States, V SORIANO, E Dapena, E Alonso, JM Echave, A Gens, JL de Justo, C Oteo, JM Rodriques-Ortiz, C Sagaseta, P Sola & a SORIANO (Eds.), *Proc. of the 14th European Conference on Soil Mechanics and Geotechnical Engineering. Rotterdam: Millpress.*

Saeki, E. & Ohki, H. 2003. A study of the screwed pile—The result of installation and loading tests and analysis of penetration mechanisms. In: Deep Foundations on Bored and Auger Piles—BAP IV, Gent.

Xu, X. & Lehane, B.M. 2005. Evaluation of end-bearing capacity of closed-ended pile in sand from cone

penetration data, *ISFOG—Gourvenec & Cassidy (Eds), Taylor & Francis Group, London*.
FGSV, Forschungsgesellschaft für Straßen- und Verkehrswesen 1992. *Merkblatt zur Felsbeschreibung für den Straßenbau.* FGSV, Arbeitsgruppe Erd- und Grundbau, Köln.
Geotechnical Engineering Office (GEO) 2006. Foundation Design and Construction, GEO Publication No. 1/2006.
ITIG 2006. A code of Practice for Risk Management of Tunnel Works.

Deep Foundations on Bored and Auger Piles – Van Impe & Van Impe (eds)
© 2009 Taylor & Francis Group, London, ISBN 978-0-415-47556-3

Pile developments

Werner Bilfinger
Vecttor Projetos Ltda. São Paulo, Brazil

ABSTRACT: Pile developments are a constant need in a competitive market like the foundation industry. It is necessary to rationally evaluate risks and the available tool is geotechnical risk management. The use of risk management in other fields of geotechnical engineering is increasing and can be seen as a valuable tool to improve foundation reliability. Geotechnical risk management in several cases is done mentally and informally by experienced engineers. The transformation of this process into documented risk management is a relatively easy task and can improve significantly foundation reliability and contractual practices. Pile technical developments are focused on better understanding behavior and its prediction, to improve reliability and allow for more cost effective solutions. Variability associated to simple pile prediction methods has not changed significantly during the last 50 years, indicating that these methods are probably not capable of further development for more precise predictions. Variability can possibly be reduced dividing lateral resistance and end bearing capacity, or using other, independent, prediction methods, like installation effort. Other ways to improve reliability is the use of Bayesian inference, combining previous general pile prediction methods with site specific testing.

1 INTRODUCTION

The increasingly competitive global market is driving industry towards two critical and opposite, thresholds: to build faster and cheaper, on one side, and, on the other side, to avoid underperformance, failures and mistakes.

For this reason, a segment of this industry is constantly searching for ways to improve and optimize the foundations of structures, which, in essence, lead to an increase in the allowable loads and/or a reduction of pile settlements, leading to proportionally cheaper foundations, without affecting the necessary safety margin. These improvements can be achieved, mainly, by two different approaches:

- Construction of "better" piles, that, using the same geometric cross section (material quantities), can support higher loads;
- Better knowledge of the behavior of existing piles, improving reliability and reducing nominal safety factors.

It is the author's opinion that deep foundation engineering—piles—can be developed focusing on better knowledge on existing pile behavior and design methodologies associated to ways of managing geotechnical risk associated to foundation engineering.

2 BACKGROUND

Piled foundations developments can be divided in three main groups:

- New pile installation concepts and types;
- Improvement of existing pile types, including design methodologies;
- New pile testing techniques and interpretation.

The development of new pile types is restricted and in the last years only few relevant developments have been proposed and presented to the geotechnical community.

The improvement of existing pile types can be divided in the following groups:

- Equipment (better performance, longer piles, etc.);
- Materials (concrete, slurries, etc.);
- Design methods.

Figures 1 and 2 below present a summary of the papers published during BAP III (van Impe, 1998) and BAP IV (van Impe, 2003), divided into following groups: case histories, new equipment, new techniques, new materials, pile testing, research—physical, research—numerical, codes and new design methods.

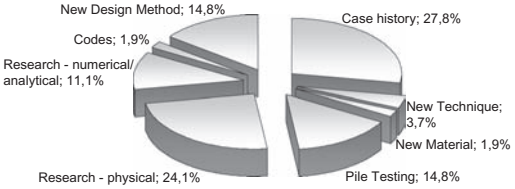

Figure 1. Summary of papers published in BAP III.

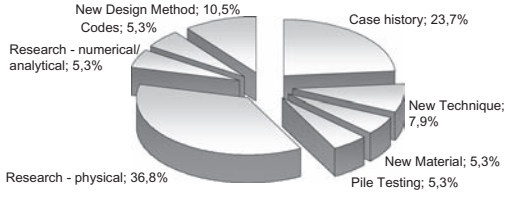

Figure 2. Summary of papers published in BAP IV.

It can be seen that in the last two BAP Conferences, little has been published related to new equipment, construction techniques and materials. More than 50% of the papers present case histories and "research—physical", associated to research performed on existing pile types to improve knowledge on pile types, mainly on the influence of different factors on pile bearing capacity and deformability.

This trend shows, in the author's opinion, that the geotechnical society is aware of the need to better understand how the existing pile types behave in distinct and complex soil-structure interaction modes, and to improve the capability to predict behavior and, therefore, reliability. Pile development, therefore, not necessarily means the development of new bored or auger piles, but mainly the better understanding of actual behavior and rational use of available information.

3 GEOTECHNICAL RISK MANAGEMENT

Claims, losses and liability problems are consuming a significant part of the possible profit that could be obtained in the foundation industry, indicating the need for actions from all sides. About 50% of the total failure costs in the construction industry may be directly or indirectly related to unexpected and unfavorable ground conditions (van Staveren, 2006). Therefore, it is not only necessary to develop piling technology, but to improve foundation industry as a whole.

Risk management is an effective management and decision tool and is widely used in several engineering activities. The introduction of risk management in geotechnical engineering is recent, becoming increasingly important. The ITIG (International Tunneling Insurer Group) published recently, together with the ITA (International Tunneling Association), a "Code of Practice for Risk Management of Tunnel Works" (ITIG, 2006), which consists in a rational way to manage risk in tunneling works. Some re-insurers are including the use of this Code in their contracts, showing that, probably in the near future, formal risk management will be almost obligatory in tunneling works. This trend, probably, will be expanded to other geotechnical works, including deep foundation engineering.

Considering that risk management will probably be "unavoidable", it is important to state that risk management does not involve complicated theories or formulation. The key tools for effective risk management are available and the only necessity is to systematic use the available information, using a relatively simple methodology.

The current practice of geotechnical risk management in the UK (ICE, 2001) is based on following steps:

- Speculate as to the geotechnical hazards that might exist on the site.
- Identify the types of construction methodology that could be used.
- Decide on the risks that could be associated with the combination of possible forms of construction methodology, and ground conditions.
- Rank the risks according to likelihood and effect.
- Decide on the type of action that is needed for risk mitigation on the basis of the severity of each risk.
- Associate each risk with a particular phase of the project.
- Identify how each risk can best be managed, and by whom.
- Record the actions taken to manage each risk.
- Reassess the severity of each risk after action has been taken.
- Review the risk register at regular intervals, to add new risks and remove risks that have been dealt with.

An almost identical concept developed by Geodelft for piling and deep foundations, called GeoQ (van Staveren, 2006), is summarized as follows:

- Gathering Information—Evaluation of possible geotechnical hazards that might exist on the site, identification of types of construction methodology that could be used.
- Identifying risks—decide on the risks that could be associated with the combination of possible forms of construction methodology and the ground conditions.
- Classifying risks—Rank the risks according to their likelihood and effect.

- Remediating risks—Decide on the type of action that is needed for risk mitigation on the basis of the severity of each risk, associate each risk with a particular phase of the project, identify how each risk can best be managed, and by whom, record the actions taken to manage each risk.
- Evaluate remaining risks—Reassess the severity of each risk after action has been taken.
- Filing in risk register.

The steps above are associated to periodic reviews, during the different project phases: feasibility studies, pre-design, design, contracting, construction and maintenance.

The 5 step procedure, described in the tunneling code of practice (ITIG, 2006), is, in the author's opinion, a simple and synthetic way for practical geotechnical risk management, applicable in all fields of activity:

- Identify hazards and associated risks, through risk assessments, that impacts on a project's outcome in terms of cost and programme, including those to third parties.
- Quantifying risks including their programme cost implications.
- Identifying pro-active actions planned to eliminate or mitigate the risks.
- Identify the methods to be utilized for the control of the risks.
- Allocating the risks to the various parties to the contract.

It is important to emphasize that at no point risk management is restricted to a specific party within the project: client, designer and constructor are all involved and should work together proactively to manage and mitigate risks.

The philosophy of sharing available information during the different project phases is, unfortunately, still not common. On the clients side, in some cases ground related risks are not fully disclosed during the bidding phase, to avoid higher bid prices. On the contractor side, in some cases profits are associated to claims due to unforeseen ground conditions. The result of these ways to handle uncertainties is often litigation, delays and a lot of resources spent with non-technical issues.

4 GEOTECHNICAL RISK MANAGEMENT IN FOUNDATION ENGINEERING

In foundation engineering, usually the following hazards should be considered:

- "Weak soil", leading to foundation failure or excessive settlements and/or horizontal displacements;
- "Aggressive soil", leading to durability problems;
- Defective construction, leading to excessive settlement or failure.

Other hazards are possible, but in most of the cases, the list above is sufficient.

Applying the 5 step procedure presented in item 3 to foundation engineering, the initial step would be:

- Risk Assessment: for a foundation project, the risk assessment starts with the soil investigation campaign, to verify strength, deformability, aggressive components, etc. During this phase, possible hazards should be identified, for example, high sulphate content in the soil (aggressive soil), soft soils that may cause negative skin friction or can generate constructive difficulties, etc.
- Quantifying risks: after preparation of a comprehensive list of all possible risk scenarios, qualitative, semi-quantitative or quantitative classification of risk is prepared, including possible impacts on cost and/or programme.
- Identifying actions to eliminate or mitigate risks: In the case of foundations, for example, in the soft soils case, risk mitigation would be consider negative skin friction in design, use a construction method that minimizes the risk of imperfections, provide pile with reinforcement to support horizontal loads, etc.
- Identification of the methods to be utilized for the control of the risks: in deep foundations, this item includes construction control, like pile cross hole integrity tests, a load test program, performance monitoring, etc.
- Allocation of the risk to the different parties: in a project, all risks have to be clearly allocated to a determined party. For example, defective construction is typically a contractor risk. Insufficient bearing capacity due to unforeseen geotechnical/geological conditions can be allocated to the designer or to the owner, but independently of the difficulties, it is a risk that has to be clearly allocated to a certain party.

A fundamental part of risk management is to register all these steps, allowing re-evaluations, corrections and adjustments. The joint tunneling code (ITIG, 2006) presents a list of documents necessary for adequate risk management. In the author's opinion, this list (eliminating some documents that may not be necessary for conventional foundation engineering) can be considered comprehensive and a good guideline for adequate geotechnical risk management:

- During the Project development phase:
  - o Site Investigation—factual report;
  - o Risk Assessment of Project options;
- During construction procurement stage:

- o Ground reference conditions;
- o Key method statement;
- o Risk assessment;
- o Tender risk register;

- Design Stages:
  - o Design brief;
  - o Schedule of third party infrastructure;
  - o Constructability reviews;

- Construction Stage:
  - o Project risk management plan;
  - o Construction stage project risk register;
  - o Method statement;
  - o Inspection and test plans;
  - o Risk assessments.

It is important to realize that in several cases the complete decision sequence is, probably, mentally performed by an experienced geotechnical consultant, without the necessity of preparation of several documents.

However, during an entire project, design and construction are increasingly becoming fragmented, different parties are involved and a complete risk awareness is not guaranteed. Therefore, the formalization process is increasingly important, and a relatively simple risk management procedure is available and easily applicable. The participation of experienced professionals continues to be fundamental for the process as a whole.

From a geotechnical point of view, in foundation engineering the most important hazards are associated to "weak soil", meaning, in other words, that accurate load-settlement/bearing capacity predictions are a key factor for successful construction and possible cost reduction without affecting safety.

A way to handle the geotechnical uncertainties technically and contractually is the GBR (Geotechnical Baseline Report), which, prior to contract, characterizes the project from a geotechnical point of view (van Staveren, 2006). Deviations of the GBR detected after contract award can be handled easily: if a determined ground behavior was not foreseen in the GBR, the contractor can be financially compensated. If, on the other side, misbehavior occurs due to construction problems, the contractor will be responsibilized.

The use of the GBR is not an universally accepted practice, but is, in the authors opinion, a valuable tool to avoid future litigation.

5 CODES

The decision processes in geotechnical engineering in general, and specifically foundation engineering design, are currently facing a gradual transition from the WSD (working stress design) approach, to the LRFD (load and resistance factor design). The need for a more rational way to consider uncertainties, substituting a global safety factor by verification of different limit states, is almost unanimous and great effort has been spend, leading, for example, to Eurocode 7 and AASHTO LRFD.

The calibration of partial resistance factors is based mainly on an adjustment to achieve equivalent global safety factors, different from structural engineering, where partial resistance factors are based on sound probabilistic approach and data. In foundation engineering, probabilistic design is still being debated (Whitman, 2000). However, there is little dispute that design can be improved integrating design components in a more logical and self consistent way (Kulhawy and Phoon, 2002). The use of reliability based design—RBD is the only available methodology, that allows a probabilistic sound approach, compatible with structural design theories. It is also a way to quantitatively manage geotechnical risks.

The need for better and more realistic calibration, using reliability based design approach shows that pile development should, at least in part, be focused on better knowledge of existing piles, design methodologies, testing techniques, etc.

Using this approach, a quantitative risk assessment is possible, allowing rational risk management, or in other words, a realistic evaluation of safety and possible margins for reducing costs. Without a probabilistic approach, risk management will continue to be, at least partially, qualitative.

6 PILE DEVELOPMENTS

Pile developments can be divided into some groups, as described in item 2. In the author's opinion and according to the amount of published papers in the last specialized conferences, the development of piles is currently focused on a better understanding of bearing capacity and load-settlement prediction and, to some extend, to improve construction reliability.

To evaluate the real possibilities of improving reliability and the capacity to predict bearing capacity and load-settlement behavior accurately, one has to consider the different factors that affect these pile characteristics.

Normally safety and reliability are affected by:

- Load uncertainties—in this paper, this issue will not be discussed;
- Material uncertainties, including strength and deformability of the pile and the surrounding material. The material uncertainties are normally divided into their intrinsic variability and those associated to representativeness, testing reproducibility, including accuracy and precision;

- Method uncertainties, associated to the design calculations and assumptions.

For practical purpose, pile behavior predictions that include all factors above, with exception of load variability, are based normally on field and laboratory testing of the foundation soil, and a model that uses these inputs. The most common soil testing performed in North-America for pile design, i.e., bearing capacity and load-settlement prediction, are SPT and CPT tests (Paikowsky, 2002). In South America, specifically in Brazil, bearing capacity predictions are based in almost all cases on SPT tests and empirical or semi-empirical correlations.

A promising new research line is under development by Odebrecht et al. (2007) and Schnaid et al. 2008: new ways to interpret SPT tests using wave propagation theory are showing interesting results for direct prediction of soil shear strength parameters. However, an extrapolation of these results to foundation engineering is not yet available.

In Europe, CPT and pressuremeter tests are the most common tools for foundation design parameter estimation.

Recent results presented by, for example, Klosinski and Rychlewski (2003) and a significant database presented by Paikowski (2002) show results of several load tests performed on piles and comparisons with results of bearing capacity prediction methods. COV (coefficients of variation) of the variable measured bearing capacity and calculated bearing capacity vary between 0,27 and 0,6.

This scatter of results of the comparison between observed and calculated bearing capacities is not significantly different from the variability observed in earlier studies by, for example, Norlund (1963), Aoki and Velloso (1975), Décourt and Quaresma (1978) and Frank (1997), leading to the conclusion that in roughly 50 years generalized formulae to predict ultimate bearing capacity have not gained significant reliability. Figure 3 presents COV associated to the databases presented by the different authors in their original papers. The data base used by Norlund in 1963 to develop the corresponding bearing capacity calculation method show a proportionally low COV, when compared to other methods. Later tests presented by Paikowsky (2002) lead to COV's between 0,22 and 0,58.

This conclusion is backed by a study by O'Neill´s (2001) about side resistance of piles, that concludes that "…much still remains to be learned... and that site specific load testing should remain an integral part of the design process for driven and drilled shafts".

Possibly, optimization can be achieved if lateral and end bearing capacity are analyzed separately: intuitively, side resistance is less affected by variability than end bearing capacity. Results of several load tests performed on different sites on driven piles confirm this statement (Bilfinger, 2002).

Figure 4 shows that the bearing capacity coefficient of variation decreases for longer piles, i.e., piles where lateral resistance is proportionally more relevant (longer piles), bearing capacity is less variable. In some, the propositions of Décourt and Quaresma (1978) use a similar approach: in their semi-empirical design methodology based on SPT blowcount, lateral resistance is factored by 1.3, while end bearing capacity is factored by 4.

A way to reduce this variability is to perform site specific load test and calibrate generalized pile behavior prediction methods to a site specific model. A theoretical sound approach is the use of Bayesian inference to combine load tests with predicted bearing capacities (Bacher and Rackwitz, 1982) (Hachich et al, 2008). But often the problem of these approaches is the necessity of performing previous load tests, preferable more than one, which in several cases is not possible. In some cases, high variability of results, even on the safe side (showing, for example, significantly higher loads than predicted), can lead to a theoretical need for higher safety factors.

Another approach is to use information from the site: a study presented by the author (Bilfinger, 2002)

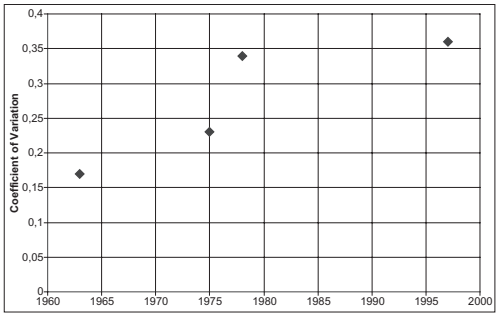

Figure 3. Coefficients of Variation of pile bearing capacity methods.

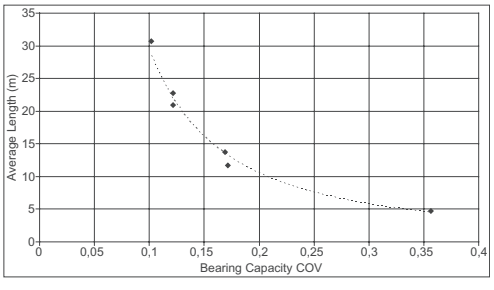

Figure 4. Pile bearing variability—coefficient of variation—as a function of pile length.

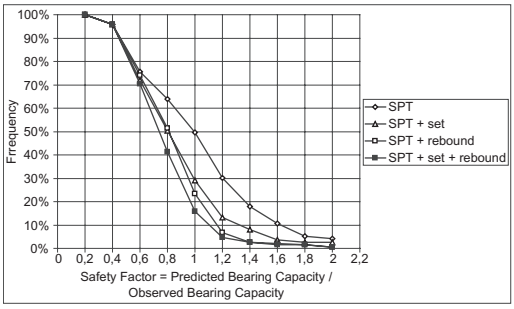

Figure 5. Safety increase due to additional pile bearing capacity prediction/control methods.

showed that for driven piles, if bearing capacity calculations were based on soil borings (SPT), a certain variability of results, and therefore, of probability of failure, should be expected. The use of complementary data related to pile installation, in this case, set and rebound due to a determined hammer and drop height, showed that variability could be reduced significantly.

Figure 5 show that if bearing capacity is based on calculations using the SPT blowcount, in this case, Décourt and Quaresma's method (1978), a certain probability of failure can be associated to a certain safety factor. If additional control methods are used, like set and/or rebound, the probability of failure for the same safety factor decreases significantly.

In the case of bored and auger piles, a direct measurement of installation parameters is more complicated, but possible. Interesting and promising results were presented by NeSmith (2003) and Saeki and Ohki (2003), where the installation effort is compared to pile bearing capacity. A statistic analysis comparing probability of failure using not only bearing capacity predictions, but adding the information of the installation effort certainly will.

The investigation of the installation parameters, in the author's opinion, is a tool to improve reliability and reduce variability. For example, a designer could make his bearing capacity predictions using SPT or CPT tests and specify a determined installation parameter. A statistical evaluation will certainly show that a combined design criteria lead to higher reliability.

From a risk management point of view, evolutions in pile behavior prediction reliability will mean, theoretically, that lower global factors of safety can be accepted. However, from a practical point of view, the risk of using a lower global factor of safety, even knowing that the probability of failure/reliability is compatible, will be taken by the involved parties only if support by a code is provided. Therefore, pile developments have to be concurrent with code developments, to allow possible cost reductions.

7 A PRACTICAL EXAMPLE

The recently finished cable stayed "Jornalista Roberto Marinho" bridge in São Paulo, Brazil, is founded on approx. 0,40 m dia. rock socketed root piles, and on 0,90 m dia. rock socketed bored piles.

The main piers foundations are the bored piles and the access bridges are founded on the root piles.

The geotechnical project was not developed using a formal risk management plan, but all design decisions can be fitted into the framework outlined in item 3. This example intends to show that it is relatively easy to use geotechnical risk management and significant possible problems can be avoided.

Subsoil in the area of the bridge can be described as being:

- Superficial uncontrolled fill layer, few meters thick;
- Recent alluvial sandy and clayey deposits, up to 10 m thick;
- Residual soil (granitic-gneissic origin);
- Transition from weathered to sound granitic gneiss.

The five step procedure described in item 3 is reproduced below, and the associated design decisions are described:

Identify hazards and associated risks, through risk assessments, that impacts on a project´s outcome in terms of cost and programme, including those to third parties:

Possible hazards identified for the foundations of the bridge were:

- Pile integrity problems due to the fill and alluvial soils;
- Insufficient bearing capacity due to insufficient embedment into the residual soil/rock;
- Aggressive groundwater;
- Insufficient concrete strength;
- Location errors during construction.

Quantifying risks including their programme cost implications. To simplify this example the cost estimative is not presented in this item.

- Pile integrity problems due to the fill and alluvial soils—relatively low probability, if adequate construction technique is used. Consequences can be significant, if not prematurely detected.
- Insufficient bearing capacity due to insufficient embedment into the residual soil/rock—if adequately designed and soil investigation campaign is representative of subsoil profile, low probability.

Consequences can be significant, if not prematurely detected.

- Aggressive groundwater—high probability due to environment. Consequences can be significant, if not prematurely detected.
- Insufficient concrete strength—low probability, because concrete will be prepared industrially and systematic control will be used. Consequences can be significant, if not prematurely detected.
- Location errors during construction—low probability. Consequences can be significant, if not prematurely detected.

Identifying pro-active actions planned to eliminate or mitigate the risks.

- Pile integrity problems due to the fill and alluvial soils—pile constructive method should be chosen, so that this risk becomes insignificant.
- Insufficient bearing capacity due to insufficient embedment into the residual soil/rock—sufficient boreholes should be perforated to allow adequate pile length estimative. For design verification/ comparison between prediction and performance, load test should be performed. Additionally, pile perforation should be controlled, verifying boring difficulties that indicate the bedrock depth.

Figure 6 beneath presents the results of the load tests performed on 2 test piles—40 cm root piles, pile 1 9,4 m long and pile 2, 11,4 m long. These piles were installed prior to foundation construction. The load tests were limited to twice the maximum structural load and performance was considered adequate.

Considering the observed behavior, pile design was considered adequate. No design optimization (i.e., proposition of shorter piles) was proposed. Possibly, the use of a Bayesian inference procedure could have lead to some optimization, but due to lack of time and willingness of the involved parties, the design as performed was considered adequate.

- Aggressive groundwater—due to the presence of aggressive groundwater, technological concrete measures should be foreseen to protect concrete from corrosion.
- Insufficient concrete strength—a test program to evaluate concrete strength should be run during pile construction.
- Location errors during construction—topography should verify pile location prior to construction.

Identify the methods to be utilized for the control of the risks.

- Pile integrity problems due to the fill and alluvial soils—constructive method should be controlled. The pile should be lined or supported by stabilizing fluid during excavation of the soil layers. For the root piles, grouting pressure should be kept high during concreting.
- Insufficient bearing capacity due to insufficient embedment into the residual soil/rock—Pile perforation should be controlled, verifying boring difficulties that indicate the bedrock depth, to allow comparison between soil profile estimative and actual profile. Complementary verification load tests should be performed.

Figure 7 presents the routine tests performed on 3 piles of the foundation.

Figure 7 shows that pile behavior can be considered adequate and in accordance with the previously performed tests.

- Aggressive groundwater—concrete quality should be controlled.
- Insufficient concrete strength—concrete quality should be controlled during pile construction.
- Location errors during construction—topography should verify pile location prior to construction.

Allocating the risks to the various parties to the contract.

- Pile integrity problems due to the fill and alluvial soils—the foundation contractor is responsible for pile integrity.
- Insufficient bearing capacity due to insufficient embedment into the residual soil/rock—the owner

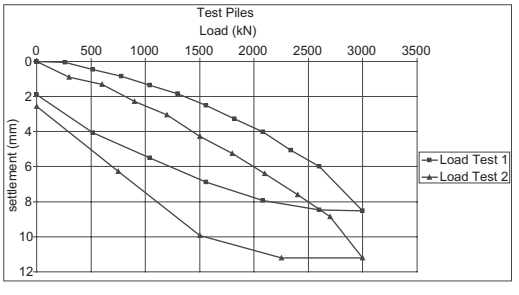

Figure 6. Load test results—prior to foundation construction.

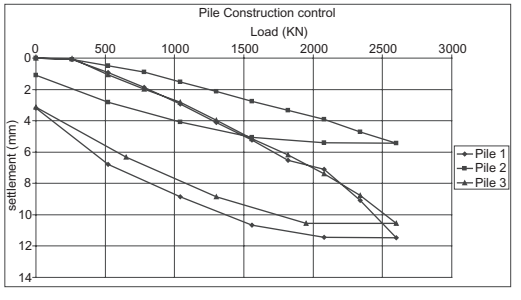

Figure 7. Routine control load test results.

is responsible for additional pile length, if bedrock elevation is different from the elevation that resulted from the site investigation campaign.
- Aggressive groundwater—the concrete supplier is responsible for concrete quality.
- Insufficient concrete strength—the concrete supplier is responsible for concrete strength.
- Location errors during construction—the contractor is responsible for adequate pile location.

The example above shows that, in a certain way, on this specific project, risk management was actually performed. The positive results were only possible due to the good relationship between owner, constructor and designer.

8 CONCLUDING REMARKS

Competitive markets are the driving forces for, on the on side, build safer and, on the other side, build cheaper.

These two apparently opposite paths can only be pursued improving knowledge about pile behavior and managing rationally risks.

Improvements of pile behavior prediction capability using the current common soil testing and pile prediction methods are difficult to achieve. The variability of the different factors affecting these methods are probably restricting reliability improvements due to their intrinsic variability.

Possible ways to improve knowledge and, therefore, reliability of piles, is the concurrent use of conventional bearing capacity prediction methods and an additional, independent, method, like, for example, measurement/specification of pile installation effort.

Rational risk management is, on the other hand, a valuable tool for all involved parties to analyze, mitigate and chare risks, explicitly allocating responsibilities. Hopefully, this tool will be used in a way that all parties can decide when and where “cheaper” can mean “better”.

ACKNOWLEDGEMENTS

The support and possibility of presenting load test results of “Jornalista Roberto Marinho” bridge by Construtora OAS is gratefully acknowledged.

REFERENCES

Aoki, N., Velloso, D.A. (1975) An Approximate Method to Estimate the Bearing Capacity of Piles. In: 5th Panamerican Conference on Soil Mechanics and Foundation Engineering, Buenos Aires.

Baecher, G.B., Rackwitz, R. (1982) Factors of Safety and Pile Load Tests. International Journal for Numerical and Analytical Methods in Geomechanics, v. 6.

Bilfinger, W. (2002) Foundation Safety Criteria of Driven Piles, considering construction control methods (*in Portuguese)*, PhD Thesis, São Paulo.

Décourt, L., Quaresma, A.R. (1978) Capacidade de Carga de Estacas a partir de Valores de SPT. In: VI COBRAMSEF, Rio de Janeiro.

Frank, R. (1997) Some comparisons of safety for axially loaded piles. In: Design of Axially Loaded Piles: European Practice.

Hachich, W.C., Falconi, F., Santos, M.S. (2008) Foundation Safety: Incorporating load test results. In: Congresso Luso-Brasileiro, Coimbra.

ICE—Institution of Civil Engineers (2001) Managing Geotechnical Risk.

ITIG (2006). A code of Practice for Risk Management of Tunnel Works

Klosinski, B., Rychlewski, P. (2003) Analysis of bearing capacity and settlement of CFA Piles. In: Deep Foundations on Bored and Auger Piles—BAP IV, Gent

Kulhawy, F.H., Phoon, K.K. (2002) Observations on geotechnical reliability-base design development in North America. In: Foundation Design Codes and Soil Investigation in view of International Harmonization and Performance, Kamakura.

Meyerhof, G.G. (1956) Penetration Tests and bearing capacity of cohesionless soils. J. Soil Mechanic and Foundation Division—ASCE, v. 82, n. SM1.

Nesmith, W.M. (2003) Installation effort as an indicator of displacement screw pile capacity. In: In: Deep Foundations on Bored and Auger Piles—BAP IV, Gent

Norlund, R. (1963) Bearing Capacity of Piles in Cohesionless Soils. Journal of the Soil Mechanics and Foundations Division—ASCE, v. 89, n. SM3.

Odebrecht, E., Schnaid, F., Rocha, M.M., Bernardes, G.P. (2007) Energy efficiency for Standard Penetration Tests. Journal of Geotechnical and Geoenvironmental Engineering, v. 133, p. 486–490.

O’neill, M.W. (2001) Side Resistance In Piles and Drilled Shafts. Journal of Geotechnical and Geoenvironmental Engineering—ASCE, v. 127, n. 1.

Paikowsky, S.G. (2002) Load and resistance factor design (LRFD) for deep foundations. In: Foundation Design Codes and Soil Investigation in view of International Harmonization and Performance, Kamakura.

Saeki, E. Ohki, H. (2003) A study of the screwed pile—The result of installation and loading tests and analysis of penetration mechanisms. In: Deep Foundations on Bored and Auger Piles—BAP IV, Gent.

Schnaid, F., Odebrecht, E., Rocha, M.M., Bernardes, G.P. (2008) Prediction of soil properties from the concepts of energy transfer in dynamic penetration tests. To be published in JGGE—ASCE.

van Impe, W. (1998) Deep Foundations on Bored and Auger Piles—BAP III, Gent.

van Impe, W. (2003) Deep Foundations on Bored and Auger Piles—BAP IV, Gent.

van Staveren, M. (2006) High Risk Control for Piling and Deep Foundations—A Systematic Approach. In: Piling and Deep Foundations—DFI 2006.

Whitman, R.V. (2000) Organizing and evaluating uncertainty in geotechnical engineering. J. Geotech. Engrg., ASCE 110(2).

Deep Foundations on Bored and Auger Piles – Van Impe & Van Impe (eds)
© 2009 Taylor & Francis Group, London, ISBN 978-0-415-47556-3

The assessment of load-settlement curve for Atlas piles correlated with CPT tests

K. Gwizdała, A. Krasiński & T. Brzozowski
Gdansk University of Technology, Poland

ABSTRACT: Rational calculations of piling foundations require reliable assessment of complete load-settlement relation for a single pile and settlements of pile groups under working loads. At the design stage when the results of load tests are unknown, the analytical methods enabling approximated determination of load-settlement curves and settlements of the whole foundation are very helpful. Currently, the recommendations included in Eurocode 7 do not precise detailed calculation methods, presenting only some general suggestions to apply local (domestic) correlations. In the paper the results of investigations of Atlas piles are presented. The piles have been installed in complex geotechnical conditions in centre of Gdansk where the subsoil is strongly layered consisting of mud and peat layers, several meters thick. Reliable load-settlement curves were obtained from static load tests. Analytical curves were calculated using load-transfer functions (for the base and shaft of pile) and have been next compared to load tests results. Application of the geotechnical parameters of natural subsoil (prior to the installation of piles) and actual load-settlement curves enabled a determination of load-transfer function parameters that, in turn, allows for a description of reliable relations for analytical assessment of load-settlement curves for engineering purposes (see also EC7).

1 INTRODUCTION

Engineers are more and more often in a situation to carry out the foundation works in difficult urban conditions, where additionally a great pressure is putting on ecological aspects of piling works. The above requirements are fulfilled, among other, by Atlas piles, the installation of which in and near Gdansk, effectively and practically confirmed their advantages.

In spite of above advantages, the estimation of bearing capacity and settlements of screwed piles, as a full displacement piles is still an open problem for engineers and researchers. Among all types of piles, the technological aspects of screwed piles have the larges influence of their bearing capacity and their work in the subsoil, and therefore that aspects have to be taken into account during design process.

In case of bored piles (with casing or CFA piles), the expected bearing capacity can be practically designed with an arbitrary diameter and length. The same regards driven piles, although there are some restrictions with regard to diameter sizes (usually up to ϕ600 mm) and pile bearing capacity (practically up to 3000 kN), mostly due to strength of the pile rod during driving process. In Poland, bored and driven piles are usually designed using simple standard recommendations consisting of tabular values of technological coefficients and soil resistances under the base and along the shaft of the pile, q and t respectively (Gwizdała, 1997).

In the case of screwed piles, the problem is more complex. The pile can not be designed for an arbitrary bearing capacity, particularly too high bearing capacity. During design stage the engineer should be aware whether an installation of screwed pile of given bearing capacity is possible to be executed by accessible devices. Present experience shows that both, tabular values of technological coefficients as well as q and t resistances existing in Polish Piling Code are not suitable for screwed piles. The design of this pile type requires more precise geotechnical data, preferably obtained from CPT or CPTU tests.

Thus, instead of tabular standard values of q and t, direct correlations between soil resistances of the penetrometer q_c and f_s and the pile resistances q and t are implemented. In these correlations the influence of pile diameter as well as soil type should be taken into account and the design procedure of bearing capacity should have upper limit (e.g. maximum value of q_c or Q_{total}) determining technologically induced application range for screwed pile.

Such design procedures for screwed piles, based on the interpretation of CPT tests have been already proposed by some authors (see e.g. Bustamante,

Gianaselli, 1993; Van Impe, 1994, 1998; Bottiau, Cortvindt, 1994). However, in Polish geotechnical conditions, the procedures require the verification by series of tests made in the filed conditions.

At present, in the Europe general concept of limit states method (ULS, SLS) is commonly accepted, Eurocode 7, EN 1997. However, general rules for piles proposed in the EC7 do not consider detailed formulae

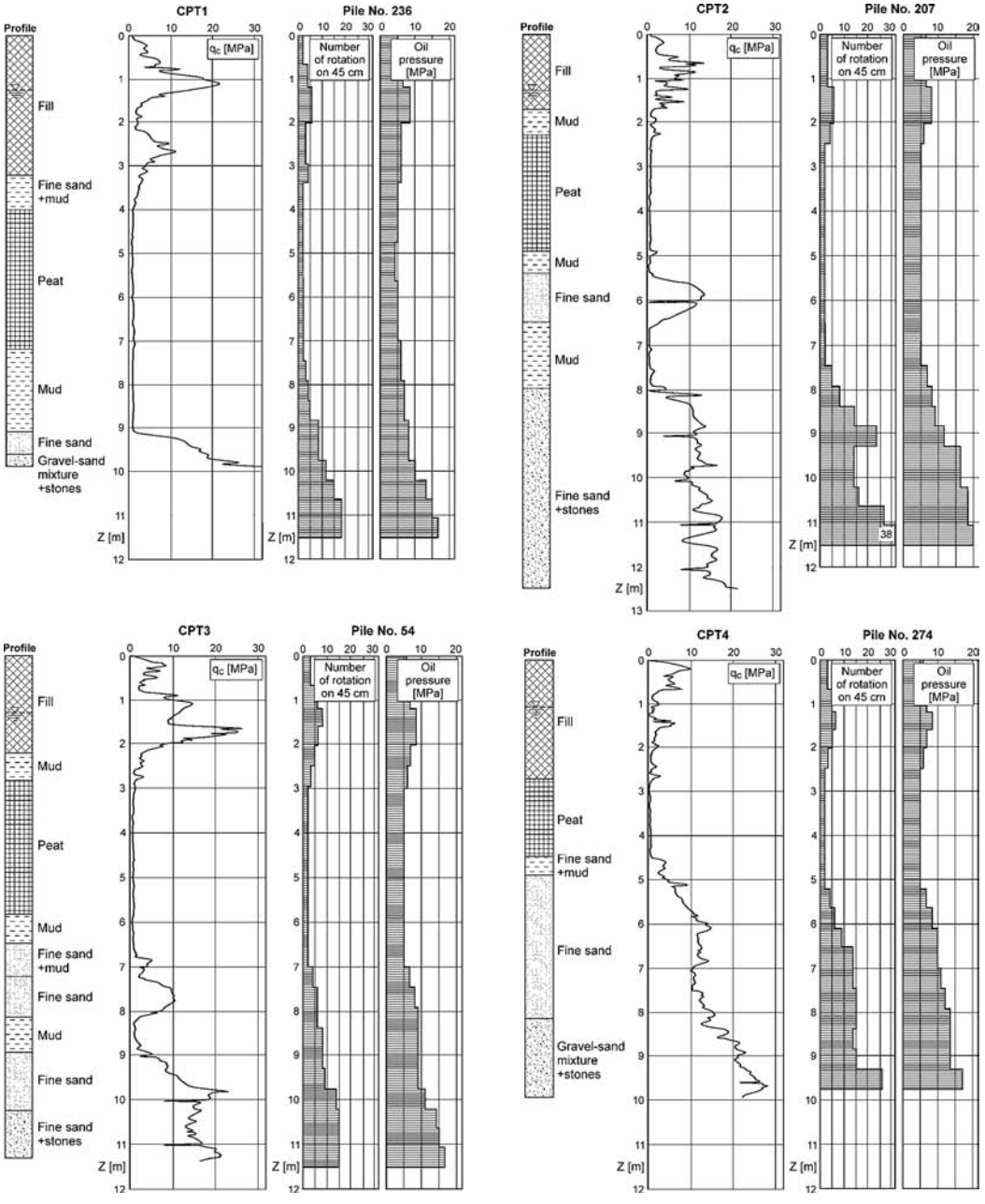

Figure 1. Geotechnical conditions and pile installation parameters.

for simple engineering calculations of bearing capacity and settlements of piles. It is rightly suggested in this case that European member countries should use national or even regional experience in this case.

2 SUBJECT OF THE PAPER

In the paper, some exemplary results of tests of Atlas piles, carried out during the foundation works for new education building at Gdansk University of Technology are presented. Actual pile characteristics expressed by load-settlement *Q-s* curves have been interpreted by back-analysis using *t-z* and *q-z* load-transfer functions. Then, interpreted ultimate t_s and q_b resistances were correlated to CPTU resistance q_c. Correlations obtained were next compared to those proposed by Bustamante what enabled to formulate final conclusions.

3 BRIEF DESCRIPTION OF THE PILE FOUNDATION AND SOIL CONDITIONS

The education building of Gdansk University of Technology has been founded on 305 Atlas piles: 188 piles diameter ϕ510/720 mm and 117 piles diameter ϕ360/530 mm. Initially, all piles have been designed for the length of L = 11.5 m, however due to high soil resistances during the pile installation part of the piles was shortened to the length of about L = 9.0 m.

Geotechnical conditions of the subsoil in the construction site were highly unfavorable because it was the area of former pond, which was filled with loose fill. Under the fill there was the layer of weak soils recognized, mostly formed by mud and peat of the thickness of 5 to 7 m. Below these soils there are sandy layers of various grain size—from fine sands to gravel with cobbles. Geotechnical recognition of the subsoil consisted of standard boreholes, dynamic tests and static penetrations (CPTUs). The results of the latter are shown in Fig. 1.

4 STATIC LOAD TESTS OF BEARING CAPACITY OF PILES

Static load tests have been performed on four piles: two piles of diameter ϕ510/720 mm and two piles of diameter ϕ360/530 mm, among which three piles were L = 11.0 m long and one pile was L = 9.5 m long (with diameter of 360/530 mm). The results of load tests in the form of *Q-s* relations were presented in Fig. 2. Please note, that the characteristics of *Q-s* relations of all piles are very similar. The piles were installed in terms of the same device and with the same, full screwing energy. Generally speaking the piles were being screwed to the depth at which q_c reached the value 15 ÷ 20 MPa.

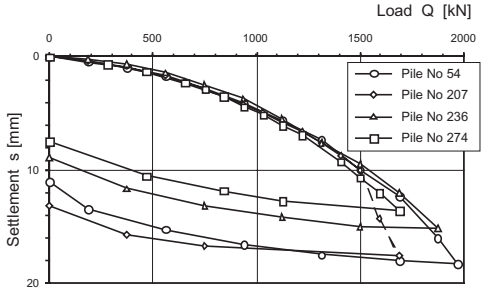

Figure 2. Load-settlement curves for all piles.

5 INTERPRETATION OF THE TEST RESULTS BY LOAD-TRANSFER FUNCTIONS

In order to construct analytical representation of load-settlement curves, the load-transfer functions method was used, see e.g. Paulos, 1980, Gwizdala, 1997. In this method, the pile is divided into elastic elements corresponding to soil layers. Soil-pile elements interaction is described by load-transfer functions: *t-z* for pile shaft and *q-z* for pile base, respectively. Practical calculations are performed in the iterative process leading to a determination of the distribution of loads along the pile length and load-settlement relation for the pile head.

Correctness of the results is verified by respective parameters describing particular load-transfer functions, such as:

– unit ultimate resistances along the pile shaft—$t_{\max}$ and under the pile base—q_f,
– non-linear initial stiffness of the pile determined in load-transfer functions,
– ultimate settlements z_v and z_f corresponding to ultimate resistances q and t.

As an initial base for further analyses, values of q and t suggested in Polish Piling Code, PN-83/B-02482 were assumed. The values roughly correspond to the technology of classical bored piles. Initial pile stiffness for t and q resistances was determined by the following, simple power functions:

– for the shaft: $t = t_{\max}\left(\frac{z}{z_v}\right)^{\alpha}$; for $z \le z_v$,

– for the base: $q = q_f\left(\frac{z}{z_f}\right)^{\beta}$; for $z \le z_f$.

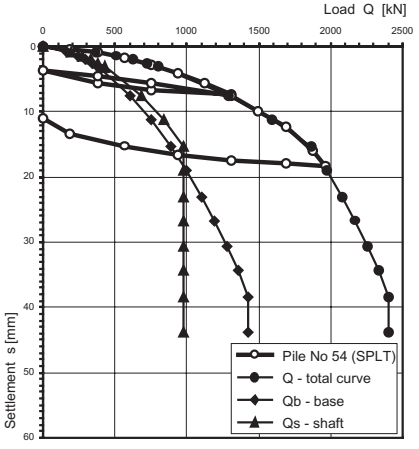

Figure 3. Load-settlement curve for Atlas pile No. 54, (ϕ510/720 mm, L = 11.0 m).

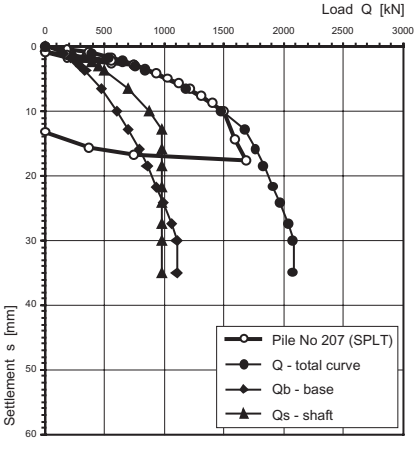

Figure 4. Load-settlement curve for Atlas pile No. 207, (ϕ360/530 mm, L = 11.0 m).

In calculations it was assumed $z_f = 0.05\ D$, $z_v = 0.01$ D, $\alpha = \beta = 0.5$ (where D—pile diameter).

Next, the base values were being corrected using back-analysis to obtain best possible correlation to load-settlement curves. In the correction process known principles (from experience) regarding the work of Atlas piles, described in the literature (e.g. Bustamante, Van-Impe) as well as technological aspects of the installation of the piles were applied. In Figs. 3, 4, 5 and 6 real load-settlement curves versus theoretical predictions are shown.

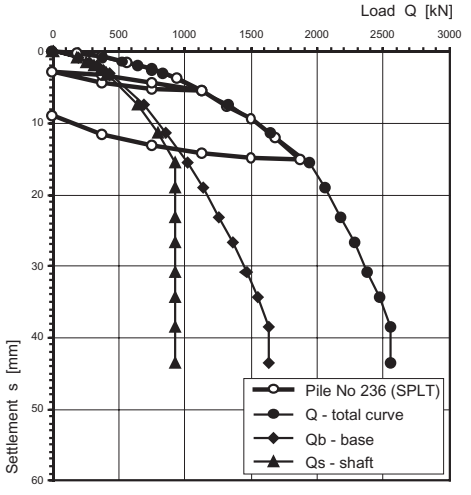

Figure 5. Load-settlement curve for Atlas pile No. 236, (ϕ510/720 mm, L = 11.0 m).

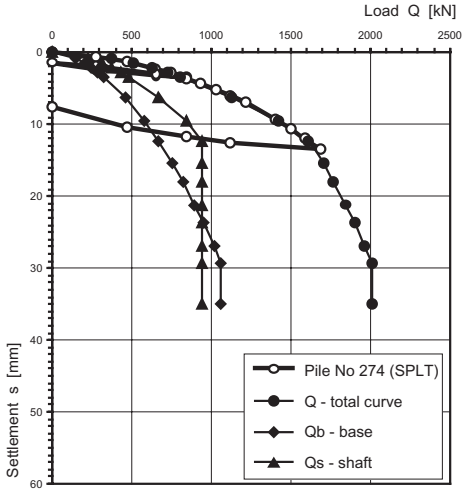

Figure 6. Load-settlement curve for Atlas pile No. 274, (ϕ360/530 mm, L = 9.5 m).

6 CORRELATIONS BETWEEN CPT TESTS AND LOAD-SETTLEMENT CURVES OF PILES

Among the basic parameters which underwent the correction the most important are the values of ultimate resistances t_{max} and q_f. These values were collated in Table 1 together with corresponding values obtained from CPTs (q_c). In this way it was possible to determine dimensionless correlations q_c / t_{max} and q_f / q_c.

The correlations were very similar for all piles but for piles with smaller diameter the correlations were

Table 1. Results of analysis.

Pile [–]	CPT [–]	Soil [–]	q_c [MPa]	q_f [kPa]	t_{max} [kPa]	q_f/q_c [–]	q_c/t_{max} [–]
No 54, ϕ510/720 mm	No. 3	Fine sand	15	3500	110	0.23	136
No 207, ϕ360/530 mm	No. 2	Fine sand	15	5000	130	0.30	115
No 236, ϕ510/720 mm	No. 1	Gravel and sand	20	4000	140	0.20	143
No 274, ϕ360/530 mm	No. 4	Gravel and sand	20	4800	160	0.24	125

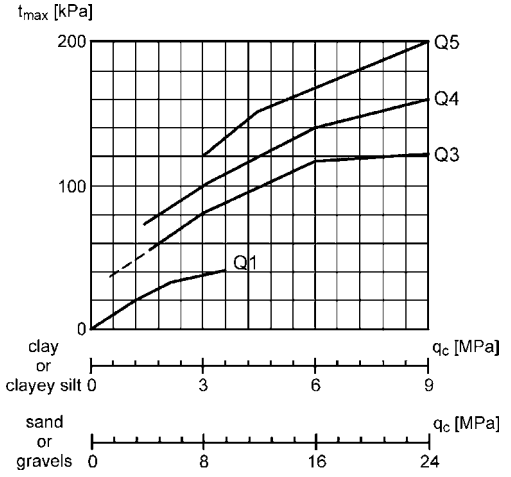

Figure 7. Unit ultimate soil resistance curves along the shaft of the pile in relation to CPT test results (Bustamante, Gianaselli, 1993).

Table 2. Selection of Q curve in relation to soil type and q_c (Bustamante, Gianaselli, 1993).

Soil	Type of curve	q_c [MPa]
Clay or clayey silt	Q1	<0.1
	Q3	>1.5
	Q4	= 3.0
Sand or gravels	Q1	<1.0
	Q4	>3.5
	Q5	>8.0

a little higher than for piles with larger diameter and a little higher for fine sand than for sand and gravel. Next, the correlations were compared with Bustamante proposal. It resulted in, that the correlations of q_c/t_{max} were similar (see Fig. 7 and Table 2) but correlations of q_f/q_c obtained in analyzed case were much smaller than in Bustamante proposal, in which for sandy soils coefficient $q_f/q_c = 0.50 \div 0.75$ is proposed.

Additionally, it should be noted, that the Atlas piles in analyzed case were installed using full screwing energy of the device. It means, that the soil resistances t_{max}, q_f are the maximum values for Atlas piles and corresponding values of $q_c = 15 \div 20$ MPa are acceptable upper limits for Atlas piles application.

7 CONCLUSIONS

The analysis of the work of Atlas piles, made by load-transfer functions of *t-z* and *q-z* type, has shown that the ultimate resistance t_{max} along the pile is up to 80% than proposed in Polish Code for bored piles installed in the same soil conditions. The base resistance q_f is also higher than in code and depends on overburden pressure, deep of the pile base and pile diameter. The increase is obviously the result of compaction and additional stresses in the subsoil induced during screwing process.

Dimensionless relationships for q_f and t_{max} resistances, referred to CPT test results (and q_f/q_c) show some common features. The relations q_c/t_{max} are in the agreement with Bustamante proposal but relations q_f/q_c are distinctly smaller than proposed by Bustamante.

The analysis suggests that the relationships obtained may be described by common procedure for design of bearing capacity of Atlas pile based on CPT test results.

Additionally, the case analysed has shown that Atlas piles of given diameter can be installed in the sandy subsoil, for which the CPT resistance fulfills the following condition: $q_c < 15 \div 20$ [MPa], taking into account also the grain size and pile diameter *D*. The condition may be treated as upper criterion of Atlas piles application.

REFERENCES

Bottiau M., Cortvindt G., 1994: Recent experience with the Omega-Pile. *Fifth International Conference on Piling and Deep Foundations*, 13–15 June, Bruges, 3.11.0–3.11.7.

Bustamante M., Gianaselli L., 1993: Design of Auger displacement piles from in situ tests. *Deep Foundations on Bored and Auger Piles*. Rotterdam, Balkema, 21–34.

De Cock, F., Imbo, R., 1994: The Atlas screw pile—A vibration free full displacement cast-in-place pile. *73d annual meeting of the USA transportation Research Board*, Washington D.C.

Gwizdała K., 1997. Polish design methods for single axially loaded piles. *ERTC3 Seminar*. Brussels. 291–306.

Gwizdała K., Dyka I., 2002: Estimation of settlements of piles in group. *Ninth International Conference on Piling and Deep Foundations*. Nice, 3–5 June 2002 Paris. 257–262.

Gwizdała K., Krasinski A., Brzozowski T., 2006: Experience gained at the application of Atlas piles in Poland. *Piling and Deep Foundations: 10th International Conference*, Amsterdam, 31st May–2nd June 2006. 460–464.

Poulos H.G, Davis E.H, 1980: *Pile foundation analysis and design*. New York: John Wiley and Sons.

Van Impe, W, F, 1994: Influence of screw pile installation parameters on the overall pile behaviour. *Workshop "Piled Foundations: full scale investigations, analysis an design"*, Naples.

Van Impe, W,F, 1988. Considerations on the auger pile design. *First International Geotechnical Seminar on Deep Foundations on Bored and Auger piles*, Ghent. 193–218.

EN 1997 (2004). *Eurocode 7. Geotechnical design*.

Polish Code PN-83/B-02482, 1983: *Foundation. Bearing capacity of piles and pile foundations*.

Deep Foundations on Bored and Auger Piles – Van Impe & Van Impe (eds)
© 2009 Taylor & Francis Group, London, ISBN 978-0-415-47556-3

A post-analysis of a large piled raft foundation constructed using reverse construction method

P. Kitiyodom, T. Matsumoto & R. Sonoda
Kanazawa University, Kanazawa, Japan

ABSTRACT: In this paper, post-analysis of the deformation of a large piled raft foundation was carried out using a three-dimensional analysis program PRAB. The soil parameters used in the analysis were obtained from the back analysis of the results of the pile load test that was conducted at the construction site. In the deformation analysis of the whole foundation, the concept of the equivalent pier was employed. The results of the analysis match well with the measured distribution of the foundation settlements.

1 INTRODUCTION

A commercial building was constructed in Kagoshima City, Japan in 2003 to 2004. The building is 7-storied building with a basement floor, having a building area of 9000 m^2, a floor area of 50000 m^2 and a maximum height of 45 m (Figure 1). The building has a composite structure consisting of steel reinforced columns and steel beams. Piled raft foundation was employed for this building to reduce the average settlement as well as the differential settlements. The raft supported by 160 piles was placed on a sandy ground The building was constructed using reverse construction method, in which construction of the superstructure (building) and the substructure (foundation) were constructed simultaneously, in order to reduce the construction period.

A static vertical pile load test was carried out at the construction site. Moreover, during the construction stage, settlements of the foundation and the water pressure beneath the raft were monitored. In this paper, post-analysis of the deformation of the foundation was carried out using a computer program PRAB that has been developed by Kitiyodom & Matsumoto (2002, 2003).

The back analysis of the results of the pile load test was carried out first to obtain the soil parameters for the analysis of the piled raft foundation. In the analysis of the piled raft foundation, in order to reduce the computation time, the concept of the equivalent pier in which a number of piles are model as an equivalent pier was employed. The results of the analysis are compared with the observed settlements of the foundation, and the validity of the concept of the equivalent pier is discussed.

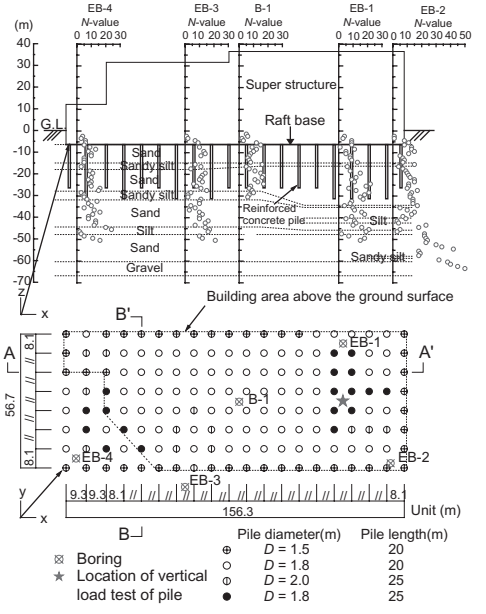

Figure 1. Elevation view of building, soil profiles, SPT-*N*-values and arrangement of piles.

2 SITE DESCRIPTION

Borehole investigations were carried out at 5 locations (EB-1 to EB-4 and B-1) within the construction site to characterise the soil conditions (Figure 1). Borehole investigations at EB-1 to EB-4 were carried out in 1993 to explore soil stratification and to obtain

distributions of SPT blow count, *N*, to depths of 50 m to 65 m. Detail borehole investigation was carried out at B-1 in 2002.

In this borehole investigation, PS-logging (elastic wave exploration) was carried out as well to estimate velocities of primary wave, V_p, and secondary wave, V_s, to a depth of 30 m below the ground level, which is nearly equal to levels of tip of piles.

The borehole investigations showed that the stratification at the construction site is almost horizontal. The soil layers to a depth of 60 m are sand or sandy silt or silt. The *N*-values are 10 to 20 to a depth of 50 m. A gravel layer having *N*-values larger than 50 exists below a depth of 60 m.

Figure 2 summarised the results of SPT at B-1 and EB-2, and PS-logging at B-1. The shear wave velocities, V_s, of the soils deeper than 30 m were estimated using an empirical equation (Equation 1) proposed by Ohta & Goto (1976):

$$V_s = 68.79 \times N^{0.171} \times H^{0.199} \times Y_g \times S_t \qquad \text{(m/s)} \qquad (1)$$

where H is the depth from G.L. (m), Y_g the geologic time coefficient, and S_t is parameter depending on soil type.

SPT *N*-values at point B-1 and EB-2 are very similar to a depth of 30 m, and it is seen that V_s measured by means of PS-logging and estimated using Equation 1 are almost identical to the depth of 30 m. Based on these results, the variation of the shear modulus at small strain level, G_0, to a depth of 63 m was estimated by means of Equation 2 and indicated in Figure 2.

$$G_0 = \rho_t V_s^2 \qquad (2)$$

where ρ_t is wet density of the soil (ρ_t = 1.6 ton/m^3 was assumed for depths greater than 30 m).

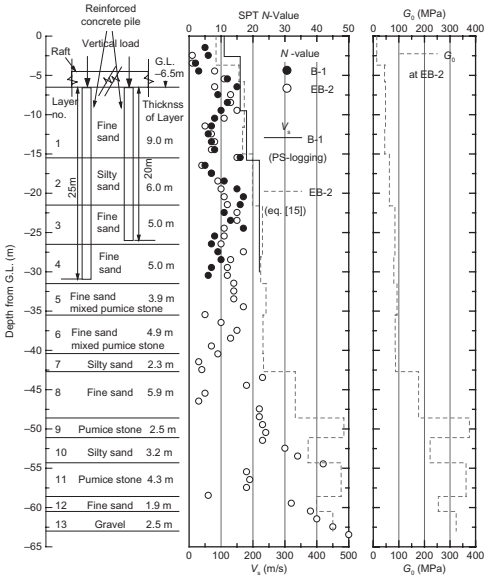

Figure 2. Modelling of foundation and ground.

3 FIELD OBSERVATIONS & PILE LOAD TEST

3.1 *Field observations*

The field observations included measurements of settlements of the raft at 45 points and water pressure beneath the raft.

Figure 3 shows the time histories of the total load from the building and measured water pressure beneath the raft. The construction of the building was completed in September 2004. The raft (mat slab of the basement floor) was completed at the end of December 2003. Hence the foundation was regarded as a pile group until the end of December 2003, and was regarded as a piled raft after that.

The raft base was located at 6.5 m below the original ground surface. The original ground water table (3.0 m below the ground level) was lowered to 7.5 m below the ground level until the end of February 2004, by means of deep wells. Then, the lowered ground water table was recovered to the original water table. The measured increase in the water pressure of 35 kPa corresponded to this recovery of the ground water table.

3.2 *Pile load test*

A test pile was constructed additionally at a location indicated by 'star' symbol in Figure 1. The test pile was a cast-in-situ concrete pile having a length of 32.0 m and a diameter of 1.0 m.

Shaft friction of the pile to a depth of 7.5 m was cut off by installing a double steel tube to this depth. Axial forces were measured at 6 levels of the pile (Figure 4) and shaft resistance at sections between the strain gauge levels was derived from the axial forces.

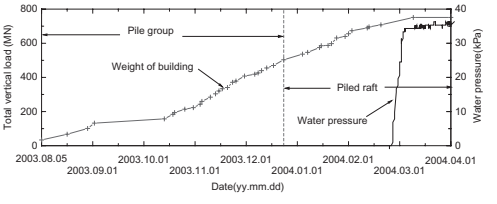

Figure 3. Time histories of the total load from the building and measured water pressure at the raft base.

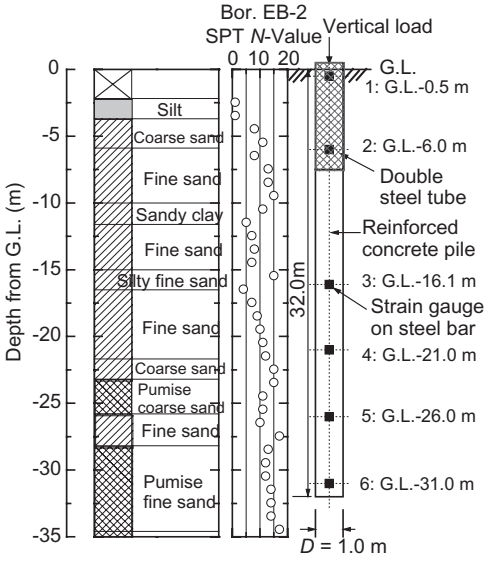

Figure 4. Seating of test pile, and soil profile and SPT-N values obtained at borehole EB-2.

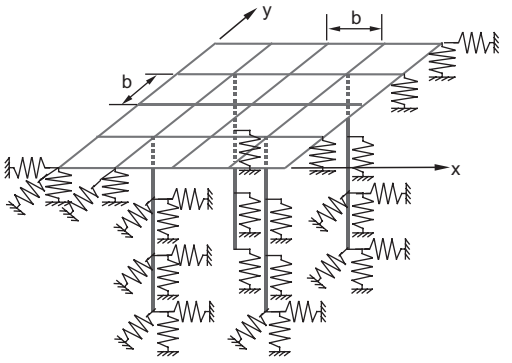

Figure 5. Modelling of piled raft foundation.

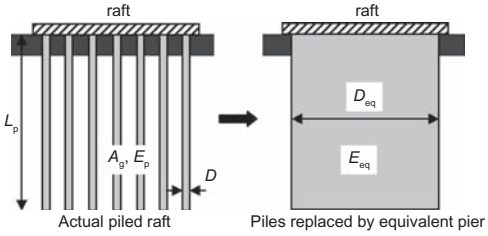

Figure 6. Concept of equivalent pier method.

4 POST-ANALYSIS

4.1 *Analytical method*

The post-analysis was carried out using a simplified three-dimensional deformation analytical program PRAB that has been developed by Kitiyodom & Matsumoto (2002, 2003). This program is capable of estimating the deformation and load distribution of piled raft foundations subjected to vertical, horizontal and moment loads, using a hybrid model in which the flexible raft is modelled as thin plates alone or beams alone or combination of thin plates and beams, the piles as elastic beams and the soil is treated as interactive springs (see Figure 5). Both the vertical and horizontal resistances of the piles as well as the raft base are incorporated into the model. Pile-soil-pile, pile-soil-raft and raft-soil-raft interactions are taken into account based on Mindlin's solutions (Mindlin, 1936) for both vertical and horizontal forces. The considered soil profile may be homogeneous semi-infinite, arbitrarily layered and/or underlain by a rigid base stratum. Note that the estimation of non-linear deformation of the foundations can be calculated by employing the bi-linear response of the soil springs.

4.2 *Equivalent pier concept*

For calculation relating to large structures supported by a number of pile groups, Poulos & Davis (1980) proposed the equivalent pier method. Horikoshi & Randolph (1999) employed this method to estimate the overall settlement of piled rafts. In this method, a number of piles are replaced by a single 'equivalent pier' as shown in Figure 6.

As suggested by Randolph (1994), the diameter of the equivalent pier, D_{eq}, can be taken as

$$D_{eq} = 2\sqrt{A_g/\pi} \tag{3}$$

where A_g is the plan area of the pile group as a block.

Young's modulus of the equivalent pier, E_{eq}, is then calculated as

$$E_{eq} = E_s + (E_p - E_s)A_{tp}/A_g \tag{4}$$

where E_p is Young's modulus of the pile, E_s the average Young's modulus of the soil penetrated by the piles, and A_{tp} is the total cross-sectional area of the piles in the group.

Randolph & Clancy (1993) discussed the applicability of the equivalent pier method and proposed an appropriate parameter to categorize as

$$R = \sqrt{ns/L_p} \tag{5}$$

where n is the number of piles and s is the pile spacing. It was shown in their work that the equivalent pier approach was suitable for values of R less than 4 and certainly for values less than 2.

4.3 *Back-analysis of vertical pile load test*

In order to determine the soil parameters appropriately, back-analysis of the vertical load test of the test pile was carried out prior to the analysis of the whole foundation. The test single pile and the ground were modelled as Figure 4. Young's modulus of the pile $E_p = 2.27 \times 10^7$ kPa was employed. The maximum shaft friction, f_{max}, of each section (see Figure 4) obtained from the static vertical pile load test results was adopted in the back-analysis.

Figure 7 shows comparison of the analysed and measured load-settlement curves of the pile head and the pile base. Good matching was obtained if the shear modulus of the soil obtained from PS-logging was reduced by a factor of 2 for the soils surrounding the pile shaft and by a factor of 5 for the soil beneath the pile base. These reductions in the shear moduli of the soils may be reasonable, considering disturbance of the soils around the pile, and difference of strain levels between the pile load test and PS-logging. Such reduction in the shear moduli of the soils around the pile are considered also in the post analysis of the whole foundation.

4.4 *Analyses of the whole foundation system*

The modelling of the foundation and the ground has been shown in Figure 2. It was judged that modelling of the ground to the depth of 63 m is needed when analysing the whole foundation because the influence of the wide length of the raft of 156 m reaches to deeper depths. Note here that SPT *N*-values for depths greater than 63 m were very large and the depth of 63 m was assumed to be a bed stratum.

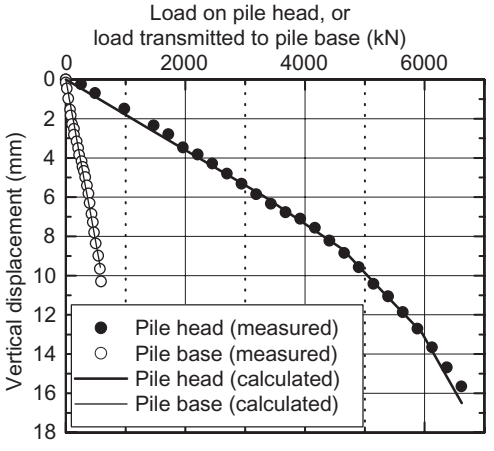

Figure 7. Comparison of load-settlement curves of the test pile.

Figure 8 shows the piles and the equivalent piers arrangement. Property of the equivalent piers are summarised in Table 1. It can be seen that the values of R in all types of equivalent piers are less than 2.

The interaction factors and soil springs at the raft nodes were calculated using the shear moduli, G_0, at small strain level shown in Figure 2, while reduced shear moduli estimated from the back-analysis of the static load test mentioned in the previous section were used for estimation of the soil springs at the pile nodes. For the estimation of the Young's modulus of a equivalent pier and soil springs at the equivalent pier nodes, the soil moduli, G_0, at small strain level were employed.

Figure 9 shows a side view of the building. In the modelling of the foundation structure, the raft was modelled by combination of thin plates and beams. The raft base was located at 6.5 m below the original

Table 1. Properties of equivalent piers.

Pier type	D_{eq}(m)	L_p(m)	E_{eq}(kPa)	R
1	11.17	20	2.51×10^6	1.27
2	20.31	20	1.76×10^6	1.90
3	11.17	25	2.52×10^6	1.14

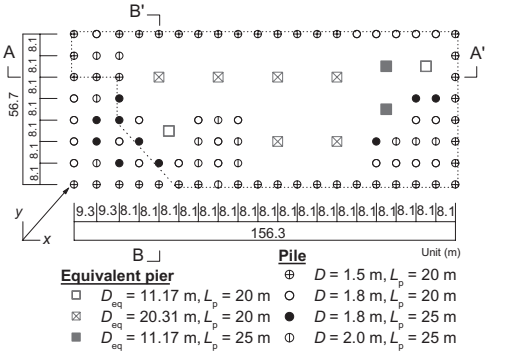

Figure 8. Arrangement of piles and equivalent piers.

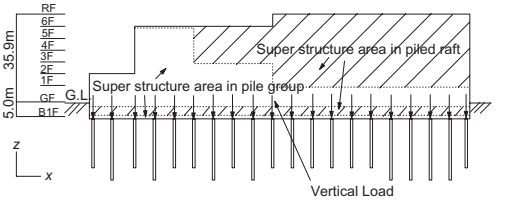

Figure 9. Construction areas of superstructure in stages of pile group and piled raft.

ground surface. In the analysis, the construction of the superstructure was divided into two stages in which the foundation acted as a pile group and as a piled raft. The hatching indicates the area of the superstructure constructed in the stage of piled raft.

In the deformation analysis of the whole structure, rigidity of the superstructure was neglected and vertical loads from the superstructure were directly applied on the raft nodes. The analysis was carried out in two stages. The first stage was the deformation analysis in stage of pile group where the raft resistance was not expected. The deformation analysis in stage of piled raft was carried out after the end of the first stage, considering the existence of the raft resistance. The stress conditions at the end of the first stage were used for the initial conditions in the second stage.

Figure 10 shows the distributions of loads on the raft. In the analysis, the loads acting on the top of the piles, which were modelled as an equivalent pier, were summed up and placed on the top of the equivalent pier node. In analysis for the stage of pile group foundation, load increments shown in Figure 10(a) were applied on the raft in 20 steps, in order to allow for the slippage of the pile and the pier shaft, and the failure of the pile and the pier base. In analysis for the stage of piled raft foundation, load increments of Figure 10(b) were applied on the raft. Note here that the ground water level was recovered at the construction stage of the piled raft as mentioned earlier. The buoyancy force due to the water pressure at the raft base was also taken into account in addition to the load increments of Figure 10(b).

Figures 11 and 12 show the distributions of calculated and measured settlements of the raft in the x-direction at y = 40.5 m (see Figure 1, section A-A') and those in the y-direction at x = 34.8 m (see Figure 1,

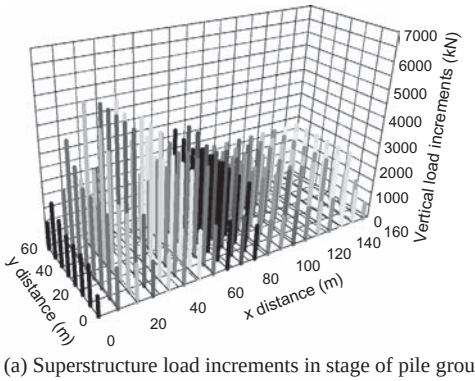

(a) Superstructure load increments in stage of pile group

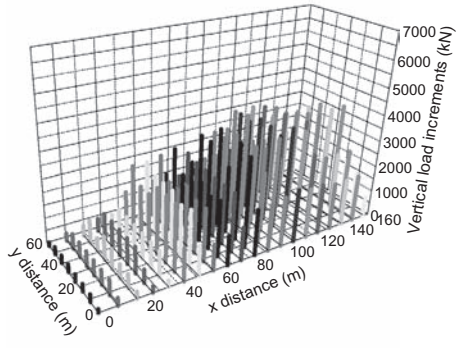

(b) Superstructure load increments in stage of piled raft

Figure 10. Distribution of loads on the raft.

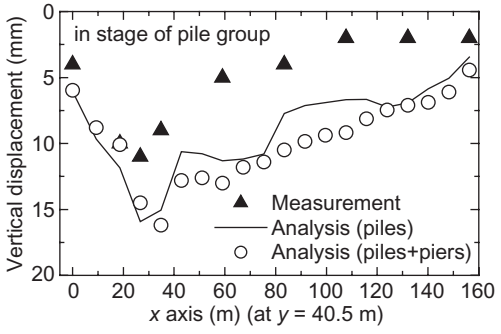

(a) Increments of settlements in stage of pile group

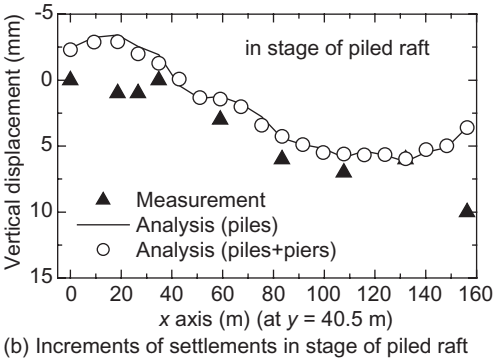

(b) Increments of settlements in stage of piled raft

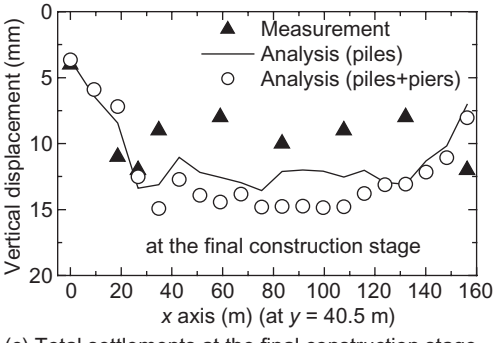

(c) Total settlements at the final construction stage

Figure 11. Calculated and measured settlements (at y = 16.2 m).

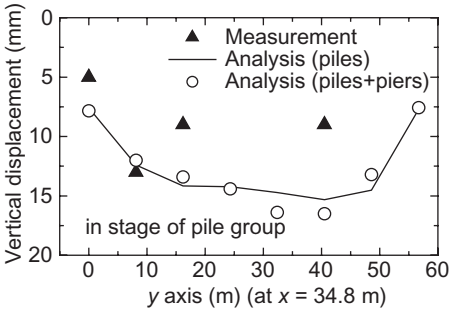

(a) Increments of settlements in stage of pile group

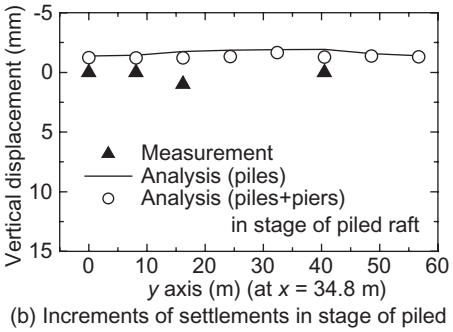

(b) Increments of settlements in stage of piled raft

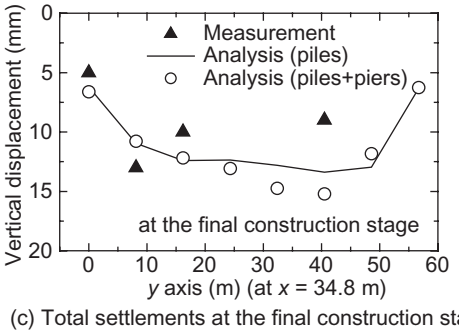

(c) Total settlements at the final construction stage

Figure 12. Calculated and measured settlements (at $x = 3\,4.8$ m).

section B-B'), respectively. Increment of settlements in stage of pile group are shown in Figures 11(a) and 12(a), those in stage of piled raft are shown in Figures 11(b) and 12(b), and the total settlements at the final construction stage are shown in Figures 11(c) and 12(c). In the figures, the calculated results of Sonoda et al. (2008) in which all of piles were modelled as piles in the analysis using PRAB are also shown. It is seen from the figure that although the analyses tends to overestimate the measured settlements in the stage of pile group foundation and underestimate the measured settlements in the stage of piled raft foundation, the analyses predicted the measured total settlements fairly well. It can be seen from the both analysis results that the analysis results using equivalent pier concept match very well with the analysis results of Sonoda et al. (2008). This demonstrates the validity to model some piles in the piled raft as the equivalent piers. Note that the calculation time using equivalent pier concept is less than 1/3 of the calculation time used in Sonoda et al. (2008).

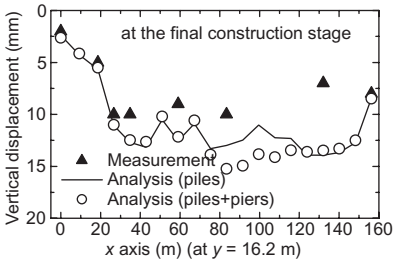

(a) Calculated and measured total settlements (at $y = 16.2$ m)

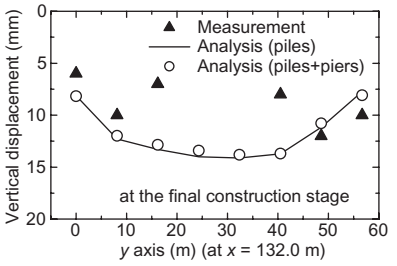

(b) Calculated and measured total settlements (at $x = 132.0$ m)

Figure 13. Calculated and measured total settlements.

Moreover, the distributions of calculated and measured total settlements of the raft are shown in Figure 13(a) for the distributions of settlements in the x-direction at $y = 16.2$ m, and in Figure 13(b) for distributions of settlements in the y-direction at $x = 132.0$ m. It is seen again from the figures that there are good agreements between the analysis results and the measured settlements.

5 CONCLUDING REMARKS

Deformation analysis of a piled raft foundation for a building constructed using reverse construction method was presented. The foundation system acted as a pile group in earlier stage and then acted as a piled raft in later construction stage in the reverse construction method. Detailed field measurements including settlements of the raft and the water pressure beneath the raft, and a static load test of a test pile were carried out during the construction work.

Post-analysis of the foundation system was carried out using a simplified three-dimensional deformation analysis method. In this paper, some of the piles were

modelled as the equivalent piers. The shear moduli of the ground were estimated from PS-logging and back analysis of the static pile load test. It was shown that the calculated settlements were acceptable for practical design purpose.

It was found from this case study that the analysis results using equivalent pier concept in which piles are modelled as equivalent piers match very well with the analysis results of the full model, and the calculation time of the analysis using equivalent pier concept are less than 1/3 of the calculation time of the full model analysis.

The above conclusions encourage the use of the simplified deformation analysis with the equivalent pier concept in the alternative designs of a large piled raft foundation.

ACKNOWLEDGEMENTS

The authors deeply thank to Kyushu Railway Company and Kagoshima Terminal Building Corporation and Yasui Architects & Engineers, Inc. for their permission to use the valuable field measurement data.

REFERENCES

Horikoshi, K. & Randolph, M.F. 1999. Estimation of overall settlement of piled rafts. *Soils and Foundations* 39(2): 59–68.

Kitiyodom, P. & Matsumoto, T. 2002. A simplified analysis method for piled raft and pile group foundations with batter piles. *International Journal for Numerical and Analytical Methods in Geomechanics* 26: 1349–1369.

Kitiyodom, P. & Matsumoto, T. 2003. A simplified analysis method for piled raft foundations in non-homogeneous soils. *International Journal for Numerical and Analytical Methods in Geomechanics* 27: 85–109.

Mindlin, R.D. 1936. Force at a point interior of a semi-infinite solid. *Physics* 7: 245–256.

Ohta, Y. & Goto, N. 1976. Estimation of S-wave velocity in terms of characteristics indices of soil. *Butsuri-Tanko Society of Exploration Geophysicists of Japan* 29(4): 31–41. (in Japanese).

Poulos, H.G. & Davis, E.H. 1980. *Pile foundation analysis and design*. New York: Wiley.

Randolph, M.F. 1994. Design methods for pile group and piled rafts. *Proc. of 13th Int. Conf. on SMFE*, New Delhi 5: 61–82.

Randolph, M.F. & Clancy, P. 1993. Efficient design of piled rafts. *Proc. of Deep Foundation on Bored and Auger Piles*, Ghent, Belgium: 119–130.

Sonoda, R., Matsumoto, T., Kitiyodom, P., Moritaka, H. & Ono, T. 2008. A case study of piled raft foundation constructed using reverse construction method and its post-analysis. *Canadian Geotechnical Journal*. (accepted)

Deep Foundations on Bored and Auger Piles – Van Impe & Van Impe (eds)
© 2009 Taylor & Francis Group, London, ISBN 978-0-415-47556-3

The DMT as tool for the monitoring of the effect of pile installation on the stress state in the soil

H. Peiffer
Ghent University—Laboratorium of Geotechnics

ABSTRACT: In the doctoral research of the author, one sub-topic was focussing on the experimental evaluation of change in stress state due to pile installation. especially measurements before, during and after pile installation were carried out. The experimental results have put the problem of prediction of the shaft capacity in a new context. The experimental results are in contradiction with simplified prediction models for evaluating the influenced zone and the magnitude of the soil stress changes.The original research mainly was focused on the measurement procedure. The procedure was worked out for the evaluation of the installation of auger cast in place piles. Afterwards the research was extended towards other types of piles, also driven piles in different types of Belgian soils.

1 INTRODUCTION

Auger cast in place piles became increasingly popular over the last 25 years. There can be listed several reasons for preferring screwel or auger piles, such as the absence of vibrations in the surrounding soil or important reduction of noise during pile installation. Moreover some of the auger pile systems are called to be of the soil displacement type, which should be reflected in a favourable load-settlement behaviour. However, the influence of pile installation on the real behaviour of the pile is very important, since the pile behviour quality seems to be extremely sensitive to it.

Nowadays one can make a global distinction between the different types of screwed or augerpiles, (fig. 1), referring to the in time rather well defined generation of screw pile developments:

- Auger piles allowing for excavating the soils during pile installation: type CFA (CFA = continous flight auger), being the first (and oldest) generation (early sixties).
- Auger piles with unique lateral displacement of the soils, second generation (seventies). Some types of pile, like the PCS-pile (PCS = "Pressured Concrete Screw") belong to both categories. Also there is a big variety in type of soils displacement is dominantly unique (in the stage of screwing down the casing) as in the Fundex-auger pile type.
- Auger piles with double soil displacement action (third generation: starting from the cighties). The basic feature is the twofold soil displacement (in both the stages of screwing in and out of the casing) as in the case of the Franki-Atlas auger pile and the latest developement such as the Omega screw pile.

Such type of classification bases on changes of the soil stresses due to installation can be extended towards other types of piles. The distinction is determined by what happens at a considered depth between the moment the pile tip or casing passes the first time (downward movement) and the moment the concrete has built up sufficient resistance to resist the horizontal possible inward soil displacements.

To evaluate the pile installation one can use a monitoring system registrating the characteristics of pile execution or execute comparable in situ test before and after pile installation. In this contribution the dilatometer is discussed as a tool for monitoring the pile

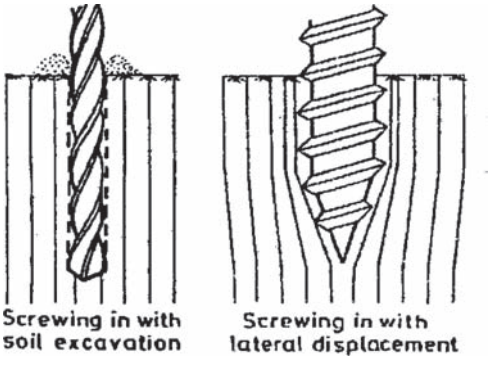

Figure 1. Different types of screwing.

installation and to evaluate the change in stress state close to the pile shaft due to such pile installation.

2 DILATOMETER TEST (DMT)

The initial scope of the dilatometer was the evaluation of the horizontal stress and stiffness of the soil close to a driven steel pile, in order to make a reliable estimation of the behaviour of a horizontally loaded pile. Extensive research programs in the years lateron resulted in an important number of correlations for the determination of a wibe spectrum of soil characteristics. Regarding the suitability of the DMT test for determination of a wibe spectrum of soil characteristics.

Regarding the suitability of the DMT test for eveluation of change in stress state inthe soil during pile installation, it is important to focus on two important features:

1) The soil distortion due to the DMT blade insertion remains small, as compared to other in situ tests, mainly because of the shape of the DMT-blade (fig. 2).
2) Based on a theoretical analysis (theory of durgunoglu and michell (1975)) it can be shown that the basic DMT parameter Kd is more sensitive to changes in Kd as compared to the CPT test results (fig. 3).

Based on this we could reasonably well expect more pronounced related to the DMT- quality of pile installation evaluation, as discussed by e.g. Van Impe (1989). One has however to take in account that the disturbed zone around the blade will influence those measurements. In the doctoral research author, the influence of the soild isturbance around the DMT

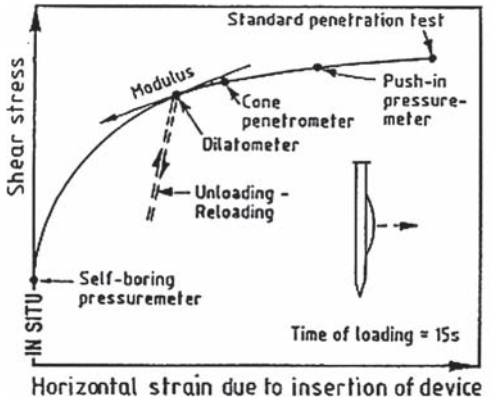

Figure 2. Qualitative estimate of insertion of in situ testing devices.

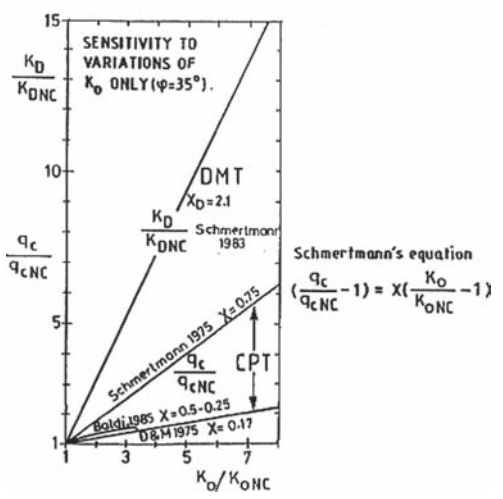

Figure 3. Sensitivity of q_c and K_D to K_0.

blade due to insertion was investigated theoretically and experimentally.

First of all one has to make a distinction between drained and undrained penetration. Fully drained penetration cours in soils with Ip (material index) greater than 1.8. Fully undrained penetrations occurs in soils with Ip smaller than 1.2.

Theoretical analysis shows that for cohesive soils, the DMT-lift-off pressure Po is dominantly determined by the pore water pressure (80 to 100% of the total stress immediately after penetration, decreasing with increasing overconsolidation to slightly overconsolidated clays (OCR < 4)). For the evaluation of change in stress state due approach (for soils with ID < 1.2.). An effective stress approach only comes in for soils with ID > 1.8. although only total stresses are known, one can use these stresses to judge (qualitatively) for the change in stress state. Indeed the excessive pore water pressure are determined by the undrained shear strength, stiffness of the soil, overconsolidation ratio and soil structure.

3 NUMERICAL AND ANALYTICAL APPROACH FOR THE DETERMINATION OF THE STRESS STATE IN THE SOIL DURING PILE INSTALLATION

The expansion of a soil cavity has been studied by an important number of authors. Only in cases of fully undrained expansion, reliable theoretical approaches are available for continuum materials. For the expansion in drained conditions, when no excessive pore water pressures are generated, or

even in partially drained conditions, however, the number of available theoretical models is still limited. Experimental results only refer to experiences with the quasi static penetration of the piezoblad, where the membrane of the dilatometerblade is replaced by a porous stone (Davidson and Boghrat, 1983). The dissipation of the execessive pore water pressure due to penetration after 1 minute was ±15% for silty soils, ±25% for sandy silts, ±80% for silty sands and 100% for sands.

3.1 *Partially drained expansion*

Datta (1982) derived from his experiments with driven piles an excess pore pressure dissipation time in coarse sand of less than 5 minutes, and in fine sillty sand of less than 45 minutes. He also measured a maximum excess pore water pressure in such soils of about 20% of the vertical overburden.

Möller and Bergdahl (1981) found for fine sand (Dr' = 80 to 90%), based on their experiments, changes in pore pressure to a distance of 5 to 7 times pile diameter. These results have to be interpreted cautiously. First of all neither the influence of the granulometry, nor of the stress state around the pile was investigated. Moreover the tests were carried out in a small sand box, height 40 cm and diameter 23 cm, for piles with diameter 2 cm. The scaling of the soil-pile stiffness, soil stresses and boundary conditions was not properly taken care for.

3.2 *Undrained expansion (in clays)*

When excess pore water pressures are generated, an additional parameter comes forward. For the un-drained expansion of a cylindrical or a spherical cavity one can refer tot Butterfield and Banerjee (1970), Vesiç (1972), Randolp and Wroth (1979), Carter et al. (1979). For our research, the results of the measurements close to piles during installation are compared with the results from theory of cylindrical expansion. Therefore we went out from cylindrical expansion, using the elastic-prefectly plastic model of Tresca for the soil. This criterium coincides with the criterium of Mohr-Coulomb for a shear angle of 0°, so for cohesive and fully saturated soils under a quick (undrained) loading.

Considering:

- the soil to be homogeneous and isotropic
- the deformations occur only in a horizontal plan
- the pore water being imcompressible
- undrained condition: a fast enough expansion in order not to have dissipation during the expansion stage.

The plastic radius Rp around the pile is given by (fig. 4).

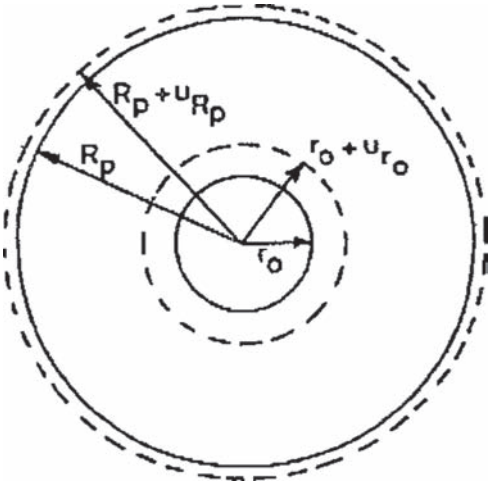

Figure 4. Cavity-expansion model.

$$R_p = \sqrt{\frac{G}{c_u} \cdot r_0} \tag{1}$$

The stresses close to the piles, in the plastic zone, are given by (r = distance at the end of expansion)

$$\Delta\sigma_{rr} = 2 \cdot c_u \cdot \ln\frac{R_p}{r} + (\tag{2}$$

$$\Delta\sigma_{\theta\theta} = 2 \cdot c_u \cdot \ln\frac{R_p}{r} - c_u \tag{3}$$

$$\Delta\sigma_{zz} = 2 \cdot c_u \cdot \ln\frac{R_p}{r} \tag{4}$$

$$\Delta u = 2 \cdot c_u \cdot \ln\frac{R_p}{r} \tag{5}$$

3.3 *Consolidation around the cavity*

One can evaluate the consolidation around a cavity using one of the following consolidation theories:

- The coupled consolidation theory (Biot (1941)), assuming that the mean total stress varies with time and the variation is determined by the variation of pore water pressures

$$\frac{E \cdot k}{3 \cdot \delta_w \cdot (1-2\nu)} \cdot \nabla^2 u = \frac{\partial u}{\partial t} - \frac{\partial p}{\partial t} \tag{6}$$

- The uncoupled consolidation theory (Terzaghi (1923) and Rendulic (1936) assuming a constant mean total stress):

$$\frac{\partial u}{\partial t} = c \cdot \nabla^2 u \tag{7}$$

4 OVERVIEW OF PILES EXAMINED

The research was originally mainly focused on the experiments determination of the stress state close to the pile shaft of srew piles of the displacement type. Besides of the torque available, also the design and the shape of the drilling tip is of big importance, not only to asily reach the bearing layer but also for the assurance of a good pile shape.

The auger tip of a screw pile of the soil displacement type has a specific shape, designed to penetrate with displacement as quickly as possible, depending on the mechanical soil properties (fig. 5).

Later on, more recently, measurements were done close to driven piles during and after installation:

– close ended tubular piles (site Aarschot)
– driven precast concrete piles (site Limelette)
– driven Franki—piles with enlarged basement

The same test procedure was followed, with measurements close to the pile during pile installation.

Later on, the measurements during installation were omitted, because of the high risk of damage of the DMT-blade and-equipment.

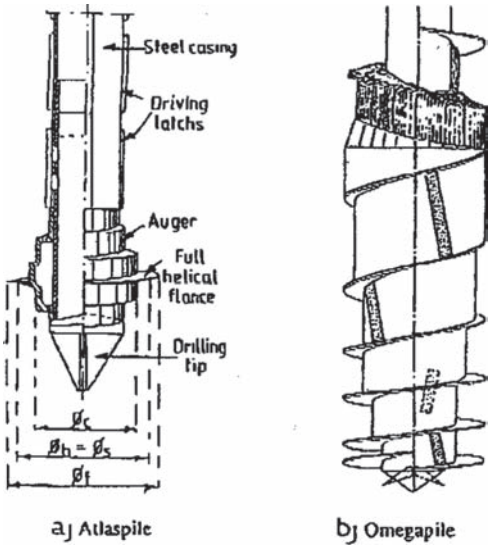

Figure 5. Different types of auger tip.

Table 1. Piles examined paper.

Type of pile	DMT before	DMT during	DMT after
Atlas	x	x	x
Omega	x	x	x
CFA	x	x	x
PCS	x	x	x
Franki (enlarged basement).	x	x	x
Tubelar (screw)	x	x	x
Tubelar (driven)	x		x
Gravel column	x	x	x
Conc. precast (driven)	x	x	x

Following piles were examined (tests executed indicated in the table 1.

5 PROCEDURE FOR THE EXPERIMENTAL DETERMINATION OF THE INFLUENCE OF PILE INSTALLATION ON THE STATE IN THE SOIL

5.1 *General considerations*

Generally, foundation piles are installed to transfer the load from surface to a deep bearing layer. The pile shaft is mainly surrounded by weak layers (weak clays, loose sandy layers). In order to obtain reliable data of the influence of pile installation on the stress state in the soil, one has to make a judicious choice for the interdistance pileshaft to DMT-blade.

This distance has to be as small as possible in order to measure important variations in horizontal stress. Preferably onde measures in the zone where plastic soil deformations have occurred. This zone is determined by:

– the diameter of the pile
– the soil characteristics (especially for cohesive soils the deformation and shear resistance characteristics and for non cohesive soils also the relative density)

Taking into account:

– the distance pile shaft to DMT-blade has to be as small as possible in order to perform reliable measurements in the plastic zone around the pile tip
– the distance to be sufficiently large on the other hand in order to avoid damage of the membrane and the blade on one hand, and to reduce the influence of non-verticality on the other hand
– the extent of the plastic zone varies with depth
– preferring only one procedure for all tests, the DMT-blade is placed at a distance smaller than the

theoretically predicted plastic radius Rp (Cavity Expansion Theory).

5.2 *Theoretical prediction for the distance DMT-blade—pile shaft*

The expression for Rp is given by (1). The Ypresian clay is a tertiary overconsolidated fissured clay. For the relation between cone resistance and undrained shear resistance, the extensive research of the Ghent University lab in this type of soil, allows for the evaluation of the Ypresian clay parameters as:

$$qc = Nk \cdot cu + \sigma_{v,0} \quad (8)$$

where $\sigma_{v,0}$ = vertical total stress at the depth considered and $N_k = 27$ for stiff fissured clay having a marine origin.

For the test site in Koekelare where the Ypresian clay was situated beneath a depth of five meters and taking in account a pile length of 13 m one can estimate c_u as follows.

$s_{v,0} = \approx 180$ kPa and qc ≈ 2.7 Mpa. This results in $c_u = 93$ kPa.

This is in good agreement with De Beer (1979): $c_u = 64 + 16.5 \cdot z$ (z = depth in meter, c_u in kPa).

For slightly overconsolidated soils, M ≈ (1.3 to 3.3) q_c of M ≈ 6.25 MPa for the test in Koekelare.

Out of the theory of elasticity one can derive $G_0 = 1.04$ MPa ($\nu = 0.40$). Eq. (1) results finally in $R_p \approx 3{,}3 \cdot r_0$. Based on this result the interdistance between pile shaft and dilatometerblade is taken equal to the pile diameter. The same interdistance is taken for non-cohesive soils because of the lack of a reliable theoretical model on the one hand and the required uniformity for the test precedure on the other hand.

6 CHANGES IN TOTAL HORIZONTAL STRESSES DURING PILE INSTALLATION—EXPERIMENTAL RESULTS—SCREWED PILE

6.1 *Omegapile at Vorst test site*

In a research program on Omega piles (Socofonda) the test site of Vorst was selected. The pile diameter was 51 cm. The dilatometerblade was placed at a distance 77 cm from the pile axis and a depth of 10.60 m. The total pile length was 25 m. Out of the available geotechnical maps the Ypresian approved to be situates between 9.60 m and 23.60 m.

On figure 6 one can see that the pressure Po reaches a first peak value the moment the auger tip passes the installation depth of the DMT-blade (downward movement). Immediately after reaching these peak values there is a considerable drop down of the total horizontale pressure. This can be explained by exceeding the tensile strenght in the soil leading to the formation of micro fissures. This results in temporary faster pre-pressure dissipation until the fissures again are closed by the inward soil deformation. This theoretical explanation is discussed under 8. Besides this, the decrease of Po is explained by decompression of the soil after the passing by of the auger, the dissipation of the excessive pore water pressure and the change in total stress state around the dilatometerblade.

6.2 *Franki-Atlaspile at Koekelare test site*

For this program the test setup is presented in figure 7. Two dilatometerblades and 1 pore water pressure transducer (CPTU-cone) were installed close to the pile, all at the same distance from the pile axis. The results are presented in figure 8 for the piles examined. One can detect only a small change is more pronounced. This probably can be explained by an inappropriate installation of the dilatometerblade (outside the plastic zone around the pile).

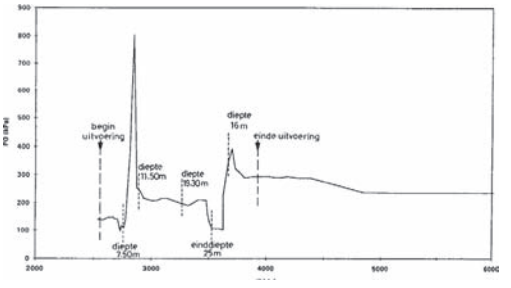

Figure 6. DMT-test installation Omegapile at Vorst test site.

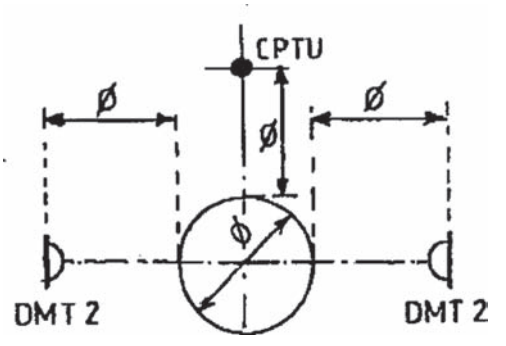

Figure 7.

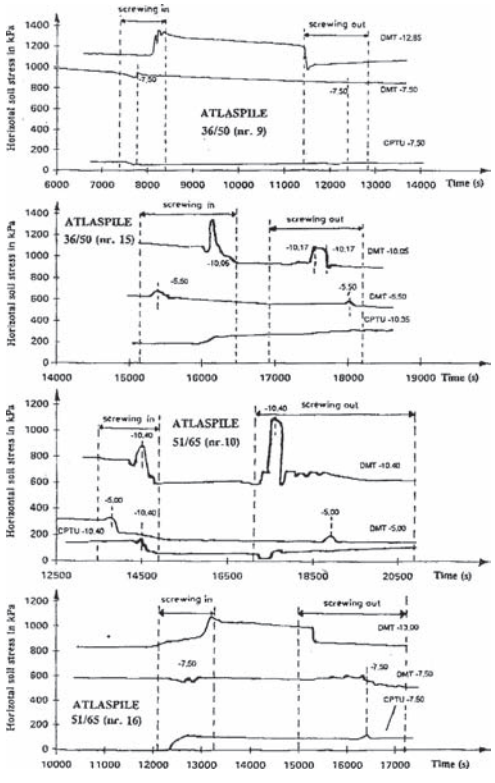

Figure 8. Results at Koekelare.

6.3 *PCS-piles in sand*

Two PSC-piles of Socofonda company were examined. The details gatherd on the folowing table.

Site	Pile length	Pile diameter	Installation depth DMT	I_D
Doel	19.07 m	0.40 m	8.5 m	2.9
Dendermonde	16.52 m	0.45 m	7.5 m	2.0

Both test programs were performed this time in a sandy soil. The DMT test measure there for predominantly during most of the pile installation period changes in effective stress around the pile. At Doel test site, the dilatometerblade was directed tangentially (deformation of the membrane perpendicular to the radius from pile axis).

6.3.1 *Doel (fig. 9)*

When the installation depth of the DMT—blade is reached, the total stress shows a sudden peak valeu, what can be explained by a sudden pore water pressure peak followed by an immediately dissipation.

Afterwards, due to arching, the tangential stress will increase because of soil decompression. During casting the concrete a similair phenomenon can be seen. At the moment the augertip passes. Pore water pressure are induced but they immediately are dissipated. At the end, when the concrete overpressure is taken away, some decrease in tangential stress is induced leading to an increase in tangential stress. One can notice that the difference in tangential stress for the upward movement is much less than daring the downward movement. This can be explained by higher decompression during the boring stage of pile execution what could be expected, since the PCS screw pile is basically only a CFA type, with some precaution on high enough vertical downward speed and pressurized concrete casting.

6.3.2 *Dendermonde (fig.10)*

Here one can see a quite similar picture as at the Doel test site. The dissipation of pore water pressure goes on however more slowly. This can be explained by the more silty sand character of the soil. A second remarkable difference comparing with the Doel test site is only a partial reduction of this radial horizontal stress after taking away the concrete over-pressure. Also this can be explained by a somewhat delayed dissipation in this soil type.

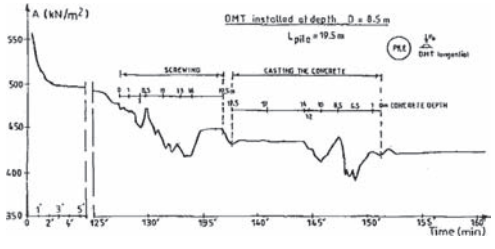

Figure 9. DMT test during pile installation of PCS-piles at Doel test site.

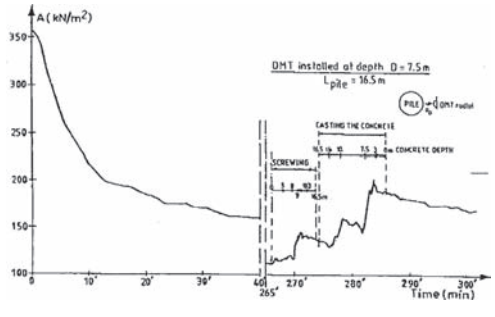

Figure 10. DMT test during pile installation of PCS-pile at Dendermonde test site.

7 COMPARISON DMT MEASUREMENTS BEFORE AND AFTER PILE INSTALLATION

The scope of these measurements was to evaluate the stress state, as finally changed by the pile installation. In figs. 11 and 12 the results of this comparative analysis are compiled. In order to evaluate these measurements, Po was normalised with respect to an approach of the mean total stress around the dilatometerblade. The normalization procedure is the same as proposed by Fretti et al. (1989):

$$P_0 = \frac{P_0}{\sigma_p} = \frac{P_0}{(\frac{P_0+\sigma}{2})} \qquad (13)$$

In this way the horizontal stress in the direction parallel to the largest DMT cross section is not take into account. This can be accepted by the fact that the stress in this direction is much smaller than Po.

7.1 *Discussion of the general pattern of the results'graph*

The normalized curve as a function of P shows some general trend. The shape is determined by:

- the stress state in the around the pile shaft before pile installation,
- the distance dilatometerblade to pile shaft
- type of pile
- the installation procedure and execution parameters of the pile
- the time lag between pile execution and the DMT-measurements (influence of the consolidation around the DMT-blade)

ID ≤ 1.2 (undrained penetration of DMT)
when we consider the mechanical overconsolidation as a measure for eventual soil improvement due to pile installation, then the degree of soil improvement decreases increasing stiffness of the cohesive saturated soil.

ID ≥ 1.8 (fully drained penetration)
For these soils the variations of the ratio of horizontal normalised stress were more pronounced. This can be explained by the fact that here directly the effective stress state is influenced. Soil decompression appeared for the omegapile from an initial normalised horizontal stress of about 1.6 on, (for the PCS-pile already from 1.2 on). This is a clear boundary for the applicability of this pile as a displacement pile. For the other pile types this as far is not yet investigated; which is a serious limitation for the determination of a reliable field of appreciation.

In fig. 12 the results for the different types of piles are presented.

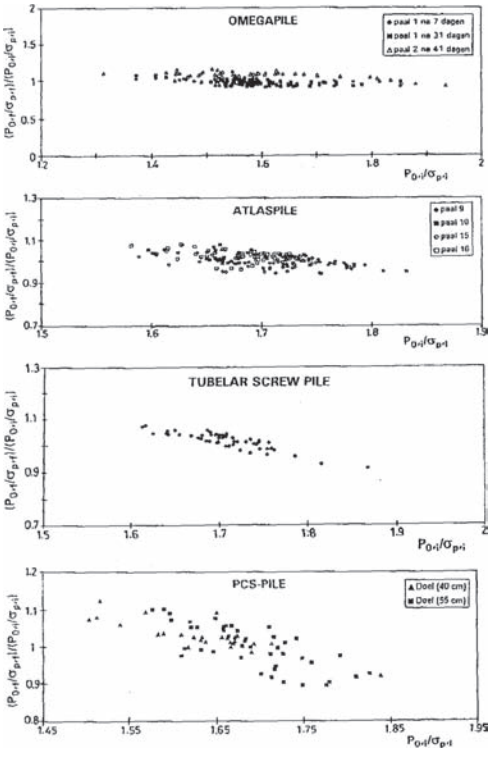

Figure 11. Changes in normalized total horizontal stress (ID ≤ 1.2).

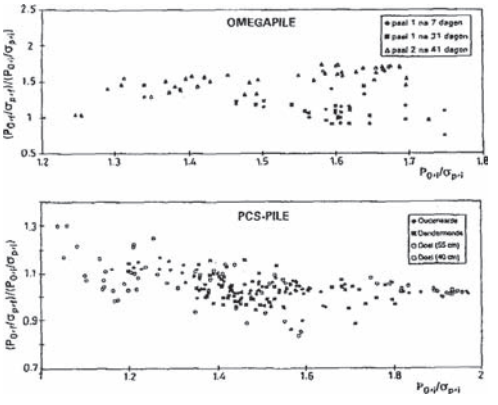

Figure 12. Changes in normalized total horizontal stress (ID ≥ 1.8).

8 EXTENSION TOWARDS SHAFT CAPACITY

An attempt was made towards the method of direct evaluation of the unit shaft capacity of piles by DMT.

For the Atlaspiles, at the Koekelare test site, evaluation of the shaft bearing capacity was available out of pile instrumentation.

This resulted in following successful preliminary, semi-empirical, relationship for the type of piles performed overthere:

$$q_{u,s} = 0.0035 \cdot P_0 \cdot K_D^{1,25} \quad (14)$$

One can expect this method to be promising also for the prediction of the unit shaft bearing capacity for other soil displacement type op piles, because for each of these types a relationship between the horizontal effective stress before and after pile execution, depending on the pile execution parameters should anyhow be quite clear. More research in this respect for the various pile types mentioned is necessary for the moment.

9 CONCLUSIONS

The execution of DMT-tests close to piles lead to better understanding of the changes in stress state in the soil due to pile installation. The DMT-test at this stage offers a qualitatively tool for the judgement of the quality level of execution of the piles. Extension of the procedure towards the direct evaluation of the shaft capacity becomes plausible and is highly recommended. It is not a real design method because estimates are obtained after the pile is executed, nor is it a real type of loading test because the bearing capacity is estimated from soil properties and not by loading the pile. It is widely recognized that pile capacity largely depends on execution next to the soil type. Hence one can not pretend to estimate the pile bearing capacity based only on measurements on the original soil. One should more rationally base such estimations on measurements on the soil parameters before and after pile installation.

REFERENCES

Baligh, M.M. & Levadoux, J.N. 1980. Pore pressure dissipation after cone penetration, MIT Report n°MITSG 80-13, p. 368.

Biot, M.A. 1941. General Theory of three dimensional consolidation, Journal of Applied Physics, vol. 12, pp.155–164.

Butterfield, R. & Banerjee, p.k. 1970. The effect of pore water pressures on the ultimate bearing capacity of driven piles. Proceedings of the 2nd South-East Asian Conference on Soil Engineering, Singapore, pp. 385–394.

Carter, J.P., Randolph, M.F. & Wroth, C.P. 1979. Stress and pore pressure changes in clay during and after expansion of a cylindrical cavity. International Journal for Numerical and Analytical Methods in Geomechanics, Vol. 3, n° 4, pp. 305–322.

Datta, M. 1982. Pore water pressure development during pile driving and its influence on driving resistance. Proceedings Conference on Behaviour of Offshore constructions, BOSS, Houston, Vol. 2, pp. 295–304.

De Beer, 1979. Historiek van het kanaal Leie-Ieper: eigenschappen en gedragingen van de Ieperiaanse klei. Tijdschrift voor openbare werken nr. 4,5en 6.

Fretti, C., Ghiona,V.N., Jamiolkowski,M., Lo Presti D. & Tortella, M.L. 1984. Dilatometer stiffness of Ticino sand. ASCE journal.

Henkel, D.J. 1961. The shear strength of a saturated remoulded clay. Proceeding Americ soc. of civil Engineering., Research Conference on shear strenght of cohesive soils.

Ladanyi. B. Expansion of a cavity in a saturated clay medium, proceeding Am. Soc. Civ. Eng., July, 89 SM 4. pp. 127–161.

Massarch, K.R. & en Broms, B.B. 1977. fracturing of soil caused by pile driving in clay. IX International Conference on soil Mechanics and Foundations Engineering, Tokyo, pp. 197–199.

Meigh, A.C. 1987. Cone penetrations testing, methode and interpretation, CIRCIA Ground Engineering Report: In-situ Testing, p. 141

Moller, B. & Bergdahl, U. 1981 Dynamic pore pressure during pile driving in fine sand Proceeding 10th International Conference on soil Mechanics and Foundation Engineering, Stockholm, Vol. 2, pp. 791–794.

Peiffer, H. 1997. Interpretatie en aanpassing van de dilatometerproef, uitgebreid tot de beoordeling van de spanningstoestand naast schroefpalen. PhD thesis, RUG.

Randolph, M.F. & Wroth C.P. 1979. An analytical solution for the consolidation around a driven pile. International Journal of Numerical and Analytical Methods in Geomechanics, pp. 361–383.

Torstensson, B.A. 1977. The pore pressure probe. Nordisk Geotekniske MOTE, Oslo, Paper n° 34, pp. 34.1–34.15.

Van Impe, W.F. 1989. Auger piles, planning and use. Conference Association of Finnish Civil Engineers (RIL), Helsinki , Finland, pp. 1–39.

Vesic, A.S. 1972. Expansion of cavities in infinite soil mass. Journal of the soil Mechanics and Foundation Division, Proceeding of the ASCE, vol. 98, SM3. pp. 265–290.

Deep Foundations on Bored and Auger Piles – Van Impe & Van Impe (eds)
© 2009 Taylor & Francis Group, London, ISBN 978-0-415-47556-3

Simulation of the performance and remediation of imperfect pile groups

H.G. Poulos
Coffey Geotechnics, Australia
University of Sydney, Australia

ABSTRACT: This paper presents a method of analysis of pile groups subjected to vertical and moment loading. It allows consideration of non-ideal situations in which not all piles in the group are the same, some piles may contain defects, and the group configuration may change during construction and operation. The paper sets out a simplified analysis which adapts closed-form solutions for axial pile head stiffness and employs a number of approximations to extend their use to more practical geotechnical profiles. In particular, it allows for piles of different length and/or diameter, piles with a soft toe, the removal of piles from the original foundation, and the insertion of new piles at some stage during the construction or loading sequences. Simplified expressions are also presented for estimation of the interaction factors for pile group settlement. The paper then describes the application of this analysis to the assessment of two high-rise buildings which experienced unacceptable differential settlements.

1 INTRODUCTION

Conventional pile group analyses almost invariably involve idealized assumptions regarding the piles, the supporting soil and the applied loadings. For example, it is usually assumed that all piles are the same length and diameter, and that they are constructed perfectly without structural or geotechnical imperfections. In addition, it is usually assumed that the pile group configuration remains unchanged during the lifetime of the building.

In reality, such assumptions are rarely if ever realized. In many groups, there are piles of different length, and some piles may contain defects arising from imperfect construction techniques. In some cases, the consequent performance of the foundation system may be sufficiently unfavourable that some form of remedial action may be necessary. For example, additional piles may be added to enhance foundation performance, or in extreme cases, some of the original piles may be cut to try and correct uneven settlement, prior to adding the extra piles.

This paper presents a method of analysis of pile groups which allows consideration of factors such as those mentioned above. It sets out a simplified analysis of pile groups which relies on the use of closed-form solutions for axial pile head stiffness, but which employs a number of approximations to extend their use to more practical geotechnical profiles than the idealized conditions considered in the original analyses.

In particular, it allows for piles of different length and/or diameter, piles with a soft toe, the removal of piles from the original foundation, and the insertion of new piles at some stage during the construction or loading sequences. Simplified expressions are also presented for estimation of the interaction factors for pile group settlement.

The application of this analysis to the assessment of two high-rise buildings which experienced unacceptable differential settlements will be described.

2 ANALYSIS METHOD

2.1 *Basic method*

The basis of the analysis, implemented by a program called PIGS, is the simplified elastic analysis of Randolph and Wroth (1978) for the stiffness of a single pile in an elastic soil mass underlain by a stiffer base layer.

Two typical piles i and j within a group are considered. For pile i, using the concept of interaction factors (Poulos and Davis, 1980), the increment of settlement at i due to an increment of load on pile j may be approximated as follows:

$$\Delta S_{ij} = \Delta P_j \, \alpha_{ij} / K_j \qquad (1)$$

where

ΔP_j = load increment on pile j
K_j = tangent stiffness of pile j
α_{ij} = interaction factor for pile j on pile i.

To allow for the non-linear response of a pile, it is assumed that the load-settlement curve for the pile is hyperbolic, so that the tangent stiffness can be expressed as follows:

$$K_j = K_{j0} (1 - R_{ij} \cdot P_j / P_{uj})^2 \quad (2)$$

where

K_{j0} = initial tangent stiffness of pile j
R_{fj} = hyperbolic factor for pile j
P_j = load acting on pile j prior to increment
P_{uj} = ultimate axial load capacity of pile j (compression value if P_j is positive, uplift value if P_j is negative).

K_{jo} is computed from the Randolph and Wroth (1978) expression, using tangent values of the soil modulus. The interaction factor α_{ij} is computed as described below.

Due to all the n piles in the group, the overall increment of settlement of pile i, ΔS_i, is:

$$\Delta S_i = \sum \Delta P_j \alpha_{ij} / K_j \quad (3)$$

Following the suggestions of Mandolini and Viggiani (1997), equation 2 is only applied to pile i, and for all other piles, $K_j = K_{jo}$, i.e. the interaction factor is applied only to the elastic component of the settlement of all piles other than the pile i itself.

Two limiting cases can then be considered: specified loads on each pile, and a rigid pile cap. For specified load on each pile in the group, equation 3 may be used directly to compute the incremental settlement of each pile. For the case of a rigid cap, equation 3 can be written for all piles in the group as follows:

$$\{\Delta S\} = [A] \{\Delta P\} \quad (4)$$

where

$\{\Delta S\}$ = vector of settlement increments
$[A]$ = matrix of values of α_{ij} / K_j
$\{\Delta P\}$ = vector of pile load increments.

To allow for the effects of having dissimilar piles in the group, or of having applied moment loadings as well as vertical loadings, consideration must be given to the rotations of the pile cap, as well as the settlements. In this case, the incremental settlement of pile i must also include components due to cap rotation. Thus, for a pile i, the incremental settlement ΔS_i is now given as follows:

$$\Delta S_i = \sum \Delta P_j \alpha_{ij} / K_j + \Delta\theta_x \cdot (x_i - x_r) + \Delta\theta_y \times (y_i - y_r) \quad (5)$$

where

$\Delta\theta_x$ = incremental rotation of rigid cap in x-direction
$\Delta\theta_y$ = incremental rotation of rigid cap in y-direction
x_i = x-coordinate of pile i
y_i = y-coordinate of pile i
x_r, y_r = are x- and y-coordinates of reference point (at which the settlement is computed).

The equilibrium equations for vertical load, moment in the x-direction, and moment in the y-direction, can be written as follows:

$$\Delta P_G = \sum \Delta P_j \quad (6)$$

$$\Delta M_x = \sum \Delta P_j \cdot (x_j - x_r) + \Delta P_G \cdot (x_g - x_r) \quad (7)$$

$$\Delta M_y = \sum \Delta P_j \cdot (x_j - x_r) + \Delta P_G \cdot (y_g - y_r) \quad (8)$$

where

ΔP_G = increment of vertical load applied to group
ΔM_x = increment of moment in x-direction applied to group
ΔM_y = increment of moment in y-direction applied to group
x_g, y_g = x and y coordinates of point of application of vertical load increment.

Equation 3 can be written for all n piles within the group, and with the three equilibrium equations, the following final equation may be obtained:

$$[Am] \cdot \{Dm\} = \{Cm\} \quad (9)$$

where

$[Am]$ = matrix containing the elements of matrix A (equation 4), and the appropriate factors from the equilibrium equations,
$\{Dm\}$ = vector of incremental pile loads (n values), the incremental settlement at the reference point, and the two incremental rotations,
$\{Cm\}$ = vector containing n zeros and the appropriate components from the equilibrium equations (6) to (8).

Equation 9 can be solved for the n incremental pile loads, the incremental settlement, and the incremental rotations in the x- and y-directions. These values are then added to the existing values to obtain the starting values for the next increment.

By putting the analysis in incremental form, it is possible to allow for changes in the loading pattern, the soil profile, and the pile group configuration during the loading process.

2.2 *Inclusion of free field soil movements*

In addition to direct axial and moment loading, it is possible that a pile group will be subjected to free-field soil movements, for example, due to the consolidation

of the soil profile under previous applied surface loading or dewatering. The presence of such free-field soil movements will modify the settlement behaviour of the pile group. An approximate analysis of such effects can be developed as set out below.
It is assumed that, if a pile i is subjected to a free-field soil surface movement S_{0i}, it will undergo an additional movement $\Delta S_{ff,i}$ given by:

$$\Delta S_{ffi} = S_{0i} \cdot \zeta_i \tag{10}$$

where ζ_i = free-field factor.

For a specified distribution of free-field soil movement with depth, ζ_i can be computed from a pile-soil interaction analysis, for example, employing the computer program PIES (Poulos, 1989).

Ignoring interaction effects from other piles, a simplifying but probably conservative assumption (Kuwabara and Poulos, 1989), the settlement of a pile i within a group can then be obtained by combining equations 3 and 10:

$$\Delta S_i = \sum \Delta P_j \, \alpha_{ij}/K_j + \Delta\theta_x \cdot (x_i - x_r) + \Delta\theta_y \cdot (y_i - y_r) + S_{0i} \cdot \zeta_i \tag{11}$$

The last term, for each pile, can then be incorporated into the vector {Cm} in equation (9), and the resulting matrix equation can then be solved for the pile loads, group settlement, and group rotations.

2.3 *Approximations for layered soil profiles*

Because of the layered nature of real geotechnical profiles, approximations are necessary in order to apply the Randolph and Wroth solutions for single pile settlement. These solutions assume a constant or linear variation with depth of the soil modulus along the pile shaft, and a single modulus values below the pile tip.

For a layered soil profile, the following procedure is adopted:

a. Along the pile shaft, an average value of soil modulus, E_{sav}, is computed as the weighted average for the soil layers in contact with the shaft, i.e.

$$E_{sav} = \sum h_k \cdot E_{sk}/L \tag{12}$$

where

h_k = thickness of a layer k along the shaft
E_{sk} = Young's modulus of layer k
L = length of pile shaft.

b. Below the base of the pile, a weighted inverse average modulus, E_{bav}, is taken, over a specified representative depth z_r (typically 3 to 5 pile diameters), i.e.

$$E_{bav} = z_r \Big/ \left(\sum W_k \, h_l / E_{sl} \right) \tag{13a}$$

where

h_l = thickness of a layer l within the representative depth z_r
W_k = weighting factor for layer k
E_{sl} = Young's modulus of layer l

The weighting factor W_k is approximated as follows:

$$W_k = 0.75 + z_k/d_b \text{ (for } z_k/d_b \le 0.25) \quad \text{or} \tag{13b}$$

$$W_k = 1.0 - (z_k/d_b - 0.25)/(z_r/d_b - 0.25) \tag{13c}$$

where z_k = depth to centre of layer k.

The summation in equation 13a is carried out over the depth z_r.

In the absence of reliable methods of estimating the bearing capacity of layered soil strata, the ultimate end bearing pressure has been assumed to be the average value, f_{be}, within the depth of influence, z_{inf}, below the pile base, i.e.

$$f_{be} = \sum f_{bj} \, h_j / z_{inf} \tag{14}$$

where f_{bj} = ultimate bearing capacity of layer j within the depth of influence.

It is recognized that this approach is approximate, but more accurate assessment would require substantially greater computational effort than is available in the present PIGS program (or indeed, in most available pile group analysis programs).

The latter two approximations have also been applied to cases where soft soil or debris has been identified as existing below the pile base.

2.4 *Interaction factors*

It has been found that the variation of the interaction factor between two piles, α with spacing can be approximated as follows:

$$\alpha = A \cdot \exp(-B \, (s/d)) \tag{15}$$

where

A, B = factors
s = centre-to-centre spacing of piles
d = diameter of piles.

Comprehensive parametric studies using the program DEFPIG (Poulos, 1990) have enabled approximations for the factors A and B to be developed, as function of the various dimensionless ratios which govern axial pile behaviour. It has been found possible to combine, with acceptable accuracy for practical purposes, the factors which depend on these dimensionless ratios to obtain the following approximations:

$$A = A_l \cdot A_b \cdot A_k \quad (16)$$

$$B = B_l \cdot B_b \cdot B_k \quad (17)$$

where

A_l, B_l = factors depending on ratio of length L to diameter d
B_b, B_b = factors depending on ratio of modulus of bearing stratum to soil along shaft
A_k, B_k = factors depending on the ratio of pile stiffness to soil stiffness.

Via curve fitting, the following expressions can be used for the above factors:

$$A_l = 0.376 + 0.0014\ (L/d) - 0.00002\ (L/d)^2 \quad (18a)$$

$$A_b = 1.254 - 0.326 \cdot \ln\ (E_b/E_s) \quad (18b)$$

$$A_k = 0.099 + 0.126 \cdot \ln\ (K) \quad (18c)$$

$$B_l = 0.116 - 0.0164 \cdot \ln\ (L/d) \quad (19a)$$

$$B_b = 0.865 + 0.164 \cdot \ln\ (E_b/E_s) \quad (19b)$$

$$B_k = 1.409 - 0.055 \cdot \ln\ (K) \quad (19c)$$

where

L = pile length
d = pile diameter
E_b = average modulus of bearing stratum below pile tip
E_s = average soil modulus along pile shaft
K = pile stiffness factor
$= E_p \cdot R_a/E_s$
E_p = Young's modulus of pile
R_a = area ratio = ratio of area of pile section to total enclosed area (=1 for solid pile).

As an alternative, the interaction factor may be expressed via the following logarithmic approximation:

$$\alpha = C + D \ln\ (s/d) \quad (20)$$

where C, D are factors, and s and d are as defined above.

By a curve fitting process, C and D may be approximated as follows:

$$C = C_1 \cdot C_b \cdot C_k \quad (21a)$$

$$D = D_1 \cdot D_b \cdot D_k \quad (21b)$$

where the various factors are analogous to those in the exponential approximations in equations 2 and 3.

In turn, the factors in equations 21a and 21b can be approximated as follows:

$$C_1 = 0.509 + [0.0007\ (L/d) - 0.00002\ (L/d)^2] \quad (22a)$$

$$C_b = 1.145 - 0.2552 \cdot \ln\ (E_b/E_s) \quad (22b)$$

$$C_k = 0.096 + 0.127 \cdot \ln\ (E_p/E_s) \quad (22c)$$

$$D_1 = 0.0242 \cdot \ln\ (L/d) - 0.209 \quad (23a)$$

$$D_b = 1.234 - 0.316 \cdot \ln\ (E_b/E_s) \quad (23b)$$

$$D_k = 0.190 + 0.114 \cdot \ln\ (E_p/E_s) \quad (23c)$$

where the various parameters are as defined above.

To examine the performance of the above approximations, a typical case has been chosen at random, in which a pile 18 m long and 0.75 m in diameter is located within a soil profile consisting of four layers, with thicknesses of 4, 6, 8 and 50 m, having Young's modulus values of 20, 50, 150 and 400 MPa respectively. The computer program DEFPIG has been used to compute the interaction factors for two cases:

1. The layered profile along the pile shaft;
2. An equivalent uniform layer with an average constant modulus of 87.8 MPa.

Figure 1 compares the approximations set out above with two sets of values computed from DEFPIG. It can be seen that:

1. The interaction factors for the equivalent uniform layer are larger than those for the layered soil profile.
2. Both approximations give a reasonable overall fit, although the exponential fit tends to underestimate the interaction factor at small spacings, while the logarithmic fit tends to overestimate the interaction factor at larger spacings.

The latter tendency can lead to over-estimates of group interaction and hence settlement. For that reason, the exponential fit has been preferred and has

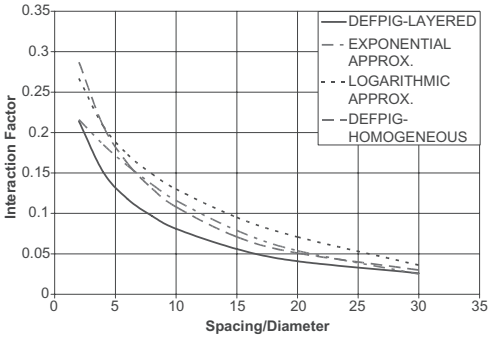

Figure 1. Comparisons between interaction factor solutions and approximations.

been coded into PIGS. Alternatively, the user can input relevant values of A and B for each particular pile type (for example, as derived from specific DEFPIG analyses).

2.5 *Interaction between dissimilar piles*

When dealing with piles of different length or diameter, the approximations developed by Poulos and Hewitt (1986) have been employed. These may be summarized as follows:

a. For piles i and j of different diameter:

$$a_{ij} \sim a_{jj} \tag{24}$$

b. For piles i and j of different length:

i. For $L_i > L_j$,

$$\alpha_{ij} \sim (\alpha_{ii} + \alpha_{jj})/2 \tag{25a}$$

ii. For $L_i < L_j$,

$$\alpha_{ij} \sim \alpha_{jj} \tag{25b}$$

where L_i and L_j = length of pile i and pile j respectively

α_{ii} = interaction factor for 2 piles of length L_i
α_{jj} = interaction factor for 2 piles of length L_j.

It must be emphasized that these approximations may not always be accurate, especially if the two piles being considered are very different in length or diameter. However, the expressions provide a useful, albeit approximate, means of considering different piles within a group, and have been coded into PIGS.

2.6 *Activation and de-activation of piles*

PIGS allows for the analysis of pile groups in which, at a specified stage of loading, piles are added, removed, or have their properties altered (for example, to simulate loss of capacity and stiffness when they are affected by tunnelling.

Piles which are added to the group (such as in an underpinning process) are "activated" at the appropriate stage, and commence to carry load from an initial specified value (usually zero). For piles which are removed from a group (e.g. by extraction or cutting), their load and incremental stiffness is reduced to zero, thus resulting in a redistribution of load among the remaining piles. For piles whose capacity and/or stiffness is altered, the new values are input by the user. If the new capacity is less than the existing load, then the load on that pile is reduced to the new capacity, and any reduction in load is then re-distributed to the other piles by the program.

2.7 *Simulation of soft toes*

The effect of a "soft toe" on the performance of a single pile can be estimated roughly by representing the soft toe as a soft layer below the base of the pile, and then using PIGS to assess the reduced stiffness and capacity of the pile. This simplification does not completely capture the behaviour of a pile with a soft toe (for which an analysis similar to that described by Poulos (2005) would be required), but it does at least provide a means of estimating the effects of the soft toe in reducing pile stiffness. A major challenge in modeling soft toes is to assess the Young's modulus, and sometimes the thickness, of the soft material at the toe.

2.8 *Simulation of structural defects in piles*

The PIGS program requires the input of the structural strength, in compression and tension, of the pile, and it then checks at each stage of the analysis whether the computed axial load exceeds these input strength values. If the load does exceed the strength, the pile is deemed to have failed structurally and the axial load is set to the strength, and further applied loads are re-distributed to the remaining unfailed piles. Piles that have, or are suspected to have, structural defects can have a lower structural strength assigned to them. Again, this is an approximate approach, as the reduction in load-carrying capacity will depend on both the location and the nature of the defects (Poulos, 2005).

3 COMPARISONS BETWEEN PIGS AND OTHER PROGRAMS FOR IDEAL PILE GROUPS

Comparisons were made between the results from PIGS and from two established and commercially available pile group programs, PIGLET (Randolph, 1987) and DEFPIG (Poulos, 1980). For this comparison, an ideal pile group in which all piles are identical was analyzed. The group contained nine piles, in a symmetrical 3×3 configuration, each 20 m long and 1 m in diameter, with a centre-to-centre spacing of 3 m in both directions. The idealized soil profile consisted of a uniform stiff clay layer 20 m deep, underlain by a very stiff layer extending to considerable depth. The drained Young's modulus values of the two layers were 50 MPa and 200 MPa respectively, while the ultimate skin friction value for the upper layer was 50 kPa. The ultimate end bearing pressure within the lower layer was 2.7 MPa. In the PIGS analysis, a hyperbolic factor R_f of 0.5 was assumed for the single piles. Two cases of loading were considered:

1. A central vertical load;
2. A central vertical load V together with a moment (equal to 2V) in the "x" direction.

The computed load-settlement behaviour obtained by PIGS, PIGLET and DEFPIG is shown in Figure 2 for the central vertical loading case. At relatively low loads, the three solutions agree closely, but as the load increases towards failure, the solution from the linear PIGLET analysis departs from the other two solutions, as would be expected. The non-linear PIGS solution gives greater settlements than the non-linear DEFPIG solution, because of the assumed hyperbolic single pile response in PIGS, whereas the DEFPIG analysis assumes, in effect, an elastic-plastic single pile response.

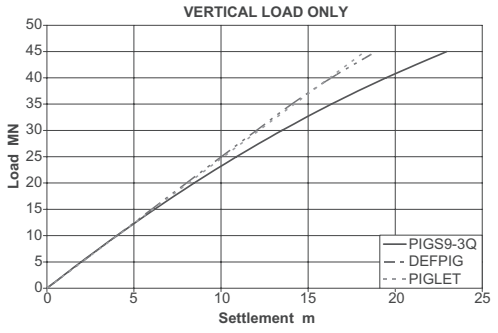

Figure 2. Comparison of load-settlement curves for vertical loading.

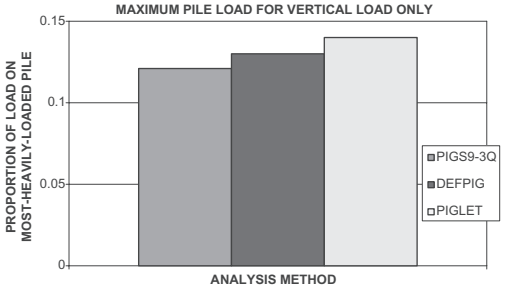

Figure 3. Comparison of computed maximum loads for vertical loading only.

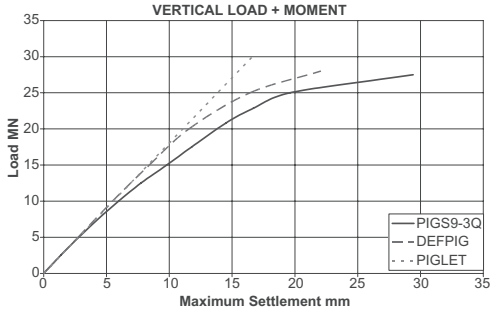

Figure 4. Comparison of load-settlement curves for combined vertical load and moment.

Figure 3 compares the computed maximum pile load within the group from a purely elastic analysis. The agreement between the three solutions is reasonably close.

Figure 4 compares the load-settlement curves for the case of combined vertical and moment loading. The agreement between the PIGS and DEFPIG load-settlement curves is again reasonable. The three analyses are also found to give similar results for the maximum pile loads.

From these comparisons, it is concluded that the simplified PIGS analysis provides a reasonable means of prediction the load-settlement behaviour of ideal pile groups.

4 APPLICATION TO BUILDINGS IN HONG KONG

4.1 *Introduction*

Construction of two high-rise residential blocks, each planned to contain about 650 apartments, was commenced in Shatin, Hong Kong, in mid-1999. Around that time, there had been revelations of improper piling practices in some projects in Hong Kong, and this gave rise to a heightened sense of awareness about building performance. In October 1999, a program of settlement monitoring was commenced on the two buildings, labelled as Blocks D and E, both of which by that stage had reached the 17th Floor. About 2 months later, it was observed that both buildings were settling unevenly, with each block tending to tilt as a rigid body. Of particular concern was the fact that there was a 6-storey secondary school very close (about 6 m) to the two blocks. Consequently, a program of investigative coring was commenced in late 1999 through a number of the bored piles supporting the buildings. As a result of this coring program, it was deduced that many of the piles for these buildings had not been constructed as per the design requirements, and not in accordance with the documented piling records. These deductions led to a thorough investigation of the foundations of the buildings and to an assessment of possible future courses of action.

The following sections describe one of the independent assessments carried out, including an evaluation of the as-built foundations, an assessment of proposed remedial measures, and a consideration of various risk factors involved in undertaking remedial works in such circumstances.

4.2 *Geotechnical conditions*

Prior to commencement of construction of Blocks D and E, a total of twenty two exploratory boreholes had been drilled in the vicinity of Blocks D and E, and Figure 5 shows a plan of the foundation piles and the borehole locations. A typical geological section is presented in Figure 6, the location of which is shown on Figure 5.

Based on the available information, the subsurface conditions for Blocks D and E comprised the following strata:

1. Fill—Highly variable ranging from silty fine sand to gravel and cobbles of granite and concrete, described as loose to dense.
2. Marine Deposit—Typically described as loose silty fine to coarse sand with some shell fragments, and also described as soft grey silty clay/clayey silt.
3. Alluvium—Highly variable unit ranging from soft sandy silt, loose silty sand to medium dense to dense gravel. This unit was typically described as firm to stiff sandy, silty clay and loose to medium dense silty, fine to coarse sand.
4. Colluvium—Material described as Colluvium was encountered in two of the boreholes and comprised sandy angular to sub-angular medium to coarse gravel.
5. Completely to highly decomposed quartz monzonite—Saprolite that was generally described as being medium dense to very dense, slightly gravelly, silty sand/sandy silt and stiff to very stiff sandy clay. Corestones of Grade II Quartz Monzonite were encountered within the Grade V/IV material in a number of the boreholes, in particular those drilled in the vicinity of Block E.
6. Moderately to slightly decomposed quartz monzonite—typically described as moderately strong to strong with medium- to widely-spaced joints.

The site was in relatively close proximity to a river, and the groundwater was typically about 2 m to 3 m below existing ground level.

4.3 *Foundation details*

As shown in Figure 5, each of the 41-storey blocks was supported on 18 bored piles, designed to be 2.3 m in shaft diameter, with a base belled out top 3.8 m. The piles were designed as end bearing piles, to be founded in Grade II (slightly weathered) granite, at a depth ranging between about 35 m and 46 m.

4.4 *Measured settlements*

When the buildings had reached the 17th storey, a program of settlement monitoring was commenced on the buildings, and Figure 7 shows typical time-settlement readings for one of the blocks. The non-uniform settlements are clearly evident from this figure. It is interesting to note that the coring investigation works caused a temporary acceleration in settlement of the buildings, which played an influential role in the ultimate decision made with respect to the buildings.

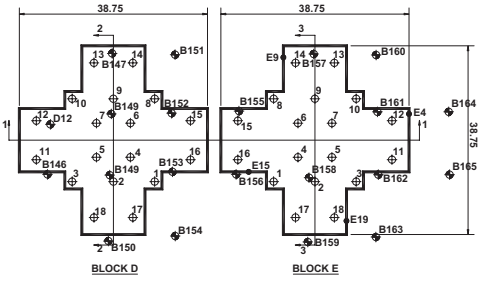

Figure 5. Plan of pile and borehole locations.

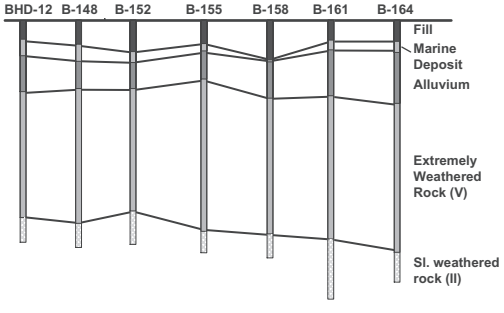

Figure 6. Geotechnical profile for section 1–1.

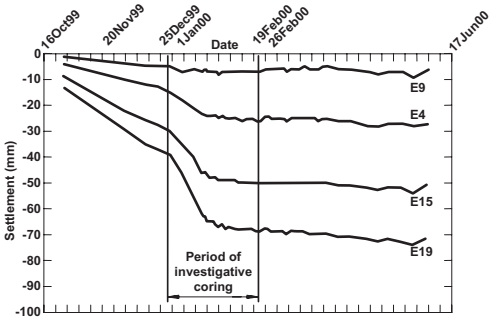

Figure 7. Time-settlement plot for typical points in Block E.

Table 1. Summary of inferred pile founding conditions from coring.

Pile founding condition	Number of piles	
	Block D	Block E
Pile founded on Grade II rock	3	1
Thin sediment layer between pile base and rock	5	1
Sediment below pile base, underlain by inferior rock	5	4
Pile founded on inferior rock, without sediments	1	12
Thick layer of soft material below pile base	4	0

4.5 *Investigative coring results*

A program of investigatory coring through the bored piles was instigated in December 1999, and this program revealed a number of deficiencies in both the pile length and the founding conditions at the base of the piles, and construction was halted at the 34th floor, very early in 2000. The conclusions of the independent consultant carrying out the coring and the assessment of pile condition are summarized in Table 1.

Only four of the total of 36 piles were compliant with the construction specifications which required founding on Grade II rock. The pile lengths were up to 16 m or more short of bedrock level. In addition to the geotechnical deficiencies, six of the concrete cores that were taken from the piles and tested showed low strengths, ranging between 22.5 MPa and 2 MPa, compared to the nominal strength of 35 MPa.

The findings of the coring investigation led to more detailed investigations of the foundation performance and of measures that could be taken to enhance this performance. One of the independent analyses, undertaken by the author, is described below.

4.6 *Analysis of building performance*

4.6.1 *Approach adopted*

The computer program PIGS was used to carry out the analyses of foundation performance for Blocks D and E. The following procedure was used:

- From the available geotechnical information, separate geotechnical models were developed for *each* of the 18 bored piles supporting each block.
- The geotechnical parameters for each of the layers within each geotechnical model were assessed initially from conventional correlations with Standard Penetration Test (SPT) data or with rock type.
- From the available coring information, models were developed for each of the piles.
- The geotechnical and pile models were input into PIGS, and the foundation behaviour under the dead loading, up to Floor 34, was analyzed.
- Because of the apparent effects of the core drilling in causing additional building settlements, an attempt was made to exclude these settlements from those due to the building load. This was done on the basis of extrapolating the measured settlement-time relationship, prior to the effects of the core drilling, to the end of January 2000, when it was assumed that the settlements due to the loads from the 34 floors of building would have been completed. For each of the settlement markers, these settlements were subtracted from the measured settlements to obtain an estimate of the settlement due to the core drilling. These settlements should be treated separately from those due to the building loads, as they would not recur if no further core drilling were done.
- The inferred pile settlements due to core drilling were then incorporated as “free-field” ground movements into the PIGS analysis for the foundation settlement behaviour. The computed settlement behaviour of the foundation, from Floor 17 (when the measurements began) to Floor 34 (when the construction halted) was compared with the measured values. The geotechnical parameters of the soil layers were modified, and the analyses repeated until a reasonable match was found between the measured and computed settlement behaviour.
- Once a reasonable match was obtained between measured and computed settlements, the foundation behaviour for various cases was analyzed via PIGS.

The settlements due to core drilling were estimated at the various settlement marker locations, for each of the two blocks. From these values, the settlement at each pile location due to the core drilling was obtained. On this basis, the assessed additional pile settlement due to the core drilling ranged between 2 and 10 mm for the piles in Block D, and between 0 and 25 mm for the piles in Block E.

It was assumed that the shaft diameter of the existing piles was 2.3 m and that there was no bell at the base of the shaft. The length of each pile was taken as the value indicated during the investigative coring, and the Young’s modulus of the pile was estimated from the measured unconfined compressive strength of the concrete cores.

For the remedial piles, it was assumed that, for an option involving additional bored piles, the shaft

and base diameters would be 2.3 m and 3.5 m respectively, and then piles would extend 0.8 m into slightly decomposed rock. For an alternative option involving prebored H-piles, the shaft diameter of the remedial piles was assumed 0.61 m. In the latter case, the piles were to be founded 9 m below the top of the slightly decomposed rock.

The assumed loadings were as follows:

Dead load—11.612 MN per floor.
Live load—2.551 MN per floor.
Moment due to wind load at 34th floor level—35.5 MNm and 529.2 MNm in the two horizontal directions.

4.6.2 *Calibration of PIGS models*

Figures 8 and 9 show the measured and computed settlements for various sections across Blocks D and E, as obtained from the final calibration runs. In order to reproduce the observed tilt, it was found necessary to introduce some eccentricity of applied loading.

While the agreement was not perfect, it was found possible to obtain a reasonable fit by adopting the following correlations with the average SPT value N:

Young's modulus: $E_s = \alpha N$ MPa
where $\alpha = 2.8$ for Block D, and 4.2 for Block E.

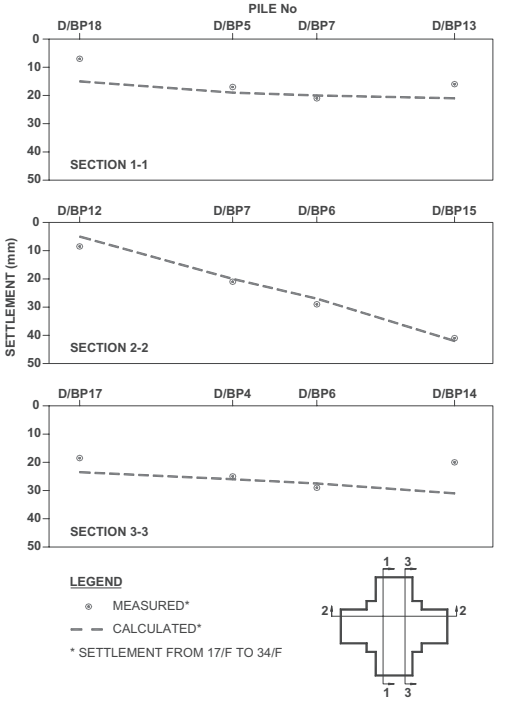

Figure 8. Measured and computed settlement profiles—Block D.

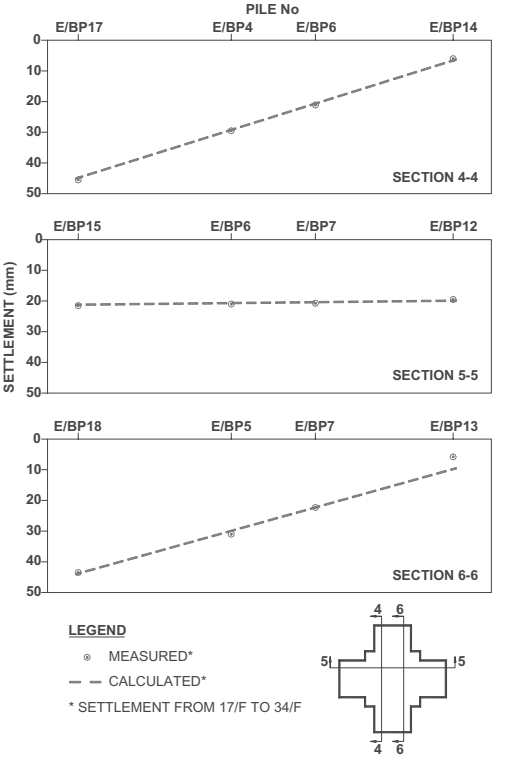

Figure 9. Measured and computed settlement profiles—Block E.

Ultimate shaft friction: $f_s = 1.0$ N kPa
Ultimate end bearing pressure: $f_b = 0.1$ N MPa.

The loading eccentricities, with respect to the geometric center of the foundation system, were as follows:

For Block D: 0.05 m in the "x" (east–west) direction, and –2.4 m in the "y" (north–south) direction.
For Block E: –1.5 m in the "x" (east–west) direction, and 0.0 m in the "y" (north–south) direction.

4.7 *Assessment of as-designed foundations*

For reference purposes, a PIGS analysis was carried out for the hypothetical case where it was assumed that the bored piles in the original foundation layout for Blocks D and E were founded 0.8 m into Grade III or better rock. In this case, no investigative core drilling settlements were applied to the piles. The following stages were modelled:

- Stage 0—Building constructed to 34 storeys
- Stage 1—Building constructed to 41 storeys (full dead load of 476.1 MN applied)
- Stage 2—Full live load of 104.6 MN applied.

Table 2. Summary of as-designed case, Block D.

Stage	Foundation factor of safety	Maximum tilt	Maximum settlement (mm)	Minimum settlement (mm)
0	4.8	1/3304	16	6
1	4.0	1/2543	20	8
2	3.3	1/1884	26	9

Table 3. Summary of PIGS analysis—Block E.

Stage	Foundation factor of safety	Maximum tilt	Maximum settlement (mm)	Minimum settlement (mm)
0	4.9	1/5519	12	7
1	4.0	1/4290	16	8
2	3.3	1/3223	20	10

The results of the analyses are summarized in Tables 2 and 3. It can be seen that had the building foundations been constructed as-designed (i.e. founded 0.8 m into Grade III or better rock), the foundation system factor of safety under full dead and live load would have been greater than 3 and the maximum overall tilts of the foundations would have been significantly less than 1/400 (in fact, less than 1/1800) for both Blocks D and E. The maximum settlement of Block D and E were estimated to be 26 mm and 20 mm respectively.

4.8 *Assessment of as-built foundations*

The PIGS program was also used to compute the behaviour of the as-built foundation systems had construction proceeded without any enhancement works. This was done by simulating the addition of dead loading for the final 7 floors to the 41st floor, and then the addition of live loading, simulating the full occupancy loading situation. Analyses were also carried to simulate the case of wind loading when the buildings were at the 34th floor level.

Table 4 shows the computed maximum and minimum settlements, the overall tilts and the overall factor of safety against failure, for each block. The following observations can be made from this table:

1. Foundation system factor of safety is less than 3 for Block D under dead loading from 41 floors.
2. Foundation system factor of safety is less than 3 for Block E under dead loading from 34 floors.
3. Failure of the Block E model occurs (overturning) under dead + live loading from 41 floors.
4. Overall tilt of Block D is greater than 1/400 under dead loading from 41 floors.
5. Overall tilt of Block E is greater than 1/400 under dead loading from 34 floors.
6. Overall tilt of Block D is greater than 1/200 under dead + live loading from 41 floors.
7. Overall tilt of Block E is greater than 1/200 under dead loading from 41 floors.
8. Maximum calculated settlement of Block D under dead loading from 41 floors is 104 mm.
9. Maximum calculated settlement of Block E under dead loading from 41 floors is 159 mm.

It was also found that several of the piles in Block D would have reached their ultimate capacity under full dead plus live load, and this would be unacceptable in relation to the client's requirements, which demand a factor of safety in excess of unity on each of the piles within the group. Indeed, the normal design requirement in Hong Kong (as stipulated by the Hong Kong Buildings Department) is that the factor of safety for each pile within a group should be at least 2. The loads in most of the piles for Block E were computed to have reached their ultimate value under full dead plus live loading. The solution for Block E was in fact unstable, indicating that rotational failure of

Table 4. Summary of computed performance for as-built foundations.

Performance measure	Loading condition	Block D	Block E
Overall factor of safety	Dead load at 34th floor	3.1	2.2
	Dead load at 41st floor	2.6	1.8
	Dead + live load at 41st floor	2.1	Failure
Overall tilt (radians)	Dead load at 34th floor	1/503	1/390
	Dead + wind load at 34th floor	1/342	1/354
	Dead load at 41st floor	1/350	1/212
	Dead + live load at 41st floor	1/204	Failure
Maximum settlement (mm)	Dead load at 34th floor	76	97
	Dead + wind load at 34th floor	96	105
	Dead load at 41st floor	104	159
	Dead + live load at 41st floor	160	Failure

the foundation would have occurred. It was therefore clear that the as-built foundations would have been inadequate to support the completed buildings.

4.9 *Assessment of remedial options*

PIGS was used to investigate a number of alternative future options, including:

- Construction of 8 new bored piles, socketted 0.8 m into Grade II or better rock, and enlargement of the pile cap.
- Construction of up to 66 new steel H-piles installed in pre-bored holes, each extending 9 m into the Grade II granite. An extended pile cap would be constructed to link the old and new foundation elements.
- Truncation of the buildings so that the existing foundation system would be adequate without any further enhancement.

Both of the first two options would require up to 5 m of excavation and dewatering. Truncation of the buildings was assessed to be technically feasible, but was not considered to be economically feasible by the owner because of the stigma of having two lower-rise buildings (12 or 13 storeys high) within a larger group of much taller buildings. Thus, the focus of the assessment of remedial options was on the use of new remedial piles to enhance the defective existing foundation system.

For the PIGS analysis of the remedial pile scheme, the following stages were modelled:

1. Stage 0—Building constructed to 34 storeys and settlement due to investigative core drilling applied to piles;
2. Stage 1—Installation of the remedial piles, and enlargement of the pile cap;
3. Stage 2—Building constructed to 41 storeys (full dead load of 476.1 MN applied);
4. Stage 3—Full live load of 104.6 MN applied.

For Block D, the maximum calculated overall tilt for the proposed remedial scheme with additional bored piles under dead + live loadings from 41 floors was 1/465 and the maximum settlement was 85 mm. The overall foundation system factor of safety was 5.3. Similar values were found for the prebored H-pile option.

For block E, the maximum calculated overall tilt under dead + live loadings from 41 floors was 1/383 and the maximum settlement was 108 mm. The overall foundation system factor of safety was 3.1.

Based on these results, it was assessed that, provided the remedial works could be executed without disturbance to the existing foundations, this remedial schemes for Blocks D and E would be theoretically adequate in reducing the overall tilts and increasing the overall foundation system factor of safety to within what may be considered as acceptable levels.

The pile loads within the original bored piles with the remediated foundation scheme were computed as part of the PIGS analysis, and it was found that, for each of the blocks, one of the piles would have reached its ultimate capacity. Under the client's design requirements, this would normally render the design unacceptable unless special dispensation was given for the unusual circumstances of this case. It should however be noted that the axial load on a pile within a group is dependent on the method of analysis used. In both cases, the computed pile loads for the remedial piles were less than the ultimate axial load capacity of the piles.

4.10 *Construction risk factors*

Despite the findings of the PIGS analysis, it was considered that there were a number of risk factors associated with any of the options involving remedial work to the existing foundations, in particular:

- The fact that such remedial operations had not previously been used for very tall buildings in Hong Kong;
- The remedial operations would in any case have to be carried out to rectify deficiencies in the capacity of the vast majority of piles in the existing foundation system;
- The difficulty of access for construction equipment within the confined spaces of the existing foundation footprints;
- The difficulty of exercising the essential precise control of construction within the confined spaces of the existing foundation footprints;
- The possible effects on the integrity of the foundation system of ground movements arising from drilling for the additional piles;
- The possible effects on the integrity of the foundation system of ground movements arising from excavation for the new pile caps;
- The possible effects on the integrity of the foundation system of ground movements arising from dewatering for construction of the new foundation elements;
- The proposed strengthening of the existing pile caps may not have been adequate, and in any case, would have been difficult to execute;
- The increased risk of damage to the adjacent school if the construction operations exacerbated the uneven settlement towards this building.

The construction of the proposed remedial measures would have been complex and would have included extensive excavation works in the vicinity of the already highly stressed foundation area of both blocks. It was considered that there would be a

potential for additional settlements of the piled foundation associated with the drilling of the additional large diameter bored piles, or of the larger number of prebored H-piles, particularly in view of the settlements experienced during the investigative coring of the foundations of Blocks D and E. There would also have been a potential for ground movements associated with the excavation, to approximately 4 m below existing ground level, required to expose the existing pile cap and allow connection with the new pile caps.

Numerical analyses were undertaken to assess the likely magnitude of the ground movements from construction, and their effects on the existing piles. A more detailed account of these analyses is given by Poulos (2004). On the basis of these analyses, it was concluded that the risks involved during the construction of the remedial works, and the potential additional settlements, were unacceptable, particularly given the proximity of the buildings to the nearby school and other existing high-rise residential blocks.

4.11 *The final decision*

In a decision that was widely publicized in Hong Kong, the decision was taken to demolish both buildings, and this was carried out in 2001–2.

5 CONCLUSIONS

This paper has presented a versatile analysis of pile group behaviour when subjected to vertical and moment loading. This analysis allows for non-ideal situations in which not all piles in the group are identical, some piles may contain defects, and the group configuration may change during the process of construction or loading.

The analysis has been used to examine the effects of the presence of defective piles within the foundation systems of the two high-rise buildings that led to their eventual demolition before the completion of construction. This was a rather extreme case of the consequences of three major construction imperfections:

Piles with a soft toe;
Piles with variable founding conditions;
Piles of variable length within a group.

The analysis revealed that enhancement of the foundation system with either additional prebored H-piles, or with additional large diameter bored piles, would provide a technically satisfactory remedial solution. However, in this particular case, the risks involved in carrying out the remedial foundation works beneath heavily loaded buildings were considered to be unacceptable, particularly in view of the potential for significant ground movements to be generated during the enhancement works. The concern over these risks was a major factor in the ultimate decision to demolish the buildings.

REFERENCES

Kuwabara, F. and Poulos, H.G. 1989. Downdrag forces in group of piles. *Jnl. Geot. Eng., ASCE*, **115**(6): 806–818.

Mandolini, A. and Viggiani, C. (1997). Settlement of piled foundations. *Geotechnique*, **47**(3): 791–816.

Poulos, H.G. (1989). Pile behaviour—Theory and application. 29th Rankine Lecture, *Geotechnique*, **39**(3): 365–415.

Poulos, H.G. 1990. *DEFPIG user's manual*. Centre for Geotechnical Research, University of Sydney, Australia.

Poulos, H.G. 2002. Prediction of Behaviour of Piled Building Foundations due to Tunnelling Operations. *Proc. 3rd Int. Symp. On Geotechnical Aspects of Underground Construction in Soft Ground*, Toulouse, Preprint Volume, 4.55–4.61.

Poulos, H.G. 2004. The consequences of defective piles for two high-rise buildings in Hong Kong. *Keynote Lecture, Proc. Int. Conf. on Structural and Geotechnical Failures, Singapore, IES.*

Poulos, H.G. 2005. Pile behavior—consequences of geological and construction imperfections. 40th Terzaghi Lecture, *J. Geot. & Geoenv. Eng., ASCE*, **131**(5): 538–563.

Poulos, H.G. and Davis, E.H. 1980. *Pile Foundation Analysis and Design*. John Wiley, New York.

Poulos, H.G. and Hewitt, C.M. 1986. Axial interaction between dissimilar piles in a group. *Proc. 3rd Int. Conf. Num. Methods in Offshore Piling*, Nantes, 253–270.

Randolph, M.F. and Wroth, C.P. 1978. Analysis Deformation of Vertically Loaded Piles. *J. Geot.. Eng., ASCE*, **104**(GT12): 1465–1488.

Randolph, M.F. 1987. *PIGLET, a computer program for the analysis and design of pile groups.* Report GEO 87036, University of Western Australia.

Deep Foundations on Bored and Auger Piles – Van Impe & Van Impe (eds)
© 2009 Taylor & Francis Group, London, ISBN 978-0-415-47556-3

Ultimate lateral load resistance of laterally loaded pile

Md. M. Rahman, Md. R. Karim, A.L. Baki & D.K. Paul
Department of Civil Engineering, RUET, Rajshahi, Bangladesh

ABSTRACT: Several methods are available for predicting ultimate lateral load resistance of laterally loaded pile. These methods often produce significantly different ultimate lateral resistance. This makes it difficult to select an appropriate method in designing/predicting ultimate lateral resistance of pile. This paper presents a review of two different methods; Meyerhof and Patra & Pise for predicting lateral resistance of pile. Then, the predicted ultimate lateral resistances by these two methods are compared with the experimental results. It is found that Meyerhof's method gives better prediction for single pile with smaller L/d ratio whereas Patra & Pise method gives better predictions for pile groups with higher L/d. Thus, none of these methods can be applicable universally for all possible conditions. Also the parametric study on ultimate lateral resistance revealed that length to diameter ratio, pile spacing, pile configuration in a pile group are important parameters for prediction of lateral load resistance.

1 INTRODUCTION

There are several approaches are available in the literature to estimate lateral load resistance of pile in sand and clay (Broms 1964; Meyerhof et al. 1981; Meyerhof and Ranjan 1972; Meyerhof and Sastry 1985; Meyerhof and Yalcin 1984; Sastry 1977; Sastry and Meyerhof 1986; Zhang et al. 2005). Also some simplified methods are proposed by Meyerhof et al. (1988) and Patra & Pise (2001) for cohesionless soil. However, these methods often produce significantly different ultimate lateral load resistance value (Zhang et al. 2005). This makes it difficult to select appropriate method when designing laterally loaded pile in cohesionless soil. A comparative study has been made in this paper between Mayerhof and Patra & Pise methods and experimental results with the intension that it could add some value on the understanding of practicing engineers. Also a parametric study is done on ultimate lateral load resistance. They are discussed in coming sections.

2 ULTIMATE LATERAL LOAD RESISTANCE

The simplified methods proposed by Meyerhof et al. (1988) and Patra & Pise (2001) has been briefly reviewed in this section. These methods are approximate with considerable assumptions. They are discussed in coming subsections.

2.1 *Meyerhof's method*

The ultimate lateral resistance of rigid pile, Q_{ur} is expressed by Meyerhof et al. (1981) as

$$Q_{ur} = 0.12\gamma dL^2 K_b \tag{1}$$

Where γ is average unit weight of sand; d is the diameter of pile; L is embedded length of pile; K_b is coefficient of net passive earth pressure on pile using an average angle of skin friction $\delta = \varphi/3$. Where φ is the angle of internal friction. However the ultimate lateral load resistance of flexible pile was presented by Meyerhof et al. (1988) as

$$Q_{ur} = 0.12\gamma dL_e^{\,2} K_b \tag{2}$$

Where L_e is the effective embedded length of flexible pile. Meyerhof and Yalcin (1984) suggested that if relative stiffness ratio K_{rs} is less than 10^{-1} to 10^{-2} then the pile can be consider as flexible pile. However, the relative stiffness, K_{rs} can be presented as

$$K_{rs} = E_p I_p / E_h L^4 \tag{3}$$

Where E_p is modulus of elasticity of pile; I_p is moment of inertia of pile; E_h is horizontal soil modulus at pile tip; L is embedded length of pile. Meyerhof et al. (1988) reported that L_e/L has an approximate functional

relationship with relative stiffness K_{rs} and it can be presented as

$$L_e/L = 1.8K_{rs}^{0.12} \quad (4)$$

However, Rahman et al. (2003) reported that L_e/L can be represent by following relation as

$$L_e/L = 1.65K_{rs}^{0.12} \quad (5)$$

2.2 *Patra & Pise method*

Patra & Pise (2001) modified the Meyerhof's equation by multiplying a constant shape factor of 3 with the line of Broms (1964)

$$Q_{ur} = 3 \times 0.12\gamma dL_e^2 K_b \quad (6)$$

2.3 *Pile group*

Patra & Pise (2001) reported that the ultimate resistance of the pile group can be represented by

$$Q_{Lg} = 2F + P_P \quad (7)$$

Where, Q_{Lg} is ultimate lateral resistance of the pile group, F is frictional resistance on the vertical plane along the side of the pile group of width equal to centre to centre distance between external piles and embedded length L and P_p passive earth pressure for the front pile as shown in Figure 1.

The frictional resistance along the side of the pile group could be approximately found as

$$F = \frac{1}{2}\gamma L^2 \times K_S S \quad (8)$$

Where, K_s is coefficient of earth pressure along the side of the piles group governing frictional resistance $[(1 - \sin\varphi)\tan\delta]$. Thus, ultimate lateral resistance of pile group, 2×1 is

$$Q_{Lg} = \gamma L^2 \left[K_s S + 0.36dK_b\right] \quad (9)$$

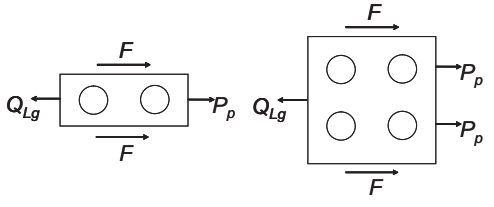

Figure 1. Free body diagram of laterally loaded pile group.

And the ultimate resistance of pile group, 2×2 can be expressed as

$$Q_{Lg} = \gamma L^2 \left[K_s S + 0.72dK_b\right] \quad (10)$$

2.4 *Group efficiency*

The efficiency of ultimate lateral resistance of pile group can be expressed as

$$\eta = \frac{Q_{Lg}}{n_1 n_2 Q_{Ls}} \quad (11)$$

Where Q_{Lg} is the ultimate lateral capacity of pile group; Q_{Ls} is the ultimate lateral capacity of single pile; n_1 is the number of rows in the pile group and n_2 is the number of columns in the pile group.

3 EXPERIMENTATION

An experimental program was designed for the verification and comparison of the above mention methods. The details of the experimental program and material properties such as sand, pile, pile cap etc. are given in following subsections.

3.1 *Foundation*

Rajshahi sand (available in north-west region in Bangladesh) is used as foundation medium. All model pile tests were done on a concrete tank of one meter in height, one meter in width and one meter in depth. Sand had a placement density of 95 lb/ft3 or 15kN/m^3 and the angle of internal friction was 37.9°. Specific gravity of the sand used in the model tank was 1.82.

3.2 *Pile and pile cap*

Aluminum alloy tube of 19 mm outer diameter and 0.81 mm wall thickness were used as model pile. To increase the pile wall friction angle, sand was added around the pile by adhesives. The average outside diameter of the rough piles were 20 mm. The embedment length-to-diameter ratios, L/d were 20, 30, and 35. Steel plate of 0.64 cm thickness was used as pile cap. The piles were attached with the pile cap by screw. The details of sand and piles properties can be found in (Rahman et al. 2003). The pile groups used in this study had configurations of 2×1 and 2×2.

3.3 *Experimental procedure*

The arrangement of test program is shown in Figure 2. The Loading arrangement was made in such a way that it acted laterally to pile or pile cap. However, it

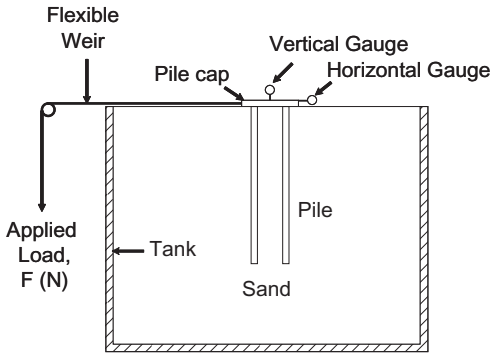

Figure 2. Experimental arrangement for laterally loaded pile.

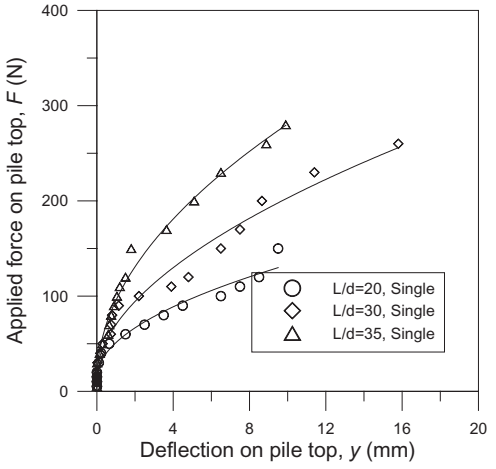

Figure 3. Load deflection curve for single piles for different L/d ratios.

was not possible to apply continuous loading but load is applied by stepping. To maintain a uniform density all through the tank depth, sand was placed in the tank from a constant height of about 0.5 m. After filling the tank, the upper surface of sand was leveled and then the pile was pushed into sand. Pile cap was then fixed on the pile top with screw connections. A 24 hours of rest period was allowed before applying any load on pile setup. The lateral load was applied to the pile cap through a pulley arrangement with flexible weir. The other end of the weir was attached to the loading apron. Load was applied by dead weight over the loading pan starting form the smallest with gradual increase in steps. To measure the lateral and vertical deflection dial gauges with a sensitivity of 0.01 mm were used. When step by step lateral loads were applied on the pile or pile group, they were deflected in the direction of the lateral load and the dial gauge readings and the corresponding loadings were recorded.

4 RESULTS

The ultimate lateral load resistance of the pile was worked out by plotting the recorded data, thus load Vs deflection curve was obtain which was non-linear in nature. Ultimate lateral resistance of the pile was obtained from the curve by double tangent method (DTM) or the point where the curve show a greater deflection without further increase in any load. The detail can be found in (Rahman et al. 2003). The curves presented in this paper are only showing the general trends. The ultimate load resistance behaviours of single pile and the pile group are presented in coming subsections.

4.1 *Single pile*

The ultimate lateral load resistance of single pile increases with increase in L/d ratio as shown in Figure 3. The ultimate load resistance of a single pile for L/d = 20 is about 107 N whereas 115.2 N predicted by Meyerhof's method and 72 N by Patra & Pise method. Thus, Patra & Pise method doesn't predict well for single pile and the prediction by Meyerhof's method is very closed to the experimental observation. However, in higher L/d, Patra & Pise method gives better prediction. The ultimate lateral load resistance of L/d = 35 is about 225 N and Patra & Pise method predicted 221.7 N whereas Meyerhof's prediction deviate by 50 N in higher side.

4.2 *Pile group, 2 × 1*

The ultimate lateral load resistance of pile group, 2 × 1 increases with increasing L/d as shown in Figure 4. It is about 117.2 N for L/d = 20 and 160 N, 250 N for L/d = 30, L/d = 35 respectively.

However, when the observed ultimate lateral resistance is compared with Mayerhof and Patra & Pise methods, it is found that the ultimate lateral load resistance predicted by Patra & Pise method gives a better prediction for pile group. Table 1. shows the detailed results for L/d = 20.

4.3 *Pile group, 2 × 2*

The load deflection curve for pile group, 2 × 2 is shown in Figure 5. This figure only shows two different L/ds and it clearly shows that ultimate lateral load resistance of pile increases with its L/d ratio. The ultimate lateral load resistances are 200 N and 300 N for L/d = 20 and L/d = 30 respectively. However, the ultimate lateral load resistances predicted by Patra-Pise methods are 190 N and 280 N respectively.

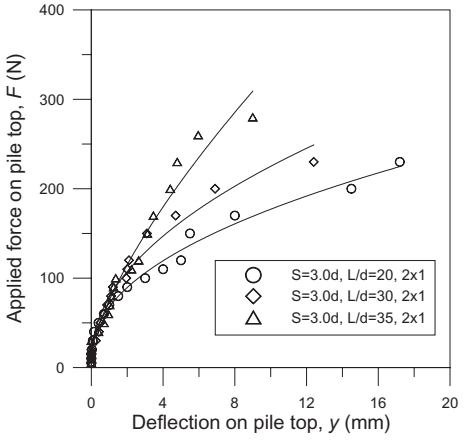

Figure 4. Load-deflection curve for pile group, 2×1.

Table 1. Comparison of lateral load resistance of pile group, 2×1 with Patra & Pise method and observed value.

L/d ratio	Spacing (d)	Observed resistance (N)	Theoretical resistance (N)
20	3.0	117.2	115.6
20	4.5	147.0	137.2
20	6.0	166.0	158.8

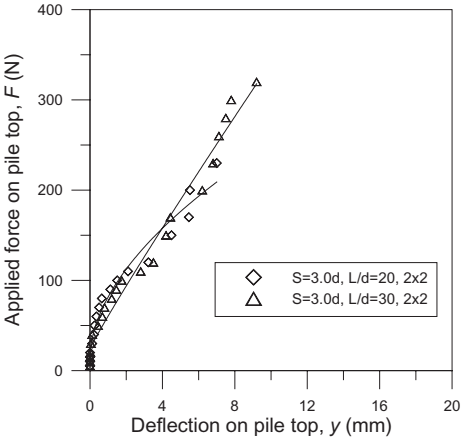

Figure 5. Load-deflection curve for pile group, 2×2.

Again, it indicates that this method could better and conservative prediction.

4.4 *Effect of pile spacing in group*

Figure 6 shows that the centre to centre distance of piles in a group has strong influence on the ultimate

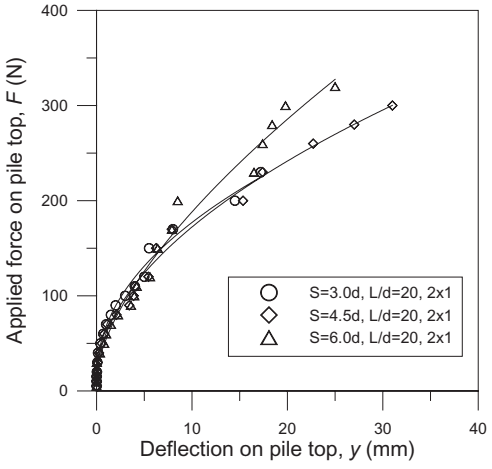

Figure 6. The effect of centre to centre distance between piles in group, 2×1.

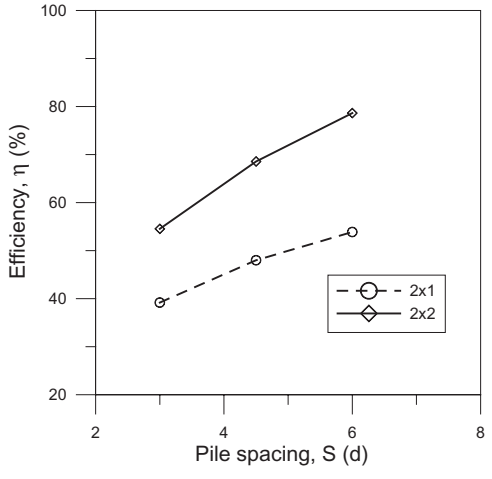

Figure 7. Variation of pile group efficiency with pile spacing between group, 2×1 and group, 2×2.

lateral resistance of pile; it increases with increasing in piles c/c distance. However, the variation with c/c distance of piles is not linear. Figure 7 shows that the increment of lateral resistance for 3.0 d to 4.5 d is higher than the increment for 4.5 d to 6.0 d.

4.5 *Group efficiency*

The efficiency of lateral load resistance for pile group is calculated by the Equation 11 and they are presented in Figure 7. It shows that the increment of group efficiency for 3.0 d to 4.5 is maximum and it reduces from 4.5 d to 6.0 d. This trend is seen in both

groups of 2×1 and 2×2. However, it is interesting to note that group efficiency for the group of 2×2 is less than for the group of 2×1. Thus, it indicates that pile spacing also very important for ultimate lateral resistance of pile.

5 CONCLUSIONS

The following conclusions are drawn from the present study:

- The ultimate lateral load resistance of pile group depends on the length to diameter ratio of pile, pile friction angle, pile group geometry, spacing of piles in a group and sand placement density. The quantitative and qualitative influence of those parameters has been investigated.
- The ultimate resistance of pile group increases with an increase in pile spacing. It has been found that resistance at 3 d spacing is less than that of 4.5 d spacing. Again resistance at 4.5 d spacing also less than that of 6 d spacing.
- Group efficiency of pile increases with an increase in pile spacing. It has also been found that the efficiency at 3 d spacing is less than that of 4.5 d and 6 d spacing.
- Finally, the prediction by Patra & Pise method can give better prediction for pile groups whereas Meyerhof's method gives better prediction for single pile. Thus, none of these can be universally used for the prediction of lateral load resistances of pile or pile group.

REFERENCES

Broms, B.B. 1964. Lateral resistance of piles in cohesionless soils. *Journal of the Soil Mechanics and Foundations Division, ASCE*, 90(SM3): 123–156.

Meyerhof, G.G., Mathur, S.K., and Valsangkar, A.J. 1981. Lateral Resistance and Deflection of Rigid Walls and Piles in Layered Soils. *Canadian Geotechnical Journal*, 18(2): 159–170.

Meyerhof, G.G., and Ranjan, G. 1972. The bearing capacity of rigid piles under inclined load in sand. I. Vertical Piles. *Canadian Geotechnical Journal*, 9, 430–446.

Meyerhof, G.G., Sastry, V., and Yalcin, A.S. 1988. Lateral Resistance and Deflection of Flexible Piles. *Canadian Geotechnical Journal*, 25(3): 511–522.

Meyerhof, G.G., and Sastry, V.V.R.N. 1985. Bearing capacity of rigid piles under eccentric and inclined loads. *Canadian Geotechnical Journal*, 22, 267–276.

Meyerhof, G.G., and Yalcin, A.S. 1984. Pile capacity for eccentric inclined load in clay. *Canadian Geotechnical Journal*, 21, 389–396.

Patra, N.R., and Pise, P.J. 2001. Ultimate lateral resistance of pile groups in sand. *Journal of Geotechnical and Geoenvironmental Engineering*, 127(6): 481–487.

Rahman, M.M., Alim, M.A., and Chowdhury, M.A.S. 2003. Investigation of lateral load resistance of laterally loaded pile in sandy soil. *4th International Conference on Bored and Auger Piles, BAPIV*, Ghent, Belgium, 209–215.

Sastry, V.V.R.N. 1977. Bearing capacity of piles in layered soil, PhD Thesis, Technical University of Nova Scotia, Halifax, NS.

Sastry, V.V.R.N., and Meyerhof, G.G. 1986. Lateral soil pressures and displacements of rigid piles in homogeneous soils under eccentric and inclined loads. *Canadian Geotechnical Journal*, 23, 281–286.

Zhang, L., Silva, F., and Grismala, R. 2005. Ultimate Lateral resistance to piles in cohesion less soils. *Journal of Geotechnical and Geoenvironmental Engineering*, 131(1): 78–83.

Deep Foundations on Bored and Auger Piles – Van Impe & Van Impe (eds)
© 2009 Taylor & Francis Group, London, ISBN 978-0-415-47556-3

A Study of end-bearing capacity mechanism of steel spiral pile

Maejima Tadashi
Research and developing division, Asahi-kasei Construction Materials Corporation

Futaki Mikio
Tsukuba building research and testing laboratory center for better living

ABSTRACT: Steel pipe pile with extended spiral steel plate at the end of the pile tip (hereinafter referred as the steel spiral pile) has some originality in its mechanism of the bearing capacity. To make clarify the mechanism of the bearing capacity with some parameters such as the soil specification of the bearing stratum, and the way of the installation of the pile, basic tests were executed, and following results were obtained. 1) Bearing capacity will be significantly weakened if bearing stratum is repeatedly stirred by the spiral plate and its shearing strength will also be deteriorated. 2) Judging from the test results, the degree of how much soil condition gives influence on the bearing capacity of the pile is linked in a proportional manner to the index of shearing strength of the stratum. 3) In the case of the steel shaft with its diameter is twice the size of steel shaft; the ratio of the distributed loading of the steel spiral is about 50% of the total loading

1 INTRODUCTION

In recent years, the steel pipe pile with extended spiral plate (hereinafter referred as the steel spiral pile) is one of typical pile foundation systems in several construction fields in Japan. First in the late 1970', it has been developed as a small sized pile system mainly for housing or residential buildings. Now this kind of pile system has developed its size variation (100 mm to over 1500 mm) and the pile installation technique, came to be the indispensable option for the selection of foundation specifications.

Asahi-kasei Construction Materials Cooperation is one of the leading companies of this field. In 1994, it obtained from the Ministry of Land and Transportation of Japan the official certification for the utilization of "EAZET System" with its superior bearing capacity strength. Since then, the bland name "EAZET" system has been leading the development of this pile system. Its pile shaft line-up ranges from 114,3 mm to 355.6 mm while spiral plate diameter from 250 mm to 800 mm.The performance of long term allowable bearing capacity by the strength of the bearing stratum is over 1200 kN at maximum. Its total construction sites topped 20 thousands in 2007.

With its distinctive features such as low-noise, low vibration, and installation without discharging surplus soil, this system can be defined as a high-performance method, enabling to monitor the condition of the soil surrounding the pile spiral plate simply by observing torque stress.

In the aspect of performance as the pile, it has strong points such as high bearing and pulling capacity mainly with the effect of the extended spiral plate. As the original feature of steel pile, it also has strong point for the horizontal resistance for the earthquake. Recent years, this pile system has drew attention for its easiness for recycling. By rotating in reverse direction, it can be withdrawn without damaging the environmental conditions and pile itself. In the trend of using limited natural resources, several practical plans are under study in a bid to find construction materials easy for recycling in the face of soaring cost of construction materials.

2 SPECIFICATIONS OF STEEL SPIRAL PILE

At the tip of the steel shaft, spiral steel plate with its diameter ranging from twice to third times as steel shaft is attached. The thickness of the spiral steel plate is chosen in accordance with the stiffness that each size of spiral plate will perform for the bearing capacity. In each steel shaft, bottom plate is attached. By attaching bottom plate, the proportional dimension of this pile can be classified as pile tip stoppage type. Other subordinate steel plates such as blade plate are attached, too. It has several functions such as to help

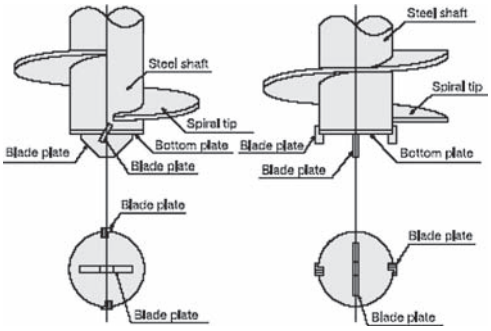

Figure 1. Specifications of the tip part of EAZET pile.

penetrate into the ground and keep the accuracy for its installation work.

As a method for the steel pile joint, we have developed the mechanical joint system with torque share type high-tension bolt used.

By using this joint system, we can not only shorten the leading time for the steel pile joint competitive to the ordinal welding joint, but also make the joint procedure more reliable one. This joint system has come to be one of the standard systems in Japanese construction field.

3 STUDY FOR THE BEARING CAPACITY MECHANISM

3.1 *On Site loading test*

For the purpose of studying the bearing capacity mechanism of this pile, we have done total 14 vertical loading tests on EAZET pile. Tests were done under different kind of soil conditions. Fig. 2 is a typical chart showing relation between the degree of loading at the tip of the pile (Pp/Ap) and that of the settlement at the tip of the pile (Sp/Dw) with its N-value in the range of 20 and 40 in cases of bearing stratums of clay, sand, and gravel. Fig. 3 shows the relation with N-value of over 40.

From the results of these tests, we can conclude that the relationship between (Pp/Ap) and (Sp/Dw) is a simple increasing curve regardless of the type of the soil or the diameter of the pile, as is often the case of steel pipe with extended spiral steel.

In case the N-value is over 40, stiffness of the settlement has no clear relation with the soil conditions even if it's on the early stage of the settlement.

This test data are showing how relationship of the (Pp/Ap) and (Sp/Dw) changes depending on the shear strength of the bearing stratum.

Fig. 4 shows the distribution of the average N value and the reaction force of the pile shaft tip and pile

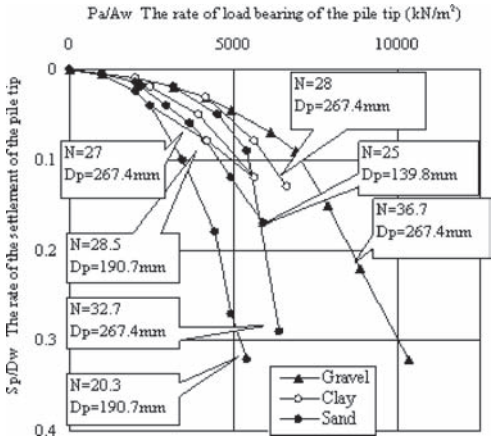

Figure 2. Normalized load-settlement curves. (0 < N < 40)

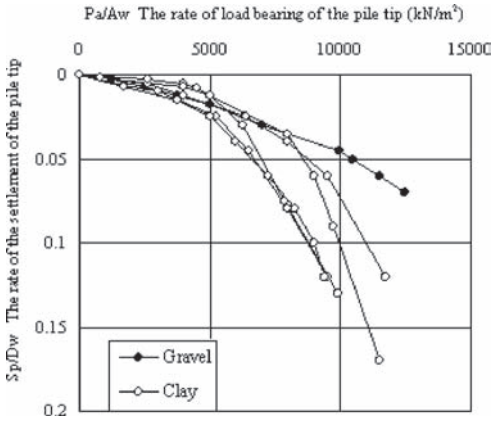

Figure 3. Normalized load-settlement curves. (40 < N)

spiral tip when its length of the settlement reaches 10% of the pile tip diameter.

As the average N-value of the pile tip increases, reaction forces of the pile shaft and pile tip also increase accordingly. Pa will reach critical point when the N-value reaches around 23, which is almost same level of the critical void rate of the sand stratum. Judging from this data, we can guess the characteristic of the soil strength has been changed after installing pile. On the other hands, regardless of the N-value, the distributed loading ratio between the pile shaft and the pile spiral plate (Pw/Pa) remains 0.5.

From these data, it can be concluded that the ratio for the reaction force from the bearing stratum between pile shaft and the pile spiral tip is 1:1 even if its rate of the area is 1:3.

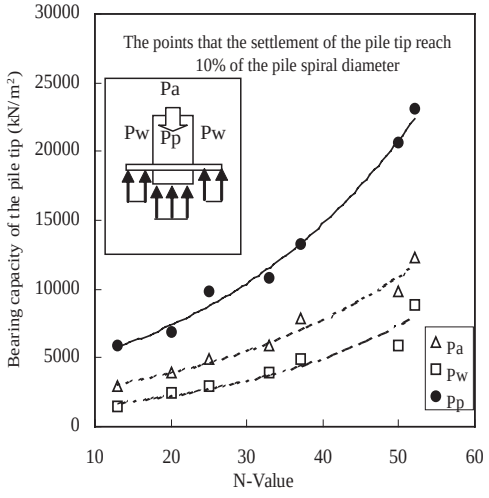

Figure 4. Load allotment rate curves.

3.2 *Analysis*

To make clarify the effect of the extended pile spiral tip, FEM analysis was conducted on the model test of the EAZET pile after the validity of the analysis being confirmed and then the distributed load at the spiral tip of the pile was studied. FEM analysis has been experimented with elasto-plasticity analysis program which takes into account the strain softening. The analysis is executed by using the model that changes the elastic modulus (such as volume elasticity or shear modulus of rigidity) depending on the mean principle stress; confining pressure.

This model was estimated axisymmetrical model and spiral steel tip part was modeled as complete circle. At the first step, we conducted the self-weight analysis to analyze initial stress and step-by-step analysis was conducted after confining pressure and forced displacement given. Thin element with small friction angle was placed at boundary face between ground and pile as joint.

Fig. 6 shows the result of the loading test simulation with the thickness of the spiral plate of 9 mm and 12 mm and also the results of the loading test that was done in the triaxial compression apparatus.

In the model experiment, the circle plate with a slit substituted the spiral plate. And axisymmetrical analysis was done by using this simplified model. Relatively similar test results were obtained from both tests.

Fig. 7 is the chart of the distribution of the bearing pressure of spiral plate with its thickness of 9 mm, showing the figures at boundary face element just beneath the steel pile spiral plate. This distribution explains that there was directional change of the maximum principal stress around the face.

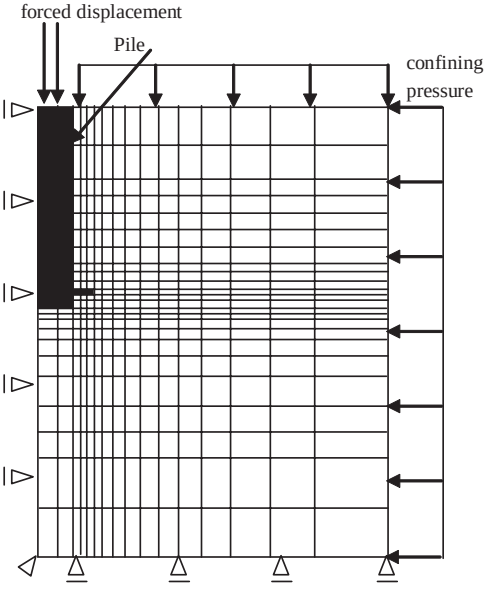

Figure 5. A model for the analysis.

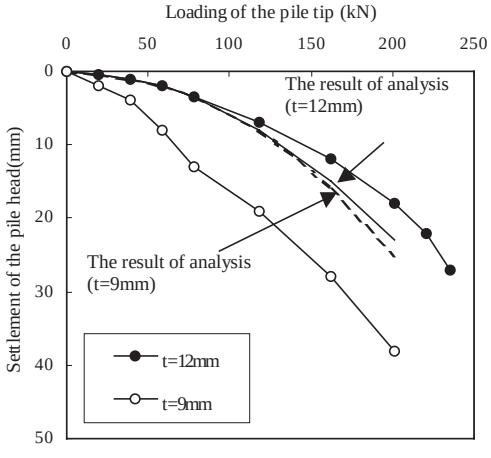

Figure 6. Pile tip load-settlement curves of analysis.

Apart from this area, the direction of the maximum principal stress for other elements of the pile is vertical and its bearing pressure is stable.

Reaction force that the spiral part covers is about 60% comparing to the pile shaft. This is because of the decrease of the effect of locked-in stress caused by the deformation of the spiral tip. The ratio for the sharing of the burden was calculated as around 0.7, which is higher than that of on site loading test. The difference has the connection with the type of the pile installing.

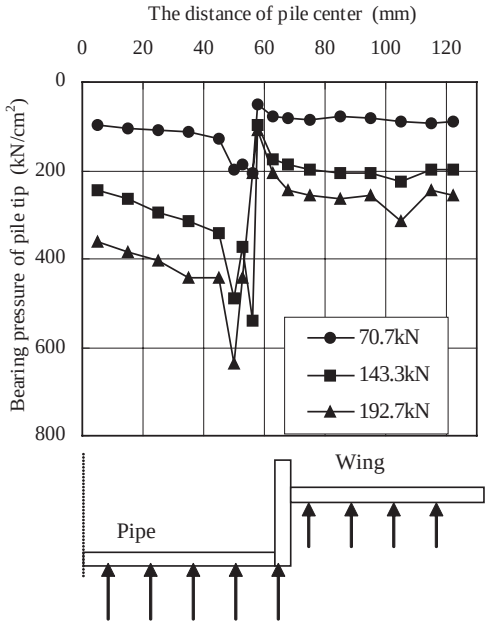

Figure 7. Distribution of the bearing pressure.

In practical use, the soil condition just beneath the pile spiral is loosened.

4 BEARING CAPACITY AND INSTALLATION METHOD

Full-size piles with extended spiral plate with different length of pitches were installed aiming to get the data of the installing speed and the bearing capacity performance under varieties of soil conditions. The specifications of the test pile are 190.7 mm in length for the pile shaft and 400 mm in diameter for the spiral plate.

Spiral pitch was set as 120 mm, 80 mm, and 60 mm.

Fig. 8 shows the results of the installing speed and the data of the standard penetration test. In the aspect of the installing speed, there was a distinctive difference. The narrower the pitch was, the speed of installing got slower. Especially at the depth of GL-8 m and GL-11 m, where the change of the characteristics of the layer was seen, there was a remarkable decrease in the rate of penetration. In the case of the pile with 60 mm pitch spiral, it took about 5 to 6 times longer than that of the pile with 120 mm pitch spiral. Fig. 9 shows the results of the loading test with different kinds of spiral pitches.

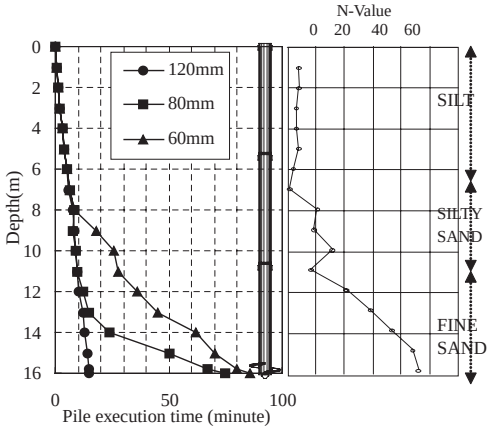

Figure 8. SPT date and time for installation by spiral pitch.

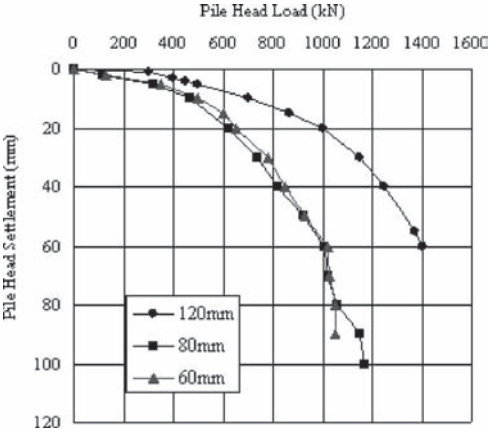

Figure 9. Pile head load-settlement curves.

Test pile No.2 and No.3, which required longer time to be installed, have almost same results in terms of relation between loading at the top of the pile and the settlement at the top of the pile. But in the No.1 pile case, it had made different transition even at the beginning of the loading test, showing outstanding stiffness toward settlement.

This difference had the close relation with the deterioration of the installing speed. The deterioration of the installing speed stirred the soil around the pile spiral tip, causing decrease not only in the shear strength of the bearing stratum, but also in the skin friction stress of the steel pile due to excessive rotation.

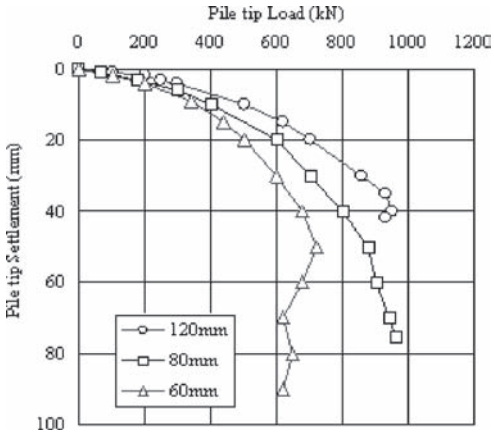

Figure 10. Pile tip load-settlement curves.

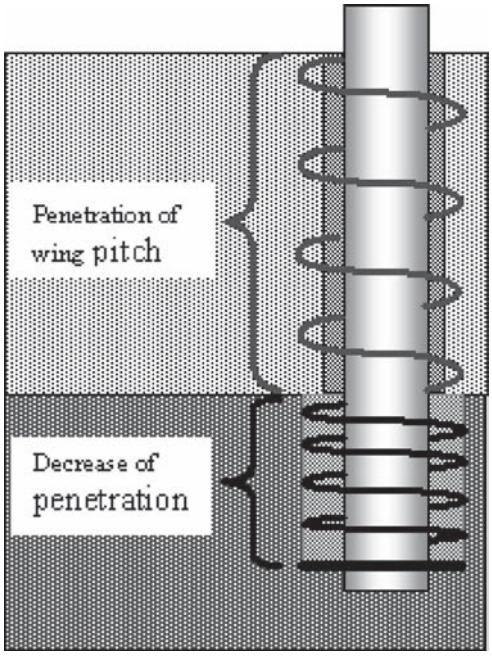

Figure 11. Penetration model of screw pile.

Summarizing the relation between the pile top loading and settlement, there is a trend that bearing capacity performance will decrease as the speed of the pile installation deteriorates.

When the length of the settlement of the tip part is 10% of that of the spiral steel, the decrease of the end bearing capacity is 70%.

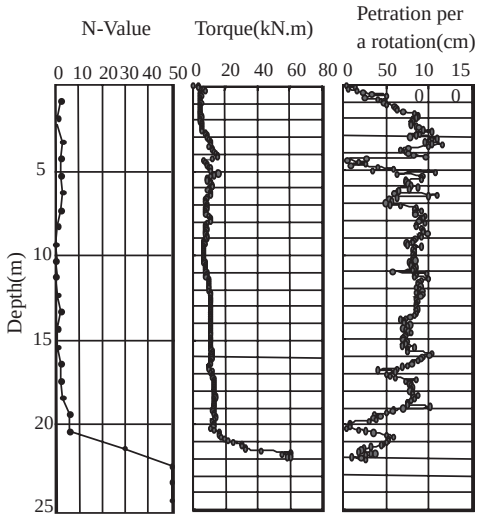

Figure 12. Installation record.

5 SUMMARY

Fig. 11 is a model drawing of the EAZET pile while Fig. 12 shows data in the installing procedure.

Receiving the driving and pushing force from the installing machine, the pile penetrates into the stratum while pushing away the soil, the volume of is the same as that of the pile shaft. In the part of the stratum with soft and weak soil condition, the pile will penetrate into the stratum down to the same depth as the pitch by rotating one round.

When the pile tip reaches near the bearing stratum, the pile installation will slow down. Excessive rotation has a direct relation with the decrease of the shearing strength of the soil, and it also leads to the deterioration of the bearing capacity performance.

Fig. 13 is the charts showing the N-value of the bearing stratum and the coefficient of end bearing capacity (with) under several soil features. With sand and gravel, a clear distinction is recognized for the distribution of the coefficient when the N-value reaches around 20. This fact will lead to a theory that the bearing capacity performance of the steel pile will differentiate depending on the dilatancy of bearing capacity.

On the other hand, in the case of clay as the bearing stratum, excessive rotation of the pile didn't affect the strength of the stratum, showing stable N-value of the stratum.

This is very interesting point from the view of the soil engineering and the fieldwork. For the understanding of these phenomena, future study is needed.

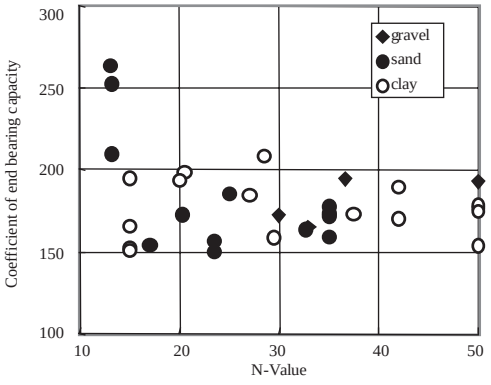

Figure 13. Relation of the N-value and coefficient of end being.

6 CONCLUSION

Steel pipe pile with spiral tip is very excellent pile system. It can install pile into soil or bearing stratum only with the effect of pushing and rotation of the pile. Compared to other pile system, this system enables to easily acknowledge the soil condition at the part of the pile tip. By observing the transition of the torque value with the machine equipment, operator is able to know when the pile reaches and starts to penetrate the bearing stratum.

Nonetheless, to get the appropriate bearing capacity performance, there are a few points that should be noted.

If too much pushing force during its operation is used for shortening leading time of the pile installation, the penetration length per round of the pile may exceed the pitch of the steel tip spiral. It may create void surrounding the soil of pile spiral tip, affecting the bearing capacity of the pile.

Another possibility is the decrease of the bearing capacity by the excessive penetration into the bearing stratum. It has a relation with the decrease of the shearing stress of the stratum with the effect of the dilatancy.

As you recognize by these studies, the bearing capacity mechanism of EAZET pile system has close relationship with the way of installing the pile. To get the appropriate performance of the pile, we not only have to do decent pile installation work, but also have to closely select a pile-installing machine.

For the machine of EAZET pile, the most important factor is torque performance of the machine. But excessive dependence on the torque performance affect the bearing stratum and its pile itself. With the experience of our on-site works during these 15 years, we also focus on another specification of the machine, such as pushing performance and machine stability and rigidity. To keep the quality and the performance of the EAZET pile system, it is indispensable for us to have good partners for the developing of the machine.

REFERENCES

Suzuki. H. et al.: Characteristics of Bearing Capacity by steel pipe pile with Tip of Spiral Wing.

Yamato. S. et al.: Penetration Characterisitcs of Rotary Penetration of steel pipe pile.

Yoshida. K. et al.: Characteristics of Bearing Capacity by steel pipe pile with Tip of Spiral Wing(part2).

DEFINITIONS OF TERMS

Dp: Diameter of the pile shaft
Dw: Diameter of the spiral steel plate of the pile
Ap: Area of the pile shaft with clogging tip
Aw: Area of the pile spiral steel plate
Qa: Ratio of the loading at the spiral tip of the steel pile
Qp: Ratio of the loading only at the shaft of the pile
Qw: Ratio of the loading at the spiral tip part of the pile without shaft part
P: load bearing at the head of the pile
Pa: load bearing at the tip of the pile
S: length of settlement at the head of the pile
Sa: length of the settlement at the tip of the pile
Ra: Ratio of the load distribution

Deep Foundations on Bored and Auger Piles – Van Impe & Van Impe (eds)
© 2009 Taylor & Francis Group, London, ISBN 978-0-415-47556-3

Urban renovation of the new marina in Rimini: Displacement piles as soil improvement and settlement reduction for the construction of a new dwelling and business centre

D. Vanni, A. Bertero, D. Attala & M. Malavolta
Trevi Group, Italy

G. Marchi & M. Marchi
Department of Civil Engineering, DISTART, University of Bologna, Italy

A. Ragazzini & L. Samorì
Enser s.r.l., Faenza (RA), Italy

ABSTRACT: Renovation and reuse of cast-off buildings in urban or former industrial areas represent a field presently encountering great development and is a continuous challenge for the ground engineering. In order to tackle the difficult logistics and the complex management of the works, innovative technologies and equipment to improve production rates, reliability of the product as well as reduced environmental impact are required. The new residential and business centre named "La prua", built in the area of the new marina in Rimini, perfectly fits in this scenario. As an alternative solution to the conventional foundation piles, a widespread soil improvement has been proposed, to be carried out under the concrete slab. Therefore, non-reinforced concrete columns have been designed to reduce the settlements of the new building foundations which are due to the compressibility of the soil layers and the buildings' loads. The results of a detailed geotechnical investigation enable us to develop geotechnical and numerical finite elements models. According to these models the columnar system has been designed through predicted total and differential settlements.

1 SITE CHARACTERIZATION

The new residential and business centre named "La prua", is presently under construction in the area of the new marina in Rimini, at a minimum distance of about 150 meter from the shoreline of Adriatic Sea. A general plan view of the project is shown in Figure 1.

The geology of the area is characterized by delta and alluvial deposits consisting predominantly of clayey and silty materials with interbedded meters thick sand layers (Upper Pleistocene—Holocene). Figure 2 shows the layout of the new two buildings called A/B/C and D/E.

According to the geology, the new buildings will be constructed over compressible marine deposits and river alluvium; previous experience clearly indicates that the main foundation problems occurred in this kind of soil are a consequence of the medium to high compressibility of the silts, clays and loose sand layers.

1.1 *Stratigraphic section*

An analysis of the subsoil stratigraphy and geotechnical properties was carried out in order to define an accurate geotechnical model. Therefore, a specific geotechnical investigation campaign was carried out, including: 6 continuous vertical boreholes (BH) to a depth of 35.0 m, 10 static penetrometer tests (CPT) and static penetrometer tests with monitoring of pore water pressure (piezocone tests, CPTu) to a depth of 25.0 m, standard penetration tests (SPT) in boreholes, extraction of several soil samples, most of which undisturbed, to be examined under further laboratory tests, to ascertain their physical and mechanical properties.

The relevant information for the stratigraphic model based on CPT's and boreholes data are shown in Figure 3 for the building A/B/C.

Data interpretation enabled to identify a rather detailed geotechnical characterisation of the subsoil

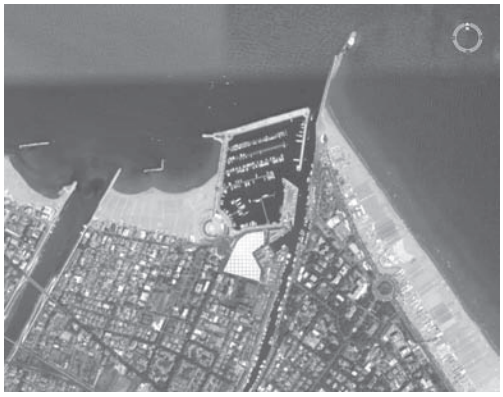

Figure 1. Site location of the new residential and business centre “La prua”, Rimini-aerial view.

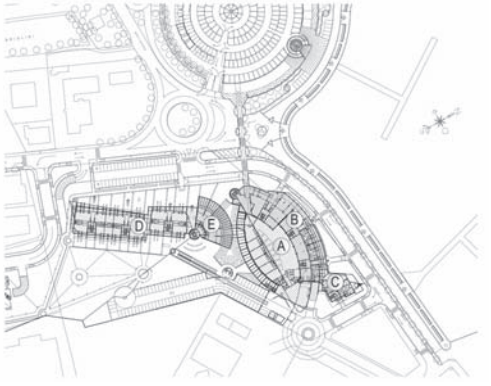

Figure 2. Plan of the new residential and business centre “La prua”, Rimini—note blocks A, B, C, D and E.

layers; the following stratigraphic units were defined:

– Unit R, from ground level to –4.5 m: anthropic fill, made of loose sand in silty matrix, with frequent inclusions of gravel; penetrometric cone resistance data from 1.0 MPa to 10.0 MPa.
– Unit A, from –4.5 m to about –8.0 m: grey-brown loose sand with clayey silt, with the presence of few centimetres-size shells; penetrometric cone resistance data from 0.5 MPa to 2.5 MPa.
– Unit B, from about –8.0 m to about –10.8 m, –14.5 m: brown medium sand, silty sand, from medium to dense, with rare inclusions of organic material; penetrometric cone resistance data from 2.0 MPa to 7.0 MPa.
– Unit C, from about –10.8 m to about –15.0 m and from about –18.0 m to about –25.0 m: grey clayey silt and silty clay, with interbedded sandy and organic layer; penetrometric cone resistance data from 0.5 MPa to 1.5 MPa.

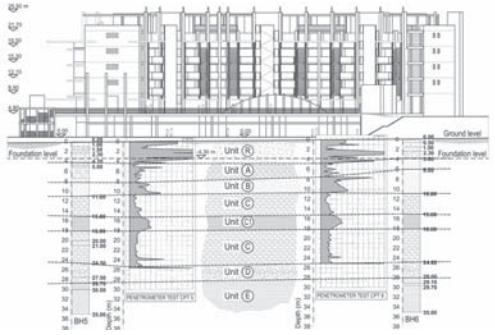

Figure 3. Stratigraphic section.

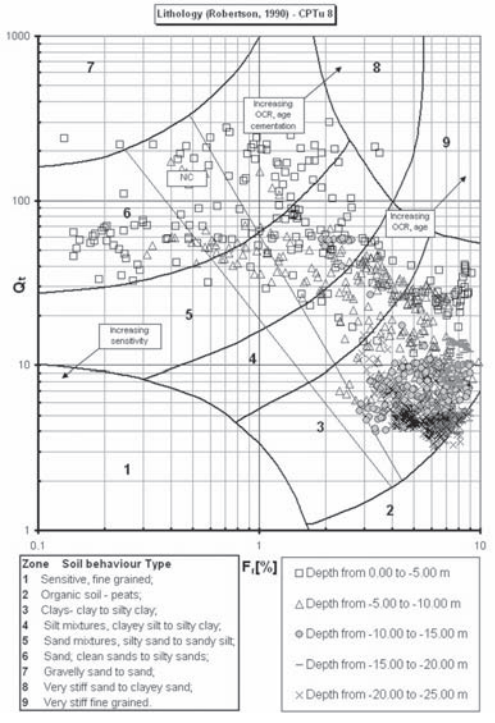

Figure 4. Soil behavior type from Robertson’s chart—CPTu.

– Unit C1, from about –15.0 m to about –18.0 m: grey-brown clayey silt and silty clay, overconsolidated for desiccation; penetrometric cone resistance data from 2.0 MPa to 4.0 MPa.
– Unit D, from about –25.0 m to about –28.0 m: gravel in sandy silt matrix, gravelly sand, gray, with diameter from few mm to 3–4 cm.
– Unit E, from about –28.0 m to about –35.0 m: grey-black clayey silt and silty clay, with organic material layer.

BH/Sample	Depth [m]	Soil description	γ_n [kN/m³]	$\gamma_{d\,dry}$ [kN/m³]	w_n [%]	LL [%]	PL [%]	PI [%]
BH1 / samp. 1	12.00-12.70	claily silt	18.90	14.20	32.48	45.10	19.60	25.50
BH1 / samp. 2	18.00-18.60	silty clay	19.80	14.30	32.11	77.20	25.50	51.70
BH1 / samp. 3	30.00-30.50	claily silt	18.80	14.30	31.74	50.30	20.80	29.50
BH2 / samp. 1	12.00-12.60	claily silt	18.60	13.70	36.13	40.40	20.00	20.40
BH2 / samp. 2	21.00-21.60	claily sandy silt	18.80	13.90	35.54	30.20	18.60	11.60
BH2 / samp. 3	30.00-30.70	claily silt	19.20	14.50	32.46	44.90	20.90	24.00
BH3 / samp. 1	11.50-12.20	claily sandy silt	18.70	13.70	36.75	41.20	19.80	21.40
BH3 / samp. 2	21.00-21.70	silty sand- sandy silt	19.10	14.40	32.41	32.00	18.20	13.80
BH4 / samp. 1	12.00-12.60	claily silt	18.80	14.10	33.44	42.80	18.90	23.90
BH4 / samp. 2	18.00-18.60	silty clay	18.90	14.10	33.90	63.90	22.80	41.10
BH5 / samp. 1	7.50-8.10	silty fine sand	18.80	13.60	38.22			
BH5 / samp. 2	12.0-12.50	claily sandy silt	18.90	14.20	33.03	47.50	20.10	27.40
BH5 / samp. 3	18.50-19.10	silty clay	19.30	13.50	38.07	71.00	24.20	46.80
BH6 / samp. 1	12.00-12.70	claily sandy silt	18.70	14.00	33.88	56.10	21.80	34.30
BH6 / samp. 2	19.00-19.70	claily silt	18.80	14.30	31.91	52.60	22.10	30.50

BH/Sample	φ_{cu} [°]	c_{cu} [kPa]	φ' [°]	c' [kPa]	c_u [kPa]	c_u [kPa]	M [kPa]
	TD consolidated undrained		TD consolidated drained		pocket penetrometer	ELL	Edometric test
BH1 / samp. 1	15.00	29.70			50.00-70.00	41.00	
BH1 / samp. 2	12.30	38.30			55.00-85.00	42.00	4883.00
BH1 / samp. 3					65.00-100.00	51.00	9523.00
BH2 / samp. 1	12.00	38.20			30.00-40.00	15.00	
BH2 / samp. 2	15.30	46.80			55.00-65.00	30.00	6339.00
BH2 / samp. 3					80.00-115.00	56.00	9936.00
BH3 / samp. 1	16.50	47.00			75.00-80.00	37.50	5519.00
BH3 / samp. 2					65.00-75.00	50.00	6228.00
BH4 / samp. 1	14.00	30.00			85.00-100.00	50.00	5357.00
BH4 / samp. 2	10.40	51.90			80.00-105.00	30.00	5074.00
BH5 / samp. 1			31.30	4.00			
BH5 / samp. 2	14.00	48.10			60.00-90.00	50.00	
BH5 / samp. 3	12.90	27.80			80.00-110.00	72.50	4583.00
BH6 / samp. 1	12.00	38.90			80.00-85.00	48.50	
BH6 / samp. 2	11.50	51.80			105.00-115.00	67.50	5108.00

Figure 5. Main physical and mechanical properties of the soil from laboratory tests.

The water table is located 1.5 ÷ 2.5 m deep in the upper stratigraphic unit.

Figure 4 shows the CPTu's data on the Robertson chart (Robertson, 1990).

1.2 *Geotechnical characterization*

Figure 5 summarizes the main geotechnical properties of soil, as deduced from laboratory tests.

In particular, in order to perform settlement calculation, the following physical, elastic and shear strength parameters in drained conditions were assumed: Unit A: $E' = 3500–5000$ kPa, $c' = 5$ kPa, $f' = 24°$; Unit B: $E' = 10{,}000–12{,}000$ kPa, $c' = 0$ kPa, $f' = 31°$; Unit C: $E' = 5000–8000$ kPa, $c' = 10$ kPa, $f' = 28°$; Unit C1: $E' = 10000–15000$ kPa, $c' = 20$ kPa, $f' = 28°$; Unit D: $E' = 35000–40000$ kPa, $c' = 0$ kPa, $f' = 36°$; Unit E: $E' = 25000–35000$ kPa, $c' = 0$ kPa, $f' = 27°$.

2 THE PROJECT

The buildings consists of interlocked multi-storey blocks (see A, B, C, D and E in Figure 2), occupying a footprint of about 100.0 m by 48.0 m for the building denoted as A/B/C, and about 115.0 m by 45.0 m for the building called D/E. Block A is 5.0 m high from the ground level, block B is 25.5 m high, block C is 19.5 m high, block D is 20.0 m high, finally block E is 25.0 m high. Both buildings have an underground floor, and the foundations consist of a 0.8–0.9 m thick concrete slab, –4.3 m deep from the ground level. The cross-section of the building A/B/C is shown in Figure 6, the plan view of the cross-section A′ in Figure 7.

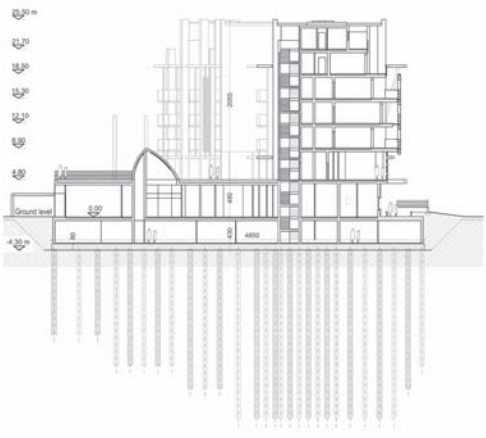

Figure 6. Section A′ of building A/B/C, with Discrepile.

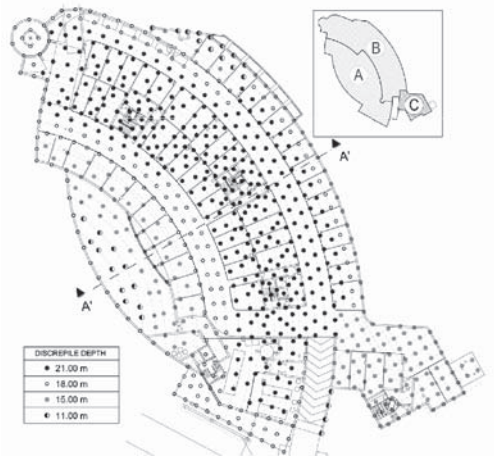

Figure 7. Plan of building A/B/C, with Discrepile.

The total asymmetric loads due to the new buildings are equivalent to an applied pressure ranging between 35.0 kPa and 230.0 kPa, with an average value of 65.0–80.0 kPa.

In order to reduce the total and differential settlements, due to the high compressibility of subsoil under the applied pressure, a widespread soil improvement has been proposed. 31,000 linear meters of non-reinforced concrete columns as settlement reducing piles have carry out under the buildings rafts. The works included about Nr. 1645 concrete columns installed using displacement technology from ground level. The columns are 600 mm in nominal diameter, and vary in length from 6.0 m to 24.0 m; the spacing between the columns varies from 2.9 to 7.4 diameters (job-site view in Figure 8).

Figure 8. Job-site view.

The arrangement of the concrete columns is designed to reduce differential settlements, using a denser array of columns in the zones where the buildings apply the greater pressure.

3 DISPLACEMENT PILES: DISCREPILE TECHNOLOGY

Some significant developments have been introduced in the recent years in displacement piles technology, in terms of tools, materials and execution method, allowing the displacement piles to spread and develop competitively on the market.

Clients, engineers and contractors appreciate the displacement piles method because it is:

– Quick and cost-effective
– Vibration-less and relatively low noise
– "clean" and environmental friendly technology, since it doesn't use bentonite slurry

The discrepiles process consists of three distinct phases, namely boring, concreting, steel reinforcement placing (Figure 9).

A special displacing tool is pushed and rotated into the soil by means of high trust and high torque. Different type and shape of displacement tools are available (Figure 10).

In unstable soils (i.e. saturated loose sand and silt), displacement piles are in general the best solution because this type of pile is able to densify the surrounding soil. In this way might be overcome the "over-augering" problems linked to the CFA (Continuous Flight Auger) technology and decompression phenomena of the ground that could result in surface

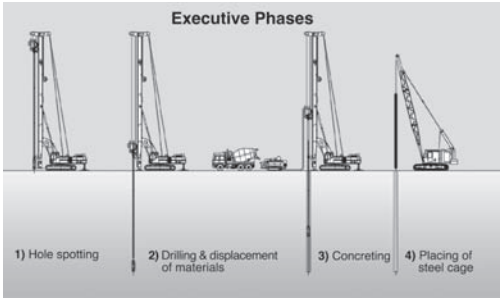

Figure 9. Discrepiles pile executive phases.

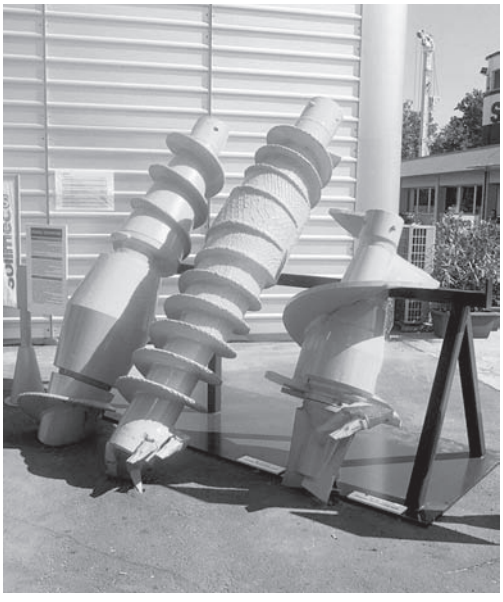

Figure 10. Displacement tools.

settlement, reduced pile bearing capacity and concrete over consumption.

The piles' diameter ranges between 400 and 600 mm, while the maximum length are 25–30 meters. Larger diameter, up to 900 mm, can be used in particulary favorable soil conditions.

The daily production is quite similar to the CFA piles, and in general it is more affected by the tool diameter and soil conditions.

If compared to CFA pile, this technique requires equipment with larger torque and thrust.

With the equipment, available on the market, the following application limits can be assumed:

– cohesive soil from soft to stiff (cu-undrained cohesion <100–120 KPa);
– loose to medium dense sand (relative density <65%)

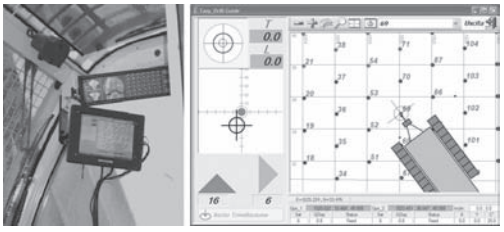

Figure 11. GPS navigation system.

This methodology represents the following advantages:

– High productivity and economical pile construction method;
– High quality of the final product (geometry, uniformity and durability);
– Improvement of the surrounding soil characteristics (in loose soils) and therefore increased piles performance in terms of bearing capacity;
– Small environmental impact (no or minimal soil removal, vibrations-free installation, working areas clean, noise emissions within the common regulations in urban areas).

Compared to CFA piles

– Reduction of the concrete over-consumption
– Risk of "over-augering" not allowed

3.1 *GPS rig positioning*

Considering the remarkable extension of the job site area, and the need to have an accurate vertical and horizontal positioning of the pile cap, a GPS device mounted on the rig (figure 11) has been adopted in conjunction with the traditional topographic survey systems. The topographic system was also used to check any soil movement (settlement or heave) occurred during the piles installation.

The implementation of GPS systems on the rig can speed up the rig positioning, and can record the actual location of each pile, allowing the possibility to prepare as-built drawing in real time. When using the GPS, the coordinates of each pile shall be uploaded to the GPS receiver on the rig. Than, the system is able to guide the operator to find the position of the selected piles on the ground and its starting elevation. Beside, the system shows all the piles already installed, avoiding mistakes or missed piles.

4 NUMERICAL MODELLING

The columnar system has been designed through predicted total and differential settlements (Fioravante et al., 2007). Therefore, a geotechnical finite element analysis of the soil foundation was performed. The aim of the modelling is the identification of the most efficient soil improvement, in terms of number and length of Discrepile, through the expected total and differential settlements.

4.1 *The models*

The plan strain FE model implemented for blocks A and B, used for the calculations, includes about 4020 elements, 32,700 nodes and about 48,200 stress point (Figure 12).

The plan strain FE model implemented for blocks D includes about 5100 elements, 41,700 nodes and about 61,600 stress point; finally axisymmetric FE model implemented for blocks E includes about 2600 elements, 21,400 nodes and about 31,500 stress point.

The analyses performed in drained conditions are non-linear and the soil is considered elastoplastic, with stress dependent stiffness according to a power law (Brinkgreve, 2002).

The costitutive model assigned to the Discrepile columns is non-linear and elastoplastic as the one used for the foundation soil, but with stiffness parameters based on non-reinforced concrete properties. Figure 13 summarizes the main geotechnical properties of soil model.

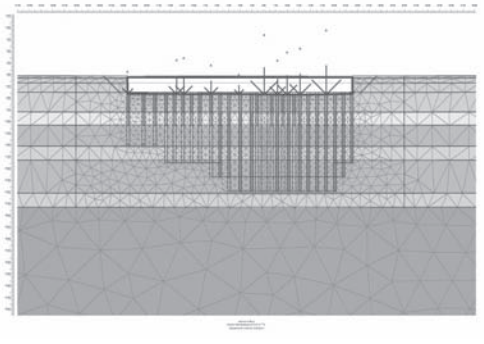

Figure 12. Plane strain model of building A/B/C, with Discrepile (deformed mesh).

HARDENING SOIL MODEL (PLAXIS FEM)								
Unit	Depth [m]	γ_{sat} [kN/m^3]	φ' [°]	c' [kPa]	ν [-]	Eoed [kPa]	Power [-]	Eur [kPa]
		Soil weight	Friction angle	Drained Cohesion	Poisson' s ratio	Plastic straining due to primary compression	Hardening soil model parameter	Elastic unloading / reloading
R	G.L./4.50 m	19.5	27.0	5.0	0.3	6000.0	0.5	25000.0
A	4.50/8.00 m	19.0	24.0	5.0	0.3	4500.0	1.0	22500.0
B	8.00/10.80 m	19.0	31.0	0.0	0.3	11500.0	0.5	57500.0
C	10.80/15.00 & 18.00/25.00 m	19.2	28.0	10.0	0.3	7500.0	1.0	22500.0
C1	15.00/18.00 m	19.5	28.0	20.0	0.3	15000.0	0.5	45000.0
D	25.00/28.00 m	20.0	36.0	0.0	0.3	40000.0	0.5	120000.0
E	28.00/35.00 m	19.5	27.0	0.0	0.3	31500.0	0.5	94500.0

Figure 13. Main physical and mechanical properties of the soil model.

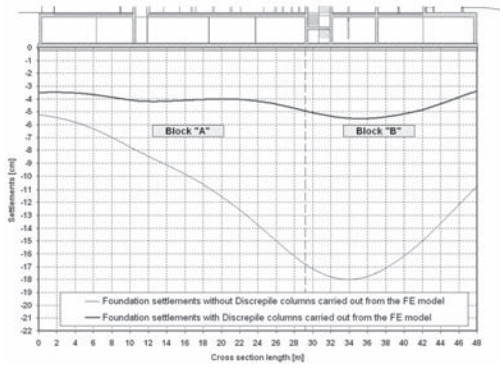

Figure 14. Foundation settlements of building A/B/C carried out from FE model.

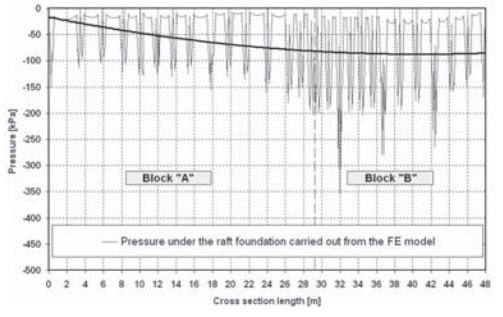

Figure 15 Pressure under the raft foundation of building A/B/C carried out from FE model.

4.2 *Results*

Figure 14 shows the vertical displacement of the foundation computed from FE model for blocks A and B, examining the case without and with soil improvement. The diagram clearly reflects the efficacy of the Discrepiles as settlement reducing piles. In fact, maximum vertical displacement vary from about 18 cm to about 5 cm, moreover differential settlements are reduced from 13 cm to 2 cm (cross section is 48.0 m long).

Some results can finally be drawn, in particular the pressure under the raft foundation carried out from FE model. As expected, the diagram in Figure 15 shows the maximum value of about 300.0 kPa on non-reinforced concrete columns and minimum value of about 40.0 kPa on soil foundation, with an average value of 70.0 kPa.

5 EXPERIMENTAL INVESTIGATIONS AND MONITORING

In order to monitor installation effects of a displacement pile on the subsoil, in situ investigations were carried out before, during and after Disrepile installation. Finally, a load test was performed on an instrumented Discrepile.

5.1 *Cone penetration tests and pore pressure measure during displacement pile installation*

The installation process may influence the stress state of the soil and hence the post-construction performance of the pile; therefore, in order to evaluate loosening of soil after Discrepile installation, some cone penetration tests have been carried out at a short distance from an installed column.

Figure 16 shows the comparison between cone penetration resistance from CPT's data, carried out before and after Discrepile installation.

Note that the change in cone penetration resistance after Discrepile installation is very small, in particular it may be due to intrinsic error in test data and/or natural soil heterogeneity.

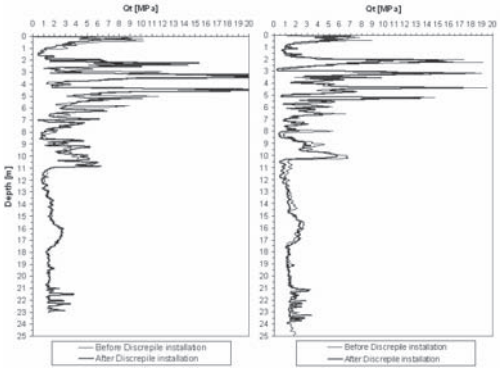

Figure 16. Cone penetration resistance before and after Discrepile installation.

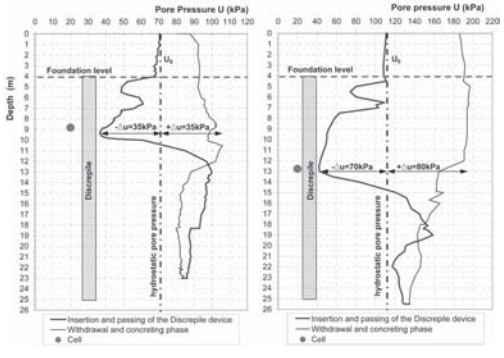

Figure 17. Pore pressure changes during Discrepile installation.

Moreover, pore pressure changes have been measured by piezocone cells during all the installation process. Figure 17 shows the collected data for two piles. Note that the pore pressure shows a decrease until the Discrepile device passes the piezometric cell then, the excess pore pressure becomes positive. This trend may be caused by two different phenomena:

– the plastic strain of the soil during the installation of the Discrepile device;
– the increment of total stress induced in the soil by the pressure of the fresh concrete in the withdrawal phase.

The analysis of the pore pressure evolution during the installation process needs further monitoring and numerical analysis, to take into account the complex stress-strain history induced in the soil by the pile installation.

5.2 *Discrepile load testing*

A load test up to failure was carried out on a preliminary installed discrepile (600 mm diameter, 20 meter long). Instrumentation was limited to an electronic load cell and settlement transducers in order to measure axial load and vertical displacement on top of pile

Figure 18. Load test configuration.

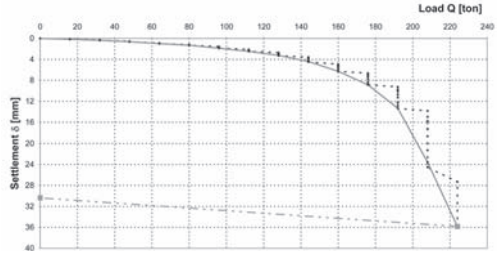

Figure 19. Load-Settlement curve.

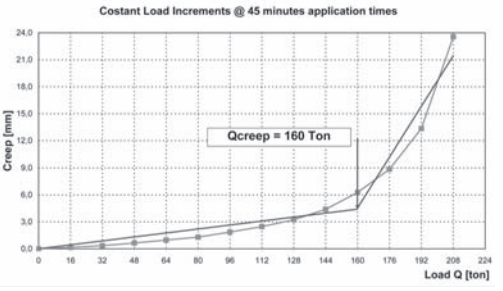

Figure 20. Creep load curve.

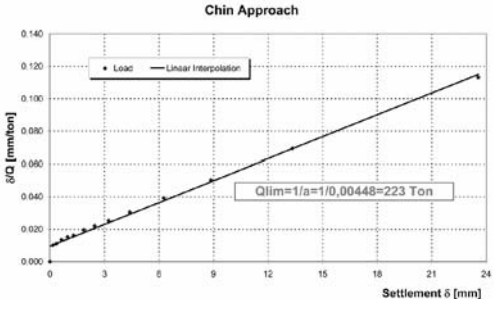

Figure 21. Chin approach.

(figure 18). The load was increased by equally spaced load steps up to failure. A total of 14 steps were required to reach the ultimate load. The load was kept constant at each step lasting a total time of 45 minutes. Settlements were measured at the beginning of each step and at 2′, 4′, 8′, 15′, 30′ and 45′. The procedure described above allows the determination of the creep load. Figure 19 shows the load-settlement behavior.

The settlement readings at every step were plotted in a semi-logarithmic graph in order to individuate the creep behavior. The creep parameter α against applied load Q is shown in figure 20. The creep parameter α increases approximately linearly with the load from the beginning of the test up to a certain limit. The behavior changes sharply for higher loads while approaching the ultimate laod. The creep limit load was individuated around 160 ton.

The ultimate load can be estimated as 223 ton (see also figure 21 which shows the result of the Chin approach to define the ultimate load).

6 CONCLUSIONS

This paper describes an advanced soil improvement intervention carried out under the foundation of a new building in a costal area (Rimini, Italy). The use of bored

or driven piles had to be avoided because they might have caused problems to the existing buildings (noise, vibrations, etc.), and to the logistics and cleanness of the works site. Therefore, as an alternate solution, a widespread soil improvement to be carried out under the concrete slab have been proposed. Non reinforced concrete columns have been designed to reduce the settlements of the new foundations, due to the compressibility of the soil layers and the new buildings loads.

Settlements analyses carried out for this case study show that use of non-reinforced columnar system, formed by Discrepile tecnology, guarantee high-efficiency soil improvement and foundation performance.

This methodology has the following advantages:

– Minimal disturbance to the soil structure;
– High quality of the final product (geometry, uniformity and durability);
– Low cost pile construction method;
– High productivity, to respect tight schedule;
– Simplification of the logistics in the job site (small equipment overall dimensions);
– Smaller environmental impact (vibrations-free installation, working areas always clean, sound emissions within the tolerance limits provided in urban areas).

REFERENCES

Brinkgreve, R.B.J., 2002. PLAXIS, Finite element code for soil and rock analyses, users manual. Rotterdam: Balkema.

Bustamante, M. and Gianeselli, L., 1982. Pile bearing capacity prediction by means of static penetrometer. Proc. ESOPT II, Amsterdam.

Butterfield, R. and Banerjee, P.K., 1971. The problem of pile group-pile cap interaction. Géotechnique, 21, number 2, pp. 135–142.

De Beer, 1971–1972. Methodes de dèduction de la capacitè portante d'un pieu à partir des rèsultats des essais de pènètration. Annales des Travaux Publics de Belgique, n.4, pp. 191–268, n.5, pp. 321–353, n.6 pp. 351–405, Brussels.

De Vos, M., Bauduin, C. and Maertens, J., 2003. The current draft of the application rules of Eurocode 7 in Belgium for the design of pile foundations, in Belgian screw piles technology: design and recent developments. Proceedings of the Second Symposium on Screw Piles, Brussels, Balkema.

Fioravante, V., Giretti, D. and Jamiolkowski, M., 2007. Physical modelling of raft on settlement reducing piles, *ASCE geotechnical special pubblication honoring Dr. John H. Schmertmann, October 2007.*

Fioravante, V., Ghionna, V.N., Jamiolkowski, M.B. and Pedroni, S., 1995. Load carrying capacity of large diameter bored piles in sand and gravel. Proc. 10th ARCSMFE, 2, 3–15.

Fleming, W.G.K., Weltman, A.J., Randolph, M.F. and Elson, W.K., 1992. Piling Engineering. Surrey University Press.

Holeyman, A. et al., 1997. Design of axially loaded piles—1997 Belgian practice, in Screw piles. Installation and design in stiff clay. edited by Holeyman A.E. Balkema, pp. 63–88.

Holeyman, A. et al., 1997. Design of axially loaded piles—Belgian practice. Proceedings of the ERTC3 seminar, Brussels.

Huybrechts, N. and Whenham, V., 2003. Pile testing campaign on the Limelette test site & installation technique of screw piles, in Belgian screw piles technology: design and recent developments. Proceedings of the Second Symposium on Screw Piles, Brussels, Balkema.

Jamiolkowski, M.B., e Sarri, H., 2000. On axial load capacity of drilled shafts in coarse grained soils. Libro Homenaje on Josè Antonio Jimènes Salas. Ministero de Fomento, Cedex, Madrid, 111–128.

Jardine, R. and Chow, F., 1996. New design methods for offshore piles marine technology Directorate. London, MTD Publication 96/103.

Mandolini, A. and Viggiani, C., 1997. Settlement of piled foundation. Géotechnique, Vol.XLVII, number 4, pp. 791–816.

Mandolini, A., Russo, G. and Viggiani, C., 2005. Pile foundations: experimental investigations, analysis and design. XVI ICSMGE, Osaka, Vol.1, pp. 177–216.

Maertens, J. and Huybrechts, N., 2003. Results of the static pile load tests at the Limelette site. In Belgian screw piles technology: design and recent developments. Proceedings of the Second Symposium on Screw Piles, Brussels, Balkema.

Nordlund, R.L., 1963. Bearing capacity of piles in cohesionless soils, JSMFD, ASCE, Vol. 89, SM3, pp. 1–36.

Poulos, H.G., 2001. Piled raft foundation: design and applications. Géotechnique, Vol.LI, number 2, pp. 95–113.

Randolph, M.F., Jamiolkowski, M.B., e Zdravkovic, L., 2004. Load carrying capacity of foundations. Advances in geotechnical engineering. The Skempton conference. ICE. Vol.1, pp. 207–240.

Reese, L.C. and O'Neill, M.W., 1999. Drilled shafts. Contruction procedures and design methods Federal Highway administration. Report FHWA-IF-99–025.

Theys, F., Maertens, J. and Maekelberg, W., 2003. Practical experinece with screw piles used for the high-speed railway in Belgium. In Belgian screw piles technology: design and recent developments. Proceedings of the Second Symposium on Screw Piles, Brussels, Balkema.

Tomlinson, M.J., 1986. Foundation design and construction. 5th edition, Longman Scientific and Technical, Wiley & Sons, New York.

Van Impe, W.F. 1994. Influence of screw pile installation parameters on the overall pile behaviour. Workshop 'Piled Foundations: Full Scale Investigations, Analysis and Design', Naples.

Van Impe, W.F., 2004. Two decades of full scale research on screw piles.

Van Impe et al., 1988. Prediction of the single bearing capacity in granular soils out of CPT results. ISOPT 1, Speciality Session, pp. 1–34, Orlando.

White, D.J. and Bolton, M.D., 2005. Comparing CPT and pile base resistance in sand. Proc. Institution of Civil Engineers, Geotechnical Engineering 158, paper 13342.

Viggiani, C., 1998. Pile groups and piled rafts behaviuor. Proc. BAPIII, Ghent, pp. 77–94.

Deep Foundations on Bored and Auger Piles – Van Impe & Van Impe (eds)
© 2009 Taylor & Francis Group, London, ISBN 978-0-415-47556-3

Re-design based on CPTs performed after pile installation

A.F. van Tol
Delft University of Technology, Delft, The Netherlands
Deltares (former GeoDelft), Delft, The Netherlands

ABSTRACT: Re-design of pile foundations based on CPT's after pile installation may be beneficial and is allowed in some design codes. For Bored and CFA piles the installation factors in the codes are in general on the safe side and a re-design based on CPT's after an optimal installation process may lead to a more cost effective design. As there is no standard procedure for such a re-design, this paper tries to formulate such a procedure. From a number of field cases it was concluded that a re-design should be based on CPT's, performed at different distances and around an installed pile and may be based on the average capacity based on CPT's after installation around the pile, taking distance effects of installation into account.

1 INTRODUCTION

CPT based design of pile foundations is a generally accepted method in areas where Cone Penetration Testing is a standard soil investigation technique. The so-called direct CPT method proved its usefulness and reliability. Several National codes in Europe apply the direct CPT method to determine the pile capacity (Cock & Legrand, 1997). Eurocode 7, part 2, Ground Investigation and Testing address this method in paragraph 4.3.4.2 and in Annex D.7 an example of the method illustrated.

The calculation procedures in different countries, like in the Dutch, the French or the Belgium method are quite similar. They distinguish between shaft and base capacity and determine the shaft and base resistance directly from the cone resistance, applying different empirical factors:

$$R_{c;i} = R_{b;i} + R_{s;I} \quad (1)$$

$$R_{b;i} = A_b \cdot q_{b;I} \quad (2)$$

$$R_{s;i} = \sum A_s \cdot q_{s;I} \quad (3)$$

where:

$R_{b;i}$ is the ultimate base capacity of the pile determined from the results of CPT i;
$R_{s;i}$ is the ultimate shaft capacity determined from the results of CPT i;
A_b is the cross sectional area of the pile base;
$q_{b;i}$ is the ultimate unit base resistance from the results of CPT i;
A_s is the circumferential area of the pile shaft in the layer in which the pile shaft friction has been assumed;
$q_{s;i}$ is the ultimate unit shaft resistance determined from the results of CPT i;

$$q_{b;i} = \alpha_b * \beta * s * q_{c;i;avg}$$

$$q_{s;i} = \alpha_s * q_{c;i;z}$$

where:

α_b, α_s are empirical factors for installation effect and soil type
β, s are geometrical factors for the pile base shape
$q_{c;i;avg}$ is the average cone resistance in a zone above and below pile base, with different averaging procedures
$q_{c;i;z}$ is the average cone resistance over a certain height, with different averaging procedures

An example of the magnitude of the empirical installation factors is presented in table 1.

Re-design based on CPT's after pile installation (with installation factors equal to 1.0) may be beneficial and is allowed in some design codes. Eurocode 7,

Table 1. Installation factor according to Dutch code.

Pile type	α_b	α_s
Displacement piles		
– precast	1.0	0.010
– cast in place	1.0	0.012
Screwed piles		
– CFA	0.8 (and $q_{c;III}$ = 2 Mpa)*	0.006
– with soil displacement	0.8	0.006
Bored piles	0.5	0.005

* In the averaging of q_c for the base resistance the value above the pile base is fixed at 2 Mpa.

part 2, Annex D.7 mentions this possibility in the note b under table D.5. For displacement piles in dense groups the significant compaction may be taken into account in a re-design. For Bored and CFA piles the installation factors in the codes are in general on the safe side to cover the uncertainties of the installation process. Therefore a re-design based on CPT's after an optimal installation process may lead to a more cost effective design. In other words, a contractor, convinced about his superior installation process may use this in a re-design based on the real performance proved with CPT's performed after the installation.

2 PROCEDURE FOR RE-DESIGN

2.1 *Approach*

There is no standard procedure for such a re-design. This paper tries to answer the following questions regarding such a procedure:

1. How many CPT's should be performed?
2. At what distances from the pile?
3. In one line or around the pile?
4. Which of the CPT's finally leads to the "real" pile capacity?

To answer the first three questions the effect of the distance between the CPT's and the installed pile and the orientation of the CPT's around the pile was assessed using the results of CPT's performed after pile installation at 10 job sites in the Netherlands, where CFA piles were installed. The results of this study are reported in Hannink & Tol (2005).

To answer the fourth question it is necessary to link the results of pile load tests to CPT's performed after installation of the pile. The objective is to determine whether the pile capacity is governed by the CPT leading to the lowest pile capacity (the idea that the weakest spot in the soil determines the strength by local failure) or by an averaging of all CPT's around the pile. To answer the fourth question two job sites were found with pile load tests and CPT's performed after pile installation.

2.2 *Distance*

Figures 1 and 2 show respectively the results of the ratio of the calculated base and shaft resistance from the CPT prior to installation and after installation at different distance and orientation around the pile. These figures are based on CPT's before and after installation on 10 job sites. The job site are depicted with different markers. It clearly visible that the installation effect differs greatly over the different sites and that in cases with a considerable

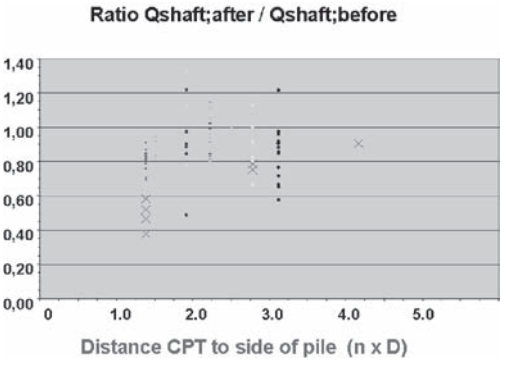

Figure 1. Ratio of calculated shaft capacity as function of distance.

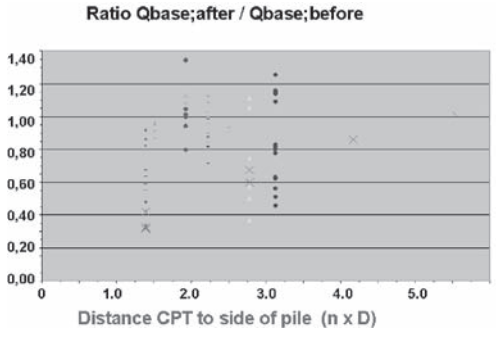

Figure 2. Ratio of calculated base capacity as function of distance.

installation effect the influence of the distance is clearly demonstrated.

2.3 *Orientation*

At one of the project sites in the southern part of The Netherlands the influence of the orientation of the CPT's made after the installation of the CFA pile was investigated. At three locations, 1 CPT was performed in the centre of the pile before installation and 4 up to 7 CPT's were performed at different distances and with different orientations. Figure 3 presents the situation. The diameter of the pile auger was 0.362 m and the base level was 8 m below reference level (mean sea level). Figure 4 shows the results of one of the three locations, where 4 CPT's were made after installation at a distance of 0.7 m, centre to centre, around the pile and the result of the CPT made before the installation. The reduction of the cone resistance due to the installation of the CFA pile is considerable and appears not to be constant over the depth and not the same in all directions.

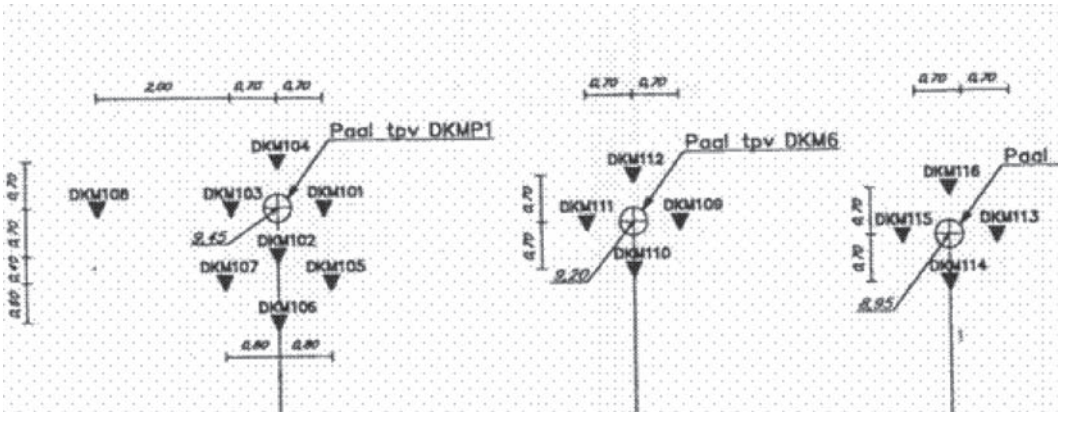

Figure 3. Position of piles and CPTs after installation.

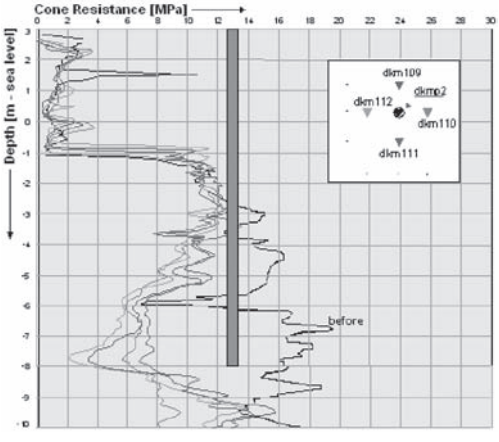

Figure 4. Four CPT's performed around an installed CFA pile at 0.70 m c.t.c.

The calculated reduction factors for the pile base vary between 0.34 and 0.59, and the reduction factors for the pile shaft vary between 0.69 and 0.76. It is obvious that the installation effect is not symmetric.

2.4 *Conclusion*

From the study of these job sites, it was concluded that the effect of installation differs strongly over the different job sites, that it is not symmetrical around the pile and that the effect decreases strongly with increasing distance. To establish the procedure for re-design based on CPT's performed after installation it seems necessary to link pile load test results to these CPT's.

3 REPRESENTATIVE CPT

Two test sites with in total four test piles were available for this study in order to answer the fourth question and to link the results of pile load tests to the calculated pile capacity based on CPT's performed after installation at different distances and around the test piles.

3.1 *Test site one*

At one of these test sites three CPT's were performed at almost the same distance but at different sides of the test pile. The CPT's were completely different: one showed an enormous decrease of the cone resistance in relation to the CPT performed prior to pile installation, because of a weak spot in the ground due to a failed pile installation. Two CPT's were similar showing a moderate decrease of cone resistance due to pile installation, see Figure 5.

Comparing the calculated pile capacity based on each CPT with the result of the static pile load test demonstrated that CPT 06 with the lowest cone resistance resulting in the lowest pile capacity does not determine the pile capacity. The measured pile shaft capacity was quite close to the average of the three calculated pile capacities based on the three CPT's around the pile, see table 2. The measured base capacity however exceeded the calculated by far. This is probably due to the specific averaging procedure according to the Dutch code. With the averaging method according to the French code (LCPC method) with 1.5 D below and above pile base the comparison shows that averaging the base capacity over the different CPT's is more in agreement with the measured base capacity, see row 4 in table 2.

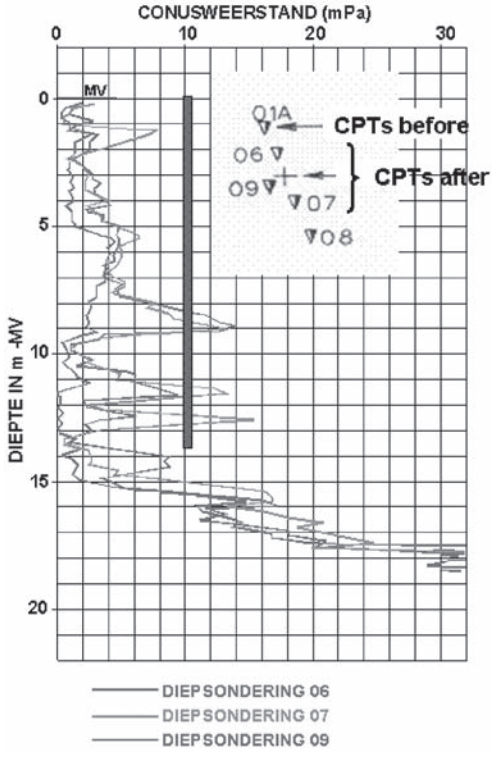

Figure 5. Position of pile and CPT's.

Table 2. Calculated base and shaft capacity compared with loads test results.

CPT	07	09	06	Average CPT	Pile load test
Shaft capacity	907	656	432	605	630
Base capacity	246	501	99	282	530
Base cap (LCPC)	278	779	159	405	530

3.2 *Test site two*

The situation at test site 2 is depicted in Figure 3. This paper describes the pile test and CPT's at the left hand site in this figure, where 8 CPT's were performed after pile installation at different distances and around the tested pile. The pile diameter is 0.362 m. One CPT was performed before installation in the centre of the pile and the CPT's after installation were made at distances of 0.70; 1.35; 1.70; 2.70 m.

A resume of the results from this test site is presented in Figure 6. The ratio between the calculated

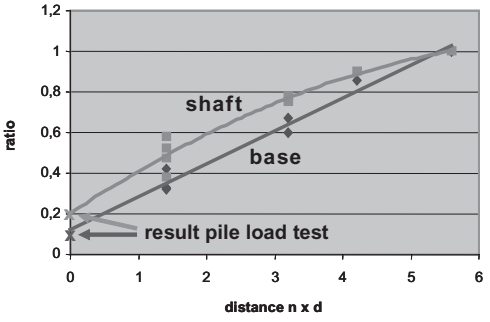

Figure 6. Ratio between the calculated $q_{b;after}/q_{b;before}$ and $q_{s;after}/q_{s;before}$ as function of the distance to the side of the pile and values from the static pile load test.

Table 3. Ratio $q_{b;after}/q_{b;before}$ and $q_{s;after}/q_{s;before}$ from the pile load test and the trend line based on calculated capacity at different distances.

Ratio	Pile load test result	Trend line
Shaft	0.20	0.20
Base	0.10	0.12

base and shaft resistance based on CPT's prior and after installation $q_{b;after}/q_{b;before}$ and $q_{s;after}/q_{s;before}$ is presented as a function of the distance to the pile, expressed in the pile diameter.

At the vertical axes the results of the pile load test are depicted, assuming that they would coincide with the results of an imaginary CPT performed at the position of the shaft. This ratio is the measured base and shaft resistance over the calculated, based on the CPT prior to installation.

It was tried to predict these values at the site of the pile (thus the measured resistance) by an extrapolation of the average calculated values at the different distances. It appears that these values can be predicted rather well with the trends lines. For the shaft a polynomial function of the second order fits the best and for the base resistance a linear function fits, see table 3.

The results from this site confirm that a re-design should be performed by averaging the CPT's around the pile and not taking the minimum. But also that the distance effect should be taken into account.

3.3 *Re-design procedure*

The installation effect is not constant around the pile, and increasing with decreasing distances from the installed pile. Based on three static pile load test and the CPT's at different distances and orientations after installation a reliable re-design can only be made when

all CPT's are taken into account. For such a re-design one should carry out CPT's at different distances as close as possible to the installed pile, and at different orientations around the pile. The calculated ultimate resistances based on these CPT's, must be plotted in a graph, base and shaft separately as a function of the distance, and the average trend line must then be drawn through these values. The extrapolated value at the side of the pile leads finally to the correct re-design value. It is obvious that this procedure is not very practical, but in case of a poor quality of the pile installation, with a severe stress relieve in the soil, it is the only way to proceed. It should be investigated whether in case of a good pile installation this procedure holds. It does of course hold if no stress relieve occurs and the CPT's before and after result in the same cone resistances.

4 CONCLUSIONS

It was concluded that:

- A re-design based on CPT's after pile installation can be beneficial, in particular in case of projects with large numbers of piles;
- For piles with soil excavation a re-design should be based on CPT's, performed at different distances and around an installed pile;
- The re-design may be based on the average capacity based on CPT's after installation around the pile, taking distance effects of installation into account.

REFERENCES

De Cock, F. & C. Legrand, 1997, Design of Axially Loaded piles, European Practice, Proceedings of the ERTC3 Seminar, Brussels, Belgium, 1997.

Everts, H.J. and H.J. Luger, 1997, *Dutch national codes for pile design.* Proceedings of the ERTC3 Seminar, Brussels, Rotterdam: Balkema.

Hannink, G. & A.F. van Tol, 2005, Reduction of the Cone Resistance caused by the installation of CFA piles, Proceedings of the XVIth International conference on Soil Mechanics and Geotechnical Engineering, pp. 1983–1987, Osaka, 2005.

Deep Foundations on Bored and Auger Piles – Van Impe & Van Impe (eds)
© 2009 Taylor & Francis Group, London, ISBN 978-0-415-47556-3

Recent case histories on monitoring settlement and load sharing of piled rafts in Japan

Kiyoshi Yamashita, Takeshi Yamada & Junji Hamada
R&D Institute, Takenaka Corporation, Chiba, Japan

ABSTRACT: Piled raft foundation has been used for more than 60 buildings in Japan including many high-rise buildings of over 100 m in height since it was first applied for a four-story building in Urawa in 1987. For designing piled rafts, it is required to consider interactions of raft-soil-pile system to predict settlement and load sharing between raft and piles. However, there exist not so many case histories on monitoring load sharing between raft and piles as well as settlement.

This paper offers recent four case histories of the piled rafts in Japan. In the buildings of 19 m to 76 m in height, field measurements were performed on the foundation settlement, axial forces of the piles and contact earth pressures as well as pore-water pressures beneath the raft from the beginning of construction to the time 9 to 32 months after the end of construction to confirm validity of the foundation design.

1 INTRODUCTION

Piled raft foundations have been frequently used in many countries because they are recognized to be able to offer a cost-effective alternative to conventional pile foundations (Randolph 1994, 2003, Poulos, 2001, Poulos et al. 2001). In Japan piled rafts have been used for more than 60 buildings including high-rise buildings of over 100 m in height since it was first applied for the four-story office building in Urawa in 1987 (Yamashita & Kakurai, 1991).

For designing piled rafts, it is required to carefully consider interactions of raft-soil-pile system to predict settlement and load sharing between raft and piles. There exist, however, not so many case histories on monitoring load sharing between raft and piles as well as settlement (Kakurai et al. 1987, Yamashita et al. 1994, Katzenbach et al. 2000, Yamashita & Yamada 2007). Thus accumulation of field evidences, especially on soil-structure interaction behaviour by monitoring full-scale structures is required to develop more reliable design methods for piled rafts (Mandolini et al. 2005).

This paper offers recent four case histories of the piled rafts in Japan. The buildings are 19 m to 76 m in height above the ground surface and completed in 2005–2007. In the buildings field measurements were performed on the foundation settlement, axial forces of the selected piles and contact earth pressures and pore-water pressures beneath the raft from the beginning of construction to the time 9 to 32 months after the end of construction to confirm validity of the foundation design. Furthermore, based on the observations of the seven case histories in all, including the previous three case histories in the present four case histories, load sharing between raft and piles in relation to pile spacing are considered.

2 ELEVEN-STORY BASE-ISOLATED OFFICE BUILDING ON MEDIUM SAND

2.1 *Building and soil condition*

The eleven-story office building of 60.8 m in height above the ground surface is located in Aich prefecture. Figure 1 shows a schematic view of the building and foundation with soil profile (Hitomi et al. 2007). The building is a steel-frame structure with base isolation system and its plan measures 80 m by 43.5 m. The foundation level is at a depth of 3.0 m, partly at a depth of 3.6 m, from the ground surface.

The subsoil consists of a diluvial loose to medium sand with SPT N-values of 10–25 to a depth of 12 m from the ground surface, underlain by alternate layers of clayey soil, medium sand-and-gravel and dense sand with SPT N-values of 10–50 to a depth of 28 m. Below a depth of 28 m there lie dense to very dense sand-and-gravel layers where a hard sandy-silt layer is inserted. The groundwater table appears at a depth of about 17 m from the ground surface. The shear wave velocity measured by a P-S logging in the

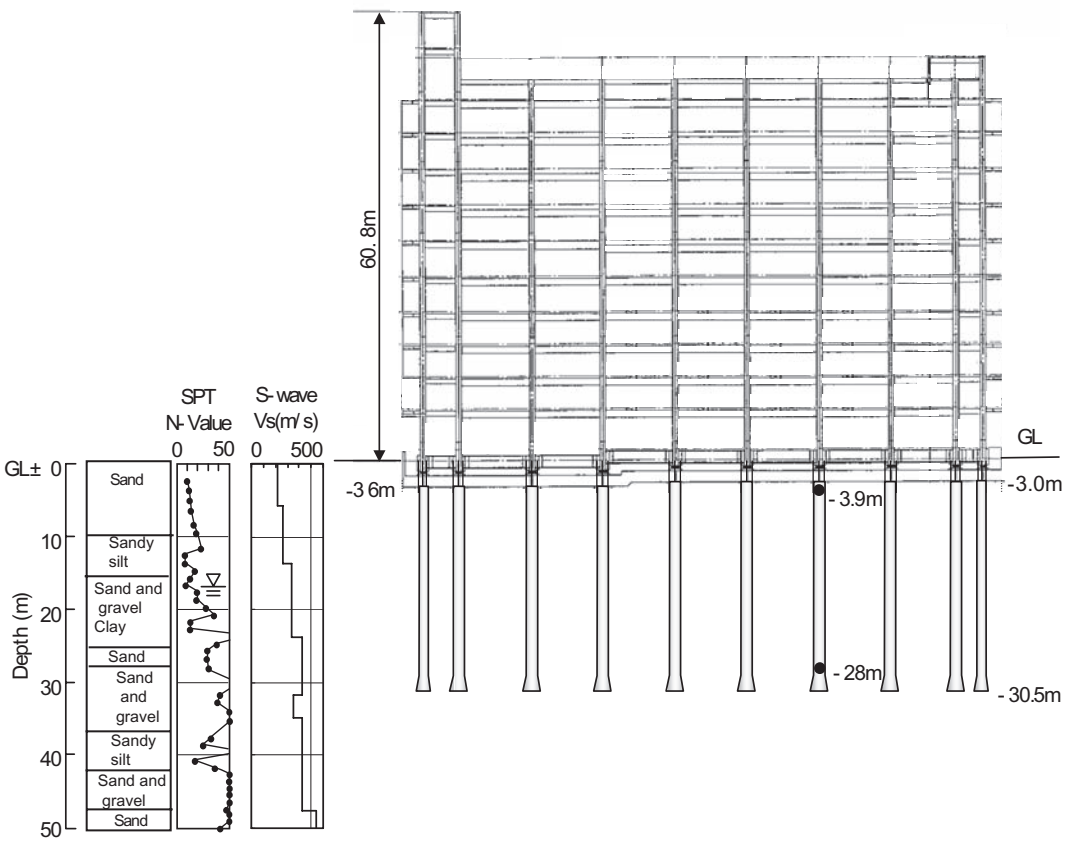

Figure 1. Schematic view of the building and foundation with soil profile.

neighboring site varies 220–260 m/s at the foundation levels to 420–540 m/s in the dense gravel layers below a depth of 28 m.

2.2 *Foundation design*

The average contact pressure allover the foundation in structural design is 145 kPa with local maximum contact pressure of 181 kPa. As the foundation levels are at a depth of 3.0 m and 3.6 m, the reinforced concrete raft is founded on loose sand with SPT N-values of about 10. Because the building has base isolation system, differential settlement of the foundation is severely restricted: the maximum inclination angle of the foundation should be less than 1/2000 radian at the serviceability limit. If raft foundation was adopted, the calculated differential settlement was not less than the allowable value. Therefore, to reduce the differential settlement, a piled raft foundation was adopted with a total number of 40 piles. The piles are cast-in-place under-reamed concrete piles of 1.1 m to 1.5 m in shaft diameter and 1.4 m to 1.8 m in toe diameter and 27.5 m, partly 26.9 m, in length. The pile toes are embedded in the dense sand-and-gravel layer below a depth of 28 m from the ground surface. Figure 2 shows a foundation plan with a layout of the piles.

2.3 *Instrumentation*

To confirm validity of the foundation design, field measurements were performed on the foundation settlement, axial forces of the pile and contact earth pressures beneath the raft from the beginning of construction to the time 32 months after the end of construction.

The locations of the monitoring devices are shown in Figure 2. A pile at the location of X7Y2 has been installed with a couple of LVDT-type strain gauges at pile head (at a depth of 3.9 m) and at pile toe (at a depth of 28.0 m) from the ground surface to investigate the load distribution along the pile. A pair of LVDT-type earth pressure cells E1 & E2 has been

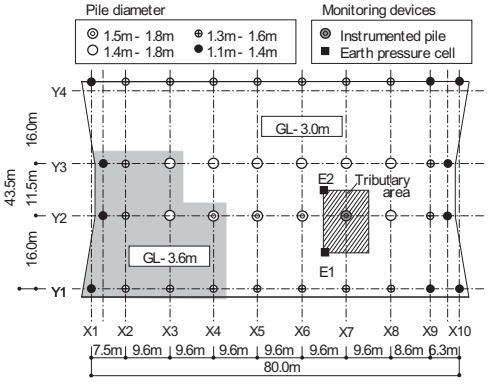

Figure 2. Layout of piles with locations of monitoring devices.

installed beneath the raft close to the instrumented pile. The settlements of the foundation were measured by an optical level at the positions of the pedestals under the rubber-bearing base isolators on the raft. The reference point was set to an existing nearby building founded on end-bearing piles.

The measurement of axial forces of the pile and the earth pressures beneath the raft started at the time just before constructing steel reinforcement for the foundation slab of 0.8 m in thickness. The measurement of the foundation settlements by an optical level began at the time just after constructing the pedestals on the raft.

2.4 *Observations*

Figure 3 shows the longitudinal settlement profiles of the foundation measured by the optical level at the time 2.5 months before the end of construction. The measured settlements were 4–10 mm and the maximum inclination angle obtained from the settlement profile was about 1/4500 radian, which is much less than the allowable value of 1/2000 radian at the serviceability limit.

Figure 4 shows development of the measured axial forces of the pile. The measured load at pile head slightly increased after the end of construction due to a live load whereas the measured load at pile toe shows almost constant value. The ratio of the pile-toe load to the pile-head load was 0.25 at the end of construction and slightly decreased to 0.20 at the time 32 months after the end of construction.

Figure 5 shows development of the measured earth pressures beneath the raft. The measured earth pressures increased due to construction to 56 kPa in E1 and 84 kPa in E2 at the end of construction. Thereafter, they slightly decreased to 39 kPa in E1 and 74 kPa in E2 at the time 32 months after the end of construction.

Figure 6 shows time-dependent load sharing between raft and the pile on the tributary area of the instrumented pile shown in Figure 2. On the tributary area it is verified that the design column load of 19.8 MN is very

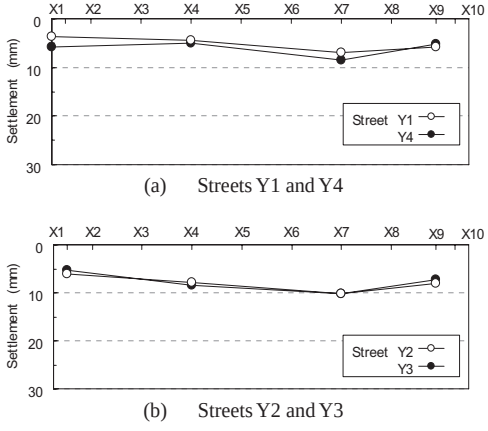

Figure 3. Measured longitudinal settlement profiles.

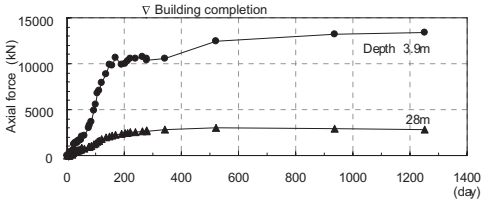

Figure 4. Measured axial forces of the pile.

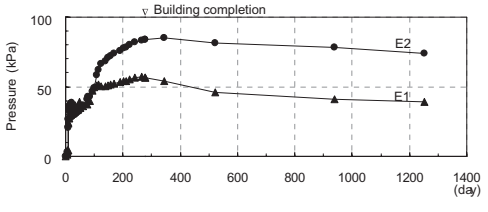

Figure 5. Measured earth pressures beneath the raft.

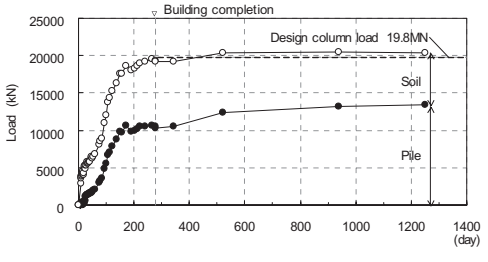

Figure 6. Time-dependent load sharing between raft and pile on the tributary area.

close to the sum of the measured pile-head load and raft load of 20.4 MN at the time 32 months after the end of construction. At this point the raft load, which corresponds to the load carried by the soil, was obtained by use of the average value of the earth pressures E1 & E2 on the tributary area. The ratio of the load carried by the piles to the net load on the tributary area was 0.54 at the end of construction and 0.66 at the time 32 months after the end of construction, where the net load is the total applied load minus buoyancy. In this case the net load is equal to the sum of the measured pile-head load and raft load because ground water level is much lower than the foundation level.

3 THIRTEEN-STORY HOSPITAL ON SOFT CLAY

3.1 *Building and soil condition*

The hospital building is located in Osaka. The building consists of a thirteen-story high-rise part of 51.3 m in height above the ground surface and a four-story low-rise part. The plan of the building measures about 55 m by 45 m. The high-rise part is a steel-frame structure while the low-rise part and the basement are reinforced concrete construction.

Figure 7 shows a schematic view of the building and foundation with soil profile (Ikeda et al. 2006). The subsoil consists of a soft alluvial stratum to a depth of 21 m from the ground surface. Below a depth of 24 m there lie a diluvial very dense sand-and-gravel layer of SPT N-values of 50 or more. The soil profile

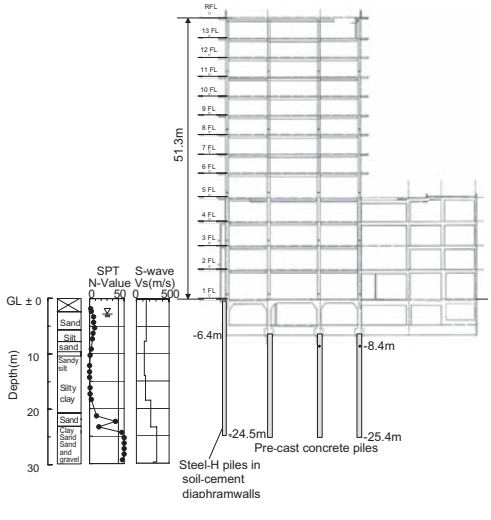

Figure 7. Schematic view of the building and foundation with soil profile.

down to a depth of 8 m is made of loose sand and silty sand with SPT N-values of 5 to 10. From a depth of 8 m to 21 m, there lie soft sandy silt and silty clay layers. The groundwater table appears at a depth of about 2.5 m from the ground surface. The shear wave velocity measured by a P-S logging in the neighboring site varies 120–150 m/s at the foundation level to 310 m/s in the dense gravel layers below a depth of 24 m from the ground surface.

3.2 *Foundation design*

The hospital building has a basement and the foundation level is at a depth of 6.4 m below the ground surface. The average contact pressure allover the foundation is 169 kPa in the high-rise part and 114 kPa in the low-rise part. In the low-rise part, raft foundation was adopted because consolidation settlement was not predicted because the consolidation yield stresses of the soft sandy silt and silty clay below the raft are slightly larger than the average contact pressure.

On the other hand in the high-rise part, piled raft foundation was proposed in order not to cause the consolidation settlement and excessive differential settlement along the interface between the high-rise part and the low-rise part. Consequently a piled raft foundation was adopted with a total number of 17 bored pre-cast concrete piles in the inside of the high-rise part with 198 steel-H piles built in the soil-cement diaphragm walls in the perimeter. The pile toes of the pre-cast concrete piles and the steel-H piles are embedded in the dense sand or sand-and-gravel layer below a depth of 24 m to ensure the end-bearing resistance. The pre-cast concrete piles are pre-tensioned and reinforced spun high-strength concrete piles of 19 m in length and 0.8 m to 1.0 m in diameter and the steel-H piles are 0.4 m by 0.2 m in cross-sectional dimension. Figure 8 shows a foundation plan with a layout of the piles.

3.3 *Instrumentation*

To confirm validity of the foundation design, field measurements were performed on the foundation settlement, axial forces of the two piles and contact earth pressures as well as pore-water pressure beneath the raft from the beginning of construction to the time 28 months after the end of construction.

The locations of the monitoring devices are shown in Figure 8. Two piles at the locations of 3C and 4C have been installed with a couple of LVDT-type strain gauges at pile head (at a depth of 8.4 m). Four earth pressure cells and a piezometer have been installed beneath the raft at a depth of 6.5 m from the ground surface: three earth pressure cells E1-E3 and a piezometer have been installed in the high-rise part and one earth pressure cell E4 in the low-rise part. The

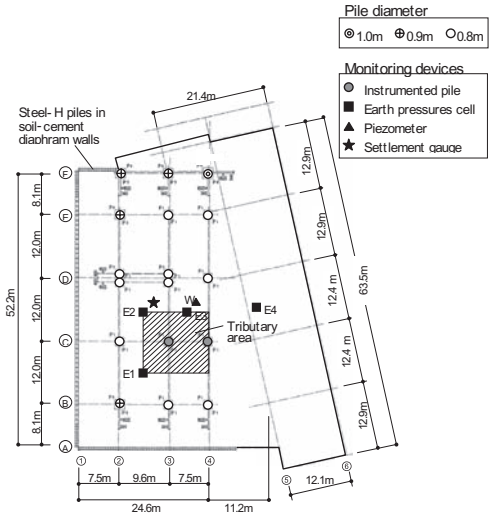

Figure 8. Layout of piles with locations of monitoring devices.

vertical ground displacement below the raft was measured at the center of the high-rise part by a differential settlement gauge. The settlement gauge in which LVDT-type transducer has been installed at a depth of 7.5 m, was reached down to the very dense sand-and-gravel layer at a depth of 27.0 m. The settlements of the foundation were measured at the selected column positions by an optical level where the reference point was set to a neighboring pier of highway viaduct.

The measurement of the vertical ground displacement below the raft started at the time just before the excavation. The measurement of axial forces of the piles, the earth pressures and pore-water pressure beneath the raft started at the time just before casting the foundation slab of 0.6 m in thickness, while the measurement of the settlements by an optical level started at the time just after casting the foundation slab.

3.4 *Observations*

Figure 9 shows the measured vertical ground displacement at a depth of 7.5 m relative to the reference point at a depth of 27.0 m from the ground surface. Before casting the foundation slab, the ground displacement showed the maximum rebound of 45 mm due to the excavation for the foundation construction. After casting the foundation slabs, the ground displacement showed downward due to the construction load. The decrease in the vertical ground displacement from the maximum rebound is assumed to be substantially equal to the settlement of the foundation just above, at a depth of 6.4 m.

Figure 10 shows the measured ground settlement at a depth of 7.5 m with the raft settlement measured at 3C by an optical level. The ground settlement increased with construction progress amounted to 18 mm at the end of construction. Thereafter, the settlement slightly increased and reached 20 mm at the time 28 months after the end of construction. The raft settlement measured by an optical level was slightly larger than the ground settlement after the end of construction, however the time-dependent settlement curve of the raft is quite similar to that of the ground.

Figure 11 shows the cross-sectional settlement profile along the street C measured by an optical level. The cross-section includes the high-rise and low-rise parts. The measured settlements were 12–23 mm at the end of construction. Thereafter, the settlements slightly increased and reached 11–25 mm at the time 28 months after the end of construction. At that time the maximum inclination angle obtained from the settlement profile was 1/1500 radian at the edge of the high-rise part, which is less than the serviceability limit of 1/1000 radian.

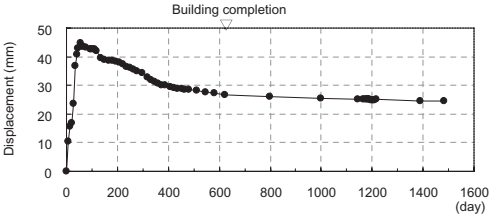

Figure 9. Measured vertical ground displacement.

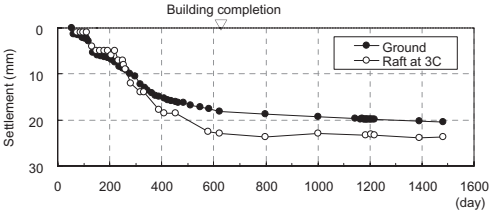

Figure 10. Measured settlement of the ground and raft.

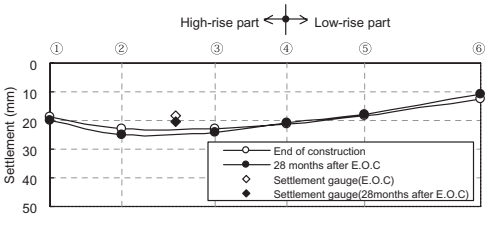

Figure 11. Measured settlement profiles along the street C.

Figure 12 shows the measured axial forces of the piles 3C and 4C. For both piles the measured load at pile head increased after the end of construction and seemed to still increase slightly at the time 28 months after the end of construction.

Figure 13 shows development of the measured earth pressures and the pore-water pressure beneath the raft. The measured earth pressures increased relatively early stage of construction and seemed to reach a state of equilibrium at the end of construction. At the time 28 months after the end of construction, the measured earth pressures of E1 to E3 in the high-rise part amounted to 75–78 kPa. At that time the measured earth pressure of E4 in the low-rise part amounted to 67 kPa, which was only slightly smaller than those in the high-rise part. The measured pore-water pressure showed almost constant value of 34–35 kPa after the end of construction.

Figure 14 shows time-dependent load sharing among the piles, soil and the buoyancy on the tributary area of the instrumented piles shown in Figure 8. On the tributary area it is verified that sum of the design load of the two columns 3C & 4C, 23.8 MN, is very close to the sum of the measured pile-head loads and the raft load of 22.1 MN at the end of construction and 24.0 MN at the time 28 months after the end of construction. The raft load, which corresponds to the sum of the effective load carried by the soil and the buoyancy, was obtained by use of the average value of the measured earth pressures E1 to E3 on the tributary area. The ratios of the load carried by the piles to the net load on the tributary area were 0.66 at the end of construction and 0.68 at the time 28 months after the end of construction. As to the ratios of the load carried by the piles to the total load on the tributary area were 0.51 at the end of construction and 0.54 at the time 28 months after the end of construction.

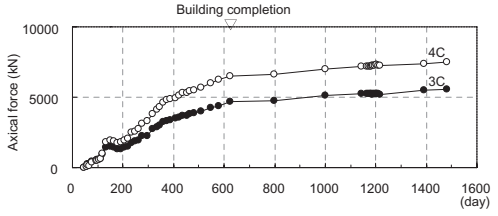

Figure 12. Measured axial forces at pile head.

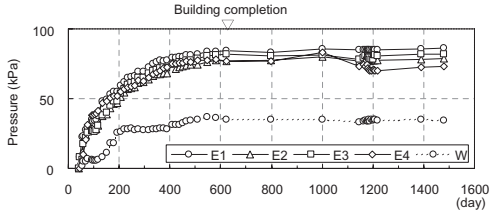

Figure 13. Measured earth pressures and pore-water pressure beneath the raft.

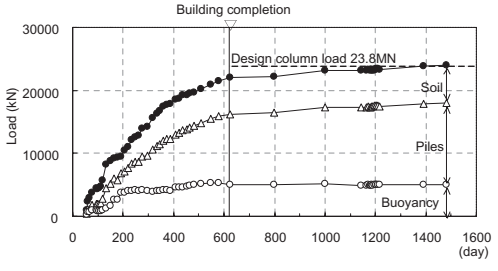

Figure 14. Time-dependent load sharing between raft and piles on the tributary area.

4 NINETEEN-STORY RESIDENTIAL TOWER ON LOOSE SAND

4.1 *Building and soil condition*

The nineteen-story reinforced-concrete residential tower of 75.8 m in height above the ground surface is located in Kagoshima prefecture. Figure 15 shows a schematic view of the building and foundation with soil profile (Nezu et al. 2008). The subsoil consists

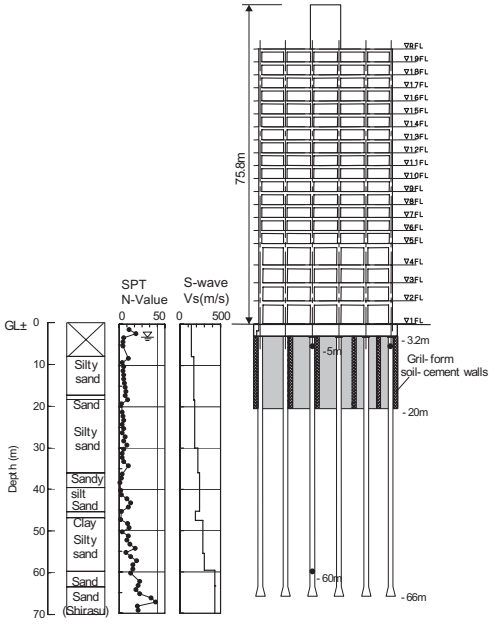

Figure 15. Schematic view of the building and foundation with soil profile.

of a loose to medium alluvial sand stratum to a depth of 63 m from the ground surface, underlain by diluvial medium to dense sand layers of SPT N-values of 20–50 to a depth of 105 m. At a top part of the diluvial stratum, there lies a Pleistocene pyroclastic fall deposit called “Shirasu” of about 10 m in thickness.

From the ground surface to a depth of 4–8 m there lies a fill made of loose sand and gravel. Below the fill to a depth of 36 m, there lie thick loose silty sand layers with SPT N-values of 4–14. The soil layers from a depth of 36 m to 47 m are made of sandy silt, fine sand with pumice and clay. From a depth of 47 m to 63 m there lies medium silty sand partially with pumice and sand. The groundwater table appears at a depth of about 3 m from the ground surface. The shear wave velocity measured by a P-S logging varies 170–220 m/s in the thick silty sand to a depth of 36 m and varies 240–300 m/s below the silty sand to a depth of 60 m. In the diluvial sand layers the shear wave velocity varies 430–520 m/s to a depth of 120 m from the ground surface.

4.2 *Foundation design*

The foundation level is at a depth of 3.2 m from the ground surface and the average contact pressure allover the foundation in structural design is 257 kPa. As the calculated overall and differential settlements were excessive if a raft foundation was adopted, a piled raft foundation was proposed to reduce the settlements of the raft foundation. However, it appears that the loose silty sand from a depth of 4–8 m to a depth of 18 m has a potential of liquefaction during an earthquake of the maximum horizontal ground-surface acceleration of over 280 Gal. To cope with the liquefiable layer, a grid-form ground improvement was introduced. In the method the grid-form soil-cement walls are constructed by deep mixing method as illustrated in Figure 16. They confine the loose silty sand by the high-modulus walls so as not to cause large shear deformation in the loose sand during strong earthquakes (Tokimatsu et al. 1996).

Consequently piled raft foundation combined with the grid-form soil-cement walls was adopted. The piled raft has a total number of 28 cast-in-place under-reamed concrete piles of 1.2 m to 1.3 m in shaft diameter and 1.8 m to 2.2 m in toe diameter. The piles are 63 m in length and embedded in the diluvial dense sand layer below a depth of 65 m. Figure 17 shows a foundation plan with a layout of the piles and the grid-form ground improvement.

4.3 *Instrumentation*

To confirm validity of the foundation design, field measurements were performed on the foundation settlement, axial forces of the selected piles and contact

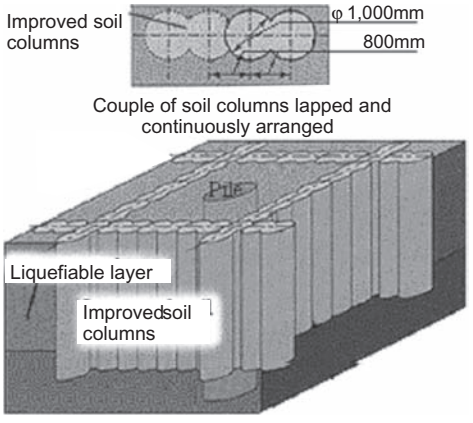

Figure 16. Grid-form ground improvement.

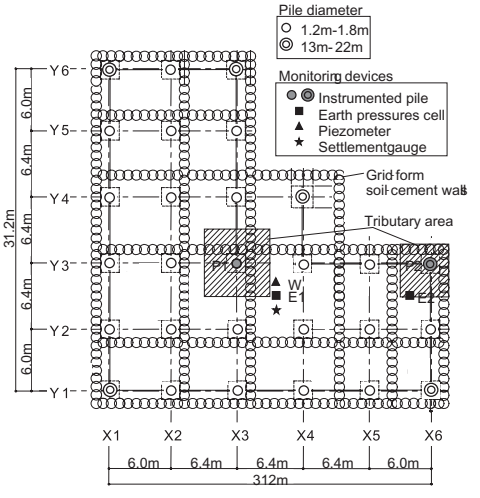

Figure 17. Layout of piles and grid-form soil-cement walls with locations of monitoring devices.

earth pressures as well as pore-water pressure beneath the raft from the beginning of construction to the time 15 months after the end of construction.

The locations of the monitoring devices are shown in Figure 17. The two piles P1 & P2 have been installed with a couple of LVDT-type strain gauges at pile head (at a depth of 5.0 m) as shown in Figure 15. Further, the pile P1 has been installed with a couple of strain gauges at pile toe (a depth of 60.0 m) to investigate the load distribution along the pile. Two earth pressure cells E1 & E2 and a piezometer have been installed beneath the raft close to the instrumented piles. The vertical ground displacements below the raft were measured by the differential settlement gauges. The LVDT-type transducers have been installed beneath

the foundation slab at a depth of 3.5 m to measure the relative displacements to the two reference points at a depth of 20 m and 80 m from the ground surface.

The measurement of axial forces of the piles, the earth pressures and pore-water pressure beneath the raft and the vertical ground displacement below the raft started at the time just after casting the foundation slab of 0.6 m in thickness.

4.4 *Observations*

Figure 18 shows the measured vertical ground displacements at a depth of 3.5 m and 20 m relative to a depth of 80 m. The measured ground displacement at a depth of 3.5 m, which is assumed to be equal to the foundation settlement, increased with construction progress and amounted to 20 mm at the end of construction. Thereafter the displacement slightly increased and reached 22 mm at the time 15 months after the end of construction. The measured ground displacement at a depth of 20 m amounted to 13 mm at the end of construction and 16 mm at the time 15 months after the end of construction.

Figure 19 shows the measured axial forces of the piles P1 & P2. For both piles the measured pile-head load slightly increased after the end of construction due to a live load. The ratio of the pile-toe load to the pile-head load in the pile P1 was 0.42 both at the end of construction and at the time 15 months after the end of construction.

Figure 20 shows development of the measured earth pressures and pore-water pressure beneath the raft. The measured earth pressures increased in early stage of construction and showed almost constant values at the time about 200 days before the end of construction and amounted to 19–22 kPa in E1 and 55–57 kPa in E2 after the end of construction. The measured pore-water pressure showed 1–5 kPa.

Figure 21 shows time-dependent load-sharing among the piles, soil and the grid-form soil-cement walls on the tributary areas of the piles P1 & P2 shown in Figure 17. In Figures 21a, b the effective load carried by the soil was obtained by use of the measured earth pressure on the tributary area where the buoyancy was neglected because the measured pore-water pressure was very small. Assuming that the actual working load

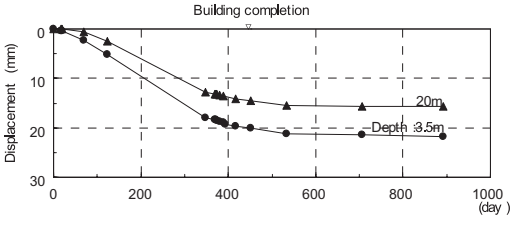

Figure 18. Measured vertical ground displacements

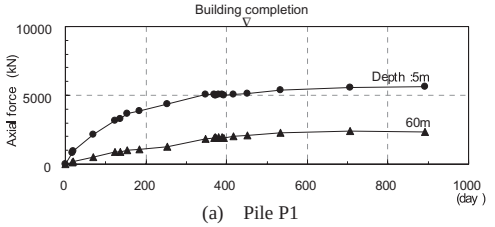

(a) Pile P1

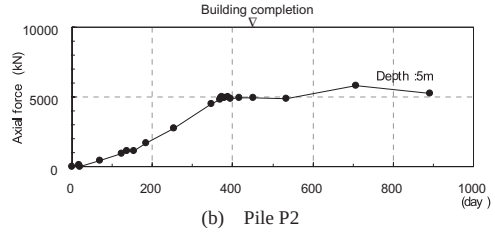

(b) Pile P2

Figure 19. Measured axial forces of the piles P1 and P2.

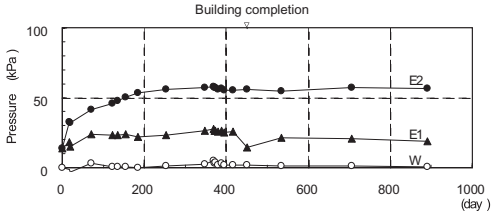

Figure 20. Measured earth pressures and pore-water pressure beneath the raft.

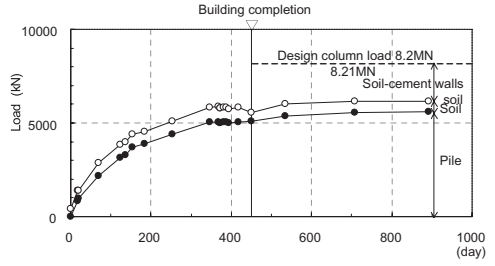

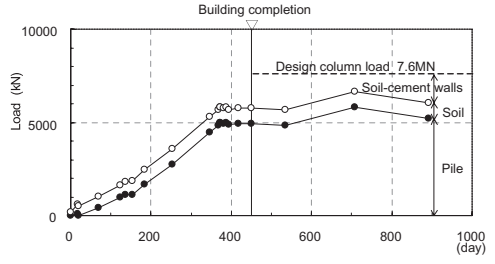

Figure 21. Time-dependent load sharing between raft and pile on the tributary area.

after the end of construction is equal to the structural design load, the ratios of the load carried by the piles to the net load on the tributary area can be obtained. The ratios are 0.63 for the pile P1 and 0.66 for the pile P2 at the end of construction, and 0.69 for the pile P1 at the time 15 months after the end of construction and 0.69–0.77 (Average value of 0.73) for the pile P2 during 8.5 to 15 months after the end of construction.

5 HADRON EXPERIMENTAL HALL ON MEDIUM TO DENSE SAND

5.1 *Building and soil condition*

The hadron experimental hall of 19 m in height above the ground surface is located in J-PARC (Japan Proton Accelerator Research Complex) in Ibaraki prefecture. The experimental hall is a steel-frame and reinforced concrete structure and a schematic view of the building and foundation with a soil profile is shown in Figure 22 (Yamada et al. 2008).

The subsoil consists of a loose to dense sand with SPT N-values of about 7 to 40 to a depth of 6 m from the ground surface, underlain by a diluvial dense sand-and-gravel of SPT N-values of 60 or more and medium to dense sand layer of SPT N-values of 20 to 60 to a depth of 16 m. From a depth of 16 m to 23 m, there lie a medium sandy silt, a loose silty sand and a dense sand layer. From a depth of 23 m to about 40 m, there lie thick sandy silt and silt layers with the unconfined compressive strength of 180–480 kPa underlain by a weathered sandy mudstone of SPT N-values of 60 or more. The groundwater table appears at a depth of about 4 m from the ground surface. The shear wave velocity measured by a P-S logging in the neighboring site varies 230–250 m/s in the medium to dense sand layer at the foundation levels to 400 m/s in the mudstone.

5.2 *Foundation design*

The hadron experimental hall consists of an experimental line, a beam line and a beam dump as shown in Figure 22. The beam line is located at the center part of the experimental hall. Both sides of the beam line there are thick concrete shielding walls of about 10 m in height. At the end part of the beam line a beam dump is located. The core part of the beam dump is made of copper to absorb the high-energy beam power safely.

The average contact pressures allover the foundation in structural design are 259 kPa in the experimental line, 350 kPa in the beam line and 442 kPa in the beam dump. The contact pressures include live

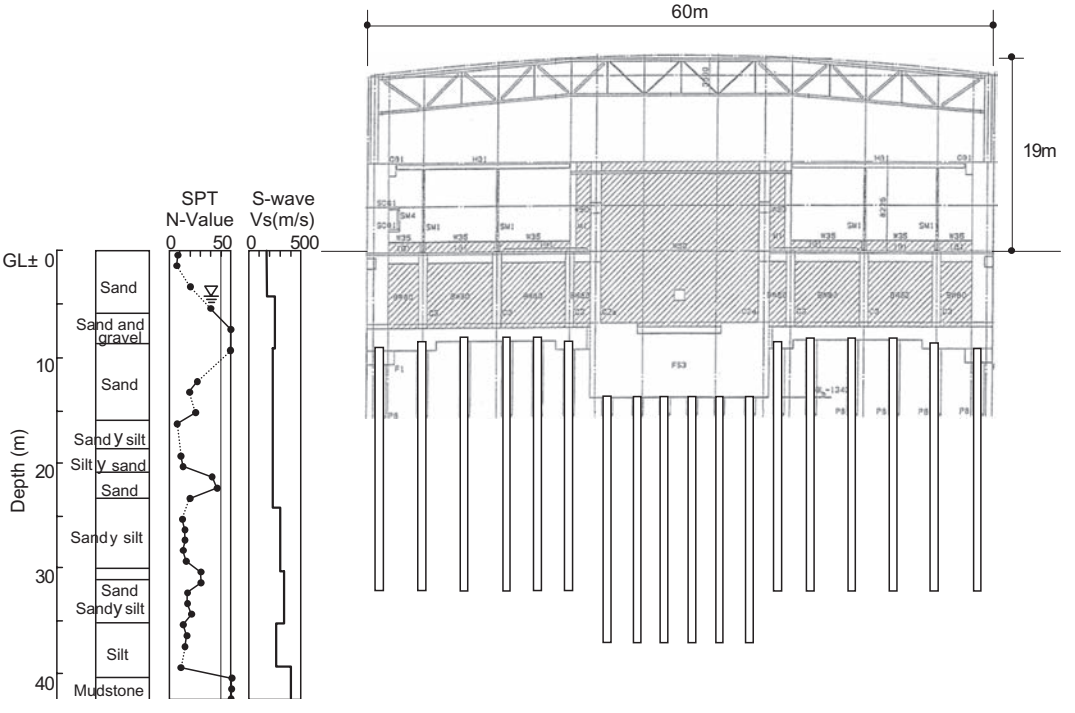

Figure 22. Schematic view of the building and foundation with soil profile.

load of 196 kPa in the experimental line and 294 kPa in the beam line and beam dump. The live load is relatively large because a lot of iron and concrete shielding blocks are set up in the experimental hall after the end of construction of the building.

The foundation levels are at a depth of 8.0 m in the experimental line, at a depth of 11.4 m in the beam line and at a depth of 13.4 m in the beam dump from the ground surface. As the reinforced concrete foundation mats are embedded in the dense sand-and-gravel and medium to dense sand, the allowable bearing capacities at the foundation levels are much higher than the average contact pressures. However, because there exist thick silt layers below a depth of 23 m, maximum settlement of the mat foundation calculated by an elastic theory was 75 mm, which exceeded an allowable value of 40 mm at the serviceability limit.

To reduce the settlement of the mat foundation within the allowable value, a piled raft foundation with a total number of 371 bored pre-cast concrete piles of 22.0–25.7 m in length and of 0.6–0.8 m in diameter (330 piles of 0.6 m, 35 piles of 0.7 m, 6 piles of 0.8 m) was adopted. The piles are pre-tensioned spun high-strength concrete piles and are sufficiently embedded in the thick silt layers to a depth of 32.0 m in the experimental line and to a depth of 37.0 m in the beam line and beam dump as shown in Figure 22. Figure 23 shows a foundation plan with a layout of the piles.

5.3 *Instrumentation*

To confirm validity of the foundation design, field measurements were performed on the ground settlement below the raft, axial forces of the piles and contact earth pressures as well as pore-water pressures beneath the raft from the beginning of construction to about 9 months after the end of construction. The locations of the monitoring devices are shown in Figure 23.

The vertical ground displacements below the raft were measured by a differential settlement gauge at the center of the beam line. The LVDT-type transducers have been installed at a depth of 12.5 m, 21.5 m, 32.0 m and 41.0 m to measure the relative displacements to the reference point at a depth of 80 m from the ground surface. The three piles of P1, P2 and P3 located in the beam line, the beam dump and the experimental line respectively have been installed with a couple of LVDT-type strain gauges at pile head and at pile toe; at a depth of 12.3 m and 36.0 m in the pile P1, at a depth of 14.3 m and 36.0 m in the pile P2 and at a depth of 8.9 m and 31.0 m in the pile P3. Further, the pile P1 has been installed a couple of strain gauges at a mid-depth of the pile, at a depth of 22.3 m. A pair of LVDT-type earth pressure cells has been installed beneath the raft in the vicinity of the instrumented piles P1, P2 and P3. In the vicinity of the piles P1 and P3 the LVDT-type piezometers have been installed.

The measurement of the axial forces of the piles and the earth pressures and pore-water pressures beneath the raft started at the time just before casting the foundation mats. The measurement of the vertical ground displacements began just before excavation for the foundation construction.

5.4 *Observations*

Figure 24 shows the relative vertical ground displacements to the reference point a depth of 80 m. Before casting the foundation mats, the ground showed rebound due to the excavation, where the maximum rebound was 18 mm at a depth of 12.5 m. After the excavation was completed, the ground displacements showed downward due to the structure load. Assuming that the vertical ground displacement at a depth of 12.5 m is equal to the settlement of the foundation just above, at a depth of 11.3 m, in the beam line, the settlement of the foundation amounted to 13 mm at the end of construction. Thereafter, the settlement slightly

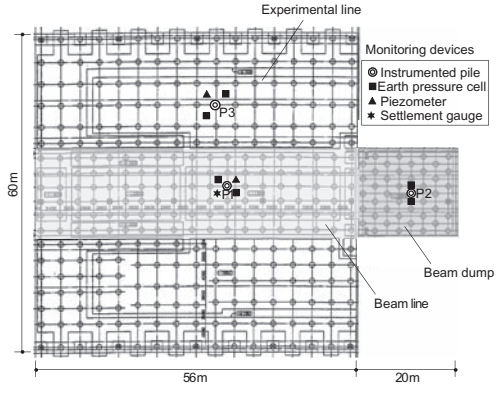

Figure 23. Layout of piles with locations of monitoring devices.

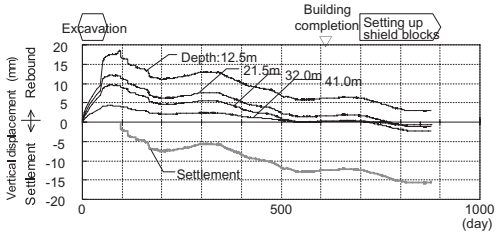

Figure 24. Measured vertical ground displacements.

increased due to live load and reached 16 mm at the time about 9 months after the end of construction.

The measured axial forces of the piles, the measured earth pressures and the pore-water pressure beneath the raft at the beam line are shown in Figure 25 and those at the beam dump are shown in Figure 26, noting that the values of the pore-water pressure at the beam dump were estimated from those at the beam line. For the pile P1 the measured load at pile-head markedly increased after the end of construction due to the live load. The measured earth pressures and pore-water pressure increased in early stage of construction. Thereafter the measured earth pressures slightly increased with construction progress whereas the pore-water pressure showed almost constant value. After the end of construction, the average value of the measured earth pressures amounted to 88–96 kPa at the beam line and 120–129 kPa at the beam dump and the pore-water pressure amounted to 61–67 kPa at the beam line. For the pile P3 at the experimental line the measured pile-head load was still very small at the time about 9 months after the end of construction.

Figure 27 shows time-dependent load sharing among the piles, soil and the buoyancy on the tributary area of the pile P1 and that of the pile P2. The ratios of the load carried by the piles to the net load on the tributary area were 0.81 for the pile P1 and 0.58 for the pile P2 at the end of construction. The net load was obtained from the sum of the measured pile-head load and the average value of the effective earth pressures on the tributary area. At the time 9 months after the end of construction

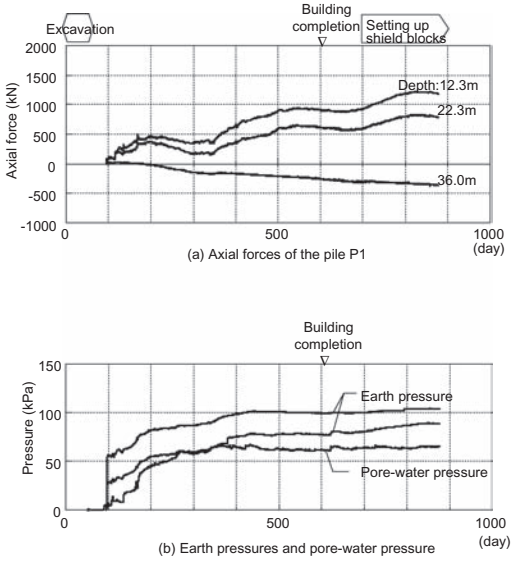

Figure 25. Measured axial forces of the pile and measured earth and pore-water pressures beneath the raft at beam line.

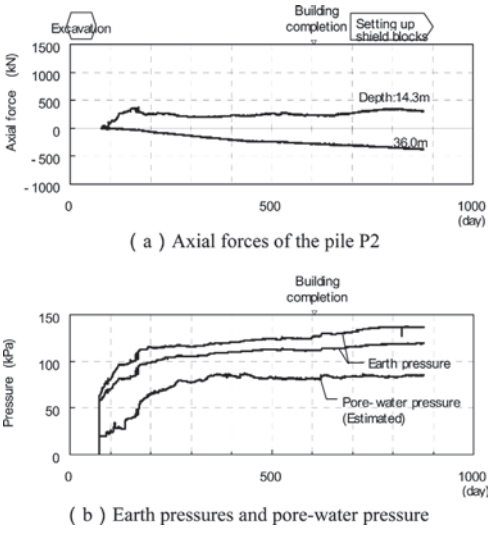

Figure 26. Measured axial forces of the pile and measured earth and pore-water pressures beneath the raft at beam dump.

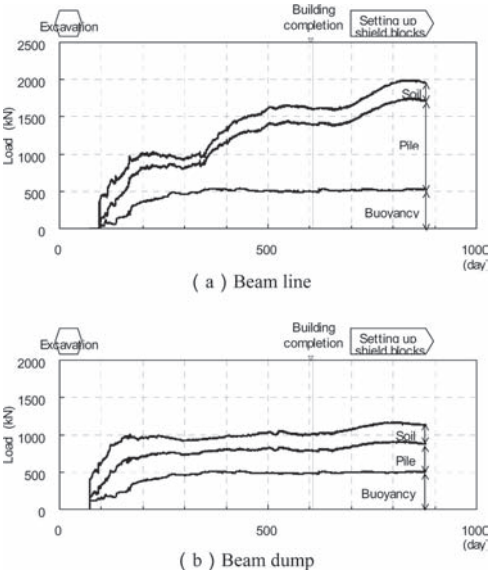

Figure 27. Time-dependent load sharing between raft and piles on the tributary area.

the ratios were 0.83 for the pile P1 and 0.60 for the pile P2. As to the ratios of the load carried by the piles to the total load on the tributary area were 0.56 for the pile P1 and 0.30 for the pile P2 at the end of construction. At the time 9 months after the end of construction the ratios were 0.60 for the pile P1 and 0.33 for the pile P2.

6 LOAD SHARING BETWEEN RAFT AND PILES

Mandolini et al. (2005) have pointed out that the simple geometrical parameter, the ratio of pile spacing to pile diameter s/d, plays a major role in load sharing between raft and piles. In Figure 28 the ratios of the load carried by the piles to the net load, α_p', in the present four case histories are plotted against s/d, where the values of α_p' correspond to those at the time 9 to 32 months after the end of construction. In Figure 28 the ratios of the load carried by the piles to the total load in the previous case histories are also plotted: a small silo (Kakurai et al. 1987), a four-story office building (Yamashita & Kakurai, 1991) and a five-story office building (Yamashita et al. 1994). In the previous case histories the ratios of the load carried by the piles to the total load are assumed to be equal to those to the net load because the groundwater tables were close to or lower than the bottom levels of the foundations. In the seven case histories in all, the three cases, the eleven-story base-isolated office building, the thirteen-story hospital and the nineteen-story residential tower, correspond to those of a raft with end-bearing piles and the other four cases correspond to those of a raft with friction piles.

The values of α_p' show a scatter but tends to decrease with increasing s/d and become nearly constant for the values of s/d above six to eight, where the values of α_p' are 0.43–0.56 for the cases of a raft with friction piles and 0.66–0.68 for those of a raft with end-bearing piles. The values of α_p' for the latter case are larger than those for the former as expected, but there is not so much difference in the values for the two cases.

7 CONCLUSIONS

Through a study on the observations of the four case histories on monitoring settlement and load sharing of the piled rafts in Japan, the following conclusions are obtained:

1. On the settlement, the maximum measured settlements ranged from 10 mm to 25 mm and the maximum inclination angle ranged 1/4500 radian to 1/1500 radian. These values are less than the allowable values at the serviceability limit.
2. On the load sharing between raft and piles, the ratios of the load carried by the piles to the net load were 0.58–0.81 at the end of construction and slightly increased to 0.60–0.83 at the time 9 to 32 months after the end of construction.
3. The ratio of the load carried by the piles to the net load, α_p', decreases with increasing pile spacing s/d and the values of α_p' become nearly constant for the values of s/d above six to eight in both cases of a raft with friction piles and a raft with end-bearing piles. The values of α_p' for the latter case are larger than those for the former, but there is not so much difference in the values for the two cases.

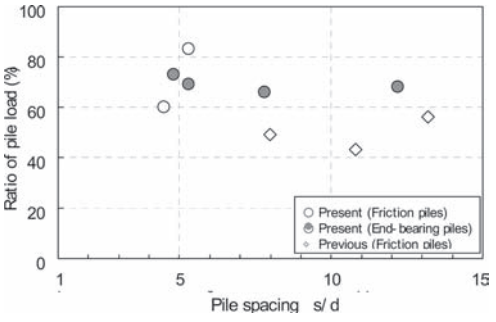

Figure 28. Ratio of load carried by piles vs. pile spacing.

ACKNOWLEDGEMENTS

The authors are very much grateful to Prof. M. Yoshioka and Mr. M. Miyahara of High Energy Accelerator Org. KEK, Mr. S. Nezu of Mitsubishi Jisho Sekkei Inc. and Mr. Y. Hitomi of Nihonsekkei Inc. for their assistance in adopting the piled rafts. The authors are also grateful to Messrs. Y. Soga, K. Shimono, H. Yamamoto, H. Ikeda, S. Yamamoto, H. Ito and H. Watanabe of Takenaka Corporation for their contribution to the structural design of the piled rafts. Our gratitude is extended to Messrs. T. Hashiba, S. Koguchi and A. Uchida of Takenaka Corporation for their efforts in the measurements of the foundation behaviour.

REFERENCES

Hitomi, Y., Yamada, T., Shimono, K., Soga, Y. & Yamashita, K. (2007): Settlement behaviour of a high-rise building with base isolation founded on a piled raft, Annual meeting AIJ, Structures 1, pp. 685–686 (in Japanese).

Ikeda, H., Yamamoto, H., Hamada, J. & Yamashita, K. (2006): Settlement behaviour of high-rise building with low-rise part founded on a piled raft on soft ground, Annual meeting AIJ, Structures 1, pp. 553–554 (in Japanese).

Kakurai, M., Yamashita, K. & Tomono, M. (1987): Settlement behavior of piled raft foundation on soft ground, Proc. 8th ARCSMFE, pp. 373–376.

Katzenbach, R., Arslan, U. & Moormann, C. (2000): Piled raft foundations projects in Germany, Design applications of raft foundations, Hemsley J.A. Editor, Thomas Telford, pp. 323–392.

Mandolini, A., Russo, G. & Viggiani, C. (2005): Pile foundations: Experimental investigations, analysis and design, Proc. 16th ICSMGE, Vol. 1, pp. 177–213.

Nezu, S., Yamashita, K., Uchida, A. & Yamamoto, S. (2008): Settlement behaviour of a high-rise condominium founded on a piled raft with grid-form ground improvement, Annual meeting AIJ, Structures 1 (in Japanese).

Poulos, H.G. (2001): Piled raft foundations: design and applications, Geotechnique 51, No.2, pp. 95–113.

Poulos, H.G., Carter, J.P. & Small, J.C. (2001): Foundations and retaining structures, Proc. 15th ICSMFE, Vol. 4, pp. 2527–2606.

Randolph, M.F. (1994): Design methods for pile groups and piled rafts, Proc. 13th ICSMFE, pp. 61–82.

Randolph, M.F. (2003): Science and empiricism in pile foundation design, The 43rd Rankine Lecture, Geotechnique Vol. 53, No.10, pp. 847–875.

Tokimatsu, K., Mizuno, H. & Kakurai, M. (1996): Building damage associated with geotechnical problems, Special Issue of Soils & Foundations, pp. 219–234.

Yamada, T., Ito, H. & Yamashita, K. (2008): Settlement behaviour on a piled raft foundation of Hadron Experimental Hall of J-PARC, Annual meeting AIJ, Structures 1 (in Japanese).

Yamashita, K. & Kakurai, M. (1991): Settlement behavior of the raft foundation with friction piles, Proc. 4th Int. Conf. on Piling and Deep Foundations, pp. 461–466.

Yamashita, K., Kakurai, M. & Yamada, T. (1994): Investigation of a piled raft foundation on stiff clay, Proc. 13th ICSMFE, Vol. 2, pp. 543–546.

Yamashita, K. & Yamada, T. (2007): Settlement and load-sharing of a piled raft foundation combined with grid-form soil-cement walls on soft ground, Proc. IWDPF 07, pp. 299–305.

Discussion session 2: Pile testing development

Deep Foundations on Bored and Auger Piles – Van Impe & Van Impe (eds)
© 2009 Taylor & Francis Group, London, ISBN 978-0-415-47556-3

Behavior of continuous flight auger piles subjected to uplift load tests in unsaturated diabasic soil

P.J.R. Albuquerque
State University of Campinas (Unicamp), Campinas, Brazil

J.A. Paschoalin Filho
Nove de Julho University (Uninove), São Paulo, Brazil

D. Carvalho
State University of Campinas (Unicamp), Campinas, Brazil

ABSTRACT: This paper presents the behavior of three continuous flight auger piles conducted in unsaturated diabasic soil submitted to uplift forces. The piles were built at the site for Experimental Studies in Soil Mechanics and Foundations at Unicamp, located in the city of Campinas, Brazil. Field tests have already been conducted at the site (SPT, CPT, DMT and PMT), as well as laboratory tests using sample soils taken from a well up to 17 m deep. The water table is not checked until a depth of 17 m. In order to check the behavior of the piles when submitted to uplift forces, slow static load tests were carried out as per the recommendations of NBR 12.131/92. The carrying capacity of these piles was also provided by means of theoretical methods, appropriate for uplift forces, and through semi-empirical methods appropriate for compression forces, considering only the portion of lateral resistance. The values estimated using the methods considered were compared to those obtained by means of load tests. One of the tested piles was extracted from the soil to be the subject of a study on its geometry.

1 INTRODUCTION

During the last few years, there have been great advances in the development of building with deep foundations, due to ever greater requirements for productivity and the constant increase in loads to be transferred to the subsoil. Because of this, foundation engineering has had to closely track this growth, developing new techniques to build deep foundations using "in situ" molded piles.

The Continuous Flight Auger (CFA) pile, built using a continuous helix auger, was first used in the United States during the fifties. In Europe, this type of pile was introduced in the seventies. In Brazil, the use of CFA piles has become a constant in medium-to-large size jobs, principally in those located in the state of São Paulo, where the largest number of companies building this type of foundation is to be found.

As the use of this pile is increasing, it becomes imperative to understand its behavior.

The interior of the state of São Paulo, where Campinas is situated, where economic growth is marked, a large number of medium-to-large construction jobs are generated, bringing about an increase in the use of these kinds of foundations, principally because the jobs are mostly industrial, where time is essential in defining the construction method.

1.1 *Continuous Flight Auger Piles—An historical review*

From the time of their introduction in the USA until the present day, significant investment has been made in CFA piles and presently they can be built up to 32 m deep, in diameters up to 1200 mm, at an available torque of up to 390 kN · m.

The CFA pile was introduced into Brazil in 1987, using locally manufactured equipment, based on foreign models, allowing the construction of 275 mm, 350 mm and 425 mm diameter piles, at a maximum depth of 15 m. In 1993, due to changes in importation laws, it was already possible to build piles of up to 1000 mm diameter and lengths of up to 25 m.

CFA piles became very popular in the eighties, due to their technical advantages, combined with relatively low cost (Brons & Kool, 1988). However, theses authors warn that the production process should receive special attention, especially with pile column

continuity, subsoil disturbance due to auger extraction and failure in weak soils due to high applied pressures that can lead to significant consumption of concrete. Moreover, they warn that the increasing competition between construction companies, with the consequent cost reduction, can lead to a reduction in quality when producing these piles.

Operator sensitivity to controlling the construction of CFA piles is the most severe limitation of these piles (Bottiau, 1993). A great deal of attention must be exercised during the entire installation process, including excavation, auger extraction and positioning the reinforcements. This author also mentions that the CFA pile was developed with the aim of eliminating one of the most important disadvantages of the bored piles: soil decompression. In field studies, using a Marchetti dilatometer, before and after building a pile, it was seen that the construction process did not cause this decompression. Bottiau (1993) emphasizes that another important advantage of the CFA pile is the possibility of continuous monitoring, which furnishes documentation on the pile´s construction.

1.2 *Uplift Capacity of deep foundations*

Uplift Capacity of piles depends on several factors such as: a) Different types, characteristics and properties of soil; b) types of piles, their executive and geometric characteristics; c) types of loading (accidental, permanent and cyclic). Orlando (1999).

Design of piles to resist uplift forces is very common in Foundation Engineering. There are many situations in which this kind of force is primarily considered, such as: foundations of electrical transmission towers, foundations that cross over extensive soils; foundations of light structures submitted to the forces of wind; etc.

There are many different theoretical methods to estimate the uplift capacity for piles. However the use of these methods is very limited. This occurs because the parameters involved with these methods are very difficult to obtain.

In addition, in many situations, these methods also present very optimistic or very conservative estimated uplift capacity values.

In Brazil, estimating uplift capacity for piles using semi-empirical methods developed for compressive forces is a common practice among foundation engineers. It is assumed in these cases that the uplift capacity should be a percentage of the total skin friction resistance of the pile when it is submitted to compression forces.

There are many different methodologies to obtain the uplift capacity of a pile. The description of these methods is recounted by many pieces of research, such as Danziger (1983), Carvalho (1991), Paschoalin Filho *et al* (2008a, 2008b), etc.

2 EXPERIMENTAL FIELD CHARACTERIZATION

The Experimental Field for Studies in Soil Mechanics and Foundations is situated at the State University of Campinas, within the boundaries of the city of Campinas, in the interior region of the state of São Paulo, Brazil. The experimental field has a total area of 400 m^2.

Several field tests, such as SPT, CPT, CPTU, Cross Hole, Marchetti Dilatometer, Refraction Seismics, Vertical Electric Investigation, were carried out in this experimental field.

Laboratory tests using disturbed samples (characterization tests) and undisturbed samples (triaxial, simple compression, odometer, permeability tests, etc.) were also carried out. Static and Dynamic Load tests in different kinds of piles, such as precast concrete piles, steel piles, root piles, omega piles, bored piles, etc. were also performed.

The local subsoil is basically composed of migmatites, in which intrusive rocks occur, from the Serra Geral Formation (diabasic), covering 98 km^2 of the Campinas region, about 14% of its area. Diabasic bodies are also found, incrusted in the Itararé Formation and in the Crystalline Complex, as “sills” and “dykes”. At the outcrops, it may be observed that the diabasic soil is quite fractured, with the formation of small blocks; the fractures are usually open or filled with clayey material.

In the experimental field a diabasic soil is present, presenting a superficial layer approximately 6.5 m thick, composed of high porosity silty-sand clay, followed by a clayey-sandy silt to a depth of 19 m; the

Table 1. Average results of the field tests.

Soil	Depth (m)	Nspt	qc (kPa)	fc (kPa)
Reddish	1	3.0	392	28
brown	2	2.7	589	19
silty-sandy	3	3.0	883	36
clay	4	4.0	1324	63
	5	5.0	1864	85
	6	6.5	2502	130
Clayey-sandy	7	6.2	2453	168
silt mix	8	7.0	2256	193
(residual soil)	9	7.6	2158	204
	10	9.2	2009	221
	11	10.2	2551	254
	12	10.2	2404	238
	13	10.0	2600	265
	14	10.4	2551	224
	15	9.5	2354	198

Key: qc and fc are, respectively, the point of resistance and lateral friction from CPT (Cone Penetration Test).

Table 2. Average geotechnical parameters obtained by laboratory tests.

Depth (m)	ρ_{nat} kN/m^3	ρ_s kN/m^3	e	c (kPa)*	ϕ^o *	R_c (kPa)
1	13.4	29.7	1.77	5	31.5	26.2
2	13	29.1	1.76	11	31.5	48.0
3	13	29.5	1.79	2	30.5	40.7
4	13	30.1	1.86	0	26.5	11.2
6	15.4	30.1	1.44	18	18.5	54.1
7	15.4	29.1	1.40	31	22.5	76.1
8	14.8	29.5	1.56	18	25.5	59.7
9	15	30.1	1.6	64	14.5	50.6
10	15.1	30.1	1.6	78	22.8	67.0
12	16.1	29.6	1.46	87	18.3	145.1
14	16.4	30.6	1.48	76	19.1	185.4
16	16.7	30.1	1.51	55	22.0	218.7

Key: ρ_{nat}, ρ_s, and, c*, Ø*, Rc are, respectively, natural specific weight, grain specific weight, void ratio, total cohesion, total friction angle, simple compression resistance.

water table is reached at 17 m. The soil of the first layer is weaker than the lower layer and is collapsible, presenting collapse ratios ranging from 2.4% to 24%, depending on the applied pressure, according to Vargas (1978). Some geotechnical characteristics of the experimental area are presented in Tables 1 and 2.

3 TEST PILES AND REACTION SYSTEM

Three Continuous Flight Auger piles were conducted at the area under study. The CFA pile dimensions are as follows: nominal diameter 0.40 m and length 12 m. The piles followed a pre-defined alignment and spacing between them was 4.80 m. Three pile head blocks were also built with dimensions of 0.70 × 0.70 × 0.70 m^3 for each pile studied.

For the execution of the CFA piles, a MAIT HR-200 drill press with a depth capacity of 32 m was used. The equipment´s torque ranged from 220 kN · m to 380 kN · m; this variation is a function of the rotation speed and diameters used.

The concrete used in piles (±240 mm slump and transportable by pump) consumed cement at a rate of 400 kgf/m^3 and aggregates (sand and fine crushed rock). For the pile head blocks, concrete with fck = 25MPa was used.

The longitudinal reinforcement of the piles was composed of 4Ø 16 mm (approximately 8.0 cm^2), 6 m in length and stirrups of Ø = 6.4 mm every 20 cm. The steel used was of the CA-50 A type.

The reaction system was composed of a reaction beam, double "I" section, designed to support loads applied on its axis, 5.3 m in length and by a steel tie-rod system composed of ST85/105 (Dywidag) special bars, 32 mm in diameter, nuts, plates and steel sleeves, all manufactured with the same material.

4 STATIC LOAD TESTS

For each CFA pile, a static load test was carried out with load maintenance. The static load tests were carried out in accordance with the guidelines established by Brazilian Standards (NBR 12.131/92).

The load applications were applied in steps of 120 kN, up to the load at which the displacements indicated a rupture of the pile. Unloading was performed in four stages.

5 THEORETICAL AND SEMI-EMPIRICAL METHODS USED FOR UPLIFT CAPACITY ESTIMATING

The carrying capacity of the studied piles was also provided by means of theoretical methods appropriate for uplift forces. The methods considered were: Meyerhoff (1973), Levacher & Sieffert (1984) and University of Grenoble according to Martin (1973).

Semi-empirical methods were also used, appropriate to compression forces, considering only the portion of lateral resistance. The methods studied were the following: Décourt & Quaresma (1978); Aoki & Velloso (1975, CPT and SPT); Antunes & Cabral (1996) and P.P. Veloso (1981).

The values estimated using the methods under consideration were compared to those obtained by means of the load tests.

6 RESULTS OF THE LOAD TESTS

The load vs. settlement curves for all CFA piles studied are shown in Figure 1. The values for ultimate load and maximum displacement for each pile are presented in Table 3.

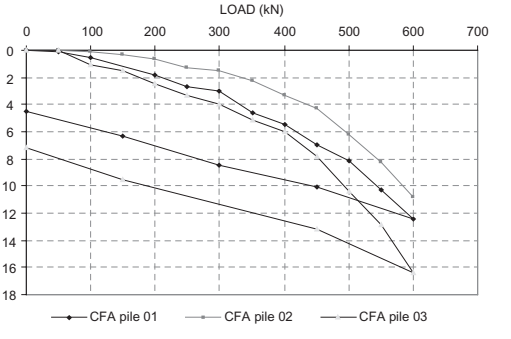

Figure 1. Load vs. settlement curves for all piles studied.

Table 3. Ultimate loads and maximum displacements reached in the loading tests.

Pile	Ultimate Load (kN)	Maximum Displacement (mm)
CFA 01	600	12.4
CFA 02	600	10.8
CFA 03	600	16.4

Table 4. Estimated ultimate loads using Van der Veen´s Method (1953).

Pile	Estimated ultimate load (kN)	Estimated ultimate load mean (kN)	Standard deviation
CFA 01	700		
CFA 02	600	667	58
CFA 03	700		

The three load tests were stopped prematurely because of the inadequacy of the reaction system. So the ultimate loads were estimated by the Van der Veen method (1953). The values of the estimated ultimate loads are presented in Table 4.

7 LATERAL RESISTANCE VALUES ESTIMATED BY SEMI-EMPIRICAL METHODS

The values for lateral resistance estimated by semi-empirical methods are presented in Table 5.

The comparison between the mean values obtained of RL_{est}/P_{load}, determined by each semi-empirical method considered, is presented in Figure 2.

In accordance with Figure 2, the method of P.P Velloso (1981) presented the mean value of $RL_{est}/P_{load\ test^*}$ closest to unity compared with the other methods. The method of Aoki & Velloso (SPT) presented the most conservative value of $RL_{est}/P_{load\ test^*}$ of all the methods studied. All methods projected lower values than those obtained through the load tests.

8 UPLIFT CAPACITY VALUES ESTIMATED BY THEORETICAL METHODS

The values for estimated uplift load capacity using the theoretical methods studied are presented in Table 6. The comparison between the mean $P_{est}/P_{load^{**}}$ values obtained, as determined by each theoretical method considered, is presented in Figure 3.

According to Figure 3, the method of Levacher & Sieffert (1984) presented the mean value of $P_{est}/P_{load\ test^{**}}$ closest to unity compared with the other theoretical methods considered. The method of Meyerhoff (1973), assuming ca = c, d = Ø, presented the mean $P_{est}/P_{load\ test^{**}}$ value which was furthest from unity. All the theoretical methods employed presented $P_{est}/P_{load\ test^{**}}$ values, on average, at least 27% higher than the actual values obtained in the load tests.

Table 5. Lateral resistance values estimated using the studied methods.

Method	Pile	Estimated ultimate load (kN)	$RL_{est}/P_{load\ test^*}$	Mean
D&Q (1996)	CFA 01	413	0.6	
	CFA 02	413	0.7	0.63
	CFA 03	413	0.6	
A&V (SPT, 1975)	CFA 01	230	0.3	
	CFA 02	230	0.4	0.33
	CFA 03	230	0.3	
A&V (CPT, 1975	CFA 01	320	0.45	
	CFA 02	320	0.5	0.47
	CFA 03	320	0.45	
A&C (1996)	CFA 01	260	0.37	
	CFA 02	260	0.4	0.38
	CFA 03	260	0.37	
P.P Vel (1981)	CFA 01	442	0.63	
	CFA 02	442	0.74	0.67
	CFA 03	442	0.63	

Key: D&Q = Décourt & Quaresma (1978); A&V = Aoki & Velloso (1975); A&C = Antumes & Cabral (1996); P.P Vel = P.P. Veloso (1981); $P_{load\ test^*}$ = Ultimate load estimated by Van der Veen´s Method (1953).

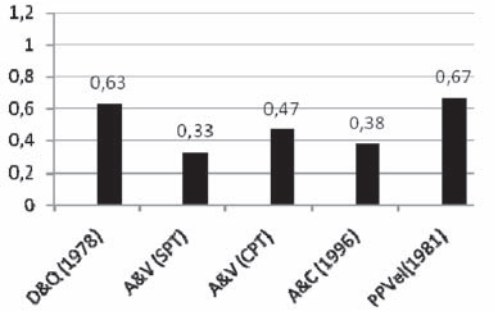

Figure 2. Mean values of RL_{est}/P_{load^*} test obtained by each semi-empirical method considered.

9 EXTRACTION OF A PILE

After performing the load tests, a pile was extracted, with the objective of knowing its geometric characteristics.

Table 6. Uplift capacity values estimated by the studied methods.

Method	Estimated ultimate load Pile (kN)		$P_{est}/P_{load\ test**}$	Mean
Meyerhoff[1] (1973)	CFA 01	1063	1.52	
	CFA 02	1063	1.77	1.6
	CFA 03	1063	1.52	
Meyerhoff[2] (1973)	CFA 01	1208	1.72	
	CFA 02	1208	2.0	1.81
	CFA 03	1208	1.72	
Levacher & Sieffert (1984)	CFA 01	844	1.2	
	CFA 02	844	1.4	1.27
	CFA 03	844	1.2	
Grenoble[#]	CFA 01	908	1.3	
	CFA 02	908	1.5	1.37
	CFA 03	908	1.3	
Grenoble[*]	CFA 01	981	1.4	
	CFA 02	981	1.6	1.47
	CFA 03	981	1.4	

Key: [1] = ca = 0.8c, δ = 0.95Ø and Ku = 1.0; [2] = ca = c, δ = Ø and Ku = 1.0; [#] = λ = 0; * = λ = –Ø/8; $P_{load\ test**}$ = Ultimate load estimated by Van der Veen´s Method (1953).

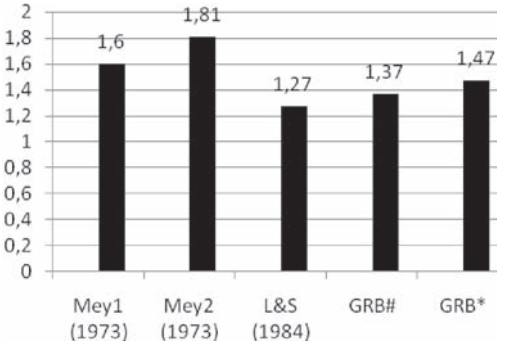

Figure 3. Mean values of P_{est}/P_{load**} test obtained by each theoretical method considered.

Figure 4. Arrangement to fix the pile.

Figure 5. Extracted pile.

For this work to be possible, a complete study was required on the possible ways of extracting the pile. Several field works were performed to make the extraction viable. All steps taken at this stage of the research are described below.

9.1 *Removal of the pile head block*

For the pile removal to be possible, the pile head block had to be demolished, to reduce the mass to be hoisted and also not to jeopardize the soil excavation along the shaft.

9.2 *Device to fix the hoist*

To permit hoisting the piles, it was seen that the most adequate means would be to fix a split metallic ring at the top of the pile. To build the ring, it was necessary to determine the pile perimeter with the objective of obtaining its diameter with maximum accuracy, so that each ring would fit perfectly onto the pile. The ring was fixed onto the pile by uniting its two parts and filling the pile-ring interface with cement slurry, to assure the connection between them. Ring details are presented in Figure 4.

9.3 *Pile extraction*

Thirty-three days after the ring was fixed, pile removal was performed. For this, it was necessary to manually excavate around its shaft. To lift the piles, an appropriate hoist was employed, since it should lift the pile at least 1 m above the ground (Figure 5).

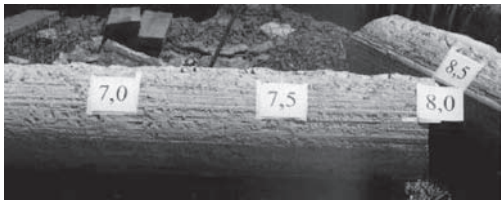

Figure 6. Crimps along the shaft.

Figure 7. Detail of the CFA pile tip.

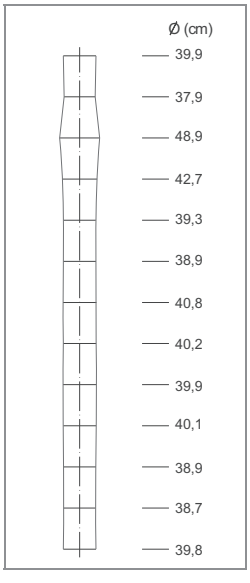

Figure 8. Detail of the CFA diameter in depth.

9.4 *Post-extraction analysis of the pile*

A complete examination of the pile was performed, revealing important data of the shaft surface, its geometry and point shape.

a. The shaft surface showed some crimps, formed by the drill, throughout the lenght of the shaft (Figure 6). Detail of the pli tip is shown in Figure 7.
b. It was been a survey of the pile perimeter and thus to get the average diameter. It was possible verify an increase of the diameter from 1.5 to 3.0 m in length (Figure 8).
c. The shaft perimeter may also be determined, thus obtaining its average diameter; it was verified that the actual diameter (40,4 cm) was on average 1% greater than the nominal diameter (40 cm).

10 CONCLUSIONS

Observing the parameters obtained through this research, the following conclusions may be reached:

a. The semi-empirical methods used in this research led to estimated values lower than the values obtained by the load tests. The method with the closest values obtained average values of 67% of the values obtained in the load tests.
b. The theoretical methods considered led to estimated uplift capacity values higher than the uplift loads obtained with the load tests.
c. The use of the theoretical methods depends on the adoption of parameters like: ca, d, Ø, etc. This situation, due to the lack of good soil value data along the length of the pile shaft, may lead to significant mistakes in uplift capacity estimates.
d. The helix auger has left crimps along the shaft. There was an increase in pile diameter between 1.5 m and 3 m depths, may have been caused by the pressure of concrete on the layer of soil weaker.

ACKNOWLEDGEMENTS

The authors would like to express their gratitude to the University of Campinas (Unicamp), Nove de Julho University (Uninove) and FAPESP by the sponsorship of this research, Brazil.

REFERENCES

Antunes, W.R., Cabral, D.A. 1996. Load capacity of continuous flight auger pile. In: Seminar of Engineering of Special Foundations. 3rd, 1996, São

Paulo-Brazil. Proceedings ... São Paulo: ABMS, v.2, 1996. pp. 105–109.

Aoki, N., Velloso, D.A. 1975. An approximate method to estimate the bearing capacity of piles. In: Pan-American Congress of Soil Mechanics and Foundation Engineering, 5th, 1975, Buenos Aires-Argentina. Proceedings … pp. 367–376.

Bottiau, M. 1993. Pile walling with the PCS Method. In: I.G.S.D.F.B.A.P., 2nd, 1993, Ghent-Belgiun. Proceedings … Rotterdam: A.A. Balkeman, 1993. pp. 185–190.

Brazilian Technical Standards Association: Static load tests: NBR 12.131/92. Rio de Janeiro: A.B.N.T., 1992. (In Portuguese).

Brons, K.F., Kool, A.F. 1988. Methods to improve the quality of auger piles. In: International Geotechnical Seminar on Deep Foundations on Bored Auger Piles, 1st, 1998, Ghent-Belgium. Proceedings … Rotterdam: A.A. Balkema, 1988, pp. 269–272.

Carvalho, D. 1991. Analysis of uplift loads of instrumented excavated piles built at experimental Field of São Carlos. 204p. Thesis. University of São Paulo. São Carlos. 1991. (In Portuguese).

Danziger, F.A.B. 1983. Load capacity of foundations submitted to vertical uplift forces. 331 p. (Dissertation) Federal University of Rio de Janeiro. 1983. (In Portuguese).

Décourt, L., Quaresma, A.R. 1978. Capacidade de carga de estacas a partir de valores de SPT. In: Brazilian Congress of Soil Mechanics and Foundation Engineering, 4th, 1978, Rio de Janeiro-Brazil. Proceedings … São Paulo: ABMS, 1978, pp. 367–376. (In Portuguese).

Levasher, D.R., Sieffert, J.G. 1984. Tests on model tension piles. Journal of Geotechnical Engineering. A.S.C.E., v.110, n12, pp. 1735–1747. Dec. 1984.

Martin, D. 1973. Calcul des pieux et foundations à dalle des pylônes de transport d'énergie électrique. Etude théorique et resultats d'essais en laboratorie et in-situ. Annales De L'Institut Technique du Bâtiment et des Travaux Publics, v. 307–308, pp. 105–130, juil.–oct.,1973.

Meyerhoff, G.G. 1973.The uplift capacity of foundations under oblique loads. Canadian Geotechnical Journal, v10 pp. 64–70, 1973.

Paschoalin Filho, J.A., Albuquerque, P.J.R.A., Carvalho, D., Nogueira, R.C.R. 2008a. Behavior of root piles submitted to uplift loads performed in diabasic soil, typical of the region of Campinas, Brazil. In: Congresso Luso-Brasileiro de Geotecnia, 4th, 2008, Porto. Portugal. Proceedings … Porto: ABMS, 2008, cd-rom (In Portuguese).

Paschoalin Filho, J.A., Pereira, M., Carvalho, D., Nogueira, R.C.R., Albuquerque, P.J.R. 2008b. Behavior of excavated piles built in diabasic soil submitted to uplift forces. In: Brazilian Congress of Agricultural Engineering, 36th, 2008, Bonito. Brazil. Proceedings … Jaboticabal: Sbea, 2008, cd-rom (In Portuguese).

Van der Veen, C. 1953. The bearing capacity of a pile. In: Procedures of Third International Conference of Soil Mechanics and Foundation Engineering. v. 2 , pp. 84–90, Zurich. 1953.

Vargas, M. 1978. Soil Mechanics. São Paulo, McGraw-Hill—Brazil Ltda. 1978. p. 509 (In Portuguese).

Deep Foundations on Bored and Auger Piles – Van Impe & Van Impe (eds)
© 2009 Taylor & Francis Group, London, ISBN 978-0-415-47556-3

Comparison of behaviour of CFA piles in London clay as determined by static, dynamic and rapid testing methods

A.P. Butcher & J.J.M. Powell
BRE, Watford,UK

M. Kightley
Testal, Derby, UK

V. Troughton
Stent Foundations, Basingstoke, UK

ABSTRACT: The determination of the capacity and load settlement behaviour of CFA piles in London clay has traditionally been achieved by static pile testing. Static pile testing is expensive and time consuming and on reuse sites may not be an option because of access or the time constraints of the redevelopment project. The Rapid Pile Performance Evaluation Resource (RaPPER) project has set out to provide guidance on testing methods for piles intended for reuse and the applicability of different testing methods to different soil types. The RaPPER project included the installation of twelve 'identical' CFA piles in London clay and the testing of the piles using Static, Dynamic and Rapid ('Statnamic') methods. This paper describes the soil conditions, the piles, the testing procedures and presents some of the initial results including the comparison of load deformation characteristics as determined from the test methods and potential developments to improve the interpretation of the rapid and dynamic tests in clay soils as applicable to the reuse of piles situation will be also discussed.

1 INTRODUCTION

The Reuse of Foundations for Urban Sites (RuFUS) project identified the difficulties of testing piles that were to be reused for capacity and load settlement performance (Butcher et al. 2007a, b). In a reuse situation where new piles are to be used with existing piles the load settlement characteristics of the new and existing piles must be similar. With the effects of ageing and load history modifying pile behaviour during the life of a foundation and often the unknown geometry of the piles, there is a need to test piles due for reuse to get their relevant performance. The RuFUS Project found that load settlement predictions based on dynamic, rapid and static tests were significantly different. Further, the relationships between the predictions from each test technique varied between soil types.

The RaPPER project began in 2007 to generate a tool to aid the selection of pile testing methods for existing foundations that were to be reused. Part of the work of the project was to install identical piles on test sites and test the piles using the different testing methods available to assess load capacity and load settlement behaviour. The first site selected was the BRE test site at Chattenden, a long term test facility on the London clay.

2 TEST SITE

The site is located at Lodge Hill Camp, Chattenden, Kent in the UK is underlain by London Clay. It was a 'green field' site initially established for research projects on the performance of foundation elements n i shrinkable clay soil (Crilly et al. 1992 & Freeman et al. 1991) these have been carried out at the site over a number of years and considerable soil information has been collected:

- The site is underlain by 30 m depth of stiff London Clay, with a desiccated crust typically up to 3 m deep, particularly near trees.
- Average c_u is 100 kPa in the upper 10 m.
- Average water content, w = 29%, in upper 15 m.
- Plasticity index, I_p = 52% in upper 10 m, rising to 60% for 10–15 m.
- Bulk density, $\gamma = 19.4$ kN/m^3.
- Water table is at approx. 1 m depth (depressed near the trees).

Some basic data found from characterisation of the site is shown in Figure 1. The upper 4 m or so is weathered brown London clay which overlays unweathered blue clay. Soil strength data is available

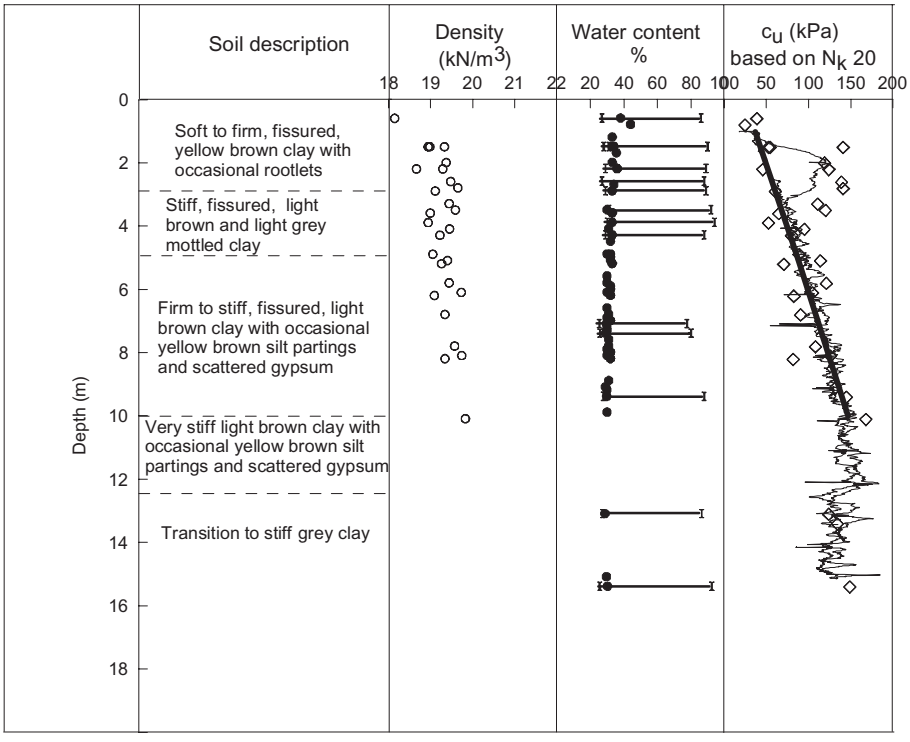

Figure 1. Typical soil properties for the Chattenden site.

from both laboratory and in situ tests and is summarised in Figure 1; it is seen that the strength increases almost linearly to about 10 m depth before continuing to increase at a much slower rate to greater depths. Note that here an N_k factor of 20 has been used to calculate strength data from the CPT in Figure 1 and this results in very similar profiles to 100 mm diameter undrained triaxial test results on thin walled pushed samples. The site has been used extensively in recent times for pile behaviour testing (Powell & Skinner 2006, Butcher 2006, Fernie et al. 2006, Powell & Brown 2006, Skinner et al. 2003).

3 TEST PILES

The intention was to design and construct a series of identical piles (as identical as could be achieved) so that 'virgin' (never previously tested) piles could be tested using the different pile testing methods.

The piles were designed so that:

- they were sufficiently large so as to model routine CFA pile construction whilst being economic to construct
- a number of similar piles could be constructed
- they would have relatively low capacities to limit the size of the reaction system.

The test piles were 450 mm diameter continuous flight auger piles installed to a depth of 9.5 m below ground level. The piles were extended above ground at the time of casting by adding a 11 mm thick steel casing of 500 mm diameter filled with concrete. All the piles were reinforced but the piles for dynamic testing included additional steel to enable them to be used as ground anchors for the static testing. Two of the piles had fibre optic strain gauges to trial their use for rapid and dynamic pile test environments but that trial will not be reported here.

The design static load capacity of the piles was to be 1000 kN.

4 TEST PROCEDURES

4.1 *Static tests*

The Static pile test where the load is applied to the pile, either in increments or continuously, with measurements made of applied load and pile head settlement. The load is usually applied using an hydraulic jack reacting against

a frame that is restrained by either kentledge or anchor piles. For the tests reported here the frame was restrained by anchor piles and a typical static pile set up is shown in Figure 2a. The test procedure used complied with the ICE Specification for Piling and Embedded Retaining Walls 2nd ed (ICE 2007). Four piles were tested, two with a maintained incremental load procedure (ML) to failure which was followed by a constant rate of penetration stage (CRP) and two tested with the CRP procedure followed by a retest using ML procedure.

The test procedure for the ML tests was to increase the load in 125 kN increments up to 500 kN, decrease the load in 125 kN increments to zero load and then increase in 125 kN increments until failure was established. The increments during loading were maintained for at least 30 minutes and then until the rate of settlement was less than 0.1 mm/hr. This criteria works well until failure is approached. In a strain softening material such as the London clay as failure is approached the rate of settlement increases. At this point it is accepted practice to reduce the load to the previously stable load increment and maintain at that level until stability returns. For the RaPPER piles when the rate of settlement reduced to less than 0.1 mm/hr the load was decreased incrementally to zero load and then a constant rate of settlement test was performed.

The test procedure for the CRP tests was to increase the load to make the pile head settle at a rate of 0.007 mm/s. The loading was continued until 50% of the design load and then unloaded. The pile was then reloaded and continued until a peak load had been reached and begun to drop back. At this point the rate of loading was increased to the safe maximum of the system, about 0.23 mm/s, for a short period to assess the effect of the rate of loading on the ultimate capacity. For the purposes of this paper the peak load reached at the standard rate of penetration has been used as the static ultimate capacity of the pile.

4.2 *Dynamic test*

The dynamic test applies a load to the pile head by a vertical impact of typical duration of less than 10 ms. This can be achieved using an impact piling hammer or in this case a guided drop weight as shown in Figure 2b. The drop weight was suspended from a crane via a free fall winch that was used lift and drop the weight to deliver the test blows. The energy from the drop weight was designed to be sufficient to fully mobilise the pile and thereby result in a permanent, i.e. non-elastic movement of the pile head. The dynamic test piles were instrumented to measure the vertical strain and acceleration of the pile at the pile head. Two sets of strain gauges and accelerometers were fixed to the pile, diametrically opposite, above ground level and at least 2 pile diameters from the pile head. The instrumentation was bolted to the steel casing and connected to a Pile Driving Analyser Model PAL-R, and the test data sent live to an office based expert for immediate inspection and analysis. The recorded strain data were then used with knowledge of the section modulus of the pile to calculate the force at the pile head and the acceleration data can be integrated with respect to time to get the pile head velocity and integrated again to get pile head settlement.

The knowledge of the section modulus and geometry of the pile enables a numerical model to be constructed to match that of the measured pile response to the vertical blow.

These analysis methods are generally based on the wave equation theory with a lump mass pile model or

(a) (b) (c)

Figure 2. Photographs of the pile tests underway: a) Static test, b) Dynamic test with sliding hammer and c) Rapid test.

a continuous pile model (CAPWAP Goble et al. 1980, TNOWAVE, Middendorp & van Wheele 1986). The software generates a pile-soil behaviour model using known engineering properties of the pile and models of the soil behaviour.

In the case of Wave Matching (CAPWAP, TNOWAVE) the soil behaviour models include an elastic-plastic model (static soil resistance) coupled to a damping model (dynamic soil resistance).

A soil-pile model is constructed in equal depth increments and the variable parameters in the soil model adjusted until the behaviour of the model matches the measured behaviour from the test.

The soil pile model was then used to give the ultimate capacity of the pile and the estimated static load settlement relationship.

4.3 *Rapid tests*

The Rapid test applies a force to the pile head over a typical duration of 120 ms through the controlled venting of high pressure gas. The gas is the product of the combustion of a fast burning fuel within a piston (fuel chamber). At the top of the piston are vents that are sealed by a load hanger retaining a reaction mass. At some point the pressure within the piston is high enough to force the reaction mass upward at accelerations in the order of 200 m/s^2. This process applies a load downwards on the test pile, resulting in pile velocities up to 1 m/s. The load applied to the pile head is measured by a dynamic load cell and the accelerations by an accelerometer. A separate optical system is used to measure and log movement of the pile head during the test relative to a remote datum.

For foundation design it is necessary to derive the 'equivalent' static load-settlement curve from the Rapid data. The most common form of which is referred to as the unloading point method (UPM) (Middendorp 2000) which tries to take account of inertia and damping effects. Other methods using curve fitting or non-linear analysis have been developed specifically to tackle the highly non-linear response of clays and fine grained soils to shearing at elevated rates (Brown 2004). The performance of the UPM analysis is typically very good where the soil is coarse grained or where the pile forms a rock socket. Unfortunately in fine grained soils (clays and silts) damping is highly nonlinear (Brown 2004), resulting in UPM over predicting ultimate static pile capacity by 50% or more. To address the soil dependent nature of UPM a series of correction or 'rate factors' have been developed (Paikowsky 2004) and given in Table 1.

It should be noted that the correction factors suggested in the Table for clay are based on a very limited number of cases which has led to reluctance by some authors to specify safety factors in clay. The use of such factors also detracts from the ethos behind the development of the UPM technique and makes user intervention necessary. This problem of interpretation in fine grained soils, the fact that a single factor can not be applied to all fine grained soils and that corrections need to account for strain dependency of damping etc, forms a major part of the RaPPER project.

Table 1. Correction factors for UPM analysis (Pailowsky 2004).

Soil type	Rate effect factor (η)	FOS* without η	FOS* with η
Rock	0.96	2.0	2.0
Sand	0.91	2.1	2.0
Silt	0.69	2.8	2.0
Clay	0.65	3.0	2.0

*FOS-Factor of safety.

The work reported here was undertaken using the Profound 4.0 MN 'Statnamic' rig Figure 2c. Brown & Hyde (2002) had recommended that the maximum load applied to a pile in a Rapid test in glacial clay should be in excess of 1.7 times the static capacity. Powell & Brown (2006) had reported that in London clay 1.75 times the static capacity had failed to fully mobilise the pile and it was then difficult to convert the test curves into equivalent static values; in fact they recommended that the equipment should have sufficient capacity to 'fully mobilise' the piles (movement in excess of 10% pile diameter). Multipliers in approaching 2 had been found previously in other glacial soils, (Powell & Brown 2009).

As a result it was to be ensured in the RaPPER testing that sufficient capacity would be available to fully mobilise the piles and the 4.0 MN Profound rig was selected.

5 TEST RESULTS

5.1 *Static test results*

Typical results from the static tests are shown in Figure 3 for one ML test (MC1) and one CRP test (MC3). The ML test specification required the rate of settlement of the pile head to be less than 0.5 mm/hour before the next load increment could be applied and similarly if a load could not be maintained then the applied load should be reduced by the same increment. The average of the ML tests was around 1050 kN and the average of the CPR tests around 1120 kN. The higher ultimate capacity shown for CRP test MC1 in Figure 3 was achieved by an increase in penetration rate to look at rate effects.

Figure 4 shows the early stages of the static tests for the first 5 mm of settlement. This plot shows that the initial modulus up to what is likely to be a working load for these piles is similar for both test

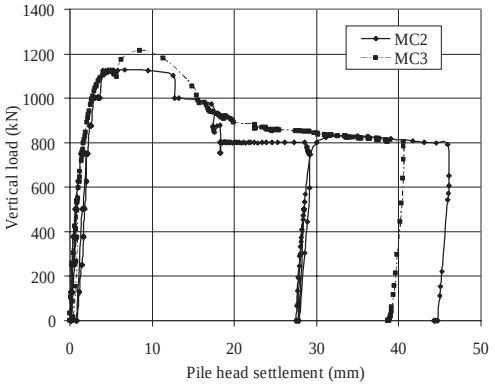

Figure 3. Static pile test results.

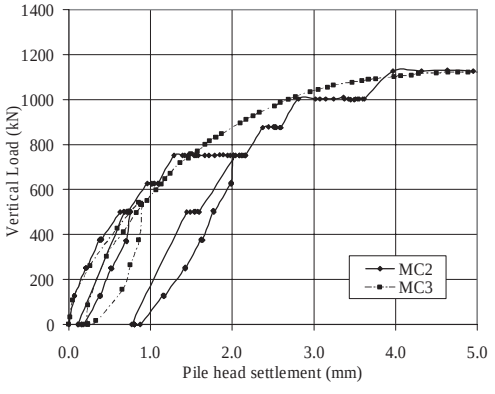

Figure 4. Static tests: Initial load settlement curves.

procedures. The CRP test forms an upper envelope to the ML test.

5.2 *Dynamic test results*

Four piles were available for dynamic testing with several series of blows made by the sliding hammer from different drop heights being applied to each pile. Rough measurements of the settlement of the pile per blow were made to compare with the analysed settlement data from the accelerometers.

Analysis was undertaken using CAPWAP software that generates the numerical models to match the measured behaviour. Initial analysis of the results assuming the piles were of uniform section and section modulus gave good signal matches but high unrealistic ultimate capacities (1450 kN to 1750 kN) and unrealistically high toe loads. Standard analysis using the as built geometry of the piles, the steel content of the cap and the elastic properties of the steel and concrete gave lower ultimate capacities but still the high toe loads. Figure 5 shows a typical output from the

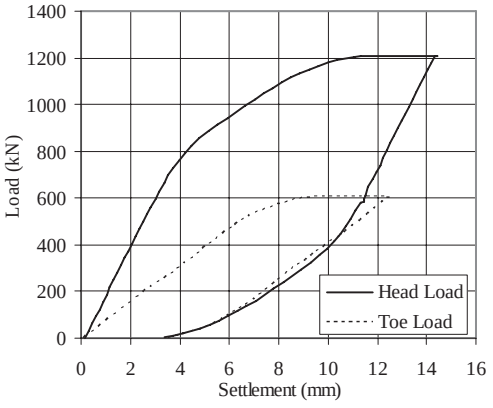

Figure 5: Typical load settlement output from a dynamic test on pile DS1 from the Standard analysis.

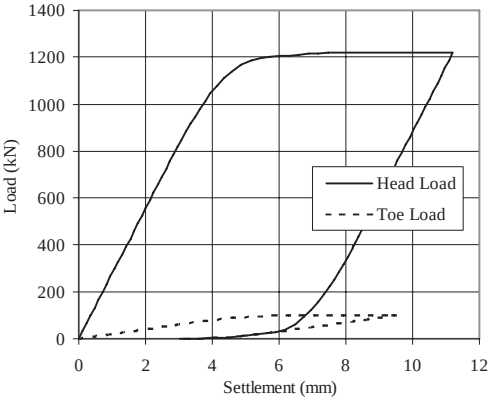

Figure 6. Typical load settlement output from a dynamic test on pile DS1 from the Standard+ analysis.

Table 2. Estimated static ultimate capacity from dynamic tests.

	Standard		Standard+	
Pile	Total kN	base kN	Total kN	base kN
DS1	1210	605	1220	100
DS2	1299	466	1299	100

test on DS1 with the standard analysis. Re-analysis by forcing the software to reduce the end bearing load and match the pile shaft friction to the CPT profile given in Figure 1, gave less good matches between the measured and CAPWAP generated behaviour but did give the expected lower toe loading and higher shaft friction elements. The effect of this re-analysis,

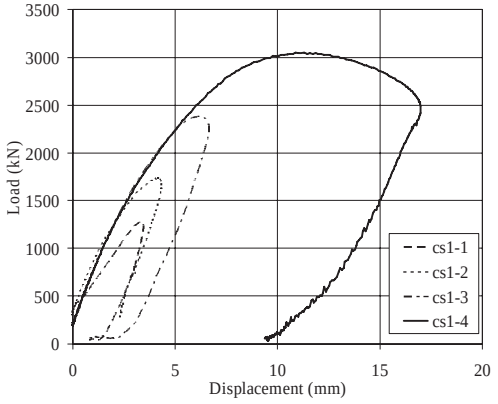

Figure 7. Rapid test results: Typical load displacement curves.

called Standard+, can be seen in Figure 6 for pile DS1. The Standard+ analysis gives a much more shaft friction dominated response as expected in these piles in stiff overconsolidated London clay. Table 2 gives the estimated static ultimate load capacity and the part of that capacity attributed to the toe of the pile from both the Standard analysis and Standard+ analysis.

5.3 *Rapid tests*

Three piles were available for Rapid testing and various loading cycles were undertaken on each of the piles. The intention was to investigate how the pile response might be affected when loaded at differing rates and with different degrees of mobilisation. As London clay is a strain softening material there will be a tendency for the pile to shed load down the pile as the loads progress towards failure (see difference between ML and CRP above) and this has to be taken into account in determining the load cycles and their possible effects on maximum capacity achieved in any test. As long as the pile is responding elastically then this should not be a problem.

Figure 7 shows some typical load cycles from Statnamic test CS1. It can be seen that only at a load in excess of 3100 kN are significant displacements generated and the pile looks to have failed. In all piles tested load cycles up to 2.5 times the static capacity failed to fully mobilise the piles and this was only achieved with loads in excess of 3 times the static capacity! The data shown are based on back calculation from accelerometer data and it would appear that significant differences were obtained between this data and that from the optical displacement system, this would have implied higher stiffnesses in the early parts of the load cycles, and this is still being investigated (similar behaviour had been found by Powell et al. 2009 but generally at lower loads and then not as dramatic as found here).

Table 3. Pile capacity from UPM with reduction factors.

	UPM kN	65% UPM kN	40% UPM kN
DC1	3360	2184	1344
R1	2360	1534	944
CS1	2600	1690	1040

Table 3 shows the capacity derived using the basic UPM method and also the UPM modified using the clay factor from Table 1.

Is can be seen that the results even with the recommended UPM reduction from Table 1 significantly overestimate the static capacities in London clay and this is consistent with the findings of Powell & Brown (2006) on smaller piles at the same site.

6 DISCUSSION

Table 4 summarises the ultimate capacities predicted from the various tests. The initial interpretations for both Dynamic and Rapid tests significantly overestimated the capacities of the piles.

For the Dynamic tests then it can be seen that initially the capacities were overestimated, on average by around 50%. Once the correct geometry and pile properties were added to the model then the average overestimate came down to just under 20% but this had to be modified further to improve the split between base and shaft. When knowledge of the expected behaviour of piles in stiff overconsolidated clays and measured soil properties were included in the analysis a more realistic pile shaft to pile toe load distribution was obtained but with a poorer match of CAPWAP and measured behaviour.

The Rapid load tests using the UPM correction of 65% overestimated capacity by around 80%. Only when using a factor around 40% do the derived loads approach those of the static ML tests and then not in all cases (DC1 requiring closer to 30%, see Table 3). An average overestimate of less than 5% is obtained. As mentioned earlier there is little data supporting the value of 65% in Table 1 and this type of correction must be related to soil type and history. Powell & Brown (2006) suggested a relationship between Plasticity Index (I_p) and the rate effect aspect of this correction but again this only has limited data to date.

The RaPPER project is concerned with assessing pile behaviour with a view to re-use. In order to successfully re-use piles knowledge of the load

Table 4. Comparison of pile capacities from different tests.

Test	average ultimate capacity kN
Dynamic - standard+	1260
Dynamic - initial	1650
Rapid (65%)	1802
Rapid (40%)	1114
Static (ML)	1065
Static (CRP)	1116

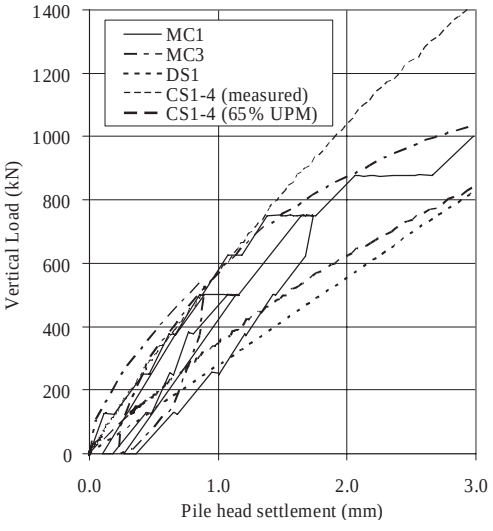

Figure 8. Comparison of test results at working loads.

settlement behaviour up to working load is essential. Figure 8 shows examples from all the test procedures in the typical working load range for the test piles up to say 50% ultimate capacity. It can be seen in the Figure that the processed and 'corrected' data from both the Dynamic (DS1) and Rapid (CS1-4) tests give a much 'softer' response in terms of load settlement. This would imply greater settlements up to working load than the static tests. It should be noted in Figure 8 that the uncorrected behaviour (shown as 'measured') from the Rapid tests closely follows the static behaviour; the UPM method and the reduction factor correction not only reduce the ultimate capacity but also the load throughout the test without any change to the displacements and hence the flatter response in the derived curves. The non-linear methods available and under development try to reduce this influence by varying the corrections throughout the test curve.

7 CONCLUSIONS

'Identical' CFA piles were installed at a test site on overconsolidated London clay for the first phase of the RaPPER project and each pile was tested by one of Dynamic, Rapid or Static test procedures.

The results showed that the difference between ultimate static load capacity from ML and CRP tests was of the order of 5–10%, typical of what might be expected as a result of 'rate' effects alone in these soils. The ultimate equivalent static capacity estimated from the Dynamic and Rapid methods using routine interpretation procedures were between 18% and 70% higher than the ML tests. With engineering knowledge and the experience of the analysts the potential was realised to bring the capacities to within between 18% and 5% of the average ultimate capacity measured in Static tests. The application of this knowledge and experience to the analysis of the test results needs to be validated and related in some way to pile and soil behaviour and a soil 'parameter' such as I_p. A rate effect alone at these high rates in the Dynamic and Rapid tests could not explain the differences. These points will be investigated further in the 2nd phase of RaPPER tests that will include CFA piles in a strain hardening stiff clay and precast piles in London clay.

It appears that the present interpretation procedures lead to load settlement stiffnesses, from the Dynamic and Rapid tests, that are significantly softer than those from the Static tests and this is concerning. However the measured Rapid data appear to give stiffnesses very close to those from the Static tests and this is consistent with data from others. (This will need to be confirmed once the differences between optical and back calculated settlement data have been resolved).

It has been shown that for Rapid tests on piles in London clay loads in excess of 3 times the static ultimate load are likely to be required to fully mobilise the piles and result in 'failure'.

There is still a need to better understand the mechanisms happening in the Dynamic and Rapid tests and to improve the models that are being used to interpret the results and to incorporate fully the pile properties and soil dependant behaviour such as loading rate effects.

REFERENCES

ASTM D4945-00 "Standard Test Method for High-Strain Dynamic Testing of Piles".

Brown, D.A. 1994. Evaluation of the static capacity of deep foundations from Statnamic testing. *ASTM geotechnical testing Journal*, Vol 17, No 4, pp. 403–414.

Brown M.J. 2004 Rapid load testing of piles in fine grained soils. PhD Thesis, University of Sheffield, UK.

Brown M.J. & Hyde A.F.L. 2006. Some observations of Statnamic pile testing. Proc. Inst. Civil Engineers: Geotechnical Engineering J., Vol 159, GE4, pp. 269–273.

Butcher, A.P. 2006. The detection of pile geometry using geophysics. in Butcher A.P., Powell, J.J.M. and Skinner. H.D. (Eds.) 2006 *Proceedings of the International Conference on the Re-use of Foundations for Urban Sites*, pp. 87–94 IHS BRE Press, Willoughby Road, Bracknell, Berks, RG12 8FB.

Butcher, A.P., Powell, J.J.M. & Skinner, H.D. 2006a (Eds). *Reuse of Foundations for Urban Projects: a best practice handbook*. IHS BRE Press, Watford, 2006. EP75.

Butcher A.P., Powell, J.J.M. & Skinner. H.D. 2006b (Eds). *Proceedings of the International Conference on the Re-use of Foundations for Urban Sites,* pp. 187–198. IHS BRE Press, Willoughby Road, Bracknell, Berks, RG12 8FB.

Crilly M.S., Driscoll R.M.C. & Chandler R.J. 1992. Seasonal ground and water movement observations from an expansive clay site in the UK. *7th Int Conf on Expansive Soils, Dallas Texas, Aug 3–5 1992,* pp 313–318.

Fernie,R. Bourne-Webb, P. Shotton, P. & Tester, P.D. 2006. Observations of pile topile and pile cap interaction at a well calibrated RuFUS test site. in Butcher A.P., Powell, J.J.M. and Skinner. H.D. (Eds.) 2006 *Proceedings of the International Conference on the Re-use of Foundations for Urban Sites,* pp. 187–198. IHS BRE Press, Willoughby Road, Bracknell, Berks, RG12 8FB.

Freeman T.J., Burford D. & Crilly M.S. 1991. Seasonal foundation movements in London Clay**.** *4th International Conference on Ground Movements and Structures, Cardiff*, July 1991, Vol 4, pp. 485–501.

Goble, G.G., Rauche, F & Likins, G.E. 1980. The analysis of pile driving—a state of the art. *International Conference on the application of Stress Wave Theory in Piles, Stokholm.*

ICE. 2007. *Specification for Piling and Embedded Retaining Walls* 2nd ed. ICE London.

Middendorp P. 2000. Statnamic the engineering of art. Proc. 6th *Int. Conf. on the Application of Stress Wave Theory to Piles*, Sao Paulo, pp. 551–561.

Middendorp, P. & van Wheele, A.F. 1986. Application and characteristic stress wave method in offshore practice. Proc. *Third Int. Conf. on Numerical Methods in Offshore piling, Nantes.*

Paikowsky S.G. 2004. Research Report NCHRP 21–08. Innovative load testing systems. Geosciences Testing and Research Inc, Massachusetts. National Cooperative Highway Research Program,

Powell J.J.M. & Brown, M,J. 2006. Statnamic pile testing for foundation reuse, in Butcher A.P., Powell, J.J.M. and Skinner. H.D. (Eds.) 2006 *Proceedings of the International Conference on the Re-use of Foundations for Urban Sites*, pp. 223–236. IHS BRE Press, Willoughby Road, Bracknell, Berks, RG12 8FB.

Powell J.J.M. & Brown, M,J. 2009. Statnamic testing of tubular Piles in a glacial clay till. In preparation.

Powell, J.J.M & Skinner, H.D. 2006. Capacity changes of bored piles with time. in Butcher A.P., Powell, J.J.M. and Skinner. H.D. (Eds.) 2006 *Proceedings of the International Conference on the Re-use of Foundations for Urban Sites*, pp. 237–248. IHS BRE Press, Willoughby Road, Bracknell, Berks, RG12 8FB.

Skinner, H., Powell, J.J.M., Morris, J. & England, M. 2003, Results from a piling trial on bored, CFA and rotary displacement piles in stiff clay. *Proc ICOO3*, Dundee, September. pp. 825–834.

Deep Foundations on Bored and Auger Piles – Van Impe & Van Impe (eds)
© 2009 Taylor & Francis Group, London, ISBN 978-0-415-47556-3

Instrumented large diameter bored piles

Armando Caputo
BRASFOND Fundações Especiais S/A
SPFE-Sociedade Portuguesa de Fundações Especiais
BRASFIX-Fundações de Obras Marítimas e Fluviais

ABSTRACT: A bridge over Tagus River in Carregado, Portugal, with extension of 11000 m of which 800 m offshore and 10200 m onshore was built, finishing in 2006. The foundations onshore were planned and were installed in bored piles, Φ 1500 mm, without using bentonite slurry, mainly for environmental reasons.

Because of the importance of the work and the need of installing approximately 1260 piles with length up to 56.00 m, it was foreseen, before the start of the job, a series of instrumented pile load tests, static and dynamic, to confirm the design assumptions and validate the solution proposed.

We intend to discuss the execution and performance of these piles facing the load tests.

1 INTRODUCTION

The construction of the bridge over the RIVER TAGUS and the access ways to the BUCELAS/ CARREGADO/IC3—A10 highway, was constructed in Portugal, in the place called Carregado.

BRISA—Auto Estradas de Portugal S.A.—has contracted for the conception works, Design and Construction, a Consortium composed by the companies: MSF, CONSTRUTORA DO TÂMEGA, LENA CONSTRUÇÕES, NOVOPCA, BENTO PEDROSO CONSTRUÇÕES and ZAGOPE,

Figure 1. Localization view of the bridge over the River Tagus—North and South bridges accesses.

called TACE—CONSTRUÇÃO DA TRAVESSIA RODOVIÁRIA DO TEJO, ACE.

The work was comprised by the NORTH—SOUTH access bridge with an approximate length of 11 km, and a section that crosses the River Tagus, which is 0.80 km long.

The North and South access ways are composed by viaducts supported by 4 ϕ 1500 mm, columns, spaced at 36.00 m. According to the design, piles compose the viaduct columns.

The quantities foreseen are:

- North Bridge (column V1 N through V3 N) 180 ϕ 1500 mm 25,00 m < L < 30,00 m
- South Bridge (column V1S through V22S) 1080 ϕ 1500 mm 25,00 m < L < 56,00 m

The bridge over the River Tagus comprises 7 columns with 10 ϕ 2200 mm each, 55,00 m long, which were installed by another company.

2 PREMISES FOR THE CHOICE OF THE CONSTRUCTION METHOD

The subsoil profile along the site is predominantly composed by an uneven superficial landfill, varying from clayey silt to silty clay, followed by a layer of gray mud. Underneath this layer, a layer of semi-coarse and coarse sand is found, including the presence of pebbles and boulders, known as "cascalheira", with an SPT blow count of around 50 blows, followed by miocenic soil formed by clay, silts and sands with SPT values higher than 60 blows. Inicial design concept for the foundations was with use of bored piles with a partial and temporary casing and stabilization of the hole with bentonit slurry or polymer down to the design depth.

The region is subject to high seismic activity, and design established that the piles should have base resistance only and, therefore, were designed with 3 ϕ into the miocenic (M1) soils.

The technical discussions about the construction methodology led to the following debates:

a. Would the slurry or the polymer be able to stabilize the excavation in the pebbles "cascalheira" area?
b. Having in consideration the environmental requirements, where should the excavated spoil, contaminated by the slurry or the polymer, be deposited?

Due to these questions, we suggested an alternative solution that was not affected by the "cascalheira" and allowed elimination of estabilizing slurry or polymer, as shown below.

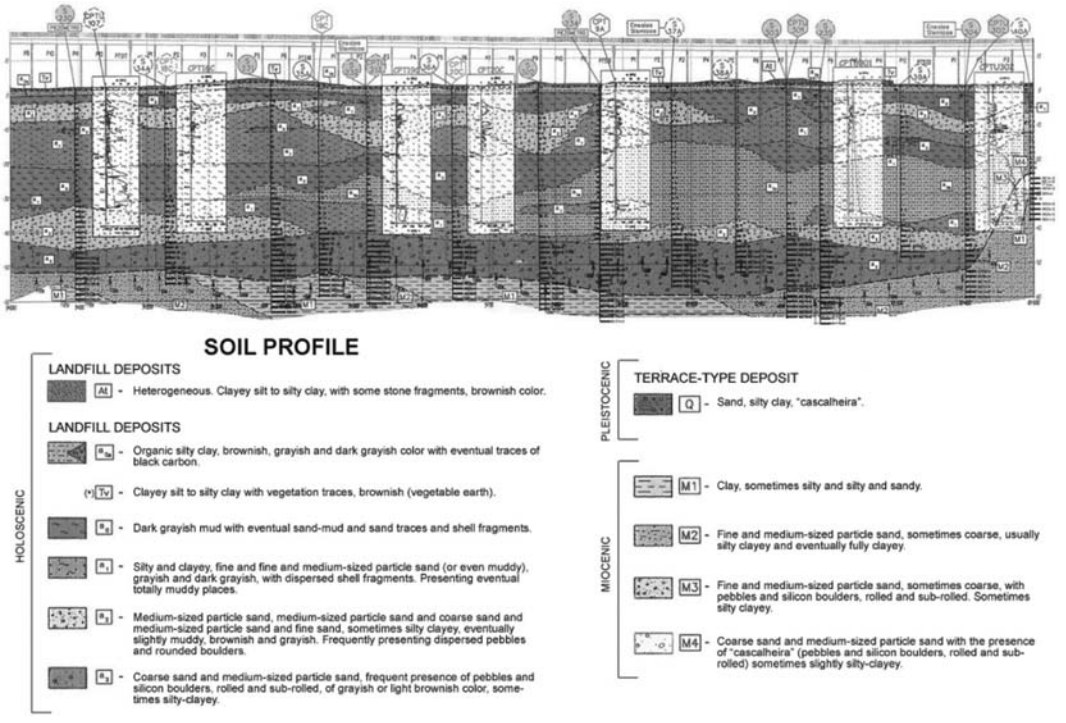

Figure 2. Longitudinal geological and geotechnical profile along the bridge alignment.

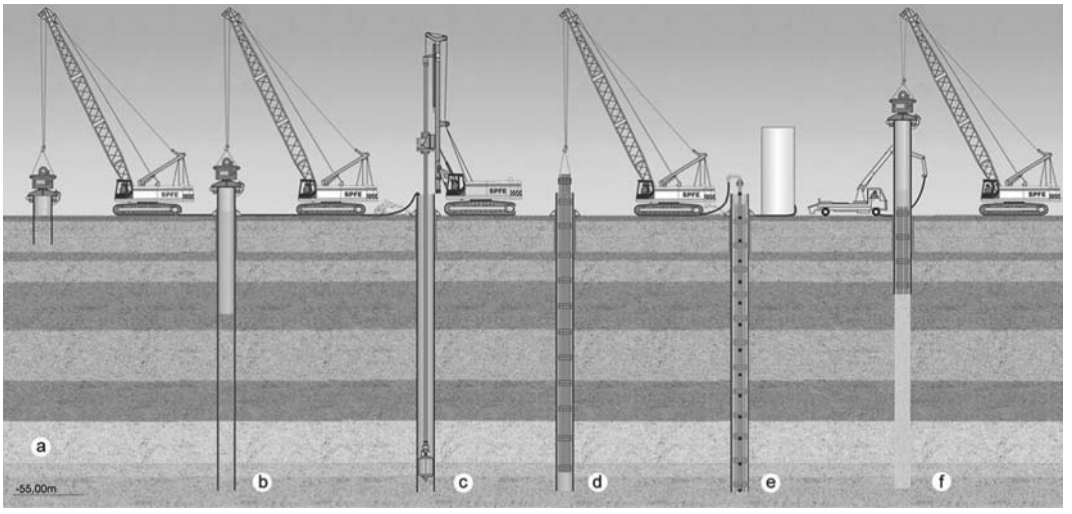

Figure 3. Construction methodology.

3 CONSTRUCTION METHODOLOGY

The construction methodology defined to install the piles is the following:

a. Placement of a guide—steel tube with 6.00 m.
b. Driving a temporary casing with the use of vibrator down to the design depth.
c. Internal cleaning of the casing up to the design depth, with a hydraulic rig.
d. Placement of the reinforcement cage in modules.
e. Cleaning the base of the pile with "air-lift".
f. Pouring of the pile concrete simultaneously with removal of the steel casing.

Note: Due to the pile length, as long as 56.00 m, the casing was driven in 3 welded elements and the inside cleaning was always carried out before the weldings.

4 INSTALLATION OF THE PILES TO BE TESTED

Having in mind the suggested solution, we proposed to perform some pile testing aimed at assessing and validating the construction methodology.

Hence, a series of instrumented static and dynamic load tests were programmed, as defined by the designer COBA, the company responsible for the project, and the interpretation of the results was assigned to IST—Instituto Superior Técnico, under the coordination of Professor Jaime Santos. The static load test was carried out by CÊGÊ, the dynamic load tests by GEOMEC and the installation of the piles was assigned to a consortium headed by SPFE—Sociedade Portuguesa de Fundações Especiais.

Table 1. Supplementary prospection.

Test	Borehole	Piezocone tests
1	S227 – km 8 + 194	SCPTU 309
2	S226 – km 7 + 904	SCPTU 308
3	S220 – km 5 + 459	SCPTU 307

Due to the importance of the tests for the construction methodology adjustment, it was decided to use, as reaction for the static load tests, piles of 1,500 mm reinforced with 12 Dywidag bars each, considering a test load up to 9600 kN.

A pile of ϕ 1500 mm with 55.00 m was also installed and tested in a dynamic test only, and another short ϕ 800 mm pile, was tested horizontally.

The load tests were carried out in 3 different locations, representative of the local subsoil condictions. For a better definition of the geological-geotechnical conditions of each of the test locations a complementary site prospection work was performed being composed by boreholes together with the SPT and SCPTU tests. Four piles were installed in each test location, always following the same construction methodology. Figure 7 shows the pile's layout:

a. Reaction piles "R" with 1500 mm-diameter;
b. Pile "E" with 800 mm-diameter for the static compression test (pile with instrumentation along the length);
c. Pile "D" with 800 mm-diameter for the dynamic test.

The distance between pile "E" and the reaction piles "R" is of about 3,50 m between centers.

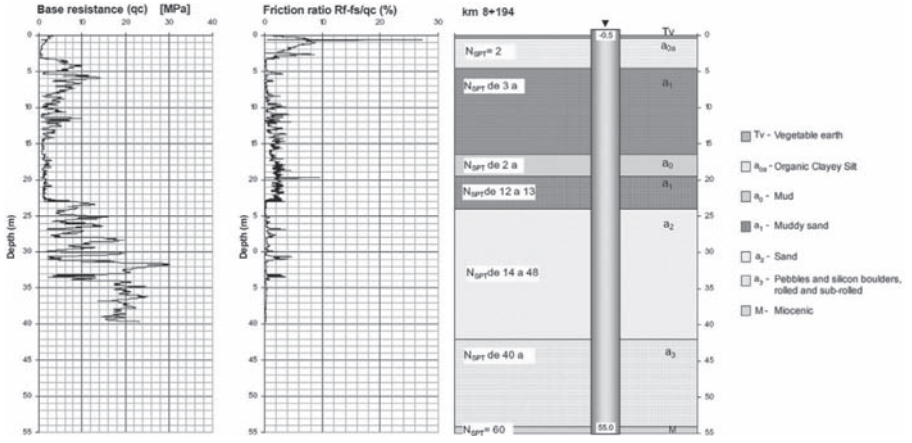

Figure 4. Test 1: Additional site investigation.

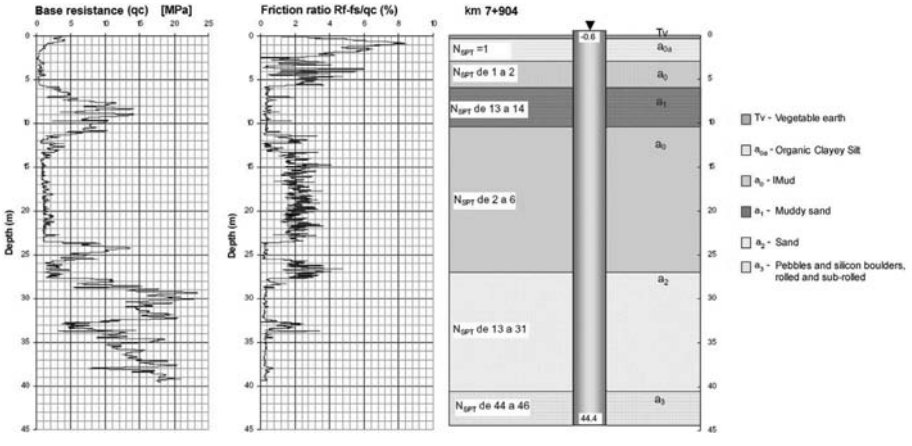

Figure 5. Test 2: Additional site investigation.

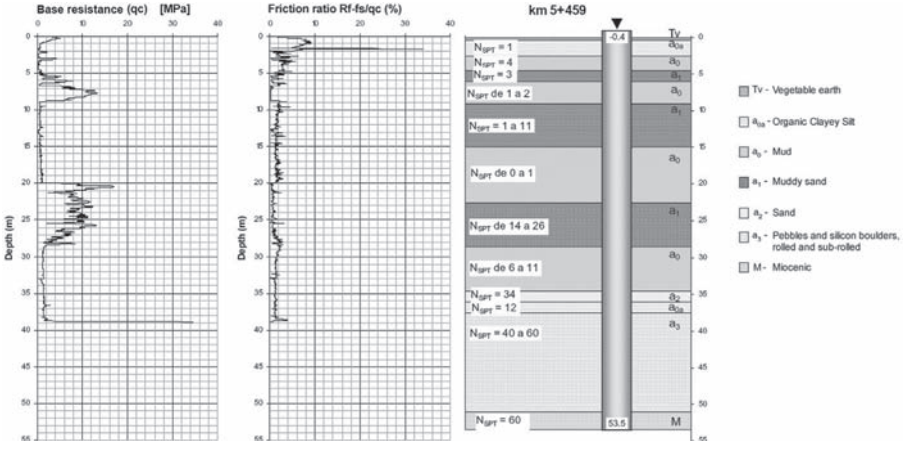

Figure 6. Test 3: Additional site investigation.

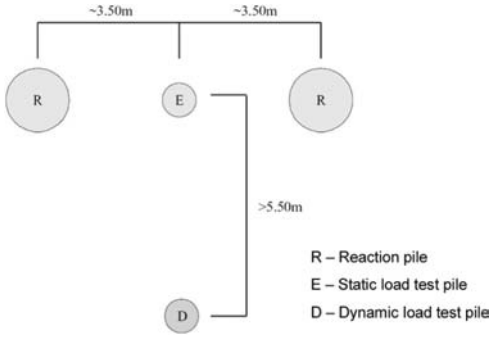

Figure 7. Layout of test piles and reaction piles.

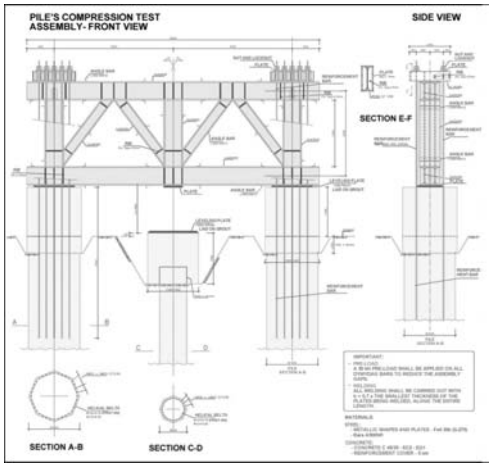

Figure 8. Pile compression test (piles ϕ 800 mm).

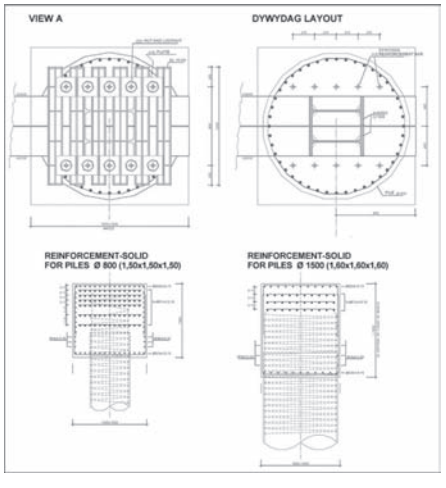

Figure 9. Pile compression test (piles ϕ 800) —Assembly, side view and sections views, details and blocks.

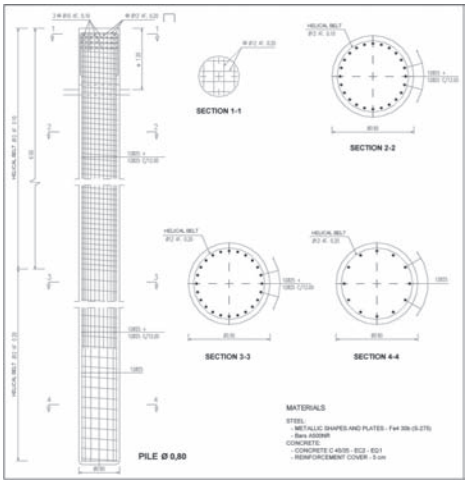

Figure 10. Test pile ϕ 800 mm.

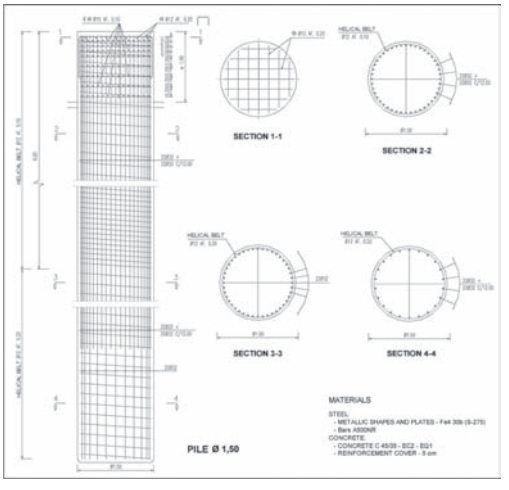

Figure 11. Test pile ϕ 1500 mm.

This value, although fulfilling the criterion of 3 times the test pile diameter, falls within: $3 \times 0.80 = 2.40$ m < 3.50 m < $3 \times 1.50 = 4.50$ m.

The piles submitted to the static compression load test, were also later tested dynamically.

The purpose of this procedure is to compare the results obtained in both tests, in piles previously loaded and in piles not yet tested by any means.

All the piles installed were also submitted to integrity tests, "cross-hole test".

5 PILE TESTS

5.1 *Test locations*

The definition of the pile foundation depth is, undoubtedly, one of the most relevant aspects of the foundation design. At this site, the foundation depth is defined by the vertical loading exclusively. In order to approach this issue, different foundation conditions were defined for the experimental piles. Table 2 shows some characteristics of the 3 test locations.

Figures 4, 5 and 6 present a summary of the informations mencioned above.

5.2 *Load plan*

According to COBA's information, the work load shall be estimated considering a normal stress of 5.5 MPa. For the test piles (ϕ 800 mm), this corresponds to a work load of approximately 2800 kN.

The maximum test load was established in 9100 kN (3.25 times the work load), where such value is limited by the reaction metallic framework resistance. Regarding the test procedure specifications proposed by COBA, the necessary changes were implemented, to take into account the stricter criteria with respect to the stabilization times.

6 TESTED PILES MONITORING

6.1 *Load measurement*

The test load was applied with the help of two hydraulic jacks. The load measurement was accomplished by using two load cells placed between the reaction structure and the hydraulic jacks, as shown in Figures 12 to 14.

6.2 *Displacement and rotation measurement*

Monitoring of the vertical displacement of the pile head was undertaken in two independent ways, intended to produce redundant readings: a) by means of transducers; b) by means of topographic readings.

Four retrievable transducers were installed on the top of the pile (over the reducer). The transducers were laid over a supporting structure built with metallic beams (Figure 14). The topographic measurements showed that the vertical displacements of this supporting structure with respect to the permanent reference level were practically negligible (lower than 1 to 2 mm) in comparison with the pile displacements.

Figure 12. Reaction system.

Figure 13. Reaction system.

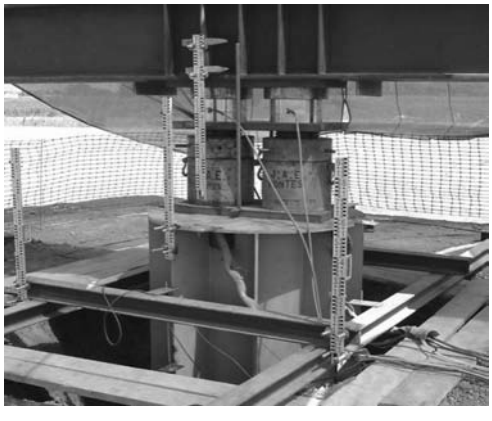

Figure 14. Reaction system (from top to bottom): metallic structure; leveling plate; load cells; leveling plates; hydraulic jacks; leveling plates; reducer (the same used in the dynamic test) and support beams for the transducers that measure the vertical displacement.

Table 2. Static vertical load tests.

Test	Bore hole	Piezocone tests	Pile end bearing condictions	Test date
1	S 227	SCPTU 309	~ 1 diameter into miocenic (M1)	10 to 12 of July 2005
2	S 226	SCPTU 308	~ 3 diameters in "cascalheiras" (a3)	15 to 17 of July 2005
3	S 220	SCPTU 307	~ 3 diameters into miocenic (M1)	23 to 25 of July 2005

During testing, the rotations on the top of the pile were also measured by means of a *tiltmeter*. The maximum values recorded in the 3 tests were respectively 0.13°, 0.30° and 0.36°, thus confirming that the loading was axial, the rotations on the top of the pile being practically negligible.

6.3 *Retrievable extensometers*

Instrumentation along the pile length allowed the determination of the mobilized resistances (base and side friction) during loading.

Figure 15. Detail of a *retrievable extensometer*.

In each test pile, 3 steel pipes were installed in the pile to attach the sensors, composed by: anchors, carbon fiber rods and retrievable transducers—*retrievable extensometers*, of Geokon (Figure 15). In use, the extensometer incorporates a string of electronic displacement sensors linked together by extension rods and designed to mesure the relative displacement between a series of pneumatically expandable anchors. The string of sensors is assembled (with variable lengths of connecting ros to enable positioning of the anchors at the required depths), inserted into the pipe and than locked in position by pneumatically actuating the various anchors, which remain fully expanded throughout the monitoring period. Figure 16 presents the anchor numbering and the symbology adopted. Table 3 and Figures 17, 18 and 19 show the anchors' localization.

Figures 17, 18 and 19, also show the subsoil profile description according to the probing profiles.

Carbon fiber rod, anchor, retrievable transducer and carbon fiber rod (from left to right).

The axial load in each elevation was estimated taking into consideration the pile's theoretical section with an 800 mm-diameter. The first instrumented level is located very close to the free surface of the excavated terrain (Figure 16), therefore, the corresponding axial load shall be the same as the load measured on the pile top. Based on this premise, it was possible to

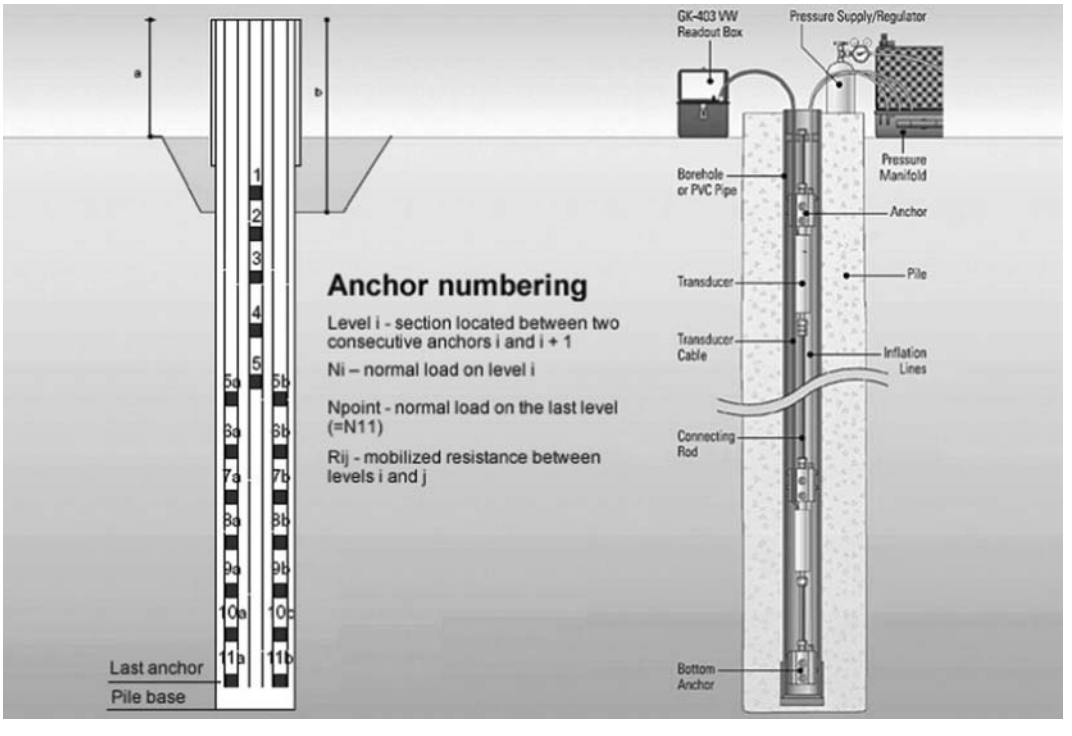

Figure 16. Anchor numbering.

Table 3. Anchors localization.

Anchor Position	Test 1 km 8 + 200 July 10 to 12/2005 a = 0.5 m; b = 2.10 m Depth regarding the surface level (m)	Test 2 km 7 + 900 July 15 to 17/2005 a = 0.6 m; b = 2.50 m Depth regarding the surface level (m)	Test 3 km 5 + 400 July 23 to 25/2005 a = 0.4 m; b = 2.00 m Depth regarding the surface level (m)
1	1.5	1.5	1.5
2	2.5	2.5	2.5
3	6.5	6.0	9.0
4	16.5	10.5	15.0
5	28.5	19.0	24.0
5a & 5b	29.0	19.0	28.0
6a & 6b	33.0	23.0	32.0
7a & 7b	37.0	27.0	36.0
8a & 8b	41.0	30.0	40.0
9a & 9b	45.0	34.0	44.0
10a & 10b	49.0	38.0	48.0
11a & 11b	53.0	42.0	52.0
12a & 12b	54.0	43.5	53.0

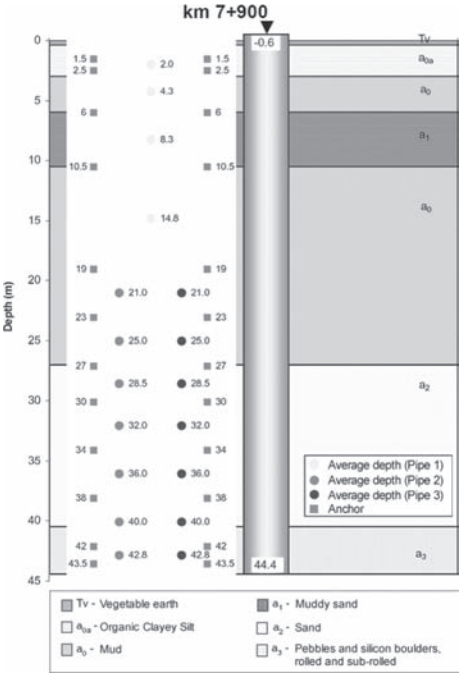

Figure 18. Test 2: Anchor location.

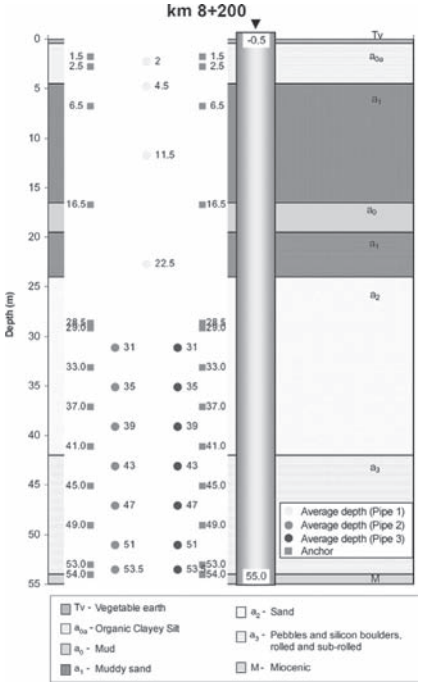

Figure 17. Test 1: Anchor location.

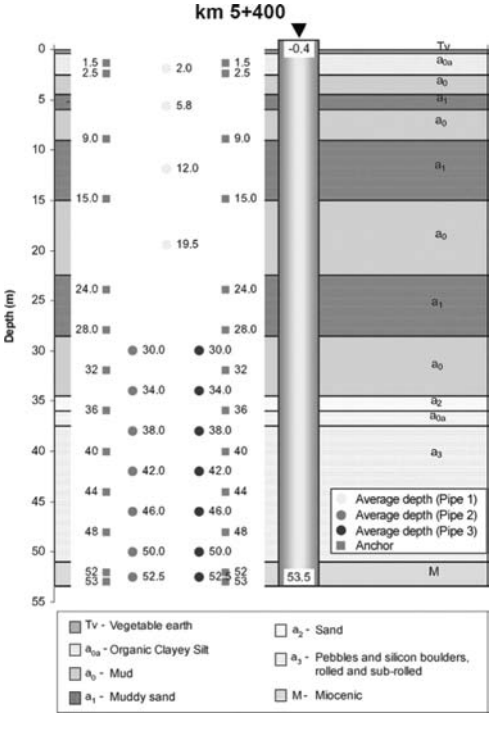

Figure 19. Test 3: Anchor location.

determine the concrete's module of elasticity (E) with respect to the deformation (ε), as shown in Table 4. It is worth pointing out that the values so obtained are in accordance with the cure time elapsed between the concrete pouring and the beginning of the test.

In Test 2 (km 7 + 900), it was not possible to apply the same methodology to estimate the modulus of elasticity. The first level record presents too much noise (mainly for the lower load levels) due to the oil pump that was installed close to the test pile. Taking in consideration the cure time, the result was simplified to E = 30 GPa.

Based on the axial load distribution along the depth, it was possible to estimate the "average" lateral resistance among levels. Figures 20, 21 and 22 represent the lateral resistance evolution (per unit area)

Table 4. Pile's modulus of elasticity.

Test	Place	Concrete pouring date	Test date	Module of elasticity
1	km 8 + 200	June 9	July 10 to 12	For $e = 2.5 \times 10 - 4$: E = 30 GPa For $2.5 \times 10 - 4 < e < 7.5 \times 10 - 4$: $E = 30 - 5 \times (e\text{-}2.5 \times 10 - 4)/(5 \times 10 - 4)$
2	km 7 + 900	June 23	July 15 to 17	E = 30 GPa
3	km 5 + 400	July 12	July 23 to 25	For $e < 10 - 4$: E = 24.5 GPa For $10 - 4 < e < 1.1 \times 10 - 3$: $E = 24.5 - 5 \times (e\text{-}10 - 4)/(7 \times 10 - 4)$

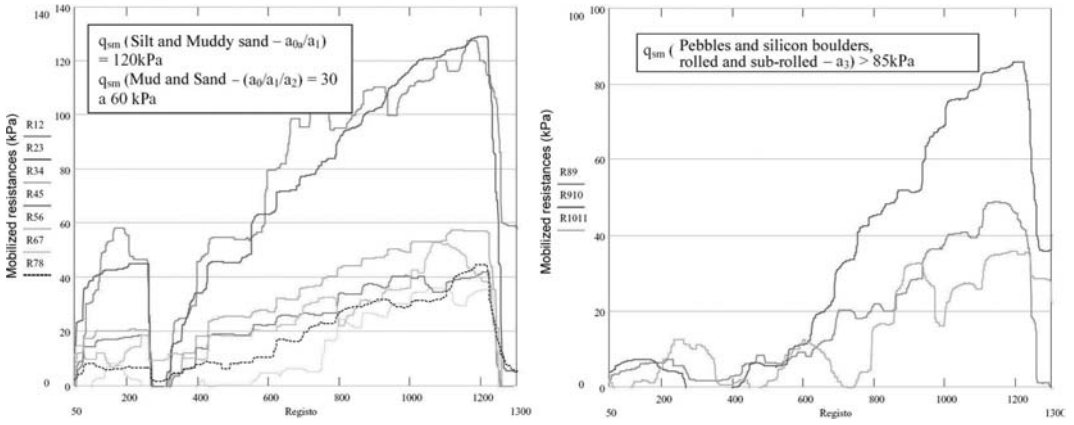

Figure 20. Test 1: Mobilized resistances (between instrumented elevations).

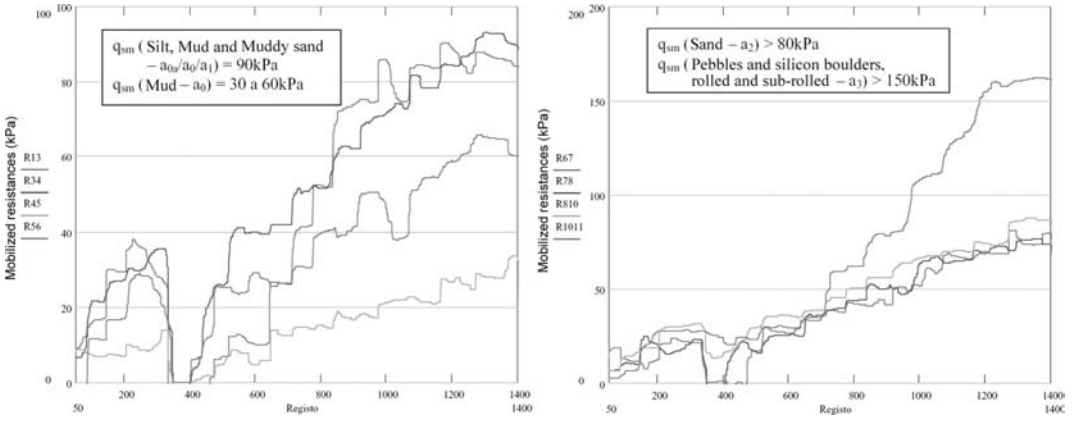

Figure 21. Test 2: Mobilized resistances (between instrumented elevations).

for tests 1, 2 and 3, respectively. These figures also present the mobilized resistances (qsm) in the different soil layers. Considering these datas, the tests point out to the following values:

6.4 *Axial load distribution along the depth*

In order to assess the contributions of the lateral and base resistances, the axial load distribution was determined for loadings 4 and 19, corresponding to the work load and to the maximum test load, respectively. The results are presented in Figures 23, 24 and 25, together with the respective geological-geotechnical conditions.

The contributions of the pile shaft and point can be represented by the values listed in Table 5. The lateral resistance contribution is notorious in any of the cases. The base contribution is limited to approximately 10% and its rigidity increases according to the improvement in the foundation conditions (refer to Table 2).

Table 5. Mobilized resistances.

Formation	Lateral resistance (kPa)
a0a/a1/a0 superficial (up to 10 m deep)	90 to 160
a0a/a1/a0 (below 10 m deep)	20 to 80
a2—sand	= 80
a3—cascalheiras	= 85 to 150
M—miocenic	= 130

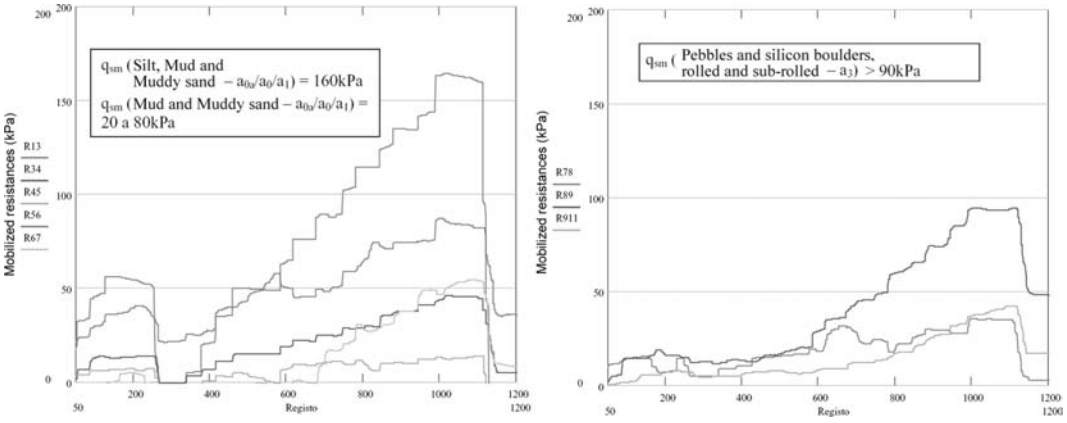

Figure 22. Test 3: Mobilized resistances (between instrumented elevations).

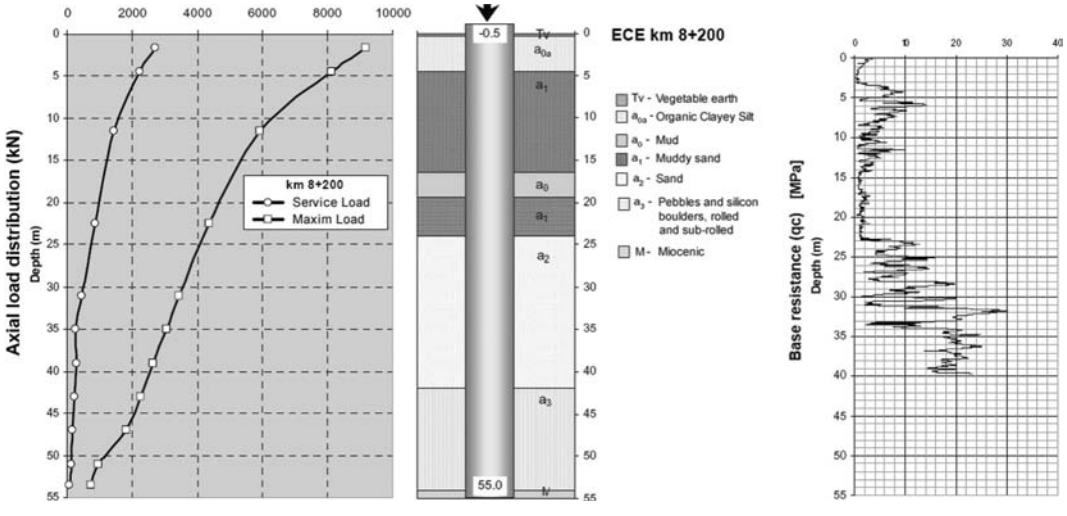

Figure 23. Test 1: Axial load distribution.

7 DYNAMIC LOADING TESTS

The performance of dynamic loading tests was suggested by the ICIST-IST's and GEOMEC's teams, being complemented by the static loading tests.

The initial test program was adjusted during the works, taking in consideration the information supplied by the static tests. Dynamic loading tests were performed in 9 experimental piles, as shown in Table 7.

The piles submitted to the static loading test (compression), were later dynamically tested. Two reaction piles were equally chosen for the dynamic loading tests.

In order to carry out the tests, the GEOMEC's and the ICIST-IST's teams conceived a specific equipment, called SIPEX—Impact System for Experimental Piles, using the free fall of two weights of 100kN each, which are capable of acting together or separately. The system is also composed by a guide tube and an attached steel cap block that is placed over the pile, acting to ensure the centered and vertical application of the impact, and also as a protection against eventual damages to the pile head (Figure 32). This equipment above is capable of testing ϕ 1500 mm-piles, but can also test lower diameter piles using a reducer (Figure 33).

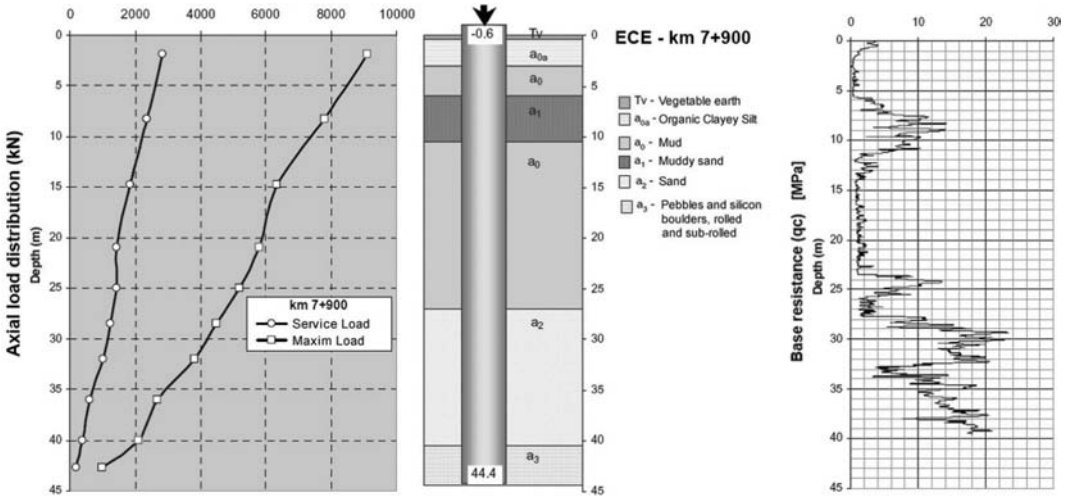

Figure 24. Test 2: Axial load distribution.

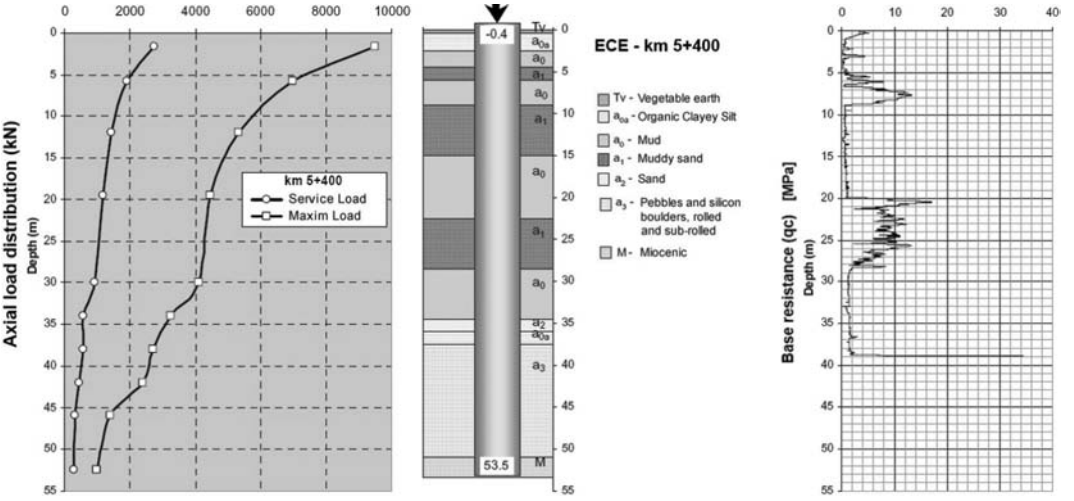

Figure 25. Test 3: Axial load distribution.

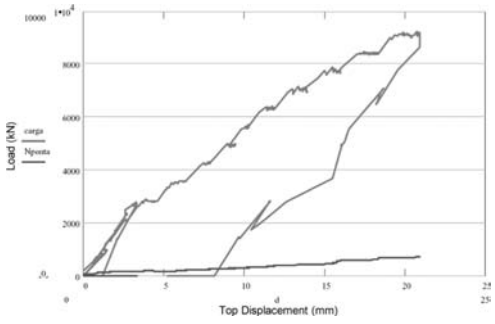

Figure 26. Test 1: Load—displacement curve.

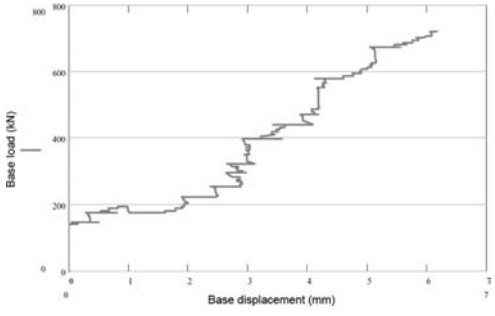

Figure 27. Test 1: Base load—displacement curve.

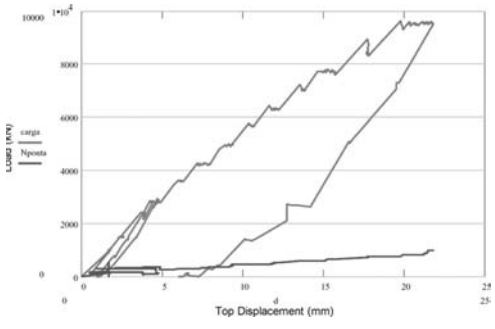

Figure 30. Test 3: Load—displacement curve.

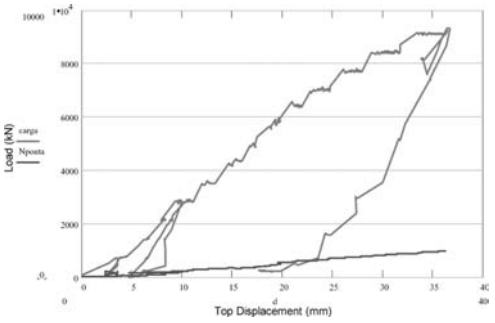

Figure 28. Test 2: Load—displacement curve.

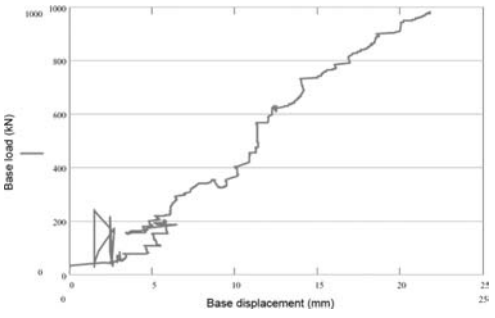

Figure 29. Test 2: Base load—displacement curve.

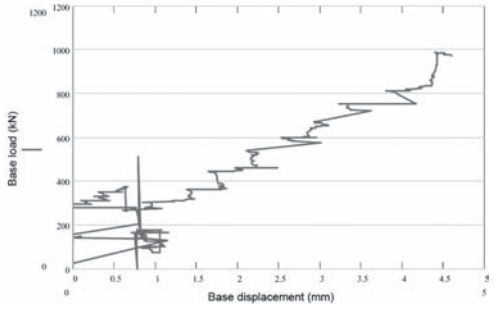

Figure 31. Test 3: Base load—displacement curve.

Table 6. Contributions of the shaft and point resistance.

Test	Average lateral resistance qs, average (kPa)	Maximum load Average lateral resistance qs, average (kPa)	Maximum load Base	Lateral	Base rigidity
1	21	65	8%	92%	~=100 000 kN/m
2	26	79	11%	89%	~=50 000 kN/m
3	19	67	10%	90%	~=200000 kN/m

Figure 32. SIPEX—Impact system for experimental piles.

Figure 33. Placement of the reducer over a ϕ 800 mm-pile.

Table 7. Dynamic loading tests performed.

Place	Diameter	No. of piles tested	Tests
Adjacent test 1	800 mm	2	i) ECE + ECD ii) ECD
Adjacent test 1	1500 mm	1	ECER + ECD
Adjacent test 2	800 mm	2	i) ECE + ECD ii) ECD
Adjacent test 3	800 mm	2	i) ECE + ECD ii) ECD
Adjacent test 3	1500 mm	2	i) ECER + ECD ii) ECD

Note: ECE—Static loading test; ECD—Dynamic loading test; ECER—Reaction pile used in the static loading test.

The test piles received a reinforced concrete extension of 1.50 m, enveloped by a steel casing. The reducer from 1.50 m to 0.80 m was also used in the static loading tests, to allow the placement of two hydraulic jacks. The system also includes rubber sheets to dampen and equalize stresses, one being placed between the pile and the attached steel cap block (or the reducer), and the other between the steel cap block and the hammer.

Figure 34. Detail of the dynamic instrumentation (at left: extensometer; at right: accelerometer.

In the tests performed, the instrumentation implementation followed two complementary lines of action:

a. in 5 ϕ 800 mm-piles and 2 ϕ 1500 mm- piles, all the transducers were installed on the surface, in 4 pairs of 1 accelerometer and 1 extensometer, placed at every 90° of the pile's perimeter (Figure 34);
b. in one of the ϕ 800 mm-piles and in one of the ϕ 1500 mm-piles, 2 accelerometers were embedded inside the pile (one at half depth and one on the point of the pile), the other measurement instruments were installed on the surface as in the remaining piles. The two embedded accelerometers were attached to the shell, during its descent through the bore.

The length of the fall and the number of blows were adjusted along the works in regard to the data collected in the field.

In most cases, a test methodology calling for an increasing fall length was implemented, so the energy transferred to the pile would also increase in consecutive blows. Such procedure allowed the assessment of the mobilized resistance evolution with the increase of the energy supplied.

Table 8 presents a summary of the results obtained in the dynamic tests, with the indication of the mobilized load (Q), the point resistance (Rb), the lateral resistance (Rs), the point contribution (%Point), the ratio between the mobilized load and the work load (Q/QS), the ratio between the lateral resistance and the maximum mobilized lateral resistance (Rs/Rs,max) and the average lateral resistance (qs, average).

The dynamic test results confirm the trends observed in the static tests. The average lateral resistance values (qs, average) are in accordance with the values obtained in the static tests (refer to Table 5), and were not affected by the pile diameter. With respect to the point contribution, the scale effect is obvious. In the 1500 mm-diameter piles the point contribution is represented by values of about 25%, while for the 800 mm-diameter piles the values were, in general, lower than 16%, either in the dynamic tests or in the static tests (<11%).

Table 8. Summary of the dynamic test results.

Place	Loading situation	Pile	Q (kN)	Rb (kN)	Rs (kN)	%Point	Q/QS	Rs/Rs,max	qs,average (kPa)
Adjacent test 1	a	E800D-3	3350	292	3058	9	1.21	0.23	23
Adjacent test 1	b	E800D-3	8967	847	8120	9	3.24	0.62	61
Adjacent test 1	c	E800D-3	15289	2100	13189	14	5.53	1.00	100
Adjacent test 1	a	E800E-3	5000	350	4650	7	1.81	0.35	34
Adjacent test 1	b	E800E-3	9059	1037	8022	11	3.28	0.60	59
Adjacent test 1	c	E800E-3	15499	2150	13349	14	5.61	1.00	98
Adjacent test 1	a	E1500R-3	9577	2347	7230	25	0.99	0.79	29
Adjacent test 1	c	E1500R-3	13413	4280	9133	32	1.38	1.00	65
Adjacent test 2	a	E800D-2	2861	469	2392	16	1.03	0.32	22
Adjacent test 2	b	E800D-2	7637	2107	5530	28	2.76	0.75	51
Adjacent test 2	c	E800D-2	9635	2233	7402	23	3.49	1.00	69
Adjacent test 2	a	E800E-2	2770	334	2436	12	1.00	0.39	23
Adjacent test 2	b/c	E800E-2	7483	1179	6304	16	2.71	1.00	59
Adjacent test 3	a	E800D-1	3980	249	3731	6	1.44	0.24	30
Adjacent test 3	b	E800D-1	8650	1392	7258	16	3.13	0.47	59
Adjacent test 3	c	E800D-1	18948	3514	15434	19	6.85	1.00	125
Adjacent test 3	a	E800E-1	5271	320	4951	6	1.91	0.50	38
Adjacent test 3	b	E800E-1	7900	937	6963	12	2.86	0.70	53
Adjacent test 3	c	E800E-1	11200	1283	9917	11	4.05	1.00	76
Adjacent test 3	a	E1500R-1	6700	1855	4845	28	0.69	0.36	25
Adjacent test 3	c	E1500R-1	17601	4251	13350	24	1.81	1.00	70
Adjacent test 3	a	E1500H-1	7948	1888	6060	24	0.82	0.47	25
Adjacent test 3	c	E1500H-1	17317	4482	12835	26	1.78	1.00	53

Loading situation: a—blow closer to the work load; b—blow closer to 3 times the work load; c—blow that mobilized the higher load

The rupture of the soil-pile system is defined when the mobilized resistance does not show up when the impact energy increases. It should be pointed out that the maximum mobilized load in the dynamic tests was fundamentally governed by the concrete resistance. In order to make possible the mobilization of the resistance of the deeper strata, it was necessary to apply high-energy impacts, which caused damages to the test piles. When this happened, the test ended (Figure 35).

Figure 35. Damage to the pile after a high-energy impact.

8 CONCLUSIONS

From the construction point of view, it can be concluded that:

- the construction methodology proposed was perfectly assessed during the pile testing.
- recovery of the large diameter and deep casing, including the vibrator, is a feasible solution when the use of bentonite slurry or polymer is not advisable or forbidden.
- the environmental restrictions can be perfectly complied with, particulary having in mind the existence of cultivated area.
- "cross-hole" tests performed in each pile allowed the reliable confirmation of the the reliable construction quality.

Based on the static and dynamic test results, it can be concluded that:

- static tests, governed by the reaction system, were carried out up to about 3.25 times the work load (in 800 mm-diameter piles).
- dynamic tests were limited by the concrete resistance (on the top of the pile) and not by the subsoil resistance. In some cases, very high load levels were achieved (6.9 and 1.8 times the work load, for the 800 mm and 1500 mm-diameter piles, respectively).
- simultaneous performance of the static and dynamic tests allowed the interpretation and

postulation of the resistances involved in the several soil layers.

- on the test locations, due to the high superficial resistance levels and the large pile length, a high lateral resistance was observed. As a result: a) the non-linearity of the system is not very significant in the load-settlement curves; b) the settlement associated to the work load is low (lower than 1 cm); c) the base contribution is also low.

REFERENCES

CAPUTO, H.P.—Mecânica dos Solos e suas Aplicações (Soil Mechanics and its Applications). Volume II.

CODUTO (1994)—Foundation Design—Principles and Practices.

MELLO, L.G. and BILFINGER, W (March/2005)—Avaliação do Método Construtivo das Estacas para as Foundações dos Viadutos de Acesso à Ponte sobre o Rio Tejo—Aspectos associados à presença de solos argilosos moles (Assessment of the Pile Building Method for the Foundations of the Access Bridges to the Bridge over the River Tagus—Aspects associated to the presence of soft clayish soils).

SANTOS, J. (Agosto/2005) IST—Instituto Superior Técnico—Tests de carga em Estacas Experimentais—Relatório de Análise (Load Tests in Experimental Piles—Analysis Report).

Ferreira,S., Rebelo,V. and Ribeiro,J. (IV Congresso Luso-Brasileiro de Geotecnia-abril/2008)-Lezíria Bridge Pile Foundations.

Deep Foundations on Bored and Auger Piles – Van Impe & Van Impe (eds)
© 2009 Taylor & Francis Group, London, ISBN 978-0-415-47556-3

Comparison between Osterberg and Statnamic load test on large diameter drilled piles

Luiz Guilherme de Mello
Escola Politécnica da Universidade de São Paulo, Brazil
Vecttor Projetos, Brazil

Guilherme Robbe
Vecttor Projetos, Brazil

Werner Bilfinger
Vecttor Projetos, Brazil

ABSTRACT: This paper's aim is to present a comparison between results obtained from two different axial compression load tests on large diameter drilled piles. It presents a quick review of available load tests techniques for large diameter drilled piles and the data from the Carlos Perez Perasso bridge foundation, where two load tests with Osterberg load cells and four tests using Statnamic's method were held; in a specific pile group, therefore in the same subsoil profile, a test of each type was performed. Results and their analysis are presented. Unit side resistance and end bearing capacities are proposed for local soils and rocks

1 LOAD TESTS

Full-scale axial load tests method vary depending basically in the way load is transferred to the pile during the test and how the resulting data is interpreted. Usual pile load tests types can be subdivided in: static maintained load, load/settlement equilibrium (staged test), quick maintained load, continuous rate of penetration, pseudo-static and dynamic tests.

In static tests loads are generally applied gradually to the pile head using a reaction system, such as anchors or piles associated with steel frames and hydraulic jacks; the Osterberg method introduced loading through flat jacks installed and concreted in different pile elevations. In dynamic tests the pile is stuck with a hammer and the resulting stress waves through the pile length are interpreted using measured strains and accelerations following an accepted theoretical framework. Pseudo-static tests usually impose a high-energy blow to the pile, of relatively long duration if compared to dynamic tests, and the energy wave along the pile is monitored and interpreted.

Once a pile is loaded during a test the immediate subsequent concern is the interpretation of the data so that the data derived and used in subsequent analysis really represents the physical conditions at the site.

When large piles have to be tested a major problem to be discussed is related to the magnitude of the loads involved, both the load to be applied by the superstructure and the test load. Special methods and equipments were developed for these cases, assuring that loads 1.5 to 2.0 times higher than the pile design load can be applied to the element being tested.

Some codes, like Eurocode 7, AASHTO or the brazilian foundation code, allow for a reduction of design factor of safety for piles if design is based on parameters back-analyzed from piles specifically installed and tested prior to commencement of the works. This is a relevant tool for site specific optimizations, leading to substantial savings in large piling works.

2 INTRODUCTION—DESCRIPTION OF THE PROJECT

The Carlos Perez Perasso bridge, over the Daule river in Quayaquil Ecuador, is 1032 m long, being founded on 11 pile groups and 2 abutments. Works for adapting the existing lanes of the bridge for the local new seismic design code[1] led, among many other specialized works, to the necessity of installing new piles and incorporating the existing pile cap to the geometry to be formed by the new pile group. The local authorities also decided to build a parallel new bridge, doubling the number of traffic lanes between Guayaquil and Entrerios.

[1] called Retrofit works.

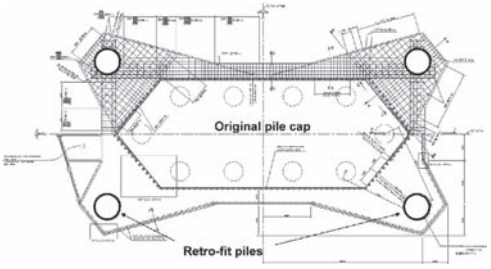

Figure 1. Pile cap of the retro-fit of the existing bridge.

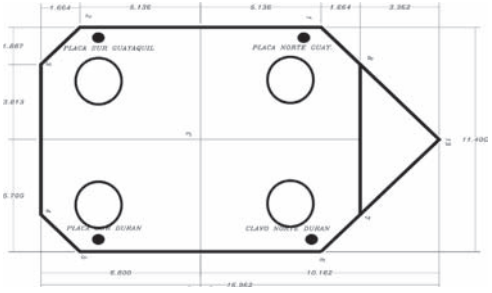

Figure 2. Typical pile cap of the new bridge.

The Designers[2] opted for large diameter cast *in situ* concrete piles and proposed, for basic design and bid purpose, lengths of piles based on documents available from the construction of the initial bridge. The large diameter piles were defined to be 2.5 m diameter steel lined during excavation, and the contractor proposed use of reverse circulation drill rigs with permanent steel casings to partial depths, without use of stabilizing bentonite slurry or other stabilizing fluids. Working loads for the 2.5 m diameter piles are in the order of 15.000 KN.

Pile installation was associated to difficult conditions, including high flow velocities due to tidal currents and typical technical and logistical problems of pile construction in Daule river.

Pile installation started from the Guayaquil abutment. The subsoil profile, as interpreted from the material excavated by the reverse circulation equipment, showed to be distinct of the subsoil profile postulated during design phase, discussions related the required pile depths led to a complementary site investigation program.

New deep boreholes were proposed and implemented, leading to at least one deep borehole per pile group, and the pile test program was anticipated and enhanced, to include tests by different procedures—static and pseudo-dynamic. As part of design, to check its hypothesis as well as to allow some decisions and improvements to be included in the on going works, the load test campaign as defined consisted of:

- Two static and instrumented Osterberg load tests;
- Four Statnamic load tests.

The tested piles are working piles, which were chosen considering the work progress, being, for the Osterberg tests piles P 9-1[3] e PD1-3 and for the Statnamic tests piles P 8-1, P 9-3, P 11-4 e PR 28-3. On one pile group, P 9, pile number 1 was tested by the Osteberg method, while pile 3 was tested using the Statnamic procedure.

3. LOCAL SUBSOIL STRATIGRAPHY

The site is located in a very complex and active tectonic context, due to its proximity to the subduction zone of the Pacific Plate under Ecuador, and the proximity to the active fault sistem of Pallatanga (Shear Zone Dolores Guayaquil, Romeral, etc). Numerous of these active faults intercept recent deposited strata in the region. Local rocks are represented by the Cretaceous age Cayo Formation rocks.

Above Cayo Formation a 60 meters thick light brown calcareous strata, with frequent silex noduli is identified as San Eduardo Formation. Above both formations, Tertiary sediments (Progresso and Subibaja Formations among others) are present, followed by younger sedimentary deposits, including sandstones, siltstones, swelling mudstones and volcanic tuffs. Their identification is complex, being frequently based on the analysis of existing fossils.

In the project area, the sands, silts and volcanic tuffs underlying the basal gravels as identified in the basic design documents, correspond to strata from the upper tertiary to the pleistocene (25 to 1,6 million years), while the strata above this gravels possibly are quaternary. In the context of the design calculations and interpretation of the load tests that follow, the representative subsoil profile of the area can be summarized as:

- superficial layer of very soft to soft sitly-clayey and clayey-silty sediments;
- sandy and clayey-sands soils of medium compact to compact consistency;
- very compact sandy layers with gravel;
- weathered rocks, with an erratic transition to sound rocks. The rock layers are very heterogeneous, with

[2]T.Y.Lin International, Consulsismica, A.E.T. and Geomatrix—CATGE Association.

[3]Nomenclature is such that the first number if the pile group number, and the second number the pile number in the group.

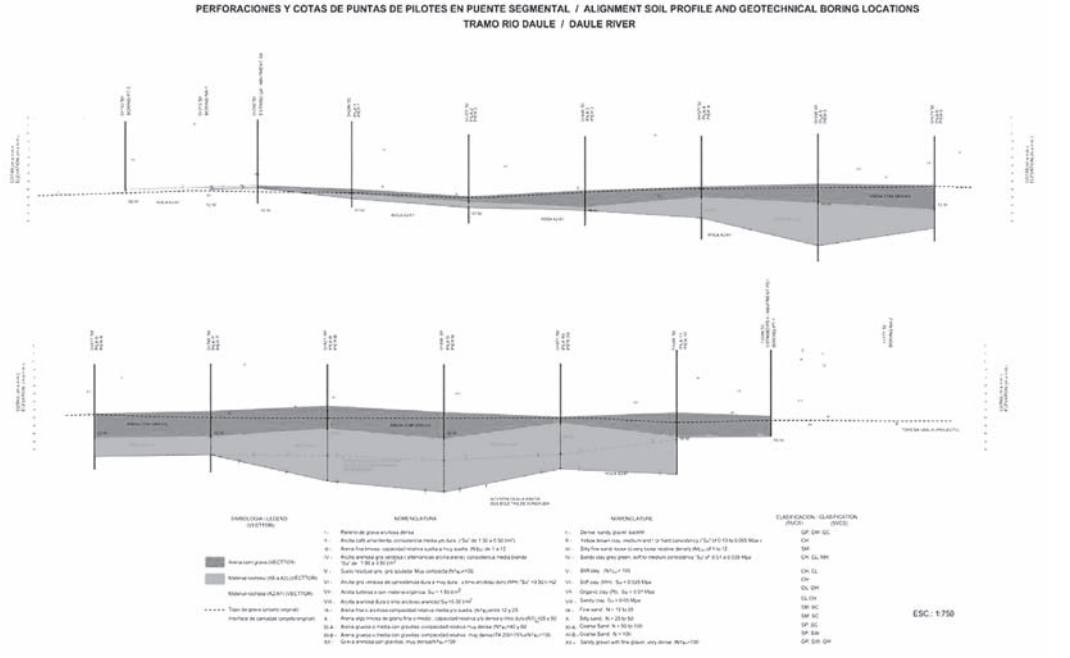

Figure 3. Longitudinal cross section of subsoil in the bridge's alignment.

very weathered materials occurring underneath sound rocks.

The simplified subsoil profile can present abrupt variations, related to the meandering of the river system, which probably has gone through many erosion/ deposition cycles.

4. PILE DESIGN METHODOLOGY

A series of *in situ* and laboratory tests were performed to back design calculations, together with percussive and drilled boreholes. Design calculations were done following ASSHTO recommendations for rock socketed piles, being calibrated by static calculations based on local experience. Adopted geomechanical design parameters were estimated from vane tests performed in the soft soil layers; direct shear and UU and CU triaxial tests held in the laboratory, associated to sample characterization tests.

5. LOAD TEST PROGRAM

The load tests performed on pile P 9-1—with an Osterberg O-cell, and on pile P 9-3—with Statnamic procedure are of particular interest for the interpretations aimed in this contribution as the subsoil profile can be assumed practically constant in the area of the pile cap for bridge column and pile group 9.

Pile P 9-1, with nominal diameter of 2,5 m, has a permanent steel casing to elevation –44 meters, as all piles constructed in water; the real volume of concrete poured in the pile was determined as being 2,5% slightly greater than the theoretical pile volume, probably associated with some caving beneath the steel casing, as the pile tip was excavated without stabilizing fluid in "*sands with gravels*" as described at the adjacent borehole.

For pile P 9-3 the same geometry and construction method was used, with a permanent steel casing to elevation –44,6 meters.. The pile tip was excavated in the same material as pile P 9-1. Unfortunately volumetric installation data is not available for this pile.

The net load-settlement behavior of this pile, as obtained from the Osterberg test, above and beneath the O-cell is presented in Figure 4, with the pile weight already subtracted from the applied loads. Figure 5 below presents the strain gauge load distribution curves interpreted for the Pile P 9-1 test. Data obtained from the Statnamic test performed on adjacent pile 9-3 is presented in the following Figure 6.

5.1 *Pile tip behavior*

The load—settlement curve interpreted from the displacement gauges installed in the pile, for pile P 9-1 tip is presented in Figure 7. The Statnamic test data performed on pile 9-3 as interpreted by the specialized subcontractor is presented in the following figure 8.

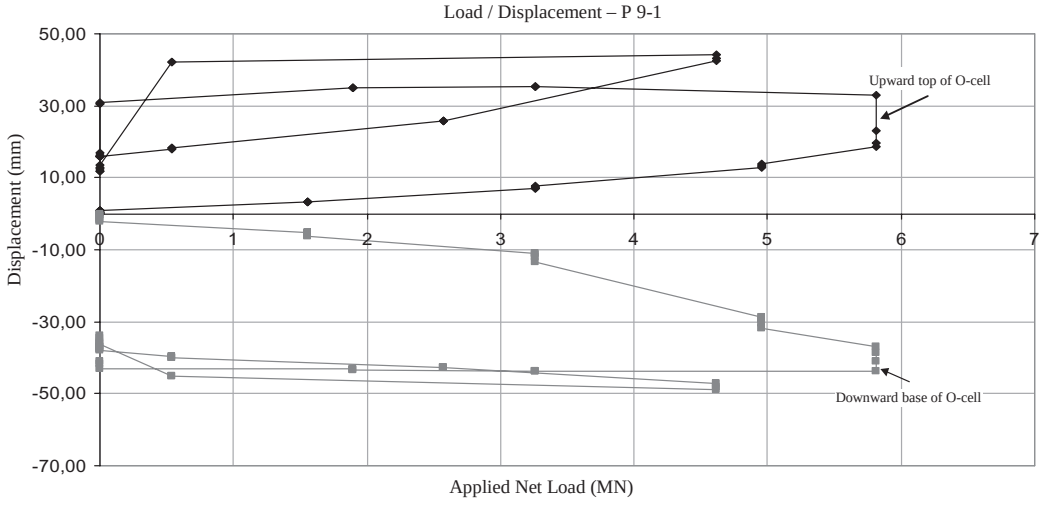

Figure 4. Net load—settlement behavior Pile P 9–1.

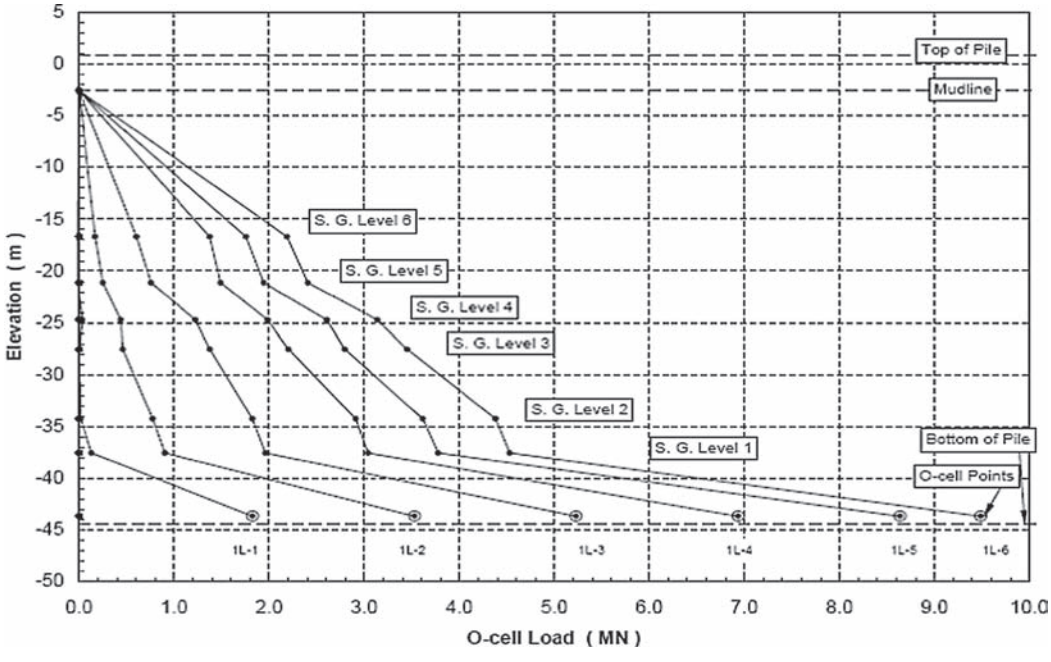

Figure 5. Interpreted load at strain gauges levels—Pile P 9–1

5.2 *Shaft behavior*

Interpretation of the load test on pile 9-1, considering a proper hypothesis for the structural concrete modulus of elasticity of 40 GPa and the theoretical pile geometry, leads to the average adhesion for each soil layer as presented in figure 9 beneath; the subsoil profile of the borehole performed in this pile group is presented at its side.

The shaft side friction as obtained in the Statnamic test performed on pile 9-3 leads to difficulties in associating consistent values directly with soil types, with some side friction values that could not, in our

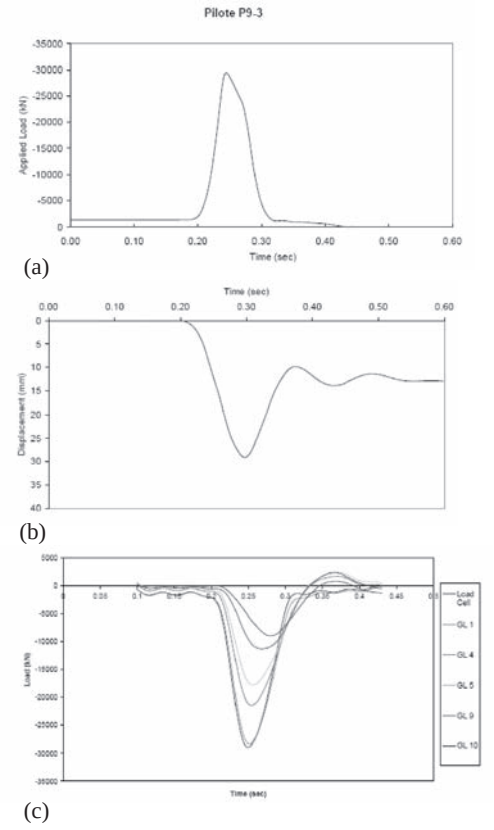

Figure 6. Routine test data as supplied by Statinamic test on Pile 9-3, including: (a) Applied load x time, (b) Pile top displacement × time, and (c) Loads at stains gauge levels × time.

Table 1. Unit side resistance and side resistance loads, as obtained in both load tests.

Soil type	Pile P 9-1 (kPa) *Osterberg test*	Pile P 9-3 (kPa) *Statnamic test*	Pile P 9-1 (kN)	Pile P 9-3 (kN)
Alluvial deposits ($N_{SPT} < 2$)	1	25	627	6704
Alluvial deposits ($N_{SPT} > 2$)	14 a 16,5	33		
Fine to medium grained sand	1	–	4243	4698
Coarse grained compact sand with gravel	78 a 90	40		

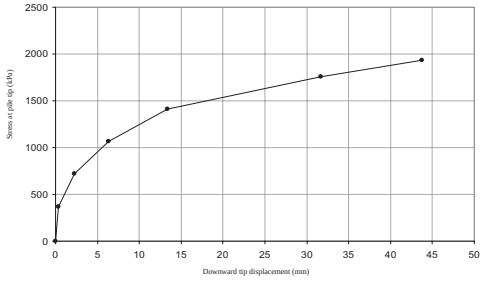

Figure 7. Pile 9-1 tip behavior.

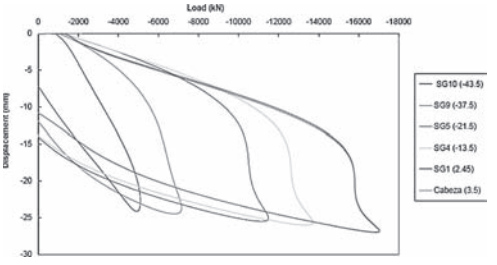

Figure 8. Interpretation of the Pile top displacement x static load of Pile 9-3, as supplied by Statnamic test.

Table 2. Mobilized load and residual displacement—Pile P 9–3.

Pile	Total mobilized load (kN)	Residual vertical displacement (mm)
P 9-3	16.8	13,4

interpretation, represent physical reality. A comparison of the plotted values, side shear resistance per "constant strata", is presented in Table 1.

6. CONCLUSIONS

The pile tip of pile 9-1 resisted to an average pressure of 1800 kPa, equivalent to a tip load of 8800 kN, values distant from full mobilization as seen in the available graphs. In summary, test on pile 9-1 mobilized a load of 14300 kN (side friction and pile tip), 60% of which associated to the pile tip. The equivalent modulus of deformability of the material at the pile tip can be postulated as being of 36,1 MPa to the stress levels applied on the pile.

For the Osterberg test performed on pile 9-1, the average side friction leads to a shaft resistance of 5500 kN, which can be associated to ultimate values, as the behavior measured in the test infers full mobilization of side friction.

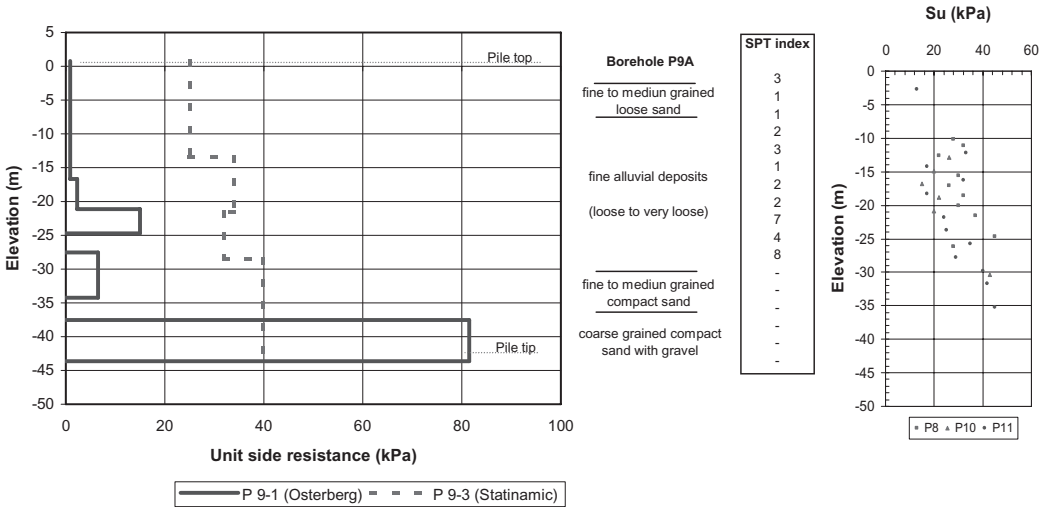

Figure 9. Average unit side resistance profile for Piles P 9-1 and P 9-3.

Table 3. Mobilized load (side friction and pile tip)—Piles P 9–1 and P 9–3.

		Side resistance		Pile Tip	
Pile	Total mobilized load (kN)	Total Mobilized (kN)	Averade unit side resistance (kPa)	Mobilized load (kN)	Average stress (Mpa)
P 9-1	14.300	4.872 (31%)	12	946 (69%)	1,93
P 9-3	16.800	11.080 (66%)	31,4	5.720 (34%)	1,1

For the Statnamic tests, the interpretation as done by the specialized subcontractor, informs that the load mobilized and the residual displacements are shown in Table 2. The interpretations developed also indicate the shaft side friction resistance as a function of depth, and the mobilized tip load, as presented in Table 3.

Load tests results indicate similar average results for the side resistance at sand and granular soils. Differences between strain gauges levels as installed in piles P 9-1 and P 9-3 lead to different average side resistance values obtained.

Failure of the pile tip was not observed during either test. Ultimate bearing capacities were estimated for piles P 9-1 and P 9-3 according to the method proposed by Reese & O`Neil (1988) for extrapolation of the pile tip *load x displacement* curves. These extrapolations indicated average ultimate bearing capacity of 4,0 and 3,3 MPa for piles P 9-1 and P 9-3, respectively, leading to ultimate pile capacity values of 24,5 and 27,3 MN.

REFERENCES

Geotecnica Cientec. "*Report on drilled pile load testing—Statinamic Method*". Report ref. I-1–05-STN.

Load Test. "*Report on drilled pile load testing—Osterberg method"*. Report ref. 2176–2/P-9–1.

M. England, W. G. K. Fleming. "*Review of foundations test methods and procedures*". Proceedings of the Institution of Civil Engineers, 1994.

USACE. Design of pile foundations—Chapter 6 "*Field pile tests*".

AASHTO. Roadway bridges, Division 1—Foundations design, item "*Load tests*"

EUROCODE 7—Geotechnical Design.

ABNT 1996—Brazilian Foundation Standard *in Portuguese.*

Deep Foundations on Bored and Auger Piles – Van Impe & Van Impe (eds)
© 2009 Taylor & Francis Group, London, ISBN 978-0-415-47556-3

Review of methods of analysis of test results from bi-directional static load tests

M. England
Loadtest, Sunbury, UK

ABSTRACT: Results from bi-directional tests are not the same as those obtained from top loading tests and although bi-directional test data often contain more geotechnical information, it is the characteristic behaviour of the head of the pile which is of interest. In order to provide an equivalent top loading characteristic, methods have been developed to enable the addition of the individual components measured.

Bi-directional loading test results automatically separate the resistance of each component which then require suitable combination and analysis to reconstruct the equivalent top load characteristic of the pile.

This paper aims to describe and review the merits of some of the direct methods currently employed and some of the analysis methods which can be used as well as the application of finite element analyses using measured behaviour.

Keywords: Loadtest, Osterberg cell, O-Cell, static load tests, bi-directional load test.

1 INTRODUCTION

Application of the method of bi-directional testing results in the foundation element under test being separated in more than one element and each is static load tested separately or in combination. For example, with a single level loading arrangement, as illustrated in the diagram of Figure 1, effectively two independent static load tests are performed simultaneously and produce two completely separate sets of results, England (2003).

Bi-directional loading tests using Osterberg cells (O-cells®) are now becoming common practice (with over 300 tests performed per year) around the world, England et al (2006), particularly where the loads to be applied are high >10MN or where it is not convenient to perform traditional top-down loading tests.

The O-cell is a hydraulically driven, high capacity, sacrificial jack-like device, installed within the foundation unit. When pressurised, it applies load in two directions: upward against skin friction and downward against either end bearing alone or end bearing plus some skin friction.

While the geotechnical information obtained directly for each of the elements tested might be sufficient, in some situations, it is found important to determine how the head of the foundation element would behave under load. This paper describes some of the methods for assessing the behaviour of the combined elements.

Multilevel tests are now performed frequently and triple level bi-directional tests have been employed on a few occasions; these cases provide an even greater challenge to recombining the behaviour of each of the components into a representative load-settlement characteristic.

The challenge is to understand the merits of the differing methods which may be used to recombine the behaviour characteristics used in assessing how the top of the foundation element would perform.

The TIMESET® analysis method, which allows back analysis of displacement-time to determine final settlement at each applied load and CEMSOLVE®, permits interpretation of friction and end bearing from load-settlement results have, until recently, only been applied to measurements of load-displacement-time recordings of the pile head during top-down static load tests.

The appropriateness of these methods is considered for the modelling of the behaviour of each element resulting from a bi-directional test; that is to model both the upper “normal friction” elements and “friction and end bearing” of the pile elements below a single level O-cell. In so doing, a method of interpretation of bi-directional test results is postulated which ensures a conservative equivalent top-load response is interpreted.

It is worth appreciating that with bi-directional testing the top of the pile/barrette need not be constructed up to ground level or even expected cut-off level for the testing, so estimates may be required regarding the elastic shortening of the column above the test element up to the desired level.

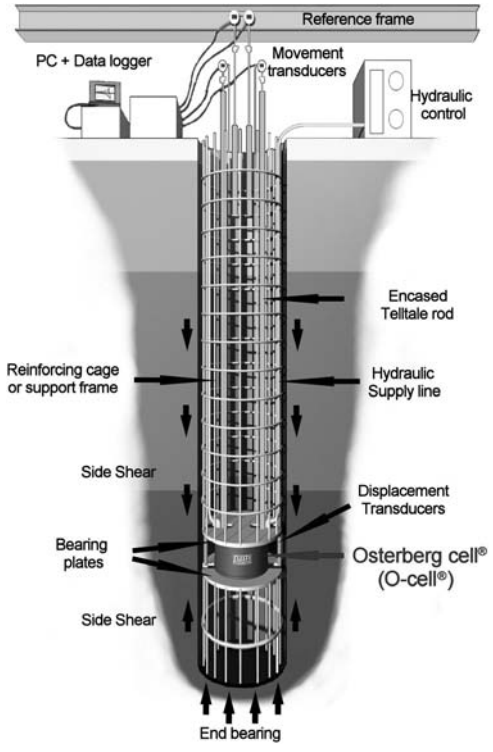

Figure 1. Single level: concept diagram.

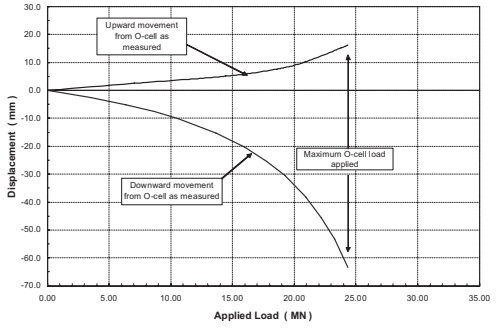

Figure 2. Typical bi-directional load test results.

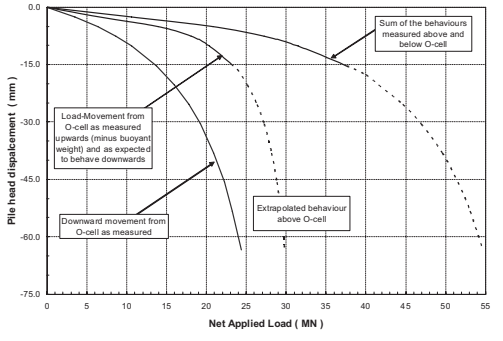

Figure 3. Sum of measured responses.

As discussed in England (2005), the compressive ultimate capacity of the behaviour of the element upwards will be assumed to be of the same ultimate skin friction as if the load were downwards, and the buoyant weight of the element will be subtracted.

2 ANALYTICAL METHOD

The data recorded during a bi-directional load test (OLT) include the elastic compressions that are part of the movement data obtained. For the purposes of illustrating the approach used, the descriptions will be limited to results from a single level O-cell assembly in which, it is expected that the upward behaviour measured is governed by skin friction and the behaviour downwards by skin friction and end bearing.

The data illustrated in Figure 2 shows a typical recording of the upward and downward displacement behaviour with respect to applied load in a single level bi-directional test up to the maximum test load applied.

To recombine the geotechnical behaviour measured (plus embedded elastic compression), the two measured components may readily be combined by adding the resultant loads for common displacements, having subtracted the buoyant weight of the element above the O-cell from the upward movement. Figure 3 illustrates the two measured behaviours to be combined along the load axes. This addition using common displacements has a slight drawback in as much as if the displacements upwards and downwards are not the same, the direct summation of the two can only be up to the smaller of the two displacements and then reliance is placed on extrapolation to project the element with the lesser movement in order to give a resulting behaviour up to a nominal load or the applied net load.

Where the upward movement is projected, this can be done with high reliability as the behaviour is normally dominated by skin friction only and a single hyperbolic curve can be made to match the recorded data.

Generally, in the design of a single level bi-directional test, the downward movement is normally expected to be larger than the movement upward; and therefore the end bearing component may be mobilized if sufficient load is applied. However, should the behaviour of the pile elements not follow

expectations, or the load be insufficient to mobilize the available skin friction downwards, projection of the downward movement is required, this can either be done using a single hyperbolic matched to the data pertinent to the end bearing behaviour (assuming the friction element is fully mobilised), using the method developed by Chin (1970), or can be done with a pair of hyperbolic functions as per Fleming (1992).

It then remains to estimate the elastic behaviour which was not present in each element during the test (referred to as the "measured behaviour curve") and then this elastic behaviour can be added to the result along the vertical axis, as illustrated below in Figure 4.

It may be noted that the elastic compression in the equivalent top load test always exceeds that mobilised in a bi-directional O-cell test.

The formulation of a simplified approximate solution in which a centroid of friction transfer is assumed to model the effect of distributed friction mobilised during the test is straightforward, Fleming (1992). The elastic component in the upward total movement measured can therefore be assessed, estimated and compared to the actual measured compression. This location of the centroid of friction transfer can also be used to assess the effect of skin friction distribution if the element were downwardly loaded, and if the element is not fully mobilised during the test, the centroid may be re-assessed for the equivalent elastic compression which would occur if the loading was at the top of the test pile if appropriate.

The elastic behaviour of the element below the O-cell is already contained within the test data so no additional influence needs to be considered.

3 MODELLING METHOD

The main difference from the method described above, where the measured behaviour is added together with respect to common displacements and the additional elastic shortening not expected to be in the test data is added to the result, is found by using Cemsolve®, Fleming (1992) in which the elastic component (measured) is also modelled leaving the geotechnical behaviour (actual friction and end bearing) to be determined; this represents the rigid element behaviour.

Once the modelled rigid behaviour of each element is obtained; these, and the elastic behaviour expected for the entire foundation element can be added together.

Figure 5 below shows a typical Cemsolve® analysis of the bottom portion of the test pile, although in this case the element of the pile below the O-cell is short and therefore the elastic component does not contribute much to the total settlement. In the analysis, it is estimated that the frictional component down is Us = 1100 kN and the ultimate end bearing Ub = 4200 kN with a base stiffness typical of clay, Eb = 48000 kN/m^2:

At the same time as the downward behaviour displayed above was recorded, the upward movement in this 1200mm diameter reinforced concrete pile was also logged and is presented in Figure 6 below.

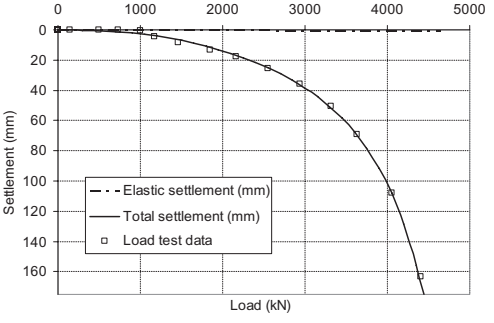

Figure 5. Cemsolve of downward movement.

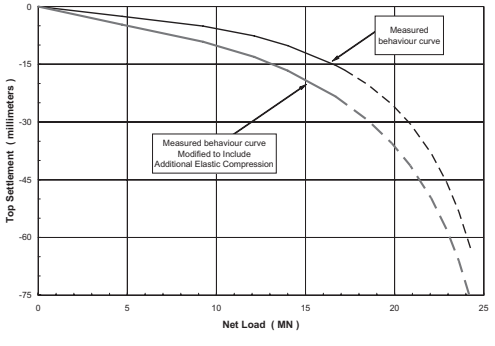

Figure 4. Additional elastic shortening.

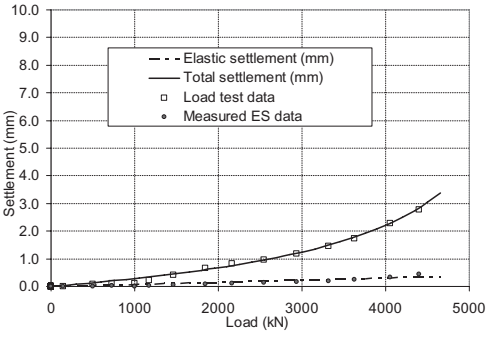

Figure 6. Cemsolve of upward movement.

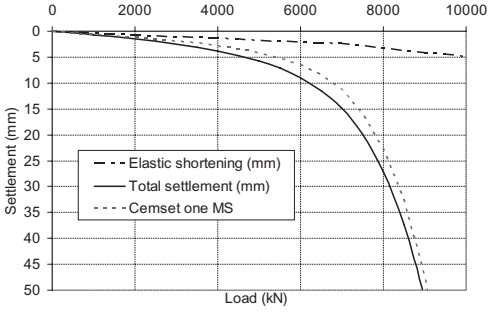

Figure 7. Cemset model with extra component.

The data points correspond to the measured upward displacement and the measured elastic shortening, the solid curve represents the modelled behaviour.

The elastic behaviour can be modelled directly from the measured data, and the remaining geotechnical behaviour can be matched using one hyperbolic function defined by Ms (flexibility factor) and Us (ultimate capacity). Buoyant weight of the upper section can be subtracted from the modelled ultimate capacity.

As pointed out in England (2005), the stiffness (flexibility factor Ms) can exhibit different values for the upward compressive behaviour in comparison to the expected downward behaviour; this can be attributed to the different boundary conditions, and therefore one may add together the modelled geotechnical behaviour measured for each element or one may choose to adopt a more typical flexibility factor expected for traditional top-down loading behaviour of foundation elements.

To illustrate the difference which may exist, the data presented in Figure 7 has also been plotted assuming a flexibility factor Ms upwards of 0.002. In this illustration, the dotted curve represents the traditional top-down loading behaviour expected and the solid line represents the summation of the modelled behaviour upwards and downwards. In essence, this approach allows for the addition of two separate hyperbolic functions for the skin friction of different ultimate capacities and one modelling the end bearing component giving a more conservative prediction of pile head behaviour.

4 FINITE ELEMENT METHOD

There are several approaches to modelling each of the elements and several different programmes which may be perfectly appropriate to model the data recorded either as just load-displacement or to include also any results from strain gauge measurements and then recombine these into predicted structural performance.

Fellenius et al. (1999) describes the use of The Advanced Geotechnical Analysis Code (AGAC) with which they have made several finite element analysis studies with this program which models the soil as an elastoplastic material and uses the bounding surface plasticity model to characterise the stress-strain-strength response of the soil. In this particular paper, the FE analysis of a 28 m deep barrette in the Guadalupe Tuff formation of the Makiti area is described. The parameters of the model were adjusted to obtain agreement with the bi-directional test results and from this model the expected top-down prediction was obtained.

Russo et al (2003) reports on their early findings of FEM analysis reporting a higher pile stiffness response from bi-directional tests when compared to top-loading; this is to be expected as the elastic shortening in a top-down loaded pile is more than that

LOADTEST employ the FB-MultiPier analysis program which is a nonlinear finite element analysis program capable of analyzing multiple interconnecting bridge pier structures. This analysis program couples nonlinear structural finite element analysis with nonlinear static soil models for axial soil behaviour to provide a robust system of analysis for coupled bridge pier structures and foundation systems. FB-MultiPier performs the generation of the finite element model internally for the geometric definition of the structure and foundation system as input graphically by the designer. Given the characteristics of the structure of the foundation element and the measured stress-strain at the pertinent levels, in a simple manner, the expected load-settlement behaviour at any elevation can be assessed with ease.

The use of Finite element or Finite difference computations to assessing the behaviour is no longer such a rare occurrence. The application finds its way into practice more regularly when the bi-directional testing methodology is applied at more than one level: In multilevel tests, the loading is necessarily done in stages, pressurising each level according to a predefined sequence relevant to the results required, and it is therefore essential to ensure the influence of previous loading stages are taken into account adequately.

5 EXPECTED ACCURACY

Direct comparisons of predicted pile head behaviour from a bi-directional test and actual is difficult to obtain reliably as separate test piles need to be installed and tested by each static loading method. In addition, the testing regime and the method of interpretation also need to be carefully chosen.

Further, because the loads applied with bi-directional tests are often far larger than those even available for top-down loading, comparisons can be a little difficult to obtain.

In principle, because bi-directional tests are full scale static loading, the results can be expected to correspond. Issues regarding softening of the ground around the bi-directional loading device only lead to conservative interpretation of the response of the soil and foundation element.

It is therefore for the engineer to assess the results obtained and how conservative these may be relative to the specification for the structure.

6 CONCLUDING REMARKS

The analysis of each separate measured response from a bi-directional test may be sufficient for many applications, but where the load-settlement response of the head of the foundation element is required, two direct methods are shown by way of example.

Where the elements of the test foundation have not been fully mobilised, the addition of the measured behaviour is perfectly suited to describing the combined behaviour of two elements.

Once one or both of the elements of a single level bi-directional test are moved sufficiently and can be modelled, the combination of the modelled elements can give a complete behaviour characteristic of the entire foundation element up to ultimate capacity.

When multilevel loading assemblies are employed within a single foundation element, it sometimes becomes imperative to find more sophisticated methods, such as Finite Element Analysis techniques to model the induced stresses in the different phases of loading.

REFERENCES

Chin, F.K. (1970) “Estimation of the ultimate load of piles from tests not carried to failure” *Proc. 2nd S.E. Asian Conf. Soil Engng. Singapore, 81–92.*

England, M. (2003). “Bi-directional static load testing—state of the art”, *Proc. Of the 4th Geotechnical Seminar on Deep Foundations on Bored and Augered piles, Ghent, Belgium pp 309–313.*

England, M. (2005). “A Conservative Method of Analysis of test results from bi-directional static load tests”*—Baltic Geotechnial Conference, October, Riga, Latvia.*

England, M. and Cheesman, P. (2006) “Recent experiences with bi-directional static load testing”, *10th DFI Conference, Amsterdam 31 May–2 June.*

Fellenius et al. (1999). “O-Cell Testing and FE Analysis of 28-m-Deep Barrette in Manila, Philippines” *in the Journal of Geotechnical and Geoenvironmental Engineering, Vol. 125, No. 7, July, p. 566.*

Fleming, W.G.K. (1992). “A new method of single pile settlement prediction and analysis”, *Geotechnique, Vol XLII, No. 3, Sept.*

Russo, G., Recinto, B., Viggiani, C. and de Sanctis, L. “A contribution to the analysis of Osterberg’s cell load test”, *Proc. Of the 4th Geotechnical Seminar on Deep Foundations on Bored and Augered piles, Ghent, Belgium pp. 331–338.*

Deep Foundations on Bored and Auger Piles – Van Impe & Van Impe (eds)
© 2009 Taylor & Francis Group, London, ISBN 978-0-415-47556-3

Physical modelling of piled raft

V. Fioravante & D. Giretti
University of Ferrara, Italy

M.B. Jamiolkowski
Technical University of Torino, Italy

ABSTRACT: The paper presents the results of centrifuge tests performed on piled raft foundation models. The model raft consisted of a circular very stiff plate; the model piles, embedded in loose saturated very fine sand, were non-displacement; some of them were instrumented with two load cells, the first at the pile head, the second at the tip or, alternatively, at mid-pile, to determine the load distribution along the shaft. The following models were tested: an un-piled rigid plate, an isolated pile and a piled raft with 1, 3, 7 and 13 piles respectively. The results of the tests carried out were analysed aimed at investigating the raft-soil-pile interaction mechanisms and at understanding how the load bearing behaviour of the piles as part of a piled raft changes compared to an isolated pile. The paper describes the experiments undertaken and some of their results.

1 INTRODUCTION

A piled raft is a composite foundation in which the raft and the piles share the total load applied by the superstructure. The raft transmits the external load partly to the piles and partly to the foundation soil, so that an interaction effect occur among piles, soil and raft (Randolph 1994, Poulos 1994, 2001, Horikoshi & Randolph 1998, Viggiani 1998, 2001, Mandolini et al. 2005, Katzenbach et al. 2000).

The load transmitted via the raft directly to the soil produces a rise in the vertical and horizontal stresses in the soil surrounding the piles and determines an increase of the piles shaft capacity, mainly in their upper part (Katzenbach et al. 2000).

The mobilisation of the shaft friction depends on the pile–soil relative displacement, which, with a rigid pile under a rigid raft, is zero at the pile head and maximum at the pile tip. As the pile settles, the shaft friction is mobilised from the bottom of the pile upwards, and reaches its limit value at a higher settlement if compared to an isolated pile (Burland 1995, Katzenbach et al. 2000, El.Mossallamy & Franke 1997).

To analyse the complex raft-soil-pile interaction behaviour, an extensive physical modelling test campaign on piled raft foundations was performed by means of the ISMGeo Geotechnical Centrifuge (IGC). The model piled raft consisted in a rigid circular steel plate founded on free-headed and close ended non-displacement piles, embedded in saturated homogeneous, very fine silica sand; some of the model piles were instrumented to evaluate the base and the shaft resistance independently. The number of piles beneath the raft was 1, 3, 7 and 13; ten loading tests were performed on piled raft models, adopting different layouts and reproducing a different pile spacing; as a comparison, two loading tests were carried out on the isolated pile.

From the results of the performed tests, the different load transmission mechanism of a pile belonging to a piled raft was quantified with respect to an isolated pile, and was investigated the influence on the load sharing mechanisms, on the pile number, on the pile spacing and on the pile position.

2 EXPERIMENTAL SET-UP

2.1 *The ISMGeo Geotechnical Centrifuge*

The model tests were carried out at the IGC. The centrifuge has a symmetrical rotating arm 6 m in diameter, 2 m in height and 1 m in width, giving a nominal radius of 2 m; the arm holds two swinging baskets carrying the model container and the counterweight. An outer fairing covers the arm, then, concurrently they rotate to reduce air resistance and perturbation during flight. The centrifuge has the potential of reaching an acceleration of 600 g at a payload of 400 kg. The model maximum dimensions are: length = 1 m, height = 0.8 m, width = 0.5 m. Additional details can be found in Baldi et al. (1988).

2.2 *Physical modelling*

Multi-g physical modelling is based on several similarity relationships between the model and the prototype, summarized in Table 1. In a model geometrically scaled down N times, and subject to a centrifuge acceleration of Ng, both stresses and strains are scaled at 1:1, displacements are reduced in the model by a factor of N and forces are reduced by a factor of N^2.

2.3 *Soil model preparation*

The geometrical scaling factor of the models was N = 100; the acceleration of 100 g was reached in correspondence to the soil surface; the acceleration field distortion was accounted for in the computation of stress distribution with depth.

Centrifuge tests were performed using FF sand (FFS), a uniform very fine sand consisting of subangular particles derived by grinding and sieving pit rocks. The main characteristic of FFS are: $\gamma_{d,min}$ = 11.58 kN/m^3, $\gamma_{d,max}$ = 14.78kN/m^3, $\phi'_{cv} = 33°$, $G_s = 2.61$, $D_{50} = 0.093$ mm, $C_U = 1.89$.

The soil model was accommodated in a cylindrical steel container, 440 mm in height and 400 mm in inside diameter, having rigid walls to avoid lateral displacements of the soil during the in flight tests. The specimen was reconstructed by pluviating the dry sand in air at a very small constant height of fall, in order to obtain a very loose specimen. After deposition, the specimen was saturated by means of an upward tap water flow, with a hydraulic gradient sufficiently small to prevent soil disturbance. As the model was subjected to the acceleration field in the centrifuge, the soil surface settled due to the consolidation; the surface settlement was measured with a displacement transducer mounted on a rigid frame fixed to the container rim. The average soil density, hereafter referred to, was evaluated at the end of the consolidation; in all models it was about the same, i.e. $D_R \approx$ 30%. The water level was monitored during the tests through two miniaturised pore pressure transducers inserted into the soil mass, one at the bottom of the container and one near the pile tips, and it was kept constant at 25 mm of depth from soil surface. A model scheme is shown in Figure 1.

The specimen uniformity and reproducibility was checked by means of two in flight static cone penetration tests (CPT) performed on dummy models; CPT's were carried out using a miniaturized electrical piezocone (diameter d_c = 11.3 mm and apex angle of 60°), penetrating at a rate of 2 mm/s. The results are shown in Figure 2, where the measured cone resistance q_c profiles are compared with those computed using an empirical correlation (Jamiolkowski et al. 2003); all data refers to prototype scale.

2.4 *Model raft and model piles*

The rigid raft foundation was modelled by means of a 88 mm in diameter (d_r) and 15 mm in thickness (t_r) steel disc. The raft-soil stiffness ratio is defined as:

$$K_{rs} = \frac{E_r}{E_s}\frac{1-\nu_s^2}{1-\nu_r^2}\left(\frac{t_r}{d_r/2}\right)^3 \quad [-] \qquad (1)$$

Table 1. Scaling factors.

Quantity	Prototype	Model
Length	N	1
Area	N^2	1
Volume	N^3	1
Velocity (projectile)	1	1
Velocity (undrained conditions)	1	N
Acceleration	1	N
Mass	N^3	1
Force	N^2	1
Energy	N^3	1
Stress	1	1
Strain	1	1
Mass Density	1	1
Energy density	1	1
Time (Dynamic)	N	1
Time (Diffusion)	N^2	1
Time (Creep)	1	1
Frequency	1	N

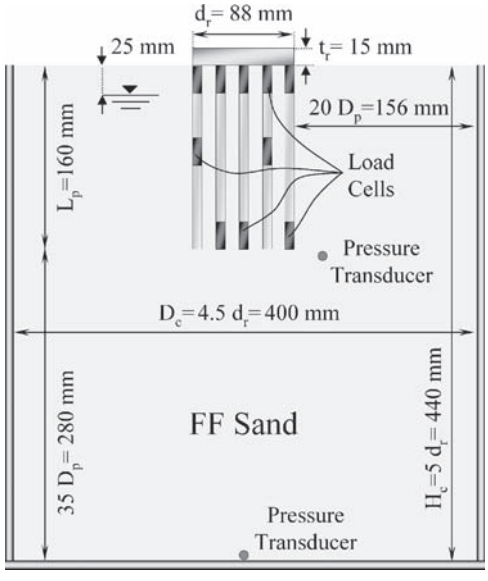

Figure 1. Centrifuge model of piled raft.

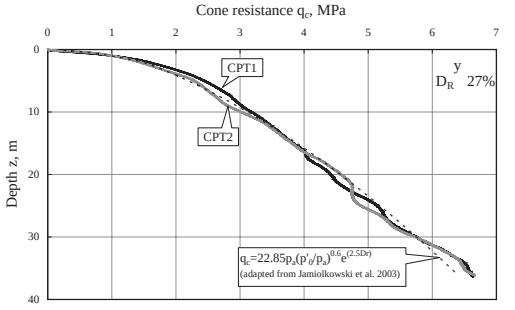

Figure 2. CPT's carried out in the centrifuge, prototype scale.

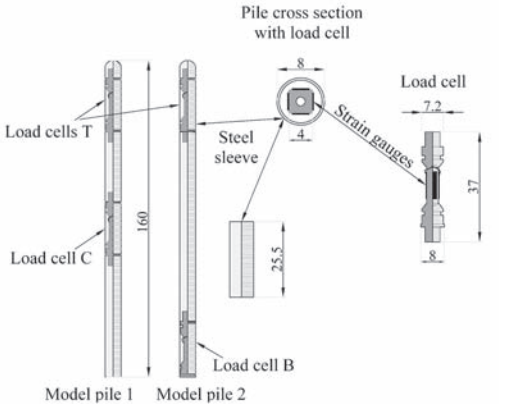

Figure 3. Instrumented model piles (all dimensions in mm).

where E_r is the steel modulus of elasticity and E_s is the soil modulus, evaluated at depth $z = d_r/2$ (Mayne & Poulos 1999), ν_s is the soil Poisson modulus and ν_r is the steel Poisson modulus. It resulted $K_{rs} >> 5$, so, according to Gorbunov-Posadov et al. (1984), Horikoshi & Randolph (1997), the raft was considered infinitely rigid. The raft settlement was measured by two vertical displacement transducers, placed in diametrically opposed positions: the average value of the measured settlements was assumed as the foundation displacement.

The close-ended and free-headed model piles, made of aluminium alloy pipes, were 8 mm in diameter (D_p) and 160 mm in length (L_p) (slenderness ratio $\lambda = 20$); the ratio $D_p/D_{50} = 86$, allowed to minimize scale effects (Garnier & Konig 1998, Foray et al. 1998, Fioravante 2002, Garnier 2002). The shaft roughness, obtained by mechanical turning and measured by a micrometrical profilometer, had an average value of $R_t = 300$ μm; the relative roughness $R_n = R_t/D_{50} = 3$ produced an angle of interface friction δ' equal to the angle of soil resistance at critical state, ϕ'_{cv}, according to Yoshimi & Kishida (1981), Kishida & Uesugi (1987), Jardine et al. (1993), Foray et al. (1995), Garnier & Konig (1998).

Some of the model piles were instrumented with miniaturised load cells; the fairly small diameter of the model piles allowed the incorporation of a maximum of two load cells per pile. The miniaturised load cells, made from stainless steel, had a square cross section as outlined in Figure 3; a couple of active strain gauges was coated with an acrylic moisture barrier on each of the four flat surfaces. The instrumented cross-section was covered by a protective stainless steel jacket to avoid soil radial stress acting on the gauges, and it was sealed with O-rings as a second moisture barrier. The instrumented piles were assembled in two configurations (models 1 and 2, as shown in Figure 3): the upper load cell, T, was placed at the pile head in both cases, the lower load cell was placed at the pile base (position B of model 2) or at mid-pile (position C, model 1). The load cells allowed measuring the axial loads transmitted from the raft to the instrumented piles at three positions along the pile length, and estimating the average load transmitted through pile shaft friction. Due to the axis-symmetry of the loads and of the geometry, it was assumed that piles placed at the same radius experienced the same load distribution with depth; therefore the results of model piles 1 and 2 were merged to compose an equivalent pile at that radius as follows:

T-C shaft resistance of model pile 1

$$Q_{S,TC}(s) = Q_T(s) + W_{P,TC} - Q_C(s) \text{ [F]} \quad (2)$$

T-B shaft resistance of model pile 2

$$Q_{S,TB}(s) = Q_T(s) + W_{P,TB} - Q_B(s) \text{ [F]} \quad (3)$$

C-B shaft resistance of the equivalent pile

$$Q_{S,CB}(s) = Q_{S,TB}(s) - Q_{S,TC}(s) \text{ [F]} \quad (4)$$

where $Q_T(s)$ = total axial load measured at pile head, assumed to have a downward positive sign; $Q_B(s)$ = base resistance, assumed to have an upward positive sign; $Q_C(s)$ = mid-pile load, assumed to have a upward positive sign; $W_{P,TB}$ = dead weight of pile segment T-B at 100 g, $W_{P,TC}$ = dead weight of pile segment T-C at 100 g; s = pile settlement. Due to the inherent rigidity of the model pile, the settlement of pile tip and pile head were assumed to be the same as the raft.

2.5 *Model piles installation*

The model piles were inserted at 1 g in the soil specimen in pre-bored holes for their full length. A very rigid frame was mounted on the container rim, to hold

Table 2. Testing programme.

Test No.	Test name	Description	No. of pile	Test layout	Spacing i/D_p	D_R (%)
1	URLT0	Unpiled raft				26
2	ND-PLT5	Isolated pile	1			31
3	ND-PLT6	Isolated pile	1			30
4	ND-PRLT5	Piled raft	1	L1		30
5	ND-PRLT6	Piled raft	3	L2	8.66	29
6	ND-PRLT7	Piled raft	3	L2	8.66	30
7	ND-PRLT8	Piled raft	7	L3	5	32
8	ND-PRLT9	Piled raft	7	L4	5	30
9	ND-PRLT10	Piled raft	13	L5	2.5–5	36
1	ND-PRLT11	Piled raft	13	L6	2.5–5	30
11	ND-PRLT12	Piled raft	3	L7	4.33	26
12	ND-PRLT13	Piled raft	7	L8	2.5	26

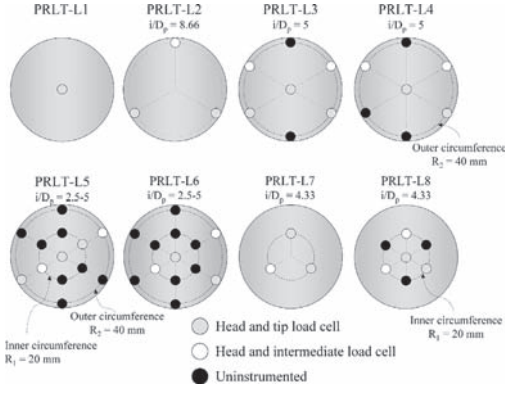

Figure 4. Layout of the tested piled rafts.

three vertical displacement transducers, one external load cell and a hydraulic actuator. Then the container was embarked on the centrifuge and accelerated to 75 g; the acceleration was kept constant until the consolidation was achieved, as monitored by the pore pressure and displacement transducers. Since the soil surface settled 1–1.5 mm more than the piles, at the end of the consolidation the piles were slightly pushed down by the raft plate to be aligned to the soil surface; then the raft was lifted up, the centrifuge speed was increased to the target value of 100 g, and a final consolidation took place. The raft plate was then slowly lowered until pile head contact was achieved again, and the loading tests were performed at a constant rate of load of 50 N/min.

The load was applied by the servo-controlled hydraulic actuator and measured by the external load cell; the pore pressure, measured near the pile tip, showed constant values during the tests, i.e. drained condition.

The residual forces, caused by the installation procedure and the in flight consolidation, were taken into account in the tests interpretation.

2.6 *Test programme*

Twelve loading tests were carried out, the isolated pile, the unpiled raft and eight different piled raft models were tested, as summarised in Table 2; the test layout are represented in Figure 4.

3 TEST RESULTS

3.1 *Stress-settlement behaviour of the piled raft*

Figure 5 illustrates the stress-settlement relationships gained from tests performed on the rafts with 1, 3, 7 and 13 piles and the test on the unpiled raft; the total applied stress, q_t, is plotted versus the measured settlement, s; all values being referred to the model scale.

The stress-settlement relationships of the piled rafts were non-linear: their slope gradually decayed with increasing settlement till yielding took place; yielding caused a sharp decrease of the stiffness, which, at large settlement, became almost steady. The yielding stress depended on the number and the position of piles: it was higher for higher pile number and for larger pile spacing. Before yielding the foundation stiffness was higher for higher pile number and for larger pile spacing; after yielding it seemed to depend only on pile spacing.

The unpiled raft showed an experimental stress-settlement curve almost linear and exhibited a lower stiffness if compared with the piled rafts. Figure 6 reports the raft secant stiffness as a function of the settlement.

3.2 *Load tests on the isolated and the single piles*

Figure 7 reports the results of the load test on the single pile beneath the raft compared with those of the isolated pile; the total load acting on pile, (Q_T), the base load capacity, (Q_B), and the mobilised shaft resistance, ($Q_{S,TB}$), are plotted as function of the pile settlement(s).

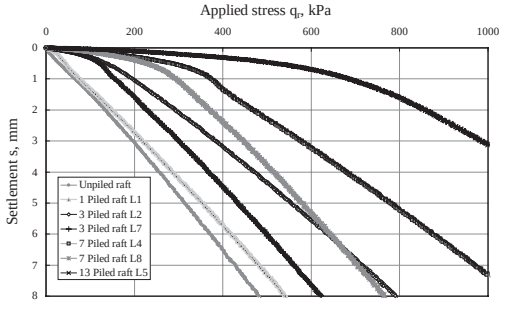

Figure 5. Stress-settlement relationships of piled rafts, model scale.

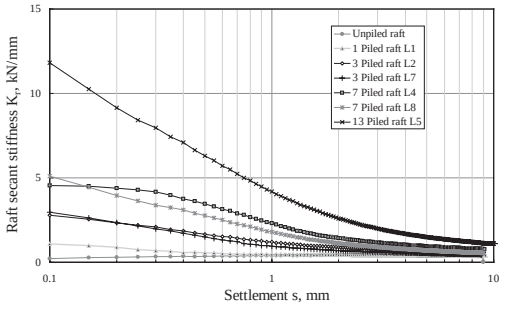

Figure 6. Piled rafts stiffness, model scale.

As to the isolated pile, the $Q_{S,TB}(s)$ relationship achieved a peak at small settlement ($s \approx 0.52$ mm), then it slightly decreased toward a steady value reached at large settlement; the mobilisation of $Q_B(s)$ was progressive and the ultimate value was reached at $s \approx 8$ mm. As result, the total load $Q_T(s)$ gradually increased with s, toward an ultimate value reached for large displacements. The pile stiffness gradually decayed with increasing settlement.

The behaviour observed for the single pile beneath the raft was more complex: the $Q_T(s)$ curve increased to a peak value, reached at small settlement, then exhibited at first a partial tendency to decrease, followed by a steady trend to increase. The peak value was 20% higher than the resistance of the isolated pile at the same displacement. Before the peak resistance was achieved, the stiffness of the pile beneath the raft was equal to that of the isolated pile; after the peak, it became almost steady, lower than the values exhibit before yielding, but anyhow greater than what exhibited by the isolated pile. The single pile $Q_B(s)$ was almost the same as the isolated pile, while the shaft friction mobilisation justified the different total load-settlement behaviour: $Q_{S,TB}(s)$ of the single pile achieved a peak at a settlement of almost 0.72 mm, then slightly decreased up to $s \approx 1.6$ mm, finally it steadily increased reaching values 30% higher the peak value at $s \approx 8$ mm. Before yielding, the single and the isolated pile exhibited the same shaft friction mobilisation rate.

3.3 *Load-transfer mechanisms of the central pile of the 7 piled rafts*

The total, base, and shaft capacity of the 7 piled rafts central pile are reported in Figures 8 and 9, as function of the pile settlement s. The pictures report also the analogous curves of the single pile.

Moving from the unconfined single pile towards the confined central pile of 7 (L4), the ultimate

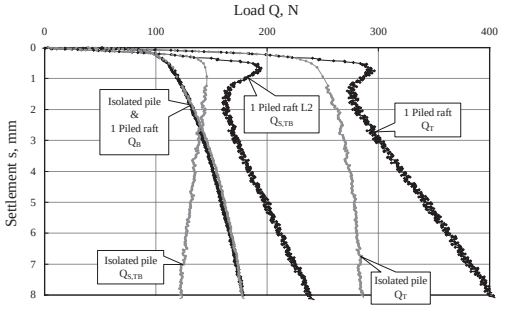

Figure 7. Load settlement behaviour of the isolated pile and the single pile beneath the raft, model scale.

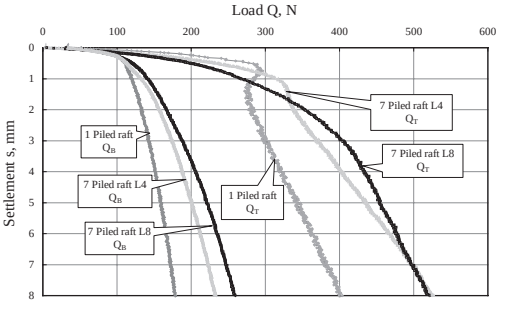

Figure 8. Total and base capacity of the central piles of the 7 piled rafts, model scale.

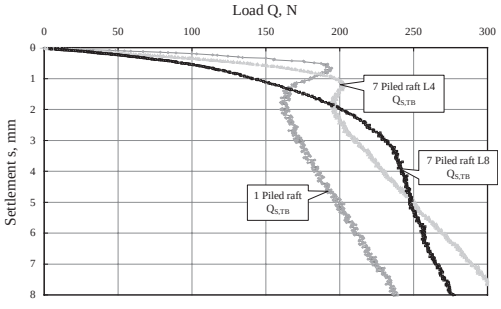

Figure 9. Shaft capacity of the central piles of the 7 piled rafts, model scale.

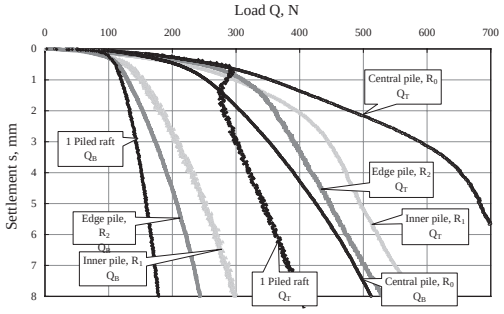

Figure 10. Total and base capacity of the piles of the 13 piled raft piles, model scale.

total load augmented, much more when the spacing reduced (L8); on the other hand the stiffness at small settlement progressively decayed. After the pile yielding took place, causing a sharp decrease of the stiffness, the bearing capacity steadily increased, at a higher rate than the single pile.

The more the central pile was confined, the more the base load capacity $Q_B(s)$ was higher than what observed for the single pile.

As to the shaft capacity shown in Figure 9, when peripheral piles were placed at the edge of the raft (L4), the $Q_{S,TB}$ peak value was slightly higher compared to the single pile, and it was achieved with a lower rate at $s \approx 1.3$ mm. After the peak, $Q_{S,TB}(s)$ increased with a steady rate, greater than that of the single pile. When the central pile was more confined (L8), the shaft capacity mobilisation took place with the lowest rate, and the shear failure, reached at $s > 3$ mm, was not much evident; the ultimate value resulted higher than that of L4 central pile. The observed increase of the ultimate capacity of the central pile was due to the increase of $Q_B(s)$ and of the ultimate shaft capacity; the increase was higher for the lower spacing layout. At the same time, the pile stiffness before yielding reduced with increasing confinement, mainly due to the lower shaft mobilisation rate.

3.4 *Load-transfer mechanisms of the 13 piled raft*

Figures 10 and 11 present the results of centrifuge tests on 13 piled raft, and compare the behaviour of the central (R_0), the inner (R_1) and the edge (R_2) pile (see Fig. 4) with that of the single pile. The ultimate pile capacity resulted higher than that of the single pile, and depended on pile position: it increased from the outer (R_2) to the central pile (R_0), due both to the increase of $Q_B(s)$ and of the ultimate shaft capacity; the central pile reached an ultimate total load higher than the central pile of the 7 pile groups. On the other hand the increasing confinement caused a reduction of the $Q_{S,TB}(s)$ mobilisation rate at small settlement.

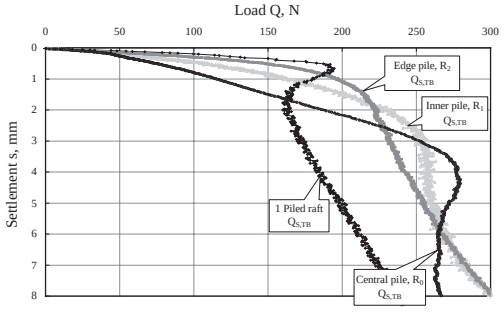

Figure 11. Shaft capacity of the piles of the 13 piled raft piles, model scale.

4 TESTS INTERPRETATION

The shaft friction mobilisation and ultimate shaft friction for a pile are governed by the behaviour of a thin zone close to the pile surface; the width of this zone depends on the pile surface roughness. When the pile is loaded, the interface zone is subjected to large plastic straining, and the soil exhibits dilative or contractive behaviour depending on its density and on the relative roughness between pile and soil (Wernick 1978, Boulon & Foray 1986, Boulon 1988, 1989). The mobilisation of the pile shaft friction, $\tau_s(s)$ depends on the relative pile-soil displacement, s; it can be expressed as follows:

$$\tau_S(s) = [\sigma'_{n0} + \Delta\sigma'_n(s)] \tan\delta' \; [FL^{-2}] \qquad (5)$$

where: σ'_{n0} = initial normal effective stress at the pile- soil interface (it depends on the initial overburden stresses and on the installation procedure); $\Delta\sigma'_n$ = change in normal effective stress during the pile loading; δ' = pile skin friction angle, equal, for a rough surface, to the angle of soil resistance at critical state, ϕ'_{cv}.

In piled raft foundations a change in the standard effective stress $\Delta\sigma'_n(s)$ can be expressed as the sum of two components:

$$\Delta\sigma'_n(s) = \Delta\sigma'_{n,d}(s) + \Delta\sigma'_{n,r}(s) \; [FL^{-2}] \quad (6)$$

where: $\Delta\sigma'_{n,d}$ (s) is due to soil dilative or a contractive behaviour in the interface zone and $\Delta\sigma'_{n,r}(s)$ is the increment in the normal effective stress caused by the load transmitted by the raft directly to the soil. $\Delta\sigma'_{n,r}(s)$ is proportional to the pressure exerted by the raft directly onto the soil and depends on the total applied load and on the load sharing mechanism between piles and raft; its value become more significant after the pile bearing capacity has been mobilised (Fioravante et al. 2008).

The results of the tests here presented have been analyzed to identify the effects of $\Delta\sigma'_{n,d}(s)$ and $\Delta\sigma'_{n,r}(s)$ on the behaviour of the piles and of the whole foundation.

In the model tests carried out, the soil-pile interface was totally rough ($R_n = 3$) and the soil dilatancy occurred, even in loose specimens. The mobilisation of the peak shaft capacity observed on the isolated pile (Fig. 7) was attributed to the dilatancy constraints of the surrounding sand; the mobilisation of $\Delta\sigma'_{n,d}$ took place at very small settlement.

The effects of $\Delta\sigma'_{n,r}$ on the single pile are illustrated in Figure 7, where the base, shaft and total capacity of the single pile beneath the raft are compared to those of the isolated pile. The peak shaft value mobilised by the single pile was higher than the one observed for the isolated pile, and after the peak, the shaft friction further increased due to the progressive increase of the load transmitted by the raft to the soil. The $Q_B(s)$ curve of the single pile was quite similar to that of the isolated pile, so the effects of the raft pressure make reference mostly to the higher part of the pile shaft.

The shaft friction mobilisation of the single pile occured at the same rate of the isolated pile, but the a greater peak value was reached at a higher settlement, due to the following mechanisms: the raft constrains caused a smaller relative pile-soil displacement in the upper part of the pile, therefore the foundation settled more to produce the full mobilisation of the shaft capacity.

The effects exerted by six peripheral piles on the bearing capacity of the 7 piled raft central pile are shown in Figures 8 and 9; in particular, the increment of $\Delta\sigma_{n,r}$, as observed for the single pile, was magnified by the confining effect exercised by peripheral piles and the ultimate shaft capacity of the central pile was enhanced. On the other hand, the interaction between pile shaft produced a stiffness decrease of the central pile. The load transmitted by the raft to the soil did not influence the base load of the single pile (Fig. 6), so the $Q_B(s)$ increase of the central pile could be attributed to base interaction effects.

Referring to the 13-piled raft, the effects of the pile position on its behaviour, is outlined in Figures 10 and 11. The ultimate shaft capacity of each pile within the group was greater than that of the single pile, and augmented moving from the outer to the central pile, but the interaction between pile shaft caused a decrease of the shaft capacity mobilisation rate, as the confinement rose. As pointed out the pile tip interaction effects increased the base load capacity.

As to the piled raft behaviour, the raft stiffness was significantly enhanced by the presence of even a few piles; before pile yielding it reflected almost entirely the stiffness of the pile group, and increased as the pile number increased. Once the pile group reached its ultimate capacity, a sharp degradation of the foundation stiffness occurred, but it remained higher than the value observed for the unpiled raft, because of the effects of $\Delta\sigma_{n,r}(s)$ on the pile shaft capacity; it depended mainly on pile spacing.

5 CONCLUDING REMARKS

The behavior of piled rafts was investigated by means of extensive centrifuge tests on the model of a circular rigid plate lying on a bed of loose very fine silica sand. Beneath the raft, non displacement model piles were installed. The testing program included: unpiled raft and rafts on 1, 3, 7 and 13 piles. In each test a number of model piles were instrumented with load cells so that the load distribution along the shaft could be estimated. Load tests on an isolated pile were also performed to establish its shaft and base load carrying capacity as well as its load-settlement relationship.

The following effects were observed:

1. The load transmitted via the raft directly to the soil produces an increase of the vertical and horizontal stresses in the soil surrounding the piles and gives rise to an increase of pile shaft capacity, both before and after yielding.
2. The raft constraints causes a smaller relative pile-soil displacement in the upper part of the piles, therefore the foundation settlement required to produce the full mobilisation of the shaft capacity augments.
3. The effect of the load transmitted by the raft to the soil is enhanced by the confinement effect exercised by adjacent piles. The more confined piles reach higher ultimate shaft friction.
4. The interaction between pile shafts produces a stiffness decrease, so that the more confined piles mobilise the ultimate shaft friction at a lower rate.
5. After yielding, the stiffness of a pile beneath the raft, although subject to decay, remained above the values observed for the isolated pile.

6. The piled raft stiffness is higher than that of the unpiled raft before as well as after yielding. Its value depends on pile number and pile spacing before yielding and only on pile spacing after yielding.

The above draws the attention to the fact that the design of piled rafts should take into account the soil-structure interaction, which significantly influences the behaviour of piles and consequently of the whole foundation.

ACKNOWLEDGMENTS

The authors appreciate the support of the technicians of the Istituto Sperimentale Modelli Geotecnici (ISMGeo) of Seriate (Bergamo).

REFERENCES

Baldi, G., Belloni, G. Maggioni, W. 1988. The ISMES Geotechnical Centrifuge. *Centrifuge 88*: 45–48. Paris, Corté J. F. Ed., Balkema, Rotterdam.

Boulon, M. Foray, P. (1986). Physical and Numerical Simulation of Lateral Shaft Friction along Offshore Piles in sand. *3rd International Conference on Numerical Methods in Offshore Piling, Nantes. Editions Technip*: 127–147. Paris.

Boulon, M. 1988. Numerical and Physical Modeling of Piles Behaviour under Monotonous and Cyclic Loading. *International Symposium on Modeling Soil-Water-Structure Interactions SOWAS '88*: 285–293. Delft, Kolkman, P.A. et al. Eds. Balkema, Rotterdam.

Boulon, M. 1989. Basic Features of Soil-Structure Interface Behaviour. *Computers and Geotechnics*, vol. 7, No. 1–2, 115–131.

Burland, J.B. 1995. Piles as Settlement Reducers. *Proc. 19th Geotechnical National Congress, AGI*. Pavia, Vol. 2, 21–34.

El.Mossallamy & Franke 1997. Piled raft: numerical modeling to simulate the behaviour of piled raft foundation. Pubblished by the authors, Darmstadt.

Fioravante, V. 2002. On the Shaft Friction Modelling of Non-Displacement Piles in Sand. *Soils and Foundations*, Vol. 42, No. 2, 23–33.

Fioravante, V., Giretti, D. Jamiolkowsi, M. 2008. Physical Modelling of Raft on Settlement Reducing Piles. *From Reserce to Practice in Geotechnical Engineering.* ASCE Geotechnical Special Publication No. 180. Laiser, Crapps, Hussein Eds.

Foray, P., Balachowski, L. Labanieh, S. 1995. Modélisation Physique des Ouvrages Géotechniques en Chambre D'étalonnage. *Colloque scientifique, Les modèles réduits en génie civil AUGC*: 55–68. Nantes. Sieffert, J.G. Ed., AUGC.

Foray, P., Balachowski, L. Raoult, G. 1998. Scale Effect in Shaft Friction due to the Localisation of Deformations. *Centrifuge '98*: 211–216. Tokyo, Kimura, Kusakabe & Takemura Eds, Balkema, Rotterdam.

Garnier, J. & Konig, D. 1998. Scale Effects in Piles and Nails Loading Tests in Sand. *Centrifuge '98*: 205–210. Tokyo, Kimura, Kusakabe & Takemura (ed.), Balkema, Rotterdam.

Garnier, J. 2002. Size Effects in Shear Interfaces. *Workshop on Constitutive and centrifuge modelling: two extremes, Monte Verità*: 5–19Springman Ed., Swets & Zeitlinger Lisse.

Gorbunov-Posadov, M.I. et al. 1984. *Analyses of Construction on Elastic Foundation. Strojizdat*, Moscow (in Russian).

Horikoshi, K. & Randolph, M.F. 1997. On the Definition of Raft-Soil Stiffness Ratio for Rectangular Raft. *Geotechnique*: Vol. 47, No. 5, 1055–1061.

Horikoshi, K. & Randolph, M.F. 1998. A Contribution to Optimum Design of Piled Raft. *Geotechnique*: Vol. 48, No. 3, 301–317.

Katzenbach, R., Arslan, U. & Moormann, C. 2000. Piled Raft Foundation in German. *Design Application of Raft Foundations:* J.A. Hemsley, Telford Ed., 323–390.

Kishida, H. & Uesugi, M. 1987. Tests of the Interface between Sand and Steel in the Simple Shear Apparatus. *Geotechnique*: Vol. 37, No. 1, 45–52.

Jamiolkowski, M., Lo Presti, D.C.F. Manassero, M. 2003. Evaluation of Relative Density and Shear Strength from CPT and DMT. *Soil Behavior and Soft Ground Construction Ladd Symposium MIT*: 201–238. Cambridge Mass. GSP No. 119, Germaine J.T. et al Eds ASCE New York.

Jardine, R.J., Lehane, B.M. Everton, S.J. 1993. Friction Coefficients for Piles in Sands and Silts. *Conference on Offshore Site Investigation and Foundation Behaviour*: 661–677. Society for Underwater Technology, London 1992, Kluwer Academic Publishers Dordrecht.

Main & Poulos 1999. Approximate Displacement Influence Factors for Elastic Shallow Foundations. *Journal of Geotechnical and Geoenvironmental Engineering* 125, No. 6, 453–460.

Mandolini, A. et al. 2005. Pile foundations: experimental investigation, analysis and design. *16th International Conference on Soil mechanics and Geotechnical Engineering*: Vol. 1, 177–213. Osaka, Millpress Rotterdam.

Poulos, H.G. 1994. An Approximate Numerical Analysis of Piled-Raft Interaction. *International Journal for Numerical and Analytical Methods in Geomechanics*: Vol. 18, No. 2, 73–92.

Poulos, H.G. 2001. Piled raft foundations: design and applications. *Geotechnique*: Vol. x, No. 2, 95–113.

Randolph, M.F. 1994. Design Methods for Pile Groups and Piled Rafst., *13th Intenational Conference on Soil Mechanics and Foundation Engineering*: Vol. 5, 61–82. New Delhi.

Viggiani, C. 1998. Pile Groups and Piled Rafts Behaviour. *3rd International Geotechnical Seminar on Deep Foundations on Bored and Auger Piles*: 77–94. Ghent, Van Impe, W.F. Ed. Millpress Rotterdam.

Viggiani, C. 2001. Analysis and Design of Piled Foundations. *1 st Arrigo Croce Lecture. Rivista Italiana di Geotecnica*: Vol. 35, No. 1, 47–75.

Wernick, E. 1978. Skin Friction of Cylindrical Anchors in Non-Cohesive Soils. *Symposium on Soil Reinforcing and Stabilising Techniques*: 201–219. New South Wales Institute of Technology Sydney.

Yoshimi, Y. & Kishida, T. 1981. Friction Between Sand and Metal Surface. *10th International Conference on Soil Mechanics and Foundation Engineering*: Vol. 1, 831–834. Stockholm.

Deep Foundations on Bored and Auger Piles – Van Impe & Van Impe (eds)
© 2009 Taylor & Francis Group, London, ISBN 978-0-415-47556-3

Some new insights with regard to load distribution in piles, based on a detailed interpretation of a large number of instrumented pile load tests

N. Huybrechts
Belgian Building Research Institute, WTCB-CSTC-BBRI, Belgium

J. Maertens
Jan Maertens & Partners bvba, Belgium
Catholic University of Leuven, KUL, Belgium

ABSTRACT: During the last decade a large number of static load tests on instrumented piles has been performed in Belgium. A number of load tests performed by the BBRI since 1997, and some former load tests are analysed in detail and compared with the recent Belgian design rules for axially loaded piles according to EC7.

1 INTRODUCTION

Since the 1970's several pile load test campaigns have been carried out in Belgium. A general overview of these test campaigns and the types of tested piles, have been given in Holeyman et al. (1997). Since 1997, a lot of supplementary scientific pile load test have been performed by the Belgium Building Research Institute (BBRI), in particular with the viewpoint to anticipate on the success of the soil displacement screw pile types on the Belgian market, and to support the establishment of a background document for pile design according to Eurocode 7 in Belgium (BBRI, 2008).

This contribution gives an overview of a number of the scientific pile load tests that have been performed by the BBRI in Belgium since 1997, and focuses in particular on the separation of the pile load in base resistance and shaft friction. Some data of former load tests on instrumented bored piles in Kallo in the 1980's have been re-analysed as well. The obtained data are compared with the recent rules for pile design in Belgium according to EC7 as described in (BBRI, 2008).

2 OVERVIEW PILE LOAD TEST CAMPAIGNS

2.1 *Pile load test campaign in Sint-Katelijne-Waver*

In Sint-Katelijne-Waver a real scale load test program on 30 piles was set up. It concerned 12 static load tests (SLT), 12 dynamic load tests (DLT) and 6 statnamic tests (STN) on 5 types of soil displacement screw piles and on precast driven piles installed in tertiary o.c. Boom clay. Figure 1 gives a typical CPT on the test site; on the same figure the two different pile installation depths (7.5 m and 11.7 m) are indicated as well.

These tests were performed in the framework of a BBRI research program (1998–2000). This project took place with the financial support of the former Belgian Federal Ministry of Economical Affairs— which is actually called the Federal Public Service Economy— and was carried out in collaboration with five Belgian piling companies (De Waal Palen, Franki Geotechnics B, Fundex, Olivier and Socofonda). A National Advisory Committee under supervision of prof. A. Holeyman (UCL) and prof. J. Maertens (KUL) guided the research program.

For a detailed overview of the test campaign set-up, the extended soil investigation campaign, the pile types, the load test procedures and the test results, reference is made to Holeyman (1998).

The normalised load settlement diagrams resulting from the instrumented load tests are summarised in figures 2 to 4.

On the vertical axis of these figures the pile head settlements are expressed as percentage of the pile base diameter. On the horizontal axis the measured pile base load $Q_{b,meas}$, the measured shaft friction $Q_{s,meas}$, and the total measured load Q_{meas} are expressed in relation to the calculated values of the ultimate pile base resistance $R_{bu,calc}$, the ultimate shaft friction

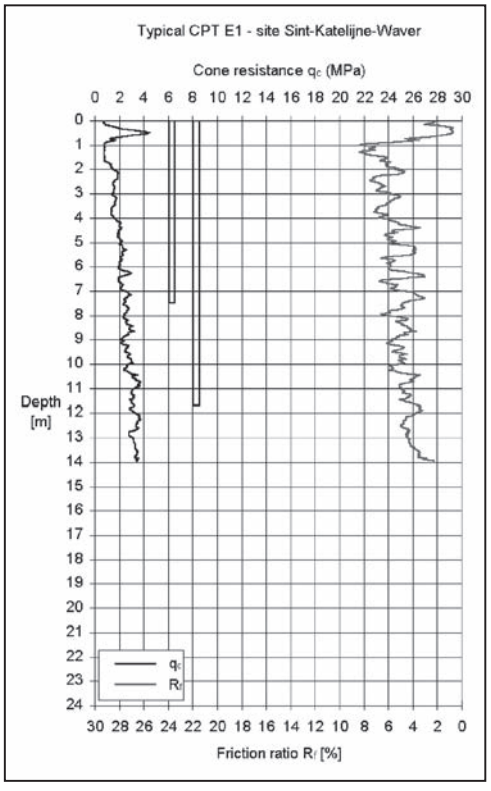

Figure 1. CPT profile and pile lengths site Sint-Katelijne-Waver.

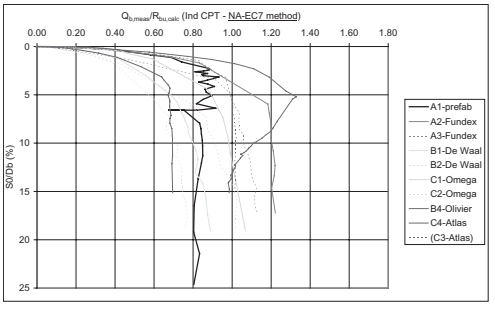

Figure 2. Normalised load settlement diagram of the pile bases in Sint-Katelijne-Waver ($\alpha_b = 0.8$ for screw piles and $\alpha_b = 1$ for driven precast piles have been applied).

$R_{su,calc}$ and the total ultimate pile resistance $R_{cu,calc}$ respectively.

These calculated values have been determined based on the CPT with electrical cone in the axis of each individual pile and according to the recent "Guidance rules for the application of EC7 in Belgium—part 1: Geotechnical design in ULS for axially loaded compression piles based on CPT" (BBRI, 2008). The formulas to determine the ultimate pile resistances are summarised below. Nominal pile dimensions as fixed in these recent design rules have been applied for the piles in Sint-Katelijne-Waver.

$$R_{cu,calc} = R_{bu,calc} + R_{su,calc} \quad (1)$$

$$R_{bu,calc} = \alpha_b \cdot \varepsilon_b \cdot \beta \cdot \lambda \cdot A_b \cdot q_b \quad (2)$$

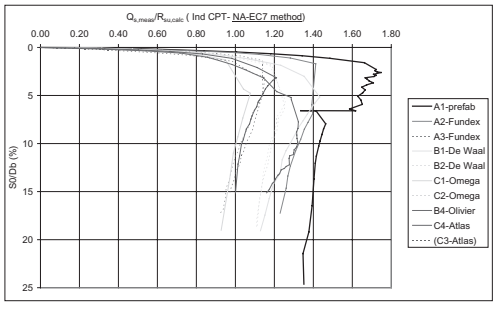

Figure 3. Normalised load settlement diagram of the piles' shaft friction in Sint-Katelijne-Waver ($\alpha_s = 0.9$ for all piles have been applied).

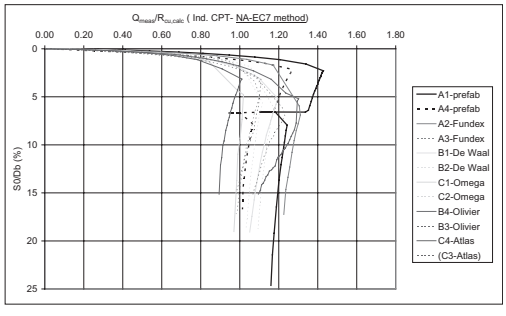

Figure 4. Normalised load settlement diagram of the total pile load in Sint-Katelijne-Waver.

Table 1. η^*_p (–) or q_s (MPa) values from BBRI (2008).

Soil type	q_c (MPa)	η^*p (–) or q_s (MPa)	R_f (%)
Clay	1–4.5	$\eta^*p = 1/30$	3–6%
	>4.5	$q_s = 0.150$	
Loam (silt)	1–6	$\eta^*p = 1/60$	2–3%
	> 6	$q_s = 0.100$	
Sandy clay/loam	1–10	$\eta^*p = 1/80$	1–2%
(silt) & clayey	>10	$q_s = 0.125$	
sand/loam (silt)			
Sand	1–10	$\eta^*p = 1/90$	<1%
	10–20	$q_s = 0.110 + 0.004*(q_c–10)$	
	>20	$q_s = 0.150$	

with

q_b (kN/m²)	ultimate unit pile base resistance, calculated from CPT results with the De Beer method
A_b (m²)	pile base cross sectional area;
α_b (–)	an installation factor: an empirical factor taking into account the method of installation of the pile and soil type.
ε_b (–)	a parameter referring to the scale dependant soil shear strength characteristics $= 1 - 0.01\left(\frac{D_{b,eq}}{D_c} - 1\right)$ in the case of fissured Tertiary Clay, but always > 0.476 $= 1$ in all other cases $D_{b,eq}$ is the diameter of the pile base; D_c is the diameter of the cone of the CPT (standard cone: 35.7 mm).
β (–)	a shape factor introduced for neither circular nor square shaped bases
λ (–)	a reduction factor for piles with an enlarged base

$$R_{su,calc} = \chi_s \cdot \Sigma(\alpha_{s,i} \cdot h_i \cdot q_{s,i}) \quad (3)$$

$q_{s,i}$ (MPa)	ultimate unit pile shaft resistance $q_{s,i} = \eta^*p,i \cdot q_{c,m,i}$
$\eta^*_{p,i}$ (–)	empirical factor depending on the soil type; values see Table 1
$q_{c,m,i}$ (MPa)	mean cone resistance (q_c) in layer i
χ_s (m)	perimeter of the shaft
$\alpha_{s,i}$	an installation factor: an empirical factor introducing the effects of pile installation method, of the nature of the shaft's material and soil structure scale effects.

For the tertiary clay site in Sint-Katelijne-Waver the following values from the recent guidance rules have been applied in the calculated values in figures 2 to 4:

- $\alpha_b = 1$ for the driven precast piles and $\alpha_b = 0.8$ for soil displacement screw piles
- ε_b: see formula before
- $\beta = \lambda = 1$ for all piles
- $\eta_p^* = 1/30$ (clay)
- $\alpha_s = 0.9$ for all piles

The measured values of the pile base resistance and shaft friction have been deduced from pile deformation measurements with a retrievable extensometer device, using the Fellenius (2001) interpretation methodology in order to deal with a non linear stress-strain behaviour of concrete.

When one takes into account that the load corresponding with a relative pile settlement of 10%D_b, with D_b the pile base diameter, has been put forward as conventional rupture load, one can conclude that:

- For the soil displacement screw piles the calculated ultimate base resistances correspond well with the measured ones, although the variation is rather high. The ultimate base resistances of these piles seem to be fully mobilised for all pile types at settlements of about 15%D_b.
- The calculated ultimate shaft resistances seem to be somewhat too pessimistic at a settlement of 10%D_b. Although, it can be stated that the ratio between measured and calculated shaft resistances evolves to 1 at larger pile displacements.
- For the driven precast piles, only one pile was instrumented. The calculated ultimate base resistance seems too optimistic, but this might partially be explained by the presence of residual stresses in the pile due to the installation. The total calculated ultimate pile capacity of the precast driven piles fits well with the measured data.

2.2 *Pile load test campaigns in Limelette (LIM I & LIM II)*

In the framework of an extension of the previous mentioned BBRI research project in 2000–2002, a similar extended real scale load test campaign on the same pile types was organised on a site in Limelette (LIM II). For details about this extended test campaign LIM II reference is made to Maertens & Huybrechts (2003).

A typical CPT on the test site is illustrated in Figure 5. The following layers have been identified:

- Quaternary loam (silt) : 1.0 m to ±6.2 m
- Sandy clay tot clayey sand : ±6.2 m to ±8.2 m
- Tertiary Ledian/Bruxellian sand = ± 8.2 m–…

The pile bases were installed in the sand layer at a depth of 9.5 m.

Similarly to the previous test campaign the normalised load settlement diagrams of the tested piles (10 soil displacement screw piles and 2 driven precast piles) are given in figures 6 to 8. On the same figures the normalised load settlement diagrams of a former test campaign in Limelette (LIM I) on three driven piles are given as well; it concerns a precast pile, a cast-in-situ pile and a closed end tubular pile.

For all the piles of the Limelette test campaigns (LIM I & LIM II), the calculated values have been determined based on the CPT with electrical cone in the axis of each individual pile and based on nominal pile dimensions as fixed in the recent design rules. For the soil layers in Limelette the following values

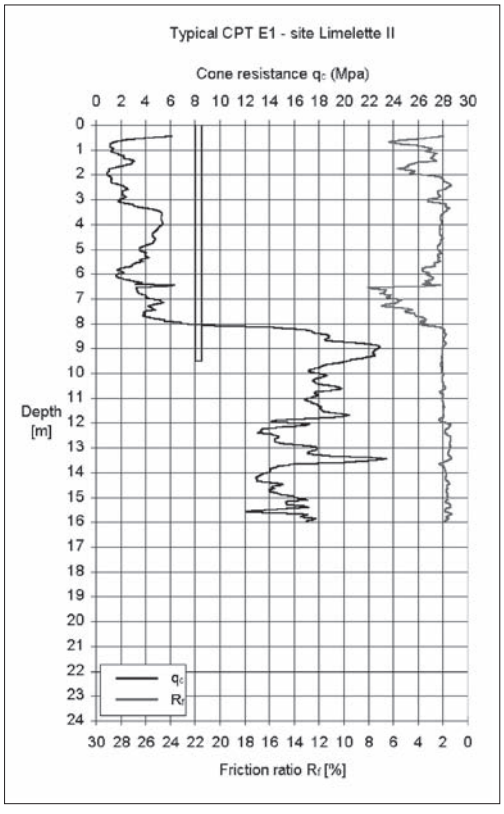

Figure 5. CPT profile an pile length site Limelette.

from the recent guidance rules have been applied in the calculated values in figures 6 to 8:

- $\alpha_b = 1$ for the driven piles and $\alpha_b = 0.7$ for soil displacement screw piles
- $\varepsilon_b = \beta = \lambda = 1$ for all piles
- $\eta_{pi}^* = 1/60$ for the loam layer at depth ±1 m to ±6.2 m
- $\eta_{pi}^* = 1/80$ for the sandy clay tot clayey sand layer (±6.2 m to ±8.2 m)
- $q_{s,i}$ (MPa) = 0.110 + 0.004 · (q_c–10) with a maximum of 0.150 MPa for the sand layer (±8.2 m to pile base)
- $\alpha_{s,i} = 0.6$ for the closed end tubular driven pile
- $\alpha_{s,i} = 1$ for the other driven piles and the soil displacement screw piles

For the LIM II test campaign, the measured values of the pile base resistance and shaft friction have been deduced from pile deformation measurements with a retrievable extensometer device, using the Fellenius (2001) interpretation methodology in order to deal with a non linear stress-strain behaviour of concrete. Furthermore, as several test piles were excavated after the load tests, the real pile dimensions

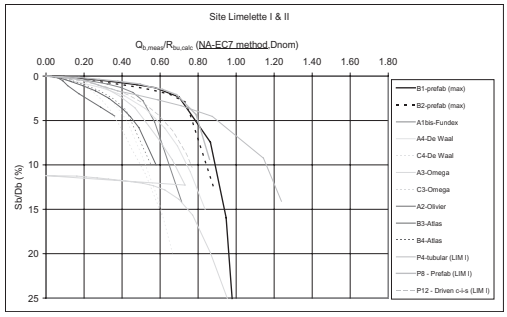

Figure 6. Normalised load settlement diagram of the pile bases in Limelette (LIM I & LIM II) ($\alpha_b = 0.7$ for screw piles and $\alpha_b = 1$ for driven piles have been applied).

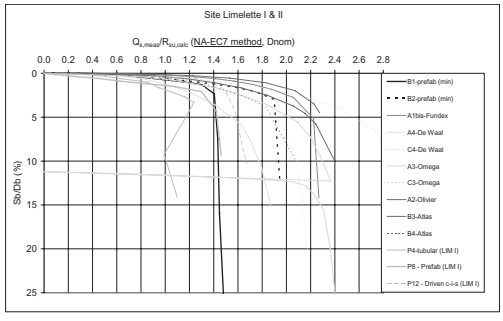

Figure 7. Normalised load settlement diagram of the piles' shaft friction in Limelette (LIM I & LIM II) ($\alpha_s = 0.6$ for tubular driven pile and $\alpha_s = 1$ for all other piles have been applied).

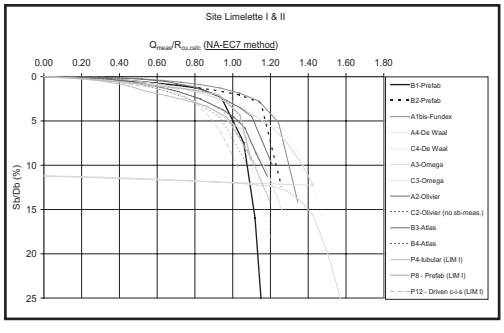

Figure 8. Normalised load settlement diagram of the total pile load in Limelette (LIM I & LIM II).

and the concrete quality with depth have been taken into account in this interpretation.

For details with regard to the LIM I test campaign reference is made to the contribution of Huybrechts & Legrand (1998).

Based on the results presented in figures 6 to 8, one can conclude that:

- When it is assumed that the ultimate resistance correspond to a settlement of 10%D_b, the calculated ultimate pile base resistances of the soil displacement screw piles seem too optimistic. It can also be deduced from figure 6 that pile settlements of 25 to 30%D_b are needed to mobilise these calculated ultimate base resistances.
- For the driven pile, the calculated ultimate base resistances seem to fit somewhat better to the measurements, but are still too optimistic. As mentioned before, residual stresses in the pile due to driving might partially explain this.
- From figure 7 it can be deduced that on the Limelette site the calculated ultimate values of the shaft resistances are far too pessimistic for all piles, in particular for the soil displacement screw piles.

2.3 *Pile load test campaign in Loenhout*

Within the framework of the construction of the high speed railway in Loenhout, (Belgium), the BBRI was asked to perform scientific pile load tests on a soil displacement screw pile of the Omega type and on a CFA pile installed with temporary casing. Details about these load tests have been reported by Theys et al. (2003).

Figure 9 illustrates the subsoil and the installation depths of one of the test piles. The following soil layers have been identified:

- Silt & clay to silty sand: 1.0 m to 3.5 m
- Sand: 3.5 m to 5.1 m
- Clay: 5.1 m to 6.3 m
- Silt: 6.3 m to 9.0 m
- Sand: 9.0 m–…

The pile bases were installed at a depth of 9.47 m for the Omega pile and 10.4 m for the CFA pile with casing.

The normalised load settlement diagrams, that have been established in the same way as the load test results of the previous test campaigns are given in Figures 10 to 12.

The calculated values have been determined based on the CPT with electrical cone in the axis of each individual pile, and based on nominal pile dimensions as fixed in the recent design rules.

For the soil layers in Loenhout the following values from the recent guidance rules have been applied in the calculated values in figures 10 to 12:

- $\alpha_b = 0.7$ for the soil displacement screw piles and $\alpha_b = 0.5$ for the CFA pile with casing
- $\varepsilon_b = \beta = \lambda = 1$ for all piles

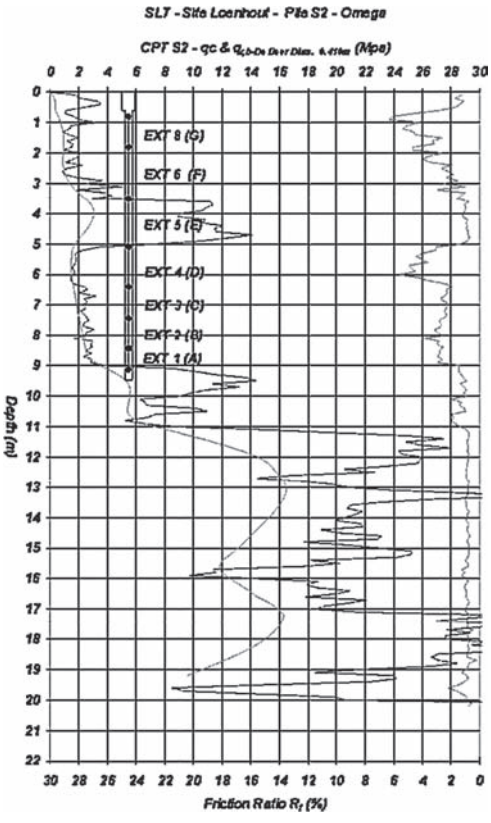

Figure 9. CPT and pile depth Omega screw pile on the Loenhout site (B).

- $\eta_{pi}^* = 1/80$ for the silt and clay to silty sand layers from 1.0 m to 3.5 m
- $\eta_{pi}^* = 1/90$ for the sand layer from 3.5 m to 5.1 m
- $\eta_{pi}^* = 1/30$ for the clay layer from 5.1 m to 6.3 m
- $\eta_{pi}^* = 1/60$ for the silt layer from 6.3 m to 9.0 m
- $q_{s,i}$ (MPa) = 0.110 + 0.004 · (q_c–10) with a maximum of 0.150 MPa for the sand layer from 9.0 m to pile base
- $\alpha_{s,i} = 1$ for the soil displacement screw pile
- $\alpha_{s,i} = 0.5$ for the CFA with casing

The measured values of the pile base resistance and shaft friction have been deduced from pile deformation measurements with a retrievable extensometer device, using the Fellenius (2001) interpretation methodology in order to deal with a non-linear stress-strain behaviour of concrete. Furthermore, as the test piles were excavated after the load tests, the real pile dimensions and the concrete quality with depth have been taken into account in this interpretation.

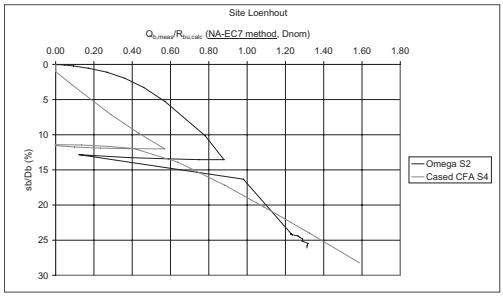

Figure 10. Normalised load settlement diagram of the pile bases in Loenhout ($\alpha_b = 0.7$ for Ω screw pile and $\alpha_b = 0.5$ for cased CFA have been applied).

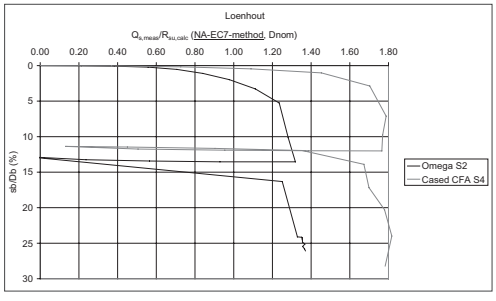

Figure 11. normalised load settlement diagram of the piles' shaft friction in Loenhout ($\alpha_{\sigma,1} = 1$ for Ω screw pile and $\alpha_{\sigma,1} = 0.5$ for cased CFA have been applied).

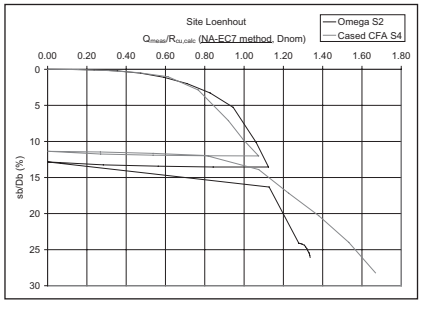

Figure 12. Normalised load settlement diagram of the total pile load in Loenhout.

From figures 10 to 12 it can be concluded that

- the calculated value of the ultimate base resistance of the soil displacement screw pile is somewhat too optimistic at a settlement of 10%D_b. The calculated ultimate value is mobilised at a displacement of 15%D_b. Beyond this pile settlement, base resistance continues to increase and is fully mobilised at a settlement of 25%D_b.
- For the CFA pile the calculated ultimate base resistance is far too optimistic at a settlement of 10%D_b.

Figure 13. Excavated CFA pile (left) with casing site Loenhout—detail of the pile base.

From figure 10 it can be stated that the base resistance continues to increase with increasing displacement and that almost no pile base resistance is mobilised in the beginning of the load test, which indicates possibly soil relaxation beneath the pile base due to an execution problem. This has been confirmed in the contribution of Theys et al. (2003), more specifically by the results of CPT performed near the pile shaft after the load tests, and by the observations of the dimensions and shape of the excavated pile (see Figure 13).

- From figure 11 it can be deduced that the calculated ultimate shaft resistances are too pessimistic for both pile types, but in particular for the CFA pile with casing.

2.4 *Pile load test campaign in Kallo*

In 1982 the Ministry of Public Works organised a load test campaign on two driven and two bored piles (performed with bentonite) on a site in Kallo (Kallo III). The tests were performed under the supervision of the former "National Pile Commission" and in collaboration with the UCL. Results of this test campaign were published in (BGGG, 1985), and by De Beer (1988).

The analysis in this contribution has however been based on the detailed test reports of UCL (1987). The influence of residual pile loads on the interpretation of the measured load distribution of the driven piles as given by De Beer (1988), has been neglected in this contribution.

Figure 14 illustrates the subsoil and the installation depths of the test piles. The following soil layers have been identified:

- Quaternary sandy silt & clay layers: –0.80 m to –3.20 m
- Tertiary Sand: –3.20 m to –14.4 m

The pile bases were installed at a depth of – 10.0 m.

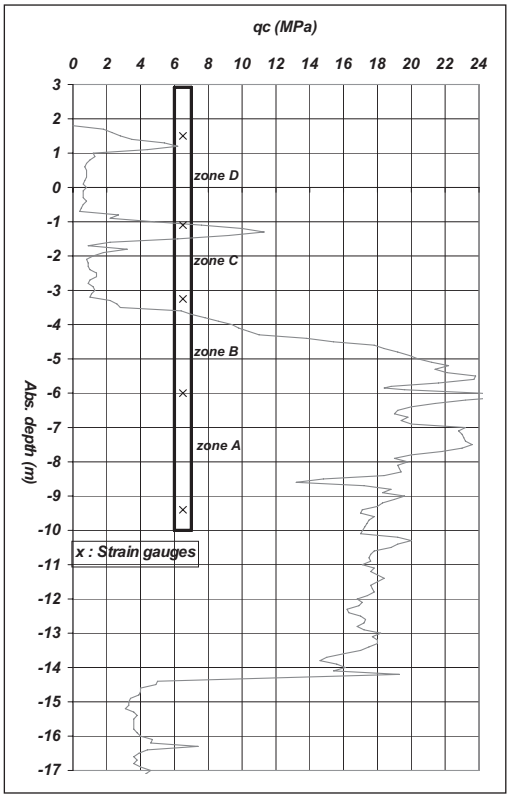

Figure 14. Typical CPT and pile lengths on the Kallo III site (B).

The normalised load settlement diagrams, that have been established in the same way as the load test results of the previous test campaigns are given in Figures 15 to 17.

The calculated values have been determined based on the CPT with electrical cone in the direct neighbourhood of the piles (±1 m distance), and based on nominal pile dimensions as fixed in the recent design rules.

For the soil layers in Kallo the following values from the recent guidance rules have been applied in the calculated values in figures 15 to 17:

- $\alpha_b = 1$ for the driven piles and $\alpha_b = 0.5$ for the bored piles
- $\varepsilon_b = \beta = \lambda = 1$ for all piles
- $\eta_{pi}^* = 1/80$ for sandy silt & sandy clay layers: –0.80 m to –3.20 m
- $q_{s,i}$ (MPa) = 0.110 + 0.004 · (q_c–10) with a maximum of 0.150 MPa for the sand layer from –3.20 m to pile base
- $\alpha_{s,i} = 0.6$ for the driven tubular piles
- $\alpha_{s,i} = 0.5$ for the bored piles

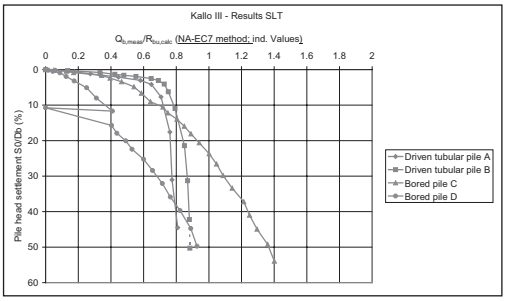

Figure 15. Normalised load settlement diagram of the pile bases in Kallo ($\alpha_b = 1$ for driven piles and $\alpha_b = 0.5$ for bored piles have been applied).

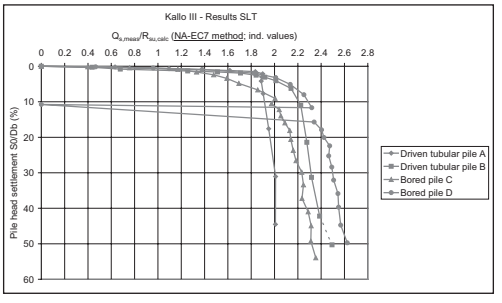

Figure 16. Normalised load settlement diagram of the piles' shaft friction in Kallo ($\alpha_{s,i} = 0.6$ for driven tubular piles and $\alpha_{s,i} = 0.5$ for bored piles have been applied).

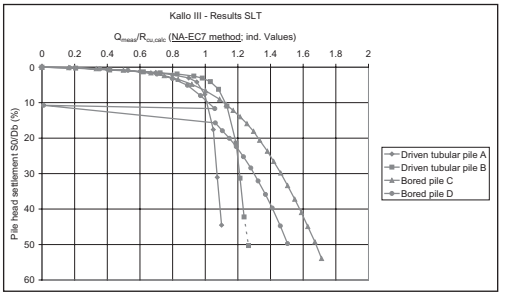

Figure 17. Normalised load settlement diagram of the total pile load in Kallo.

The measured values of the pile base resistance and shaft friction have been based on the values given in UCL (1987).

Based on figures 15 to 17 one can conclude that

- For the bored piles the calculated ultimate base resistance is far too optimistic at a settlement of 10%D_b. From figure 15 it can be stated that the base resistance continues to increase even at very

large pile displacements (up to 50%D_b). This is quite normal as, due to the large displacements, the piles become more a displacement pile.
- For the driven piles, the calculated ultimate values of the base resistances seem to fit somewhat better to the measurements, but are still too optimistic. As mentioned before, residual stresses in the pile due to driving might partially explain this.
- For both pile types, the calculated shaft friction is far too pessimistic.

3 GENERAL CONCLUSIONS

Several instrumented pile load tests performed in Belgium by the BBRI since 1997, as well as some former load tests have been analysed. Pile base resistances and shaft friction deduced from these tests have been compared with calculated values following the new design rules for piles in Belgium in BBRI (2008). In general it can be concluded that

- In tertiary clay a good agreement seems to exist between calculated and measured values of the ultimate base resistance and shaft friction for soil displacement screw piles and for precast driven piles. Recent tests on instrumented bored piles in tertiary Ypresian clay, which are not subject of this contribution, seem to confirm this for bored piles as well.
- With regard to the ultimate base resistance in sand, it can be stated that for driven piles the design rules seem to be somewhat optimistic, although the effect of residual stresses might explain this partially. For soil displacement screw piles the design rules are too optimistic when it is assumed that the ultimate base resistance corresponds to a settlement of 10%D_b. The calculated ultimate base resistance seems rather to be mobilised at settlements of 15 to 25%D_b. For bored piles, the calculated values are far too optimistic at a settlement of 10%D_b and continue to mobilise pile base resistance until very large pile displacements.
- The calculated ultimate shaft friction in silt and sand seem to be too pessimistic for all piles, in particular for the soil displacement screw piles and the bored piles. This seems to compensate for the cases in the previous points were the prediction of the ultimate pile base resistance is too optimistic (at 10%D_b).
- More instrumented pile load tests of high quality on different pile types in different soil types are needed to assess in the future in a more accurate way the real load distribution along piles.

REFERENCES

BBRI, 1998–2000 & 2000–2002. Soil displacement screw piles—calibration of calculation methods and automatisation of the static load test procedure: stage 1—friction piles & stage 2—end-bearing piles. Research programs subsidised by the Belgian Federal Ministry of Economical Affairs, convention numbers CC-CIF-562 and CC-CI-756.

BBRI, 2008. Richtlijnen voor de toepassing van Eurocode 7 in België. Deel 1: het grondmechanisch ontwerp in uiterste grenstoestand van axiaal op druk belaste funderingspalen/Directives pour l'application de l'Eurocode 7 en Belgique. Partie 1: Dimensionnement géotechnique à l'état limite ultime de pieux sous charge axiale de compression. Document available in Dutch and French on www.tis-sft.wtcb.be and www.bggg-gbms.be (English version will be available by mid-2008).

BGGG-GBMS, 1985. Belgian Geotechnical Volume published for the 1985 Golden Jubilee of the International Society for Soil Mechanics and Foundation Engineering (ISSMFE), by Belcotec and Belgian Member Society of ISSMFE. Brussels, 1985.

De Beer, E. 1971–1972. Méthodes de deduction de la capacité portante d'un pieu à partir des resultants des essays de penetration. Annales des Travaux Publics de Belgique, N° 4 (p191–268), 5 (p321–353), 6 (p351–405). Bruxelles).

De Beer, E. 1988. Different behaviour of bored and driven piles, proceedings of the Deep Foundations on Bored and Auger Piles Conference, Ghent, 1988.

Fellenius, B.H. 2001 From strain measurement to load in an instrumented pile, Geotechnical News, March 2001.

Holeyman, A., Bauduin, C., Bottiau, M., Debacker, P., De Cock, F., Dupont, E., Hilde, J.L., Legrand, C., Huybrechts, N., Mengé, P. & Simon, G., 1997. Design of axially loaded piles—Belgian practice. Proceedings of the ERTC3 seminar, Brussels.

Huybrechts, N & Legrand, C. 1998. Static and dynamic pile loading tests on different types of driven piles in Limelette, DFI 98 Conference, Vienna.

Swets & Zeitlinger, 2001. Holeyman A. (ed.). Screw Piles : installation and design in stiff clay, Lisse (The Netherlands).

Swets & Zeitlinger, 2003. Maertens, J. & Huybrechts, N. (eds.). Belgian Screw Pile Technology: Design and Recent Developments, Lisse (The Netherlands).

Theys, F., Maertens J & Maekelberg, W. 2003. Practical experience with screw piles used for the high-speed railway in Belgium, Proceedings of the 2nd symposium on screw piles, May 2003, Brussels.

UCL—Laboratoire du Génie Civil, Etude du Pouvoir portant des pieux—Chantier de Kallo, Rapport des essais 265/1-84, Juin 1987.

Deep Foundations on Bored and Auger Piles – Van Impe & Van Impe (eds)
© 2009 Taylor & Francis Group, London, ISBN 978-0-415-47556-3

Field tests with drilled shafts in tension in frictional soil

Sven Krabbenhoft & Lars Damkilde
Esbjerg Institute of Technology, Aalborg University, Esbjerg, Denmark

Allan Andersen
ISC Consulting Engineers, Kolding, Denmark

ABSTRACT: Three series of ten piles each have been installed. The lengths of the piles varied from 2 m to 6 m and the diameters were 14 cm, 25 cm and 60 cm. The piles were constructed above the ground water table using continuous flight augers and the concrete was placed by gravity free fall. All piles were tested to failure in axial uplift and the load-displacement relations were recorded and the results from the tests have been compared with theoretical values based on current design practice and the methods proposed by Fleming et al. and Reese & O'Neill seem to produce the best match with the test results.

1 INTRODUCTION

Piles in frictional soils subject to uplift forces carry their load by skin friction forces, which develop on the sides of the pile. These side resistance forces are normally computed using an empirical formula, of which a large number exist. The purpose of the present project is to compare the uplift capacities found by some of the most common codes and standards and also to see how well these values match with results from field tests. This project has been dealing with three different codes and standards and a striking thing is the fact, that according to some codes, the carrying capacity in uplift is almost independent of the strength of the soil, provided the quality of the soil is above a certain lower limit, whereas other methods put much more emphasis on the strength of the soil. This is quite remarkable, as all methods are based on results from field tests.

This point has been investigated by comparing the results from the present project with results from tests carried out in loose sand with bored piles of similar size.

Another point of interest, which has been dealt with, is to verify the significance of the diameter of the pile on the unit side resistance.

The present paper deals with the results of three test series with bored piles of different diameters in dense sand. Altogether 30 piles have been tested.

2 THE TESTING PROGRAMME

2.1 *The testing area and soil conditions*

The testing area is situated on the campus of Esbjerg Institute of Technology, Aalborg University, in Esbjerg, Denmark and the piles were placed in a grid of 4×4 metres. Three series of piles were cast and each series consisted of ten piles, of which the lengths varied from 2 metres to 6 metres at one metre intervals and two piles of each length were cast. The diameter of the piles in the three series were 14 cm, 25 cm and 60 cm.The borings, which were uncased, were carried out using a continuous flight auger at a depth of maximum 6 m and samples were taken at 1 m intervals. The ground water table was just only touched in the deepest borings and thus the water did not cause any practical problems.

The samples, which were all disturbed, have shown very homogeneous soil conditions and they all consisted of alluvial quartz sand from the ice age named Saale.

The grading of the sand has been determined on 3 different samples taken out in 3 different borings at depths of 2 metres, 4 metres and of 5 metres. The grading curves of the 3 samples were almost identical.

The mean grain size d_{50} is app. 0.22 mm, the coefficient of uniformity C is equal to 1.8 and the specific gravity of the quartz sand is 2.621.

Table 1. Soil characteristics.

Depth in m	N	Id	φ_{tr}
0,0 – 1,0	14	0.48	40
1,0 – 2,0	17	0.58	40
2,0 – 3,0	17	0.57	39
3,0 – 4,0	26	0.66	40
4,0 – 5,0	54	0.95	44
5,0 – 6,0	57	0.97	44

Average values for void ratios of the 3 samples: $e_{max} = 0.764$, $e_{min} = 0.467$.

Because of the homogeneous soil conditions just 1 SPT boring was carried out and the SPT blow count—using the below equations (1) and (2)—have resulted in the values for the relative densities and friction angles shown in table 1.

On the basis of the SPT tests the sand is characterized as dense and very dense.

$$I_d = \sqrt{\frac{N}{60 + 25 \cdot \log(d_{50})}} \quad (1)$$

In this equation—Kulhawy & Mayne (1990)—I_d is the relative density, d_{50} is mean grain size in mm and N is the SPT blow count.

The peak triaxial angle of friction has been calculated using the equation suggested by Bolton (1986):

$$\varphi_{tr} = \varphi_{cv} + 3 \cdot (I_d \cdot [10 - \ln(p')] - 1) \quad (2)$$

In this equation I_d is the relative density, p' is the mean principal effective stress at failure, which is approximately equal to twice the value of the vertical effective stress S'_z, (Rollins et al. 2005) and ϕ_{cv} is the friction angle at constant volume, which is taken to be 33° for quartz sand, Bolton (1986).

3 CONSTRUCTION OF PILES

In the open holes left by the continuous flight augers, one or more 20 mm reinforcing bars were put in position, and the concrete was placed by gravity free fall. The quality of the concrete was 25 MPa with a high degree of workability (flow value = 530 mm) and when the hole within a few minutes had been filled to the ground level, a high strength steel bolt of length 2 m was installed to a height of 1 m above the top of the concrete; that is the lap length with the reinforcing bars is 1 m. For the 14 cm piles a 16 mm bolt was used and for the 25 cm piles and the shorter of the 60 cm piles a 24 mm bolt was used. For the longer of the 60 cm piles a 32 mm 950/1050 WR Dywidag bar was used over the entire length of the piles projecting 1 metre above the top of the piles. Two piles of each length were constructed. Construction of the 14 cm piles and the 25 cm piles took place in February 2006 and the 60 cm piles were cast in June 2006.

4 TESTING OF PILES

The uplift tests of the 14 and 25 cm piles were carried out in May 2006 and the 60 cm piles were tested in September 2006. The load was applied to the piles by a hollow ram hydraulic jack resting on two steel beams, which for the 14 cm and 25 cm piles were of the type IPE 240 of length 6 m supported at either end by 100×200 mm timber. For the 60 cm piles 2 beams of the type HE 240B were used. The distance between the supports for the 60 cm piles was 2,1 metres for the 2 and 3 metre piles, 1,6 metre for the 4 metre piles, 1,35 metre for the 5 metre piles and 1,1 metre for the 6 metre piles. The purpose of the two longitudinal beams was to transfer as little additional horizontal forces to the piles as possible. As described later in this paper, account has been taken of the additional horizontal forces, caused by the vertical reactions from the beams. During the test the load was recorded using a pressure transmitter of the type Danfoss MBS 33 and for the vertical displacements were used two displacement transducers of the type HBM W20TK fixed on a separate steel beam. Both pressure transmitter and displacement transducers were calibrated before the tests started. The displacements of the piles were taken as the average of the two transducer readings. The load was raised continuously and the rate of displacement was app. 3 mm pr. minute. All the test values were recorded by means of a datalogger of the type Spider 8 from HBM. The set up of the load test for the smaller piles is shown in figure 1.

Figure 1. Load test arrangement.

5 TEST RESULTS

The results of the tests are shown in figures 2, 3 and 4.

The vertical reaction forces, transmitted from the steel beams to the ground, will cause additional horizontal forces on the sides of the piles, which again are giving rise to an apparent increase in the uplift capacity. This increase in the uplift capacity must, together with the selfweight of the pile, be deducted from the force applied by the hydraulic jack to give the true capacity of the pile. The additional horizontal forces, caused by the vertical reactions from the supporting beams, have been calculated in the following way:

The additional, vertical stresses $S_{v,z,b}$ at the depth z in the centreline of the pile due to the reactions from the supporting beams are calculated according to the theory of elasticity, (Aysen 2005) and the horizontal stresses $S_{h,z,b}$ on the pile is found from the equation:

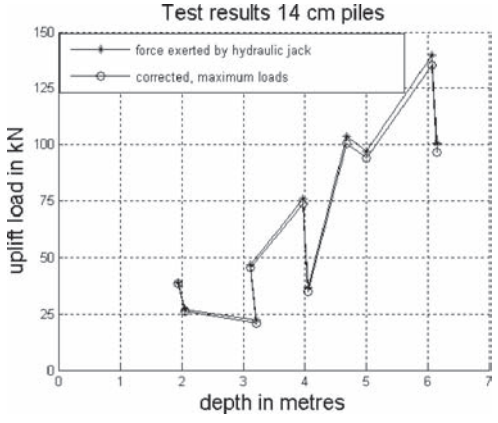

Figure 2. Test results of 14 cm piles.

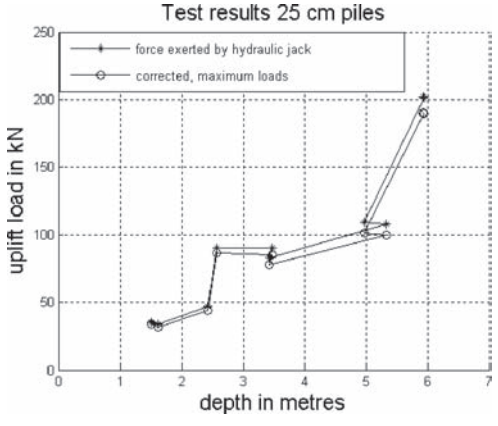

Figure 3. Test results of 25 cm piles.

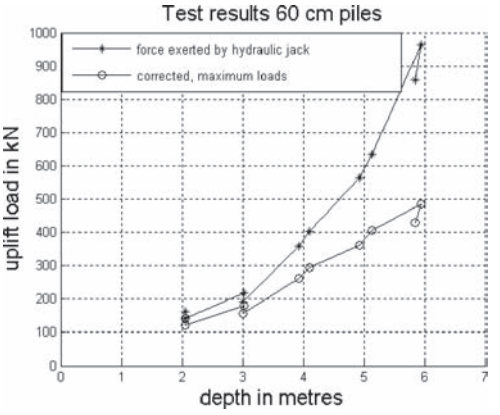

Figure 4. Test results of 60 cm piles.

$$\sigma_{h,z,b} = K(z) \cdot \sigma_{v,z,b} \tag{3}$$

In this equation $K(z)$ is the earth pressure coefficient, which is assumed to vary with the depth below ground level.

The side resistance of a pile can be calculated from the general equation, Kulhawy (1991):

$$Q_s = \int_0^L K(z) \cdot z \cdot \gamma' \cdot \tan\delta \cdot \pi \cdot d \cdot dz \tag{4}$$

where L is the length of pile, d the diameter of pile, γ' the effective soil unit weight, $K(z)$ the coefficient of earth pressure ($K = S'_h / S'_v$) S'_h being the effective horizontal and S'_v the effective vertical pressure at depth z and d = interface friction angle. For cast-in-place concrete a rough interface develops resulting in $d = f$. The value of Q_s is found from equation (5) in which Q_s is equal to the expression on the left hand side of the equal sign.

$$\int_0^L K(z) \cdot z \cdot \gamma' \cdot \tan\delta \cdot \pi \cdot d \cdot dz = Q_{jack} - Q_g - \int_0^L K(z) \cdot \sigma_{v,z,b} \cdot \tan\delta \cdot \pi \cdot d \cdot dz \tag{5}$$

In this equation Q_{jack} is the force exerted by the hydraulic jack, Q_g is the selfweight of the pile, $S_{v,z,b}$ is the vertical stress caused by the force from the hydraulic jack—equation (3)—and $K(z)$ is the earth pressure coefficient.

Form figures 2 and 3 it can be seen, that the correction due to the vertical forces from the reactions of the beams is almost negligible for the 14 cm and 25 cm piles, because the supporting beams here had a length of 6 metres, whereas the supporting beams for

the 60 cm piles had a much shorter span, leading to a substantial correction which is shown in figure 4.

The earth pressure coefficient K is as mentioned before assumed to vary with depth and for the test piles it turned out to be appropriate to express this variation by the equation:

$$K(z) = K_u \cdot \exp(-p \cdot \sqrt{z}) \tag{6}$$

where K_u is the coefficient at ground level and z the distance measured from the ground level.

Back calculations of the K values for the test data have yielded the following values for K_u and p for $z <$ 6 metres:

14 cm piles : $K_u = 2{,}8892$, $p = 0.5917$
25 cm piles : $K_u = 4.3214$, $p = 0.9345$
60 cm piles : $K_u = 4.6247$, $p = 0.8801$

In figure 5 a graphical representation of the variation in K with depth is shown and as can be seen, there is no significant difference between the K values and thus the unit side resistance is in practical terms independent of the diameter of the test piles.

5 BEARING CAPACITIES ACCORDING TO STANDARDS

5.1 *British/American methods*

Fleming et al. (1992) suggest the unit side friction f_s to be calculated from the equation:

$$f_s = \sigma'_r \cdot \tan\delta = K \cdot \sigma'_v \cdot \tan\delta \tag{7}$$

where $K = 0.90$ for all sands and 0.6 in silt; S'_v is the vertical effective stress and d the angle of friction in the interface between the soil and the pile and can be taken to be in the interval f_{cv} and f_{peak} No distinction is made between the values in tension and compression and in this study a value of d equal to the average $f_{peak} = 41°$. has been used.

On the basis of tests with 41 piles Reese & O'Neill (1988), have suggested the unit side friction to be calculated from the equation:

$$f_s = \beta \cdot \sigma'_z \tag{8}$$

in which $\beta = 1.5–0.245 \cdot z^{0.5}$ and z is the depth below ground level and S'_z is the vertical effective stress. It is assumed, that $0.25 <$ ß <1.20 and $f_s < 200$ kPa. For SPT values lower than 15, O'Neill has later recommended to scale down the side resistance by the factor N/15 (O'Neill, 1994).

The values according to the above mentioned methods, together with the fitted values of the test results using the calculated values of K_u and p are summarized in figures 6, 7 and 8. In figure 9 are shown the fitted results from a test series of ten bored piles in loose sand with a diameter of 14 cm, carried out by the authors in 2006, (Krabbenhoft et al. 2006). Also in figure 9 are shown the capacities computed according to the above mentioned methods.

5.2 *The German code of practice—DIN 4014*

This code is based on a large number of tests for both cased and uncased borings and the unit side friction on the shaft may be related to the results obtained from a SPT test using the following equation:

$$f_s = a \cdot N \tag{9}$$

in which f_s is the unit side resistance in kN/m^2 and N is the SPT blow count. The factor a takes on a value 4.14 for coarse sand and 2.73 for fine sand. The value

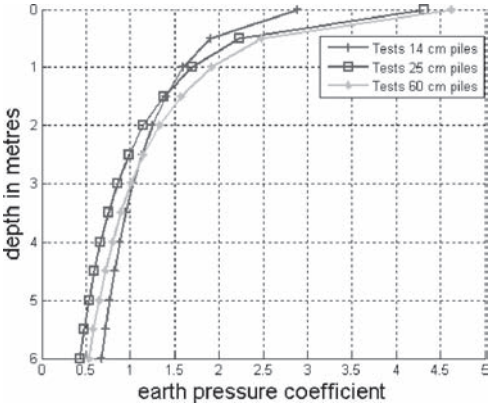

Figure 5. Variation of earth pressure coefficient K.

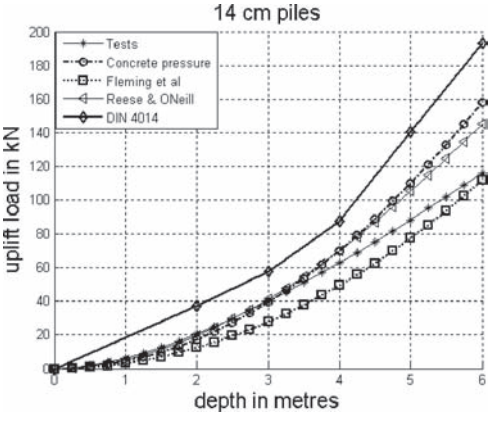

Figure 6. 14 cm piles in dense sand.

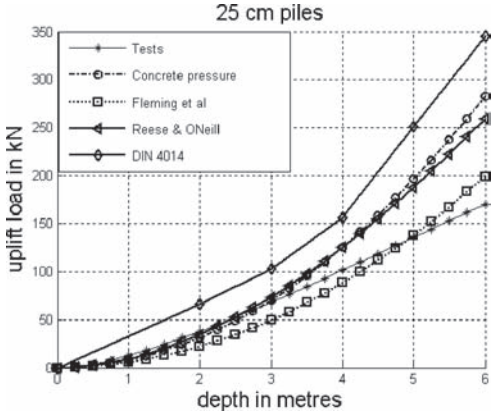

Figure 7. 25 cm piles in dense sand.

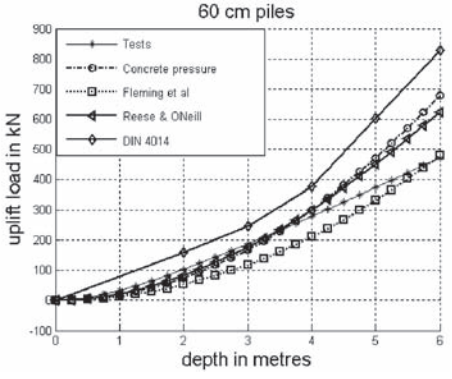

Figure 8. 60 cm piles in dense sand.

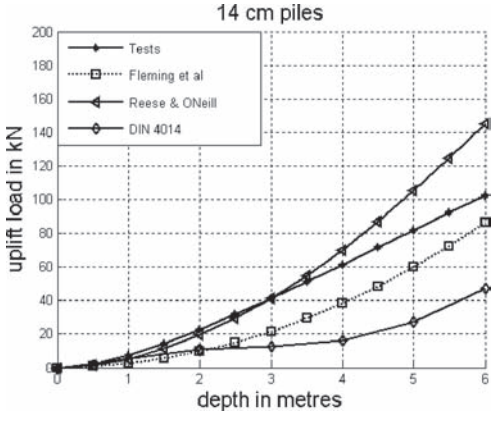

Figure 9. 14 cm piles in loose sand.

of f_s should not be taken greater than 120 kN/m^2. For the piles in this test a = 2.73 has been used and the calculated values to DIN 4014 code are indicated in figures 6, 7 and 8. For the DIN values in figure 9 a value of a = 4,14 has been used. The low values in figure 9, predicted by the German Code, are due to very low SPT values.

Also in the figures 6, 7, 8 is shown the uplift capacity of the piles assuming the lateral pressure on the pile being equal to the pressure from the concrete during casting. It is interesting to see, how close these values lie to the Reese & O'Neill values.

6 COMPARISON OF MEASURED AND COMPUTED VALUES

From the graphs in the figures 6–8 it can be seen, that the German Code DIN 4014 is yielding the highest predicted ultimate values and the second largest predicted results are reached by the Reese and O'Neill method. The test results are in general in the interval between the capacities recommended by Reese and O'Neill and Fleming et al. and closer to the former for the shorter piles and closer to the latter for the longer piles.

The relatively high SPT blow counts reflect at the strongest on the DIN 4014 values, whereas the Reese and O'Neill values are independent of the SPT for $N > 15$ blows.

By comparing the fitted test values for the 14 cm piles in dense sand (figure 6) with the fitted test values for the 14 cm piles in loose sand (figure 9), it can be seen, that the values in dense sand on the average are only slightly above the values in loose sand indicating, that the relative density of the sand only plays a minor role in estimating the uplift capacity. Also from figure 9 it can be seen, that the test results in loose sand in general are in the interval between the values predicted by the Reese and O'Neill method and the Fleming Method.

7 CONCLUSIONS

Load tests on thirty piles with diameters 14 cm, 25 cm and 60 cm in dense sand have shown, that the diameter of the pile has no significant effect on the unit side resistance. Also by comparison with tests carried out in loose sand it can be concluded, that the uplift capacity of a bored pile is only to a smaller degree dependent upon the strength of the soil and this in line with both the method proposed by Fleming et al. and the Reese & O'Neill method.

The method proposed by Reese & O'Neill produces the best match with the test results for the shorter piles and for the longer piles the Fleming method gives values closer to the test values.

The German Code of practice DIN 4014 produces results which for a loose sand strongly understimates and for a dense sand overestimates the capacity of a bored pile.

ACKNOWLEDGEMENTS

The authors wish to thank civil engineer B.Sc. Svend Karkov and civil engineer B.Sc. Jesper Jorgensen for skilful and careful work in connection with the tests and the Lida and Oskar Nielsen Foundation for a substantial, financial support. Also the work carried out by the soil exploration company Jysk Geoteknik during construction of the piles is highly appreciated.

REFERENCES

Aysen, A. 2005. *Soil Mechanics*. Taylor & Francis Group, London and New York.

Bolton, M.D. 1986. The Strength and Dilatancy of Sands. *Geotechnique*, Vol. 36, No. 1, 65–78.

DIN 4014, *Bohrpfähle*. March 1990.

Fleming, W.G.K., Weltman, A.J., Randolph, M.F. & Elson, W.K. 1992. *Piling Engineering*. Taylor & Francis Group, London and New York.

Krabbenhoft, S., Clausen, J. & Damkilde, L. 2006. Tension Tests on bored piles in sand. *ELU—ULS 2006. International symposium on the ultimate limit states of geotechnical structures.*

Kulhawy, F.H. & Mayne, P.W. 1990. *Manual on estimating properties for foundation design. Rep. No. EPRI EL-6800, Electric Power Research Institute, Palo Alto, Calif.* 2–25.

Kulhawy, F.D. 1991. Drilled Shaft Foundations. *Foundation Engineering Handbook, 2nd Ed., H. Y. Fang, ed., Van Nostrand-Reinhold, New York.*

O'Neill, M.W. 1994. *Drilled Shafts*. Proc., International Conf. on Design and Construction of Deep Foundations, Fed. Highway Admin., Washington, D.C., Vol. 1, 185–206.

Reese, L.C. & O'Neill, M.W. 1988. *Drilled Shafts: Construction procedures and design methods. Pub. No. FHWA-HI-88–042,U.S.Dept.of Transportation, Washington, D.C.*, 564–564.

Rollins, K.M., Clayton, R.J., Mikesell, R.C. & Blaise, B.C. 2005. Drilled Shaft Side Friction in Gravelly Soils. *Journal of Geotechnical and Geoenvironmental Engineering,* Vol. 131, No. 8, August 1, 2005.

Deep Foundations on Bored and Auger Piles – Van Impe & Van Impe (eds)
© 2009 Taylor & Francis Group, London, ISBN 978-0-415-47556-3

Bi-directional instrumented load test of a pile bored in Guinea Bissau

F. Rocher-Lacoste
Université Paris Est, LCPC, MSRGI, Paris, France

M. Bustamante
MB Fondations, Saint-Cloud, France

M. England
LOADTEST Limited, Sunbury on Thames, Middlesex, UK

ABSTRACT: On July 2nd, 2007, LOADTEST ltd., the LCPC and MB-Foundations performed a static loading test with an Osterberg-cell on a bored pile of 1600 mm diameter. The 56.50 metre deep test pile constructed by Trevi Spa for Soares da Costa group, was in Guinea Bissau near the Cacheu River. This test was conducted to validate the design of the foundations of the Sao Vicente bridge; a project undertaken by the Ministry of Public Works of the Republic of Guinea Bissau and funded by the European Development Fund. The pile were loaded statically using the O-cell® bi-directional method 25 days after concreting. The piles were also instrumented using LCPC removable extensometers. This paper provides a very brief presentation of the bridge project and the test pile instrumentation: LCPC removable extensometers and O-cell® instrumentation. The results are detailed and analyzed herein and the combined use of these two instrumentation systems is a world première.

1 INTRODUCTION

As part of the Trans-Africa road project, the Ministry of Public Works of the Republic of Guinea Bissau and the European Development Fund set out to build a 620 metre long bridge over the Cacheu River. In order to evaluate the foundation design for the future São Vicente Bridge, it was decided to make a static load test using the Osterberg Method. To obtain additional information on the behaviour of the test pile, a complementary instrumentation system using the LCPC removable extensometer string (Bustamante & Doix 1991) was deployed.

The 1600 mm diameter bored test pile was constructed to a depth of 56.50 metres at a location near the river. This pile was also used to validate the drilling method for the project.

2 SITE SUB-SURFACE CONDITIONS

Many geological investigations were necessary (on land and in the river) to attempt to accurately determine the soil characteristics. The contract specified the use of the Menard pressuremeter method.

Table 1. General sub-surface description.

NGGB Level [m]	Description	Pressure limit average (Mpa)
+3.0 to +2.0	Backfill/ working platform	0.05
+2.0 to –7.9	Soft silt	0.1
–7.9 to –25.65	Clay	1.0
–25.65 to –51.35	Sands	2.0
–51.35 to –53.5	Compact clay	2.5

The sub-surface stratigraphy at the general location of the test pile and the Menard pressure limit (pl, results of pressuremeter test) were reported to Table 1.

3 TEST PILE CONSTRUCTION

Trevi Spa, employed by Grupo Soares da Costa S.A., began excavating the dedicated test pile on June 5, 2007 and performed the final cleanout and concreting on June 7, 2007. The 1600 mm test pile was excavated to a tip elevation of –53.50 m, under bentonite. The pile was started with a 1624 mm O.D. casing, installed by vibratory driving with a Soilmec VS-8.

Figure 1. Link Belt LS-418 with Soilmec RT3-ST.

Figure 2. The reinforcing cage with the O-cell.

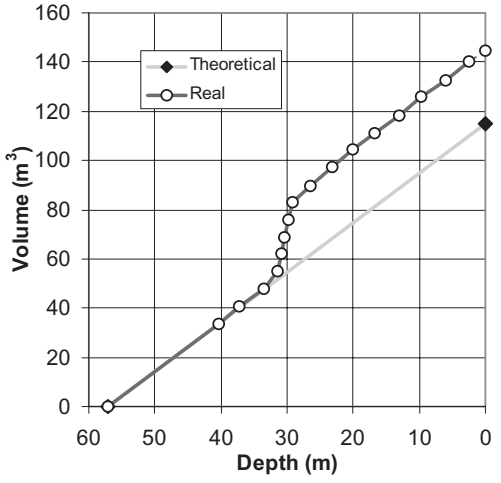

Figure 3. Concreting curves (real and theoretical).

To perform the piling operations, Trevi Spa utilized a Link Belt LS-418 drilling system attached to a Soilmec RT3-ST, see Figure 1. The bottom of the pile was airlifted after drilling. After cleaning the base, the reinforcing cage with attached O-cell® assembly (Fig. 2) was inserted into the excavation and temporarily supported from the steel casing.

Concrete was then delivered into the pile by a 300 mm O.D. pipe into the base of the pile.

The Figure 3 presents a comparison between the theoretical and the real concrete curves. There was an expected soft layer between approximately 33 and 29 metres where the over consumption of concrete required an additional 35 m^3 of concrete. This over consumption coincided with a level of grey sand, where the Menard pressure limit indicated less than 1 MPa.

4 OSTERBERG CELL TESTING

4.1 *Pile instrumentation*

Test pile instrumentation and assembly was carried out under the direction of LOADTEST with the assistance of LCPC and MB-Foundations. The loading assembly consisted of one 670 mm O-cell located 10.50 metres above the toe of the pile, see Figure 4. The Osterberg cell was calibrated to 13.6 MN and then welded closed prior to shipping by the manufacturer, American Equipment and Fabricating Corporation.

O-cell® testing instrumentation included four Linear Vibrating Wire Displacement Transducers (LVWDTs, Geokon Model 4450) positioned between the lower and upper plates of the O-cell assembly to measure expansion. Two telltale casings were attached to the reinforcing cage, diametrically opposed, extending from the top

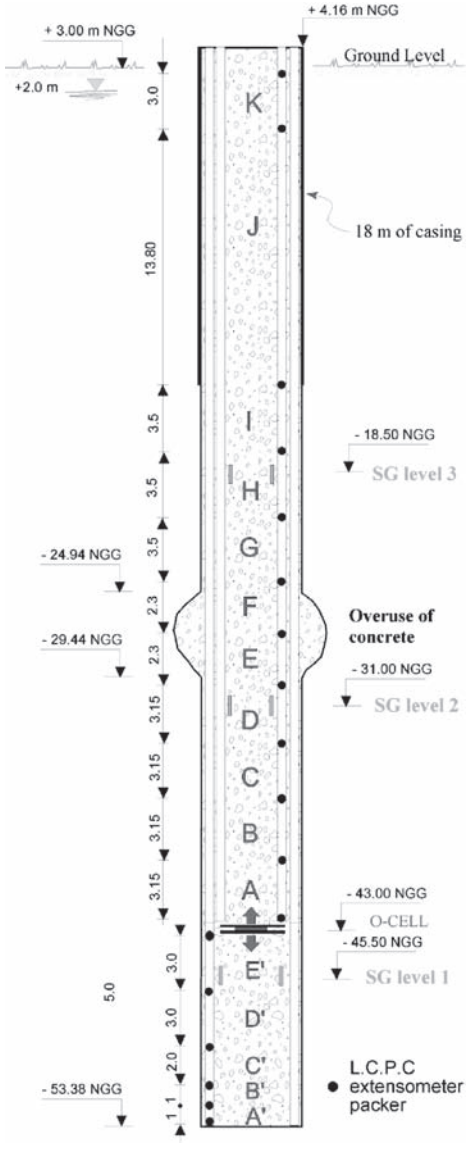

Figure 4. Schematic section of the test pile.

of the O-cell assembly to beyond the top of concrete to measure the total pile compression. Strain gauges were used to assess the side shear load transfer of the pile above and below the O-cell assembly. One level of two "sister bar" vibrating wire strain gauges (Geokon Model 4911) was installed, diametrically opposed, in the pile below the base of the O-cell assembly and two levels of two gauges were installed in the pile above it.

All telltale casings were constructed using a nominal 25 mm O.D. embedded steel pipe and 6 mm internal steel telltale rod.

Figure 5. Two LVDTs: one monitoring the top of pile from the reference beam and the pile compression above the O-cell.

Two lengths of steel pipe were also installed, extending from the top of the pile to the top of the bottom plate, to vent the break in the pile formed by the expansion of the O-cells. The O cell assembly was attached normal to the reinforcing cage on the ground and when lifted to vertical, racking of the cage caused a tilt of the assembly across the cage which was measured as 65 mm. This tilt would correspond to a required correction to the applied load of only 0.11% and was ignored.

4.2 *Test arrangement*

Throughout the load test, key elements of pile response were monitored using the equipment and instruments described herein. Pile compression was measured using 6 mm telltales installed in the 25 mm steel pipes and monitored by Linear Voltage Displacement Transducers (LVDTs). Two LVDTs attached to a reference system were used to monitor the top of pile movement, see Figure 5.

The reference system consisted of an 11.5 m 300 × 300 mm H-beam welded between a pile casing one end and a buried steel beam upright at a height of approximately 1.25 m. The supports were located approximately three pile diameters from the centre of the test pile. The beam was not shaded during the test. An automated digital survey level (Leica NA 3003) monitored the reference beam for movement during testing from a distance of approximately 15.85 metres to a precision of ±0.01 mm. A maximum upward movement of 4.62 mm was observed for the reference beam; this was assumed to be due to environmental effects and not settlement of the reference system which had been assembled two days prior to the start of the test.

Both a Bourdon pressure gauge and a vibrating wire pressure transducer were used to measure the pressure applied to the O-cell at each load interval. The pressure transducer was used for manually setting and maintaining loads and real time plotting. The Bourdon pressure gauge readings were used as a check on the transducer and for data analysis. There was close agreement between the Bourdon gauge and the pressure transducer.

In addition to the requirements for bi-directional testing, allowance was made during construction of the cage for the installation of up to two removable extensometer strings, to be monitored and reported on by LCPC as required. One string was intended to be used for the pile element above the O-cell arrangement and one for below. The extensometers defined a total of 16 measuring sections, see Figure 4.

4.3 *Data acquisition*

All the installed O-cell instrumentation was connected through a data logger (Data Electronics 515 GeoLogger) to a laptop computer allowing data to be recorded and stored automatically at 30 second intervals and displayed in real time. The same laptop computer synchronized to the data logging system was used to acquire the Leica NA3003 data.

The data acquisition of the strain gauges within the removable extensometer string was conducted manually.

4.4 *Testing procedures*

The test was begun by pressurizing the O-cell in order to break the tack welds that hold it closed (for handling and for placement in the pile) and to form the fracture plane in the concrete surrounding the base of the O-cell.

After the break occurred, the pressure was immediately released and the testing started. Zero readings for all instrumentation were taken prior to the preliminary weld-breaking load-unload cycle, which in this case involved a maximum applied pressure of 200 psi (1.38 MPa) to the O-cell.

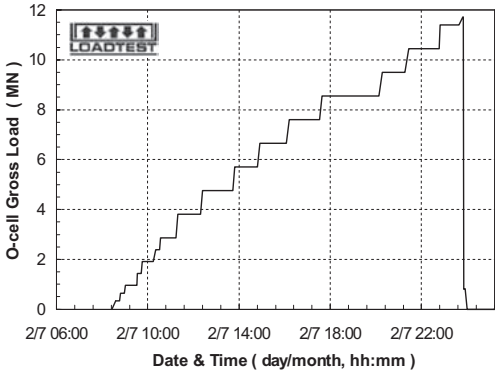

Figure 6. O-cell load increment—time plot.

The Osterberg cell load test was conducted as follows: The 670 mm diameter O-cell, with its base located 10.50 metres above the base of pile, was pressurized to assess the combined end bearing and lower side shear characteristics of the pile section below the O-cell using the skin friction above as reaction. The O-cell was pressurized in 17 loading steps up to 51.02 MPa (7400 psi) resulting in a bi-directional gross O cell load of 11.4 MN (Fig. 6).

Each successive scheduled load increment was maintained constant for a minimum of 30 minutes and up to a maximum of 180 minutes while automatically maintaining the O-cell pressure constant until a creep criterion of less than 0.05 mm per 10 minutes in each direction was met. The data logger automatically recorded the instrument readings every 30 seconds.

5 TEST RESULTS AND ANALYSES

On 2nd July 2007, LCPC and LOADTEST performed the static loading test. Figure 7 shows the instrumented pile head during the test.

The loads applied by the O-cell act in two opposing directions, resisted by the capacity of the pile above and below. It can be considered that the O-cell does not impose an additional upward load until its expansion force exceeds the buoyant weight of the pile above the O-cell. Therefore, net load, which is defined as gross O cell load minus the buoyant weight of the pile above, is used to determine skin friction resistance above the O-cell and to construct the equivalent top-loaded load-settlement curve. For this test a pile buoyant weight of 1.47 MN above the O-cell was used.

5.1 *Ultimate resistance*

With a settlement value $S_0 = 85.94$ mm, using a failure criteria of 1/10th of the pile diameter as the total settlement, the ultimate resistance Rc of the pile was not

Figure 7. Pile Head with instrumentations.

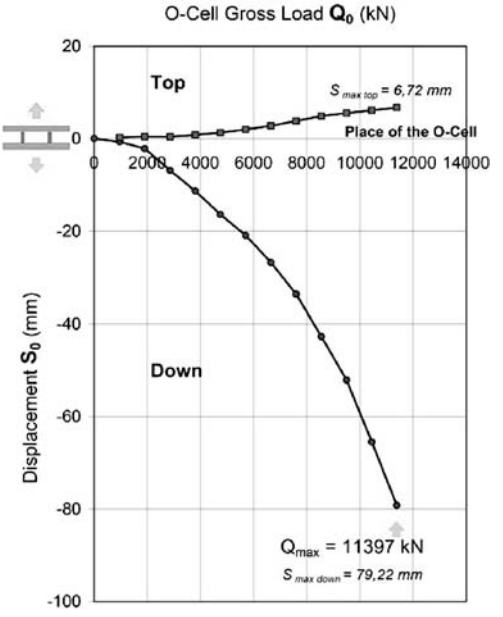

Figure 8. Load settlement curves.

achieved under the maximum load test of 22.8 MN (2280 t). By using the method of Chin (Chin 1970, Fleming 1992), we can estimate the ultimate resistance to be about 30 MN.

The maximum downward applied load was 11.7 MN which occurred at the last load interval. At this loading, the average downward movement of the O-cell base was 79.2 mm after correction due to reference beam movement.

The maximum upward applied gross load was 11.7 MN. At this loading, the upward movement of the top of the O-cell was 6.7 mm. Figure 8 shows the combined load settlement curves in both directions.

5.2 *Skin friction resistance*

The different strain gauge systems employed during the O cell loading test gave similar results.

5.2.1 *Above the O-cell*

The upward movement of the pile (Fig. 8) and the strain gauge micro-strain results (Fig. 9) have been analyzed to determine the characteristic skin friction values.

The analysis of the two strain gauges (SG 2 & 3) shows a maximum mobilized unit skin friction of:

q_s = 33 kPa at 21.5 m depth in the clay.
q_s = 62 kPa at 34 m, in sand.

The upward movement of the pile (Fig. 8) and the removable extensometer micro-strain results (Fig. 10) have been analyzed to determine the skin friction distribution. The analysis of the stain gauges within

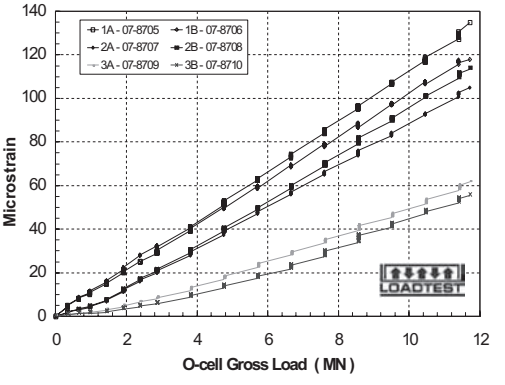

Figure 9. Strain guage micro-strain results (me) (SG 1a. 1b, 2a 2b, 3a & 3b).

the removable extensometer string give unit skin friction values of:

q_s = 80 kPa from 17 to 21.5 m depth, clay level,
q_s = 60 kPa from 21.5 to 24 m, it is for sand,
q_s = 65 kPa from 32.1 to 35.25 m, sand,
q_s = 110 kPa from 35.25 to 38.4 m, sand,
q_s = 60 kPa from 38.4 to 41.55 m, sandy clay,
q_s = 50 kPa from 41.55 to 44.7 m, sand.

This analysis is presented in Figure 11.

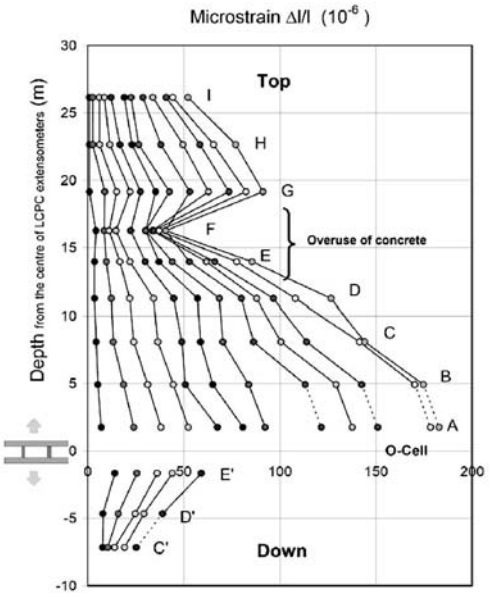

Figure 10. Removable extensometer micro-strain results.

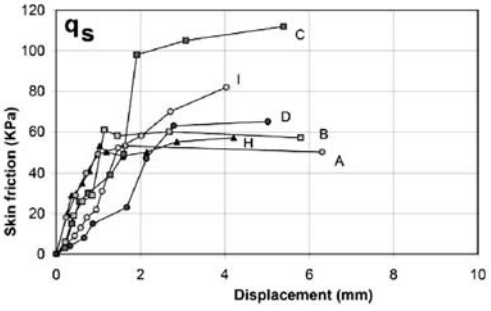

Figure 11. Mobilization of shaft resistance along the pile above the O-cell.

5.2.2 *Below the O-cell*

During the load increment of 4.76 MN, water caused an electrical problem and it was decide to stop the acquisition of the removable extensometer below the O-cell. If the results of the removable extensometer are extrapolated from the strain distribution previously determined, (SG level 1) it is possible to estimate the toe resistance of the pile as 22.8 MN and a total skin friction of approximately 7.2 MN.

The analysis of the strain gauge (SG 1) indicates a unit skin friction of: q_s = 72 kPa at 48.5 m depth in sand at the end of the test.

The interpretation of extensometer measurements made by the LCPC and MB Foundations identified unit skin friction q_s for different levels along the pile (Fig. 10). The comparison between the measured values and those taken from curves recommended by the French norms (Fascicle 62 Title V) shows the validity of the values taken in the foundations design notes (determination of the length of the piles) of Soares da Costa group.

6 CONCLUSION

The pile behaviour measured downwards allows the ultimate capacity to be determined and a total bearing capacity below the O-cell of 22.5 MN (asymptotic definition) is deduced.

The most interesting conclusion made from this test is that it has been proved possible to construct the pile with LCPC removable extensometer and use the O-cell methodology to implement the loading. Due to the low cost of implementing the O-cell test it has proved more economical than a traditional top-down axial static loading test.

The use of the removable extensometer in determining unit skin friction along the pile has been proved beneficial in determining whether to slightly modify the method of pile design analysis and also provided a nice insight into the effect of the oversize cross section.

The combined use of these two instrumentation systems is a world première and we hope to make further tests and create a database.

ACKNOWLEDGEMENT

The authors wish to give a special thanks to all workers of Trevi Spa and Soares da Costa group for the excellent performance of their work.

REFERENCES

Bustamante M., Doix B., 1991. A new model of LCP removable extensometer. Proceeding 4th international conference on piling and deep foundation, Stresa, 7–12 April. Ed.: Balkema.

Chin F.K., 1970. Estimation of the ultimate load of piles not carried to failure, Proc. 2nd Southeast Asian Conf. on Soil Engineering, pp. 81–90.

Fleming W.G.K., 1992. A new method for single pile settlement prediction and analysis, Geotechnique 42, No. 3, pp. 411–425.

Fascicule 62—Titre V. Règles techniques de conception et de calcul des fondations des ouvrages de génie civil. Cahier des clauses techniques générales applicables aux marchés publics de travaux. 1993. Ministère de l'Equipement, du logement et des transports. Paris. Textes officiels (in French).

Deep Foundations on Bored and Auger Piles – Van Impe & Van Impe (eds)
© 2009 Taylor & Francis Group, London, ISBN 978-0-415-47556-3

Static field load test on foundations: Case study of rigid inclusions

Alain Le Kouby & Frédéric Rocher-Lacoste
Université Paris-Est, LCPC, MSRGI, Paris, France

Serge Lambert
Keller Fondations Speciales, France

Philippe Liausu
Menard Soltraitement, France

ABSTRACT: Within the French research project ASIRI (Soil Improvement by the technique of rigid inclusions), 420 mm in diameter and 6.50 m long rigid inclusions were built following two installation methods; drilling with or without removal of soil. The LCPC has been entrusted with the static field load test of the two types of columns which aimed at comparing their bearing capacity as well as the distribution of load along the columns.

1 INTRODUCTION

The French national research project ASIRI (Soil Improvement by the technique of rigid inclusions) aims at developing new design methods for soil improved by the technique of rigid inclusions. An experimental site has been chosen at Saint Ouen l'Aumone which was characterized by a 7–11 m thick layer of soft soil underlying by a substratum. On this test area, a embankment was built on a soft soil reinforced by rigid inclusions and monitored (Simon and Schlosser, 2005).

In addition, load tests were carried out on two single Ø 420 mm and 6.50 m long columns built following two methods; drilling with and without removal of soil (Rocher-Lacoste and Le Kouby, 2006).

The results of these two tests will help to understand and to model the behaviour of the rigid inclusions beneath the embankment: embankment underlied by soil reinforced by rigid inclusions.

The Laboratoire Central des Ponts et Chaussées (LCPC) was entrusted to achieve field load tests on these two single rigid inclusions. These tests aimed at studying the influence of the installation method on the response of the columns; the bearing capacity, the settlement of a column for a given load; which could correspond to load transferred to the columns by the embankment and the distribution of load along the column.

In this paper, at first, we analyze the main information on the soil campaign and the building up of columns. Secondly, we analyze the results of the loading tests in terms of bearing capacity and load distribution along the columns (shaft friction and tip resistance).

2 SOIL INVESTIGATION

The soil campaign carried out on the experimental site made us identify two different layers: a first soft layer (low mechanical characteristics) with a thickness encompassed between 7 and 11 m and the substratum underneath. Besides, heterogeneities within the first layer appeared due to numerous removal of soils along the years. The last soil campaign outlined, from the cuttings and boreholes, the following layers near the place the field load tests on columns were undertaken:

From 0 to 3.40 m: a clayey sand layer,
From 3.40 m to 4.30 m: a clay layer,
From 4.30 m to 7.30 m: a peat layer,
From 7.40 m: compact sand.

The water table was estimated at 3 m.

Pressumeter tests were carried out and allowed us to identify the range of the depth of the substratum but were not satisfactory in terms of measured limit and creep pressures. This is the reason why, we are not showing the results of these tests.

3 RIGID INCLUSIONS

The rigid inclusion technique enters the soil reinforcement technique as they are founded on the soft

layer and not on the substratum. In addition, contrary to the pile, they are not connected to a slab. They can eventually be overlaid by a distribution layer (or not) under an embankment.

The rigid inclusions tested in this research project were built by two contractors. KELLER FOUNDATIONS built up the rigid inclusions drilled without removal of soil on 11 May 2006 (Figure 1). MENARD SOLTRAITEMENT built up the rigid inclusions drilled with removal of soils on 18 May 2006 (Figure 2).

Figure 1. KELLER FOUNDATIONS—Column P1.

Figure 2. MENARD SOLTRAITEMENT—Column P2.

Both inclusions were tested until failure through field load tests carried out on 26–28 June 2006 i.e. one month after they had been built up.

The rigid inclusions were 420 mm in diameter and 6.50 m long. A closed ended steel tube was jacked in the center of the inclusion after the concrete had been injected in the column. This steel tube will be used to set up the removal extensometer during the test phase and had the following characteristics: a length of 7 m and an external diameter of 60 mm, an internal diameter of 52 mm i.e. a thickness of 4 mm.

Besides, a column head (dimension 400 mm $\times$ 400 mm $\times$ 400 mm) was built to ensure a good contact

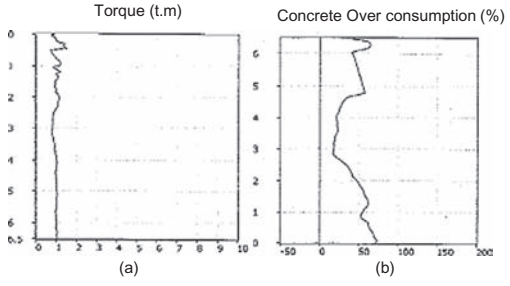

Figure 3. Drilling parameters of rigid inclusion P1 drilled without removal of soil (a) torque and (b) injected concrete volume.

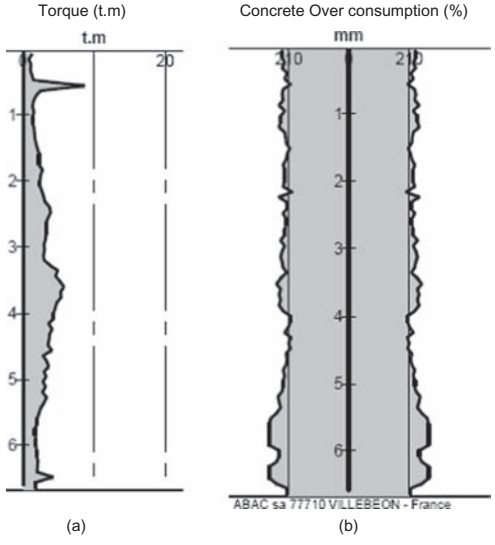

Figure 4. Drilling parameters of rigid inclusion P2 drilled with removal of soil (a) torque and (b) injected concrete volume.

and a good vertical load transfer between the jack and the head of the rigid inclusion (Figure 5).

On Figures 3 and 4, the drilling parameters, especially the torque and the injected concrete volume, are shown. We can notice that the energy (torque) used to drill was much more important in the case of the inclusion drilled with removal of soil P2 (about 5 t.m) in comparison to the other column P1 (1 t.m). The range of the torque for the other columns built up was similar. In addition, as far as the over consumption of concrete is concerned, it was less important for the column drilled with removal of soil P2 (25.39%) in comparison to P1 (47.21%).

Therefore the geometry of the columns was to be adjusted in the analysis.

Many other columns were built on the test site. The difference of overconsumption of concrete between the two techniques was not always of the same range. Nevertheless, the overconsumption of concrete was generally superior to 20% for both types of column.

4 MONITORING BY LCPC

4.1 *Reaction frame*

Two field load tests were realized.

For each of these tests, an independent reaction frame was set up. It consisted in a steel beam laying on wood beams and linked to four bars DYWIDAG 22 mm and consequently to four reaction piles 420 mm. They work in tension when the column was tested in compression. The limit tension resistance of the DYWIDAG bar was 2 MN. The anchors were built on 11 May 2006. This system was designed to resist a limit tension load of 3 MN.

MENARD SOLTRAITEMENT provided the reaction frame, set up by the LCPC. On Figure 5, we show the reaction frame used for column P1.

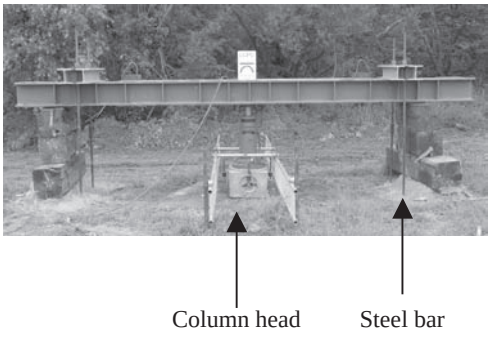

Figure 5. Reaction frame.

Table 1. Planning of the tests.

Type of inclusion	Building phase	Load test	Set up of concrete (days)
P1	11 May 2006	28 June 2006	48
P2	18 May 2006	27 June 2006	40

P1: Drilling without removal of soil.
P2: Drilling with removal of soil.

4.2 *Load application, sensors and deformation gauges*

The loads are applied through a hydraulic jack of 2 MN capacity and 200 mm displacement range. At the head of the jack, we position a load sensor. A steering joint is set up between the load sensor and the hydraulic jack to avoid bending moments.

– The column head displacement were measured with the help of four dial gauges with a accuracy of 1/100 mm.
– The deformation $\Delta l/l$ were measured through the technique of the removable extensometer of the LPC. The column was then divided into 6 segments of measures within the close ended 52/60 steel tube.

4.3 *Load program*

For each of the load test, the columns were loaded following the LPC procedure (Bustamante & et al., 1991, 1996 and 2001). The load phase consisted in applying constant incremental load of 25 kN until failure. Table 1 summarizes the planning of the tests.

5 LOAD TESTS AND RESULTS OF TESTS

For both single inclusions of the ASIRI research project, load tests were carried out on the 27–28 June 2006. The failure loads were obtained for both inclusions i.e. the loads were measured until the column settled by 10% of its diameter.

5.1 *Column head load and loading curves*

The load-displacement curves for both columns P1 and P2 are shown on Figure 6.

– For the rigid inclusion drilled without removal of soil (P1), 16 load steps of 25 kN were necessary. The failure progressively occurred. Maximum load reached was 400 kN, which also corresponds to the the limit load (Qu) of the inclusion at 10% diameter displacement. Indeed, for that load, the

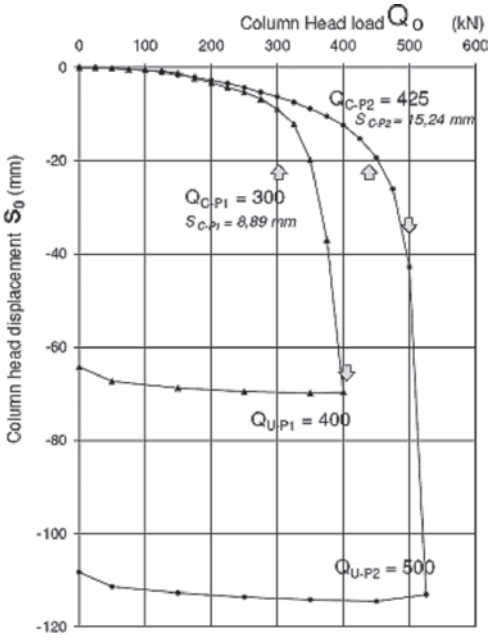

Figure 6. head displacement (S_0) —head load de charge Q_0 for inclusion P1 (no removal) and inclusion P2 (removal).

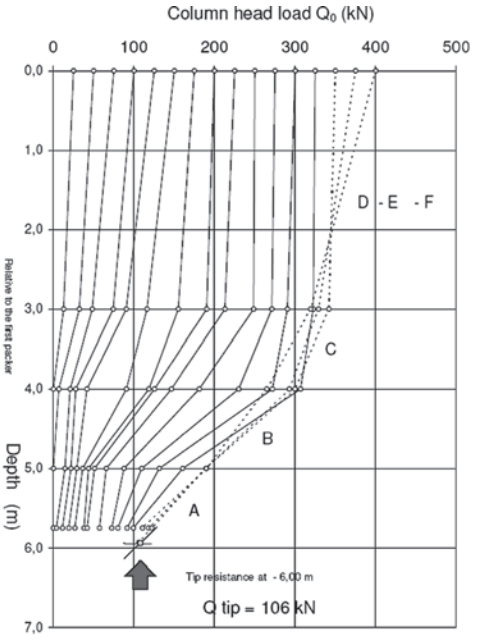

Figure 7a. Distribution of load along the column P1—drilled without removal of soil.

rate of displacement significantly increased. The test was stopped at a column head displacement S_0 of 70 mm. The creep load Qc is about 300 kN (Figure 7). We only present the case of column P1.

– For the column drilled with removal of soil (P2), twenty load steps of 25 kN were necessary and the maximum load reached was 500 kN.The limit load was also of of 500 kN as the settlement measured for that load largely overran the 10% diameter and reached S_0 = 110 mm. The creep load obtained was about 425 kN (Figure 6).

The influence of the installation method was obviously significant in terms of bearing capacity as the rigid inclusion drilled with removal of soil was able to carry a maximum load 25% higher than the inclusion drilled without removal of soil. This result is consistent with the design methods.

5.2 *Removal extensometer measures—distribution of loads*

5.2.1 *Rigid inclusion P1—no removal of soil*

The analyze of the distribution of loads along the rigid inclusion and their mobilization were made from the unit deformations ε and are shown on Figures 7 (a) and (b). The results showed a small distribution of load from the top to the depth of 4 m and beyond, the column acted as it was expected. As far as shaft

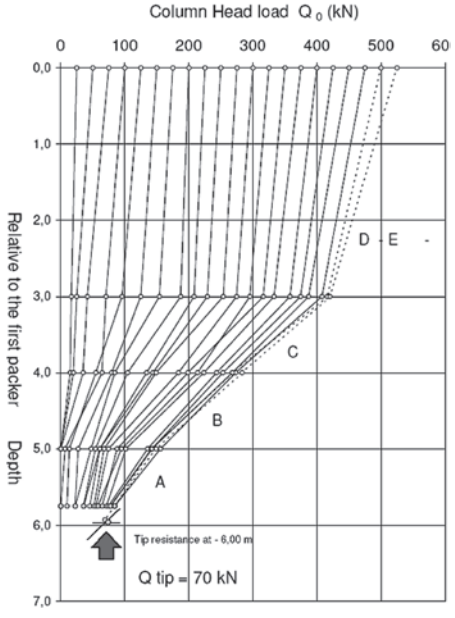

Figure 7b. Distribution of load along the column P2—drilled with removal of soil.

friction is concerned (Figure 9), 73% of the maximum load was taken from the shaft (Qs = 294 kN) and 27% of the load by the tip (Qp = 106 kN). The mobilization curves of shaft friction for the different levels A—B—C—D—E—F are represented on figure 9; calculated for the theoretical side surface (for a diameter of 420 mm) of the column. The values of shaft friction at different levels calculated from the deformation of gauges are: levels D, E and F qs ≈ 25 kPa, level C qs ≈ 40 kPa, level B qs ≈ 90 kPa, level A, qs ≈ 55 kPa. We can suppose that the steel tube and the concrete were unsealed during the higher load steps which were difficult to analyze.

5.2.2 *Inclusion P2—removal of soil*

The distribution of loads along the rigid inclusion were made from the unit deformations ε and showed the same shape as for rigid inclusion P1. The results showed a small distribution of load from the top to the depth of 3 m and beyond, the column acted as it was expected. As far as shaft friction is concerned (Figure 10), 86% of the maximum load was taken from the shaft (Q_s = 430 kN) and 14% of the load by the tip (Qp = 70 kN). The mobilization curves of shaft friction for the different levels A—B—C—D—E—F

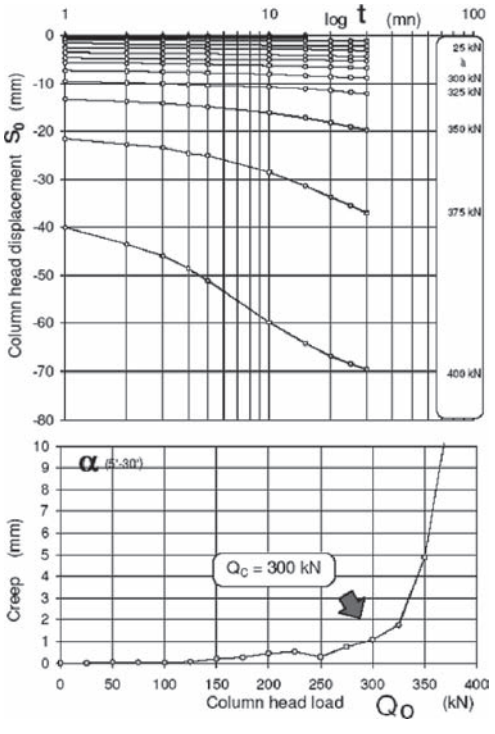

Figure 8. Determination of creep load—column P1—drilled without removal of soil.

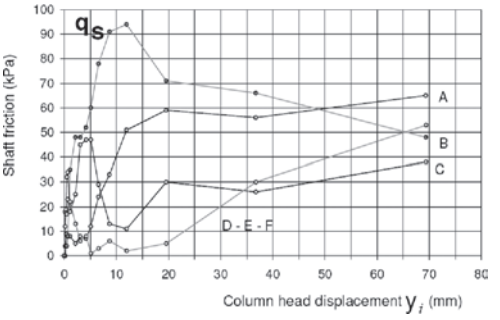

Figure 9. Rigid inclusion drilled without removal of soil (P1).

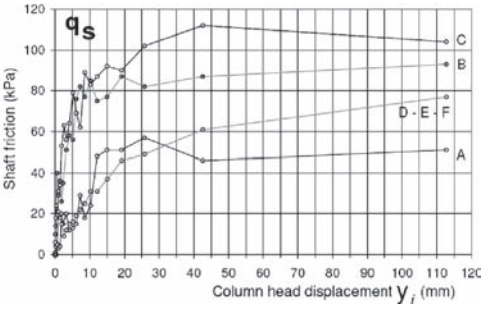

Figure 10. Rigid inclusion drilled with removal of soil (P2).

are represented on figure 10; calculated for the theoretical side surface (for a diameter of 420 mm) of the column. The values of shaft friction at different levels calculated from the deformation of gauges are : levels D, E and F qs ≈ 45 kPa, level C qs ≈ 90 kPa, level B qs ≈ 80 kPa, level A, qs ≈ 50 kPa.

For column P1, we can notice that the distribution of load along the column P1 was low small from level F to level C but from level B to the tip the biggest part of the load is carried. Nevertheless, for column P2, the load carried by the three levels D, E and F was low and increased a lot from level C to the tip. It illustrated a difference between the two installation methods.

The column drilled with removal of soil P2 showed stronger values (double) of shaft friction than column P1 on the first 4 m. Beyond, the values of shaft friction measured were in the same range showing no significant difference; an observation that has also been made at the level of the tip.

Indeed, as far as tip resistance is concerned, no significant difference was noticed between the two columns. Some reasons could be the difficulty during the building phase to get a good tip in a soft soil and the fact that we do not exactly know where the over consumption of concrete was located in both columns.

Table 2. Limit, creep loads and settlements.

Type of inclusion	Limit load Q_u (kN)	Creep load Q_c (kN)	Settlement under Q_c (mm)
Rigid inclusion P1	400	300	8,89
Rigid inclusion P2	500	425	15,24

6 CONCLUSIONS

The load tests carried out on rigid inclusions drilled without and with removal of soil allowed us to compare the influence of the installation method in terms of bearing capacity as well as distribution of load along the inclusions in a soft soil.

The results showed that the column built with removal of soil carried a load 25% higher that the other column; a result consistent with the design.

Besides, the creep loads were 40% higher in the case of the column built with removal of soil (table 2). Therefore, this technique should provide a better response in terms of settlement in service state.

The shaft friction mobilized in the case of the inclusion drilled without removal of soil was smaller than the other column in the first four meters but beyond, the values were similar.

Besides, the tip resistance calculated in both cases showed similar values (106 kN for column P1 and 70 kN for column P2). As for maximum load, the steel tube might unsealed from the concrete, the tip resistance was difficult to be determined precisely.

We are not able to compare the values of shaft friction and tip resistance we have determined to the design methods as we were not satisfied with the results of the pressumeter tests carried out near the column load tests.

At last, the installation method described as drilling without removal of soil could be expected as having a smoother mechanical response than the other method (drilling with removal of soil). Nevertheless, this technique can be used in zones that allows small displacement of the soil corresponding to small disturbance of the surrounding buildings.

REFERENCES

Bustamante M., Doix B. 1991. A new model of LPC removable extensometer. Proceedings of the 4th International on Deep Foundation (DFI), pp. 475–480.

Bustamante M., Gianeselli L. 1996. Méthode d'essai n°45—Recommandations pour la préparation d'un essai de chargement statique de pieu instrumenté à l'aide d'un extensomètre LPC. Laboratoire Central des Ponts et Chaussées, Paris.

Bustamante M., Gianeselli L. 2001. Méthode d'essai n° 34. La mesure des déformations à l'aide des extensomètres amovibles LPC. Laboratoire Central des Ponts et Chaussées, Paris.

Fascicule 62—Titre V 1994. Règles techniques de conception et de calcul des fondations des ouvrages de génie civil. Cahier des clauses techniques générales applicables aux marchés publics de travaux. 1993. Ministère de l'équipement, du logement et des transports. Paris.

Rocher-Lacoste F., Le Kouby A. 2006. Interprétation des essais de chargements réalisés à Saint Ouen l'Aumône. IREX, Projet ASIRI, LC/06/ASI/14.

Simon, B., Schlosser, F. 2005. Soil reinforcement by vertical stiff inclusions in France. Symp. Rigid Inclusion in difficult subsoil conditions, 11–12 mayo, Mexico, 22 p.

Deep Foundations on Bored and Auger Piles – Van Impe & Van Impe (eds)
© 2009 Taylor & Francis Group, London, ISBN 978-0-415-47556-3

Vertical and horizontal static load tests on bored piles in Dubrovnik

Jan Masopust
FG Consult, s.r.o. Praha, Czech Republic
Technical University Brno, Czech Republic

ABSTRACT: The paper deals with the results of two static pile tests of vertical load up to 15,0 MN and four pile tests of lateral load up to 1,5 MN on bored piles in Dubrovnik, Croatia. The piles were fitted with the 1500 mm diameter steel liner along the shaft length in quaternary sediments and fixed in bedrock without casing with the diameter of 1800 mm. Two tested piles were fully instrumented, e.g. the distribution of normal stress in pile shaft was monitored. The static load tests showed an excellent vertical load-bearing capacity of both piles, which showed only negligible deformation at the maximum test load. The horizontal deformations were much larger due to the technology used in the construction of these piles.

Keywords: Bored pile, Static load test, Limit state of serviceability.

1 INTRODUCTION

The paper deals with the results of two static pile tests of vertical load up to 15,0 MN and four pile tests of lateral load up to 1,5 MN on bored piles in Dubrovnik, Croatia, where the new passenger port would be built. The drilling and geophysical survey has shown that the bedrock on the site is formed by light grey to light brown limestones and dolomites of granular structure; the rock is tectonically fractured and weathered, with occasional larger cracks and tiny caverns and pockets filled with clay. The limestones and dolomites are affected by a weathering process. The assumed depth of the bedrock at the test piles location is 14,0–17,0 m. The overlying soils are formed by Quaternary sediments and recent fills. The Quaternary sediments are represented by clays of medium plasticity and hard to stiff consistency with thickness varying from 1 to 5 m. Recent marine sediments are formed by silt and sand with organic material, of soft consistence. The Port quay is built on backfilled material and rockfill of varying grain size. The underground water level (e.g. sea level) is in the depth of 2,0 m.

2 TEST PILES

All preliminary test piles e.g. TP-V1 and TP-V2 (vertical load tests), TP-H1 and TP-H2 (horizontal load tests) were of 1500 mm diameter, enlarged in the bedrock to 1800 mm diameter base. The piles were fitted along the shaft length in quaternary sediments with the 1500 mm diameter steel liner, that had the total length 14,2 to 17,0 m, the length of pile shaft in limestone layer was 4,5 m. In case of axial static load test the steel test bridge was anchored by 12 temporary $8 \times 0{,}6''$ strand anchors total length of 30,0 m—fixed in the bedrock for the length of 10 m (Figure 1). In case of lateral load test the testing set comprised of the steel strut equipment with the bearing capacity of 2,0 MN, which strutted the pair of test piles (Figure 2). Some dates of test piles are shown in the Table 1.

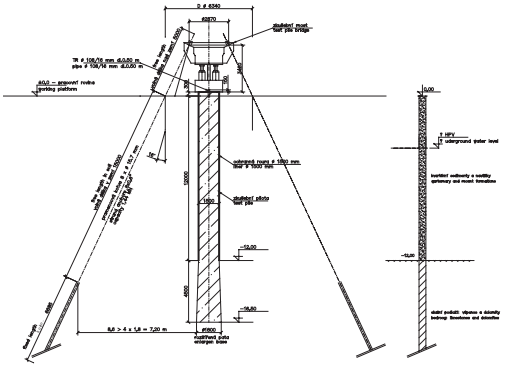

Figure 1. Configuration of axial load test on the pile TP-V1.

3 AXIAL STATIC LOAD TESTS

The static load test set comprised of the following elements (Figure 3):

– bored test pile of 1500 mm diameter, enlarged in the bedrock to a 1800 mm diameter base, fitted

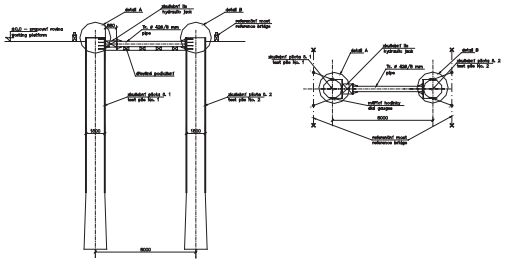

Figure 2. Configuration of horizontal load test.

Table 1. Characteristics of the test piles.

Test pile	Total length of pile	Length of steel liner	Date of pile constr.	Date of pile test	Geological profile
TP-V1	18,70	14,20	10.–11. 05/06	07.07. 2006	0–10 : fill 10–11,5 : mud 11,5–14,2 : stiff to solid clay 14,2 : limestone
TP-V2	21,50	17,00	05.–11. 05/06	12.– 13. 07/06	0–11 : fill 11–15,5 : mud 15,5–17,0 : stiff to solid clay 17,0 : limestone
TP-H1	18,70	14,00	27.–29. 04/06	10.–11. 07/06	Like TP-V1
TP-H2	21,30	16,50	04.–06. 05/06	14.–15. 07/06	Like TP-V2

along the entire length with a 1500 mm diameter steel liner, with the measurement of stress along the pile shaft,
- 12 temporary 8 × 0,6″ strand anchors, total length of 30,0 m with the single load capacity of 1,44 MN,
- steel test bridge of 22,0 MN load bearing capacity with a set of 3 hydraulic jacks,
- reference bridge for electronic measurements of settlement in 4 points on the pile head with accuracy 0,1 mm,
- actual check equipment for measuring forces acting on the pile and for settlement measurements, connected to a control computer.

The static load tests on piles TP-V1 and TP-V2 were performed with the loading and unloading steps, which were applied in accordance with the test plan. Deformations stabilised very quickly and without any problems. In case of test pile TP-V1 one anchor at 13,5 MN applied load failed (the anchor No. 9 was ripped and the load redistributed to the remaining anchors). Due to the anchor failure a decision was

Figure 3. Axial static load test on the pile TP-V1.

made for safety reasons not to continue with the test and the planned final 15,0 MN load step was not carried out. The static load test on pile TP-V2 was performed in accordance with the test plan up to design load of 15,0 MN. The total settlement at 15,0 MN load was 9,32 mm, of which permanent deformation after unloading was 4,48 mm (48%) and elastic deformation 52% (Figure 4).

According to Eurocode EC 7, chapter 7, pile design load-bearing capacity $R_{c,d}$ can be determined from comparable results (at least 2 static load tests performed in similar geotechnical environments):

- measured load-bearing capacity $R_{c,m}$ = 13,5 MN and 15,0 MN, respectively,
- characteristic bearing capacity $R_{c,k} = \min[(R_{c,m})_{mean}/\xi_1; (R_{c,m})_{min}/\xi_2]$, i.e.
- $(R_{c,m})_{mean}$ = 14,25; $R_{c,k}$ = 14,25/1,3 = 10,96 MN
- $(R_{c,m})_{min}$ = 13,5; $R'_{c,k}$ = 13,5/1,2 = 11,25 MN

a. combination 1: (A1 + M1 + R1)
design b.c. $R_{c,d} = R_{c,k}/\gamma_t = 10,96/1,15 = \underline{9,53\ MN}$
(coeff. A1 must be applied γ_G = 1,35 and $\gamma_Q = 1,50$),

b. combination 2: (A2 + M1 + R4)
design b.c. $R_{c,d} = R_{c,k}/\gamma_t$ = 10,96/1,50 = $\underline{7,31\ MN}$ (coeff. A2 must be applied γ_G = 1,00 and γ_Q = 1,30).

More interesting is the analysis of the load distribution along the pile shaft according to stress measurement in full instrumented test pile TP-V1 (Figure 5).

On the basis of measured distribution curves in course of static load test it is possible to create the diagrams of the relation of the skin friction and tip resistance on the pile head settlement (Figures 6 and 7).

The relationship between load and deformation of bored pile is distinctly non-linear. It was the reason

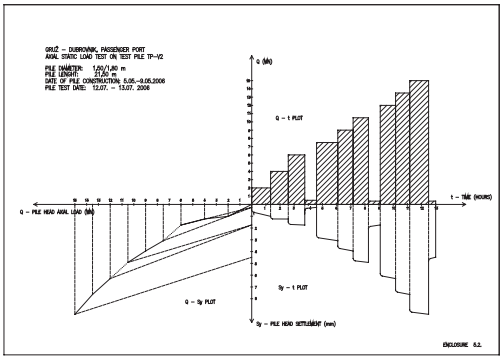

Figure 4. Load-settlement curve of test pile TP-V2.

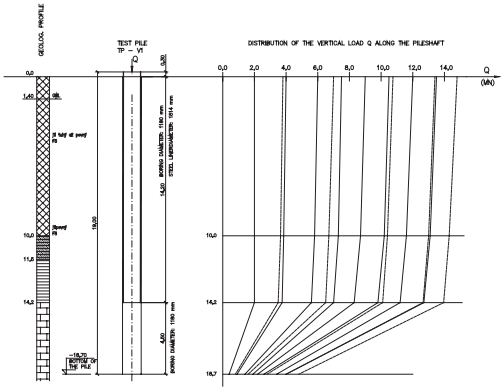

Figure 5. Load distribution curves along the pile shaft, test pile TP-V1.

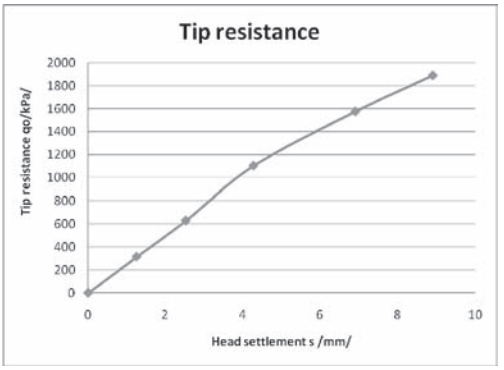

Figure 6. Tip resistance depending on pile head settlement.

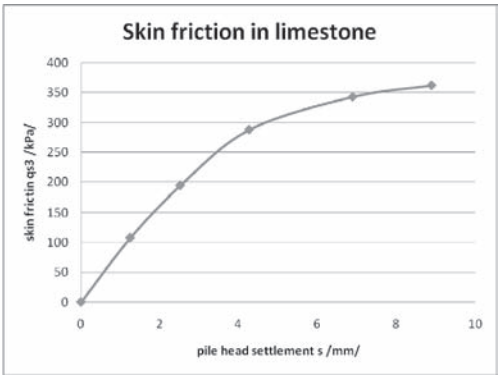

Figure 7. Skin friction in bedrock (limestone).

for the acceptance of rheological model of foundation soil characterized by pressiometric modulus of soil deformation E_s and rheological coefficient of soil structure *a*. The rheological coefficient *a* depends on compression strength and stress-strain relationship for the weak rocks. Using the non linear relationship according to computing model [Masopust, (2003)], we receive following data for the skin friction, tip resistance and limit settlements:

- $q_{s1,lim}$ = 13,60 kPa (limit skin friction in the 1. layer—fill—with reducing by the steel liner),
- $q_{s2,lim}$ = 20,60 kPa (limit skin friction in the 2. layer—mud—with reducing by the steel liner),
- $q_{s3,lim}$ = 372,00 kPa (limit skin friction in the 3. layer—weathered limestones and dolomites),
- q_0 = 3153,00 kPa (tip resistance in bedrock for the pile head settlement of 10 mm),
- $s_{s1,lim}$ = 19,40 mm (limit settlement for maximal skin friction in 1. layer),
- $s_{s2,lim}$ = 23,00 mm (limit settlement for maximal skin friction in 2. layer),
- $s_{s3,lim}$ = 8,90 mm (limit settlement for maximal skin friction in 3. layer—bedrock).

The conformity between actual load settlement curve and results of computing model is very good.

4 HORIZONTAL STATIC LOAD TESTS

The tests were performed on two pairs of piles. The first pile was already used for vertical load and the other one was performed specially for horizontal test. The test set comprised of the following elements:

- bored test pile of 1500 mm diameter, enlarged in the bedrock to an 1800 mm diameter base, fitted along the entire length with 1500 mm steel liner; distance between pile axes is 8,0 m,
- steel strut equipment consisting of steel plates on pile heads, ball joint, hydraulic jack of 2,0 MN capacity (Figures 2 and 8),

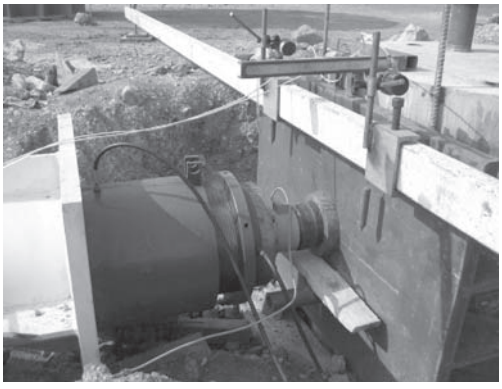

Figure 8. Detail of the hydraulic jack and reference bridge in case of horizontal load test.

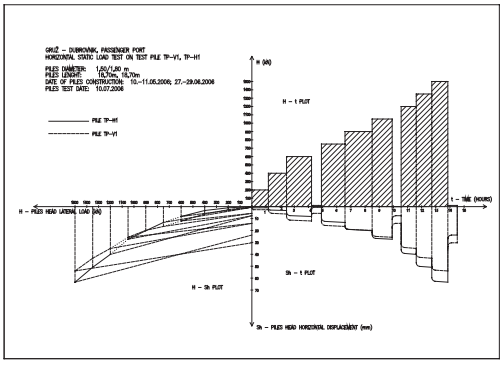

Figure 9. Horizontal load test on the piles TP-V1 and TP-H1.

– reference bridge for measuring horizontal deformation of both piles in 2 points on the pile head (measurement accuracy 0,1 mm),
– actual measuring and check equipment for measuring forces acting on the piles.

The test results of piles TP-V1 and TP-H1 show growing and considerable horizontal deformation of both pile heads with minimum differences—within 18% (Figure 9). Total deformation at 1,50 MN for pile TP-V1 and TP-H1 reached 54,00 mm and 63,40 mm respectively of which the permanent deformation after unloading was 30,36 mm (56%) and 23,85 mm (38%) respectively In case of horizontal load test on piles TP-V2 and TP-H2 the results were similar. Total deformation at 1,50 MN for pile TP-V2 and TP-H2 reached 58,48 mm and 68,25 mm respectively of which the permanent deformation after unloading was 31,44 mm (54%) and 3,29 mm (55%) respectively. The total deformation of every pile was caused by the pile construction technology used, when a space of undetermined size formed around the post-installed 1514 mm protective liner along the length of 10–14 m of the pile shaft, filled with compressible material the properties of which could not be accurately determined. Insufficient horizontal resistance of this fill is the main reason for these large horizontal deformations of the pile heads.

No uniform methodology (according to Eurocode 7) exists for determining of the design bearing capacity, because the 1. limit state is not suitable for the analysis. Only the limit state of serviceability is suitable it means, the permissible horizontal deformations of the pile heads must be known. In case, that the permissible deformation is 25 mm, the design horizontal bearing capacity reaches:

a. combination 1: A1 + M1 + R1
   $H_{c,d} = 810$ kN,
b. combination 2: A2 + M1 + R4
   $H_{c,d} = 621$ kN.

5 CONCLUSIONS

Four static load tests were performed on drilled piles at the Dubrovnik Passenger Port construction site. The results show the following:

– an excellent vertical load-bearing capacity of piles TP-V1 and TP-V2, which even at the maximum test load showed only negligible deformation,
– relatively large horizontal deformation of piles caused by the not suitable technology used in the construction of these piles.

ACKNOWLEDGEMENTS

The author is pleased to acknowledge the support of the MSM (research project 0021830519).

REFERENCES

Masopust, J.: *Design of axially loaded bored single piles.* Proceedings of the 4th International Geotechnical Seminar, Ghent, Belgium, June 2003, pp. 203–208,

Masopust, J.: *Gruž—Dubrovnik, Passenger Port. Final report on Results of Pile Static Load Tests.* FG Consult, Praha, 08/2006.

Deep Foundations on Bored and Auger Piles – Van Impe & Van Impe (eds)
© 2009 Taylor & Francis Group, London, ISBN 978-0-415-47556-3

High capacity bored piles in soft volcanic rock—experiences based on single- and multi-level tests

Chr. Moormann
Smoltczyk & Partner GmbH, Stuttgart, Germany

R. Saul
Leonhardt, Andrä + Partner GmbH, Stuttgart, Germany

ABSTRACT: The 'Puente Centenario' is the second bridge crossing the famous Panama Canal in Central America. The cable-stayed bridge with two 185 m high pylons and a main span of 420 m crosses the Canal in the area of the 100 m deep Gaillard Cut, the narrowest part of the Canal. Besides basalt flows the subsoil consists of very heterogeneous soft rocks of volcanic debris causing long-term creep behaviour and landslides moving. The foundation design for the new bridge is presented with a focus on the deep foundations and the pile load-tests using Osterberg cells. The pile tests were executed as single- and multi-level tests resulting in new experiences on the pile behaviour in soft volcanic rock. A special focus will be set on the evaluation of the results of single-level and multi-level tests comparing the behaviour of pile segments at different stages. The results of single-level tests will be compared with the results of multi-level tests.

Keywords: deep foundation, axial pile load tests, Osterberg Cells, volcanic soft rocks.

1 INTRODUCTION

For the improvement of the infrastructure in the Canal Zone of Panama in Central America it was decided to construct a second bridge crossing the Panama Canal. The bridge with a total length of 1,050 m was designed as cable stayed bridge crossing the 100 m deep Gaillard trench of the Canal (Fig. 1). As the bridge is just the second link over the Canal it will be of special relevance for the connection between North and South America ('Interamerican Highway'). The foundation design for the pylons and piers of the bridge was influenced by the very heterogeneous subsoil conditions predominated by soft rocks of volcanic debris (McCullough 1977, Stewart 1984).

For the pile foundations in the soft volcanic rocks originally very long bored piles were planned. In order to optimize these deep foundations pile load tests were executed using the Osterberg test-method. The tests allow a comparison of single- and multi-level tests with O'cells and result in new experiences on the pile behaviour in the soft volcanic rock of Panama.

2 PANAMA CANAL: 100 YEARS HISTORY

The 81.6 km long Panama Canal is the shortest connection between the Atlantic and Pacific Ocean and one of the main important sea-paths in the world being of major economic and strategic importance. The Canal with a width of 90 m to 300 m starts next to Colón at the Caribbean Sea. At the Gatun locks the vessels are raised by 26 m before entering the Gatun Lake. It follows the passage through the Gaillard resp. Culebra Cut, a 13.7 km long and up to 100 m deep cut that was carved through the rock and shale of the Continental Divide. At the south end of the Gaillard Cut the vessels are lowered back to sea level at two sets of locks before leaving the Canal next to Panama City.

The Gaillard Cut was the main hurdle for the construction of the Panama Canal. A first attempt by the French engineer de Lesseps to cross the Isthmus with a sea-level canal was brought to financial ruin in 1889 due to technical difficulties and tropical diseases. An U.S.-effort undertook the construction of a canal 26 m above sea level. Lasting ten years, the labor of more than 75,000 men and new excavation techniques in the Gaillard Cut (Fig. 2) to complete the job successfully in 1914. But the Isthmus' unique geology made landslides a constant menace: in 1915 the Canal was temporarily closed due to a large landslide.

Presently studies are conducted to expand the Canal and to build new locks for 'Post-Panamax' vessels.

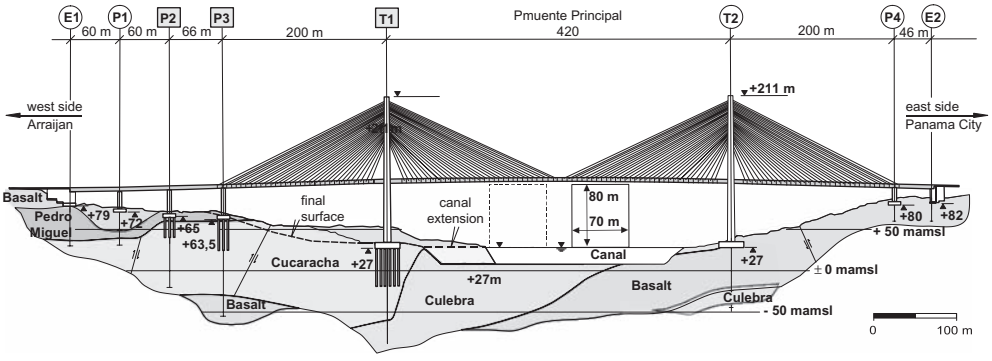

Figure 1. Longitudinal section of the new 'Puente Centenario' crossing the Panama Canal with subsoil conditions.

Figure 2. Panama Canal: excavation work using trains in the deep Gaillard Cut, 1911.

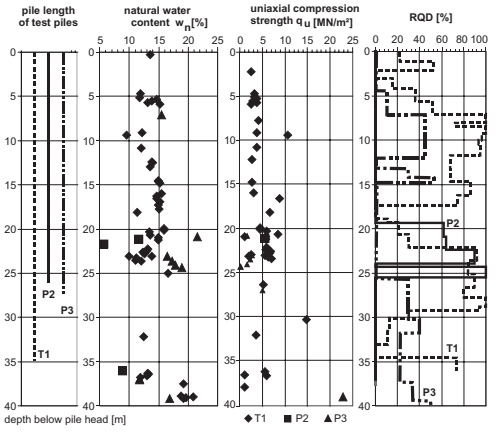

Figure 3. Results of laboratory tests and RQD-values (Deere 1964) for axes T1, P2 and P3 in the Cucaracha-Formation.

3 NEW BRIDGE 'PUENTE CENTENARIO'

So far the Canal dividing Panama into two parts could be crossed only by a steel-made bridge next to Panama City. For the improvement of the infrastructure it was decided to construct a second bridge crossing the Canal at the deep Gaillard Cut with its complex geology. The 'Puente Centenario' with a total length of 1,050 m and a main span of 420 m was designed as cable stayed bridge made of pre-stressed concrete (Fig. 1). Two 184 m high pylons and four piers support the carriageway suspended in a height of 80 m above Canal-level.

After a construction period of only two years the 'Puente Centenario' was opened in August 2004.

4 SUBSOIL CONDITIONS

The subsoil conditions being mainly of volcanic debris are very complex and vary along the bridge axis with strong or fractured basalt at the east side but also with soft rock of the Culebra and Cucaracha Formation at the west side of the Canal (Fig. 1).

The andesitic basalts, that are mainly of late Miocene age, occur as sills, dikes, plugs and flows. The basalt is a dark, fine-grained igneous rock. The sound rock of the basalt has been classified as very hard and very strong rock (rock hardness RH-5, in parts RH-4) with uniaxial compression strengths of q_u = 75 MN/m² in average. The basalt is widely to moderately jointed. The joints are closed or filled with calcite.

The Culebra and Cucaracha Formations are a very heterogeneous 'soft rock' of middle-early Miocene in age. The soft rocks are a terrestrial deposit of volcanic debris from intense, explosive activity. The formations consist of weak andesitic materials that are predominantly weak clay shales. These clay shales are locally bentonitic and interbedded with fine tuffaceous sandstones and pebble conglomerates. All of the formation has been altered and hydrates and slakes on exposure to air. It is cut by basalt dikes. The

Table 1. Results of soil investigation and laboratory tests for the axes with deep foundations in soft volcanic rocks (Cucaracha-Formation).

		P2	P3	T1
Natural water content	$\overline{w}_n$[%]	12	16	14
Uniaxial compression strength	$\overline{q}_u$ [MN/m²]	6.5	5.8	6.0
Rock Quality Designation	RQD [%]	15	18	53
Rock Mass Rating	RMR [-]	10	10–15	40
Density	γ/γ' [kN/m³]	22/12	22/12	22/12
Shear strength	φ' [°]	20	20	30
Cohesion	c' [kN/m²]	50	60	100
Bulk modulus	E_s [MN/m²]	110	130	200

clay shales comprise about 60% of the formation; they are not true shales, but are compact, massively bedded, variably waxy or soapy, altered tuffs in which the original, unstable, glassy particles of volcanic ash have been broken down into clay minerals. The clay shales are of soft to medium hardness (RH-1 to RH-3). The rocks are with numerous, irregular oriented slickensides, minute fractures caused by volumetric changes as a result of alteration and in some areas due to faulting. This means that the Culebra and Cucaracha Formation are very heterogeneous soft rocks varying considerably within short distance, that for practical purposes cannot be stratified but rather considered, as far as engineering properties are concerned, as single subsoil package. The soil investigation mainly comprises classification tests. In this context Figure 3 shows the results of laboratory and field parameters varying in a wide range at the three axes P2, P3 and T1 of the new Panama Canal Crossing. Table 1 summaries the results of soil investigations and laboratory tests. In average the results indicate for axes P2 and P3 worse rock quality as for axis T1.

5 FOUNDATION CONCEPT

The foundation design for the pylons and piers of the 'Puente Cetenario' based on AASHTO and was mainly influenced by

- the very heterogeneous, in part also 'chaotic' geological situation in the Gaillard Cut,

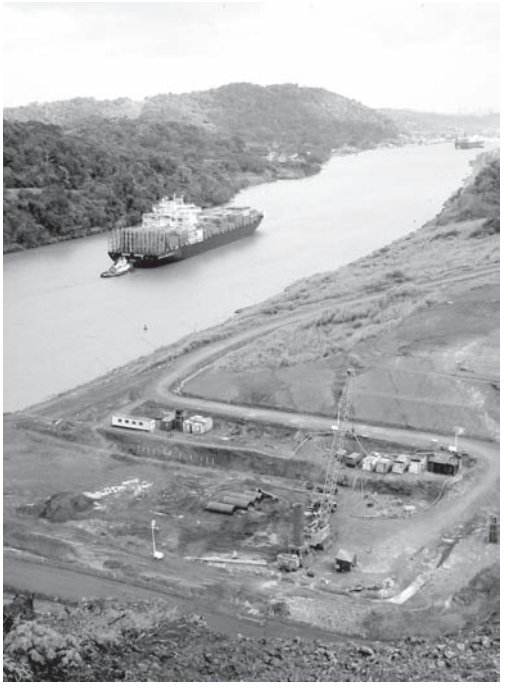

Figure 4. Piling work for pylon T1 next to the Panama Canal.

- the time-dependent behaviour and landslide moving of the slopes as the section of the Gaillard Cut was and continues to be the Canal's most susceptible area in terms of landslides,
- the impact of heavy earthquakes that was specified as an acceleration of 0.33 g in vertical and horizontal direction,
- high structure loads (e.g. axis T1: max. vertical load 525 MN),
- the short construction time, that demands for a technical and economic optimization of the bridge foundation.

5.1 *Shallow foundations*

At the east side of the Canal a flat foundation on sound basalt was designed for the axes T2, P4 and E2. Following the approach of AASHTO specifications the allowable bearing capacity in basalt was correlated to the uniaxial compression strength of the rock and the rock indices RQD and RMR (Bieniawski 1974, Hoeck 1983). Considering the local boundary conditions, especially the slope situation and the irregular jointing of the basalt rock mass the allowable contact pressure was limited to $\sigma_0 = 5.0$ MN/m² in strong

basalt. During execution the shallow foundations faces some unexpected aspects due to the variation of the fracturing of the basalt and to the limit extension of the basalt occurring in flows.

5.2 *Deep foundations*

In the Culebra and Cucaracha Formations at the west side of the Canal (Fig. 1) pile foundations were planned for axes P2, P3 and T1 with 9, 15 and 32 piles. Bored cast in situ piles with a diameter of 2.0 m and lengths up to 35 m were executed. The experiences with bored piles of this dimension were limited in Panama and no pile load tests were available in these volcanic rocks at all. For that reason three static pile load tests were planned, one test at each axis. As test-loads of more than 50 MN could not been realized using a top loading, the pile shafts were divided into segments and loaded by means of Osterberg Cells placed in the pile shaft (Osterberg 1989, 1998). For axis T1 and P2 multi-level tests with two levels of 4 to 5 O'cells were planned as for axis P3 a single-level test with one level of three heavy O´cells should be performed (Fig. 5). A successful application of the Osterberg-concept demands for a relative balance between the pile-segments loaded bi-directionally by the O´cells. In cases where no preliminary experiences in similar soils are available as in Panama, this might be a demanding task especially for multi-level tests.

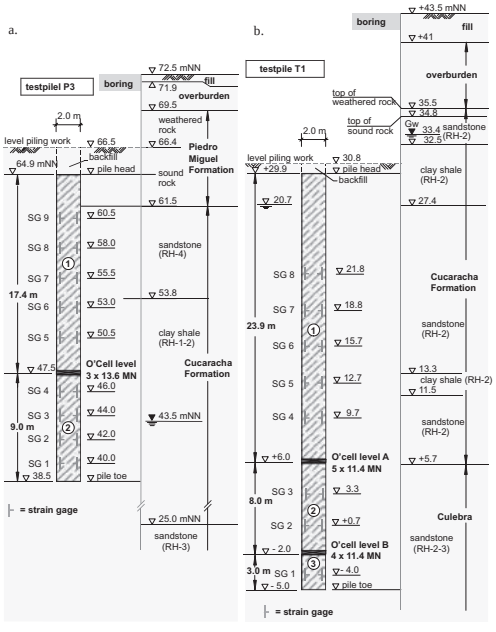

Figure 5. Single- and multi-level tests in the Cucaracha-Formation: test arrangement for test piles at axes P3 and T1.

During the execution of a single-level test there is only one stage, as the execution of multi-level tests (Fig. 5b) comprises several stages e.g. testing the lowest segment 3 vs. segments 1 and 2 (stage 1), the middle segment 2 vs. segment 1 (stage 2a) and finally the upper segment 1 vs. segments 2 and 3 (stage 2b). In stage 3 O'cell level A and B were both activated stressing segment 2 in order to determine the Elastic modulus of pile's concrete in situ.

Also the pile load tests were executed as quick-load tests with observation times of only 10 minutes per load step in accordance to the ASTM D 1143-recommendation, at chosen load steps the observation time was extended in order to fit European experiences with maintained-load tests (WG 2.1, 1998) and to investigate reliably the time-dependent displacement behaviour of the soft rocks and the creep behaviour.

The results of the single-level test at test pile P3 (Figs. 5a, 6) show typical parabolic curves. For a maximum test load of 31 MN the heave of the upper pile segment is with 1.6 cm smaller than the settlement of the lower pile segment with 2.5 cm. The ultimate skin friction recalculated from strain gages varies between 70 kN/m² and 535 kN/m² along the pile shaft.

During stage 1 of the multi-level test at test pile T1 the lowest pile segment shows a typical behaviour for tip resistance in soft soils (Figs. 5, 7a): at the begin the skin friction is mobilized by small deformations. The destruction of the inter-logging at the interfaces leads to increasing deformations. The mobilization of the tip resistance causes again a stiffening of the load-settlement behaviour. During this stage at the two upper segments a skin friction of q_s = 130 kN/m² was mobilized by a displacement of 5 mm. During stage 2a the behaviour of the middle segment was influenced by the impressed stresses of stage 1 (Fig. 7b). In stage 2b with the O'cells closed in level B a maximum load of 42 MN was applied in level A caus-

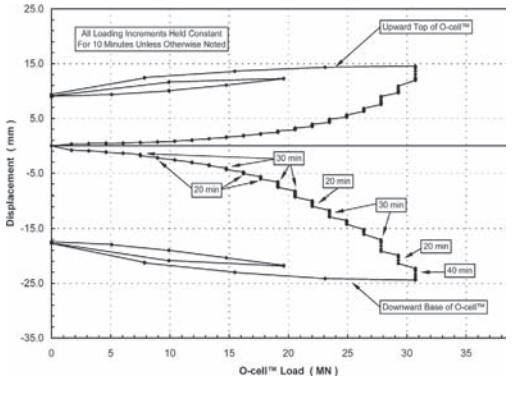

Figure 6. Single-level test pile P3: load-displacement curve.

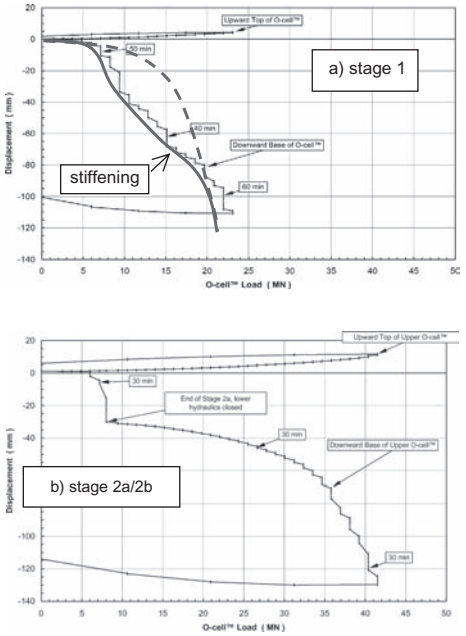

Figure 7. Multi-level test pile T1: load-displacement curves.

ing a heave of 12 mm of the upper segment 1 (q_s = 100 kN/m² to 450 kN/m²) and a settlement of 120 mm of the segments 2 and 3.

During the load test of pile P2, originally planned to be also a multi-level test, the ultimate limit load of the lower and the two upper pile segments was reached already during stage 1 of the test. So the test was ended as single-level test.

Analysing the results of Osterberg-tests the load-settlement curve of an equivalent top-loaded pile can be recalculated. The calculated bearing capacity of the test piles as well as the ultimate skin friction and tip resistance is documented in Table 2. For the specification of the ultimate bearing capacity of a pile no international acknowledged criteria are available (Tomlinson 1994). For that reason different approaches were used. The criterion of ASTM D 1143, a displacement rate of 0.25 mm/h was exceeded in the short-time load steps. Following the German recommendations (WG 2.1 1998), the ultimate bearing capacity was defined to be reached for a creep value $k_s = (s_2 - s_1)/\log(t_2/t_1) \geq 2.0$ mm. Applying this approach e.g. on test pile P2 for $k_s = 2.0$ mm the ultimate bearing capacity of segments 1 and 2 is determined to 12.5 MN (Fig. 8). Considering also segment 3 the ultimate bearing capacity of the whole pile is about 20 MN. By the Swedish pile-commission or the Building Code or the approach of Chin (1979) the bearing capacity of test pile P2 is calculated to 23 MN.

Table 2. Results of the three static pile load tests in the Cucaracha-Formation.

Test pile	P2	P3	T1
pile length l [m]	26 m	26.4 m	34.9 m
ultimate bearing capacity R_1 eq. top load	20 MN	52 MN	53 MN
ultimate skin friction $q_{s,f}$ in the Cucaracha-Formation			
measured min. $q_{s,f}$/ max. $q_{s,f}$	80 kN/m²/ 560 kN/m²	70 kN/m²/ 520 kN/m²	65 kN/m²/ 450 kN/m²
$q_{s,f}$ used for design	30 kN/m²/ 100 kN/m² (1)	100 kN/m²/ 250 kN/m² (1)	250 kN/m²
maximum tip resistance $q_{b,max}$			
measured $q_{b,max}$	– (2)	7,500 kN/m²	4,600 kN/m²
$q_{b,max}$ used for design	2,000 kN/m (3)	5,000 kN/m²	400 kN/m²

(1) Limit skin friction varies along pile shaft.
(2) Results for segment 3 could not be divided into skin friction and tip resistance.
(3) Calculated tip resistance for displacement needed to mobilize limit skin friction.

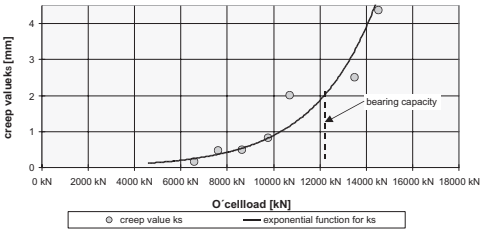

Figure 8. Creep value k_s for upper segments 1 and 2 of test pile P2 during phase 1.

6 SINGLE- AND MULTI-LEVEL TESTS WITH O'CELLS: A COMPARISON

Comparing the experiences gained by the three pile load tests for the new Panama bridge the following results can be concluded:

- One of the main preconditions for a successful pile load test using Osterberg-cells is a concept that divides the pile shaft in segments in such a way that the segments loaded bi-directionally by the

O´cells will be in a relative balance during the pile test with similar displacements up- and downward. Here multi-level tests with several test stages offer more flexibility to adapt the test procedure to the real pile behaviour even during test execution. So even in cases where the pile behaviour differs from prognosis the chance is greater that the ultimate bearing capacity of the pile can be investigated.

- On the other hand a single-level test is once and for all finished, when the bearing capacity of one of the two segments is reached, the bearing potential of the second segment remains unknown.
- For that reason it is often necessary to extrapolate the load-settlement curve of one of the both segments by analyzing single-level tests.
- The analysis of the results of a single-level test, e.g. calculation of the load-settlement curve of an equivalent top-loaded pile and of the bearing capacity is much more easier than for a multi-level test.
- Multi-level tests with several stages offer the possibility to stress a single segment twice in the same direction (repeated loading) or with changing load-direction first up- and then downward or vice versa.
- And finally economic aspects have to be considered: as multi-level tests need a greater number of O'cells they are more expensive than a single-level test.

7 CONCLUSIONS

The foundation design for the new cable stayed bridge 'Puente Centenario' crossing the Panama Canal was influenced by the complex geological situation in the deep Gaillard Cut. For the deep foundation of three axes static pile load tests were executed using the Osterberg method. The results show:

- In the soft volcanic rocks of the Cucaracha and Culebra Formation the skin friction scatter in a wide range depending on the irregular distributed clay shales and sandstone layer. Also all indices indicate for axes P2 and P3 similar conditions (Table 1), the results for test pile P2 are much worse than for pile P3 (Table 2).
- By the analysis of load tests using the Osterberg-method time-dependent effects often are neglected. For the evaluation of the load-settlement curve of an equivalent top-loaded pile only the criterion of a comparable displacement is considered. Varying durations of different load steps might influence the load-settlement behaviour determined in this way.
- As load tests with O'cells usually are executed as Quick-load tests further research work is required to consider creep effects.

REFERENCES

ASTM American Society for Testing and Materials 1994. *ASTM D 1143–81: Standard test method for piles under static axial compressive load.* Reapproved 1994.

AASHTO American Association of State Highway and Transportation Officials 2002. *Standard Specifications for Highway Bridges*. 16th Ed., 1996, Interims Revisions 2002, Washington.

Bieniawski, Z.T., Rock mass classification in rock engineering. *Proc. Symp. on Exploration for Rock Engineering*, Vol. 1, 97–106, 1974.

Chin, F.K., Diagnosis of pile condition. *Geotechnical Engineering*, Vol. 9, 85–104, 1978.

Deere, D.U., Technical description of rock cores for engineering purposes. *Rock Mechanics and Engineering Geology*, Vol. 1, No. 1, 17–22, 1964.

Hoeck, E., *Strength of jointed rock masses.* Rankine Lecture, Imperial College of Science and Technology, London, March 1, 1983.

McCullough, J.O., *The Path Between the Seas—The Creation of the Panama Canal 1870–1914.* Touchstone Book, Simon and Schuster (eds.), New York, 698 pp., 1977.

Osterberg, J.O., New device for load testing driven piles and drilled shafts separates friction and end bearing. *Int. Conf. on Piling and Deep Foundations*, London, Balkema, 421–431, 1989.

Osterberg, J.O., The Osterberg load test method for bored and driven piles: the first ten years. *7th Int. Conf. on Piling and Deep Foundations · DFI 98*, 15–17 June 1998, Wien, 1.28.1–1.28.11, 1998.

Stewart, J. *Description of formations found in Gaillard Cut.* Panama Canal Commission, 1984.

Tomlinson, M.J., *Pile design and construction practice.* E & FN Spon, London, 1994.

WG Working Group 2.1 of the German Society of Geotechnics, *Recommendations for static and dynamic axial pile load tests*, 1998.

Deep Foundations on Bored and Auger Piles – Van Impe & Van Impe (eds)
© 2009 Taylor & Francis Group, London, ISBN 978-0-415-47556-3

Foundation of a high speed railway track by comparing different pile load tests

M. Raithel & A. Kirchner
Kempfert + Partner Geotechnik, Würzburg/Kassel, Germany

A. Kneißl
Max Bögl Bauunternehmung GmbH & Co. KG, Neumarkt, Germany

ABSTRACT: In China a high speed railway track with a slab track superstructure and a length of about 115 km is currently being built near Beijing. As a so-called "trial track" about 10 km of railway track were constructed in advance. About 9.6 km of this track run on a structure consisting of bridges. The other 400 m run on an embankment. All structures are founded on roughly 2800 large-diameter bored piles as well as 1500 cased-in-place auger piles and 500 precast driven piles. Due to the high requirements concerning settlement of the foundation, the bearing behaviour of the foundation was tested with load tests on the different pile types. For a realistic prognosis of the remaining settlement after installation of the slab track, analytical and numerical calculations based on the load test results were executed considering the effect of pile groups.

1 INTRODUCTION

In the course of the planned modernisation of the Railway system until the year 2020, the People's Republic of China presses ahead with the construction of new high speed railway tracks for passenger transportation. One of the first tracks is the connection between Beijing and the upcoming city of Tianjin, south-east of the capital. This railway track with a total length of 115 km is planned to go into service before the start of the Olympic Games 2008.

The superstructure of the line will consist of the concrete slab track system of the German company Max Bögl, but the design of the project as well as the construction works are executed by a Chinese Design Department and Chinese construction companies.

For the trial track near Tianjin with a length of about 10 km, the company Max Bögl assumed technical responsibility, in order to make sure that the requirements of the slab track system and design speed of 350 km/h are kept by the foundation method. Consequently, particularly high demands were made on the geotechnical consultancy and design especially in consideration of the necessary special foundation methods.

2 PROJECT

About 9.6 km of the trial track run on a structure consisting of single-span and multi-span bridges generally built by precast box beam elements with standard lengths of 24 and 33 m (Figs. 1–2).

Between sections with single-span elements, the bridges sometimes have to cross distances up to 100 m. Those bridges were poured-in-place.

The precast bridge elements were fabricated in field plants, which are distributed along the railway line (Fig. 1). With a special raise construction the elements were lifted onto the bridge and distributed on top of the already finished bridge sections to their final position, where they were installed according to the so-called FSPLM (Full Span Pre-cast Launching Method).

The slab track superstructure system "System Bögl" consists of laterally tensioned, prefabricated slabs with mounted rail fastenings. Each slab has a length of 6.45 m, a width of 2.55 m, a height of

Figure 1. Precast box beam during dismantling from formwork.

Figure 2. Bridge pier. Installation of box beams.

Figure 3. Angular retaining wall (earth structure).

0.20 m and weight of about 9 tons. After installation the slabs are connected, so that they become an infinite slab with a high resistance against longitudinal and lateral displacement.

Due to subsoil conditions and the requirements of the superstructure regarding settlement, all structures (bridges and earth structures) were deeply founded on piles. The piers are generally founded on 8 to 12 large-diameter bored piles (1.0 to 1.75 m) with lengths up to 70 m (av. length about 45 m).

Like all earth structures of this railway line, the 400 m earth structure section belonging to the trial track is founded on cast-in-place auger piles and precast driven piles (av. length about 28 m). The load transfer from the embankment to the foundation follows via a reinforced concrete slab. In some parts of the earth structures (as the part of trial track), the embankments are retained by angular walls (Fig. 3).

3 GEOLOGY AND STRATIFICATION

The North China Plain consists of sediments of alluvial loess and sand deposed by rivers from the western mountains. The area is characterised by tectonic stress, which every now and then leads to heavy earthquakes like the one in July 1976, when the most devastating earthquake of the 20th century took place in Tangshan, 140 km east of Beijing. This earthquake also affected Beijing, Tianjin and other cities of the region seriously.

The entire railway track lies just a few meters above sea level.

For site investigation borings including Standard Penetration Tests (SPT) were carried out nearly at every bridge pier down to a depths of 55 m—occasionally 85 m—below ground surface.

The investigation showed that the in-situ subsoil consists mainly of clay and silt with an organic content. Down to a depth of about 20 to 25 m below ground surface, the cohesive soil is of soft to stiff consistency. Below, in depths down to 50 to 80 m, the consistency changes to medium stiff to stiff.

There are also several cone penetration tests with profiles down to 35 m available. The cone resistance varies between q_c = 0.2–1 MN/m² in the softer cohesive layers. Generally there is an increase of sounding resistance with depth, but cone resistances of more than q_c = 2 MN/m² were only encountered in depths of more than 30 m.

Layers of fine sand with varying contents of silt may be embedded in the cohesive subsoil at different depths.

The groundwater level was encountered directly beneath the ground surface.

4 PILE LOAD TESTS

4.1 *General*

For verification of the actual bearing capacities of the piles, load tests on single piles in the area of the trial track were conducted.

Thus 4 large-diameter bored piles with lengths of 50 and 70 m and diameters of 1.0 and 1.5 m,

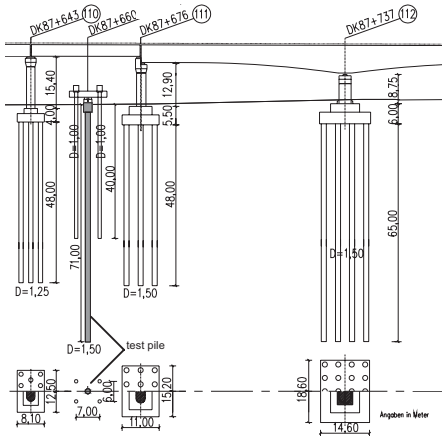

Figure 4. Position of the pile load test in the area of a 3-span bridge.

respectively, and in the area of the earth structure, 2 cast-in-place auger piles and 2 driven piles with lengths between 26 and 30 m were tested.

The pile load tests were executed in accordance with the technical recommendations of EA-Pfähle (DGGT 2007).

With the aid of special measuring equipment, it was planned to measure the development of the skin friction resistance in the different soil layers as well as the increase of the pile base resistance, in order to be able to transfer the derived characteristic pile resistances to other parts of the railway line. Furthermore the results of the pile load tests were needed for the determination of the settlement behaviour of the pile groups.

Figure 5. Tent for protecting the equipment. Top of a test pile with hydraulic jacks.

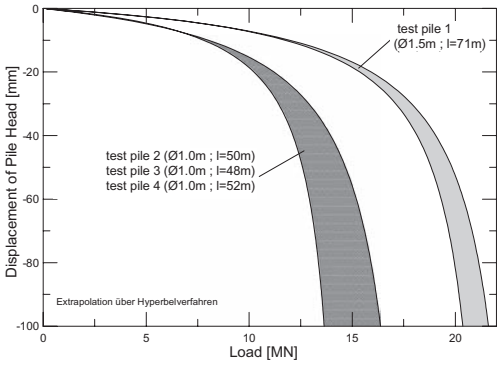

Figure 6. Extrapolated load-settlement curves.

4.2 *Load tests of large-diameter piles*

The pile foundation of the bridge is loaded primarily vertically due to dead loads of the structure, traffic loads and covering material above the pile caps.

The locations of the pile load tests were chosen to give a representative overview of the trial track. Furthermore the pile load tests were chosen in adjacencies to structures, which are very sensitive to settlements, e.g. the 3-span bridge with a maximum span length of 100 m (Fig. 4).

For the counter bearing constructions, cross beams fixed by anchor piles were installed above the test piles. The load-controlled test forces were applied to the piles by 5 to 6 hydraulic jacks (Fig. 5).

This test configuration provided maximum test loads of about 13 MN.

The measurement of pile head displacement of the test and anchor piles were carried out by digital displacement transducers mounted on reference beams that were controlled by precise levelling. The measurement of skin friction development with depth, i.e. with the length of the pile, was realised by electric strain gauges installed at the reinforcement cage at different depths of the test pile and one anchor pile.

The pile test was driven load-controlled in 4 equal load steps until the future working load was reached. Afterwards the pile was unloaded and then reloaded in steps till the maximum test load was reached.

The evaluation was carried out with regard to load-settlement curves, ultimate loads and ultimate skin friction. The measured load-settlement curve was extrapolated according to the hyperbola method (Kempfert & Smoltczyk 2001) in order to obtain the ultimate pile resistance (cp. Fig. 6). Due to the

Table 1. Settlements at working load and extrapolated ultimate pile resistances.

Test pile	Max. test load [MN]	Range of working loads		Ultimate pile resistance (extrapolated)	
		Load [MN]	Settlement [mm]	Lower margin [MN]	Upper margin [MN]
1: ∅ 1.5 m l = 71 m	12.7	7–8	4.2–5.2	20.9	22.3
2: ∅ 1.0 m l = 50 m	11.0	3–4	3.1–3.8	14.6	15.8
3: ∅ 1.0 m l = 48 m	11.3	3–4	3.0–3.6	13.6	15.8
4: ∅ 1.0 m l = 52 m	9.8	3–4	2.6–3.4	14.7	16.4

fact that the measured load-settlement curve is just a small part of the extrapolation, a range of ultimate loads could be determined by using different hyperbolas (Table 1).

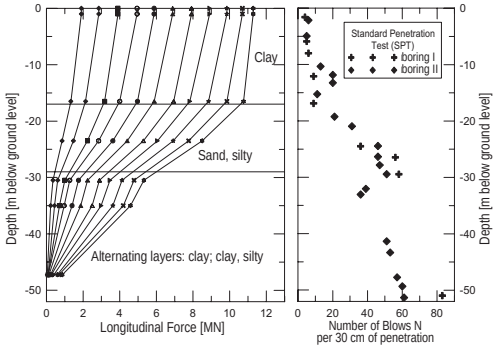

Figure 7. Force versus depth (test pile 3).

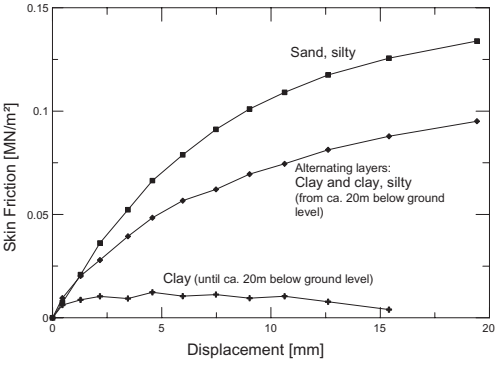

Figure 8. Skin friction versus displacement (test pile 3).

Table 2. Ultimate skin friction.

Depth below surface [m]	Soil layers	Ultimate skin friction [MN/m²]
0–20	Alternating layers: clay, silty and clay	0.010
20–70	Alternating layers: clay, silty and clay	0.055
20–70	Silt, sandy	0.065
0–70	Fine sand/sand, silty	0.100

In Figure 7 the measured axial force development of test pile 1 in combination with SPT-sounding results can be seen. The skin friction vs. displacement of the same test pile is illustrated in Figure 8. Table 2 shows the ultimate skin friction determined from all pile load test results.

Thus for the first 20 m below ground surface only small amounts of skin friction could be activated. The SPTs confirm this outcome. The pile load test results furthermore showed that due to the comparatively long piles and due to the existing subsoil conditions only negligible base resistances of $\sigma_b = 1 - 1.5$ MN/m² could be activated.

4.3 *Load tests of driven and auger piles*

The earth structures were installed completely on precast driven piles and on so-called Cement-Flyash-Gravel piles (CFG-piles), known in Germany as cast-in-place auger piles.

Considering a pile grid with distances of about 1,5 × 1,5 m, the maximum load that a single pile under the finished embankment must bear was determined at 0.4 MN.

The test equipment was configured for a maximum test load of 2 MN.

The evaluation was carried out with regard to the load-settlement curve and ultimate pile resistance. For the proof of serviceability, particularly the settlements at working load (0.4 MN) were of main interest (Table 3).

5 TRANSFER OF THE TEST RESULTS TO PILE GROUPS

With regard to the examination of the deformation behaviour of the track in its entirety, the settlements of the deep foundations of the piers and earth structures were estimated considering the interactions between the piles (pile group effect).

For the description of the load-settlement behaviour of pile groups, analytical, numerical or empirical calculation methods are known. In addition to the calculation method they also differ in accuracy, required input parameters and calculation effort. Two practical calculation methods have been presented lately (Rudolf 2005, Lutz et al. 2006) which allow an easy estimation of the deformation behaviour of a group consisting of compression piles.

Since the required amount of input parameters is significantly less, in the first instance the deformation behaviour of the pile groups was determined with the nomogram method according to Rudolf (2005). Due to the high requirements concerning the settlement prognosis, further numerical finite elements calculations were carried out in order to verify the

Table 3. Pile test results of CFG- and driven piles.

Test pile	Max. test load [MN]	Range of working loads		Ultimate pile resistance (extrapolated)	
		Load [MN]	Settlement [mm]	Lower margin [MN]	Upper margin [MN]
Driven piles: ∅ 45 cm, l = 30 m					
A[1]	1.82	0.4	2.0	2.6	2.9
B[1, 2]	2.00	0.4	2.2	≤2.0	
CFG-piles: ∅ 40 cm, l = 28 m					
C[3]	1.50[4]	0.4	1.7	2.0	2.3
D[3]	1.25[4]	0.45	1.5	2.0	2.2

[1] ultimate settlement 4.5 cm; [2] ultimate settlement reached; [3] ultimate settlement 4.0 cm; [4] pile head failure.

estimations. The pile load tests were first simulated numerically and the results were then compared with the measured values. After adjusting the numerical calculation model to the real conditions, the load settlement behaviour of decisive pile groups was calculated.

The calculations of the 3-dimensional model were done with the FE-program PLAXIS 3D Tunnel 1.2.

At the given conditions, both constitutive equations, the Mohr-Coulomb (MC) and Harding Soil Model (HSM), can be used. Since comparative calculations in this case showed similar results for both material models, the more simple constitutive equation of Mohr-Coulomb (linear elastic—ideal plastic) was used in order to reduce the calculation time and input parameters.

For an additional verification of the applied calculation program and model, examples from literature (Rudolf 2005) were re-calculated using the same parameters and conditions. Especially in the range of the working loads, the re-calculated load deformation behaviour of single piles as well as of pile groups matched the results of the calculations from literature very well.

Due to the limits of the used FEM programme, the circular piles had to be transformed into square elements. Since in this project almost the entire load is transferred into the subsoil by skin friction, the dimensions of quadratic pile element in the calculation was chosen so that skin surface is equal to the skin surface of the real, circular pile.

As shown in Table 4, both calculation methods (nomogram method, 3D-FEM) showed good accordance when considering a single pile. For the existing conditions, the applicability of the nomogram method could thus be verified. The group factor G_S is the ratio of the settlement of the pile group s_G versus the settlement of the single pile s_S ($G_S = s_G/s_S$).

Nevertheless, the FE calculations show that the particular settlement depressions of different pile groups can superimpose, due to the comparatively long piles

Table 4. Comparison of the analytically and numerically calculated settlements and group factors at working loads.

	Calculated total settlement [mm] group factor G_S[–]	
	Nomogram method acc. to Rudolf (2005)	FEM Plaxis 3D
Pier of 1-span bridge	s = 15 mm G_S = 4.0	s = 20 mm G_S = 5.0[2]
Center pier of 3-span bridge	s = 20 mm G_S = 4.5	s = 25 mm G_S = 5.5[2]
Earth structure	s = 20 mm G_S =14[1]	–

[1] more favorable conditions expected due to linear structure.
[2] incl. superimposition of settlement depressions.

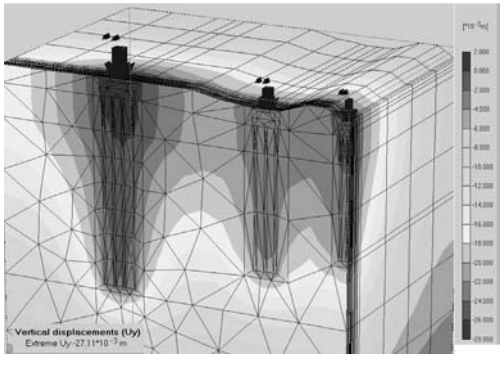

Figure 9. PLAXIS print-out of 3-span bridge. Vertical deformations at final state incl. traffic.

(Fig. 9). Hence, it results in an increase of the calculated total settlements of the particular pile groups. But since the subsoil is comparatively homogenous, it is not expected that settlement differences of major

influence between the different piers will occur, it is rather expected that the settlements will spread uniformly between the piers.

6 INSTALLATION OF LARGE-DIAMETER BORED PILES

Due to time restrictions, it was necessary to use 45 drilling rigs at the same time on the trial track. Thus different boring methods were applied but in general all construction methods were carried out slurry-supported. Beside the dry rotary drill method with drill bucket (Fig. 10), the direct flush drilling method (Fig. 11) and suction bore method (Fig. 12) were also used.

In Europe these methods are seldom used and there is only little practical knowledge. In Asia, however, these methods are well known and especially in China the flushing and suction drilling are the most common methods for pile construction (Aubel 2004).

In contrast to dry drilling methods where the soil is loosened and removed by the cutter head (in this case: the drill bucket), when using wet drilling methods the soil is cut by the drilling head and then transported by flushing.

The direct flush drilling method and the suction bore method differ mainly by the path the bore mud takes. Hence with the direct flush drilling method the bore mud is lifted with the flushing between the bore hole wall and the drill pipe. At the suction drilling method the mud takes the other direction: the flushing flows down outside from the drilling rods, through the cutter head and is lifted inside of the drill pipe.

Especially with the suction drilling method long piles and great diameters can be constructed, e.g. 80 m with a diameter of 1.5 m in the area of the trial track.

Due to the decisive load case “earthquake”, the uppermost 25 m of the piles are reinforced. With the aid of large cranes the reinforcement cages were installed in one piece.

Figure 10. Dry rotary drilling with drill bucket.

Figure 11. Direct rotary flush drilling with vane cutter ∅ 1,0 m.

Figure 12. Suction drill rigs.

Figure 13. Chipping off the pile heads.

Figure 14. Driven pile. CFG-pile production. Small Pict.: hollow stem of auger (∅ 10 –12 cm).

After the chip off of the pile heads (Fig. 13), all piles were checked for reasons of quality assurance by integrity tests. Piles with lengths of less than 50 m were tested by "low-strain" method. Here a stroke is applied by an impact hammer at the pile head and the reflection behaviour as well as the velocity of spread is measured/controlled by accelerometers gauges. Piles with lengths of more than 50 m were equipped with measuring pipes, so that the piles could be checked for integrity by ultrasonic ("cross-hole" method).

7 INSTALLATION OF DRIVEN AND AUGER PILES

The driven piles (pre-stressed centrifugally-cast concrete piles with a diameter of 45 cm) were driven by a diesel ram (Fig. 14). They consist of 3 pile pieces with a length of 10 m each. The pieces were connected by electrical welding.

The cast-in-placed auger piles, that were carried out in this project—the so-called CFG piles, were bored with a continuous hollow stem auger with an outer diameter of 40 cm (Fig.14). The maximum construction depths is limited to 28 m. The inner tube of the auger has a diameter of 10 to 12 cm and can be capped at the bottom. After having reached the final depth, the auger is pulled without rotation and concrete is filled through the inner tube.

8 CONCLUSION

Meanwhile the high speed railway track is completed and test operation has begun. The high speed railway track can go into service according to schedule at the Olympic Games 2008 in Beijing.

During construction and the test operation to date, settlement measurements were executed. The measurements confirm the calculations: in large sections the measured settlements are in accordance with the settlement prognosis. In conclusion this means that the interaction of piles of a pile group has to be considered and cannot be neglected.

REFERENCES

Aubel, P. 2004. Die Baulose 260 und 270 der Taiwan High Speed Railway. WISSENPORTAL baumaschine.de.

DGGT—Deutsche Gesellschaft für Geotechnik (ed.) 2007. *Empfehlungen für des Arbeitskreises "Pfähle", EA-Pfähle.* Berlin: Ernst & Sohn.

Kempfert, H-G., Eigenbrod, K.D. & Smoltczyk, U. 2001. Pile foundations. In Ulrich Smoltczyk (ed.), *Geotechnical Engineering Handbook Volume 3: Elements and Structures.* Berlin: Ernst & Sohn.

Lutz, B., El-Mossallamy, Y., Richter, Th. 2006. Ein einfaches, für die Handrechnung geeignetes Berechnungsverfahren zur Ab-schätzung des globalen Last-Setzungsverhaltens von Kombinierten Pfahl-Plattengründungen. *Bauingenieur 2:* 61–66.

Randolph, M.F., Wroth, C.P. 1979. An analysis of a vertical deformation of pile groups. *Geotechnique No. 4:* 423–439.

Rudolf, M. 2005. Beanspruchung und Verformung von Gründungskonstruktionen auf Pfahlrosten und Pfahlgruppen unter Berücksichtigung des Teilsicherheitskonzepts. *Schriftenreihe Geotechnik, Heft 17.* Kassel: University of Kassel.

Deep Foundations on Bored and Auger Piles – Van Impe & Van Impe (eds)
© 2009 Taylor & Francis Group, London, ISBN 978-0-415-47556-3

Numerical simulations for a testpile

K. Thooft & K. Vanfroyenhoven
De Nayer University College—Association Leuven Catholic University, Sint Katelijne Waver, Belgium

ABSTRACT: Test pile regulations stipulate a minimum waiting time for pile load testing to allow for the hardening of the concrete and to allow for a sufficient amount of soil consolidation because of soil disturbance due to the pile installation process.

This paper deals with a number of numerical simulations using Plaxis 7.2 to check the influence of this waiting time or consolidation time on the actual pile load test results. To obtain a proper calibration for the model the actual pile load tests performed at the Sint Katelijne Waver test site for friction piles in stiff over-consolidated Boom clay as well as other test results for the same site are used. An effort is made to model the lateral soil displacement during pile installation and its influence in load-settlement behaviour of the pile.

1 INTRODUCTION

Test pile regulations stipulate a minimum waiting time for pile load testing to allow for the hardening of the concrete and to allow for a sufficient amount of soil consolidation because of soil disturbance due to the pile installation process.

The authors made use of a comprehensive testing program on auger piles to calibrate the soil parameters for use with the Hardening Soil Model in Plaxis 7.2. In a first stage the results of c.u. triaxial tests are used to calibrate the material parameters. The remaining model parameters such as the interface parameter and the radial displacement occurring during pile execution was calibrated by using the pile load test data (pile load versus axial displacement data). The fully calibrated model was then used to model consolidation and to check for the effect of consolidation time between pile installation and pile testing.

2 SOIL PROFILE AT THE TEST SITE

As a part of a research into the mechanical behaviour of auger piles in Belgian soils a comprehensive testing program was set up and conducted for stiff clays by the BBRI involving 5 types of auger piles and one type of prefabricated driven pile as reference. The Sint Katelijne Waver site was selected because of the presence of a thick and homogenous layer of Boom clay. For a detailed description of the site the reader is referred to Mengé, 2001. Figure 1 gives a typical CPT-diagram that is representative for the test site.

It can be seen that the soil profile consists of a thin silty sand layer above a thick deposit of Tertiary over-consolidated stiff Boom Clay.

3 CALIBRATION FOR THE TRIAXIAL TESTS

As a part of the testing program undisturbed soil samples from depths of 4.5 m–4.9 m, 8.5 m–8.9 m,

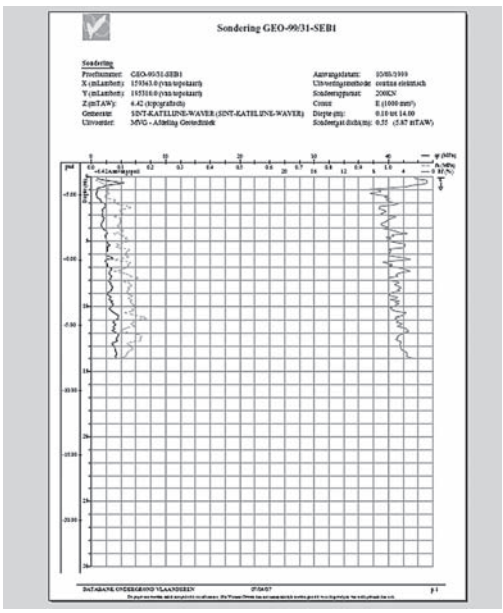

Figure 1. CPT-test for Sint Katelijne Waver.

10.5 m–10.9 m and 13.5 m–13.9 m were subjected to c.u.-triaxial tests.

The authors used these test results to perform a calibration calculation for the Hardening Soil Model within Plaxis 7.2. With respect to the geometry of the test a axisymmetric model was used with 6-node elements. For the 4 c.u. tests , and thus for the 12 soil samples calculation runs were made to correspond to the real testing results as closely as possible. The multiplier approach was selected to accommodate for the isotropic cell load and subsequent consolidation as well as for the strain controlled loading process to failure. A number of soil parameters were assigned starting values, adopting γ_n = 16 kN/m², γ_{sat} = 18 kN/m³ and a permeability of 0.001 mm/day or 1.16 10^{-11} m/s. The shear resistance parameter values were directly derived from the c.u-test data as $\varphi' = 28°11'$ and $c' = 22$ kN/m². The dilatancy angle $\psi = 0°$ for associated flow was adopted. Finally the stress dependency power m = 0.5 was assumed in the relation $E = \sigma'^m$. For other essential model parameters a large number of calculation runs was made, varying parameters between a lower bound and an upper bound as summarized in Table 1.

Figures 2 and 3 represent some of the results in a stress-strain plot. The accented and square marked values are the measured data in the triaxial test. The diamond marked values are the simulation results.

The calibration results allow for a good simulation of both the initial small strain stiffness and of the large strain behaviour. The pore pressure buildup as a function of axial strain was also measured but was not taken into account in the calibration process through numerical simulations.

Table 1. Parameter combinations for calibration.

Parameter	Upper bound	Lower bound	Number of steps	Selected value
E_{50} (N/mm²)	100	5	15	7.5
E_{oed} (N/mm²)	160	7	25	9
E_{ur} (N/mm²)	420	15	25	22.5
ν	0.45	0.15	10	0.2
R_f	1	0.8	15	0.9

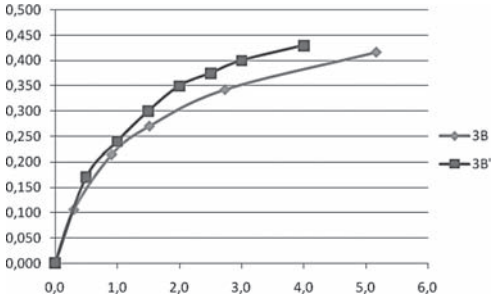

Figure 2. Simulation versus triaxial test for the sample at 10.5 m depth.

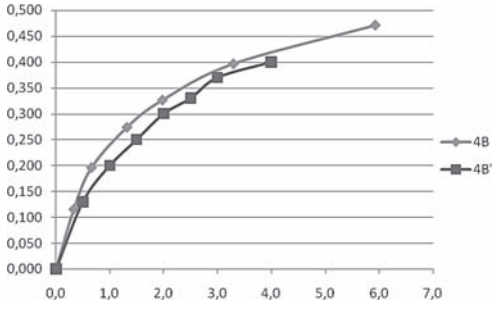

Figure 3. Simulation versus triaxial test for the sample at 13.5 m depth.

4 DETAILS ABOUT THE TEST PILES

As mentioned in paragraph 2 the testing program consisted out of 2 static load tests, two dynamic load tests and one statnamic load test on each of 5 types of auger piles (Atlas, Fundex, De Waal GVS, Socofonda Omega and Olivier) and on a prefabricated driven pile as a reference test. Each pile was statically loaded approximately 90 to 120 days after pile installation. Based upon an expected bearing capacity and failure load (calculated by the De Beer method) piles of approximately 11 m to 12 m length were installed.

During the load test the pile head load was increased to failure in 10 steps. Each load was kept constant for 60 minutes and was then increased. After reaching the maximum load the pile was unloaded in 5 steps, with each load maintained constant for 10 minutes to measure the pile head rebound during unloading.

Each pile was fitted with extensometers, allowing to separate end bearing and shaft friction during the loading process. The extensometer data were not used in the calculations in this paper.

Some essential data on every pile are given in Table 2.

The characteristic compressive strength f_{ck} of the pile concrete was determined at the age of the concrete during pile loading. The elasticity modulus of the concrete E_{cm} at he same time is not given in Table 2, but can be calculated through equation 1, with f_{ck} and E_{cm} both expressed in N/mm².

$$E_{cm} = 9500\,(f_{ck} + 8)^{1/3} \qquad (1)$$

5 CALIBRATION FOR THE PILE TESTS

For every pile in Table 1 a similar axisymmetric calculation was made in Plaxis 7.2 with the Hardening

Table 2. Pile characteristics.

Pile	Age at testing (days)	f_{ck} (N/mm²)	L (m)	D (m)	Load step (kN)
Prefab	90	79.5	11.58	0.395	160
Fundex	97	42.1	11.50	0.380	140
GVS	102	46.1	11.73	0.410	130
Olivier	106	39.5	11.68	0.510	250
Omega	109	52.7	11.83	0.410	160
Atlas	114	46.5	11.76	0.510	260

Table 3. Calibration results for the piles.

Pile	Interface strength ratio	Lateral soil displacement
Prefab	0.6	1 cm
Fundex	0.5	2 cm
GVS	0.5	1 cm
Olivier	0.5	2 cm
Omega	0.8	2 cm
Atlas	0.9	2 cm

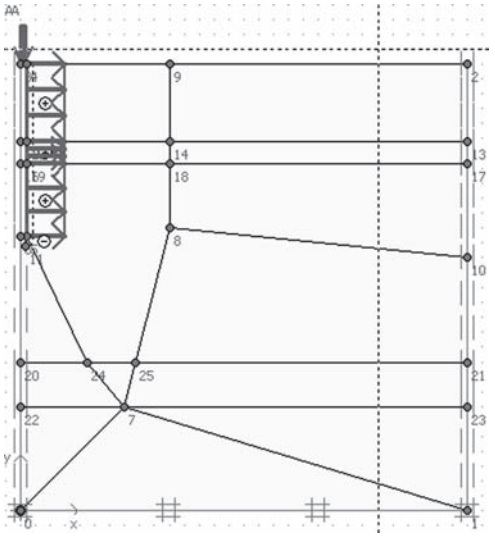

Figure 4. Plaxis model for the pile.

Soil model with the calibration data discussed in paragraph 3 and listed in Table 1. Locally, around the pile, a denser mesh was generated as suggested in the geometrical model in Figure 4.

The pile was modelled as a combination of a beam (tubular steel section) filled with concrete with the appropriate material parameters, leaving the horizontal effective stress in the soil around the pile constant.

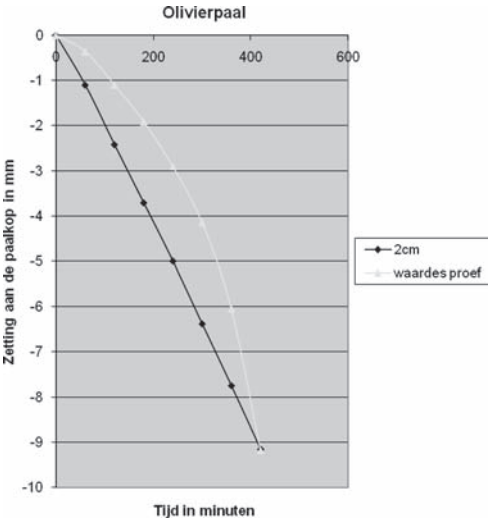

Figure 5. Simulation versus load test data for the Olivier pile.

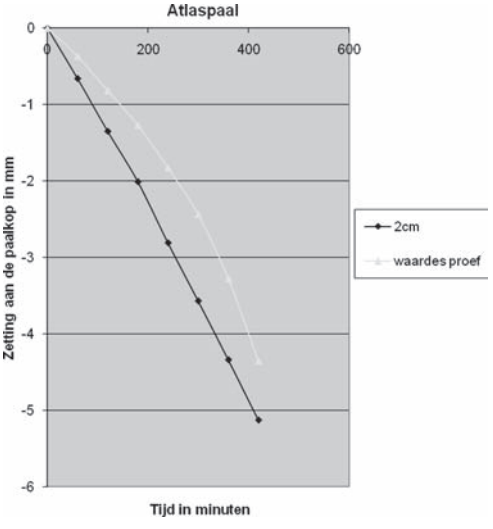

Figure 6. Simulation versus load test data for the Atlas pile.

An interface was defined to allow for shaft friction and displacement along the pile shaft to develop. During the substitution of soil by concrete there was no possibility to develop an extra amount of effective horizontal stress: to accommodate for the soil displacement during installation of the displacement auger piles an (to be determined) amount of lateral displacement was defined as an extra loading situation.

The following modelling steps were made in Plaxis 7.2 after generating pore water pressures and effective

stresses from a ground water table coinciding with the ground level.

- substitution of soil by concrete (staged construction)
- lateral expansion of the pile body to simulate the displacement character of the pile
- consolidation for 90 to 120 days, according to the actual pile loading time schedule
- alternating steps (multiplier) of applying one load step and subsequent consolidation, both in loading and unloading.

The calibration process for the test piles essentially comprised the determination of 2 supplementary parameters: the necessary amount of lateral displacement to accommodate for the displacement character of the pile and the interface strength adopted. The selected values for every pile to obtain a best fit between simulation results and test data are found in Table 3.

Figures 5 and 6 give an example of the simulation results as a load-settlement curve in comparison to the actual load test data for the Olivier pile and for the Atlas pile. The diamond marked values represent the simulation; The triangle marked values represent the load test data.

6 EFFECTS OF PILE AGE AT THE MOMENT OF THE PILE LOADING TEST

To model the influence of the pile age at the moment of pile load testing only the duration of the consolidation process, following the lateral soil displacement along the pile shaft is varied. All other data for the soil and for the pile as discussed in previous paragraphs and as listed in Tables 1, 2 and 3 were used without changes. Also the finite element model for every pile in Plaxis 7.2 was used without changes.

Table 4 lists the corresponding calculated pile head settlement for the different pile types in case of an immediate loading test without any consolidation and after a consolidation time of 1 week, 2 weeks, 1 month, 6 months and 1 year.

The E-modulus of the concrete was kept invariable for all the calculations: no allowance was mode for the increasing stiffness of the concrete during the hardening of the concrete.

Only consolidation time was varied, taking into account soil consolidation after pile installation. It can be seen in Table 4 that there is hardly any significant change with time in calculated pile head settlements for the Sint Katelijne Waver test site.

One can therefore conclude that as far as soil consolidation is concerned no specific waiting time larger then 1 or 2 weeks should be taken into account.

Other technological considerations should of course be taken into account: one needs approximately one month for the hardening of the cast in place concrete for the auger displacement pile. Another month should be allowed for the hardening of the concrete in the cast in situ concrete block at the pile head that will transmit the forces of the hydraulic jack to the pile during load testing.

Table 4. Calculated pile head settlements (in mm) for various consolidation durations.

Pile	Load (kN)	No wait	1 week	2 weeks	1 mth	6 mths	1 yr
Prefab	1600	59	59	56	57	57	57
Fundex	1120	50	51	51	51	48	49
GVS	1300	61	60	58	59	59	55
Olivier	1750	81	89	89	81	90	88
Omega	1280	32	32	31	31	31	31
Atlas	1820	41	41	40	36	36	41

7 EFFECTS OF THE PILE LOADING TEST PROCEDURE

Finally, in a last series of simulations the pile load testing procedure was changed. Instead of undrained loading in 10 steps, followed each by a one hour consolidation period, as done in paragraph 6, similar calculations were made with an undrained loading to failure in one step without intermediate consolidation, enabling a test to be run in as little as one hour. This “fast” pile loading test was again modelled for a pile immediately after pile installation and lateral soil displacement and for consolidation durations of 1 week, 2 weeks, 1 month, 6 months and 1 year as in the preceding paragraph. Table 5 lists the corresponding calculated pile head settlements.

Comparing Tables 4 and 5 it can clearly be seen that the pile load procedure is very important. The “fast” pile load testing procedure results in a significantly larger value for the pile head settlement.

Table 6 compares tables 4 and 5 by listing the ratio (in %) of the calculated pile head settlement for the “fast” test to the calculated pile head settlement for the conventional test. Averaging the values per pile one finds the following ratios:

- prefabricated: 298%
- Fundex: 128%
- De Waal GVS: 101%
- Olivier: 123%
- Omega: 97%
- Atlas: 143%

Averaging the values per column (load testing time after pile installation) one finds the following ratios:

- no waiting time: 146%
- 1 week waiting time: 143%

Table 5. Calculated pile head settlements (in mm) for various consolidation durations for a “fast” pile loading test.

Pile	Load (kN)	No wait	1 week	2 weeks	1 mth	6 mths	1 yr
Prefab	1600	171	170	169	172	174	173
Fundex	1120	64	64	65	63	64	63
GVS	1300	59	59	59	59	59	59
Olivier	1750	106	106	106	106	106	106
Omega	1280	31	28	31	31	31	31
Atlas	1820	55	56	56	56	56	56

Table 6. Ratio in % of calculated pile head settlements for a “fast” pile loading test to those in a conventional test.

Pile	No wait	1 week	2 weeks	1 month	6 months	1 year
Prefab	290	288	302	302	305	304
Fundex	128	125	127	124	133	129
GVS	97	98	102	100	100	107
Olivier	131	119	119	131	118	120
Omega	97	88	100	100	100	100
Atlas	134	137	140	156	156	137

– 2 weeks waiting time: 148%
– 1 month waiting time: 152%
– 6 months waiting time: 152%
– 1 year waiting time: 149%

It can clearly be seen that on average the “fast” test yields deformations that are approximately 50% higher (with a large variation according to pile type) then the conventional test. The pile testing procedure and more specific the buildup rate of pile head load seems a more important parameter then the waiting time before load testing.

The differences between the standard pile load test and the “fast” version is significant for most pile types as stated above. Only in the case of the De Waal GVS and Omega piles there is surprisingly hardly any difference at all. This is a topic for further research.

Figures 7 and 8 give the calculated load settlement curves for the Olivier and Atlas piles respectively both for the standard pile load test and for the fast pile load test compared to actual recorded pile head settlements in the pile load test.

8 CONCLUSIONS

Using a finite element program (Plaxis 7.2) it was shown that one can use the Hardening Soil Model to simulate existing test data from c.u. tests and test load data of pile load tests for an acceptable calibration of a finite element model.

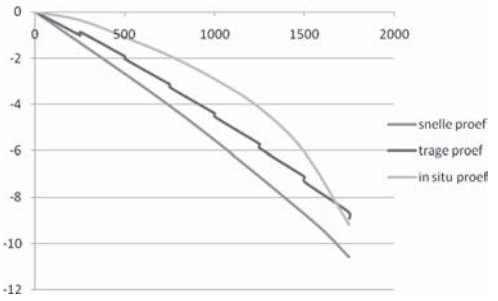

Figure 7. Load—settlement for the Olivier pile: measured and calculated values for the standard and fast test variations.

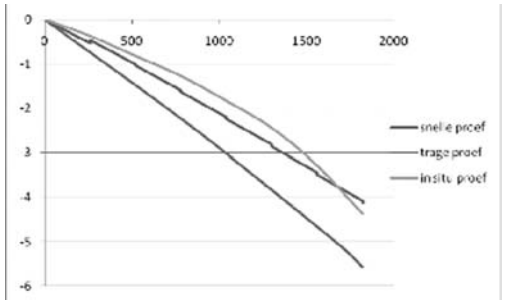

Figure 8. Load—settlement for the Atlas pile: measured and calculated values for the standard and fast test variations.

After these preliminary calibrations, numerical simulations were made varying the pile load testing procedure and varying the consolidation time between pile installation and pile load testing. It was found that consolidation time has little influence beyond a 2 week to 1 month waiting time, coinciding with standard pile loading test practice; no supplementary waiting time should thus be taken into account or prescribed.

It was also shown, however, that the pile load testing procedure and duration has a considerable effect on the expected load settlement data. Pile loading procedure should therefore be described in detail and followed accurately.

REFERENCES

Mengé P., Soil investigation results at Sint-Katelijne-Waver (Belgium), Screw piles installation and design, Brussels, 2001.

Vanfroyenhoven, K., Modelleren triaxiaalproeven en paalbelastingsproeven Sint-Katelijne-Waver in verband met het tijdstip van belasten na installatie van de paal, Masterthesis (in Dutch), De Nayer University College Sint Katelijne Waver, 2008.

Deep Foundations on Bored and Auger Piles – Van Impe & Van Impe (eds)
© 2009 Taylor & Francis Group, London, ISBN 978-0-415-47556-3

Interpretation and misinterpretation of Cross Hole Sonic Logging test results

H.T. Williams & I. Jones
Testconsult Limited, Warrington, Cheshire, UK

ABSTRACT: Cross-Hole Sonic Logging (CSL) is one of the most powerful methods of assessing the integrity and quality of cast in place foundations. It offers many advantages over low strain methods, in particular the ability to determine the vertical and lateral extent of anomalies at any depth. In recent years 2 and 3 dimensional tomography is being applied to results to present a graphical visualisation of results, which are easy for engineers to understand. In addition first arrival times can be automatically picked from response signals. However, without understanding how these new developments are created, there is a real danger that results can be misinterpreted. This paper explores the causes and effects of real and apparent defects in cast in place piles on cross-hole sonic logging results.

1 INTRODUCTION

Cross-Hole Sonic Logging has been a common method of assessing cast in place concrete foundations since the 1960's. It is now used extensively throughout the world and on many significant construction projects.

Its popularity can be attributed to two main factors—firstly, there is no depth limitation to the method and secondly, the apparent ease of interpreting results, compared with low strain type integrity tests.

However, if the equipment operator is not able to view all of the raw data and select appropriate filters, it can be possible to come to the wrong conclusion and interpret results incorrectly. Is has not been unknown for piles to be condemned and replaced, because of problems with tube installation, such as:

- Tube debonding
- Poor tube joints
- Joint wrapping
- Bent tubes

These can all appear to alter the first arrival time of the signal, even though the true velocity of the signal in concrete between the tubes is normal.

This paper investigates the ways of differentiating between true pile shaft defects and tube defects when interpreting sonic logging results.

2 SONIC LOGGING INTERPRETATION

The principle of cross-hole ultrasonic logging is very simple, in that it measure the time taken for a signal to travel from one transducer to another, between tubes cast into concrete. The time will depend on the distance between transducers and the material between the transducers. The further apart the transducers and the lower the density of material, the longer the transit time.

In homogenous concrete, free of defects, the velocity of sound is constant and in the order of 4000 m/sec. Concrete containing soil inclusions, bentonite, honeycombing etc has a lower sound propagation velocity. This means that measurements of wave speed or transit time can be used as a non destructive method of assessing the quality of buried concrete foundations. Anomalies in the concrete are indicated by a change in signal arrival time or amplitude. A typical signal is shown in Figure 2.

More recently cross-hole tomography techniques have been used to produce both two and three

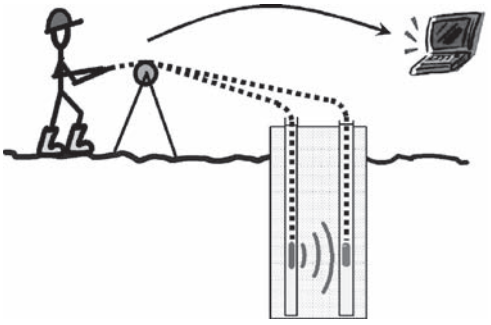

Figure 1. Simple CSL schematic.

dimensional images of the pile shaft. Anomalies are shown as different shaded coloured area on a visual representation of the pile shaft.

A waterfall plot is usually produced, which is effectively a profile built up from modulated signals, taken from each test level, see Figure 3.

The wave speed of ultrasonic waves in concrete is given by:

$$V^2 = \frac{E\,(1-\mu)}{\rho(1+\mu)\,(1-2\mu)} \qquad (1)$$

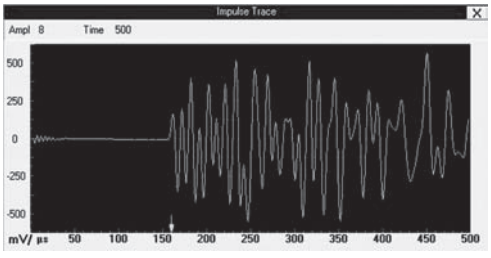

Figure 2. Typical CSL signal.

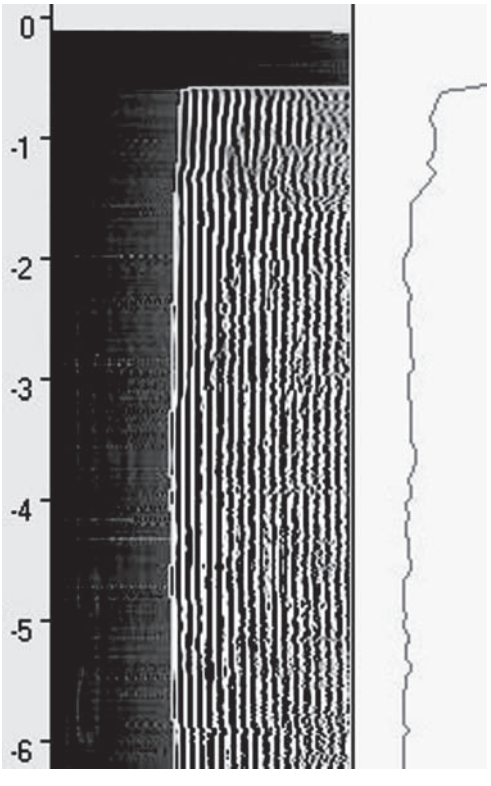

Figure 3. Typical CSL waterfall plot.

where: V = wave speed, ρ = density, E = dynamic modulus & μ = Poisson's ratio

In practice, the transducers are placed in water filled tubes, cast into the concrete. So the signal actually has to pass through water/tube and tube/concrete interfaces twice on it's journey.

First Cautionary Note: Each interface has the potential to alter the quality of the signal, independently from the quality of concrete between the tubes—the very thing we are trying to assess!

2.1 *What is a significant change in First Arrival Time (FAT)?*

Correlations between test results and excavated/cored defects indicate that an increase in FAT of 20% or more is significant. This corresponds to a 17% reduction in apparent signal velocity. So, concrete with a normal velocity of 4000 m/sec would reduce to 3320 m/sec.

Reductions in FAT of less than 10% are not considered to be significant. This corresponds to a 9% reduction in apparent signal velocity. So, concrete with a normal velocity of 4000 m/sec would reduce to 3640 m/sec.

Reductions in FAT between 10–20% are of intermediate significance and the total number of profiles should be taken into consideration. 2 and 3D tomography can be of assistance in visualising the lateral extent of anomalies.

Figure 4 shows 3 profiles from a test result showing a significant increase in transit time. The FAT has increased between 57–76% indicating a significant defect over a vertical zone of approx 1 m. By presenting results alongside each other, it is visually apparent that the anomalies are connected. Signal energy has also decreased by approx 20–24 dB.

It is important to view the individual signal within defective zones, to ensure that the automatic FAT calculation is taken from the correct first arrival. Figure 5, below, shows a damped signal, however the first arrival is still visible. It may be appropriate

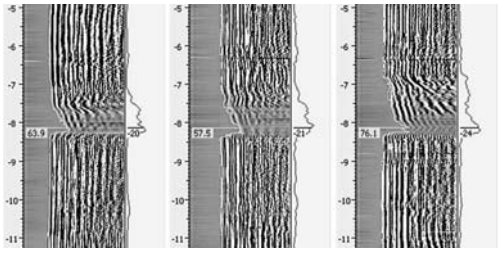

Figure 4. Significant mid-shaft defect found in a retaining wall in New Zealand.

to re-test a signal such as this with a higher signal amplification.

2.2 *Base defects*

Figure 6 shows a result from a pile with contamination at the base. This type of defect tends to occur with tremied piles cast under bentonite, when it is difficult to clean the base.

The signal does not disappear suddenly, but gradually increases in transit time. This could indicate peripheral contamination; however with an increase in excess of 150% it is probably significant enough to affect the whole of the pile section. This was confirmed by the other 5 profiles.

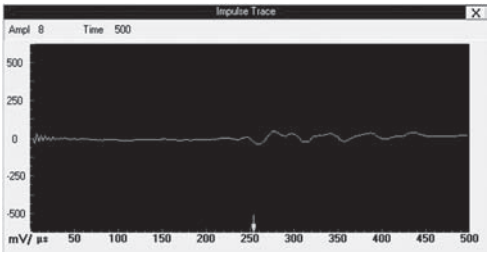

Figure 5. Damped signal.

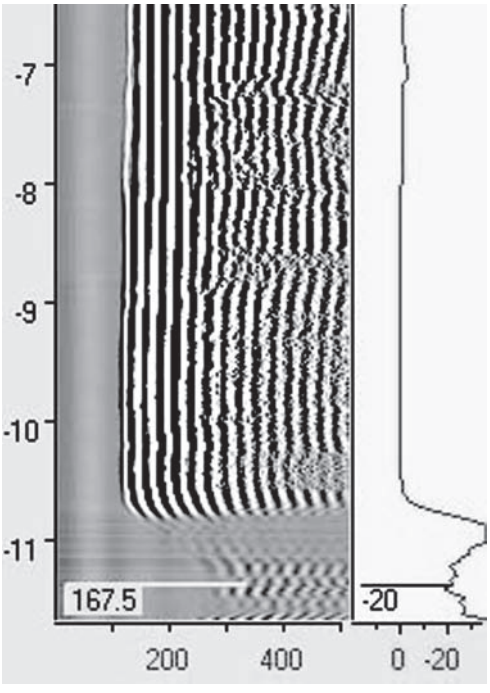

Figure 6. CSL profile of base defect in London.

2.3 *Measurement of concrete velocity and bent tubes*

It is not uncommon for CSL to be used to determine concrete velocity and hence give an indication of concrete modulus. However, the test does not measure velocity directly, it measures the transit time between the probes. Converting this to velocity involves assuming a path length. The path length is only known accurately at the top of the pile, where the distance between tubes can be accurately measured. In practice the tubes can bend over the length of the pile, giving rise to gradual changes in transmission time. If the path length is assumed to be constant, then velocity calculations will be incorrect and misleading. If the tube spacing is known, an *apparent* velocity can be calculated by dividing the tube spacing by the transit time. It must be remembered however, that this apparent velocity includes the water and the tubes. It should also be noted that a signal travelling around a void could yield the same velocity as one travelling through a zone of low modulus material.

Figures 7a & 7b, show the results for a pile with bent tubes. Figure 7a shows a maximum increase in transit time of 43%. Assuming that the tubes are straight this would correspond to a reduction in concrete velocity of 30%, i.e. to 2800 m/sec if normal velocity is 4000 m/sec. This would be comparable to much weaker concrete. This is clearly misleading and could lead to the pile being condemned incorrectly. The corresponding profile shown in Figure 7b shows a matching reduction in transit time. It is unlikely that concrete properties have increased so dramatically!

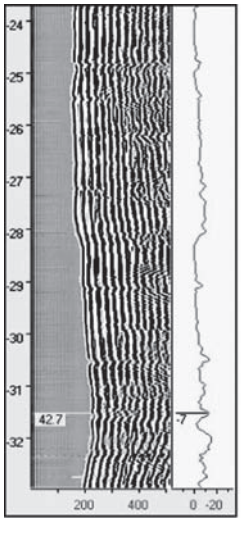

Figure 7a. Tubes bend out.

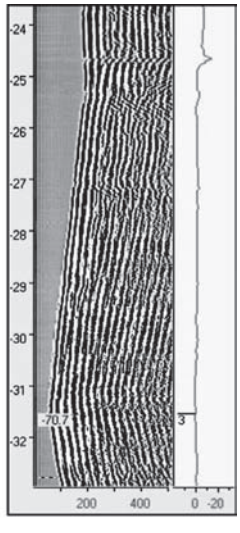

Figure 7b. Tubes bend in.

As a general guide if tubes are bent, signal transit time will tend to change gradually. If the tube is severely bent or kinked, it is unlikely the transducer will pass anyway. The increase may also be matched by an opposing decrease by other profiles. Increases in transit time caused by voids or contamination, tend to appear more abruptly.

Second Cautionary Note: Calculation of concrete velocity from sonic logging results should be treated with caution, and clearly state they are apparent.

2.4 *Firsta arrival time versus signal energy*

Most modern CSL systems have the ability to view not just the individual signal, but also a modulated waterfall plot. A first arrival time (FAT) can then usually be determined and plotted out against depth (on some systems this is all that is displayed). The energy in the signal can also be calculated by measuring the area under the curve and plotted out against depth.

First Arrival time is generally considered to be the most important measurement with CSL. For this reason it is important to understand exactly where it is being measured. On modern digital systems, the FAT is measured automatically. It does this by setting two signal amplitude thresholds. The lower threshold is set to ignore background signal noise. The upper threshold is set to catch the first significant signal arrival.

A problem can occur if you are testing a large diameter pile or diaphragm wall unit with a large path length, especially if the system is not sensitive enough or emitter strength is insufficient. Because of the higher signal to noise ratio, the selection of a correct threshold is imperative for a correct FAT measurement. If it is set too high, it will miss the true first arrival and falsely indicate a problem.

Another reason for a low signal to background noise ratio is tube debonding. Where tube debonding occurs, the actual path length of the signal through concrete is unchanged. A small gap is introduced between the tube and the concrete, which effectively reduces the amplitude of the signal.

Signal amplitude is therefore of secondary importance to FAT and cannot be relied upon on its own, as a measure of concrete quality. It can however be used to back up FAT measurements. Figure 8 shows a sonic logging test result from a pile with tube debonding over the upper 5 m of pile shaft. Signal amplitude is clearly significantly reduced, however the first arrival can be seen, albeit very faintly on the waterfall plot.

Figure 8b shows the FAT and Energy plots using a correctly selected low threshold, however Figure 8c shows the same result with the threshold set too high. The signal at its most damped part has been incorrectly interpreted as having a 72% increase in signal transit time. On its own it could have lead to an incorrect interpretation. For this reason it is much more reliable to assess anomalous areas by viewing the waterfall plot and also the individual signal.

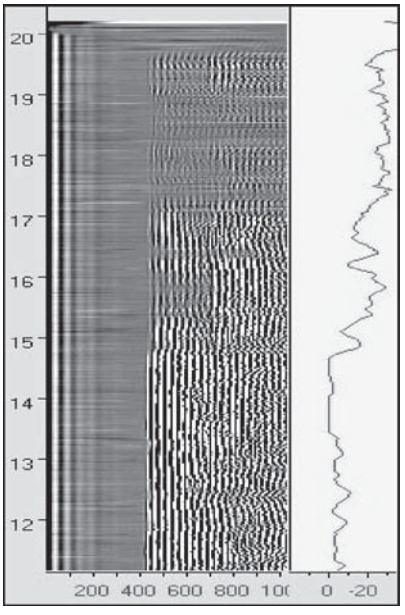

Figure 8a. CSL result for pile with de-bonded tubes over the upper 5 m of pile.

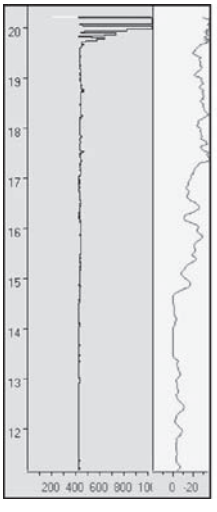

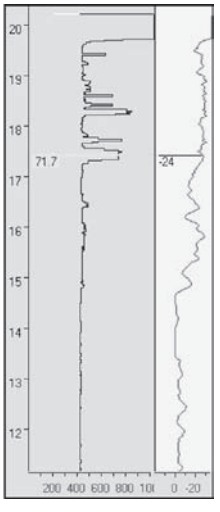

Figure 8b. Good threshold. Figure 8c. High threshold.

Plastic tubes have a tendency to de-bond from concrete more readily than steel. They are also more prone to damage during breading out. For this reason metal tubes generally give better results. On deeper piles, plastic tubing may also suffer from heat of hydration or pressure and collapse.

Third Cautionary Note: Do not rely purely on plots of first arrival against depth

2.5 *Vertical resolution—distance apart of readings*

This varies from system to system. The smaller the vertical interval between readings, then the smaller the defect you will be able to detect, without staggering probes. Some systems take a reading every 20 cm, whereas other take readings every 1 or 2 cm. Whilst it is quite difficult to detect horizontal cracks in concrete piles with CSL, due to signal skipping, with 1 cm spacing it is more likely you will detect some change in signal. With the power and memory of current computers, testing and storing results at 1 cm intervals is no longer an issue and is probably best used as standard.

2.6 *Poor joints?*

Screwed and socketed steel tubing is the best. Welded joints can lead to transducers becoming stuck (very expensive!) or unable to pass. Another problem that can be encountered are wrapped joints. Site engineers in good faith may wrap joints with densotape type material to ensure a waterproof joint, unaware that the signal find it difficult to pass through this interface. Figure 9 shows a CSL result from such a case. This was clearly identified however by the precisely spaced anomalies—coinciding with the joint spacing!

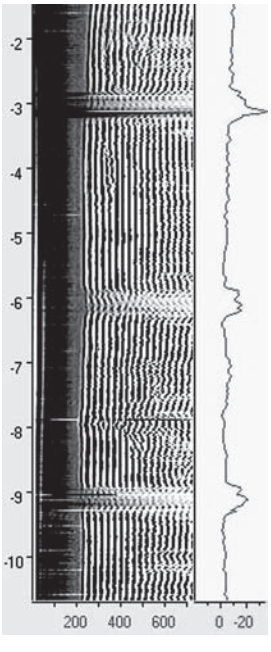

Figure 9. Pile with lagged joints at 3 m intervals.

2.7 *What is signal skipping?*

As you would expect, signals tend to take the shortest and easiest route wherever possible. If the transducers are aligned exactly on the same level as a very thin crack, then the signal will simply travel up the tube a little and through the good concrete above or below. Even if the probes are staggered this will occur, although a slight shift in FAT and signal energy may be observed.

2.8 *So how can thin cracks be detected?*

It is recommended that low strain integrity testing is used if cracks are suspected. The signal from this type of test is unable to pass cracks and is travelling in the vertical plane rather than horizontally. This does presume however that there is good access to the top of the concrete.

2.9 *When to test?*

7 days is the recommended minimum time that concrete should be left to cure before testing. However, assuming that you are not relying on the test to measure concrete velocity (which would be inadvisable as discussed above), CSL can be used as a comparative test and used to test concrete piles at 3 days. This would be purely to check that signal transit times are constant and no changes exist. If that is the case then anomalous areas are not likely to suddenly appear. If however, an area of increased FAT is measured, it would be advisable to re-test the pile again after at least 7 days, during which time concrete strength may have improved.

2.10 *Tube layout—what are you missing?*

The main drawback of CSL, is the requirement to pre-install tubes in foundations during construction (although in emergencies it is possible to core or drill holes in concrete for testing). The layout and number of tubes must therefore be chosen to suit the information that is required by the engineer. For example, if 3 tubes are used and attached equidistant to the reinforcement cage, then only 3 profiles are possible and it is impossible to take a measurement across the centre of the pile. This may be critical if the pile is tremied, when core defects are more likely to occur. With 4 tubes, 6 profiles are possible, around the periphery and across the cores—which is why it is the most widely used configuration.

On diaphragm walls, the tube layout will again depend on panel dimensions. It is recommended however that tube spacing does not exceed 1.5 m to ensure good strength signals.

The more tubes, the better the lateral extent of defects can be determined.

2.11 *Tomography—how useful is it?*

As a quick overview of where anomalous areas are, tomography software is a useful tool. 2D tomography can also give you a clearer idea of the lateral extent. However, they do not give an actual measurement of change in FAT. To do this, you must be able to ideally view each individual signal or if not a good waterfall plot. A simple FAT plot is no good unless you are confident it picked correctly—see section 2.4 above.

First arrival time is king and should be the main basis of all interpretation and used to quantify the severity of defects—along with the number of profiles affected at the same depth.

2.12 *Operator error*

The most common operator errors are:

- Starting tests with slack cables
- Carrying out tests without transducers level
- Not topping up tubes with water on long piles
- Pulling transducers up too fast

When commencing tests, particularly on longer piles, the slack should be taken out of cables and held just in tension before taking data. Figure 10 shows a result with approx 400 mm of cable slack, which is evidenced by a perfectly aligned modulated signal at the base. The winch is moving but the transducers are not lifting. This will produce a test profile longer than the actual pile.

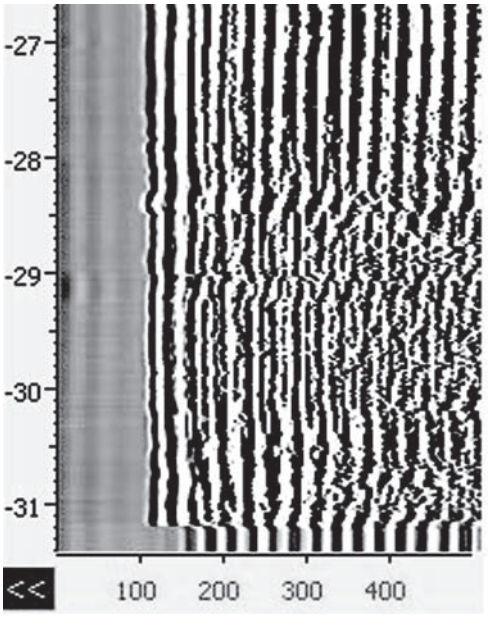

Figure 10. Cable slack at base of pile.

To ensure that the transducers are level, they should either be lowered together to the base, or when at the base, the signal should be viewed, and one transducer raised and lowered until the transit time is at a minimum (this is best done say 2 m from the base, in case of base contamination.

Many systems have a maximum speed that transducers can be raised. The signal acquisition time should be such that data is processed and stored before the next signal is triggered. This is governed usually by warning lights, however with much faster computers being available, this is less of a problem. If warning lights are ignored however, signals may not to stored or processed, before the next one is acquired. This would lead to shorter profiles than expected.

On long piles, the cables will displace quite a lot of water. It is therefore necessary to top up the tubes being tested, before the transducers reach the top. The signal will not transmit through air and part of the pile profile will be lost if the water level is low.

To ensure that the full length of the pile is tested, we would recommend that the tube length is plumbed with a tape measure (if a metal weight the same size of the transducer is used, it may prevent jammed transducers). The tube top level and pile toe level should also be determined. By comparing all reading it is possible to confirm that the tubes go to the base of the pile, that the tubes are not blocked and that the tested length is correct.

3 CONCLUSIONS

In this paper, the interpretation of cross-hole sonic logging results has been discussed and potential pitfalls have been explored. Incorrect interpretation can be caused by many factors if care is not taken.

Users should not rely too heavily on calculated values such as apparent signal velocity, automatically picked first arrival time plots, signal energy plots and tomography profiles. Whilst these do give valuable additional information, the severity of any anomaly should always be assessed mainly on the change in first arrival time, so the original signal should always be available for interpretation after testing.

Where anomalies are suspected, the possibility of this being caused by the tube bonding, joints, loss of water, lagging, or bending should also be considered.

REFERENCES

Stain, R.T. and Williams, H.T. (1991). “Interpretation of Sonic Coring Results: a research project”, Proceedings of the 4th International Conference on Piling and Deep Foundations, Stressa. Vol. 1, pp. 633–640.

Turner, M.J. (1997). Ciria Report 144, “Integrity testing in piling practice”.

Discussion session 3: Pile execution developments & equipment

Deep Foundations on Bored and Auger Piles – Van Impe & Van Impe (eds)
© 2009 Taylor & Francis Group, London, ISBN 978-0-415-47556-3

Durability of cast-in-situ piles

E. Dapena
Geotechnics Laboratory, CEDEX and U.P.M., Spain

P. Alaejos
Materials Laboratory, CEDEX and U.P.M., Spain

L. Prieto
Rodio, Spain

G. Marote
Terrabauer, Spain

ABSTRACT: The execution of excavated piles is a process that can affect the performance of these structural elements and therefore also affect the stability of the structure they support. On the one hand there is the type of concrete to be used, which needs to retain its fluidity during the pile filling process, and on the other, the concrete casting process allowing the pile to be considered as a structural unit capable of transmitting the loads of the structure to the ground in the manner contemplated in the design, as also the fact that it has the correct durability. Bearing in mind that in Spain the responsibilities of execution are regularly shared by the general construction firm and the specialist pile building firm, the research organisation CEDEX belonging to the Spanish Ministry for Development and AETESS, the Association of Special Foundations Firms, are preparing a "Practical Guide on Concrete for Special Foundations" to enable piles to be built with the relevant guarantees for their performance to meet the Design terms assigned. This document is still at the drafting stage and its chapters will cover the materials comprising the concretes and their dosage, durability and quality control. There will also be a chapter on self-compacting concrete (SCC). This paper reports on some aspects referring to the durability of cast-in-situ concrete piles.

1 INTRODUCTION

The reference Standard for executing cast-in-drilled-hole concrete piles in Spain is UNE-EN 1536 ("Execution of special geotechnical works. Drilled piles"). This Standard applies to the construction of piles moulded on site by means of excavation and that form a structural element for load transmission. Piles can be circular in shape, quasi circular or rectangular. The reference Standard for executing concrete screen walls is UNE-EN 1538 ("Execution of special geotechnical works. Screen walls").

The concrete for these structures must have some special features allowing it to meet design specifications while at the same time allowing easy casting on site. The main determining factors for the casting of these concretes, Marote (2006), are as follows:

– casting using tremie tube with an interior diameter generally less than 300 mm;
– high concreting depths with the consequent free-fall of concrete by gravity from substantial heights or else by the use of pumping systems (utilised for the concreting of continuous flight augur piles and rotary bored piles);
– concreting in many cases under water or drilling mud;
– presence of armoured cages with small spaces between longitudinal and cross rods;
– in some cases, prolonged concreting times, maintaining the fluid consistency of the concrete.

The appropriate concrete for these determining execution factors therefore requires a series of properties specified in CTE (2006):

– not easily segregatable;
– high plasticity and good cohesion;
– great fluidity;

– capacity to seal without needing compaction;
– great workability during the pouring process, including the removal stage, where appropriate, of provisional casing.

The materials used to produce the concrete and their dosage should be selected to obtain a concrete that possesses these properties in addition to the strength and durability parameters demanded by the design.

2 PILE DURABILITY

Firstly, any possible aggressive environments will have to be defined which the concrete for special foundations could encounter, followed by detailing of the conditions to be met by the concrete involved in each one of these environments in order for it to reach its useful life without any excessive degradation. The Spanish Concrete Code (2007) guarantees the durability of the structure by laying down a set of specifications relative to the properties and dosage of the constituent materials, to the impermeability of the concrete, the thickness for covering armouring and the maximum crack aperture; finally, special protection measures can be applied in specific cases.

3 DEFINITION OF AGGRESSIVE ENVIRONMENTS

The different environments piles can be subjected to are defined by the set of physical or chemical conditions to which the concrete is exposed and that may be capable of provoking its degradation.

Tables 1, 2 and 3 classify the environments and their aggressivity following the EHE criteria.

Table 1 classifies the general environments, atmospheric I and II, marine III, and the environments involving chlorinated waters other than seawater, IV, swimming pools, purifying plant, etc.

Table 2 classifies the specific environments created by the dumping of industrial waste or soils that can produce a chemical attack on the piles.

This environment Q, or chemical attack, can in turn be broken down into three subcategories (Qa, Qb and Qc), depending on the increasing degree of aggressivity of the surrounding waters or ground. The classification of the chemical aggressivity of the ground or water is given in Table 2. Bearing in mind that piles are structures that are buried or in contact with the ground, if this or groundwater are aggressive they will affect their stability.

Waters exist with a low pH in the effluent of certain chemical plant (waters containing nitric, hydro-chloric or sulphuric acids, for instance) or the result of food waste (which can produce acetic, formic or lactic acids) or drinks (soft drinks contain carbonic acid). High CO_2

Table 1. General Atmosphere Classes.

Class	Designation	Description
Regular low humidity	I	Interiors of buildings
Regular high humidity	IIa	Damp interiors w >65% Exteriors exposed to rainfall >600 mm/year Elements buried in non-aggressive soils: foundations and basement walls
Regular medium humidity	IIb	Exteriors exposed to rainfall <600 mm
Marine above tidal run	IIIa	Structures near coastal areas Structures above tidal runs
Marine submerged	IIIb	Submerged marine structures
Marine within tidal run	IIIc	Structures in tidal run areas Structures in splash areas
Non-marine chlorinated water	IV	Structures in contact with chlorinated water not comprising seawater

Table 2. Specific classes of environment causing chemical attack on the ground or industrial water.

		Environment class		
		Qa	Qb	Qc
Aggressive medium	Parameters	Weak attack	Medium attack	Heavy attack
Water	pH value	6.5–5.5	5.5–4.5	<4.5
	Aggressive CO_2 (mg CO_2/l)	15–40	40–100	>100
	Ammonium ion (mg NH_4^+/l)	15–30	30–60	>60
	Magnesium ion (mg Mg_2^+/l)	300–1000	1000–3000	>3000
	Sulphate ion (mg SO_4^{2-}/l)	200–600	600–3000	>3000
	Dry residue (mg/l)	75–150	50–75	<50
Soil	Baumann-Gully acidity (ml/kg of soil)	> 200	(*)	(*)
	Sulphate ion (mg SO_4^{2-}/kg of dry soil)	2000–3000	3000–12000	>12000

(*) These conditions do not occur in practice.

Table 3. Specific environment classes affected by frost or erosion.

Class	Designation	Description
Frost	H	Structures at high altitudes in damp zones
Ice treated with deicing salts	F	Structures in cold zones where use of deicing salts is necessary
Erosion	E	Structural elements subjected to erosion or cavitation

contents may also occur in some natural waters, for example when they have been in contact with animal or vegetable waste. Chlorides and ammonium sulphates are regular components of fertilizers and the farming industry. Magnesium compounds (chlorides, sulphates or bicarbonates) are easily found in groundwater, in seawater and in some industrial effluents. Some soils containing salts, particularly sulphates—gypsiferous marls and gypsums for instance—also contain chlorides. Finally, the dry residue content in the water gives us an idea of its purity and therefore of its capacity for lixiviating the concrete; in mountainous areas, for example, snowmelt can give rise to increased purity of the water in rivers.

Contaminated water and ground can constitute an additional risk to the chemical aggressivity in the above table. For instance they may have a retarding effect or induce changes in the structure of the concrete owing to the presence of heavy metals, AENOR (2000).

Finally, Table 3 gives three types of specific environment referred to piles and other structural elements, located in areas with relative winter atmospheric humidity in excess of 75% and that can be subjected to temperatures below –5ºC, environment H. Structural elements in areas where de-icing salts are used to clear frost/ice, environment F, and structural elements in areas subject to erosion, environment E. Where piles are concerned, this last environment is typical of bridge foundations in river beds, which scour the foundations under flooding conditions, and the entrained material itself that subjects the surface of the piles to erosion.

4 PROTECTING CAST-IN-SITU PILES AGAINST ENVIRONMENTAL AGGRESSIVITY

By way of general practice, piles are protected from surrounding environmental attack by increasing the compacity of the concrete and the armouring cover.

For cast-in-situ concrete piles the EHE stipulates that minimum cover must be 70 mm.

For foundations not directly concreted against the ground, in lost-sleeve piles for instance, the minimum cover required over armouring is a function of the environment involved. In all cases, UNE-EN 1536 Standard demands a minimum cover of 40 mm. In Type III marine environments, or in aggressive soils, environment Q, cover thicknesses can be as much as 70 mm. In environments Qb and Qc, the Spanish EHE stipulates that the designer must fix the minimum cover.

In order to increase the compacity of the concrete, the water/cement ratio is limited and a minimum cement content per cubic metre is set, as shown in Table 4, and the use of cements resistant to sulphate action (SR) or seawater action (MR) is mandatory if the piles will be subjected to these environments.

In terms of cement type, higher impermeability is obtained in concretes made of cements incorporating additives than that obtained in analogous conditions with Portland cement, meaning that the time it takes for the aggressive agent to reach the armouring is much longer and, consequently, its use is highly beneficial for improving the durability of the concrete. By way of conclusion, under environment Q the recommendation is to use cements incorporating puzzolanic or blast furnace slag additives.

It is also forbidden for the armouring to be allowed to come into contact with other metals with a very different galvanic potential. This aspect becomes specially important in the selection of the material for the separators and the wire tying the steel rods.

In the event that the concrete will be in contact with highly acidic water (pH < 3), some type of protection must be provided as no concrete is capable of resisting this acidity in the long term. Additional recommendations for protecting the concrete of piles subjected to acidic environments can be found in Neville (1981), ACI (2005) and Alaejos & Bermúdez (2003).

5 CONCLUSIONS

The durability of cast-in-situ piles is an extremely important aspect to bear in mind in the execution process owing to the aggressivity of certain environments in which the piles are built.

The classification of these environments is given in Tables 1, 2 and 3.

Well executed piles, particularly with the collaboration of a very low consistency (self-compacting concrete) and the right dosage, plus the use of special cements as a function of the particular environment involved, can guarantee a good performance for the pile concrete.

Table 4. Characteristics of the concrete in reinforced concrete piles affected by different environments. EHE (2007)

Environment	Environment type	Max w/c	Minimum cement kg/m^3
Regular interiors, buildings	I	0.65	250
Damp interiors: w < 65%		0.60	275
Exteriors under rainfall			
>600 mm	IIa		
Buried elements			
Exteriors under rainfall	IIb		
<600 mm	H	0.55	300
High altitude structures			
Structures in coastal areas	IIIa		
Structures above tidal runs	E	0.50	300
Structures subject to erosion			
Submerged marine structures	IIIb		
Structures in contact with:		0.50	325
– chlorinated water	IV		
– deicing salts	F		
– low aggressivity industrial waters: low pH 6.5–5.5	Qa		
– soils with sulphates, SO_4 of 2 to 3 g/kg			
Structures in contact with:			
– medium aggressivity industrial waters.		0.50	350
Average pH 5.5–4.5	Qb		
– soils with sulphates; $SO_4^=$ of 3 to 12 g/kg			
Structures in tidal runs and in:			
– high aggressivity industrial waters: high pH < 4.5	IIIc	0.45	350
– soils with sulphates, $SO_4^=$ greater than 12 g/kg	Qc		

w/c: water:cement ratio.

The maximum water/cement ratio permitted in the concrete, as a function of the type of environment involved, and the minimum cement content, also for each environment, are given in Table 4. This highlights that for piles built at sea or cast on gypsiferous soils, the maximum water/cement ratio is 0.50 or 0.45 if the piles are subjected to tidal runs. The minimum cement content is 300 kg/m^3 in piles built above tidal runs, or 350 kg/m^3 in piles built in tidal run areas or in gypsiferous soils.

It is general practice to require a minimum cover of 70 mm for the piles.

REFERENCES

ACI (2003). Guide to Durable Concrete. ACI 201.2R-92. En *ACI Manual of Concrete Practice Part 1: Materials and General Properties of Concrete.* Detroit: Ed. American Concrete Institute.

ACI (2006c). Design, manufacture and installation of concrete piles. ACI 543R. In *ACI Manual of Concrete Practice. Part 6*. Detroit: Ed. American Concrete Institute.

AENOR (2000). *Ejecución de trabajos especiales de geotecnia. Pilotes perforados. NORMA UNE-EN 1536.* Madrid: Ed. AENOR.

Aguado, A. et al. (1996). *Diagnóstico de daños y reparación de obras hidráulicas de concrete*. (Monografías 19). Colegio de Ingenieros de Caminos, Canales y Puertos.

Alaejos, M.P. & Bermúdez, M.A. (2003). *Durabilidad y procesos de degradación del hormigón de presas. Estudio Bibliográfico.* Monografía M-76. Centro de Estudios y Experimentación de Obras Públicas. Madrid.

CTE (2006). Código Técnico de la Edificación. Documento Básico SE-C. Seguridad estructural. Cimientos (2006).

EHE (2007) Ministerio de Fomento (2007). *Propuesta de modificación de la Instrucción EHE. Document 0*.

Marote, G. (1006). *Aspectos fundamentales de los materiales que intervienen en la ejecución de pantallas*. AETOS—AETESS Technical Meeting, Madrid, 26 September, 2006.

Neville, A. M. (1981). *Properties of concrete*.—Longman Scientific & Technical (pages. 433 to 528).

PG3 Ministerio de Obras Públicas (2002). Pantallas continuas de hormigón armado moldeadas "*in situ*". In *Pliego de prescripciones técnicas generales para obras de carreteras y puentes*.

RC-03 Ministerio de la Presidencia (2004). *Instrucción para la recepción de cementos (RC-03)*. Madrid.

RILEM. *Corrosion of steel in concrete. Report of the Technical Committee 60-CSC*.: P. Schiessl.

Deep Foundations on Bored and Auger Piles – Van Impe & Van Impe (eds)
© 2009 Taylor & Francis Group, London, ISBN 978-0-415-47556-3

Statistical analysis of CFA piles construction

A. Mandolini
Second University of Naples, Italy

G. Russo
University of Cassino, Italy

ABSTRACT: For the construction of a large treatment plant in Poggiomarino (Napoli, Italy) a large number of bored CFA piles (more than 1000) was installed in a loose silty sand soil deposit. All the parameters recorded during the installation of the piles (rate of revolution, rate of penetration, etc.) have been used in order to carry out a statistical analysis of the construction. Since the piles construction is very similar to an industrial process (due to either the large number of piles involved or the highly repetitive construction phases), in the paper an analysis of CFA piles construction has been performed by means of statistical process control methods. The close dependency between the construction parameters and the geotechnical variability of the subsoil has been considered. Control charts of the mean and the standard deviation of the selected executive parameters have been developed referring to a small piles subgroup. The analysis points out the strong dependency of the control limits by the position of the piles selected to set up the control charts. It has been demonstrated the dependency of the statistical "in control/out of control" of the construction process of a single pile on the location in the installation area.

1 INTRODUCTION

The construction of a civil work can be regarded as an industrial process aimed to realize the planned design. The correspondence between the design and the work as built depends largely on the procedures performed during construction. These procedures should be adequate to the scopes and carefully controlled in order to meet the design specifications. Control procedures therefore play a central role for the quality of the construction. The control activity should not be only intended to the final satisfaction of design specifications, but also aimed to the intervention on the construction process in maintaining the standard requirements of the product. The use of proper analysis instruments of process control, largely involved in industrial process control, are particularly attractive also referred to civil construction processes.

In the paper statistical process control methods have been applied to the analysis of Continuous Flight Auger (CFA) bored piles construction. More than one thousands CFA piles were built for a huge treatement plant in the south-west area of the Napoli area in Italy (Mandolini & Falconio 2001, Mandolini et al., 2002). The construction parameters during the penetration and during the extraction of the screw were continuously monitored and recorded. Since the piles construction is very similar to an industrial process (due to either the large number of piles involved or the highly repetitive construction phases), all the recorded data have been analysed by means of statistical process control methods. The close dependency between those parameters and the geotechnical variability of the subsoil has been considered (Mandolini & Russo 2007). The control charts (Shewhart 1939) of the mean and the standard deviation of the selected construction parameter have been developed referring to a small piles subgroup. As stated by Woodall (2000), control charts may be used either *a posteriori*, in order to determine whether or not a given process has been in statistical control, or during production, in order to manage the process detecting changes in samples taken sequentially over time. In the present study the control chart method is applied to simulate an on line control of the construction process. Aim of the study is to develop a practical method of controlling the CFA piles construction by means of specific control charts, to be implemented in future applications.

2 STATISTICAL PROCESS CONTROL

In the statistical process control methods the control parameters are regarded as normally distributed

random variables. If the variability of the control variables is normal, the process is considered to be in statistical control (Fig. 1a). In this case the variability of the parameters is inherent, i.e. it cannot be eliminated acting on the process. If assignable causes (operator, machines, procedures) influence the process, then the variability differs from the normal and the process is dragged out of statistical control (Fig. 1b). Assignable causes can be eliminated by intervention on the process.

The Shewhart control charts are used in order to highlight the variability of a statistical process. Two types of control charts are required in order to investigate the features of a statistical process: the first one is the mean control chart, that shows the process variability, and the second one is the standard deviation control chart that describes the variability inside a single sample. The mean control chart is obtained by plotting the mean values $\bar{x}_1$ of samples with dimension n as a function of the sample number, on a diagram in which three control lines are reported: namely the upper control line (UCL), the lower control line (LCL) and the central line (CL). The process is defined in control, if $\bar{x}_1$ systematically falls inside the control interval. If, on the contrary, $\bar{x}_1$ falls out of the control interval, it means that the process is dragged out of control by specific factors affecting the normal variation of the control parameters.

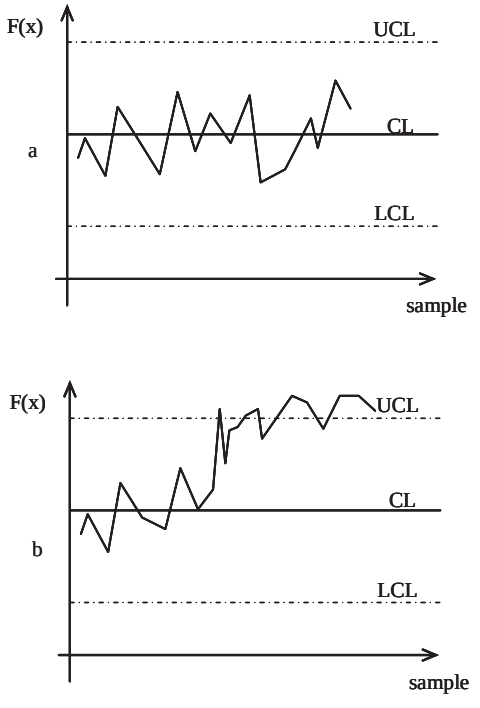

Figure 1. In control process (a); out of control process (b)

If the statistical distribution of the population is known, the control limits of a mean control chart are defined by:

$$\begin{cases} UCL = \mu + k\sigma_{\bar{x}} \\ CL = \mu \\ LCL = \mu - k\sigma_{\bar{x}} \end{cases} \quad (1)$$

where μ is the mean, σ the standard deviation of the population and k is the interval extension. The latter is set as a multiple of the standard deviation and a value $k = 3\sigma$ is usually chosen, because 99.73% of the elements pertaining to a normally distributed population fall in the $(\mu \pm 3\sigma)$ interval.

In most cases, however, the mean and the standard deviation of the population are unknown, and thus the control limits of the mean control chart are estimated from the sample distribution as follows:

$$\begin{cases} UCL = \bar{\bar{x}} + \dfrac{3}{c_4\sqrt{n}}\bar{s} \\ CL = \bar{\bar{x}} \\ LCL = \bar{\bar{x}} - \dfrac{3}{c_4\sqrt{n}}\bar{s} \end{cases} \quad (2)$$

where $\bar{\bar{x}}$ is the mean of sample means, $\bar{s}$ is the mean standard deviation, c_4 is a function of the sample dimension n with the expression

$$c_4 = \frac{4(n-1)}{4n-3} \quad (3)$$

In the same case, the standard deviation control chart has the following parameters:

$$\begin{cases} UCL = 1 + \dfrac{3\bar{s}}{c_4\sqrt{2(n-1)}} \\ CL = \bar{s} \\ LCL = 1 - \dfrac{3\bar{s}}{c_4\sqrt{2(n-1)}} \end{cases} \quad (4)$$

3 CASE HISTORY

The Poggiomarino treatment plant is placed in the valley of the Sarno river, south-west of Napoli (Fig. 2). It is formed by a complex of structures, in which the biological treatment plant, considered in the present study, is about 60 m in width and 100 m in length.

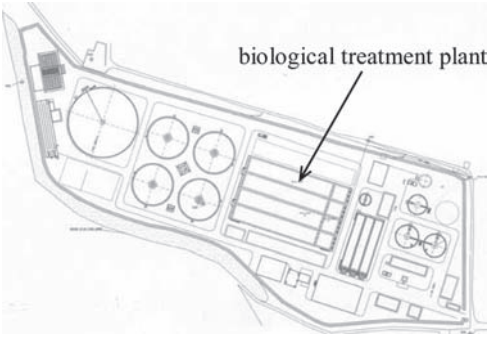

Figure 2. The Poggiomarino treatment plant.

Figure 3. Foundation of the biological treatment plant.

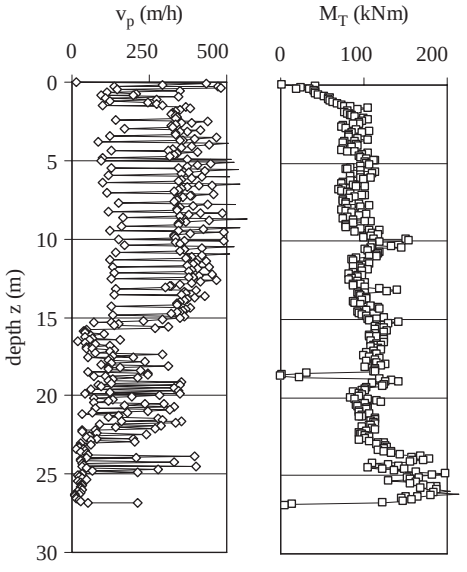

Figure 4. Typical profiles of construction parameters rate of penetration v_p and torque M_T

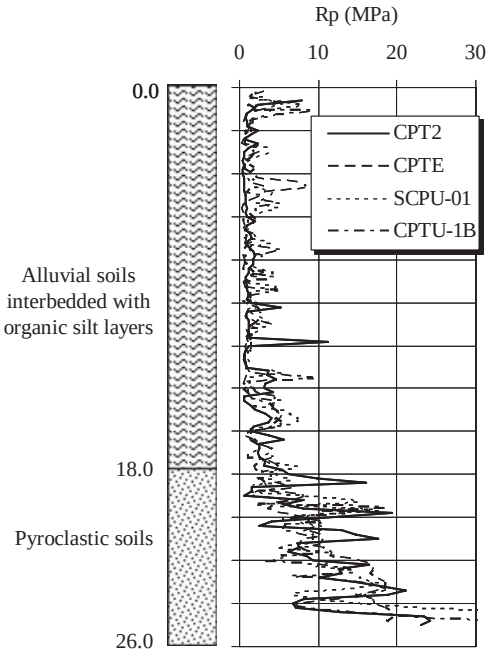

Figure 5. Subsoil profile

About 1000 CFA piles were used for the foundation of the plant (Fig. 3). The piles diameter is 0.80 m and the length is about 27 m, with a 2.5 m distance between the pile axes.

The drilling machine (Casagrande C600, total weight 1000 kN, hydraulic rotary with a maximum torque $M_{T,max}$ = 220 kNm) was provided with instruments for the continuous monitoring of the construction parameters during the penetration (rate of revolution n, rate of penetration v_p and torque M_T) and during the extraction of the screw (concrete flow Q_C and retrieval rate v_R). These parameter have been recorded every 0.08 m along the pile length. In Figure 4 typical profiles of rate of penetration and torque are represented.

Geotechnical properties of the subsoil were investigated by means of boreholes, cone penetration tests (CPT), piezocone tests (CPTU) and seismic piezocone tests; laboratory tests on undisturbed samples were carried in order to determine physical and mechanical properties of the soils (Mandolini et al., 2002).

The subsoil conditions (Fig. 5) are mainly formed by alluvial soils of pyroclastic origin, interbedded with organic silt layers, on a base formation of pyroclastic soils. This configuration results relatively uniform in horizontal direction. The groundwater level fluctuates between 1.2 m and 1.6 m below the ground surface.

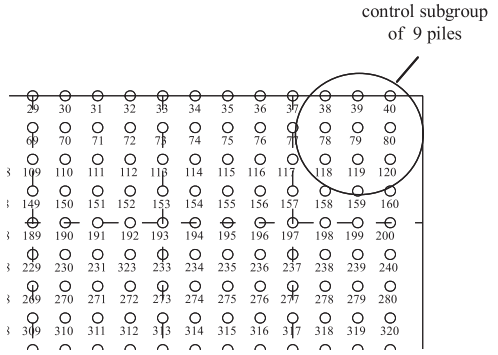

Figure 6. Location of the control piles subgroup.

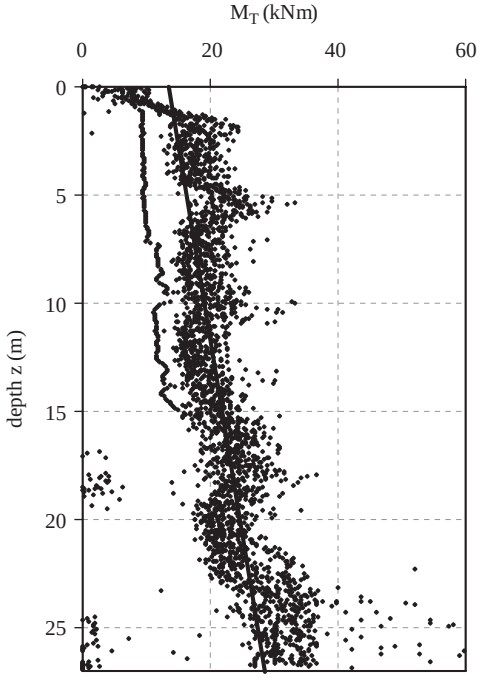

Figure 7. Average trend evaluation of torque M_T

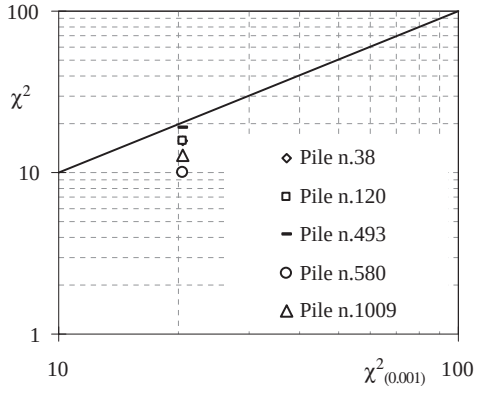

Figure 8. Chi-squared test results

Table 1. Control limits.

	Mean (kNm)	Standard deviation (kNm)
UCL	0.966	6.840
CL	–0.045	6.162
LCL	–1.055	5.454

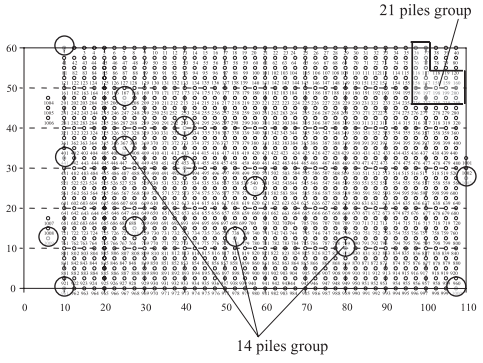

Figure 9. Location of two piles group selected for the statistical process control

4 STATISTICAL ANALYSIS OF CFA PILES CONSTRUCTION

An on line control of the pile construction has been simulated in the study. Control charts of the relevant construction parameters were set up to analyze the construction of piles subgroups.

The torque M_T is directly linked to the soil properties. A minimum torque is necessary to allow the screw penetrating in the subsoil, then the torque is variable with depth. The variation is characterised by an increase with depth, with fluctuations due to local features of the subsoil, and it depends on the location of the vertical in the considered area. This spatial variability of the torque have been managed hypothesizing that the variable $x(z)$ is composed of a deterministic part, function of depth and called trend $t(z)$, and a random part called residual $r(z)$ (Jaksa et al., 1997, Phoon et al., 2003):

$$x(z) = t(z) + r(z) \tag{5}$$

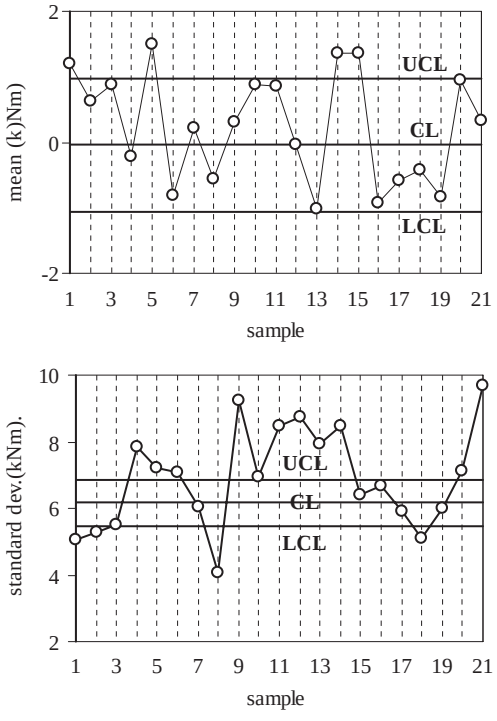

Figure 10. Control charts for 21 piles group.

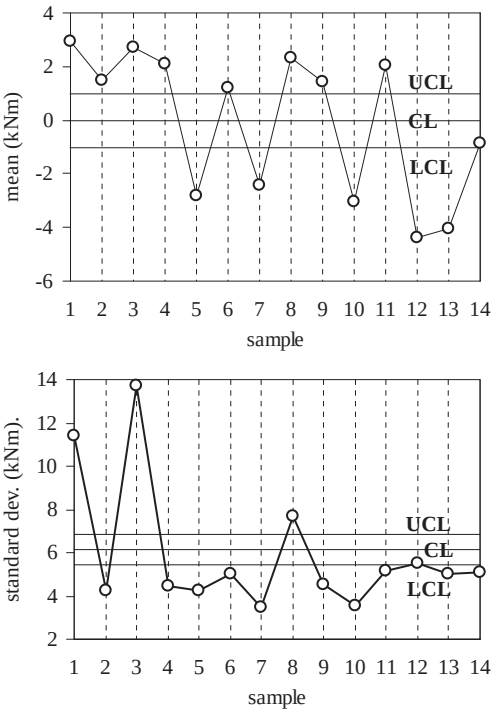

Figure 11. Control charts for 14 piles group.

Residuals are characterised by mean value equal to zero. The deterministic trend has been evaluated by means of a linear regression based on least square method. The statistical process control has been implemented with reference to the residuals of torque.

The control charts were defined referring to a small subgroup of n. 9 piles. The construction process of these piles was considered in statistical control, as usual of the statistical process control methods (Montgomery, 1999). In Figure 6 the location of the subgroup in the foundation area is reported. The average trend $\overline{t(z)}$ of torque M_T as a function of depth z was evaluated (Fig. 7) for the subgroup. Residuals of torque were then calculated for each pile of the subgroup from eq. (5) as follows:

$$r(z) = x(z) - t(z) \tag{6}$$

A chi-squared test was performed in order to verify the normality of the torque residuals distribution of few piles in the area, since normality is a necessary requirement to perform statistical process control by means of control charts. In Figure 8 it is evidenced that the residuals distribution is normal with a significance level of 99%.

The limits of the mean and standard deviation control charts were then calculated referring to expressions (2) and (4), based on the torque residuals of the piles subgroup selected. In Table 1 these limits are reported.

The on line control is based on the comparison between the mean and standard deviation values of the torque residuals pertaining to piles not included in the subgroup and the control limits. Two piles group were analysed in order to simulate the on line control (Fig. 9). The first is a 21 piles group located nearby the control subgroup, while the second is formed by 14 piles randomly selected in the foundation and located far from the control subgroup.

Figure 10 shows the mean and standard deviation control charts for the 21 piles group. With reference to the mean chart, the process is characterised by a fluctuation of the values mainly inside the control interval (with the exception of some values), indicating the overall statistical control of the construction process. The scattering of standard deviations showed by the standard deviation chart involves the high variability of residuals inside each sample of torque residuals.

Referring to 14 piles group, the mean and standard deviation control charts highlight the statistical out of control of the construction process with reference to the fixed control limits (Fig. 11). The values fall

systematically out of the control interval, referring to both mean and standard deviation values. It can be argued that the control interval does not represent the statistical process for the selected 14 piles group. The engineering properties of soils exhibit variability from one location to another, even within apparently homogeneous profiles. This divergence of properties, termed spatial variability, is characterised by more related (i.e. autocorrelated) values at adjacent locations than those at larger distance lags. In this case, the spatial variability of the soil properties influences directly the torque values, and it is evident that the control charts are not suitable for the statistical control of piles located at relatively great distance from the control group. In order to make this method suitable, an update of the control limits should be systematically performed during the construction phase. It means that new control limits should be evaluated as the distance of the piles to be controlled from the control group increases. The frequency of the control limits update depends on the gradient of the decay of the autocorrelation of the soil parameters.

5 CONCLUSIONS

In the paper the results of a statistical analysis of the construction of CFA piles have been reported. The case history of the construction of an important huge treatment plant in Poggiomarino (Naples) has been adopted due to the overall uniformity of the subsoil conditions, and due to the large number of bored CFA piles installed. During the construction the main installation parameters were measured with a high frequency of recording.

The analysis has been performed by means of statistical process control methods. Control charts of the mean and the standard deviation of the selected construction parameters have been developed in order to simulate an on line control of the process. In the case a small subgroup of piles has been selected in order to evaluate the control interval. The analysis has been developed referring to the torque parameter M_T, due to its direct dependency on the subsoil properties. The monitoring data were filtered in order to take account of the spatial variability of the subsoil properties, operating a de-trending of data and considering for the analysis only the residuals (i.e. random component of the data) and their distributions.

With reference to the control interval evaluated on the small piles subgroup, the process is in statistical control for piles located nearby the selected subgroup, while is out of statistical control for piles located at great distance. This result points out the strong dependency of the construction parameters on the spatial variability of the subsoil properties. It is therefore necessary a systematic upgrade of the control interval for a proper application of an on line statistical process control.

At this stage the analysis has been pointed out the suitability of the statistical process control to the construction of CFA pile, provided that an extended monitoring of the relevant parameters should be performed. From the practical standpoint, the correct implementation of such a control method requires a careful analysis of the spatial variability of the subsoil properties in the area of interest. In this way the control interval can be upgraded depending on the location where the construction is taking place. Further investigations are required in order to link the quality control of the construction with the expected performance of the CFA piles.

REFERENCES

Croce, P. & Russo, G. 2002. Statistical analysis of earth dam construction. *International Conference of Numerical Methods in Geotechnical Engineering*, NUMGE 2002, Paris.

Jaksa, M.B., Brooker, P.I. & Kaggwa, W.S. 1997. Inaccuracies associated with estimating random measurement errors. *J. Geotech. Geoenviron. Eng.*, ASCE, 123 (5), 393–401.

Mandolini, A., Ramondini, M., Russo, G. & Viggiani, C. 2002. Full scale loading tests on instrumented CFA piles. *Deep Foundation Congress*, GeoInstitute of the ASCE, Orlando, Florida, 1088–1096.

Mandolini, A. & Russo, G. 2007. Controllo statistico della costruzione di pali CFA. *Associazione Geotecnica Italiana. XXIII Convegno Nazionale di Geotecnica*. Padova, 593–599.

Montgomery, D.C. 1996. *Introduction to Statistical Quality Control*. J. Wiley & Sons, New York.

Phoon, K.-K. & Kulhawy, F.H. 1999. Characterization of geo-technical variability. *Canadian Geotechnical. Journal*, 36 (4), 612–624.

Shewhart, W.A. 1939. Statistical Method from the Viewpoint of Quality Control. *Graduate School of the Department of Agriculture*, Washington D.C. (published by Dover Publications, 1986, Mineola, N.Y.).

Woodall, W.H. 2000. Controversies and contradictions in statistical process control. *Journal of Quality Technology*, 32 (4), 341–350.

Deep Foundations on Bored and Auger Piles – Van Impe & Van Impe (eds)
© 2009 Taylor & Francis Group, London, ISBN 978-0-415-47556-3

Installation effort, current calculation methods and uses in design and construction in the US

W. Morgan NeSmith Jr.
Berkel & Company Contractors, Inc., Atlanta GA, USA

Willie M. NeSmith, P.E.
Berkel & Company Contractors, Inc., Birmingham AL, USA

ABSTRACT: For BAP IV, one of the authors (NeSmith, 2003) presented a paper in which the concept of Installation Effort (IE) was introduced, and the potential uses of IE as an indicator of stratigraphy and displacement screw pile capacity were described. Since that time, there have been a number of developments in this field including: improvements in the acquisition of data required to calculate IE; the real time presentation of IE data during pile installation; modifications to the calculation of IE and Cumulative IE; and refinements in the relationship between Cumulative IE and pile capacity. These developments have facilitated the application of IE as a practical tool for design, and for control of production pile installation. This paper describes these developments, provides an overview of the database of Installation Effort vs. Capacity collected by the authors, and demonstrates the calculation, presentation and use of IE and Cumulative IE on recent foundation construction projects in the US.

Keywords: displacement screw piles, installation effort

1 UPDATED ACQUISITION OF DATA

The data acquisition system used by Berkel in 2003 was an analog system with a limited number of available signal inputs. Recording grout pressure for quality assurance during pile casting used one of the available inputs, leaving two remaining inputs for data recorded during drilling tool penetration. These were used for recording of stem depth and KDK pressure (the hydraulic fluid pressure applied to the rotary head). Since then, this system has been replaced by a digital system which allows for greater flexibility in the number of inputs that can be acquired and recorded. Two primary additional inputs have been added. The first was the measurement of grout volume during pile casting by means of a flow meter. More recently, the recording of drill stem rotation during pile penetration has been recorded as well. Figure 1 shows a typical drilling platform and the location of these sensors. A detailed description of the data acquisition system can be found in the 2002 paper by the authors.

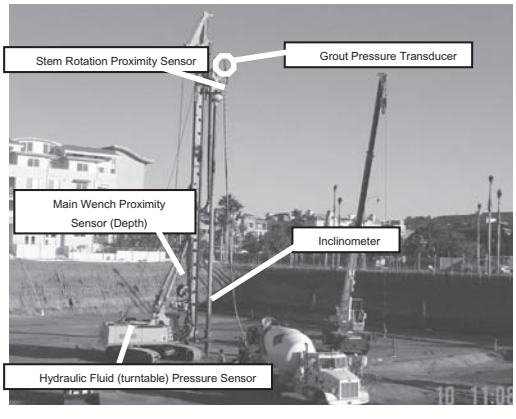

Figure 1. Data recorded on drilling platform.

More importantly, the switch to the digital acquisition system increased the flexibility of the presentation of recorded data, allowing for real time display of data as well as real-time calculation and display of the Installation Effort described herein. This led to improvements in data display for both the drilling platform operator and the piling inspector. The results of these improvements to the data acquisition system are discussed in the following sections.

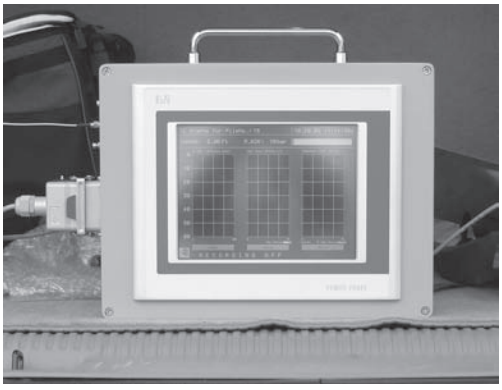

Figure 2. Wireless remote monitor.

2 CALCULATION OF IE AND REAL TIME DISPLAY OF INSTALLATION DATA

The method of calculating Installation Effort as a function of drilling tool penetration rate and torque (as estimated from the KDK Pressure) was described in the previous paper. This calculation method is still in use. IE values are calculated at every 1-second recording interval based on the KDK Pressure and Penetration Rate recorded at that interval. Plots of IE vs. depth are produced in real-time in the field and continue to provide excellent agreement with stratigraphic representations from Cone Penetration Tests. This agreement has extended beyond the original database to a variety of geologies.

Berkel incorporated a larger monitor for the pile inspector to increase the amount of data displayed during pile production (Figure 2). In addition, this remote monitor communicates with the computer on the drilling platform wirelessly, doing away with the need for the inspector to move the monitor with the drilling platform. More recently, the on-board system has been modified so that the remote data can be viewed on a standard laptop computer rather than a dedicated monitor.

Figure 3 shows the main screen and engineering screen as viewed on the wireless monitor or laptop. The main screen includes general pile information such as date and time, pile number, current depth, etc. as well as graphical representations of KDK and grout pressures.

The engineering screen shows plots of KDK Pressure, Penetration Rate, Installation Effort and Cumulative Installation Effort vs. depth as drilling tool penetration occurs. This real-time display allows the inspector to observe the stratigraphy at the pile location and adjust the pile toe level as appropriate. It also allows the inspector to view Cumulative IE as it is developed to verify that the effort required for pile

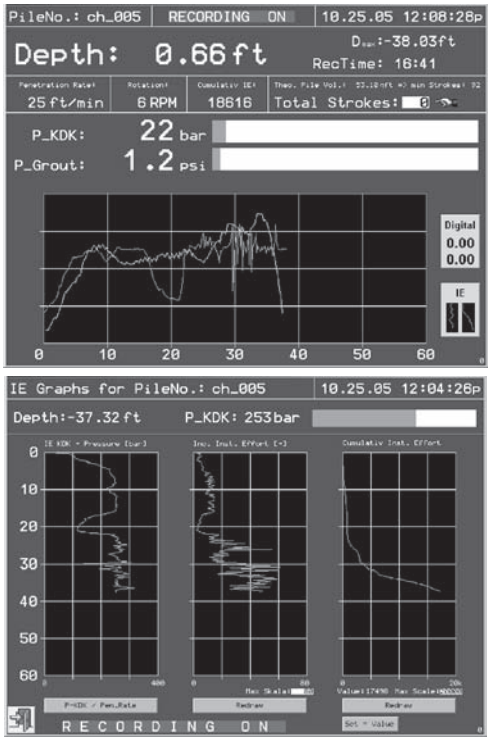

Figure 3. Main and engineering screen of wireless remote monitor.

installation meets the specifications developed during the design and load test phases of the project.

3 UPDATED CALCULATION OF CUMULATIVE INSTALLATION EFFORT

In the 2003 paper, the term SumIE was introduced. As the name would indicate, this was an estimate of the total Installation Effort as the sum of the IE values recorded at 1-second intervals during penetration of the drilling tool. The consistent relationship between SumIE and Capacity was also demonstrated; however this relationship could not be extended to shaft capacity or toe capacity. A study of the Total IE developed during pile penetration (SumIE vs. Depth) indicated that the SumIE was heavily weighted by dense and hard layers and subsequently underestimated the contribution to capacity of loose or soft layers while severely overestimating the contribution to capacity of hard or dense layers. This also resulted in difficulty when trying to use IE to predict the capacity of variable pile lengths.

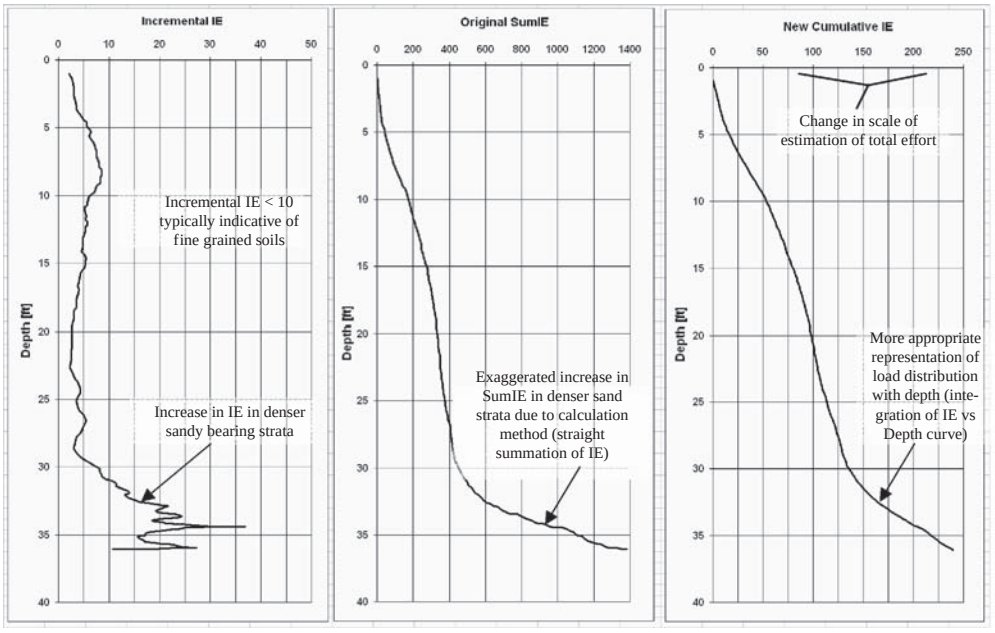

Figure 4. Example incremental IE profile with calculated SumIE and cumulative IE profiles.

Drilling data is recorded and IE is calculated at 1-second intervals. When the drilling tool encounters a hard or dense layer, the SumIE calculation is affected in two ways. First, the individual IE values calculated in that strata increase (as one would expect with an increase in density). Second, because drilling slows down in these layers and because these calculations are performed on a time interval, more IE values are recorded per unit length in these layers than in softer or looser layers. These additional recordings per unit length of penetration are what produce the exaggerated SumIE in dense and hard materials. An example of this calculation from an IE vs. Capacity profile is shown in Figure 4.

Cumulative IE was proposed as an alternative estimation of the total effort during pile penetration. Instead of a straight summation of recorded Installation Effort values, each value is weighted according to the length from the previous calculation depth; in effect an integration, rather than a summation, of the IE vs. Depth plot. The result is a much smoother Cumulative IE vs. Depth plot which does not exaggerate the influence of hard or dense layers (Figure 4).

Additionally, Cumulative IE shows a good correlation with shaft capacity, as one might expect considering that IE is calculated at 1-second intervals along the shaft of the pile.

4 CUMULATIVE IE DATABASE

In 2002, Berkel's database of Installation Effort vs. Capacity consisted of 15 test piles from 9 project sites. The current database consists of 111 load tests from 48 project sites (Figure 5). The mean relationship and plus/minus one standard deviation are also shown.

Figure 5 also includes an example of load test results from two example projects and the resulting design Cumulative IE vs. Capacity line for Example A. This is typical of Berkel's current design process; the load test results from a project site are plotted on the entire database and the mean relationship is adjusted to fit the load test results for that particular site and to develop the relationship for use in final design of production piles on that project.

Typically, displacement piles in loose and medium dense sands have Cumulative IE and capacity relationships that fall within the plus/minus one standard deviation range of the database shown. As fines contents increase and density decreases, the relationship tends to move to below the minus one standard deviation line. This is due to the decrease in shaft resistance developed in these materials for the same amount of effort expended by the drilling platform AND the lower toe capacities developed by piles in these materials as well. Example B on Figure 5 shows

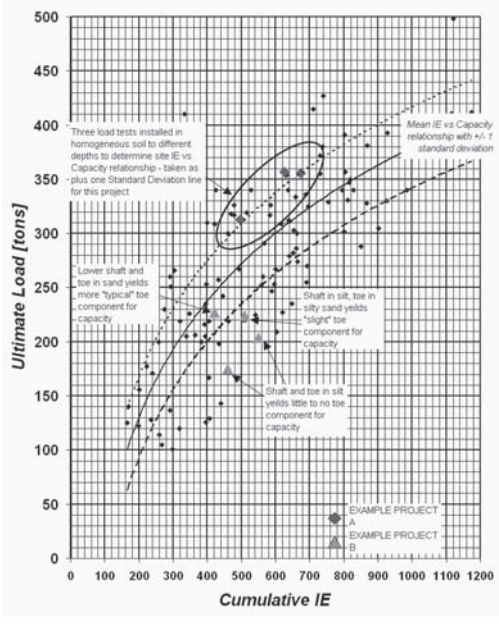

Figure 5. Database of Cumulative IE vs. ultimate load and two example projects.

four load tests from a project site with two load tests with the entire shaft and toe in a sandy silt; one load test with the shaft in this silt and the toe in a slightly cleaner sand; and one load test with the bottom of the shaft as well as the toe in cleaner sandy material. The movement of the Cumulative IE–Capacity relationship from below the minus one standard deviation line to about the mean relationship as soil type and density change is illustrated in this example. Piles installed in denser and cleaner sands tend to have an IE–Capacity relationship that falls towards the plus one standard deviation line. Piles that fall well above this line have typically been installed with the pile toe in dense cemented sands or gravels resulting in toe capacities in excess of what is developed in the majority of the displacement screw piles installed in North America.

5 USE OF CUMULATIVE IE

The development of the calculation of Cumulative IE vs. depth and the expansion of the IE–Capacity database are significant tools in the design of displacement screw piles. The database can be used to set final test pile depths based on the Cumulative IE developed by probe and reaction piles installed prior to test pile installation. IE–Capacity relationships from the test pile program can be used to set Cumulative IE values for pile termination during production. This is becoming a more common pile termination criterion as the database has expanded.

In addition, Berkel often uses the Cumulative IE vs. Depth curve (Fig. 4) to evaluate the segmental capacity of pile shafts and to adjust production pile IE or depth requirements based on these segmental capacities. The most common application of this is on projects with deep excavations in some areas of the project site—for elevator pits or shear walls for example. Typically, an adjusted pile capacity is developed considering the loss of Cumulative IE from the material that will be excavated and the final Cumulative IE required for these piles is adjusted if necessary. This has often eliminated the need for production piles to be extended by a length equal to the depth of excavation, as is a common solution to the problem above. Instead, production piles need only be extended to compensate for the IE developed in the excavated material. As production piles often bear in denser materials than are in place nearer the ground surface, this typically results in shorter production piles than might be required if the Cumulative IE data was not available. In fact, Cumulative IE is much better suited to setting production pile lengths based on the conditions at each pile location than the historically used approach of using a required effective pile length for all production piles. The result is a more efficient and economical development of pile toe elevations across the project site.

6 FUTURE RESEARCH

Currently Installation Effort is calculated as a function of KDK Pressure and Penetration Rate. When this relationship was developed, it produced a typically operator-independent IE calculation. However, there have been recent improvements in the efficiency with which hydraulic fluid pressure (KDK Pressure) is applied to the rotation head of the drilling tool. The result is that the manner in which an operator installs piles (aggressively vs. passively for example) can have a more pronounced effect on the IE calculated during pile installation.

It is considered that revising the IE calculation to include rotation rate (a more recent) in conjunction with KDK Pressure, and thus using a more accurate reflection of torque than KDK pressure alone, may alleviate this issue. The addition of rotations as a parameter monitored and recorded by Berkel's data acquisition system will provide data to evaluate this matter.

Berkel also installs Partial Displacement Screw Piles that utilize a continuous flight auger with a

large diameter drilling stem with the same installation platforms used to install Displacement Screw Piles. Typically, the IE–Capacity relationship for Partial Displacement Screw Piles plots significantly lower than the minus one standard deviation line shown on Figure 5. However, early research indicates that the overall IE–Capacity relationship of these piles conforms to the trend exhibited by the Displacement Pile database, but producing lower capacities at similar installation efforts. Currently, Berkel typically plots Partial Displacement test pile results on the Displacement Pile database and adjusts the mean line to the test pile results, similar to the example application for Displacement Piles discussed previously. As more Partial Displacement Pile load tests are performed, a new database will be developed specific to partial displacement piles for comparison to the current database.

Berkel has recently installed automated monitoring equipment similar to that described in the forgoing on crane mounted (non-fixed mast) drilling platforms for continuous flight auger piles. Very little data is currently available for crane-mounted drilling platforms but early results clearly indicate the need to incorporate rotation rate and total rotations (as one would probably expect) to any estimation of effort expended during penetration and the relating of this effort to pile capacity.

REFERENCES

NeSmith, W.M. (2002). "Static Capacity Analysis of Augered, Pressure-Injected Displacement Piles". *ASCE Geotechnical Special Publication No. 116*, Proceedings from DEEP FOUNDATIONS 2002. Orlando, FL. pp. 1174–1186

NeSmith, W.M. (2003). "Installation Effort as an Indicator of Displacement Screw Pile Capacity" Proceedings of the 4th International Conference on Bored and Augered Piles (BAP IV). Ghent, Belgium, June 2003.

NeSmith, W.M. and NeSmith, W.M. (2006). "Anatomy of a Data Acquisition System for Drilled Displacement Piles". Proceedings of the the American Society of Civil Engineers GeoCongress 2006. Atlanta GA USA. 26 February–01 March 2006.

NeSmith, W.M. and NeSmith W.M. (2006). "Application of Data Acquired During Drilled Displacement Pile Installation." Proceedings of the American Society of Civil Engineers GeoCongress 2006. Atlanta GA USA. 26 February–01 March 2006.

Deep Foundations on Bored and Auger Piles – Van Impe & Van Impe (eds)
© 2009 Taylor & Francis Group, London, ISBN 978-0-415-47556-3

Design and construction aspects of piled foundations for Eureka Tower Project

Jim Slatter & Slav Tchepak
Vibropile (Aust) Pty Ltd, Melbourne, Australia

ABSTRACT: The Eureka Tower project involved the construction of a 300 m high 92-storey tower, the world's tallest apartment tower at the time, located in Melbourne's Southbank area. An unusual feature of the building is its slenderness, having a height to base ratio of 6 to 1. The construction of the foundations for the project proved to be a challenging task.

The geological conditions at the site were complex, highly variable and posed significant construction and technical difficulties, with two layers of high to very high strength basalt above high strength Silurian Siltstone bedrock at a depth of approximately 35 m. The ground water table occurred at 2 m depth and the upper and lower basalt layers were not continuous across the site. To add to the complexity, the loadings imposed on the foundations by the structure were high. The lower basalt provided a suitable founding medium, provided that sufficient thickness was available to ensure that settlements of underlying soils were within acceptable limits. This was difficult to define because of the discontinuous nature of the lower basalt and the variable thickness of that stratum.

The foundation solution that ultimately proved to be the most cost-effective was a combination of CFA piles founded on the very high strength lower basalt flow and Bored piles constructed under bentonite drilling fluid founded in the high strength Siltstone when there was insufficient thickness of the lower basalt. This paper discusses the design and construction aspects of the piled foundations for these challenging conditions, including the additional site investigation required to define areas appropriate for each pile type; construction of the piles and the special techniques required to ensure clean bases for the heavily loaded piles; and the testing regime that comprised Statnamic and Dynamic pile loading tests.

1 INTRODUCTION

The site for the 92 storey apartment building was originally an industrial area. Because of its proximity to the CBD of Melbourne and the Yarra River, the area rapidly evolved to commercial and apartment usage. Extensive geotechnical work had been carried out for previous developments on the site, which were abandoned, partly because of the costs of providing economical foundation solutions for multi-storey developments in the challenging soil conditions. Local builder Grocon proposed a 92 storey apartment building which presented even greater challenges for the structural, geotechnical and piling engineers to provide an economical foundation system given the high loadings that result from such tall structures. The structure had a relatively small footprint, resulting in a height to base ratio of 6 to 1. The top of the tower can flex up to 600 mm in high winds with resulting oscillations being dampened by two 300 ML water tanks on levels 90 and 91.

The builder, Grocon, in conjunction with consulting structural engineers Connell Mott MacDonald and geotechnical consultants Golder Associates, issued documentation for the tower foundations comprising bored piles socketed into the strong Silurian bedrock. Initially the piling work was priced on the "conforming" solutions utilising bored methods, the equipment and expertise for which needed to be imported due to the requirement to penetrate up to 8 m of massive, very high strength Basalt at up to 1.5 m diameter. The costs of the conforming solutions considerably exceeded budget expectations both in terms of cost and program and the project was at significant risk of not proceeding.

2 SITE GEOLOGY

The geological conditions at the site are complex and difficult. It is not possible to provide a simple tabulation of soil types with depth, nor will reproduction

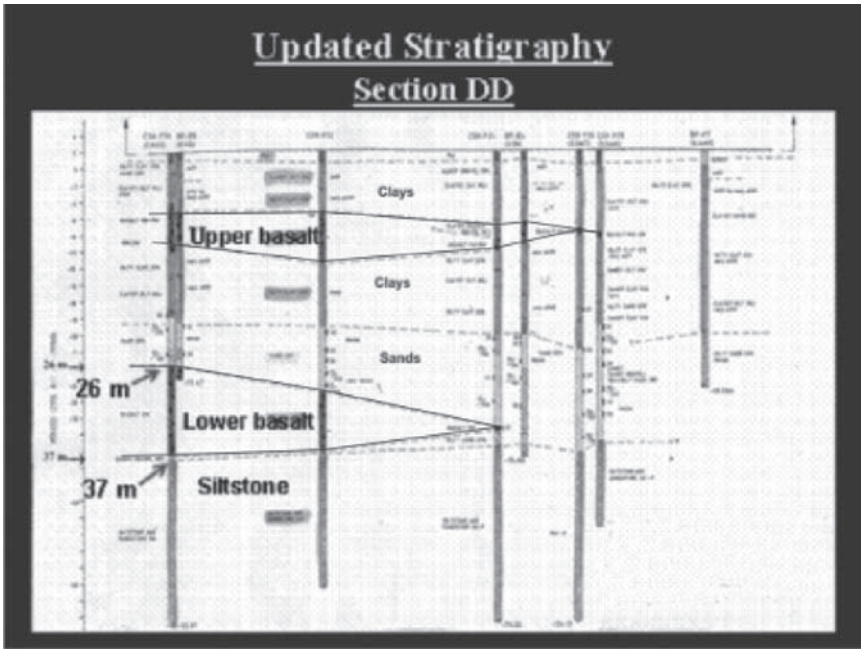

Figure 1. Section DD.

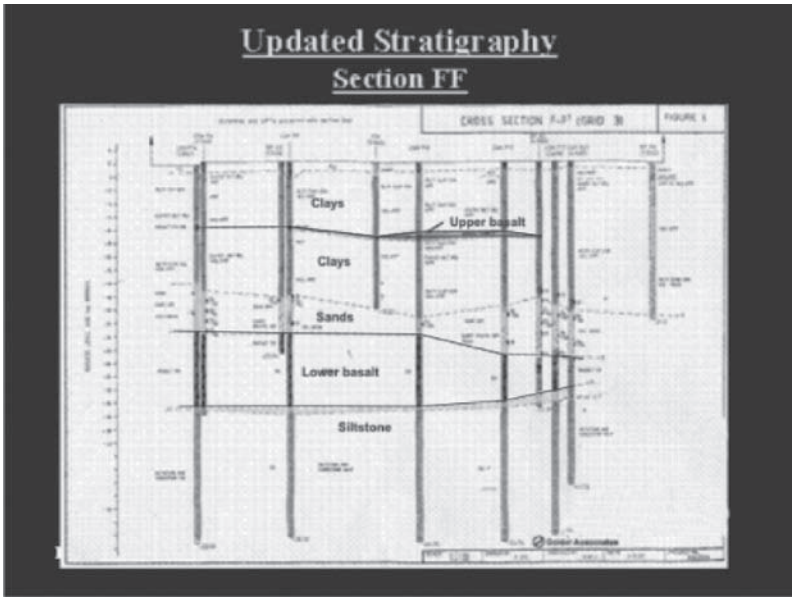

Figure 2. Section FF.

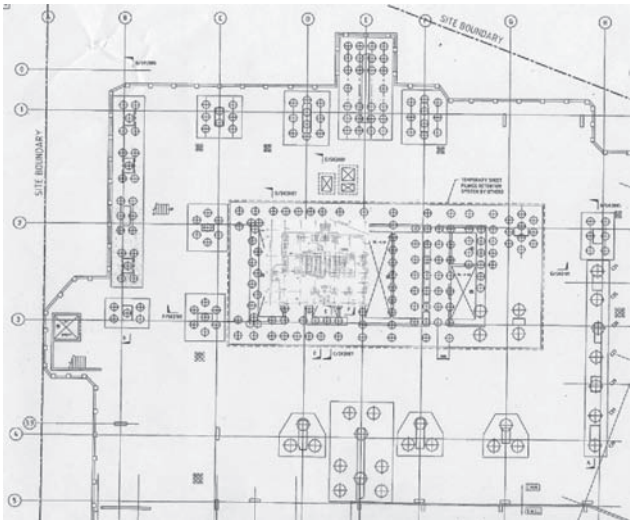

Figure 3. Final layout of CFA & bored piles.

of bore logs provide a realistic depiction of the geotechnical conditions. The geological complexity of the site was primarily due to two layers of basalt occurring above the Silurian Siltstone bedrock that occurs at a depth of about 35 to 37 m depth.

The upper basalt is "sandwiched" between layers of clay that varied in consistency from soft to very stiff. The upper basalt varied in thickness from zero to about 8 m and was typically of high strength, 80 to 100 MPa and most commonly highly fractured, with fracture spacings typically not greater than 300 mm

The lower layer of basalt was generally overlain by dense sands and gravels, occasionally underlain by the same sand and gravel strata or occasionally sitting directly on the siltstone bedrock. The lower basalt was of very high strength, indicated by testing to be in excess of 200 MPa and tended to be massive. The ground water table occurred at 2 m depth.

Neither the upper or lower basalts were continuous across the site.

The siltstone bedrock was typically a strong rock (up to 80 MPa), with the upper 1 to 2 m being relatively highly jointed before becoming massive in formation.

Cross sections from the relatively small site are shown in Figs. 1 and 2 that highlight the variability in soil conditions.

3 DESIGN CONSIDERATIONS

Founding piles or pile groups on the upper, highly fractured basalt was not an option because of the high loads, which would result in excessive settlement of foundations due to the compressible soils underlying the upper basalt.

By contrast the massive lower basalt provided a suitable founding medium, provided that sufficient thickness was available to ensure that settlements of underlying soils were within acceptable limits. This was difficult to define because of the discontinuous nature of the lower basalt and the variable thickness of that stratum. As a consequence, an extensive geotechnical investigation was performed by the geotechnical engineer to better characterise the condition and extent of the lower basalt with a view to revising the foundation solution.

The geotechnical design responsibility remained with the geotechnical engineer, who determined that a minimum of 5 m of strong lower basalt would be required to ensure satisfactory performance of piles founded in that stratum. Where 5 m of basalt was not available, piles would need to be bored through the basalt and socketed into the underlying strong siltstone.

A variety of solutions were considered including:

- An initial proposal to utilise 76 No. 1500 m dia piles socketed into siltstone
- 110 No. 1200 mm dia bored piles socketed into siltstone

Foundation solutions included construction utilising conventional and reverse circulation drilling methods. Interestingly, because of the difficulties of penetrating the very high strength basalts in particular, costs were found to be cheaper for a larger number of 1200 mm dia piles compared to 1500 mm solutions, especially when relatively high strength

concrete (70 MPa) was used and piles loaded up to the safe structural limits of the pile shafts for both piletypes. A solution was then proposed by the piling contractor to use high capacity CFA piles founded on the lower basalts where possible, with 1200 mm dia bored piles socketed into siltstone where the lower basalts were less than 5 m thick. This solution was found to be significantly cheaper than all-bored pile solutions and offered considerable savings in construction programme. A final solution incorporating the following was adopted:

- 243 No. CFA piles 750 mm dia founded on the lower basalt, to a unit pile design (i.e. ultimate) load of 9250 kN (corresponding to a working load of approximately 6800 kN).
- 28 No.1200 mm dia bored piles socketed in siltstone for ultimate loads of up to 32 MN (working load approximately 25 MN). An allowable stress was adopted as 20 MPa in the basalt. The design of bored piles in the siltstone was done using the program ROCKET to ensure that estimated settlements of those piles would be compatible with bored piles founded in the basalt. Consequently the settlement at the top of the siltstone socket was restricted to 6 mm and resulted in sockets of 4.5 m length.

4 CONSTRUCTION ISSUES

A number of issues had to be addressed, including:

- Proving the performance of CFA piles would be in accordance within specified criteria by load testing those piles.
- Confirming the constructability of the bored piles, to enable confirmation of production rates and pricing structure of those piles.
- Confirming that construction procedures for bored piles founded in either the basalt or the siltstone will be satisfactory and that those procedures can be implemented on a routine basis should the CFA trials not meet expectations.

In addition to the above technical considerations, the site was also extremely congested due to the multiple concurrent activities which were had to be scheduled in order to meet the extremely challenging construction program. As a result, site management was critically important and the movement of each item of plant needed to be carefully co-ordinated in order to prevent clashes (see Figure 4).

4.1 *CFA piles*

During the course of production piling approximately 75% of the piles required predrilling through the upper basalt layer using crane mounted drilling rigs. After predrilling, the excavation was backfilled with cement stabilised sand, ready for construction of CFA piles. Predrilling of clustered piles was be sequenced such that following casting of any pile in the cluster, subsequent predrilling for the next pile would not take place for at least three days.

Figure 4. Site congestion was a major concern.

CFA piles were drilled to effective refusal to found on top of the lower basalt and constructed using concrete injection techniques. Due to the sloping surface and negligible weathering profile of the lower basalt, specially designed rock drilling heads had to be adopted to ensure that CFA piles were adequately seated into the very high strength lower basalt. Every aspect of pile construction was fully monitored by on-board computers to ensure the highest quality construction.

4.2 *Bored Piles*

Bored piles required drilling through up to two layers of high to very high strength basalt to socket into the high strength siltstone. Construction under bentonite drilling fluid was adopted as the most economical approach to the difficult conditions.

The sockets were formed using conventional rotary drilling methods however extremely high

powered machines were required. A 55 tm crane mount drill was required to core through the very high strength basalt (Fig. 5). To facilitate base cleanliness, a series of purpose built tools were developed. Firstly a pilot hole/sump was formed centrally at the base of the 1200 mm diameter socket, a second tool was then deployed to mill a flat surface (or ledge) at the base of the pile (Fig. 6) and finally a third tool was used to sweep any debris on the milled ledge into the sump thus providing a high degree of cleanliness on the load bearing ledge at the pile toe (Fig. 7).

The sump, which was formed by coring and chiselling was 600 mm diameter and 600 mm length. The purpose of the sump was to attract base debris during construction, ensuring the remaining 75% of base area to fully utilise end-bearing. Socket walls were grooved in accordance with the requirements of the ROCKET analyses, namely, a minimum 5.5 mm deep by 6 mm wide groove at 100 mm spacing.

Piles were concreted within 24 hours of completion of socket drilling, with socket grooving and desanding (to ensure a maximum sand content of 1%) operations carried out on the same day as concreting. Socket inspections by underwater video camera proved the efficacy of construction methods in providing a clean pile base that would satisfactorily support the high loadings.

5 PILE TESTING

An initial trial piling programme was instigated to confirm the veracity of the proposed CFA construction technique and to confirm the estimated construction programme. Two non-production CFA piles were constructed and load tested to destruction. While it was understood that all production CFA piles would be drilled to effective refusal, one

Figure 5. Coring of basalt.

Figure 6. Ledge, milling & sump coring tool.

Figure 7. Ledge sweeping tool.

test pile was purposely terminated as soon as the auger reached the lower basalt, while the other was drilled to refusal. The purpose of the former was to simulate the potential effects of partial contact with the basalt.

5.1 *Bored piles*

Load tests were not done on any bored piles, however a remote socket inspection device (SID) was used on two bored piles to verify the cleanliness of the milled and swept ledge, and the pile sump. The results of the SID inspections proved that unique construction procedure adopted for the pile toes had met the design objectives and that the ledge had been cleaned to satisfactorily high levels. On this basis the construction procedure for all future bore piles on the project was approved and strict QA procedures were implemented to ensure that these procedures were adhered to.

5.2 *CFA piles*

The two trial CFA piles were subjected to load testing by Statnamic and dynamic methods. Dynamic tests were carried out using a drop hammer of 20 tonne mass after completion the Statnamic tests. The costs of doing Statnamic testing precluded testing of a large number of piles on the project, so the purpose of the subsequent dynamic tests on the trial piles was to gain a correlation with Statnamic and provide confidence in dynamic methods for future routine testing of production piles. The results of the loading tests on the trial piles are shown in Fig. 8.

The results of the comparative tests indicated a slightly less stiff response from the dynamic tests compared to the Statnamic tests. However the performance of the piles for both tests was satisfactory. The magnitude of the mobilised loads during the tests was not sufficient to conclusively prove the difference in drilling methods. Although the piles were to be tested to destruction, it was not possible to impart sufficient energy during the tests to damage the piles.

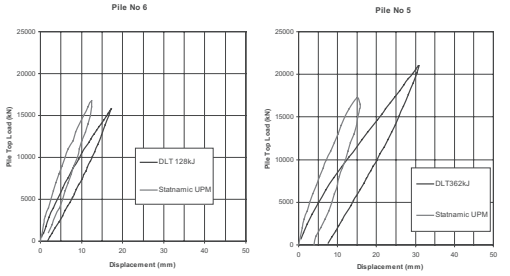

Figure 8. Comparative statnamic and dynamic load tests.

During routine piling an additional 5% of the piles were tested dynamically, with all results between the bounds of the DLT results indicated in Fig. 8. All parties were satisfied that the load testing regime was satisfactory given the level of QA available from the computerised monitoring of every CFA pile.

6 CONCLUDING REMARKS

A cost-effective and innovative solution for the foundations for the Eureka Tower project was brought about by co-operation between consulting structural and geotechnical engineers and piling contractors in what were extremely difficult geotechnical conditions. The application of different pile types and construction techniques was novel and innovative and resulted in the final cost of the foundations being reduced by over 30% and the program reduced by approximately 3 months. The construction was performed in difficult circumstances compounded by the restricted space available on site. In this manner, the skills of all parties were utilised, to the benefit of the project.

REFERENCES

Seidel, J.P. 2000. Rocket 3.0 Manual. Monash University. Melbourne.

Golder Associates. 2001. Report on geotechnical investigation. Eureka Tower. South Bank. No 01615054.

Deep Foundations on Bored and Auger Piles – Van Impe & Van Impe (eds)
© 2009 Taylor & Francis Group, London, ISBN 978-0-415-47556-3

M6 Mossband Viaduct, Carlisle, United Kingdom, long SFA piles installed with low-headroom Rigs

Erwin Stötzer
BAUER Maschinen GmbH, Schrobenhausen, Germany

Franz-Werner Gerressen
BAUER Maschinen GmbH, Schrobenhausen, Germany

Joachim Urs Müller
BAUER Maschinen GmbH, Schrobenhausen, Germany

ABSTRACT: As part of the M6 Motorway Extension Scheme near the English City of Carlisle and the Scottish Town of Gretna Green, bored pile foundations were required for the construction of a new motorway bridge over the West Coast Main Line between London and Glasgow. A special aspect of the project was strict compliance with the safety regulations of the rail track operator Network Rail, which required in particular the deployment of plant and machinery that had been specially adapted for the task and the requirements. To comply with the height restrictions imposed on the plant ranging from 7.50 m to 10.0 m, two conventional BAUER MG 20 rotary drilling rigs were reduced in height and deployed to install 20,000 linear meters of foundation piles using the Segmental Flight Auger (SFA) technique, a variation of the continous flight auger pile with auger extensions. After the completion of a four week long programme of trials, training and pile testing on site, over one thousand piles with lengths over 28.0 m were installed successfully over a construction period of 7 months.

1 GENERAL PROJECT DESCRIPTION

As part of the M6 Motorway Extension Scheme between Carlisle and Gretna Green near the English/ Scottish border, the existing 4-lane Mossband Viaduct over the West Coast Main Line from London to Glasgow, which is in a very poor condition, is being replaced by a new motorway bridge. The removal of this 9 km long dual carrigeway, the last remaining bottleneck, known for many years as the Cumberland Gap, will after completion of the construction works provide a continuous motorway link not only between Southern England and Central Scotland, but between Europe and Scotland. The total investment for this project amounts to circa 180 Mio €.

In line with the safety culture prevalent in England today, the entire project is characterised by an extremely sensitive approach towards Health and Safety (HSE) Regulations as well as regulations for the protection of the environment. In addition, the project has to cope with the very severe conditions imposed by the British rail track operator "Network Rail" who cannot accept any risk or restrictions in train operations as a result of the construction activities. This is reflected in both the structural design and the technical concepts for the entire structure as well as the safety regulations and the construction concepts.

1.1 *Client: Highways Agency*

The Highways Agency is an Executive Agency of the Department for Transport (DfT), and is responsible for operating, maintaining and improving the strategic road network on behalf of the Secretary of State for Transport.

1.2 *Engineer: Capita Symonds consulting*

Capita Symonds is one of the UK's leading consultancies and provides a broad range of professional services, covering the design, engineering, construction and infrastructure market.

1.3 *Main contractor: Carillion Roads*

Carillion Roads is a business unit of the multinational construction corporation Carillion plc and undertakes road construction and maintenance activities in the UK.

1.4 *Piling subcontractor: Carillion Piling Ltd.*

Carillion Piling is the foundation specialist of Carillion plc. It developed from the former independent company Mowlem Piling.

2 FOUNDATION CONCEPT

The foundation concept developed by Capita Symonds Consulting for the bridge structure and its adjoining embankments consists of a multiple foundation system, which comprises the following components:

- 143 No. Bored piles of 1500 mm diameter as foundation for the main bridge structure.
- 1055 No. SFA (Segmental Flight Auger) piles of 510 mm diameter, spaced at 1.90 m, as foundation piles for the adjoining embankments in the vicinity of the large diameter bored piles.
- 3820 No. Vibrated Concrete Columns (VCC) of 500 mm diameter, spaced at 2.50 m, as foundation elements in the transition area of the existing old road.

The underlying idea of this tripartite foundation system is a gradual transition from the stiff foundations of the bridge structure with its large diameter bored piles to the more flexible embankment structures, resulting in uniform settlement behaviour across the entire structure. In the vicinity of the large diameter bored piles, the Engineer also specified the use of a rotary drilling technique in preference to displacement and vibratory techniques. As the load-bearing horizon for the piles varies in depth across the site, piles ranging in length from 14.0 m to 28.0 m had to be installed. The design bearing capacity of the piles equates to a working load of 100 tonnes.

3 GEOLOGY

The site is located in North-West England, near the Scottish border. In the immediate vicinity of the site, the River Esk flows into the flats and marshes of the upper "Solway Firth" which forms a kind of tide-dependent inland water with the Irish Sea.

The ground conditions are characterised by a sandstone formation at varying depths, with inter-bedded layers of weathered sandstone and dense sands. Across the site, the sandstone horizon drops from a level of around 14.0 m below platform level to a depth of around 28.0 m below platform level. In the structural design concept, this highly variable horizon has been specified as foundation level for the SFA piles. The sandstone formation is overlain by a sequence of alluvial soils, comprising layers of soft clays, peat and gravel of varying thickness.

4 PLANT AND EQUIPMENT

As a result of the extremely restrictive and conservative safety regulations of the British rail track operator "Network Rail", drilling rigs and cranes may only be deployed adjacent to the railway line after thorough stability checks have been carried out and drilling rigs, in particular, may not move freely around the site. To determine operating heights and operational limitations of freely moving plant near the track, the principle of "mast height = distance to loading gauge of railway" has been defined as a rule-of-thumb.

With regard to the installation of the 143 large diameter bored piles adjacent to the railway line, it meant that the plant used (rotary drilling rigs and lifting cranes) had to be anchored firmly to a massive reinforced concrete beam that stretched across the whole site. The height restriction described above could not be applied as the fully cased bored piles were constructed by the kelly drilling technique. In respect of the SFA piles, the construction of an anchor beam was impracticable due to the large number of piles and their grid formation across the site. The unacceptably high number of rig moves and what would have been an elaborate and costly anchor beam system required an alternative approach with regard to the type of plant being deployed and made it necessary to deviate from traditional plant concepts and construction processes.

Network Rail's requirement to equate the maximum height of the rigs with the distance to the load gauge of the railway, resulted in the height of the rigs being limited in some areas of the site to a maximum of between 7.50 m and 10.00 m. This limitation and the structural necessity to install bored piles using the rotary drilling technique, resulted in a new challenge with regard to the selection—in close consultation with the contractor Carillion Piling—of the most suitable type of plant and construction process.

To comply with the specifications for the plant, the mast geometry on two BAUER MG 20 rotary drilling rigs was modified and, as illustrated in Fig. 1 and on site in fig. 2, both masts were reduced to their smallest possible height of 7.50 m and 9.95 m.

Based on the BAUER MBG 12, which is already well established in the market, the BAUER MG 20 drilling rig with its torque converter and system of four hydraulically operated outriggers, has been designed for the special requirements of the so-called single-pass techniques, such as the classic Continuous Flight Auger (CFA) and the Full or Partial Displacement Pile (FDP/PDP) systems. The rigs are equipped as standard with a chain operated crowd system that can be easily adapted to suit any length of mast, eliminating the need for structural changes on the hoist winch or adjustments in the length of the ropes.

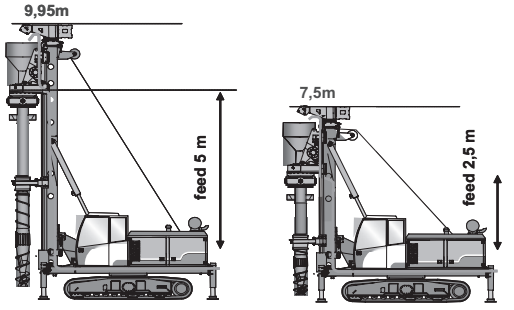

Figure 1. Modified BAUER MG 20 drilling rigs.

Electronic aids, such as the so-called “drill/ extraction assistants”, can be employed to achieve an optimal rate of penetration during drilling and control the placement of concrete during extraction of the auger.

The structural modifications on individual mast sections were made in such a way, that both rigs can at any time be rigged up again to their full operating height of 16.00 m without extensive retrofitting being required. The modular mast design of the MG 20 makes it possible for a 2-man crew to change the length of the mast on site within half a day.

These modifications resulted in drilling rigs with maximum operating heights of 7.50 m and 9.95 m that, in spite of their height restrictions, are capable of installing SFA piles cost-effectively to depths of up to 28.00 m.

Figure 2. Site set up.

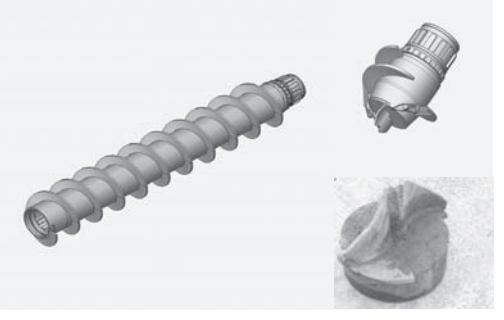

Figure 3. Auger, starter auger, sacrificial bit.

5 DRILLING TECHNIQUE

The concept of the SFA drilling technique is based on elements of the well-known BAUER Full displacement Pile (FDP) system with a sacrificial bit. Both the drill stems and starter auger sections, see fig. 3, were employed after some modifications. To achieve the required diameter of 510 mm, a new auger flight was welded onto the 318 mm diameter hollow drill stem. Officially, the pile is classified as a CFA pile.

Due to the ratio of drill stem diameter to auger diameter, and the smaller amount of spoil being excavated compared with the CFA process, this technique can be classified, however, as a partial displacement system.

The reduced rig heights and the resultant much shorter crowd lengths of 2.95 m and 5.60 m set new challenges for the design of the drilling tools and the joints between individual auger sections, as well as the general organisation of auxiliary activities.

Individual auger sections with standard lengths of 2.50 m and 5.00 m were selected as drilling tools.

As with the displacement piling system, the SFA augers, which are stored on a purpose-built rack that can be picked up and moved by the drilling rig, are inserted into the drill string on demand. A patented system of wedges is used to secure the joint between individual auger sections, capable of transferring both torque and extraction forces. It also facilitates the rapid insertion and removal of auger sections, as required, to a maximum drilling depth of up to 28.00 m.

The installation of SFA piles is generally carried out in the construction sequence detailed below:

- Set up rig over current pile position and place guide plate.
- Insert sacrificial bit into hollow drill stem of starter auger.
- Drill first auger section into the ground.
- Disconnect auger section from rotary drive adapter and pick up next auger section from the auger rack positioned on the working platform alongside or at the rear of the rig.
- Place next auger section on top of previously installed section, insert wedges and secure with bolts to obtain a positive connection between individual components.

– Drill second auger section into the ground.
– Repeat this process until the specified depth has been attained or the criteria for terminating drilling as a result of the auger having reached the load-bearing soil formation have been fulfilled.
– After attainment of the terminal depth, the drill string is raised by approx. 10–15 cm to enable the sacrificial bit to drop out of the hollow drill stem of the starter auger.
– Concrete, which is placed through a hopper mounted at the top of the KDK rotary drive, is placed in the pile purely under gravity, which means that the concrete pump cannot build up pressure in the drill stem of the auger. Before withdrawing the auger, the drill stem and hopper are simply filled with concrete to a predetermined level indicated by a mark on the inside of the hopper. Fill level control is by way of a camera mounted on the rim of the hopper enabling the rig operator to monitor the level of concrete accurately on his screen.
– Auger withdrawal. The auger should only be withdrawn by a constant predetermined amount. Depending on the length of the segment, the auger section is disconnected and stored in the rack and the hopper is again filled with concrete. This ensures that the concrete pressure inside the drill stem is always adequate and an excessive rate of withdrawal during concrete placement is prevented.
– Depending on the diameter and layout of the reinforcement cage, it is possible to install a full length cage in the centre of the pile through the hollow drill stem prior to placing concrete. Alternatively, the cage is inserted into the fresh concrete of the completed pile, similar to CFA piles, with the use of the auxiliary winch or auxiliary equipment.
– To break the auger, the auger sections remaining in the ground are first secured in a pile gate to obtain a stable and vertical position for the removal of the wedges and to prevent the remaining drill string from sinking into the concrete when reconnecting it to the rotary drive adapter.
– After breaking and before storing the auger in the rack, the drill stem of the auger, the hopper and the male and female sections of the auger must be thoroughly cleaned using the high pressure jetting device mounted at the front of the rig.

In suitable, displaceable, soft cohesive soils with an undrained shear strength of Cu > 15 N/mm² but not exceeding 70 N/mm², piles of specified lengths can be constructed cost-effectively and at a uniform quality despite the height restrictions of the rigs. The pile bore is always supported either by the drilling tool or a column of concrete.

Compared to the construction of conventional CFA piles, placing concrete under gravitational pressure through a hopper attached to the rig prevents bulging or necking of the pile shaft. Concrete overbreak can thus be reduced to normal levels of around 15% of the theoretical pile volume, particularly in soils with interbedded layers of organic material.

Permanent visual monitoring of concrete levels in the drill stem enables auger sections to be disconnected without interrupting the concreting process.

Based on the experience gained from the pile tests carried out at the start of the contract and the production data recorded by the data acquisition system inside the rigs during initial pile installation, it was possible to define criteria in close consultation with the Engineer and the Client, which made it possible for the rig operators to identify the foundation horizon at its varying levels and thus terminate the drilling process accordingly.

The attainment of the load bearing foundation level was identified by the rig operators based on the following criteria:

– Penetration rate of auger <0.20 m/min.
– Torque min. 50% of available
– Crowd force min. 50% of available

These values had to be maintained for a period of up to 2 minutes, in order to prevent the premature termination of the drilling process as a result of a possible underground obstruction.

All necessary pile production data are displayed for the rig operators on a control monitor and stored in the onboard computer. They form the basis for a comprehensive documentation and quality assurance system, as illustrated by the example in Fig. 4 below.

6 PILE LOAD TESTS

As is usual on projects of this size and complexity, a series of pile load tests was carried out on contract piles in advance of the main piling works. The Client's representative and the Engineer stipulated a test load of 150% of the specified working load of the piles.

As part of the acceptance procedure, the quality of every working pile was checked by way of an integrity test.

The load test set up shown in fig. 5, designed for a maximum test load of 250 tonnes, is an advancement of the type of test arrangements used to date. The construction of the load spreader beam and reaction system is designed in such way that the entire unit can be moved on site by a single crane.

A further novelty is the newly developed reaction system. This consists of a set of re-usable screw piles (l = 12.00 m), which are installed by the drilling rig and are removed again after completion of the pile test. The load transfer is effected by the auger flights at the toe of the piles.

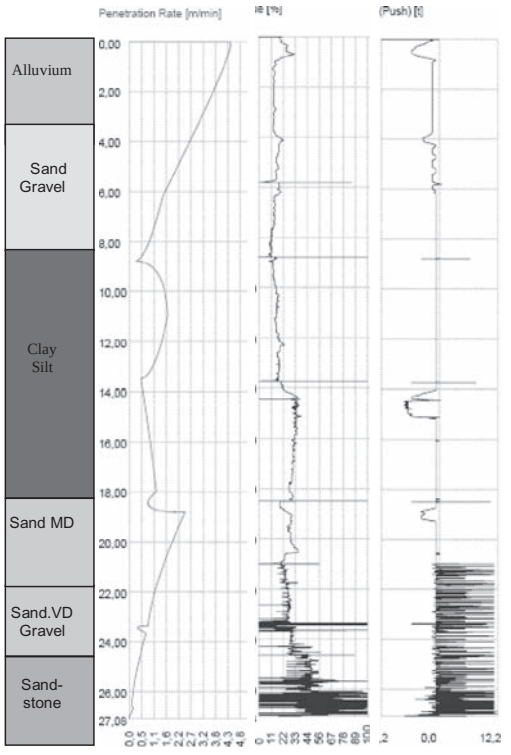

Figure 4. Torque diagram.

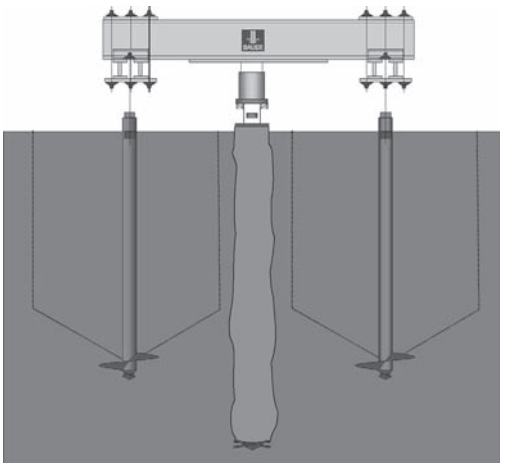

Figure 5. Diagram of pile load test set up.

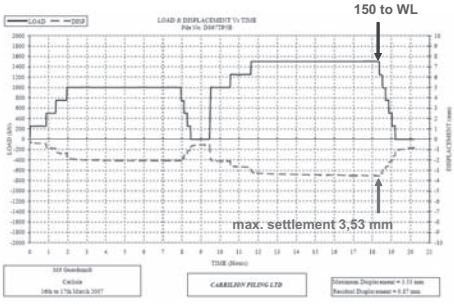

Figure 6. Load-settlement diagram.

The advantages of this new test arrangement include not only short periods for setting up and moving, but also a greater flexibility in its application. Testing can commence as soon as the installation of the test set up has been completed over the pile. Waiting times for the attainment of minimum concrete strengths in the reaction system are eliminated.

The load-settlement diagrams for the piles tested to 150% of their specified working load ahead of the main piling works showed that actual pile settlements were well below specified maximum settlement values. Fig. 6 shows the load-settlement diagram for one of the load-tested working piles.

All five load tests showed similarly good test results. The design of the remaining working piles was, however, not revised by the Engineer, although this might have resulted in larger pile spacing and, thus, a reduced number of piles.

7 CONCLUSIONS

The project was successfully completed within the specified time scale and by meeting all scheduled milestones. Both the technique and the modifications carried out on the rigs fully proved themselves under real site conditions. An evaluation of the production data for the whole project shows, that in these severely restricted conditions outputs of around 50 m per shift were achieved by the 7.5 m high unit and around 72 m per shift by the 9.95 m high version.

In comparison with conventional techniques and projects having to be carried out in restricted headroom conditions, this project has clearly demonstrated that even the most difficult tasks can be accomplished in close cooperation with all project stakeholders.

Investment in the right plant and tools on the M6 Mossband Viaduct contract has demonstrated that special tasks require special and innovative solutions. Other projects requiring to be carried out under similar height restrictions are already under consideration.

Discussion session 4: Energy pile concepts

Deep Foundations on Bored and Auger Piles – Van Impe & Van Impe (eds)
© 2009 Taylor & Francis Group, London, ISBN 978-0-415-47556-3

Tunnels and foundations as energy sources—Practical applications in Austria

D. Adam
Geotechnik Adam ZT GmbH, Brunn am Gebirge, Austria

ABSTRACT: Concrete structures of cut-and-cover tunnels like bored piles and diaphragm walls as well as tunnel linings of mined tunnels can be used as absorber elements for ground heat exchange. Absorber pipes are installed within concrete elements and a heat carrier fluid is circulated through the system. Practical applications have been designed and constructed in Austria, e.g. at the Vienna metro extension U2 and most recently at the new Lainzer tunnel at lot LT44. This promising technology leads to a reduction of fossil energy consumption at moderate installation costs and low operation costs.

1 INTRODUCTION AND PRINCIPLES OF GEOTHERMAL HEAT UTILIZATION

The subsurface of Earth contains an enormous potential of geothermal energy that can be used for heating and cooling purposes. In particular with the development of the earth-coupled heat pump it became possible to open up the geothermal energy present in the ground.

In the 1980's deep foundations were first used for geothermal heat extraction by placing heat absorber pipes in concrete elements which are in close contact with the ground. At first foundation slabs, then driven precast piles and later bored piles and diaphragm walls have been successfully activated for heating and cooling purposes (Brandl & Markiewicz 2001, Brandl & Adam 2002, Adam & Markiewicz 2003).

The basic requirement for the use of geothermal energy is a widely constant temperature of the ground at a depth of approximately 10 to 15 m. In most European climate zones, this temperature varies between 10 to 15°C and remains constant up to a depth of approximately 50 m. Heat pumps and/or cooling machines are connected between the absorber pipes within the concrete elements (primary circuit) and the heating/cooling systems of the buildings (secondary circuit) which adapt the temperature to a suitable level for HVAC applications (around 6 to 50°C). Modern heat pumps have an efficiency (coefficient of operation, COP) of at least 4, meaning that ¼ of electric energy and ¾ of geothermal energy can be added up to 4/4 directly usable energy (for heating operation).

Two different operation schemes for the use of geothermal energy from deep foundations are possible:

- Exclusive geothermal energy extraction or energy input.
- Alternating seasonal operation with heating and cooling storage.

For exclusive geothermal energy extraction the energy flow takes place only in one direction, e.g. for heating purposes during winter. The seasonal operation however uses the thermodynamic inertia of the soil in order to store thermal energy in the ground for a later operation with reversed energy flow. Consequently, the seasonal operation can produce energy equilibrium in the ground over a complete heating/cooling period of a year. A geothermal cooling system extracts heat energy from the building either via an air-cooling system or a water-based cooling system, which can be integrated in ceilings and walls. The cooling machine acts like a `reverse' heat pump and the thermal energy can be stored in the ground. Geothermal energy applications which need a very low service temperature can also be operated in "free heating" or "free cooling" mode. The necessary energy input then is limited to the electricity required to operate a circulation pump, because no heat pump is needed to raise the temperature level. For buildings, this technology can now be considered as state-of-the-art. During the last years, engineers have investigated how the technology can be applied to tunnels. In comparison with foundations of buildings, a substantially larger ground volume can be activated for geothermal heat exchange. Additionally, tunnels with a high

overburden can have a significantly higher temperature of the surrounding ground, resulting in a better performance of the geothermal system. However, shallow tunnels, i.e. metro tunnels, can also be used profitably for geothermal heat extraction due to their urban location. The installation of absorber pipes in the concrete structure of a tunnel is different for cut-and-cover tunnels and mined tunnels. For cut-and-cover tunnels, the well-experienced methods already used in deep foundations can be used: installation of absorber pipes in bored piles, diaphragm walls and in or under base slabs. However, the use of mined tunnels as heat exchanger elements has been a new challenge for engineers. While the existing methods can be applied for the installation of absorber systems in the tunnel invert, a completely new technology had to be developed for the lining of the tunnel.

2 GEOTHERMAL PROJECTS IN AUSTRIA

Since the year 2000 several geothermal projects in combination with infrastructure projects have been carried out or are currently under construction in Austria. The first project to be carried out was the testing plant at lot LT24 of the Lainzer tunnel. It went under construction in 2001 and the initial operation started in spring 2004. Other full-scale applications are currently being constructed at four stations of the U2 metro extension (since spring 2003), where e.g. diaphragm walls and foundation slabs serve as heat exchangers. In 2003 an innovative testing plant started at lot LT22 of the Lainzer tunnel, where the worldwide first "energy geotextile" has been installed. Most recently—in February 2006—the construction of an energy plant has begun at lot LT44 of the Lainzer tunnel.

2.1 *Testing plant at lot LT24 of the Lainzer tunnel*

The testing plant LT24 was the first application worldwide, where the existing absorber technology already successfully used for foundations of buildings was applied to bored piles of a cut & cover tunnel (see Figure 1). The plant comprises 59 "energy piles" with a diameter of 1.2 m and an average pile length of 17.1 m. The energy piles are equipped with absorber pipes that are connected to a service room (see Figure 2). There the absorber pipes are connected to collection pipes which lead to 6 heat pump units in an adjacent school building in order to heat the school. The testing project was financed in cooperation with the following companies: ÖBB Bau AG (former HL-AG), Railway Infrastructure Services Company (SCHIG mbH), the Austrian Federal Ministry of Transport, Innovation and Technology (BMVIT) and EnergieComfort GmbH. The design was done by iC consulenten ZT GmbH in close cooperation with the Institute for Soil Mechanics and Geotechnical Engineering, Vienna University of Technology.

Figure 1. Connection points at pile heads of "energy piles".

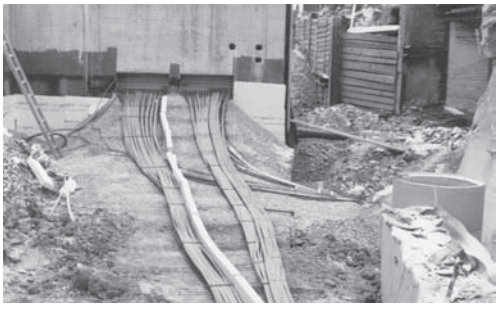

Figure 2. Absorber pipes and measurement cables.

The initial operation of the energy plant started in February 2004 with a first testing period. About 70 MWh of heating energy could be extracted from the energy piles during the first months of operation. Since autumn 2004 the energy system provides the adjacent school with geothermal heat. During the second heating period in winter 2004/05 a total amount of 186.2 MWh of geothermal heat was extracted, while in 2005/06 an amount of 193.9 MWh was gained. This amount of geothermal energy corresponds closely to the predicted maximum performance per heating season (see Figure 3).

2.2 *Testing plant at lot LT22 of the Lainzer tunnel*

The geothermal utilization of tunnels excavated according to the "New Austrian Tunneling Method" requires special absorber elements. In construction lot LT22 of the Lainzer tunnel a completely new technology has been developed for the thermal activation of the concrete lining (Markiewicz & Adam 2003). Absorber pipes were first attached to non-woven geosynthetics out of site and then placed between the

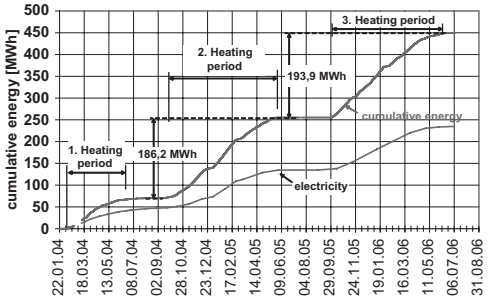

Figure 3. Extracted energy and consumption of electricity of testing plant LT24.

Figure 4. Detail of the four absorber loops with collection pipe.

Figure 5. Energy geotextile at lot LT22 of the Lainzer tunnel.

primary and secondary lining of the tunnel (see Figure 4 and Figure 5).

This technology makes prefabrication possible and provides for an easier installation method on site. Similarly to the testing plant LT24, sophisticated measurement instrumentation (temperature sensors, heat carrier flow measurement, etc.) has been installed for detailed investigation. The initial operation of the energy plant started in February 2004 with a first heat extraction. However, the testing plant can be run in both heating and cooling operation. As the extracted energy is not used for specific heating purposes, further investigation can be carried out until the tunnel is put into operation. Therefore different operation scenarios are still run in order to obtain the most effective settings of this geothermal system.

2.3 *Utilization at the Viennese metro line extension U2*

The Viennese metro line U2 will be extended in a first phase from the existing station Schottenring to Vienna's football stadium in the 2nd district and from there in two additional phases to the 22nd district to the former airfield Aspern (see Figure 6).

Four new metro stations and tunnel tubes will be heated and cooled by geothermal energy. At the construction lots U2/1 Schottenring, U2/2 Taborstrasse, U2/3 Praterstern and U2/4 Messe deep foundations such as piles, diaphragm walls, base slabs and tunnel inverts are utilized as "energy foundations". Absorber pipes are attached to the reinforcements of structural elements and connected via manifolds to the service rooms. Depending on its final heating/cooling purpose the temperature level is raised to a certain level by heat pumps and/or cooling machines. After completion of the civil works, the responsibility for the geothermal facility usually is turned over from the contractor to a company which installs the HVAC equipment.

An accurate definition of the contractual and technical interface between these companies, combined with acceptance inspections, is therefore essential. Engineers and geothermal designers will accompany the energy plants in the first operational years and optimize them in close cooperation with the client.

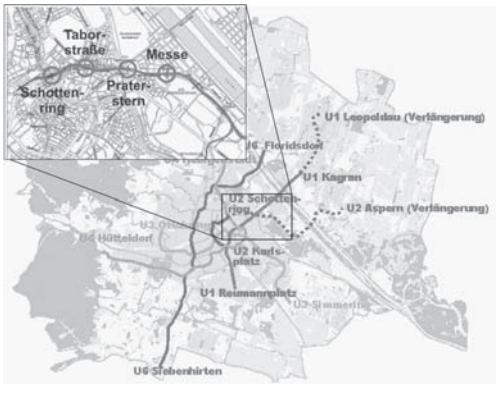

Figure 6. Site plan of U2 line extension, circles show stations equipped with geothermal energy plants.

The first trial operation of some plants will start in fall 2007, while the normal operation is expected to start in spring 2008.

2.4 *Design and construction of geothermal energy plant at lot LT44 of the Lainzer tunnel*

Large sections of the Lainzer tunnel project are situated close or below urban regions of Vienna. Consequently, there have been early considerations about a geothermal utilization at lot LT44 of the tunnel. The pharma company Boehringer-Ingelheim is situated close to the lot LT44. For further extensions of their company grounds, Boehringer-Ingelheim showed great interest in this form of regenerative energy. Therefore feasibility and economical studies were carried out to find the adequate size of geothermal absorber plant.

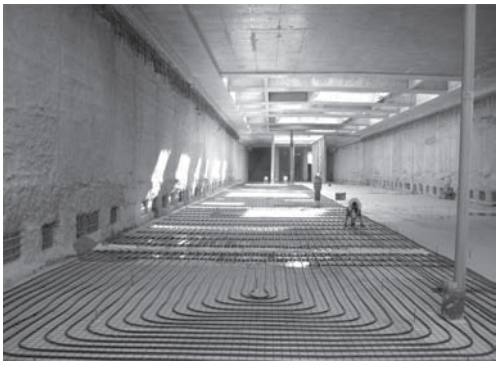

Figure 7. Base slab of station "U2/4 Messe" equipped with absorber pipes.

Figure 8. NATM driven station tube at "U2/2 Taborstraße" with thermal activation of tunnel invert.

2.5 *Research project absorber optimization*

The costs of absorber plants mainly depend on the amount of installed piping material and the equipped absorber area. For an absorber plant the most important design task is to optimize the amount of extracted energy at least construction costs. Some years ago, this optimization task could only be done by expensive test installations with different absorber distances, the expected thermal loads and boundary conditions in the place of installation. The ongoing development of computational physical modeling programs has enabled a much cheaper and more effective optimization of this problem. With the experience from former geothermal energy systems and the necessary data for the design of the energy plant LT44 a new research project was started in spring 2005 for the economical optimization of absorber plants (iC consulenten *et al.*, unpubl.). This project was supported by the municipal authorities of Vienna—EU strategy and economical development (Department 27).

The research project was carried out for different absorber elements—base slabs and diaphragm walls—with geometrical and thermal conditions fitting lot LT44 (see Figure 9). From the tender design prices were available for all parts of the energy plant. These prices could be separated into costs depending on the equipped absorber area and prices depending on the length of installed absorber pipes for both diaphragm walls and base slabs.

Examples for costs depending on absorber area:

- Number of connection points at the diaphragm walls.
- Total installation costs (exclusive manifolds) from the service room to the customer (main piping, valves, thermal insulation, etc.). These costs depend on the design power of the plant, which depends itself on the total absorber area.
- Additional costs due to interference of absorber installation and construction of diaphragm walls or bottom slabs.
- Design fees of the absorber plant.

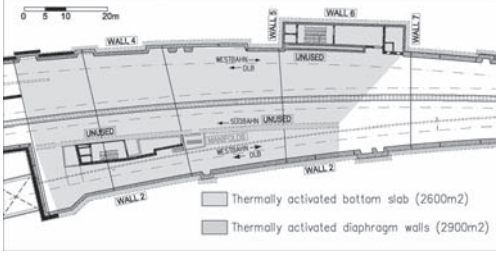

Figure 9. Ground view of the cut-and-cover section at lot LT44 with thermo-active elements.

Examples for costs depending on installed absorber length:

- Costs per meter of absorber pipe
- Number of Manifolds
- Amount of heat carrier fluid

Starting from these costs, simulations could be performed to calculate the heating and cooling performance of absorber elements at different absorber distances (see models on Figure 10 and Figure 11). With larger absorber distance, the thermal power will decrease as well as the installation costs (depending on installed absorber length), tending to an optimum.

Several boundary conditions had to be defined:

- Annual atmospheric temperature (from meteorological measurements)
- Annual tunnel air temperature (derived from measurements at tunnels with similar conditions)
- Thermal properties of soil, concrete elements and heat carrier fluid
- Temperature curves of the heat carrier
- Initial conditions (temperatures)

The amortization period was calculated for each absorber distance using a price of extracted geothermal energy of 25 €/MWh to find an optimum. The optimization curve with optimum absorber distance for diaphragm walls can be found in Figure12.

This approach shows one possible way for the economical optimization of geothermal energy plants. The calculated optimum absorber distances are valid only for the geometrical, economical and thermal boundary conditions at energy plant LT44. For other geothermal systems the results may differ considerably. However, the introduced method can be applied to any geothermal energy system installed in foundation elements.

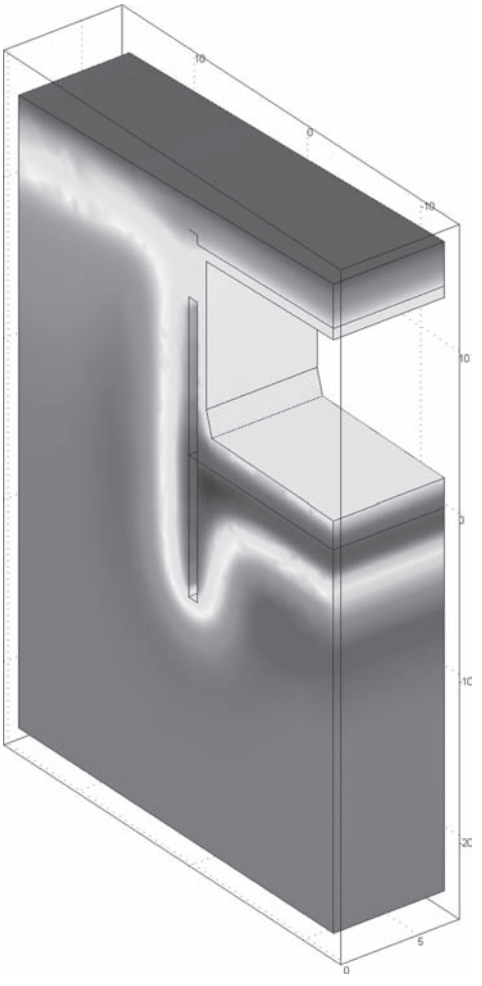

Figure 10. Finite-element simulation model for absorber distance optimization.

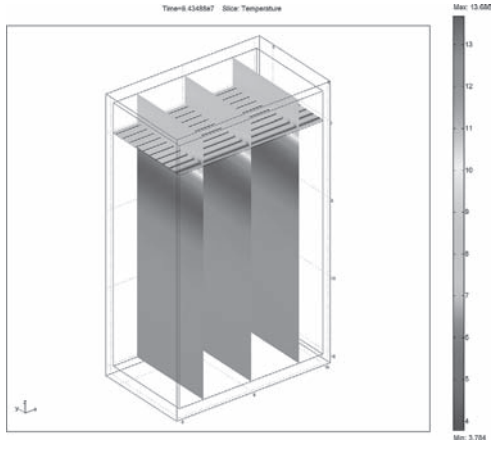

Figure 11. Detail of the base slab simulation model.

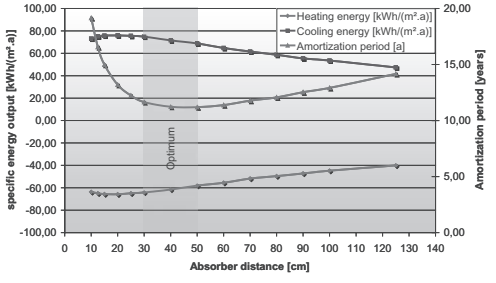

Figure 12. Results of the absorber distance optimization with range of optimum distance leading to least amortization periods.

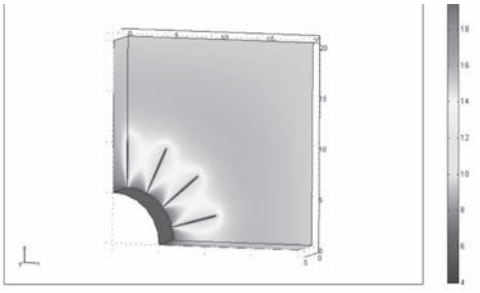

Figure 13. Finite-element simulation results for energy anchors placed in a tunnel and for a retaining structure.

As geothermal absorber plants are always in economical competition with other energy sources like natural gas, fossil oil or municipal heating, economical optimization is an important task for the designer in the future.

2.6 *Development of energy anchors*

In the scope of a research program performed at the Vienna University of Technology a new absorber element has been developed for tunnels, retaining walls etc. Anchors are an important structural element to support the tunnel excavation forming an arch-like structure around the tunnel as well as for retaining structures (Figure 13).

Thus, energy anchor prototypes were produced and tested in the laboratory.

Both numerical simulations and practical application in a large-scale field test have proven the applicability of the energy anchor being an additional promising structural geothermal energy absorber element (Oberhauser 2006).

3 CONCLUSION

There are numerous possibilities for the utilization of thermo-active concrete elements for heating and cooling purposes. Particularly urban tunnels can provide with clean, regenerative energy when used as heat exchangers. The overburden of these tunnels is usually low and the distances to the customers are short. This energy source is especially interesting for newly established buildings with mixed residential and commercial use and a considerably cooling demand. In addition, metro stations as well have an internal energy demand, because various premises have to be heated and cooled. The geothermal utilization of tunnels offers benefits to all involved. Geothermal energy is an environmentally friendly, economical and renewable energy source, which is independent to fossil fuels and contributes to climate protection and to the fulfillments of international obligations (Kyoto Protocol).

The customer of the geothermal energy receives a pipe-bound, pollution free energy source with all benefits of such systems. Additionally, geothermal energy will represent a more economical form of energy in the medium term compared to fossil energy sources, especially if corresponding political measures are taken. For the owner of the tunnel geothermal energy offers additional income from a structure that is needed anyway, therefore lowering the operating costs. Furthermore this application can result in a positive public image of infrastructure projects because of the pollution-free and innovative character of geothermal facilities.

REFERENCES

Adam, D. Markiewicz, R. 2003. Geothermische Energienutzung im Bauwesen. Heft 54/Oktober 2003. Vienna: Österreichische Vereinigung für Beton- und Bautechnik.

Brandl, H. Adam. D. 2002. Die Nutzung geothermischer Energie mittels erdberührter Bauteile. In: *Festschrift der Universität für Architektur* "Geotechnique" Vol. XL (1999–2001), Sofia, Bulgary.

Brandl, H. Markiewicz, R. 2001. Geothermische Nutzung von Bauwerksfundierungen ("Energiefundierungen"). In: *ÖIAZ*, 146. Jg., Heft 5–6/2001, Vienna, Austria.

iC consulenten ZT GmbH, Institute for Soil Mechanics and Geotechnical Engineering, Vienna University of Technology 2005. *Wirtschaftliche Optimierung von Tunnelthermie®—Absorberanlagen, Grundlagenuntersuchung und Planungsleitfaden*, sponsered by MA27, unpublished, Vienna, Austria.

Markiewicz, R. Adam, D. 2003. Utilization of Geothermal Energy using earth coupled Structures—Theoretical and Experimental Investigations, Case Histories. In: *Geotechnical Problems With Man-Made And Man Influenced Grounds. XIIIth European Conference on Soil Mechanics and Geotechnical Engineering*, Volume 2, 25–28th August 2003, Prague.

Oberhauser, A. 2006. *Verfahrens- und Komponentenentwicklung zur Planung von Tunnelthermie®—Anlagen*, PhD-thesis (in German), Vienna University of Technology.

Deep Foundations on Bored and Auger Piles – Van Impe & Van Impe (eds)
© 2009 Taylor & Francis Group, London, ISBN 978-0-415-47556-3

Investigations on the mechanical behaviour of a Heat Exchanger Pile

L. Laloui & M. Nuth
Soil Mechanics Laboratory, Ecole Polytechnique Fédérale de Lausanne (EPFL), Switzerland

ABSTRACT: The geothermal use of concrete geostructures (piles, walls and slabs) is an environmentally friendly way of cooling and heating buildings. With such geothermal structures, it is possible to transfer energy from the ground to fluid-filled pipes cast in concrete and then to building environments. A comprehensive research work was carried out at the EPFL (Switzerland) to improve the knowledge in the field of geothermal structures and to quantify the thermal influence on the bearing capacity of heat exchanger piles. In this paper, some features of the behaviour of a pile subjected to thermo-mechanical loads are presented. Numerical finite element results are supported by in-situ measured values.

1 INTRODUCTION

This paper deals with the development of a new sustainable technology for the intermittent storage of energy in soils. The goal of our research work is to contribute, by a geotechnical approach, to obtaining reliable, environmentally and resource friendly heating and cooling of residential, office and commercial buildings at low additional cost. The idea behind energetic geostructures is to take advantage of the thermal storage capacity of the ground as an energy storage system by using the foundation of a building (e.g. piles or retaining walls). The key factor in the sustainability of such system is the use of the building elements which are already needed for structural reasons. The parallel combination of several heat exchanger piles, hydraulically connected and linked to a heat pump, permits the extraction of warmth from the ground to satisfy the need for heat in winter and to expel excess heat resulting from air conditioning in summer (Figure 1). With this geothermal use of geostructures, buildings can be cooled at minimal cost and cheaply heated with a heat pump, using the available geothermal energy in the ground and the natural thermal properties of the concrete. From a geotechnical point of view, heating of foundations may also have an important advantage in the improvement of the soil characteristics (Cekerevac and Laloui, 2004). This may result in a reduction in foundation cost. Another potentially significant practical and technological aspect concerns our recently obtained results showing that the thermal pre-treatment of clays may have a very positive effect on their resilience under cyclic loading, which results in higher resistance of the buildings against earthquakes (Laloui et al., 2005). In any case, freezing of the piles is to be avoided by continuous monitoring and control systems to prevent thaw-induced defects.

The heat exchanger technology, although very successful in Switzerland (e.g. Zürich Airport) and world-wide (more than 300 installations in Europe), faces the lack of rational knowledge of the thermal effects on the behaviour of the foundations. In particular, no analytical, physical or numerical tools are yet available to consider the complex interactions between thermal storage and the mechanical behav-

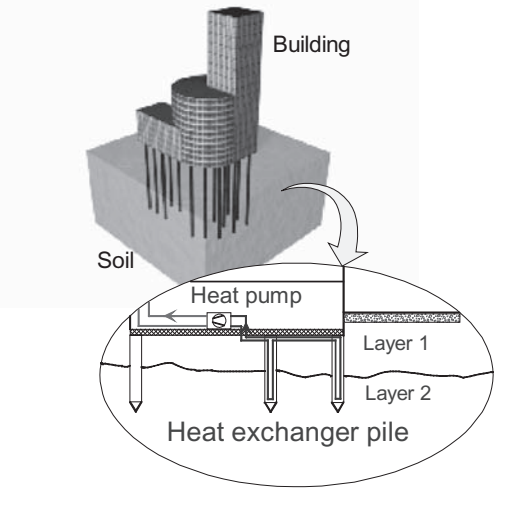

Figure 1. Schematic representation of a heat exchanger pile system.

iour of geostructures. This paper highlights some features of the behaviour of a heat exchanger pile. The thermal transfers in the pile and soil will not be quantified here.

2 EXPERIMENTAL IN SITU TEST ON A HEAT EXCHANGER PILE

2.1 *Test site*

A four storey building under construction at the Swiss Federal Institute of Technology (EPFL) in Lausanne (Switzerland) was chosen for an in-situ test of a heat exchanger pile (Laloui et al., 2003). The building is 100 m in length and 30 m in width and is founded on 97 piles approximately 25 m in length. The tested pile was located at the side of the building. The drilled pile diameter was 88 cm and the length was 25.8 m. The schematic soil stratigraphy profile is presented in Figure 2. The groundwater table in this zone is very close to the ground surface. Polyethylene (PE) tubes were installed vertically in the reinforcing structure with a U-shaped configuration to permit the circulation of the heat-carrying fluid. The instrumentation chosen for the measurement of strain (Inaudi et al., 2000), temperature and load in this in situ test was made up of 58 gauges placed as indicated in Figure 2.

2.2 *Loading history*

Seven thermo-mechanical loading conditions were applied to the pile. The loading principle was to apply a mechanical load (dead weight of superstructure at the construction of each storey) and a temperature variation controlled by a heating device. The two types of loads were applied separately and alternately in order to decouple the thermal and mechanical effects. Test 1 differs from the others with regard to the free displacement boundary condition of the pile head. For the other tests, the pile was blocked in its movement by the applied mechanical load (weight of the building under construction).

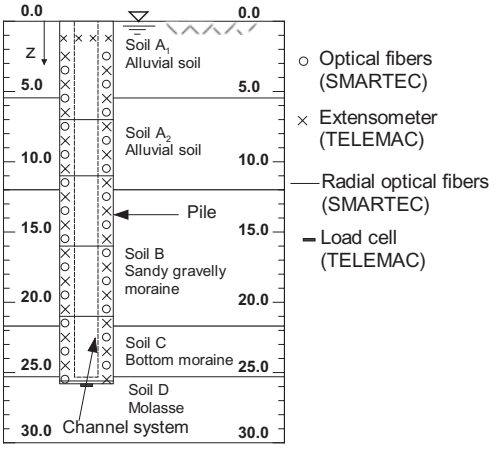

Figure 2. Soil profile and instrumentation of the tested pile.

3 FINITE ELEMENT MODEL

A thermo-hydro-mechanical (THM) model for saturated porous media is used to simulate the behaviour of the heat exchanger pile and the surrounding soils.

Readers may refer to (Laloui 1993, Laloui et al., 2006) for the complete mathematical formulation. It is chosen to model a single vertical pile using an axisymmetric geometry (Figure 3). The finite element nodes of the pile and the soil at the interface are assumed to have no relative movement. The contact area being modeled as the soil material, a refinement of the finite element mesh around this zone is required.

3.1 *Material characteristics*

Due to the length limitation of the paper, the material parameters are not given here. The interested reader may find them in Laloui et al. (2006). The soil is represented by five layers obeying the Drucker-Prager thermo-elastoplastic model. The pile itself is modelled with solid elements and behaves as a thermo-elastic material. The mechanical parameters were determined from triaxial tests at three confining pressures for each soil layer. The pile is considered impervious, as is the layer D (molasse formation) while the other soil layers are considered drained. The horizontal permeability coefficients were determined from in situ measurements and isotropic permeability was further assumed. The thermal parameters were estimated based on the geotechnical characteristics while the porosity of each layer was determined experimentally.

3.2 *Initial and boundary conditions*

Besides the mechanical boundary conditions defined in Figure 3, the hydraulic boundary conditions were imposed as follows:

- Layer D and pile are impervious (undrained conditions)
- Elsewhere, layers are saturated with the water table located at the top surface. Drainage takes place at the top surface and at the right hand side of the mesh.

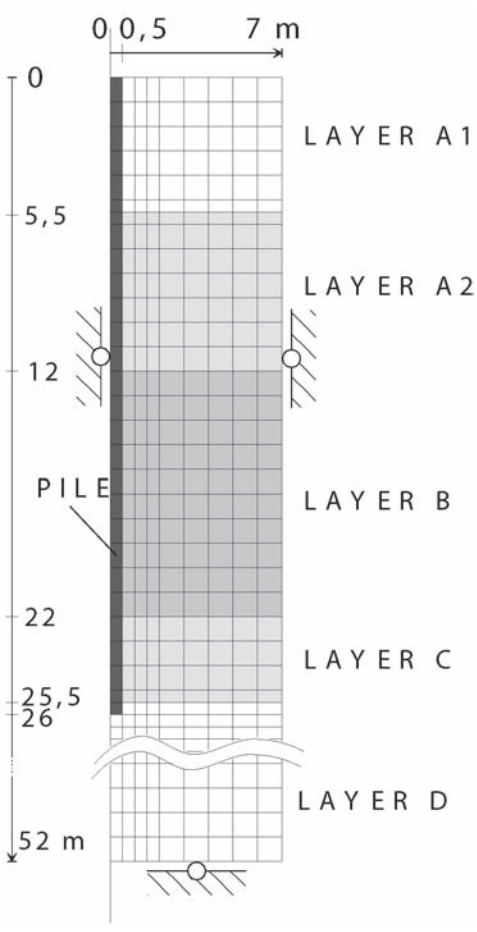

Figure 3. Finite element mesh (534 elements) and mechanical boundary conditions.

The thermal boundary conditions consist in allowing the heat to flow through the right-hand side of the mesh as well as through the bottom of the mesh.

Constant temperatures were imposed on the top surface of the mesh and the heat flux was supposed null along the axis of symmetry.

4 NUMERICAL/EXPERIMENTAL RESULTS

In this section, some of the finite element results are presented and compared with the experimental ones. We mainly focus here on the behaviour of the concrete pile. For the presented example the considered thermal loading in the pile is a heating-cooling cycle: 12 days of heating with a variation of temperature of 21°C then 16 days of cooling (Figure 4).

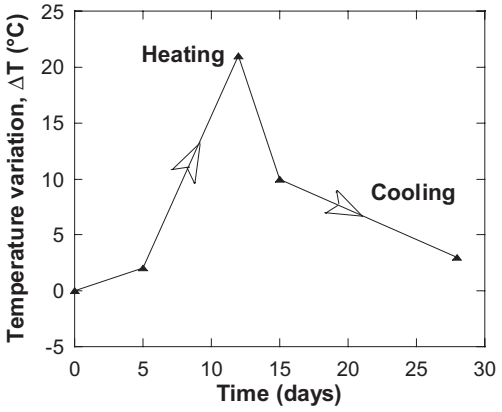

Figure 4. Temperature values imposed in the pile.

4.1 *Thermal strains*

In the case of Test 1, the thermal heating-cooling cycle was applied to the pile. No mechanical load was imposed at the pile top and the pile was free to move upwards. The imposed thermal field generated strains. Figure 5a compares the simulated thermo-elastic vertical strains with respect to the measured ones for the heating and cooling periods. Strains are not uniform during the heating period and are influenced by the friction along the pile shaft. In fact, the measurements show different straining according to the type of surrounding soil, and the layer boundaries (A, B, C and D) may be identified in Figure 5a. The model is able to reproduce this effect.

Thermo-elastic linear behaviour is observed and computed during the cooling phase. This reversibility means that the displacement of the pile with respect to the soil has not yet reached the threshold where the friction would no longer permit the pile to return to its initial state. The modeled radial strains fit the measured ones well, as may be seen for one of them (at depth of 16 m) in Figure 5b. The radial strain behaviour shows that lateral contact is still maintained between the pile and the ground after a thermal cycle.

It should be noted here that the final temperature values are different from the initial ones; this explains why the strains do not return to zero at the end of the heating-cooling cycle.

4.2 *Induced thermo-mechanical stresses*

In the case where the pile is not entirely free to move (e.g. due to side friction or blocked head and toe), part or all of the induced thermal deformation will be prevented. The constrained strains produce thermal stresses. Figure 6 gives the vertical stress profile

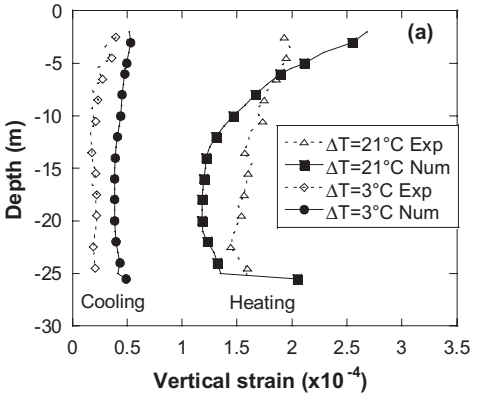

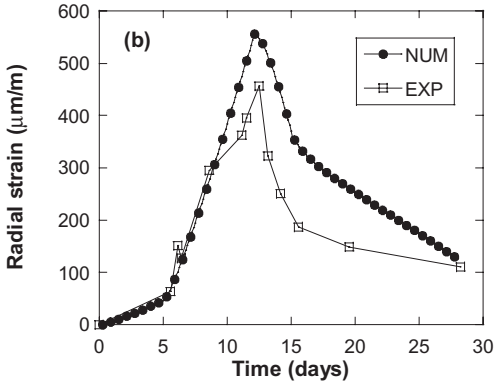

Figure 5. Thermal strains in the pile during a heating and cooling period.

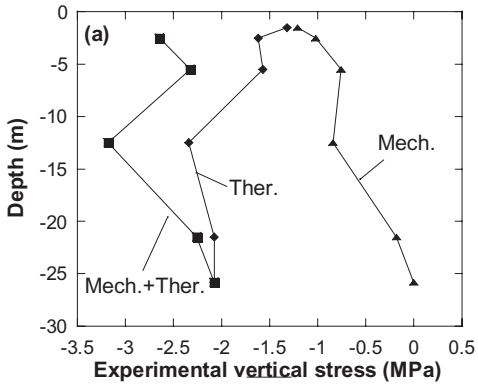

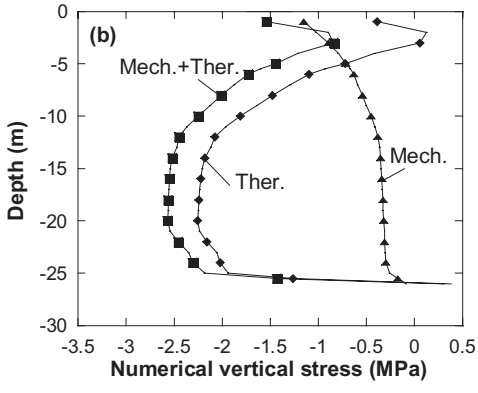

Figure 6. Thermo-mechanical vertical stresses in the pile (ΔT = 13.4°C): (a) experimental results; (b) numerical simulations.

along the pile axis due to the thermo-mechanical load in the case where the building is constructed.

The experimental results clearly show the differences between the effects of the mechanical and the thermal loading (Figure 6a). Even though the mechanical axial stress is large at the pile top (on the order of 1.3 MPa) and diminishes with depth (the toe carries almost no load), the thermal load is larger and rather uniform. This results in an overstress on the order of 1.2 MPa at the pile head and strongly loads the toe (2 MPa). An analysis of other tests shows that a temperature increment of 1°C results in an additional temperature-induced load on the order of 100 kN.

As a consequence, the total axial load in the pile is twice as large as the one due to purely mechanical loading, with a large vertical stress in the toe. The numerical model is able to reproduce the decrease in the mechanical vertical stresses with depth as well as the increase in the thermally-induced vertical stresses with depth (Figure 6b).

5 CONCLUSION

Using experimental results from local full-size in-situ test of one heat exchanger pile, a coupled displacement-temperature finite element analysis was carried out. It was assumed that : i. the concrete and the soil were governed by a thermo-elastoplastic law, and ii. the heat flow followed Fourier's law. The numerical calculations reproduce quite well the experimental results.

The thermo elastic straining of the pile presents the following main behaviours:

i. The pile deformation depends on the type of surrounding soil.

ii. Whereas the mechanical load affects mostly the top of the pile, the thermal load creates rather large axial stresses at the toe.

REFERENCES

Cekerevac, C. & Laloui., L. 2004. “Experimental study of the thermal effects on the mechanical behaviour of a clay”. *International Journal of Numerical and Analytical Methods in Geomechanics*, 28, p. 209–228.

Inaudi, D., Laloui, L. & Steinmann, G. 2000. “Looking below the surface”. *Concrete Engineering International*, 4(3).

Laloui, L. 1993. *Modélisation du comportement thermo-hydro-mécanique des milieux poreux anelastiques*. Doctoral Thesis, Ecole Centrale Paris.

Laloui, L., Cekerevac, C. & Vulliet, L. 2005. « Non-isothermal Modelling of the Cyclic Mechanical Behaviour of MC Clay ». *Proceedings of the 11th International Conference of IACMAG*, Torino, pp. 377–384.

Laloui L., Nuth M. & Vulliet L. 2006. “Experimental and numerical investigations of the behaviour of a heat exchanger pile”. *International Journal for Numerical and Analytical Methods in Geomechanics*, 30(8) pp. 763–781.

Laloui, L., Moreni, M. &Vulliet, L. 2003. “Comportement d’un pieu bi-fonction, fondation et échangeur de chaleur”. *Canadian Geotechnical Journal*, 40(2), p. 388–402.

Deep Foundations on Bored and Auger Piles – Van Impe & Van Impe (eds)
© 2009 Taylor & Francis Group, London, ISBN 978-0-415-47556-3

Energy piles in Scotland

D.J. Lennon
Stent Foundations Limited, Balmore, UK

E. Watt
Stent Foundations Limited, Balmore, UK

T.P. Suckling
Stent Foundations Limited, Basingstoke, UK

ABSTRACT: Comparative thermal conductivity testing of piles and a borehole are described. The results of installation and testing of both precast concrete and steel driven energy piles are presented. There is currently no standard UK specification for thermal conductivity testing and the three tests de-scribed were all undertaken using different procedures. It is demonstrated that piles can be used to measure the thermal properties of the ground. Foundation piles which incorporate a ground source pipe can offer a cost effective sustainable method of providing heat energy for a wide range of construction developments. Procurement and the construction sequence must be properly planned and managed to give the Client the best value for money.

1 INTRODUCTION

The sustainable use of resources is now an important part of the construction process. In the United Kingdom (UK) statutory requirements currently require a proportion of the energy usage of any new building to be provided from a renewable source. In the future the proportion required is likely to increase and when at levels above 10% ground source energy storage systems are likely to become viable in many cases.

Designers of piles have the opportunity to specify energy piles whenever piles are required to provide structural support to any building. However, it is currently very difficult to ensure that energy piles are compatible with the architectural, structural and energy design requirements unless introduced into the building design concept at an early stage.

Full scale thermal testing of in-situ piles is unfortunately still rare in the UK. Comparative tests are described on a driven concrete pile, a driven steel pile and on a pushed-in plastic coaxial pipe, all installed on a test site in Balmore, Scotland. This is the first time ever worldwide that side-by-side thermal tests on piles and a pushed-in coaxial pipe have been undertaken, and also the first time that such tests have been carried out on piles in Scotland.

2 GROUND SOURCE ENERGY SYSTEMS

The heat pump for the extraction of ground source energy was invented in the 19th Century. In Europe ground temperature is reasonably constant below about 8 m depth. This phenomenon can be used in the design of seasonal thermal ground storage, with excess energy transferred between a building and the ground throughout the year as the seasons and the building's energy requirements change.

The available energy capacity from the ground beneath or surrounding any building depends on factors including geometry, geology, groundwater and groundwater flow. Other aspects such as whether the ground surface is covered and thus not able to receive replenishing solar energy also influence the available ground source energy. Every project will thus be different and a calculation is essential for each and every building.

3 ENERGY PILES

Energy piles can be either bored or driven piles, normally comprising reinforced concrete. The piles contain plastic pipes which transport a heat transfer fluid. From the pile heads these pipes are connected to a network of pipes leading to the heat exchanger within the building. The double use of piles to provide both

structural support and to realise ground source energy has been successfully employed in central Europe since the 1980s. The first such use of piles in the UK did not take place until the 21st Century.

An important component of the economic viability of energy piles is that the length of pile appropriate for structural and geotechnical capacity is then used to provide the energy, i.e. piles should not be lengthened purely for energy purposes.

4 BALMORE TEST SITE GEOLOGY

Balmore lies in the valley of the River Kelvin to the north of Glasgow, a short distance west of the town of Torrance. The area is underlain by Drift deposits comprising glacial till and glaciofluvial sands and gravels, with alluvium in the Kelvin Valley. Beneath the Drift deposits is Carboniferous (Namurian) bedrock. Groundwater is encountered 0.75 m below ground level, flowing downhill towards the river.

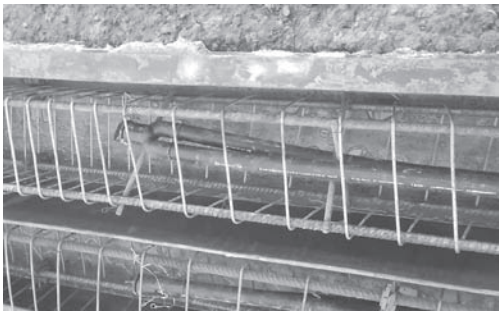

Figure 1. Precast energy pile before casting concrete.

Figure 2. Heads of precast energy piles before casting.

5 TEST PILE DETAILS

Two 12 m long precast concrete piles were manufactured with a plastic U-tube embedded in the centre of the pile (Figure 1). The 270 mm square piles were fabricated in the normal way, but with the plastic tube held in position using a cross piece shear link reinforcing bar.

Piles were manufactured with 32 mm diameter HDPE plastic pipe cast inside with the top of the pipes 200 mm from the pile head in one pile and 500 mm from the pile head in a second pile (Figure 2). This was to investigate whether there was any difference in the handling and driving characteristics of the piles, compared to a standard pile.

Figure 3. Driving of precast concrete energy piles.

Figure 4. Driven steel energy pile.

An 18 m standard pile (i.e. without pipes) was pitched and driven into the ground. This was achieved by a 6 m length driven in first, followed by joining a 12 m length on top. Second and third piles were then driven, similarly with a 6 m standard section but followed by a 12 m energy pile section attached to the top (Figure 3). All piles had a driven length of about 17 m with approximately 1 m pile left upstanding.

All piles withstood pitch and drive conditions for the different configurations of plastic tube location, and for loose and hard driving, and no differences were observed between the standard pile and the two energy piles.

In addition to the three precast concrete piles, a steel tubular pile of 244 mm diameter with a welded closed end steel shoe was also driven 17 m into the ground. A plastic U-tube, similar to before, was installed full depth and a standard cementitious grout was used to fill the pile (Figure 4).

All of the above test piles were driven during June 2007.

6 PUSHED-IN PIPE DETAILS

During August 2007, Lankelma Ltd were employed to install a pushed-in coaxial pipe (Figure 5). The borehole was advanced by cone-penetrometer pushing techniques and the 40 mm/25 mm outside diameter HDPE plastic pipe was installed to 15.8 m depth. It is presumed that after installation the soils have collapsed against the outer wall of the coaxial pipe. There is no borehole backfilling or grouting between the closed coaxial pipe and the borehole wall.

7 THERMAL CONDUCTIVITY TESTING

The testing procedure for a thermal conductivity test needs to be able to differentiate between the thermal resistance of the pile or borehole and the thermal conductivity of the ground. The general arrangement of the testing apparatus is shown in Figure 6.

The procedure is to inject heat at a constant flow rate into the pile or borehole, whilst measuring the change with time of the inlet and outlet water temperature. After sufficient time the effects of thermal storage in the plastic tube and in the pile or borehole will be overcome, and after this any temperature rise will be due only to the conductivity of the ground. The most common approach is then to plot the mean of the inlet and outlet temperatures against log time, and when the plot becomes linear the slope of this portion is used to estimate the thermal conductivity of the ground. It should be noted that there is currently no standard UK procedure or specification for thermal conductivity testing.

Figure 5. Coaxial pipe being installed.

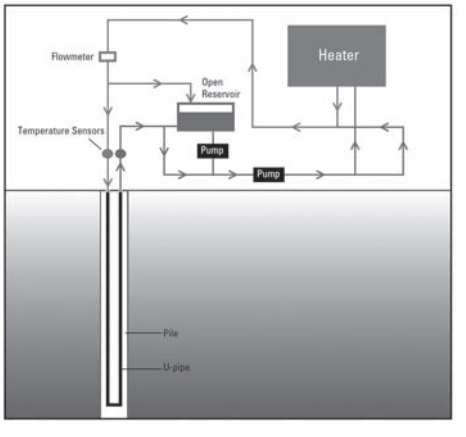

Figure 6. General arrangement for a thermal conductivity test.

8 THERMAL CONDUCTIVITY TEST RESULTS FOR THE PILES

A testing company was employed to undertake testing of the piles. Only one of the concrete energy piles, the one manufactured with the pipe cast 200 mm from the pile head, was tested (Figures 7 and 8) plus the steel pile (Figures 9 and 10).

Figure 7. Thermal test on concrete pile.

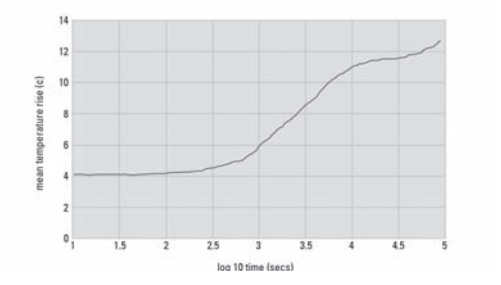

Figure 8. Test result for concrete pile.

For the test on the concrete pile, the testing company quoted that the ground thermal conductivity is 2.56 Wm-1K-1 with the thermal resistance of the pile being 0.17KmW-1. For the test on the steel pile, quoted values for the ground thermal conductivity are 2.37 Wm-1K-1 and the thermal resistance of the pile 0.11 KmW-1.

9 THERMAL CONDUCTIVITY TEST RESULTS FOR THE PUSHED-IN PIPE

Another testing company was employed to undertake testing of the borehole (Figures 11 and 12), which was located 10 m from the nearest pile.

For the test on the borehole, this testing company quoted that the ground thermal conductivity is 2.1 ± 0.5 Wm-1K-1 with the thermal resistance of the

Figure 9. Thermal test on steel pile.

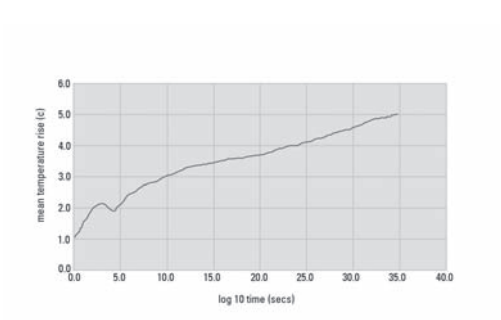

Figure 10. Test result for steel pile.

Figure 11. Thermal test on pushed-in pipe.

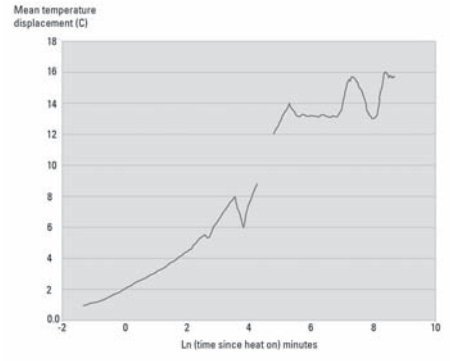

Figure 12. Test result for pushed-in pipe.

borehole being in the range 0.005 to 0.11 KmW-1. It was stated that the latter portion of the test data indicated that global thermal conductivity of the ground could be as high as 7 Wm-1K-1, due to advection with the flow of groundwater. This borehole was expected to be able to exchange 1 kW of heat with the ground over 3 days.

10 REVIEW OF RESULTS

Measured ground thermal conductivity values are;

- concrete pile; 2.56 Wm-1K-1
- steel pile; 2.37 Wm-1K-1
- borehole; 2.1 ± 0.5 Wm-1K-1.

Measured thermal resistances are;

- concrete pile; 0.17KmW-1
- steel pile; 0.11KmW-1
- borehole; 0.005 to 0.11KmW-1.

The values of ground thermal conductivity range 1.6 to 2.6 Wm-1K-1. Moisture content has a significant influence on measured values and published data can be summarised as;

saturated clay <2.5 Wm-1K-1
saturated sand <3.5 Wm-1K-1
concrete 1.3 Wm-1K-1
water 0.6 Wm-1K-1.

Thus the results from the three tests all appear to be reasonable although it is not known which particular value would be most appropriate for design.

The borehole offers least resistance to the transfer of heat between the fluid in the plastic pipe and the ground. The concrete pile offers more resistance than the grout filled steel tubular pile.

11 PROCUREMENT PROCESS AND CO-ORDINATION OF SUBCONTRACTORS

The management of building works involving ground source heating systems can quickly become complex if the multiple specialist disciplines are not controlled from one source. There are two project management models developing in the UK at present and these are described below;

(1) Led by the Engineer

Here a typical project organization would involve a) the Client with a Quantity Surveyor, b) the Structural Engineer, c) the Mechanical and Electrical Consultant, d) Main Contractor, e) Ground Source Installation Contractor, f) Ground Source Designer, g) Heat Exchanger Supplier, h) Foundations Contractor and i) Site investigation Contractor.

It is best if the Structural Engineer and the Mechanical and Electrical Consultant are the same organisation. This organisation then needs to be capable of managing the Ground Source Installation Contractor, Heat Exchanger Supplier, Foundations Contractor and the Site investigation Contractor. Interfaces of responsibility reduce if the Mechanical and Electrical Consultant is the designer for both internal heating and cooling plant, including air-conditioning, and for external ground source energy supply. Problems commonly arise in this model when one contractor cannot provide the full range of services specified, or when the specification is inconsistent or incomplete.

For example, the Site Investigation Contractor may also be able to provide the services of Ground Source Installation Contractor. Alternatively, the Foundations Contractor may be able to provide the services of both Site Investigation Contractor and Ground Source Installation Contractor. Here the Foundations Contractor may claim that he can also provide the services of Heat Exchanger Supplier, however in reality this will be another supplier. It is clear that the Ground Source Installation Contractor, Ground Source Designer and Heat Exchanger Supplier require a very close working relationship. For example the flow rate and carrier fluid used, combined with the characteristics of the ground and the ground-pipe contact material, will all have a direct influence on the ability of the heat exchanger to work at full capacity.

(2) Led by the Contractor

The second model is contractor led and here the Main Contractor is responsible for the management of design and build specialists. The ideal scenario is once again that Structural Engineer and the Mechanical and Electrical Consultant are the same organisation. The Mechanical and Electrical Consultant calculates and provides the heating and cooling load requirements for the building and prepares tender documents which require a heating, cooling and

ventilation solution. The clarity of these documents is essential.

The Ground Source Installation Contractor could be a single source design and installation service, incorporating Ground Source Designer and Heat Exchanger Supplier. It would be possible for Ground Source Installation Contractor, Ground Source Designer, Heat Exchanger Supplier, Foundations Contractor and the Site investigation Contractor to work together to provide one package of works. It is also possible that the Ground Source Installation Contractor can provide associated specialist construction services such as underfloor heating pipe installation including the screed and finishes.

In both project management models, it is critical that the overlap between the ground source system installation and substructure construction is planned. At tender stage in the Contractor led model, the Ground Source Installation Contractor should include written proposals for installation and connection methods. The pile head preparation (for energy piles) or the borehole head connection, together with trenching, pipe-laying, backfill materials, timescales and plant involved need to be described in detail. Attendances required from the Main Contractor by each party can then be identified.

12 PILE INSTALLATION AND CONNECTIONS

Typically the material used for a ground source system is HDPE plastic pipe. The ground loop can be installed in a borehole or cast into a pile, or it can be pushed directly into the ground. When drilled boreholes are used it is important to note that thermally enhanced grout is required to improve thermal conductivity between the pipework and the ground. A bentonite backfill will act as an insulator and inhibit heat conduction.

When heat exchangers are operational they are pumping the carrier fluid through a pipe network. The pipe network requires to be sealed at all connections and should be pressure tested continuously as part of the installation works. The best and quickest method of jointing the pipework is by fusion welding. This process involves melting a collar onto two butt ended sections of the pipe. Fusion welding is an electrical technique which creates a full circumference seal if used with purpose made equipment.

When carrier fluid in a closed pipe loop is likely to be exposed to very low temperatures it will be necessary to ensure that freezing does not occur. Antifreeze is often included in the fluid to overcome this. Properly sealed pipework will provide efficient flow to the heat pump and avoid any possible contamination of groundwater. The use of antifreeze in the carrier fluid raises the issue of ground contamination in the event that pipes leak or burst. The Environment Agency in the UK may restrict which types can be used in the future. A future ban on standard antifreeze types may mean that existing systems need to replace their fluid which could be a large expense for industrial scale systems currently in operation.

If boreholes or energy piles are to be adopted within the footprint of a proposed building, there is a large construction phase interface between the substructure construction and the pipe laying and trenching works. When pipework is within the building footprint, the installation head manifold needs to be constructed and the pipework should then be taken by the shortest route into a single trench. This trench can then be routed straight to the plant room. This is the quickest method of clearing the substructure such that pile caps can be constructed. This requires a clearly defined order of responsibility for pile head preparation, trenching, pipelaying, backfilling and pile cap construction including manifold protection.

Alternatively, if the borehole field or energy pile array (where the piles are not to be loaded) is located outside of the building footprint, the trenching and pipe laying operation will have no interface with the substructure and could be simultaneous to pile cap construction. If an energy pile array is used, there is no structural head preparation. The pipework can then be placed and the pile head buried.

13 CONCLUSIONS

Comparative thermal conductivity testing of piles and a borehole are described. The results of installation and testing of both precast concrete and steel driven energy piles are presented.

There is currently no standard UK specification for thermal conductivity testing and the three tests described were all undertaken using different procedures.

It is demonstrated that piles can be used to measure the thermal properties of the ground and this form of testing could be considered in future to be included as an additional part of any proposed programme of pile load testing.

Foundation piles which incorporate a ground source pipe can offer a cost effective sustainable method of providing heat energy for a wide range of construction developments. However, procurement and the construction sequence must be properly planned and managed to give the Client the best value for money.

REFERENCES

Brandl, H., 1998, Energy piles for heating and cooling buildings, 7th International Conference on Piling and Deep Foundations, Vienna, Austria.

Ennigkeit, A. and Katzenbach, R., 2001, The double use of piles as foundation and heat exchanging elements, 15th International Conference on Soil Mechanics and Geotechnical Engineering, Istanbul, Turkey.

Suckling, T.P. and Smith, P., 2002, Environmentally friendly geothermal piles at Keble College, Oxford, UK, Deep Foundations Institute Conference, Nice, France.

Suckling, T.P. and Cannon, R., 2004, Energy piles for Pallant House Art Gallery, Chichester, UK, Ground Engineering, July.

Lennon, D.J., Watt, E. and Suckling, T.P, 2009, Thermal response tests on driven piles and a pushed-in pipe at Balmore, Scotland, Thermal Characteristics of the Ground, Geotechnique Symposium in Print.

Deep Foundations on Bored and Auger Piles – Van Impe & Van Impe (eds)
© 2009 Taylor & Francis Group, London, ISBN 978-0-415-47556-3

Author index

We all should request the fundamental right to be wrong, especially when related to discussions on very difficult and specialized topics such as the screw or bore pile-soil interaction problem.

The outcome of such discussion sessions however generally results in a remarkable levelling up of our understanding. This cannot be acquired without an intensive interplay among academicians, design specialists and contractors.

Although progressing very well over the last years, the design criteria for bored and auger piles are still not fully under control and in acceptable synergism with the real pile foundation behaviour. The economic situation over the past couple of years in many countries worldwide, had some braking influence on several research minded initiatives linked to the deep foundation engineering. On the other hand, such strong and difficult competitive market, also favorized the ingenuity of the contractor's world. A striking example of such development is linked to the ideas on energy piles; a topic discussed as well in these proceedings.

CRC Press
Taylor & Francis Group
an **informa** business
www.crcpress.com

6000 Broken Sound Parkway, NW
Suite 300, Boca Raton, FL 33487
Schipholweg 107C
2316 XC Leiden, NL
2 Park Square, Milton Park
Abingdon, Oxon OX14 4RN, UK

ISBN-13: 978-0-415-47556-3
9 780415 475563

an **informa** business